HR Wallingford
Working with water

# Lake Michigan beach protection

## 2D physical modelling final report

DKR6353-RT002-R01-00 January 2021

# Document information

| | |
|---|---|
| Document permissions | Confidential - client |
| Project number | DKR6353 |
| Project name | Lake Michigan beach protection |
| Report title | 3D physical model final report |
| Report number | RT002 |
| Release number | R01-00 |
| Report date | January 2021 |
| Client | SmithGroup |
| Client representative | Margaret Boshek |
| Project manager | Dr Tim Pullen |
| Project director | Dr Terry Stewart |

# Document history

| Date | Release | Prepared | Approved | Authorised | Notes |
|---|---|---|---|---|---|
| 22 Jan 2021 | 01-00 | IDC | TAP | TPS | |

# Document authorisation

Prepared

Approved

Authorised

© HR Wallingford Ltd

This report has been prepared for HR Wallingford's client and not for any other person. Only our client should rely upon the contents of this report and any methods or results which are contained within it and then only for the purposes for which the report was originally prepared. We accept no liability for any loss or damage suffered by any person who has relied on the contents of this report, other than our client.

This report may contain material or information obtained from other people. We accept no liability for any loss or damage suffered by any person, including our client, as a result of any error or inaccuracy in third party material or information which is included within this report.

To the extent that this report contains information or material which is the output of general research it should not be relied upon by any person, including our client, for a specific purpose. If you are not HR Wallingford's client and you wish to use the information or material in this report for a specific purpose, you should contact us for advice.

# Executive Summary

Lake Michigan recently experienced record breaking high water levels and the sandy shoreline of Illinois Beach State Park, Lake Michigan has eroded significantly, damaging and threatening rare wetlands. SmithGroup are designing a coastal protection scheme to stabilise the shoreline at the park. The scheme will include beach nourishment and beach control structures. These will be shore-connected and detached breakwaters, both armoured with heavy grades of natural rock. HR Wallingford was approached by SmithGroup to undertake 2 dimensional (2D) and 3 dimensional (3D) physical modelling to investigate the stability of the rock armour on the breakwaters, assess their wave transmission and the response of the nourished beaches.

A 2-dimensional physical modelling study (DKR6353_RT001-R01-00) preceded the work described here, in which a wide range of structures were tested for wave transmission. The purpose of those tests was to optimise the breakwater cross-sections and confirm the stability of the principal rock grade to be used in the most exposed locations. The data collected for the optimised cross-sections were used by SmithGroup to inform the size and orientation of the beach control structures used during the 3-dimensional physical modelling campaigns described here.

Beach State Park, Lake Michigan includes three distinct areas (Area 1: North Beach, Area 2: Camp Logan, and Area 3: Swimming Beach) and for each of these a separate physical modelling campaign was commissioned. In each case, the modelling programme consisted of two phases: firstly, the optimisation of the beach control structures to stabilise the beach and reduce sediment drift during persistent morphological wave conditions; secondly, confirmation tests were run to assess the stability of the rock armoured beach control structures under extreme wave and water level conditions.

This report includes details on the background to the study, the methods, techniques and facilities used, and the wave conditions and water levels used throughout the testing campaign. This information is contained within the first four Sections of this report, and each of the next three Sections describe in detail the design, test programme and results for each of the three separate model studies. The general procedure for each being the same and commenced with the optimisation of the beach control structures using proxies for the armoured rubble mounds and lightweight anthracite sediment. This was tested with a generic morphological wave condition that was able to mobilise the anthracite without affecting the beach response due to wave breaking significantly. The assessment for each layout was carried out by comparing and contrasting scanned and photographic beach plan shapes. Following the optimisation of the beach control structure layout, the proxy armoured structures and the anthracite beaches were removed from the model, and fully scaled model armour breakwaters were then constructed and the beach material was replaced with modelling sand. A full suite of armour stability and beach storm response tests were then run from two directions using a series of storm conditions.

## Area 1 – North Beach (Section 5)

The Area 1 model examined the North Beach area of Lake Michigan. To the north of this area, are harder engineered structures that are holding the coastline, whilst to the immediate south, there is significant and ongoing beach erosion with a net north to south sediment drift driven predominantly by North East waves. The first phase of the model included a northern breakwater to hold the coastline adjacent to the Winthrop Yacht Club, followed by a series of shore detached groynes to encourage the development of salients and tombolos to arrest or reduce the north-south sediment drift.

Once the stable configuration had been identified, the lightweight modelling sediment was replaced with a fine grained modelling sand with the correct density. The final configuration of proxy armourstone structures was replaced with correctly sized and scaled model rock structures, and the whole was then tested with a sequence of six wave and water level conditions from both the North East and South East wave directions.

A total of ten beach control structures of various cross-sections and armourstone grades were utilised for the final configuration. It is demonstrated that a stable beach can be maintained with a reduced north-south sediment drift using the final configuration. The beaches remained static during most of the stability tests, however for the extreme high water 1:10 and 1:100 return period storms, a wide crest at the beach could not be maintained and there was a net transfer of sediment to the immediate hinterland.

The beach control structures resistance to wave action during the stability test programme, demonstrated that all structures, with some exceptions, were substantially intact at the end of the testing campaign. Where damage was noticeable and exceeded recommended damage levels, that information was passed forward to the following models and the rock grades were modified accordingly.

## Area 2 – Camp Logan (Section 6)

The Area 2 model examined the Camp Logan area of Lake Michigan, situated to the South of Area 1. To the north of this area is Kellogg Creek which creates a small headland into the lake. To the immediate south, there is significant and ongoing beach erosion with a net north to south sediment drift driven predominantly by North East waves, as in Area 1. The first phase of the model included a northern breakwater coming from the small headland to hold the coastline adjacent to Kellogg Creek, followed by a series of shore detached groynes to encourage the development of salients and tombolos to arrest or reduce the north-south sediment drift. As with Area 1, this was done using sandbags to act as proxies for armourstone breakwaters and allowed multiple configurations to be examined using a lightweight modelling sediment. This was tested with a generic Morphological wave condition that was able to mobilise the modelling sediment without affecting the beach response due to wave breaking significantly.

Once a stable configuration had been identified, then as with Area 1, the lightweight modelling sediment was replaced with a fine grained modelling sand with the correct density. Then seven beach control structures of various cross-sections and armourstone grades were utilised for the final configuration. It is demonstrated that a stable beach can be maintained with a reduced north-south sediment drift using the final configuration. The beaches remained static during the stability tests, with a wide crest at the beach maintained throughout.

The beach control structures resistance to wave action during the stability test programme, again demonstrated that all structures, with some exceptions, were substantially intact at the end of the testing campaign.

## Area 2 – Swimming Beach (Section 7)

The Area 3 model examined the Swimming Beach area of Lake Michigan, situated some distance to the South of Area 2. In the North of this area is the swimming beach and to the South is a hotel and wedding venue complex currently protected by hard engineered structures. To the area immediately south of the modelled area, there is significant and ongoing beach erosion with a net north to south sediment drift driven predominantly by North East waves, as in Area 1 and 2. The first phase of the model included a series of shore detached groynes and encourage the development of salients and tombolos to arrest or reduce the north-south sediment drift.

As with the previous two models, and following confirmation of a stable configuration, the modelling sediment was changed, and correctly sized and scaled model rock structures were constructed. This included five

beach control structures of various cross-sections and armourstone grades. It is demonstrated that a stable beach can be maintained with a reduced north-south sediment drift using the final configuration. The beaches remained static during the stability tests, with a wide crest at the beach maintained throughout. All structures were substantially intact at the end of the testing campaign.

# Contents

Executive Summary

1. Introduction 1
   - 1.1. Project overview 1
   - 1.2. Objectives and scope of study 1
   - 1.3. Modelling overview 1
   - 1.4. Report outline 2
2. Test facilities and methods 4
   - 2.1. Model scale 4
   - 2.2. Wave basin and bathymetry 4
   - 2.3. Model construction 5
   - 2.4. Model materials 6
     - 2.4.1. Model rock grades and scaling 6
     - 2.4.2. Mobile material scaling 8
   - 2.5. Wave calibration 11
     - 2.5.1. Morphological wave conditions 11
     - 2.5.2. Stability wave conditions 12
   - 2.6. Beach morphology measurements 13
     - 2.6.1. 3D laser scanning 13
     - 2.6.2. Photographic time-lapse beach evolution mapping 14
   - 2.7. Dye tracing measurements 14
   - 2.8. Armour stability measurement and performance criteria 14
     - 2.8.1. Performance criteria 15
3. Wave conditions and water levels 16
   - 3.1. Morphological test conditions 16
     - 3.1.1. Morphologically significant wave direction 16
     - 3.1.2. Selection of test conditions 23
   - 3.2. Stability test conditions 24
4. Test programme 25
5. Area 1 – North Beach 27
   - 5.1. Wave basin layout 27
     - 5.1.1. Area 1 beach material placement 27
   - 5.2. Test sections 32
     - 5.2.1. Morphological testing 32
     - 5.2.2. Stability testing 32
   - 5.3. Wave calibration results 37
   - 5.4. Morphological tests results – anthracite beach 40
   - 5.5. Dye tracing tests 45
   - 5.6. Storm response and morphological tests results – sand beach 45
     - 5.6.1. Storm response from NE conditions 45

5.6.2. Storm response from SE conditions ..... 46
5.6.3. Morphological response from SE ..... 47
5.6.4. Morphological response from NE ..... 48
5.7. Stability test results ..... 50
5.8. Summary ..... 59
6. Area 2 – Camp Logan ..... 60
6.1. Wave basin layout ..... 60
6.1.1. Area 2 beach material placement ..... 60
6.2. Test sections ..... 64
6.2.1. Morphological testing ..... 64
6.2.2. Stability testing ..... 64
6.3. Wave calibration results ..... 73
6.4. Morphological tests results – anthracite beach ..... 75
6.5. Dye tracing tests ..... 80
6.6. Kellogg Creek tests ..... 80
6.6.1. Phase 1 dye tracing optimisation tests ..... 80
6.6.2. Phase 2 morphological confirmation tests ..... 84
6.7. Storm response tests results – sand beach ..... 86
6.7.1. Storm response from SE conditions ..... 86
6.7.2. Storm response from NE conditions ..... 87
6.8. Stability test results ..... 88
6.9. Summary ..... 97
7. Area 3 – Swimming Beach ..... 98
7.1. Wave basin layout ..... 98
7.1.1. Area 3 beach material placement ..... 98
7.2. Test sections ..... 102
7.2.1. Morphological testing ..... 102
7.2.2. Stability testing ..... 102
7.3. Wave calibration results ..... 107
7.4. Morphological tests results – anthracite beach ..... 109
7.5. Dye tracing tests ..... 114
7.6. Storm response tests results – sand beach ..... 114
7.6.1. Storm response from SE conditions ..... 114
7.6.2. Storm response from NE conditions ..... 115
7.7. Stability test results ..... 117
7.8. Summary ..... 124
8. Summary ..... 125
9. References ..... 126
Appendices ..... 127
A. Rock grading curves
B. Area 1 – North Beach: morphological and stability photographs and scan data

C. Area 2 – Camp Logan: morphological and stability photographs and scan data

D. Area 3 – Swimming Beach: morphological and stability photographs and scan data

## Figures

Figure 1.1: Study location ..... 3
Figure 2.1: Model bathymetry under construction – Area 1 model ..... 5
Figure 2.2: Wave condition WC_HIGH_WL from Area 2 model, showing significant transfer of Incident spectral wave energy due to wave breaking against the idealised Target spectrum ..... 13
Figure 3.1: Area 1 wave rose, percentage occurrence excluding calms ..... 18
Figure 3.2: Area 1 calculation of morphologically significant direction (61°N, 0 nett drift) ..... 18
Figure 3.3: Area 2 wave rose, percentage occurrence excluding calms ..... 20
Figure 3.4: Area 2 calculation of morphologically significant direction (65°N, 0 nett drift) ..... 20
Figure 3.5: Area 3 wave rose, percentage occurrence excluding calms ..... 22
Figure 3.6: Area 3 calculation of morphologically significant direction (65°N, 0 nett drift) ..... 22
Figure 5.1: Arrangement of beach-normal templates for initial anthracite beach placement for Area 1 ..... 28
Figure 5.2: Area 1 basin layout showing the location of the wave gauges during the anthracite morphological tests ..... 29
Figure 5.3: Wave gauge locations for Area 1 stability and sand beach morphological tests ..... 30
Figure 5.4: Initial layout of Area 1 beach control structures for morphological tests ..... 31
Figure 5.5: Layout drawing of beach control structures for stability tests ..... 33
Figure 5.6: BW1-1 cross-section for stability tests ..... 33
Figure 5.7: BW1-1 long-section for stability tests ..... 34
Figure 5.8: BW1-2 cross-section for stability tests ..... 34
Figure 5.9: BW1-3 cross-section for stability tests ..... 34
Figure 5.10: BW1-4 cross-section for stability tests ..... 35
Figure 5.11: BW1-4 long-section for stability tests ..... 35
Figure 5.12: BW1-5, 1-6 and 1-8 cross-section for stability tests ..... 35
Figure 5.13: BW1-5 long-section for stability tests ..... 35
Figure 5.14: BW1-6 long-section for stability tests ..... 36
Figure 5.15: BW1-7 and 1-10 cross-section for stability tests ..... 36
Figure 5.16: BW1-7 and 1-10 saddle cross-section for stability tests ..... 36
Figure 5.17: BW1-7 long-section for stability tests ..... 36
Figure 5.18: BW1-8 long-section for stability tests ..... 37
Figure 5.19: BW1-9 long-section for stability tests ..... 37
Figure 5.20: BW1-10 long-section for stability tests ..... 37
Figure 5.21: BW1-10 Fish Tail long-section for stability tests ..... 37
Figure 5.22: Fish Tail cross-sections for stability tests (BW1-6, 1-8, 1-9 and 1-10) ..... 37
Figure 5.23: Area 1 Morph_03 spectral plot ..... 39
Figure 5.24: Area 1 Morph_03 Rayleigh plot ..... 39
Figure 5.25: Post-test scan data for Area 1 Configuration 22 (Scan26), solid area post-test beach, structures in magenta ..... 40
Figure 5.26: Pre (top) and post-test (bottom) photographs from ‘North’ view for Area 1 Configuration 01 ..... 41

Figure 5.27: Pre (top) and post-test (bottom) photographs from 'South' view for Area 1 Configuration 01 ..... 42
Figure 5.28: Pre (top) and post-test (bottom) photographs from 'North' view for Area 1 Configuration 22 ..... 43
Figure 5.29: Pre (top) and post-test (bottom) photographs from 'South' view for Area 1 Configuration 22 ..... 44
Figure 5.30: Area 1 stability post Test Part 04 beach scan data, SWL 585.2 ft IGLD 85 (pre-test scan in green, post-test scan in red, structure outline in green) ..... 46
Figure 5.31: Area 1 stability post Test Part 06 beach scan data, SWL 582.2 ft IGLD 85 (pre-test scan in green, post-test scan in red, structure outline in green) ..... 46
Figure 5.32: Area 1 beach scan data post Morph_SE_01, SWL 579.2 ft IGLD 85 (pre-test scan in yellow, post-test scan in orange, structure outline in green) ..... 47
Figure 5.33: Area 1 beach scan data post Morph_SE_02, SWL 582.4 ft IGLD 85 (pre-test scan in green, post-test scan in purple, structure outline in green) ..... 48
Figure 5.34: Area 1 beach scan data post 6 hr (1 hr model) test of Morph_03, SWL 582.4 ft IGLD 85 (pre-test scan in dark blue, post-test scan in green, structure outline in green) ..... 49
Figure 5.35: Area 1 beach scan data post 59 hr (10 hrs model) test of Morph_03, SWL 582.4 ft IGLD 85 (pre-test scan in dark blue, post-test scan in cyan, structure outline in green) ..... 49
Figure 5.36: Area 1 stability analysis panels ..... 51
Figure 6.1: Area 2 basin layout showing wave gauge locations for anthracite morphological tests ..... 61
Figure 6.2: Wave gauge locations for Area 2 stability and sand beach storm response tests ..... 62
Figure 6.3: Initial layout of Area 2 beach control structures for morphological tests ..... 63
Figure 6.4: Layout drawing of beach control structures for stability tests (armour grades given in key) ..... 65
Figure 6.5: BW2-1 trunk cross-section for stability tests ..... 65
Figure 6.6: BW2-1 seaward end cross-section for stability tests ..... 66
Figure 6.7: BW2-1 long-section for stability tests (seaward end only) ..... 66
Figure 6.8: BW2-2 trunk cross-section for stability tests ..... 66
Figure 6.9: BW2-3 trunk cross-section for stability tests ..... 67
Figure 6.10: BW2-4 trunk cross-section for stability tests ..... 67
Figure 6.11: BW2-4 long-section for stability tests ..... 67
Figure 6.12: BW2-5a trunk cross-section for stability tests ..... 68
Figure 6.13: BW2-5b trunk cross-section for stability tests ..... 68
Figure 6.14: BW2-5 long-section for stability tests ..... 68
Figure 6.15: BW2-6 trunk cross-section for stability tests ..... 69
Figure 6.16: BW2-6 long-section for stability tests ..... 69
Figure 6.17: BW2-7 trunk cross-section for stability tests ..... 69
Figure 6.18: Fishtail generic cross-section for stability tests ..... 70
Figure 6.19: Healthy Port Futures fortified ridge (4) trunk cross-section for stability tests ..... 70
Figure 6.20: Healthy Port Futures basic ridge (5) trunk cross-section for stability tests ..... 71
Figure 6.21: Healthy Port Futures habitat ridge, deformed, (6) trunk cross-section for stability tests ..... 71
Figure 6.22: Healthy Port Futures layout ..... 72
Figure 6.23: Area 2 Morph_03 spectral plot ..... 74
Figure 6.24: Area 2 Morph_03 Rayleigh plot ..... 74
Figure 6.25: Post-test scan data for Area 2 Configuration 17, solid area post-test beach, structures in magenta with spot-heights given for key locations ..... 75

Figure 6.26: Pre (top) and post-test (bottom) photographs from 'North' view for Area 2 Configuration 01 ..... 76
Figure 6.27: Pre (top) and post-test (bottom) photographs from 'South' view for Area 2 Configuration 01 ..... 77
Figure 6.28: Pre (top) and post-test (bottom) photographs from 'North' view for Area 2 Configuration 17 ..... 78
Figure 6.29: Pre (top) and post-test (bottom) photographs from 'South' view for Area 2 Configuration 17 ..... 79
Figure 6.30: Kellogg Creek Configuration 1 – showing initial dye placement ..... 81
Figure 6.31: Kellogg Creek Configuration 2 – showing initial dye placement ..... 81
Figure 6.32: Kellogg Creek Configuration 3 – showing initial dye placement ..... 82
Figure 6.33: Kellogg Creek Configuration 4 – showing initial dye placement ..... 82
Figure 6.34: Kellogg Creek Configuration 4 with additional beach material – showing initial dye placement ..... 83
Figure 6.35: Kellogg Creek Configuration 5 – showing initial dye placement ..... 83
Figure 6.36: Kellogg Creek Configuration 6 – showing initial dye placement ..... 84
Figure 6.37: Kellogg Creek morphological test pre-test photograph ..... 85
Figure 6.38: Kellogg Creek morphological test post-test photograph ..... 85
Figure 6.39: Area 2 stability post Test Part 02 beach scan data, SWL 582.2 ft IGLD 85 (pre-test scan in green, post-test scan in red, structure outline in green) ..... 86
Figure 6.40: Area 2 stability post Test Part 04 beach scan data, SWL 583.3 ft IGLD 85 (pre-test scan in green, post-test scan in red, structure outline in green) ..... 87
Figure 6.41: Area 2 stability post Test Part 06 beach scan data, SWL 585.2 ft IGLD 85 (pre-test scan in green, post-test scan in red, structure outline in green) ..... 87
Figure 6.42: Area 2 stability analysis panels ..... 89
Figure 7.1: Area 3 basin layout showing wave gauge locations for anthracite morphological tests ..... 99
Figure 7.2: Wave gauge locations for Area 3 stability and sand beach storm response tests ..... 100
Figure 7.3: Initial layout of Area 3 beach control structures for morphological tests ..... 101
Figure 7.4: Layout drawing of beach control structures for stability tests (armour grades given in key) ..... 103
Figure 7.5: BW3-1 2-4 t armour cross-section ..... 103
Figure 7.6: BW3-1 1-2 t armour cross-section (also section for BW3-2 and BW3-3) ..... 104
Figure 7.7: BW3-1 0.5-1 t armour cross-section (also section for BW3-2 and BW3-3) ..... 104
Figure 7.8: BW3-2 2-4 t armour cross-section (also section for BW3-3) ..... 105
Figure 7.9: BW3-3 3-6 t armour cross-section ..... 105
Figure 7.10: BW3-4 2-4 t armour cross-section ..... 106
Figure 7.11: BW3-1 1-2 t armour cross-section ..... 106
Figure 7.12: BW3-5 1-2 t armour cross-section ..... 107
Figure 7.13: Area 3 Morph_03 spectral plot ..... 108
Figure 7.14: Area 3 Morph_03 Rayleigh plot ..... 108
Figure 7.15: Post-test scan data for Area 3 Configuration 34, solid area post-test beach, structures in orange with spot-heights given for key locations ..... 109
Figure 7.16: Pre (top) and post-test (bottom) photographs from 'North' view for Area 3 Configuration 01 ..... 110
Figure 7.17: Pre (top) and post-test (bottom) photographs from 'South' view for Area 3 Configuration 01 ..... 111

Figure 7.18: Pre (top) and post-test (bottom) photographs from 'North' view for Area 3 Configuration 34 ..... 112
Figure 7.19: Pre (top) and post-test (bottom) photographs from 'South' view for Area 3 Configuration 34 ..... 113
Figure 7.20: Area 3 stability Test Part 01 beach scan data, SWL 579.2 ft IGLD 85 (pre-test scan in green, post-test scan in red, structure outline in green) ..... 115
Figure 7.21: Area 3 stability Test Part 02 beach scan data, SWL 582.2 ft IGLD 85 (pre-test scan in green, post-test scan in red, structure outline in green) ..... 115
Figure 7.22: Area 3 stability Test Part 03 beach scan data, SWL 576.0 ft IGLD 85 (pre-test scan in green, post-test scan in red, structure outline in green) ..... 116
Figure 7.23: Area 3 stability Test Part 04 beach scan data, SWL 583.3 ft IGLD 85 (pre-test scan in green, post-test scan in red, structure outline in green) ..... 116
Figure 7.24: Area 3 stability Test Part 05 beach scan data, SWL 585.2 ft IGLD 85 (pre-test scan in green, post-test scan in red, structure outline in green) ..... 116
Figure 7.25: Area 3 stability Test Part 06 beach scan data, SWL 585.2 ft IGLD 85 (pre-test scan in green, post-test scan in red, structure outline in green) ..... 116
Figure 7.26: Area 3 stability analysis panels ..... 118

## Tables

Table 2.1: Target rock grading characteristics in kg prototype ..... 6
Table 2.2: Target rock grading characteristics in lbs prototype ..... 7
Table 2.3: Design values of the damage parameter, $S_d$, for armour stone in a double layer with a slope of 1:1.5 ..... 15
Table 3.1: Morphologically significant wave directions by Area ..... 16
Table 3.2: Area 1 scatter table (Hs vs θ), percentage occurrence excluding calms ..... 17
Table 3.3: Area 2 scatter table (Hs vs θ), percentage occurrence excluding calms ..... 19
Table 3.4: Area 3 scatter table (Hs vs θ), percentage occurrence excluding calms ..... 21
Table 3.5: Morphological test conditions, as defined on 565 ft IGLD 85 contour ..... 23
Table 3.6: Stability test conditions, as defined on 565 ft IGLD 85 contour ..... 24
Table 4.1: Area 1 stability test sequence of wave conditions ..... 25
Table 4.2: Area 2 and 3 stability test sequence of wave conditions ..... 26
Table 5.1: Results of Area 1 morphological wave calibration at 565 ft IGLD 85 contour ..... 38
Table 5.2: Results of Area 1 stability wave calibration at 565 ft IGLD 85 contour ..... 38
Table 5.3: Area 1 sand beach Test Part and scan record ..... 45
Table 5.4: BW1-1 cumulative number of rocks displaced ..... 52
Table 5.5: BW1-1 damage parameter $S_d$ ..... 52
Table 5.6: BW1-2 cumulative number of rocks displaced ..... 53
Table 5.7: BW1-2 damage parameter $S_d$ ..... 53
Table 5.8: BW1-3 cumulative number of rocks displaced ..... 54
Table 5.9: BW1-3 damage parameter $S_d$ ..... 54
Table 5.10: BW1-4 cumulative number of rocks displaced ..... 55
Table 5.11: BW1-4 damage parameter $S_d$ ..... 55
Table 5.12: BW1-5 cumulative number of rocks displaced ..... 56
Table 5.13: BW1-5 damage parameter $S_d$ ..... 56
Table 5.14: BW1-8 cumulative number of rocks displaced ..... 57
Table 5.15: BW1-8 damage parameter $S_d$ ..... 57

Table 5.16: BW1-10 cumulative number of rocks displaced ....58
Table 5.17: BW1-10 damage parameter $S_d$ ....58
Table 6.1: Results of Area 2 morphological wave calibration at 565 ft IGLD 85 contour ....73
Table 6.2: Results of Area 2 stability wave calibration at 565 ft IGLD 85 contour ....73
Table 6.3: Area 2 sand beach Test Part and scan record ....86
Table 6.4: BW2-1 cumulative number of rocks displaced ....90
Table 6.5: BW2-1 damage parameter $S_d$ ....90
Table 6.6: BW2-2 cumulative number of rocks displaced ....91
Table 6.7: BW2-2 damage parameter $S_d$ ....91
Table 6.8: BW2-3 cumulative number of rocks displaced ....92
Table 6.9: BW2-3 damage parameter $S_d$ ....92
Table 6.10: BW2-4 cumulative number of rocks displaced ....93
Table 6.11: BW2-4 damage parameter $S_d$ ....93
Table 6.12: BW2-5 cumulative number of rocks displaced ....94
Table 6.13: BW2-5 damage parameter $S_d$ ....94
Table 6.14: BW2-6 cumulative number of rocks displaced ....95
Table 6.15: BW2-6 damage parameter $S_d$ ....95
Table 6.16: BW2-7 cumulative number of rocks displaced ....96
Table 6.17: BW2-7 damage parameter $S_d$ ....96
Table 7.1: Results of Area 3 morphological wave calibration at 565 ft IGLD 85 contour ....107
Table 7.2: Area 3 sand beach Test Part and scan record ....114
Table 7.3: BW3-1 cumulative number of rocks displaced ....119
Table 7.4: BW3-1 damage parameter $S_d$ ....119
Table 7.5: BW3-2 cumulative number of rocks displaced ....120
Table 7.6: BW3-2 damage parameter $S_d$ ....120
Table 7.7: BW3-3 cumulative number of rocks displaced ....121
Table 7.8: BW3-3 damage parameter $S_d$ ....121
Table 7.9: BW3-4 cumulative number of rocks displaced ....122
Table 7.10: BW3-4 damage parameter $S_d$ ....122
Table 7.11: BW3-5 cumulative number of rocks displaced ....123
Table 7.12: BW3-5 damage parameter $S_d$ ....123

# 1. Introduction

## 1.1. Project overview

Lake Michigan recently experienced record breaking high water levels and the sandy shoreline of Illinois Beach State Park, Lake Michigan has eroded significantly, damaging and threatening rare wetlands. SmithGroup are designing a coastal protection scheme to stabilise the shoreline at the park. The scheme will include beach nourishment and beach control structures. These will be shore-connected and detached breakwaters, both armoured with heavy grades of natural rock. HR Wallingford was approached by SmithGroup to undertake 2 dimensional (2D) and 3 dimensional (3D) physical modelling to investigate the stability of the rock armour on the breakwaters, assess their wave transmission and the response of the nourished beaches.

The 2D and 3D models examined three distinct areas - Area 1: North Beach, Area 2: Camp Logan, and Area 3: Swimming Beach. The overall study location is shown in Figure 1.1. Separate 3D physical models were undertaken for each Area. Each model initially optimised the shore-connected and detached breakwaters to provide the optimum protection for the beach material and then confirmed the stability of these optimised structures. This report describes the 3D physical modelling study of all three Areas.

Related reports:

- 2D physical modelling study final report – DKR6353-RT001-R01-00, January 2021.

## 1.2. Objectives and scope of study

3D physical model tests were required to optimise and validate the shore-connected and detached breakwater designs by examining the following parameters:

- The plan shape of the beach resulting from the different configurations of beach control structures;
- The stability of the primary rock armour layers of the beach control structures.

The vertical datum used in the study is International Great Lakes Datum 1985 (ft IGLD 85). All values given in this report are in prototype dimensions unless stated otherwise. Unless stated otherwise all length values are in feet (ft). The rock grades used in this study substantially conform to the grades specified in the CIRIA Rock Manual (2007) and are presented in metric tonnes; a table of equivalent US lbs for the final tested rocks grades is given in Table 2.2. All values given in this report are in prototype dimensions unless stated otherwise.

## 1.3. Modelling overview

The 3D physical modelling campaign described in this report started with Area 1 (North Beach), then Area 2 (Camp Logan) and concluded with Area 3 (Swimming Beach). Each model began with the optimisation of the beach control structures using proxies for armoured rubble mounds and lightweight anthracite sediment. Assessment for each layout was carried out by comparing and contrasting scanned and photographic beach plan shape. Further data on the efficacy of each layout was gleaned by using dye tracing to indicate the presence of potentially high and dangerous currents.

Following optimisation of the beach control structure layout, the proxy armoured structures and the anthracite beaches were removed from the model. Fully scaled model armour breakwaters were then constructed and the beach material was replaced with modelling sand. A full suite of armour stability and beach storm response tests were then run from two directions using a series of storm conditions. At the conclusion of each Area model, the armour performance of each beach control structure was assessed.

## 1.4. Report outline

This Report describes the main objectives of the 3D physical modelling and some basic information about the project in Section 1. Section 2 covers the model design, the facility used in the study and outlines the test methods and measurements. Section 3 describes the test conditions with the test programme following in Section 4. Sections 5, 6 and 7 cover the specific setup, structures, wave calibrations and results for Area 1, 2, and 3 respectively. Each Section starts with a brief introduction and concludes with a summary specific to each Area covered. Section 8 provides a short summary of the 3D physical modelling study.

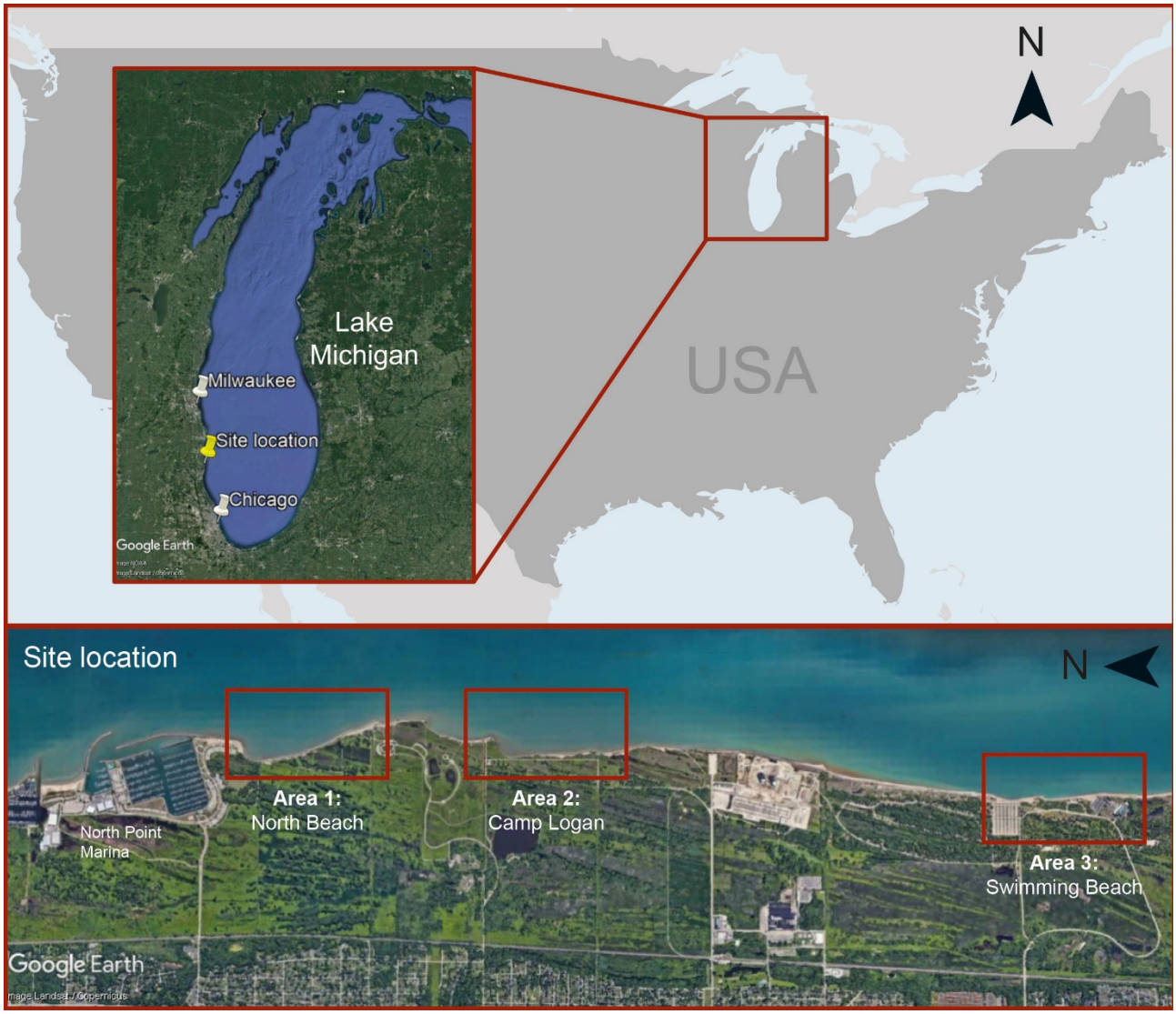


Figure 1.1: Study location

*Source: Google Earth*

# 2. Test facilities and methods

The main modelling methodologies and descriptions of the materials used are described in this section and are applicable to all three Area models. Specific details for a particular Area are provided within the section dedicated to that Area later in the report, Sections 5, 6 and 7 for Area 1, 2 and 3 respectively.

## 2.1. Model scale

The Froude scaling law is applied to physical models where gravity is the predominant factor in the fluid motion. Wave models, since wave motion is essentially a gravitational phenomenon, are therefore designed according to this law. Froude's law states that the Froude number, Fr, should be the same in model and prototype, where Fr is defined as:

$$Fr = \frac{u}{\sqrt{gL}} \qquad 2.1$$

where u is a characteristic velocity, g is the acceleration due to gravity and L is a characteristic length.

Wave models are not distorted, having the same horizontal and vertical scale. The linear scale of the model, to which the bathymetry and structures were constructed, is known as the geometric scale, $\lambda$. The Froudian scaling relationships for various different parameters are outlined below:

| | | | |
|---|---|---|---|
| Length | $\lambda$ | Time | $\lambda^{1/2}$ |
| Velocity | $\lambda^{1/2}$ | Force | $\lambda^{3}$ |
| Volume | $\lambda^{3}$ | Acceleration | 1 |
| Overtopping | $\lambda^{3/2}$ | | |

In the design of a physical model of this type, the principle concern is to ensure that the main aspects of wave-structure interaction are reproduced faithfully at a scale that avoids significant scale effects. The test section must also be of a practical size to be handled in the facility selected and with the resources available. The depth of water at the paddle must be deep enough to produce the required offshore wave heights. The level of the bathymetry at the paddle was chosen as 540 ft IGLD 85 which provides a water depth ranging between h = 36 and 45 ft over the range of still water levels covered by the study, which is more than sufficient to generate the largest wave height required at the calibration point (565 ft IGLD 85 contour), $H_{m0}$ = 12 ft. The model scale for all three Area models was set at 1:35.

## 2.2. Wave basin and bathymetry

Testing was carried out across a total of four of HR Wallingford's 3D model basins, which each have a maximum working depth of 1.0 m (metric model terms). Temporary mortar bathymetries were constructed in each basin and represented the prototype seabed down to a depth of 560 ft IGLD 85 for all three models, as shown during construction of the Area 1 model in Figure 2.1. Above the 570 ft IGLD 85 contour, the bathymetry was formed using mobile bed sediment. The bathymetry for all three models was modelled using primarily *12324-C-SURV.dwg* with additional information provided in specific photographs and surveys for each Area. The wave paddle was situated on a level of 540 ft IGLD 85 and a 1:20 approach slope was used to connect the representative bathymetry with the basin floor. The full layout of each model is provided in the relevant Sections below (Sections 5, 6 and 7).

According to the HYDRALAB III guidelines on the physical modelling of breakwaters (HYDRALAB III, 2007), the extent and depth of the bathymetry was sufficient to reproduce the near-shore processes of shoaling and breaking in the area of interest. The basin walls were lined with wave-absorbing shingle beaches to absorb waves during sea state calibration and model testing.

The waves were generated by piston type paddles, controlled by HR Wallingford's Merlin software. The paddle operation includes a steering function which allowed waves to be generated at angles to primary axis of orientation. This function was used to steer the waves to achieve the correct incident wave direction as defined at the calibration point on the 565 ft IGLD 85 contour. Vertical steel wave-guides were used to contain the waves within the modelled area, and which were also aligned with the incident wave direction.

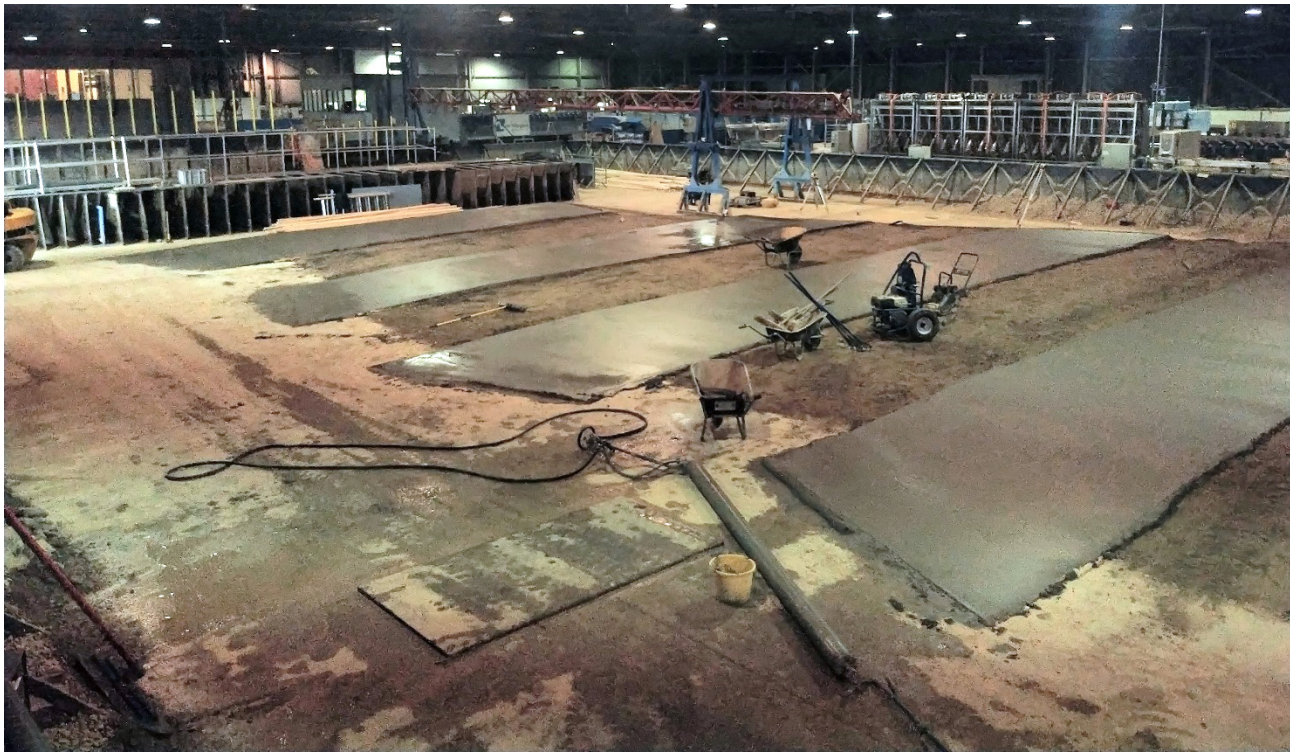

Figure 2.1: Model bathymetry under construction – Area 1 model

## 2.3. Model construction

The existing seabed for each Area modelled was represented by a solid mortar bathymetry, covering the area defined in the basin layout drawings given in the relevant Sections below (Sections 5, 6 and 7). Figure 2.1 shows the Area 1 model bathymetry under construction. For all three models, the beach control structures were constructed initially from sandbags and concrete blocks to allow their layout to be rapidly changed during the morphological testing phase. Following the optimisation of the layout of the control structures, fully scaled / armour structures were built from crushed rock appropriately sorted to reproduce the prototype material (Section 2.4.1). All material placement methods seek to reproduce the effect of standard prototype construction techniques. The core and filter layers were placed into position using hand held scoops to profiles controlled by templates that were levelled into position on the basin bathymetry.

Primary armour rocks were individually placed ensuring that each rock had a minimum of three points of contact in its layer.

The placement of the anthracite and sand beach materials varied among the different models dependent on the results and experience from previous tests (such as morphological tests), and on specific characteristics for each Area. The placement methods are described in the relevant Sections below (Sections 5, 6 and 7).

## 2.4. Model materials

### 2.4.1. Model rock grades and scaling

The rock gradings used throughout all three Area models are specified in Table 2.1 in kg prototype and in lbs prototype in Table 2.2. All rock materials have an equivalent prototype density of 2.65 tonne/m$^3$. All core and underlayer materials were scaled to reproduce the correct degree of permeability to fluid flow (permeability scaled rock). This scaling method involves making the material slightly larger than it would be if purely geometric scaling were to be applied. Details of the scaling method are given below. The model rock classes were prepared by sieving and mixing standard crushed grades. Grading curves of all armour grade prepared model rock classes are plotted in Appendix A.

All rock armour material was scaled to reproduce the stability of the armour layer correctly. This scaling method involves correcting for both the differences in density between prototype and model rock and prototype and model water. Details of the scaling method are given below. The model rock classes were prepared by weighing individual rocks on a sorting machine.

Table 2.1: Target rock grading characteristics in kg prototype

| Class | ELL (kg) | NLL (kg) | $M_{50}$ (kg) | NUL (kg) | EUL (kg) |
|---|---|---|---|---|---|
| 6-9 tonne | 4200 | 6000 | 8038 | 9000 | 13500 |
| 3-6 tonne | 2100 | 3000 | 4945 | 6000 | 9000 |
| 2-4 tonne | 1400 | 2000 | 3297 | 4000 | 6000 |
| 1-2 tonne | 700 | 1000 | 1648 | 2000 | 3000 |
| 0.5-1 tonne | 350 | 500 | 824 | 1000 | 1500 |
| 0.25-0.5 tonne | 175 | 250 | 412 | 500 | 750 |
| 450-4250 lbs | 143 | 204 | 1031 | 1928 | 2892 |
| 250-2750 lbs | 79 | 113 | 639 | 1247 | 1871 |
| 150-1600 lbs | 49 | 70 | 380 | 730 | 1095 |
| 100-950 lbs | 32 | 45 | 229 | 430 | 645 |
| 50-550 lbs | 16 | 23 | 121 | 230 | 345 |
| 20-250 lbs | 6 | 9 | 56 | 113 | 170 |
| Core | 1 | n/a | n/a | n/a | 500 |

*Source: Various documents and emails from SmithGroup providing the NLL and NUL values, remainder calculated using standard relationships given in the CIRIA Rock Manual (2007)*

Table 2.2: Target rock grading characteristics in lbs prototype

| Class | ELL (lbs) | NLL (lbs) | $M_{50}$ (lbs) | NUL (lbs) | EUL (lbs) |
|---|---|---|---|---|---|
| 6-9 tonne | 9259 | 13228 | 17720 | 19842 | 29762 |
| 3-6 tonne | 4630 | 6614 | 10902 | 13228 | 19842 |
| 2-4 tonne | 3086 | 4409 | 7268 | 8818 | 13228 |
| 1-2 tonne | 1543 | 2205 | 3634 | 4409 | 6614 |
| 0.5-1 tonne | 772 | 1102 | 1817 | 2205 | 3307 |
| 0.25-0.5 tonne | 386 | 551 | 909 | 1102 | 1653 |
| 450-4250 lbs | 315 | 450 | 2272 | 4250 | 6375 |
| 250-2750 lbs | 175 | 250 | 1409 | 2750 | 4125 |
| 150-1600 lbs | 108 | 150 | 837 | 1600 | 2414 |
| 100-950 lbs | 69 | 100 | 505 | 950 | 1422 |
| 50-550 lbs | 35 | 50 | 267 | 550 | 761 |
| 20-250 lbs | 14 | 20 | 124 | 250 | 375 |
| Core | 2 | n/a | n/a | n/a | 1102 |

### Rock scaling for permeability

In order to reproduce the permeability of the materials realistically, it was necessary to compensate for the scale effects which result from the use of Froude's scaling law. Work by Jensen and Klinting (1983) suggests a method of compensating for scale effects due to laminar flow by applying a correction factor to the ordinary geometric scale when determining rock sizes. The calculation of the correction factor uses a special Reynolds number, $\xi_p$, which is defined as the ratio of turbulent to laminar hydraulic gradients. The special Reynolds number is defined as:

$$\xi_p = \left(\frac{\beta_o}{\alpha_o}\right)\frac{1}{(n(1-n)^2)}U_p\frac{d}{v} \qquad 2.2$$

where $\alpha_o$ and ß$_o$ are constants derived from experiments; $n$ is the porosity of the prototype rock mound; $d$ is the size of the prototype rock; $v$ is the kinematic viscosity of water; and $U_p$ is the maximum velocity in the prototype mound.

The ratio of rock size in prototype to model, $K$, is then given by:

$$K = \left(\frac{\xi_p}{2\sqrt{\lambda}}\right)\left[\left(\frac{1+4\lambda^{\frac{3}{2}}(1+\xi_p)}{{\xi_p}^2}\right)^{\frac{1}{2}} - 1\right] \qquad 2.3$$

where $\lambda$ is the geometric scale. Throughout this analysis it is assumed that the porosity of model and prototype rock is identical.

To enable the above equations to be used in calculating a correction factor, certain assumptions have been made. Experimental work by Engelund, (1953) suggested values for the empirical coefficients of $\alpha_o$ = 1500 and ß$_o$ = 3.6. The maximum prototype velocity in the mound was estimated at 0.5-1.0 m/s from simple calculations of wave velocities and comparisons with velocities calculated by a mathematical model of flow in

rubble mounds. The porosity of the rock mound, *n*, used the standard value of 37% (The Rock Manual, CIRIA, 2007).

### Rock scaling for stability

Differences between the density of the model and prototype armour rock, and between the model and prototype fluids, mean that, without compensation, the stability of the armour in the model would be different from that in the prototype. It was therefore necessary to correct the size of rock to be used in the model, so that it exhibits the same stability characteristics as the prototype.

A correction factor for density may be derived by reference to the Hudson equation (CERC, 1984) which states:

$$M\alpha \frac{\rho_s H_s^3}{\left(\frac{\rho_s}{\rho_f} - 1\right)^3 \cot\theta} \qquad 2.4$$

where $M$ is the mass of the armour unit, $H_s$ is the significant wave height, $\theta$ is the structure slope angle to the horizontal, $\rho_s$ is the density of the armour and $\rho_f$ is the density of the displacing fluid.

The correction factor ($C_f$) for the armour mass may thus be calculated from the following equation:

$$M_m = M_p \frac{C_f}{\lambda^3} \qquad 2.5$$

where $\lambda$ is the model scale. This leads to the following expression for the correction factor:

$$C_f = \frac{\rho_{sm}}{\rho_{sp}} \left[ \left( \frac{\rho_{sp}}{\rho_{fp}} - 1 \right) / \left( \frac{\rho_{sm}}{\rho_{fm}} - 1 \right) \right]^3 \qquad 2.6$$

where the subscripts $p$ and $m$ respectively refer to parameters in the prototype and model.

## 2.4.2. Mobile material scaling

The ability of a physical model to reproduce prototype beach behaviour successfully is limited by scale and model effects. The scale effects inherent in mobile bed physical models arise from the fact that it is not possible to achieve similitude in the main sediment transport processes, which are:

- The permeability of the beach, which governs beach slope.
- The relative magnitudes of the onshore and offshore motion, which determines whether the beach erodes or accretes.
- The threshold of motion, which ensures that the beach material is mobile.

Although scale effects cannot be eliminated from mobile bed physical models, we attempt to minimise them within the constraints imposed by the requirements of the study by selecting the most appropriate modelling material. The primary objective of the morphological tests was to reproduce beach plan shape, so it was important that the model sediment was mobile in all areas where the prototype sediment will be expected to be mobile. For the confirmation (stability) tests the cross-shore profile was important, as was the ability of the beach to respond correctly to the larger wave conditions required for the stability tests.

For coastal scale models, it is often important to achieve similarity of the cross-shore equilibrium bed profiles between prototype and model, particularly in the surf zone. This means that the dimensionless parameters describing equilibrium profile behaviour should be the same in model and prototype. Dean (1985) reasoned,

that in an undistorted model, the fall trajectory of a suspended particle must be geometrically similar to the equivalent prototype trajectory and fall with a time proportional to the prototype fall time. This can be accomplished by ensuring similarity of the fall speed parameter between the prototype and the model. The fall speed parameter (Dean number) is described as:

$$D_w = \frac{H_{m0}}{w_s \; T_{m,0,2}} \qquad 2.7$$

where $H_{m0}$ is the significant wave height, $T_{m0,2}$ is the mean spectral wave period and $w_s$ is the settling velocity (or sediment fall speed).

Noda (1971) and Kamphuis (1983) suggested that in order to reproduce correctly a surf-zone profile response in a model scale study, the fall speed parameter needs to be preserved between prototype and the geometrically undistorted model, with the hydrodynamics being scaled by the Froude criterion (as discussed in Section 2.1). Therefore, in order to produce the correct beach response in a mobile bed model, the model should satisfy the following criteria:

- Geometrically undistorted model (all lengths are scaled by the geometric length scale);
- Hydrodynamics scaled according to Froude similarity;
- Similarity of the fall speed parameter between prototype and model;
- Model large enough ($D_{50}$ > 0.008mm) to preclude significant viscous, surface tension and cohesive sediment effects so that the effect of wave breaking is properly simulated.

The prototype beach material is not well characterised, however previous numerical modelling work on the project has assumed $D_{50}$ ~ 0.3mm (*RPT 2019-0913 Illinois Beach Shoreline Protection v0 - Design Report.pdf*), representing a sand beach, although it is known that there are gravels present in many areas (*RPT 2019-0913 Illinois Beach Shoreline Protection v0 - Design Report.pdf*). A $D_{50}$ = 0.3mm suggests that the equivalent geometrically scaled model (1:35) material would be $D_{50}$ ~ 0.01mm. This would be close to silt and the sediment movement could be controlled by cohesive (electrostatic) forces. The following section describes the method used to scale the model sediment by maintaining the similarity of the fall speed parameter between prototype and model and at the same time precluding significant viscous scale effects.

### Similarity of the fall speed parameter between prototype and model

Sediments will move onshore or offshore depending on the fall speed parameter, for $D_w$ <1 then the sediment moves onshore and if $D_w$ > 1 then offshore movement occurs. For the correct reproduction of the relative magnitudes of onshore/offshore movement, it is therefore necessary to maintain similitude of the Dean number between model and prototype.

The first step is therefore to estimate the Dean number for the prototype conditions. For the present study, the prototype settling velocity ($w_s$) was estimated by using the method of Soulsby (1997). The settling velocity of a sand grain in water is determined by its diameter, its density and the viscosity of the water.

$$w_s = \frac{\nu}{D_{50}} \left[ (10.36^2 + 1.049 D_*^3)^{0.5} - 10.36 \right] \qquad 2.8$$

where $D^*$ is the dimensionless grain size:

$$D_* = \left[ \frac{g(s-1)}{\nu^2} \right]^{\frac{1}{3}} D_{50} \qquad 2.9$$

and where $g$ is the acceleration due to gravity, $v$ is the kinematic viscosity of water (1.31E-6 $m^2/s$), $D_{50}$ is the median sieve diameter of the grains and $s$ is the ratio of densities of grain and water ($s$ = 2.6).

Once the prototype settling velocity is calculated, the prototype fall speed parameter is determined from Equation 2.8. Two potential modelling materials were considered: low density anthracite (in models terms $D_{50}$ = 0.85mm, $\rho$ = 1,389kg/$m^3$) and a full density sand (in model terms $D_{50}$ = 0.11mm, $\rho$ = 2,650kg/$m^3$), which is approximately the finest sand that can be used before cohesive effects begin to affect the model.

### Depth of closure

In the design of the model beach material, it is important to represent the cross-shore performance of the model beach as closely as possible to the prototype conditions. One of the most important parameters is the depth of closure ($D_c$), i.e., the depth at which the wave conditions can no longer change the profile. At this depth, the sediments will still be subject to movement, however, there will not be a perceptible change in profile. This means that a well-designed model material will be able to reproduce the correct depth of closure in the model study and therefore be mobilised at water depths similar to those in the prototype.

In order to guarantee that the sediment model will be mobilised under the morphological wave condition (less severe wave conditions), the prototype depth of closure and the model sediment threshold of motion were assessed. The same process was undertaken for the more severe stability conditions.

The prototype depth of closure was estimated by using Haliermeier's (1978 - 1981) expression:

$$D_c = 2.28H_{m0} - 68.5\left(\frac{H_{m0}^2}{gT_{m0,2}^2}\right) \qquad 2.10$$

where $H_{m0}$ is the significant wave height, $T_{m0,2}$ is the mean spectral wave period and $g$ is the acceleration due to gravity.

Behind the beach control structures, the wave heights diminished in the sheltered waters. Therefore, it was important to consider the movement of the material under small wave heights. For example: a sheltered wave height of $H_{m0}$ = 1.6 ft and period $T_{m0,2}$ = 10.5s. The estimated prototype depth of closure was $D_c$ = 1.6 ft. For a larger wave height from the stability testing ($H_{m0}$ = 4.9 ft and period $T_{m0,2}$ = 10.5s), the estimated prototype depth of closure was $D_c$ = 10.8 ft.

### Shields parameter

The initiation of sediment motion can only be triggered when the bed shear-stress induced by the flow exceeds a certain threshold critical value. The sediments will hence move if $\tau_w > \tau_{cr}$, where $\tau_w$ is the total bed shear stress amplitude and $\tau_{cr}$ is the threshold bed shear stress.

A precise measure of the threshold of motion can be given in terms of bed shear-stress by using the well-known threshold Shields parameter (see Soulsby, 1997):

$$\theta_{cr} = \frac{\tau_{cr}}{g\,(\rho_s - \rho)D_{50}} \qquad 2.11$$

where $\tau_{cr}$ is the threshold bed shear stress, $g$ is the acceleration due to gravity, $D_{50}$ is the median sieve diameter, and $\rho$ and $\rho_s$ are the grain and water densities, respectively.

For this study, the improved equation of Soulsby and Whitehouse (1997) was used to predict the Shields parameter:

$$\theta_{cr} = \frac{0.30}{1 + 1.2D_*} + 0.055\,[1 - \exp(-0.020D_*)] \qquad 2.12$$

where $D_*$ is the dimensionless grain size (Equation 2.9). From this equation (2.12) the value of $\theta_{cr}$ is obtained and can be used in Equation 2.11 to find $\tau_{cr}$.

While the bed shear stress produced by the hydrodynamic action of the waves is:

$$\tau_w = 0.5\,\rho f_w U_w \qquad 2.13$$

where $\rho$ is the water density, $f_w$ is the wave friction factor and $U_w$ is the bottom orbital velocity. To initiate the transport the fluid stresses $\tau_w$ have to overcome the inertia of the particles resisting on the bed $\tau_{cr}$.

For the present study, the sheltered morphological wave condition ($H_{m0}$ = 1.6 ft and $T_{m0,2}$ = 10.5s) and sheltered stability condition ($H_{m0}$ = 4.9 ft and $T_{m0,2}$ = 10.5s) were used to estimate the bottom model orbital velocities at different water depths and hence derive the bed shear stress produced by the hydrodynamic action of the waves $\tau_w$. The results showed that the anthracite mobilised more easily and to a greater depth than the sand, while the sand gave a closer match to the Dean fall speed parameter ($D_w$). The anthracite was therefore chosen for the morphological tests, and the sand for the stability (conformation) tests.

## 2.5. Wave calibration

### 2.5.1. Morphological wave conditions

All morphological sea-states were defined by their spectral wave height, $H_{m0}$, peak period, $T_p$, still water level, *SWL*, peak enhancement factor, $\gamma$, and storm/test duration. Morphological wave conditions were calibrated in the basin after construction of the model bathymetry, but before construction of the model structures, to minimise corruption of the incident waves by reflections. The objective of the calibration process was to produce the wave conditions at the 565 ft IGLD 85 contour in each Area model. The target calibration conditions are discussed in Section 3 of this report and the results of the wave calibrations are given in the relative Area Sections below (Sections 5.3, 6.3 and 7.3).

Calibration was an iterative process: the amplitude of the signal driving the wave generator was adjusted until the spectral significant wave height measured at the calibration point was within ±5% of the target significant wave height, in prototype. For each wave condition, an in-line array of four wave gauges was used to measure the incident wave. Time histories recorded by each gauge in the array were analysed spectrally by HR Wallingford's HR-Daq software to give the following parameters:

- Significant incident spectral wave height, $H_{m0i}$;
- The mean spectral wave period, $T_{m0,2}$, defined using the zeroth and 2nd moments of the frequency spectrum;
- The spectral wave period, $T_{m-1,0}$, defined using the inverse and zeroth moments of the frequency spectrum.

The data recorded by the array was analysed to separate the incident and reflected wave spectra, and determine the incident significant wave height, $H_{m0i}$. For each sea condition, the wave generation produced non-repeating wave sequences, with durations equal to not less than 1,000 times the mean wave period, $T_{m0,2}$, of the target spectrum. This gave a statistically significant sample for the wave calibration analysis. The wave gauges were scanned at an interval of $T_p$ / 48.

The reflection analysis was based on measuring the wave height at the four wave-gauge array (at differing and known gauge spacings in constant water depth). The method calculates the incident and reflected wave spectral energy and the reflection coefficients at frequencies spread across the frequency range. The reflection coefficient was calculated using the following equation:

$$C_r = \sqrt{\frac{m_{0r}}{m_{0i}}} \quad 2.14$$

where $m_{0i}$ and $m_{0r}$ are the incident and reflected wave spectral energy, respectively.

The total wave height ($H_{Tot}$) is therefore expressed as:

$$H_{Tot} = \sqrt{H_{m0i}^2 + H_{m0r}^2} \quad 2.15$$

and this can be expressed in terms of the incident wave height ($H_{m0i}$) as:

$$H_{Tot} = \sqrt{H_{m0i}^2 + (C_r^i H_{m0i})^2} \quad 2.16$$

and so,

$$H_{m0i} = \frac{H_{Tot}}{\sqrt{1 + C_r^2}} \quad 2.17$$

One of the wave gauges was used to specify the calibrated wave condition at the 565 ft IGLD 85 contour, after the application of the wave reflection coefficient.

### 2.5.2. Stability wave conditions

All stability test sea-states were defined by their spectral wave height, $H_{m0}$, peak period, $T_p$, still water level, *SWL*, peak enhancement factor, $\gamma$, and storm/test duration. Stability wave conditions were calibrated in the basin after construction of the model bathymetry, but before construction of the model structures, to minimise corruption of the incident waves by reflections. The objective of the calibration process was to produce the wave conditions at the toe of the structure. The target calibration conditions are discussed in Section 3 of this report and the results of the wave calibrations are given in the relative Area Section below (Section 5.3, 6.3 and 7.3).

The general procedure for wave calibration is an iterative process whereby the amplitude of the signal driving the wave generator is adjusted until the spectral significant wave height measured at the calibration point is within ±5% of the target significant wave height, in prototype as described above in Section 2.5.1 for the morphological wave conditions.

For all three 3D models, as with the 2D modelling study (DKR6353-RT001, HR Wallingford 2021), all the stability test wave conditions were breaking as they transferred from offshore to the calibration point. This was as expected as it was known that the waves would be affected by depth limited breaking. As waves break, there is a loss and transfer of energy within each frequency band, with the subsequent result that the recorded spectra no longer represents that generated offshore at the paddle or the target spectra. As an example, for wave condition WC_HIGH_WL (see Table 3.6) from the Area 2 model, the wave spectrum recorded during wave calibration is shown in Figure 2.2. Under these circumstances, the spectral significant wave height ($H_{m0}$) calculated from the measured spectrum will be significantly different from the $H_{m0}$ calculated form the target spectrum, it being defined by the integration under spectrum ($m_0$).

The criterion for the calibration of the wave conditions for the stability tests, was therefore to take the measured value of $H_{1/3}$, and compared with the $H_s$ values supplied by SmithGroup (presented in the calibration results sections for each Area, Sections 5.3, 6.3 and 7.3). This calibration method was discussed and agreed with SmithGroup's onsite representative during the wave calibration process once the heavily broken nature of the wave conditions was understood.

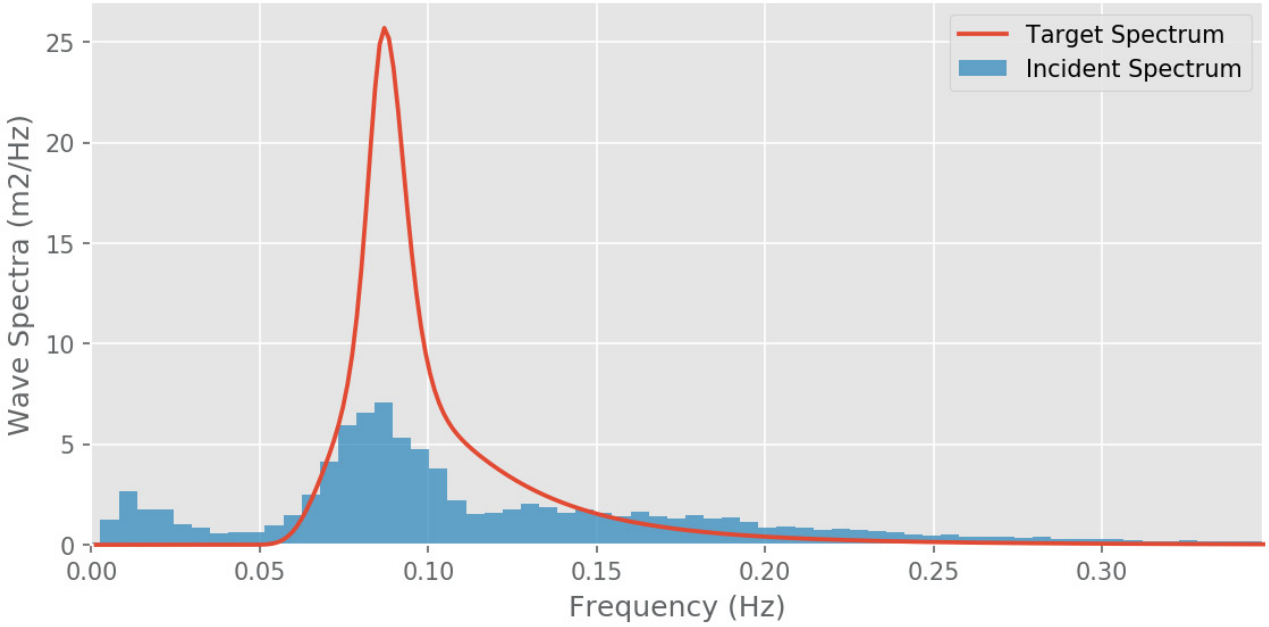


Figure 2.2: Wave condition WC_HIGH_WL from Area 2 model, showing significant transfer of Incident spectral wave energy due to wave breaking against the idealised Target spectrum

## 2.6. Beach morphology measurements

### 2.6.1. 3D laser scanning

A 3D terrestrial laser scanner was used to scan the beach and beach control structure layout. The laser scanner produced a 3D point cloud representing the beach which was used to compare pre and post-test beach plan shapes. The point cloud data was used to take measurements of the evolution of the *SWL* at the beach. This provided a continuous beach plan shape rather than isolated point measurements. The position of the beach control structures was also taken from the laser scans. Full laser scans were taken:

- at the start of a test series;
- after a morphological test when the SmithGroup on-site representatives required, and;
- after the stability (confirmation) tests.

Laser scan data from key stages in the evolution of the beach control structures is provided for each Area in Sections 5, 6 and 7 and Appendices B, C and D. The data has also been provided to SmithGroup on-site representatives in AutoCAD format separately to this report.

### 2.6.2. Photographic time-lapse beach evolution mapping

A photographic overview of the beach was taken at approximately 3 minute (30s model) intervals throughout testing. The photographs can be overlain to monitor movement of the *SWL* and plan shape of the beach. Pre and post-test photographs of the various stages in control structure optimisations for each Area are provided in Appendix B, C and D for Areas 1, 2, and 3 respectively.

## 2.7. Dye tracing measurements

At various points during the modelling, the SmithGroup on-site representatives, supported by HR Wallingford staff, undertook dye tracing observations. These were primarily used to track cross-shore currents and to assess the potential for both high currents and sediment transport around key features. For the Kellogg Creek testing as part of the Area 2 modelling (Section 6.5), the dye movement was tracked with time-lapse photographs. For other dye tracing observations, the SmithGroup on-site representatives placed the dye at locations of interest and observed the movement whilst a test was running. These observations were then used by the SmithGroup on-site representatives in the optimisation of the beach control structures. No formal data was recorded by HR Wallingford for these observational dye tracing tests.

## 2.8. Armour stability measurement and performance criteria

Rocks displaced from the armour layer and toe were counted using an overlay photograph technique. Photographs were taken from fixed camera positions before and after each test. The images were superimposed and compared to identify instances of rock extraction. The images were sent separately to the SmithGroup representatives on-site at HR Wallingford.

Following assessment of the number of rocks displaced the damage parameter $N_{od}$ was calculated for the armour layer and then converted to an $S_d$ approximation. The $S_d$ calculated damage parameters are reported in Sections 5, 6 and 7 for Areas 1, 2, and 3 respectively.

The $N_{od}$ number is determined using Equation 2.18 and is defined as the number of displaced stones in a strip of width one nominal rock diameter ($D_{n50}$):

$$N_{od} = \frac{N_{displ}}{B/D_{n50}} \qquad 2.18$$

where $N_{displ}$ is the number of displaced stones, $B$ is the width of the test section; determined at the centreline of each section and $D_{n50}$ is the nominal stone diameter exceeded by 50% of the stones by total mass.

The damage parameter $S_d$ can be estimated from $N_{od}$ through use of Equation VI-5-61 in CEM (2002), reproduced here as Equation 2.19.

$$N_d = G(1 - n_v)S_d \qquad 2.19$$

where $G$ is the gradation factor usually between 1.2 and 1.6 for rock armour and $n_v$ is porosity; taken to be 0.37. CEM (2002) and Via-Estrem *et al* (2013) suggest using the approximation shown in Equation 2.20, which, for this study, corresponds to a conservative approach to the gradation factor, G ≈ 1.2. Equation 2.20 has been used universally throughout the stability analysis of all three Area models to convert $N_{od}$ values to $S_d$.

$$S_d = 1.4N_{od} \qquad 2.20$$

### 2.8.1. Performance criteria

Stability performance criteria was not provided to HR Wallingford for this study. To allow assessment of the stability of the armour layers on the beach control structures, HR Wallingford have assumed the values from Table 5.23 of the Rock Manual (CIRIA, 2007) to provide standard performance criteria in terms of $S_d$, reproduced here in Table 2.3. The $S_d$ damage parameter was not measured directly within this study so has been estimated from the $N_{od}$ damage parameter as described in Section 2.8 above.

Table 2.3: Design values of the damage parameter, $S_d$, for armour stone in a double layer with a slope of 1:1.5

| Damage level | $S_d$ (-) |
|---|---|
| Start of damage | 2 |
| Intermediate damage | 3-5 |
| Failure | 8 |

*Source: CIRIA, 2007*

# 3. Wave conditions and water levels

## 3.1. Morphological test conditions

### 3.1.1. Morphologically significant wave direction

SmithGroup provided 35 years' worth of wave data for each of the three Areas for directions 0 - 180°, binned in 11.25°, 0.5m, 1s increments at the 565 ft IGLD 85 contour matching the calibration point used in each Area model. These are summarised for each Area as scatter tables and as wave roses below. The wave climate data was used by HR Wallingford to derive the morphologically significant direction. This is the single direction that can be used to simulate the nett effect of the wave climate in terms of longshore drift on the beach. It takes account of the frequency of occurrence of each sea state and its capacity to generate drift, using HR Wallingford's DRCALC model.

Longshore drift on a beach is caused primarily by waves breaking at an angle to the coast, with the rate of transport depending on the wave height at breaking and the angle between the wave direction and shore-normal. DRCALC calculates the total potential longshore drift using the CERC formula (CERC, 1984) by transforming each wave condition from the wave prediction point towards the breaking depth. The morphologically significant direction is, in effect, the direction normal to the hypothetical beach alignment that would result in zero nett drift in the annual wave climate. The calculations are concerned purely with potential drift on an open beach, making no attempt to predict the actual drift rates, and the beach-normal direction is adjusted until the potential drift in each direction is balanced. The morphologically significant direction for each Area is given in Table 3.1.

The wave data are summarised in scatter Table 3.2, Table 3.3 and Table 3.4 for Area 1, 2 and 3 and as a wave rose in Figure 3.1, Figure 3.3 and Figure 3.5 respectively. As can be seen, the inshore wave climate is dominated by waves approaching from a relatively narrow range of directions at around 40°N for all three Areas. Figure 3.2 illustrates the nett drift results for Area 1, with the morphologically significant direction at 61°N. The nett drift results for Area 1 and 2 are shown in Figure 3.4 and Figure 3.6 respectively and both have a morphologically significant direction at 65°N.

Table 3.1: Morphologically significant wave directions by Area

| Area | Morphologically significant wave direction (°N) |
|---|---|
| Area 1: North Beach | 61 |
| Area 2: Camp Logan | 65 |
| Area 3: Swimming Beach | 65 |

Table 3.2: Area 1 scatter table (Hs vs θ), percentage occurrence excluding calms

| Direction (°N) | Hs = 0.5m | Hs = 1.0m | Hs = 1.5m | Hs = 2.0m | Hs = 2.5m | Hs = 3.0m | Hs = 3.5m | Hs = 4.0m | Total |
|---|---|---|---|---|---|---|---|---|---|
| 0 | 0 | 0 | 0 | 0 | 0 | 0 | 0 | 0 | 0 |
| 10 | 0 | 0 | 0 | 0 | 0 | 0 | 0 | 0 | 0 |
| 20 | 1486 | 25 | 0 | 0 | 0 | 0 | 0 | 0 | 1511 |
| 30 | 13396 | 921 | 5 | 0 | 0 | 0 | 0 | 0 | 14322 |
| 40 | 32621 | 12903 | 2776 | 17 | 0 | 0 | 0 | 0 | 48317 |
| 50 | 6270 | 6647 | 5328 | 972 | 302 | 39 | 0 | 0 | 19558 |
| 60 | 3012 | 1316 | 758 | 760 | 251 | 224 | 96 | 52 | 6469 |
| 70 | 2633 | 1224 | 495 | 193 | 71 | 36 | 5 | 3 | 4660 |
| 80 | 2282 | 1115 | 494 | 181 | 58 | 34 | 8 | 12 | 4184 |
| 90 | 2341 | 1189 | 422 | 173 | 39 | 22 | 10 | 5 | 4201 |
| 100 | 2261 | 1109 | 296 | 148 | 43 | 11 | 6 | 0 | 3874 |
| 110 | 2546 | 1180 | 313 | 99 | 15 | 11 | 0 | 0 | 4164 |
| 120 | 2638 | 1185 | 423 | 186 | 25 | 0 | 0 | 0 | 4457 |
| 130 | 3909 | 2627 | 981 | 132 | 0 | 0 | 0 | 0 | 7649 |
| 140 | 9648 | 6207 | 413 | 0 | 0 | 0 | 0 | 0 | 16268 |
| 150 | 12645 | 1738 | 0 | 0 | 0 | 0 | 0 | 0 | 14383 |
| 160 | 3783 | 0 | 0 | 0 | 0 | 0 | 0 | 0 | 3783 |
| 170 | 0 | 0 | 0 | 0 | 0 | 0 | 0 | 0 | 0 |
| 180 | 0 | 0 | 0 | 0 | 0 | 0 | 0 | 0 | 0 |

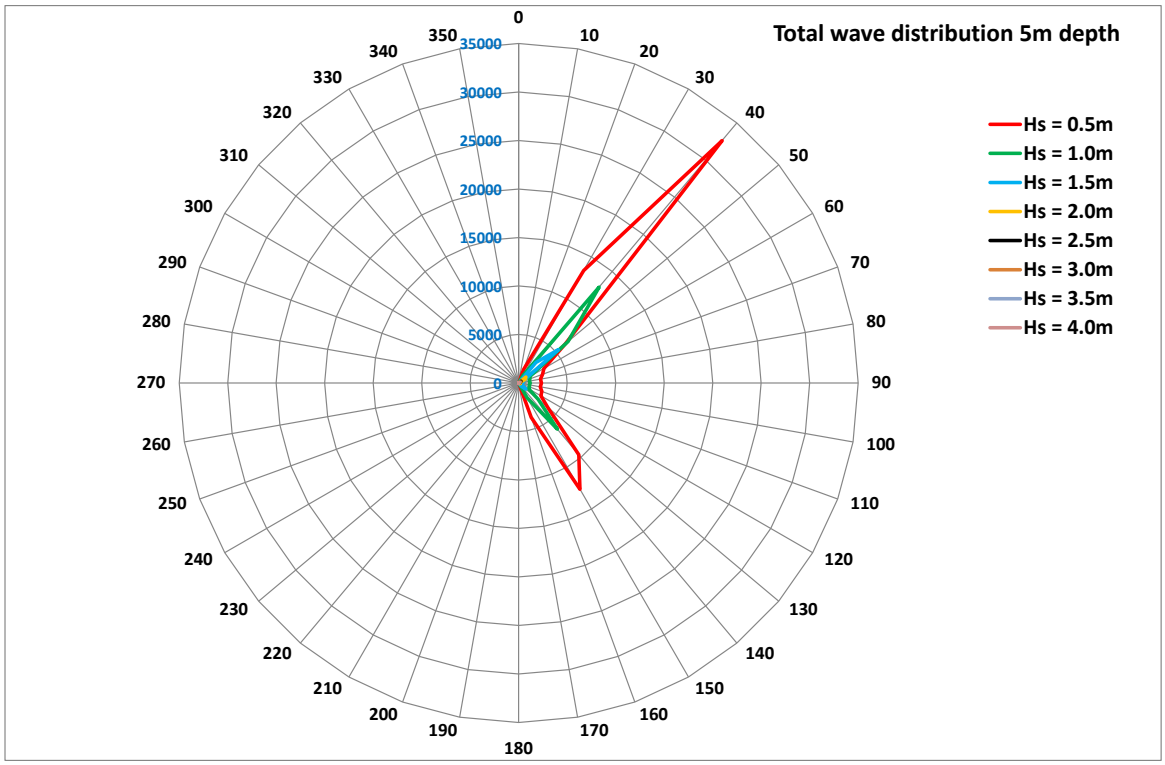


Figure 3.1: Area 1 wave rose, percentage occurrence excluding calms

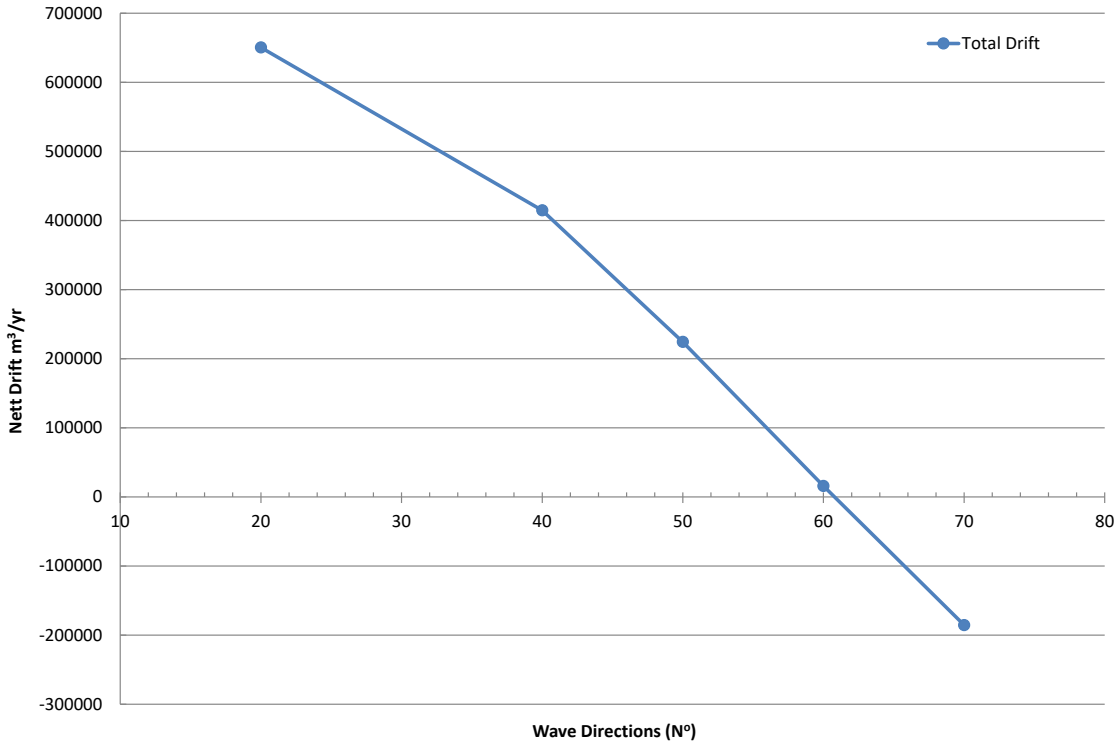


Figure 3.2: Area 1 calculation of morphologically significant direction (61°N, 0 nett drift)

Table 3.3: Area 2 scatter table (Hs vs θ), percentage occurrence excluding calms

| Direction (°N) | Hs = 0.5m | Hs = 1.0m | Hs = 1.5m | Hs = 2.0m | Hs = 2.5m | Hs = 3.0m | Hs = 3.5m | Hs = 4.0m | Total |
|---|---|---|---|---|---|---|---|---|---|
| 0 | 0 | 0 | 0 | 0 | 0 | 0 | 0 | 0 | 0 |
| 10 | 0 | 0 | 0 | 0 | 0 | 0 | 0 | 0 | 0 |
| 20 | 1486 | 25 | 0 | 0 | 0 | 0 | 0 | 0 | 1511 |
| 30 | 13396 | 921 | 5 | 0 | 0 | 0 | 0 | 0 | 14322 |
| 40 | 32621 | 12903 | 2776 | 17 | 0 | 0 | 0 | 0 | 48317 |
| 50 | 6270 | 6647 | 5328 | 972 | 302 | 39 | 0 | 0 | 19558 |
| 60 | 3012 | 1316 | 758 | 760 | 251 | 224 | 96 | 52 | 6469 |
| 70 | 2633 | 1224 | 495 | 193 | 71 | 36 | 5 | 3 | 4660 |
| 80 | 2282 | 1115 | 494 | 181 | 58 | 34 | 8 | 12 | 4184 |
| 90 | 2341 | 1189 | 422 | 173 | 39 | 22 | 10 | 5 | 4201 |
| 100 | 2261 | 1109 | 296 | 148 | 43 | 11 | 6 | 0 | 3874 |
| 110 | 2546 | 1180 | 313 | 99 | 15 | 11 | 0 | 0 | 4164 |
| 120 | 2638 | 1185 | 423 | 186 | 25 | 0 | 0 | 0 | 4457 |
| 130 | 3909 | 2627 | 981 | 132 | 0 | 0 | 0 | 0 | 7649 |
| 140 | 9648 | 6207 | 413 | 0 | 0 | 0 | 0 | 0 | 16268 |
| 150 | 12645 | 1738 | 0 | 0 | 0 | 0 | 0 | 0 | 14383 |
| 160 | 3783 | 0 | 0 | 0 | 0 | 0 | 0 | 0 | 3783 |
| 170 | 0 | 0 | 0 | 0 | 0 | 0 | 0 | 0 | 0 |
| 180 | 0 | 0 | 0 | 0 | 0 | 0 | 0 | 0 | 0 |

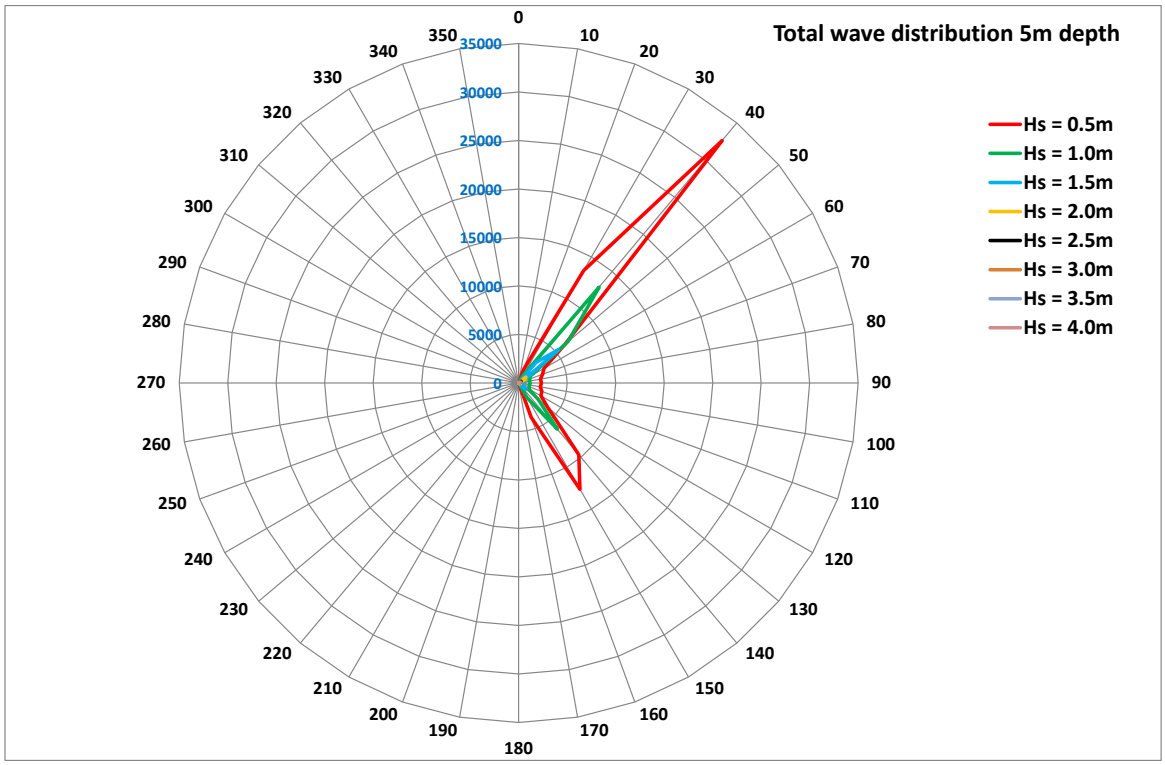


Figure 3.3: Area 2 wave rose, percentage occurrence excluding calms

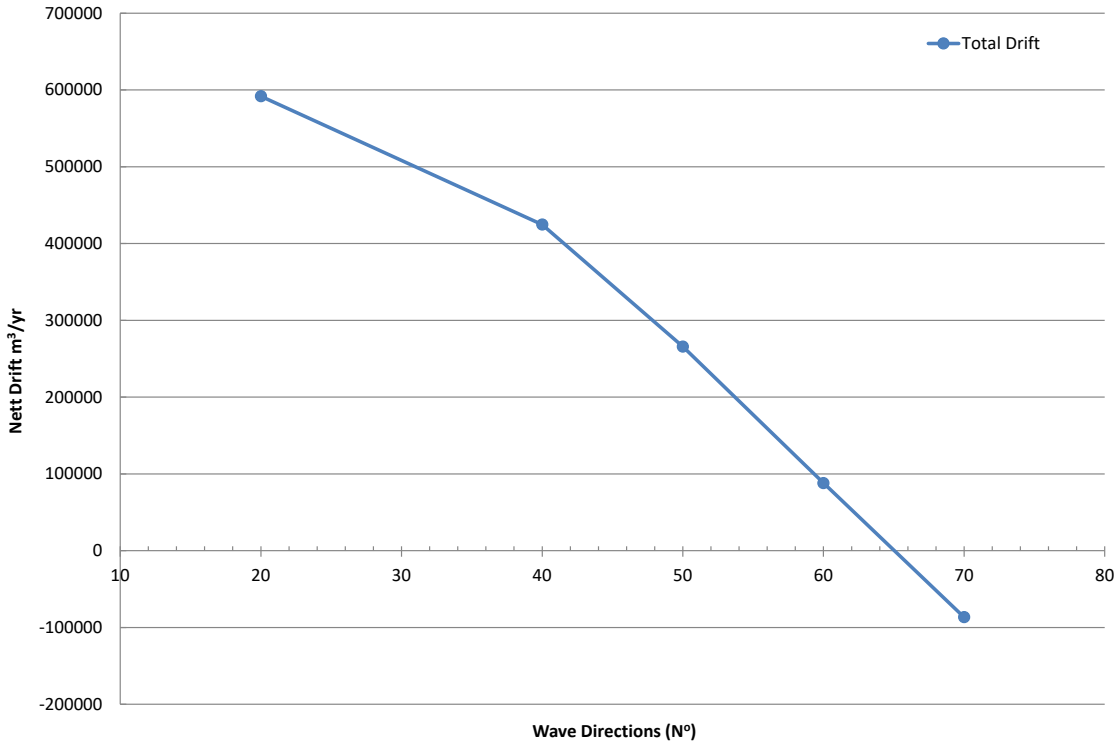


Figure 3.4: Area 2 calculation of morphologically significant direction (65°N, 0 nett drift)

Table 3.4: Area 3 scatter table (Hs vs θ), percentage occurrence excluding calms

| Direction (°N) | Hs = 0.5m | Hs = 1.0m | Hs = 1.5m | Hs = 2.0m | Hs = 2.5m | Hs = 3.0m | Hs = 3.5m | Hs = 4.0m | Total |
|---|---|---|---|---|---|---|---|---|---|
| 0 | 0 | 0 | 0 | 0 | 0 | 0 | 0 | 0 | 0 |
| 10 | 0 | 0 | 0 | 0 | 0 | 0 | 0 | 0 | 0 |
| 20 | 0 | 4 | 0 | 0 | 0 | 0 | 0 | 0 | 4 |
| 30 | 6194 | 288 | 0 | 0 | 0 | 0 | 0 | 0 | 6482 |
| 40 | 31341 | 5399 | 253 | 0 | 0 | 0 | 0 | 0 | 36993 |
| 50 | 16135 | 13865 | 6027 | 360 | 17 | 0 | 0 | 0 | 36404 |
| 60 | 1792 | 3581 | 2585 | 1365 | 536 | 232 | 145 | 38 | 10274 |
| 70 | 1349 | 2505 | 498 | 209 | 68 | 40 | 5 | 6 | 4680 |
| 80 | 1227 | 2170 | 494 | 181 | 58 | 29 | 13 | 12 | 4184 |
| 90 | 2341 | 1189 | 422 | 173 | 39 | 22 | 10 | 5 | 4201 |
| 100 | 2261 | 1108 | 296 | 148 | 43 | 7 | 6 | 0 | 3869 |
| 110 | 1212 | 2512 | 313 | 93 | 14 | 15 | 0 | 0 | 4159 |
| 120 | 1114 | 1152 | 296 | 176 | 22 | 0 | 0 | 0 | 2760 |
| 130 | 1563 | 2916 | 559 | 120 | 19 | 0 | 0 | 0 | 5177 |
| 140 | 3213 | 5571 | 1223 | 13 | 0 | 0 | 0 | 0 | 10020 |
| 150 | 15291 | 5492 | 29 | 0 | 0 | 0 | 0 | 0 | 20812 |
| 160 | 7763 | 18 | 0 | 0 | 0 | 0 | 0 | 0 | 7781 |
| 170 | 0 | 0 | 0 | 0 | 0 | 0 | 0 | 0 | 0 |
| 180 | 0 | 0 | 0 | 0 | 0 | 0 | 0 | 0 | 0 |

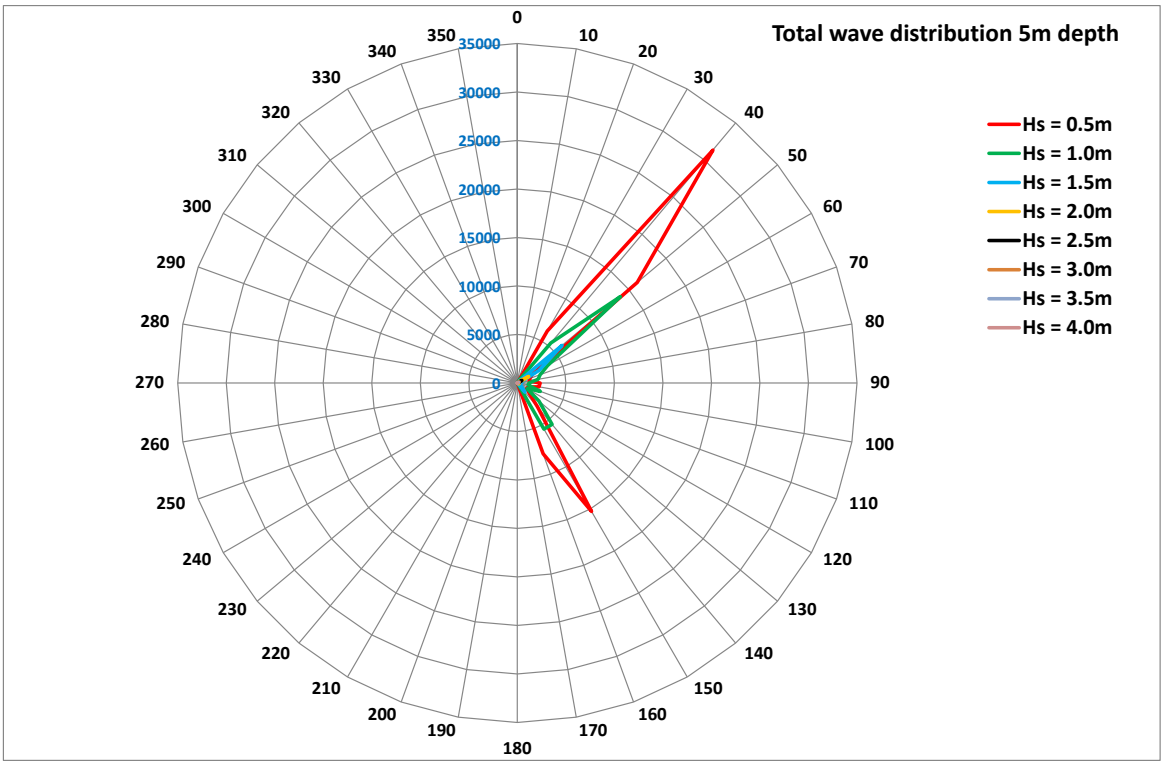


Figure 3.5: Area 3 wave rose, percentage occurrence excluding calms

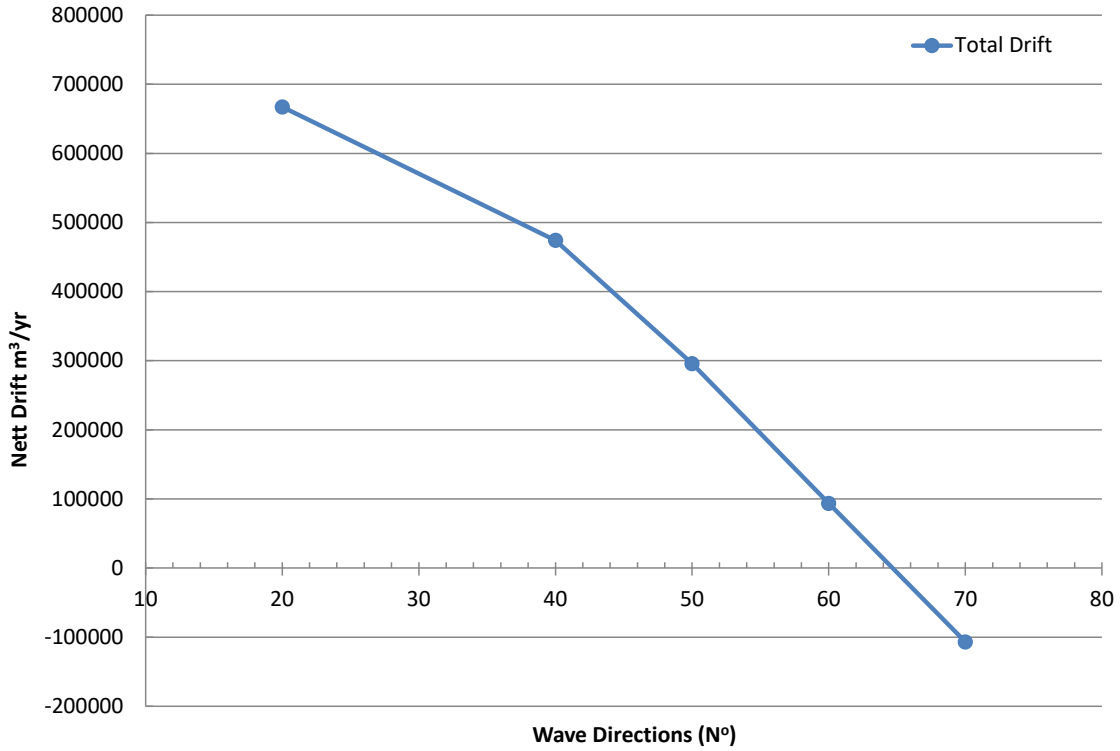


Figure 3.6: Area 3 calculation of morphologically significant direction (65°N, 0 nett drift)

### 3.1.2. Selection of test conditions

The morphological test conditions had to be energetic enough to mobilise the model sediment and to make the beach respond within a reasonable time, but not so energetic as to cause non-typical responses. A significant wave height of $H_{m0}$ = 8.2 ft was initially selected for the tests. This was to ensure that the beach material would be mobile and provide results quickly, i.e. fewer waves required to reach equilibrium than if a smaller wave height was used.

During the Area 1 model wave calibration process (Section 2.5.1), the mobile beach was present to allow an initial assessment of the ability of the waves to mobilise the beach. This process demonstrated that the initial wave height ($H_{m0}$ = 8.2 ft) was too large and successively smaller wave heights were tried, as shown in Table 3.5. The most promising condition, and the one taken forward for the morphological tests in all three Area models was Morph_03 ($H_{m0}$ = 4.9 ft). A JONSWAP spectra with a peak enhancement factor of $\gamma$ = 3.3 was assumed for all conditions, and the condition was tested with a still water level (*SWL*) of 582.4 ft IGLD 85.

Table 3.5: Morphological test conditions, as defined on 565 ft IGLD 85 contour

| Wave condition | Return period | SWL (ft IGLD 85) | $H_{m0}$ (ft) | $T_p$ (s) | θ (°N) |
|---|---|---|---|---|---|
| Morph_01 | Morphological | 582.4 | 8.2 | 9.0 | 61* |
| Morph_02 | Morphological | 582.4 | 6.6 | 9.0 | 61* |
| Morph_03 | Morphological | 582.4 | 4.9 | 9.0 | 61 or 65# |

*Note: All spectral shapes JONSWAP with γ = 3.3*

** Condition only run in Area 1*

*# 61°N in Area 1 and 65°N in Area 2 and 3*

## 3.2. Stability test conditions

The wave conditions for the stability tests are shown in Table 3.6 and were provided initially for the 2D physical modelling study (email "12324 - 2D Flume Stability Testing" on 03/09/2020). These conditions have been adopted for the North East, 61 or 65°N wave direction for Area 1 or Area 2 and 3 respectively. These wave directions were selected as they were consistent with the morphological tests, and are within the main storm wave sectors identified in *Results_CalibrationPoint_Extremes - mrb review.xlsx*. The South East wave direction conditions were confirmed in email "FW: 12324 - Extreme Waves" on 24/09/2020. A JONSWAP spectra with a peak enhancement factor of $\gamma = 3.3$ was used for all conditions.

Table 3.6: Stability test conditions, as defined on 565 ft IGLD 85 contour

| Wave condition | Return period | SWL (ft IGLD 85) | $H_{m0}$ (ft) | $T_p$ (s) | θ (°N) |
|---|---|---|---|---|---|
| WC_HIGH_WL | 1:100 | 583.3 | 11.2 | 11.5 | 61 or 65[#] |
| WC_LOW_WL | 1:100 | 576.0 | 6.6 | 11.5 | 61 or 65[#] |
| WC_EXT_WL_01 | 1:10 | 585.2 | 11.2 | 10.0 | 61 or 65[#] |
| WC_EXT_WL_02 | 1:100 | 585.2 | 12.1 | 11.5 | 61 or 65[#] |
| WC_HIGH_WL_SE | 1:100 | 582.2 | 6.2 | 7.5 | 130 |
| WC_LOW_WL_SE | 1:100 | 579.2 | 6.2 | 7.5 | 130 |

*Note: All spectral shapes JONSWAP with γ = 3.3*

*[#] 61°N in Area 1 and 65°N in Area 2 and 3*

*Source: Results_CalibrationPoint_Extremes - mrb review.xlsx and email: "FW: 12324 - Extreme Waves", 24/09/2020*

The nomenclature used in Table 3.6 is primarily used for cross referencing across the various models and Test Parts. The first four conditions in Table 3.6 are the stability waves from the North East (NE) direction and do not include the suffix NE; the final two South East conditions do include the suffix SE to differentiate them. Although varying slightly for the two directions, the wave conditions are further categorised according to the water level (including surge). These are LOW, HIGH and Extreme (EXT), with the most onerous conditions being WC_EXT_WL_, where 01 is the 1:10 year return period and 02 the 1:100 year return period event.

# 4. Test programme

The 3D physical modelling studies started with Area 1 (North Beach), then Area 2 (Camp Logan) and concluded with Area 3 (Swimming Beach). Each model followed a similar programme consisting of morphological tests with an anthracite beach to optimise the layout of the beach control structures, followed by beach response tests with a sand beach and then stability testing of the beach control structures under storm conditions.

All morphological tests (for both anthracite and sand beaches and for all three Areas) were conducted with the Morph_03 wave condition (Table 3.5) and the test lengths were determined by the rate of beach evolution (tests were run until the beach plan shape reached equilibrium) or by the SmithGroup on-site representatives. The length of time each configuration was tested is provided in the corresponding results Section (Sections 5, 6 and 7). Any dye tracing work undertaken by the SmithGroup on site representatives (see Section 2.7) on the three Area models was conducted during anthracite beach morphological tests before changing the beach material to sand for the confirmation tests.

The stability tests were conducted following calibration of the stability wave conditions in each Area model. The sand beach was placed along with the beach control structures which were constructed from correctly scaled armourstone to assess the stability. The structures were not repaired between Test Parts, resulting in cumulative damage throughout the Test Series. Each stability Test Part lasted for 3000 waves (3000 x $T_{m0,2}$), a minimum of 5 hrs prototype. The order of wave conditions for the Area 1 model is given in Table 4.1, and for Area 2 and Area 3 in Table 4.2.

Within the Area 1 model morphological tests were undertaken with the sand beach following the storm response tests. This was an additional request from the SmithGroup on-site representatives to confirm that the change in model beach material, required for the storm response tests, would provide consistent results with the anthracite material used for the optimisation. As discussed in Section 2.4.2, the sand is not an ideal material to use with the smaller morphological wave condition. With the smaller condition longer testing times are required to reach equilibrium plan shape which matches that achieved in a much shorter time with the anthracite material.

Table 4.1: Area 1 stability test sequence of wave conditions

| Test Part | Wave condition | Return period | SWL (ft IGLD 85) | Target significant wave height, $H_{m0}$ (ft) | Target peak wave period, $T_p$ (s) | Wave direction (°N) |
|---|---|---|---|---|---|---|
| 01 | WC_LOW_WL | 1:100 | 576.0 | 6.6 | 11.5 | 61 |
| 02 | WC_HIGH_WL | 1:100 | 583.3 | 11.2 | 11.5 | 61 |
| 03 | WC_EXT_WL_01 | 1:10 | 585.2 | 11.2 | 10.0 | 61 |
| 04 | WC_EXT_WL_02 | 1:100 | 585.2 | 12.1 | 11.5 | 61 |
| 05 | WC_LOW_WL_SE | 1:100 | 579.2 | 6.2 | 7.5 | 130 |
| 06 | WC_HIGH_WL_SE | 1:100 | 582.2 | 6.2 | 7.5 | 130 |

Table 4.2: Area 2 and 3 stability test sequence of wave conditions

| Test Part | Wave condition | Return period | SWL (ft IGLD 85) | Target significant wave height, $H_{m0}$ (ft) | Target peak wave period, $T_p$ (s) | Wave direction (°N) |
|---|---|---|---|---|---|---|
| 01 | WC_LOW_WL_SE | 1:100 | 579.2 | 6.2 | 7.5 | 130 |
| 02 | WC_HIGH_WL_SE | 1:100 | 582.2 | 6.2 | 7.5 | 130 |
| 03 | WC_LOW_WL | 1:100 | 576.0 | 6.6 | 11.5 | 65 |
| 04 | WC_HIGH_WL | 1:100 | 583.3 | 11.2 | 11.5 | 65 |
| 05 | WC_EXT_WL_01 | 1:10 | 585.2 | 11.2 | 10.0 | 65 |
| 06 | WC_EXT_WL_02 | 1:100 | 585.2 | 12.1 | 11.5 | 65 |

# 5. Area 1 – North Beach

The Area 1 model examined the North Beach area of Lake Michigan. To the north of this area, are harder engineered structures that are holding the coastline, whilst to the immediate south, there is significant and ongoing beach erosion with a net north to south sediment drift driven predominantly by North East waves. The first phase of the model included a northern breakwater to hold the coastline adjacent to the Winthrop Yacht Club, followed by a series of shore detached groynes to encourage the development of salients and tombolos to arrest or reduce the north-south sediment drift. This was done using sandbags to act as proxies for armourstone breakwaters and allowed multiple configurations to be examined using a lightweight modelling sediment. This was tested with a generic morphological wave condition that was able to mobilise the modelling sediment without affecting the beach response due to wave breaking significantly.

Once a stable configuration had been identified, then the lightweight modelling sediment was replaced with a fine grained modelling sand with the correct density. The final configuration of proxy armourstone structures was replaced with correctly sized and scaled model rock structures, and the whole was then tested with a sequence of six wave and water level conditions from both the North East and South East wave directions. This section describes the model set up, the wave calibrations, the morphological beach testing and the structural stability for Area 1. Some key observations are given in Section 5.8.

## 5.1. Wave basin layout

The Area 1 model testing was carried out in HR Wallingford's Wave Basin E which is 38 m long by 25 m wide and has a maximum working depth of 1.0 m (all dimensions in metric model terms). The bathymetry design and construction is described in Section 2.2, and the full basin layout is shown in Figure 5.2.

The location of the wave gauges for the anthracite morphological tests are shown in Figure 5.2 and for the sand morphological and stability tests in Figure 5.3.

### 5.1.1. Area 1 beach material placement

The anthracite beach material (refer to Section 2.4.2) was initially placed according to an idealised profile consisting of a 1:15 slope from 570 ft IGLD 85 to 582 ft IGLD 85, then a 1:26 slope to 584 ft IGLD 85 and a 1:42 slope to 585 ft IGLD 85. The profile was used to manufacture beach-normal wooden templates. The templates were arranged along the model beach as indicated in Figure 5.1 (blue lines) and then levelled into position using an optical dumpy level. Beach material was then placed and screeded to these templates to create the initial beach cross shore profile and plan-shape. The templates were then removed and the gaps between them were filled.

The sand beach material was placed according to an idealised profile with a 1:15 slope from the 570 ft IGLD 85 contour to an elevation of 586 ft IGLD 85. The profile was used to manufacture beach-normal wooden templates. The toe of each template was placed on the 570 ft IGLD 85 contour and then levelled into position before creating the beaches with fine modelling sand.

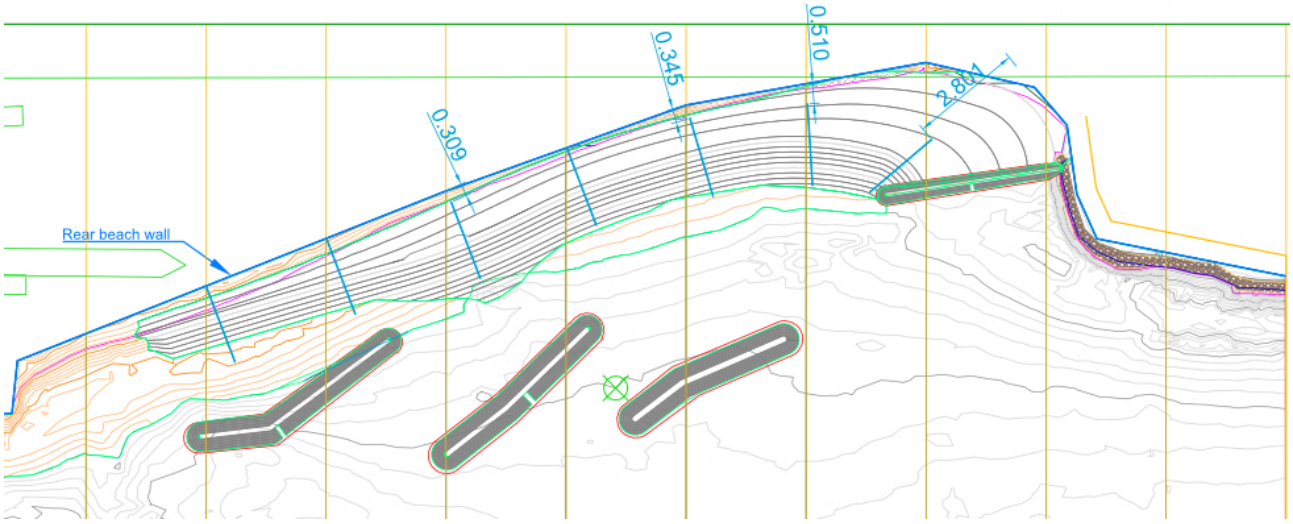


Figure 5.1: Arrangement of beach-normal templates for initial anthracite beach placement for Area 1

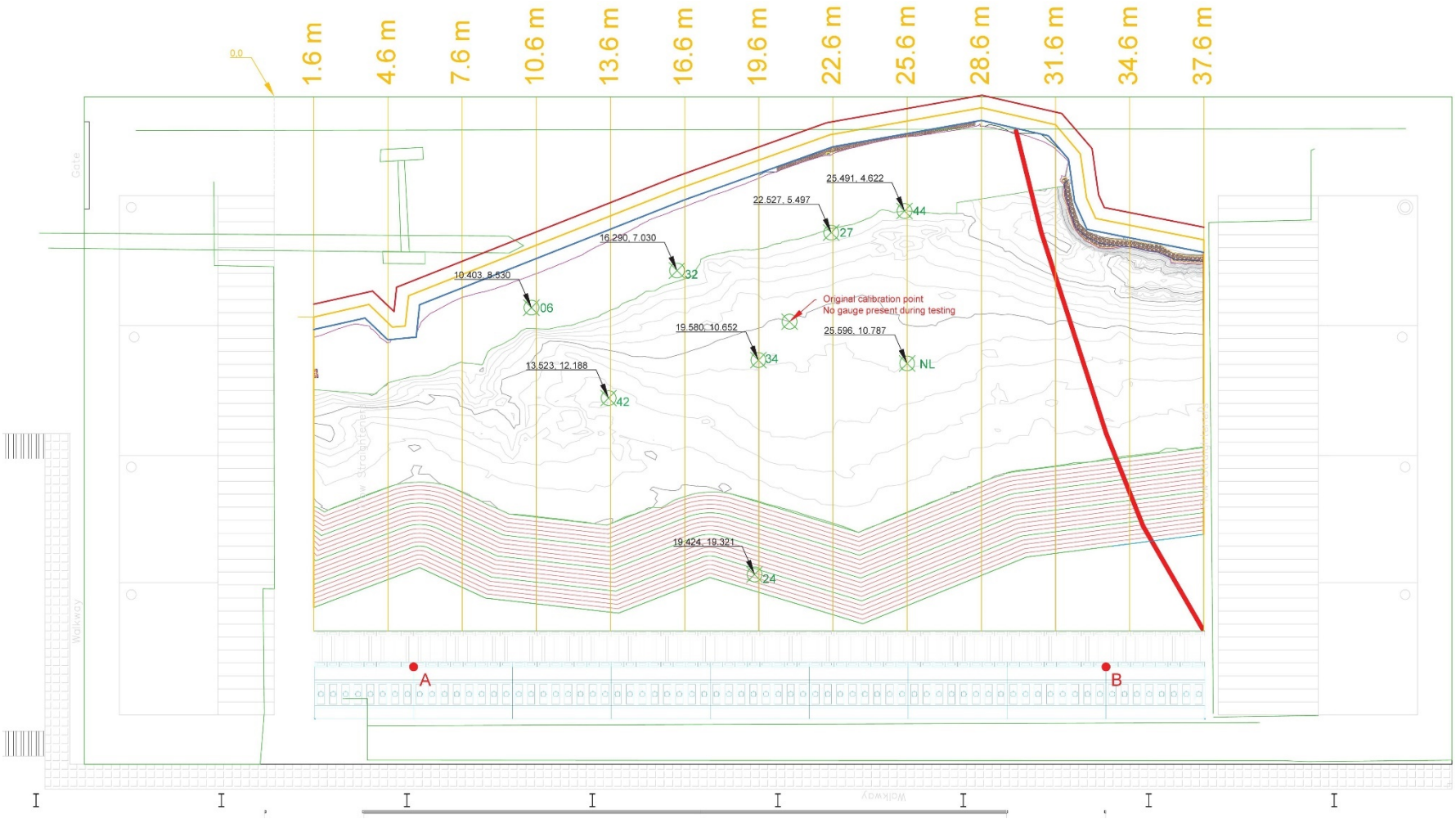


Figure 5.2: Area 1 basin layout showing the location of the wave gauges during the anthracite morphological tests

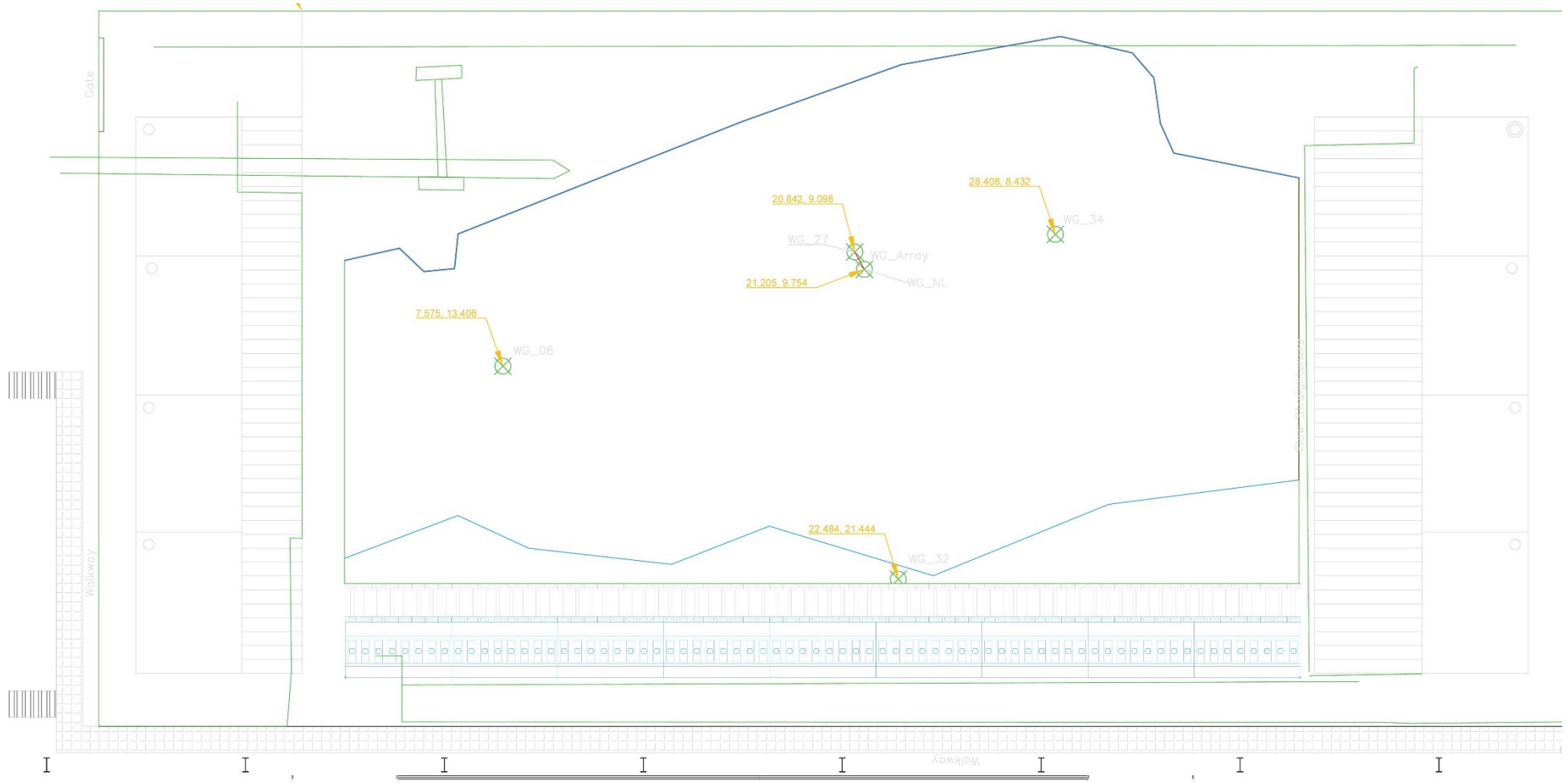


Figure 5.3: Wave gauge locations for Area 1 stability and sand beach morphological tests

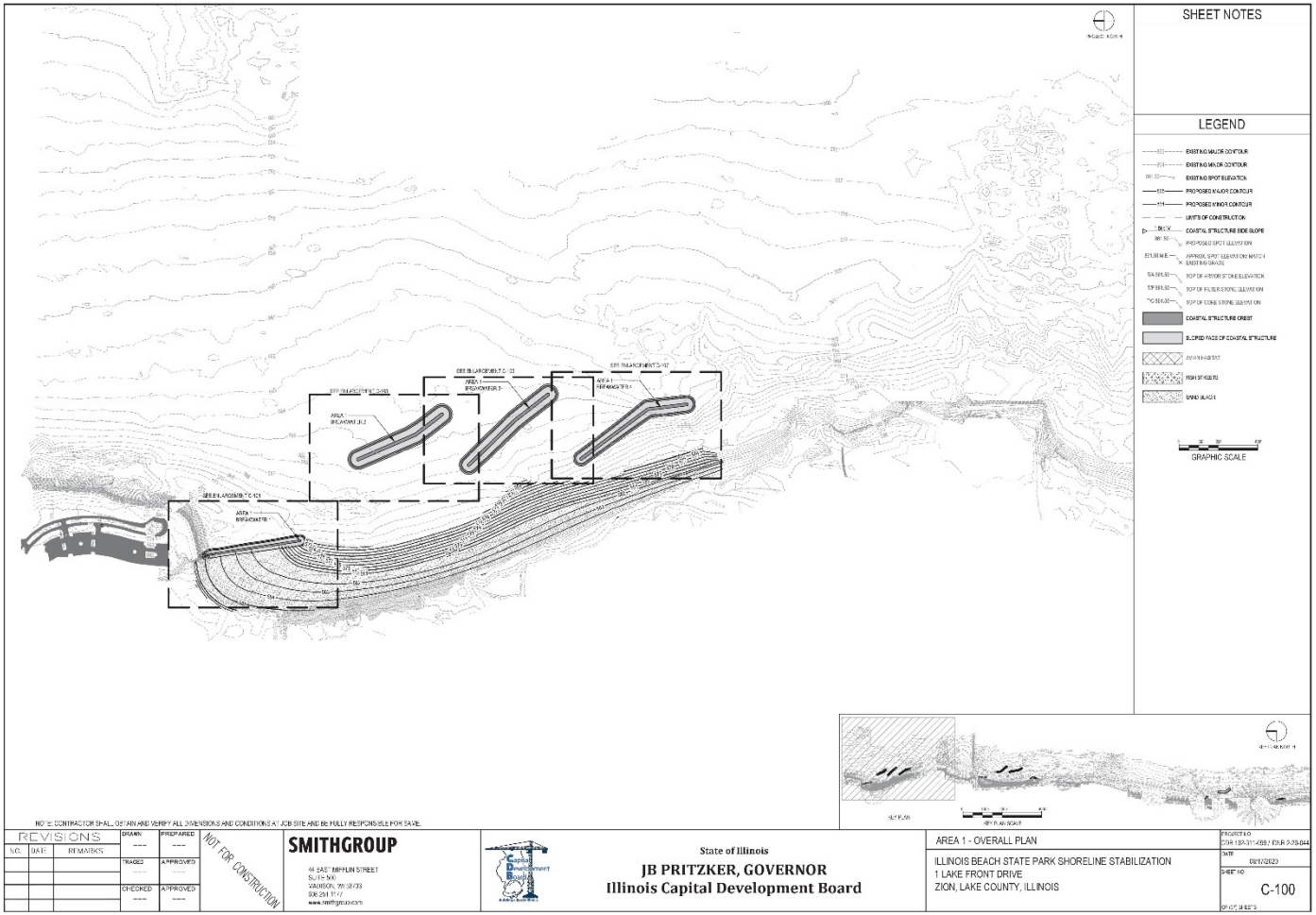


Figure 5.4: Initial layout of Area 1 beach control structures for morphological tests

*Source: 2020-0617 Illinois Beach State Park Shoreline Stabilization.pdf*

## 5.2. Test sections

### 5.2.1. Morphological testing

The beach control structures were optimised during the morphological tests. The initial layout of the beach control structures is shown in Figure 5.4, provided in *2020-0617 Illinois Beach State Park Shoreline Stabilization.pdf*. The intermediate layouts were directed by SmithGroup's on-site representatives based on the results of the preceding tests. The modifications were often small and iterative in nature, and were often only tested for short durations until a layout was showing promising results and subject to a full morphological test. Photographs and scan records of the significant intermediate structures are given in Appendix B.1, with a summary provided in Section 5.4. There were often no specific drawings for these intermediate structures as they were developed within the physical model. The final layout of the control structures was taken forward for the confirmation (stability) tests. The details of these structures are provided in Section 5.2.2.

### 5.2.2. Stability testing

The beach control structures for the stability tests were provided in *Scan 25-26 - Sections - w LONGS.dwg*, and are reproduced in Figure 5.5 to Figure 5.22. The plan layout is shown in Figure 5.5 and the cross-sections and long-sections in Figure 5.6 to Figure 5.22. The rock grades used for the stability tests are given in Table 2.1. The grading curves of the prepared model rock classes are given Appendix A. The stability tests focussed specifically on beach control structures BW1-1, 2, 3, 4, 5, 8 and 10. Note: as discussed in Sections 1.2 and 2.4.1, all rock grades use metric tonnes, and so, for example, the primary armour shown in Figure 5.6 as 0.5-1 Ton was modelled as 500-1000kg.

Figure 5.5: Layout drawing of beach control structures for stability tests

*Source: Scan 25-26 - Sections - w LONGS.dwg*

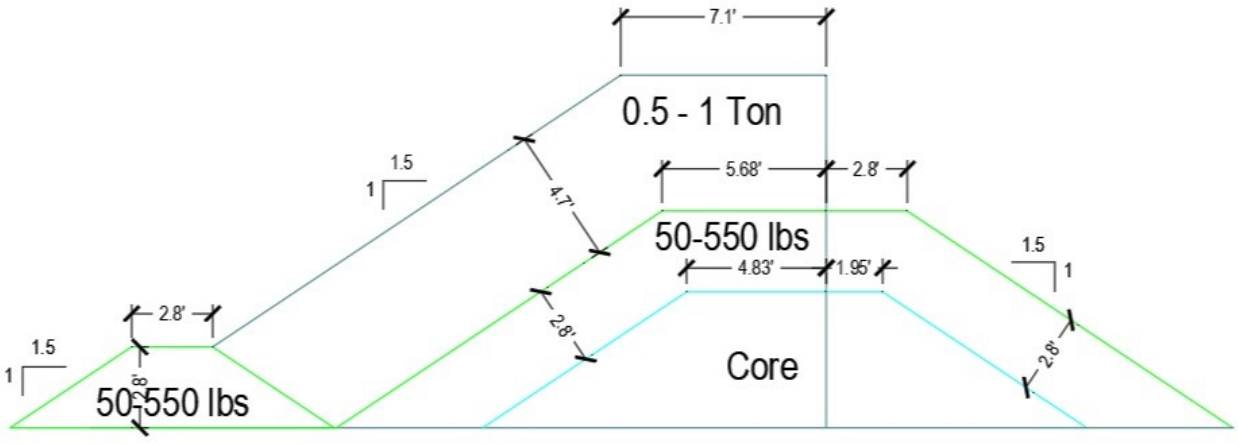


Figure 5.6: BW1-1 cross-section for stability tests

*Source: Scan 25-26 - Sections - w LONGS.dwg*

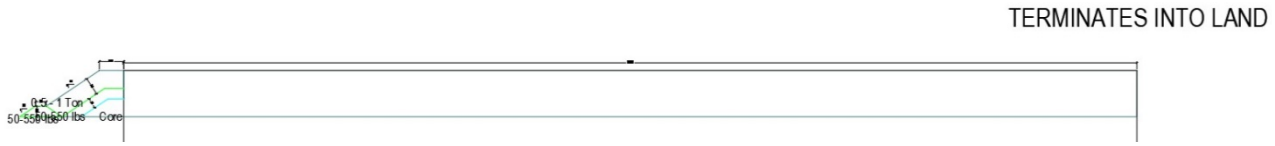


Figure 5.7: BW1-1 long-section for stability tests

*Source: Scan 25-26 - Sections - w LONGS.dwg*

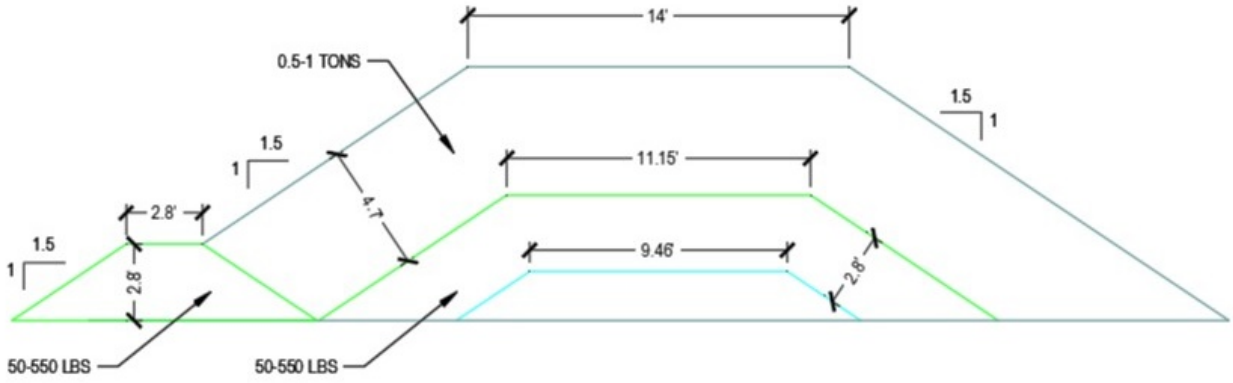


Figure 5.8: BW1-2 cross-section for stability tests

*Source: Scan 25-26 - Sections - w LONGS.dwg*

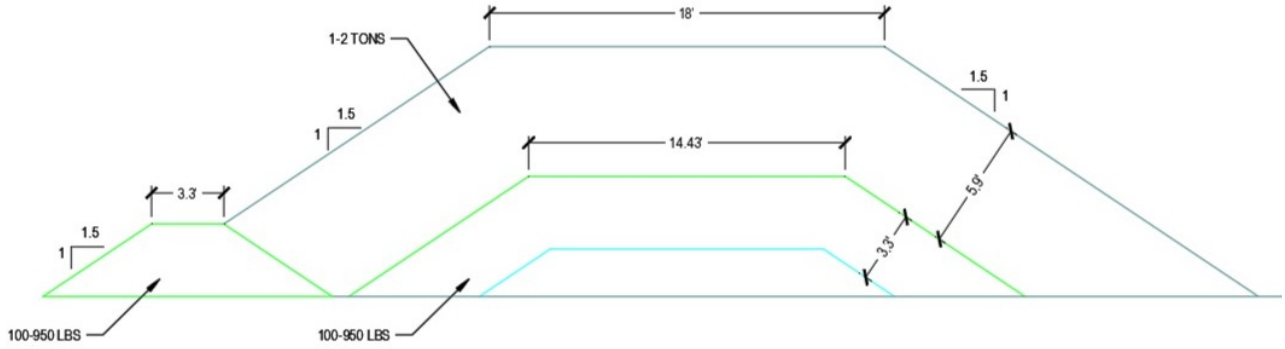


Figure 5.9: BW1-3 cross-section for stability tests

*Source: Scan 25-26 - Sections - w LONGS.dwg*

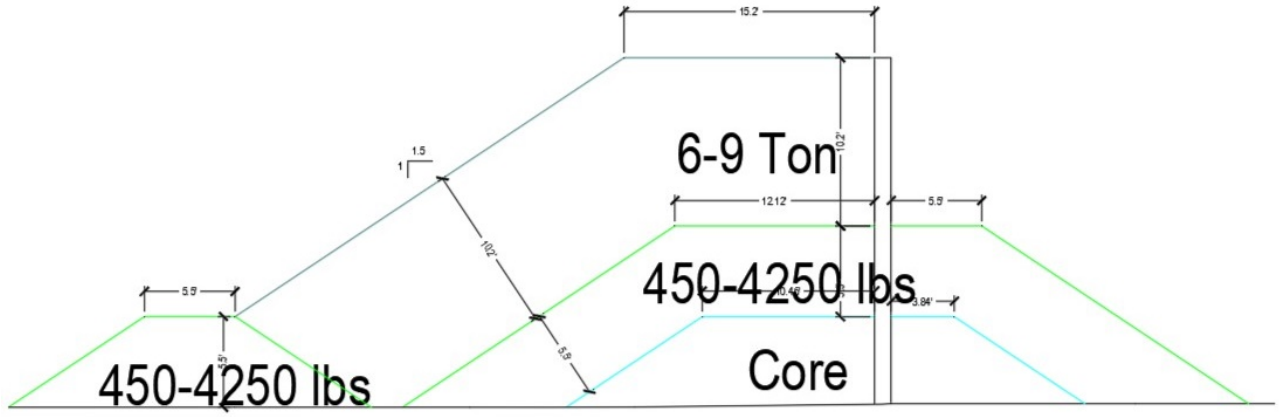


Figure 5.10: BW1-4 cross-section for stability tests

*Source: Scan 25-26 - Sections - w LONGS.dwg*

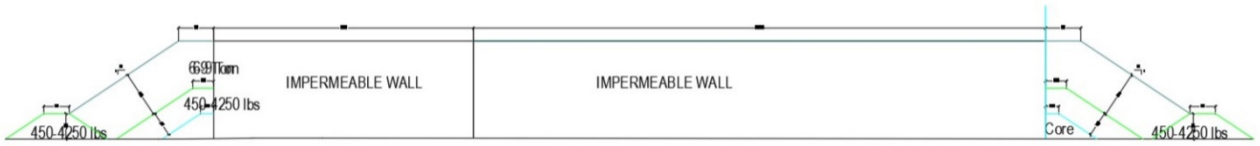


Figure 5.11: BW1-4 long-section for stability tests

*Source: Scan 25-26 - Sections - w LONGS.dwg*

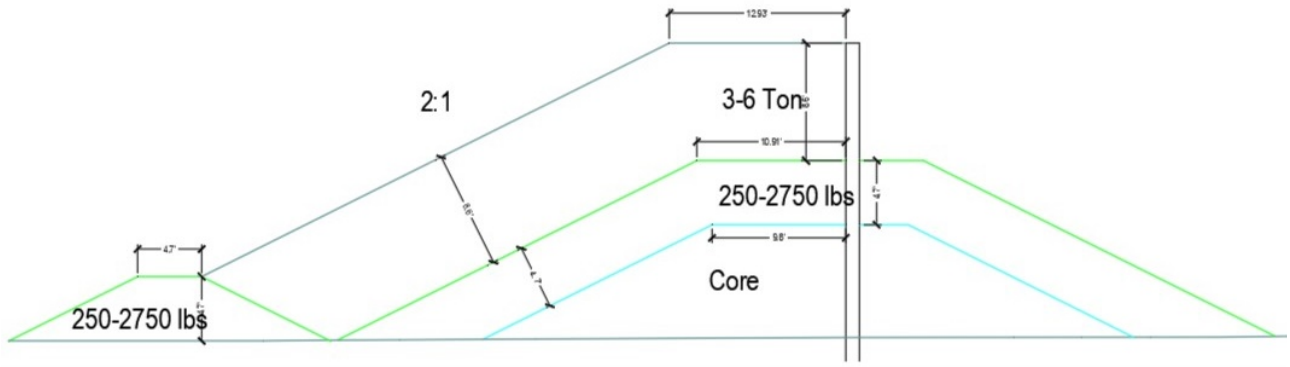


Figure 5.12: BW1-5, 1-6 and 1-8 cross-section for stability tests

*Source: Scan 25-26 - Sections - w LONGS.dwg*

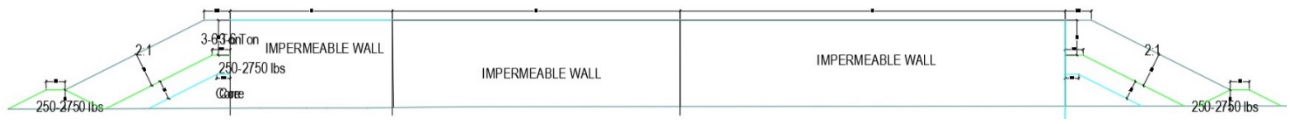


Figure 5.13: BW1-5 long-section for stability tests

*Source: Scan 25-26 - Sections - w LONGS.dwg*

Figure 5.14: BW1-6 long-section for stability tests

*Source: Scan 25-26 - Sections - w LONGS.dwg*

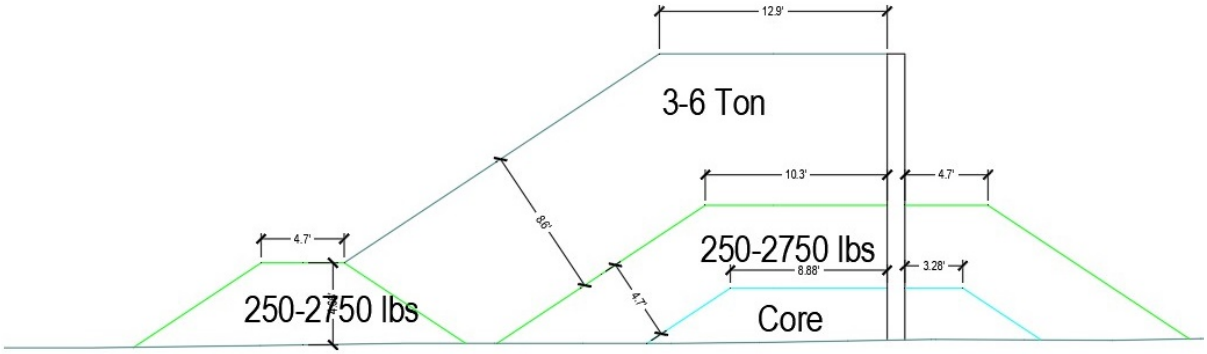


Figure 5.15: BW1-7 and 1-10 cross-section for stability tests

*Source: Scan 25-26 - Sections - w LONGS.dwg*

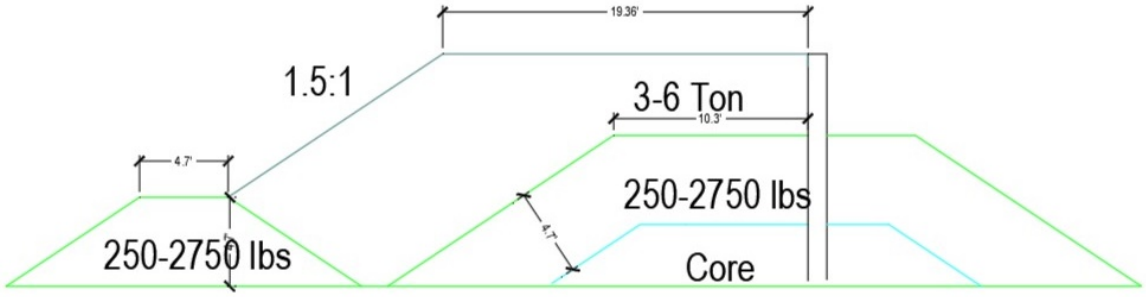


Figure 5.16: BW1-7 and 1-10 saddle cross-section for stability tests

*Source: Scan 25-26 - Sections - w LONGS.dwg*

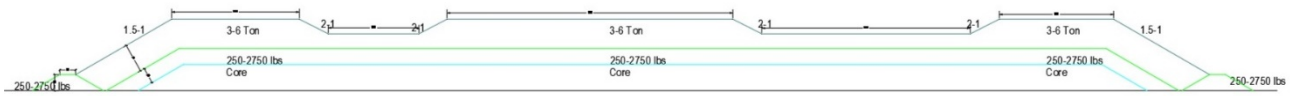


Figure 5.17: BW1-7 long-section for stability tests

*Source: Scan 25-26 - Sections - w LONGS.dwg*

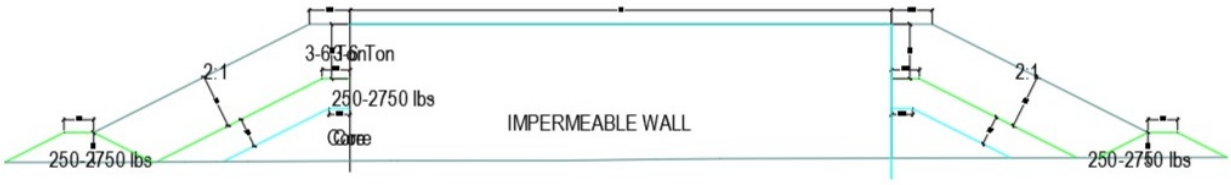


Figure 5.18: BW1-8 long-section for stability tests

*Source: Scan 25-26 - Sections - w LONGS.dwg*

Figure 5.19: BW1-9 long-section for stability tests

*Source: Scan 25-26 - Sections - w LONGS.dwg*

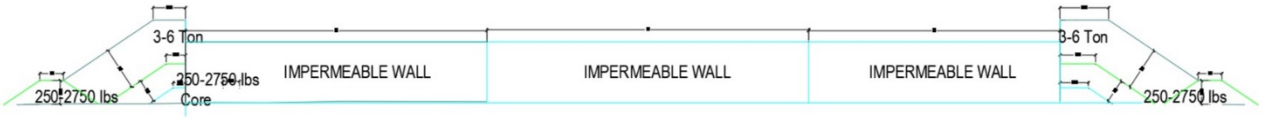


Figure 5.20: BW1-10 long-section for stability tests

*Source: Scan 25-26 - Sections - w LONGS.dwg*

Figure 5.21: BW1-10 Fish Tail long-section for stability tests

*Source: Scan 25-26 - Sections - w LONGS.dwg*

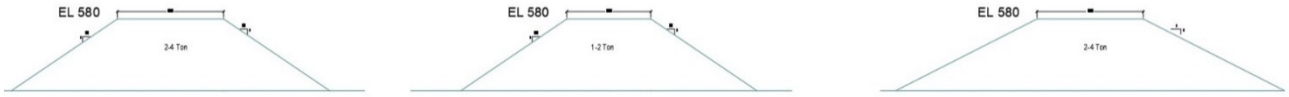


Figure 5.22: Fish Tail cross-sections for stability tests (BW1-6, 1-8, 1-9 and 1-10)

*Source: Scan 25-26 - Sections - w LONGS.dwg*

## 5.3. Wave calibration results

The results of the wave calibrations are summarised in Table 5.1 for the morphological condition and Table 5.2 for the stability conditions. These were determined at the calibration point (565 ft IGLD 85 contour, see Figure 5.2) using the methods outlined in Section 2.5. The tables present the target wave heights ($H_{m0}$) and periods ($T_p$) at the calibration point, along with the measured $H_{m0}$ (morphological condition) or $H_{1/3}$

(storm conditions) as discussed in Section 2.5. The spectral and Rayleigh plots for the morphological condition are reproduced in Figure 5.23 and Figure 5.24, respectively.

The South East (130°N) stability test conditions were not calibrated prior to construction of the model structures so as to accelerate the testing programme. The same paddle settings (input files, timeseries and gain etc.) were carried over from the North East conditions and were then run for the first time during testing. Due to an oversight, no wave data were recorded during the stability tests for Area 1. The wave heights given in Table 5.2 for the Southeast conditions have been estimated from the Area 2 measured wave heights which used the same wave paddle settings and a similar bathymetry. The Northeast conditions in both models were compared and the resultant relationship applied to the Southeast waves.

Table 5.1: Results of Area 1 morphological wave calibration at 565 ft IGLD 85 contour

| Wave condition | Target | | Measured |
|---|---|---|---|
| | $H_{m0}$ (ft) | $T_p$ (s) | $H_{m0}$ (ft) |
| Morph_03 | 4.9 | 9.0 | 5.1 |

Table 5.2: Results of Area 1 stability wave calibration at 565 ft IGLD 85 contour

| Wave condition | Direction (°N) | Target | | Measured |
|---|---|---|---|---|
| | | $H_{m0}$ (ft) | $T_p$ (s) | $H_{1/3}$ (ft) |
| WC_EXT_WL_01 | 61 | 11.2 | 10.0 | 11.4 |
| WC_EXT_WL_02 | 61 | 12.1 | 11.5 | 12.3 |
| WC_HIGH_WL | 61 | 11.2 | 11.5 | 11.3 |
| WC_LOW_WL | 61 | 6.6 | 11.5 | 6.3 |
| WC_HIGH_WL_SE | 130 | 6.2 | 7.5 | 5.1* |
| WC_LOW_WL_SE | 130 | 6.2 | 7.5 | 3.2* |

*Note: * Wave heights estimated from Area 2 wave data as described in the text above.*

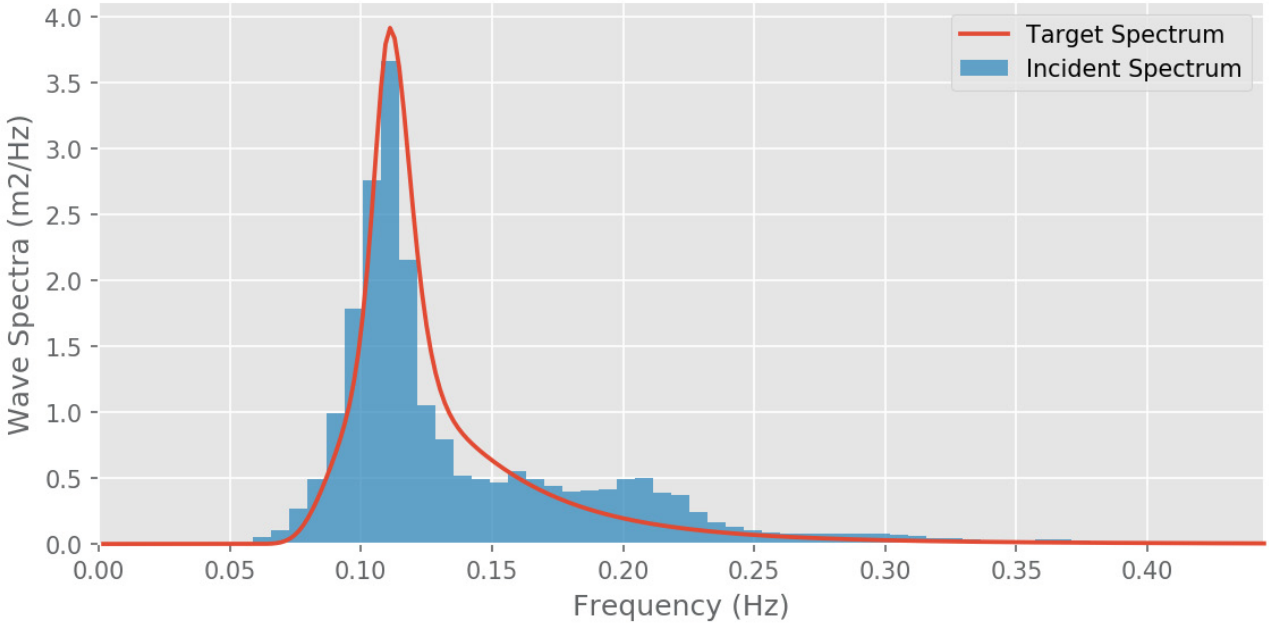


Figure 5.23: Area 1 Morph_03 spectral plot

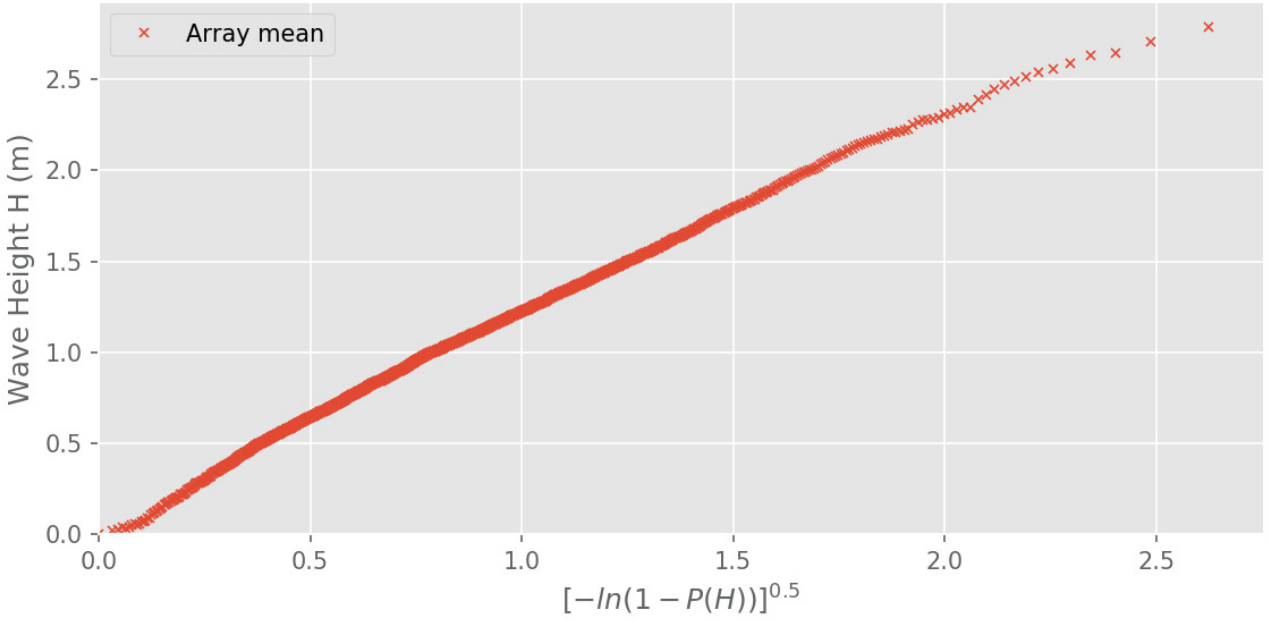


Figure 5.24: Area 1 Morph_03 Rayleigh plot

## 5.4. Morphological tests results – anthracite beach

The starting point for the Area 1 beach control structures optimisation was Configuration 01, and was provided in *2020-0617 Illinois Beach State Park Shoreline Stabilization.pdf* (Figure 5.4). This configuration was tested for 1.5 hrs then two 3 hr tests (15 minutes then 2 x 30 minutes model). The pre and post-test photographs from the 'North' and 'South' time-lapse camera views are shown in Figure 5.26 and Figure 5.27. The layout consisted of three long detached breakwaters with a predominantly Northwest-Southeast alignment and a shore connected breakwater at the Northern end of the Area 1 site, close to North Point Marina.

The optimisation moved through a further 21 configurations to arrive at the optimised layout, Configuration 22. A complete description of all the configurations leading to the development of the optimised layout are provided in Appendix B.1. Configuration 22 consisted of ten shorter structures, all with a predominantly shore-parallel orientation. Nine of the breakwaters were detached and were a combination of submerged and emergent, with and without fishtails. The original shore connected breakwater was retained but with a much shorter length. The pre and post-test photographs from the 'North' and 'South' time-lapse camera views are shown in Figure 5.28 and Figure 5.29. The post-test scan data, including the structure outlines, is shown in Figure 5.25. This configuration was tested once for 3 hr tests (30 minutes model). All tests were undertaken with the Morph03 wave condition (Table 3.5).

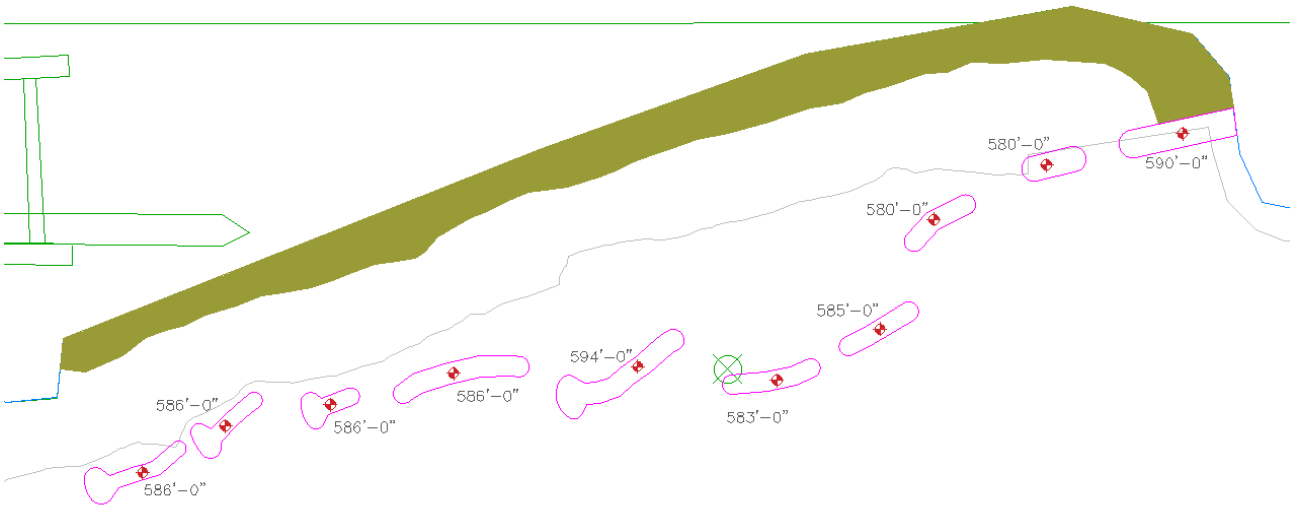


Figure 5.25: Post-test scan data for Area 1 Configuration 22 (Scan26), solid area post-test beach, structures in magenta

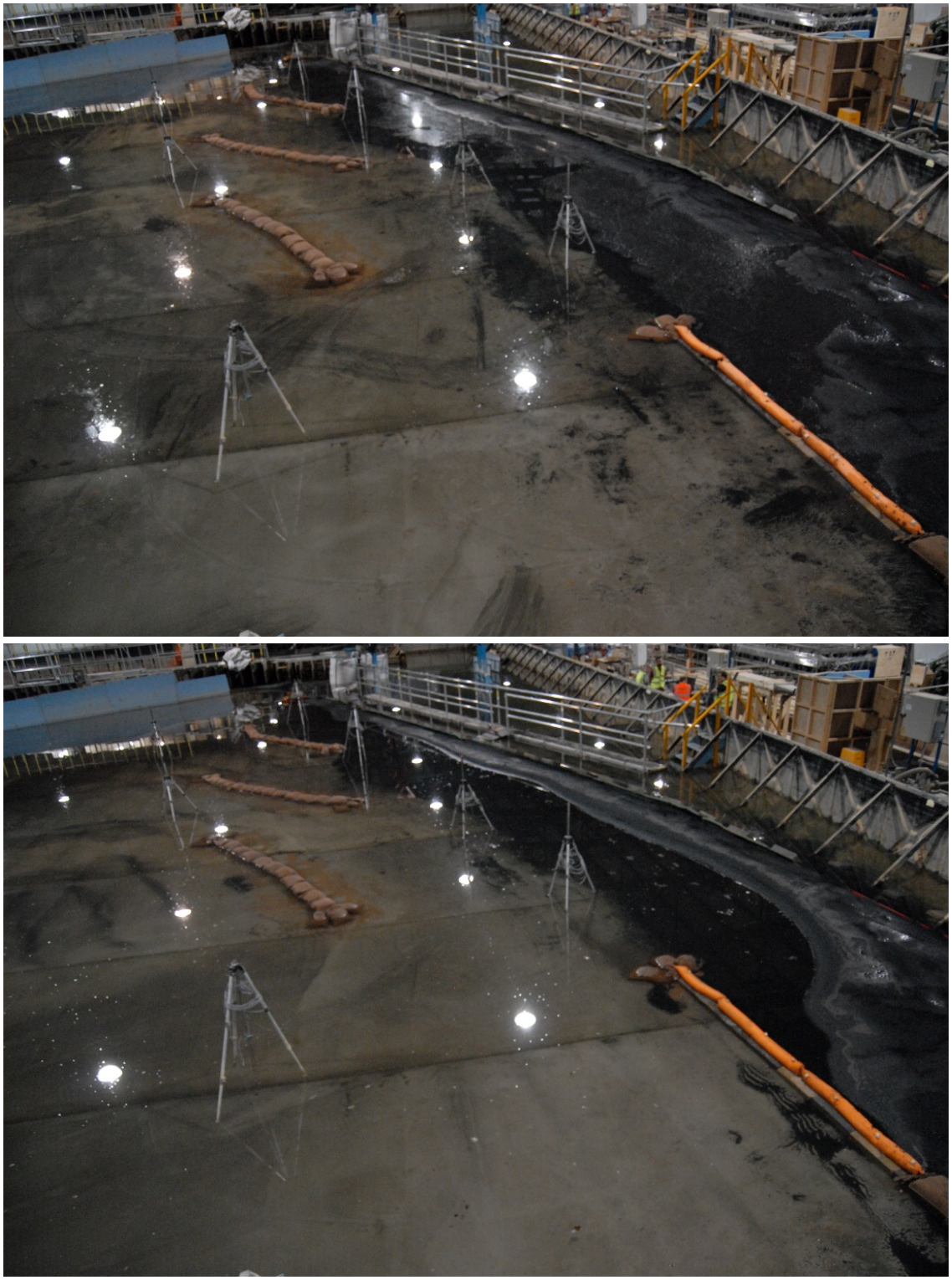

Figure 5.26: Pre (top) and post-test (bottom) photographs from 'North' view for Area 1 Configuration 01

Figure 5.27: Pre (top) and post-test (bottom) photographs from 'South' view for Area 1 Configuration 01

Figure 5.28: Pre (top) and post-test (bottom) photographs from 'North' view for Area 1 Configuration 22

Figure 5.29: Pre (top) and post-test (bottom) photographs from 'South' view for Area 1 Configuration 22

## 5.5. Dye tracing tests

At various points during the anthracite morphological tests the SmithGroup on-site representatives undertook dye tracing tests to observe cross-shore currents and to assess the potential for both high currents and sediment transport around key features (see Section 2.7). The current patterns observed by SmithGroup on-site representatives aided their development and optimisation of the beach control structures. No formal data was recorded by HR Wallingford for these observational dye tracing tests.

## 5.6. Storm response and morphological tests results – sand beach

Following the completion of the anthracite beach morphological tests, the anthracite beach was replaced with a sand beach to confirm the results from the anthracite beach and to allow the beach response to storm conditions to be checked during the stability tests. The storm response tests were conducted first (alongside the structure stability tests, Section 5.7), followed by morphological tests from the South East (130°N) and finally from the North East (61°N). The test order, including when scans were taken and the beach re-profiled is provided in Table 5.3.

Table 5.3: Area 1 sand beach Test Part and scan record

| Activity | Type | Scan |
|---|---|---|
| Initial placement of sand beach | Setup | Pre-test |
| Stability Test Part 01 - WC_LOW_WL | Test Part | No |
| Stability Test Part 02 - WC_HIGH_WL | Test Part | No |
| Stability Test Part 03 - WC_EXT_WL_01 | Test Part | No |
| Stability Test Part 04 - WC_EXT_WL_02 | Test Part | Post-test |
| Stability Test Part 05 - WC_LOW_WL_SE | Test Part | No |
| Stability Test Part 06 - WC_HIGH_WL_SE | Test Part | Post-test |
| Beach re-profiled to initial placement profile | setup | Pre-test |
| Morphological test from SE - *SWL* = 579.2 ft IGLD 85 | Test Part | Post-test |
| Morphological test from SE - *SWL* = 582.4 ft IGLD 85 | Test Part | Post-test |
| Morphological test from NE – Morph_03 (6 hrs) | Test Part | Post-test |
| Morphological test from NE – Morph_03 (59 hrs) | Test Part | Post-test |

### 5.6.1. Storm response from NE conditions

The storm response of the sand beach to the four Northeast storm conditions is shown in Figure 5.30. It compares the plan shape of the beach pre-test with that post all Northeast Test Parts 01 to 04 (scan post WC_EXT_WL_02). The beach recedes (reduces in width) throughout the progressive storm tests, each storm eroding the beach further. Following Test Part 04 there is still some beach above the SWL along the length modelled for Area 1. This series of storm tests, primarily run to assess the armour stability of the beach control structures, represents an extreme case as four full storm conditions have been tested by this point, replicating something that is unlikely to occur in prototype.

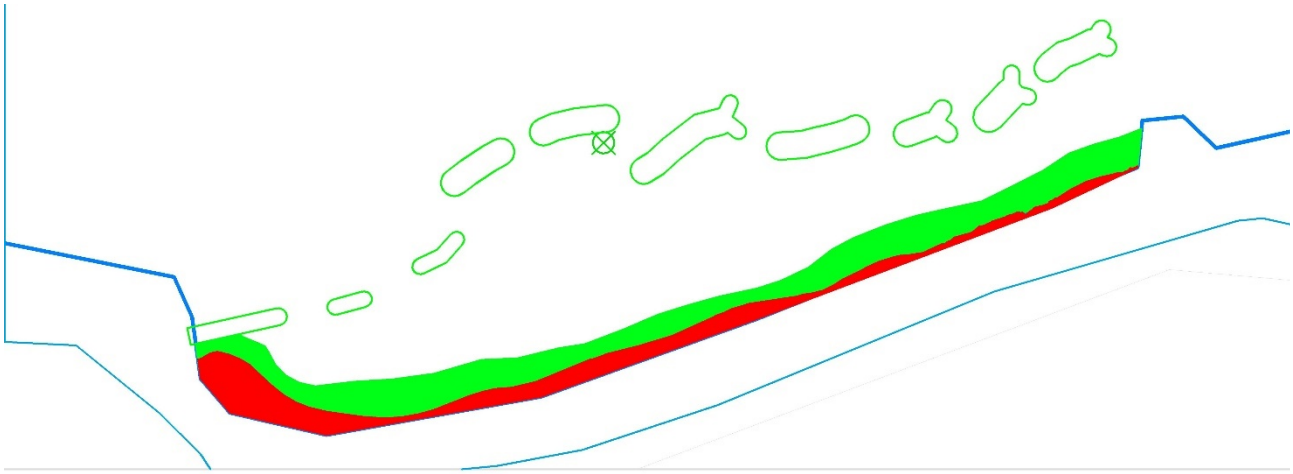

Figure 5.30: Area 1 stability post Test Part 04 beach scan data, SWL 585.2 ft IGLD 85 (pre-test scan in green, post-test scan in red, structure outline in green)

### 5.6.2. Storm response from SE conditions

The storm response of the sand beach after both Southeast storm conditions is shown in Figure 5.31. There is little change in the plan shape of the beach at the SWL (582.2 ft IGLD 85) after the smaller (relative to the Northeast) Southeast storm tests.

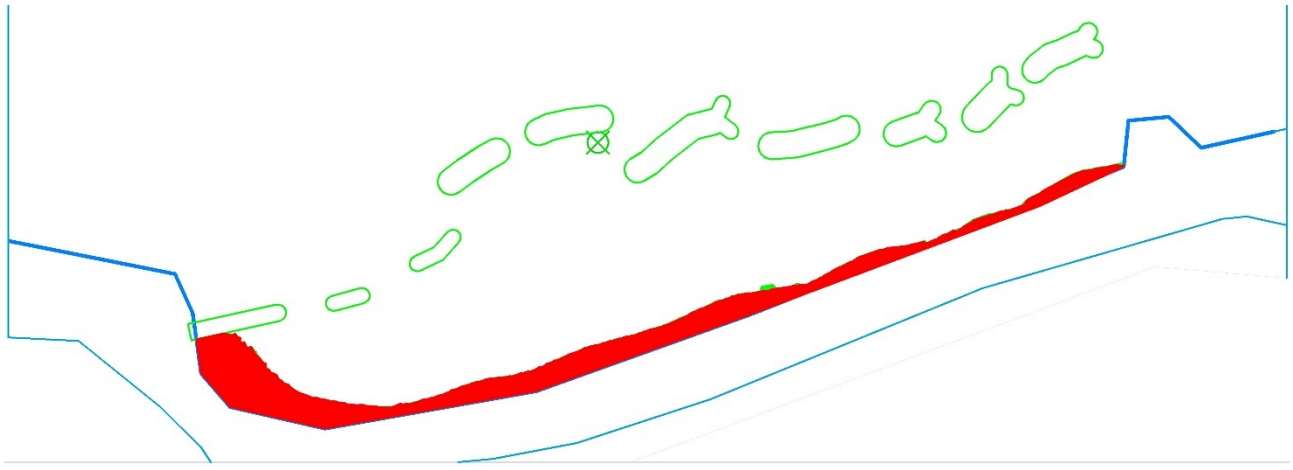

Figure 5.31: Area 1 stability post Test Part 06 beach scan data, SWL 582.2 ft IGLD 85 (pre-test scan in green, post-test scan in red, structure outline in green)

### 5.6.3. Morphological response from SE

Following the storm response tests, the sand beach response to the morphological wave conditions (Morph_03) was investigated. As discussed in Section 4, this was to provide confidence to the SmithGroup on-site representatives that the change in model beach material, required for the storm response tests, would provide consistent results with the anthracite material used for the optimisation.

The sand beach response to two relatively short morphological tests from the Southeast are shown in Figure 5.32 and Figure 5.33. Both use a modified Morph_03 condition from 130°N. The first Test Part, at the request of the SmithGroup on site representatives, used a SWL of 579.2 ft IGLD 85 (Figure 5.32), and the second used the same SWL used throughout the anthracite morphological tests (582.4 ft IGLD 85, Figure 5.33).

Both tests show an accretion of material at the elevation around the SWL as would be expected following the storm conditions run in the preceding Test Parts, particularly in the Northern end of the model as material is transported cross-shore from the South to the North by the Southeast wave conditions.

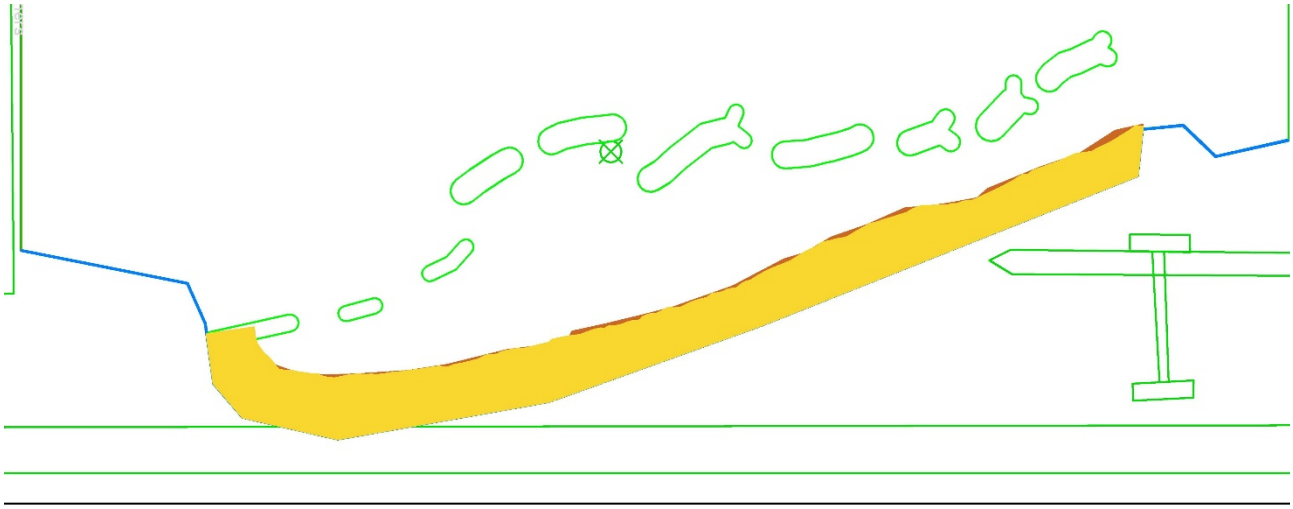

Figure 5.32: Area 1 beach scan data post Morph_SE_01, SWL 579.2 ft IGLD 85 (pre-test scan in yellow, post-test scan in orange, structure outline in green)

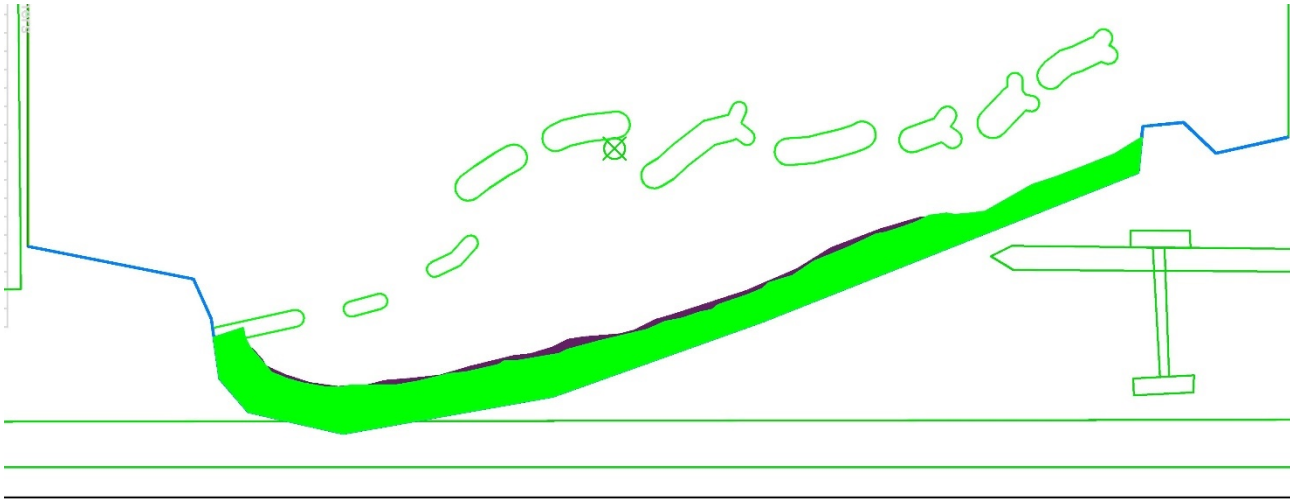

Figure 5.33: Area 1 beach scan data post Morph_SE_02, SWL 582.4 ft IGLD 85 (pre-test scan in green, post-test scan in purple, structure outline in green)

### 5.6.4. Morphological response from NE

After completion of the Southeast morphological Test Parts (Section 5.6.3), two Test Parts were run from the Northeast using the Morph_03 condition. The sand beach response to a 6 hour test (1 hr model) and a 59 hour test (10 hrs model) are shown respectively in Figure 5.34 and Figure 5.35. As expected the 6 hour tests shows little movement of the sand (Figure 5.34) as discussed in Sections 2.4.2 and 5.6.3. Figure 5.34 does show some transport of material North to South, again as expected with the switch in wave direction from the Southeast to the Northeast.

Following the longer (59 hour) second Test Part there is more movement of the sand beach, showing accretion of material at the elevation around the SWL compared to the pre-test plan shape and further movement of material from the North to the South.

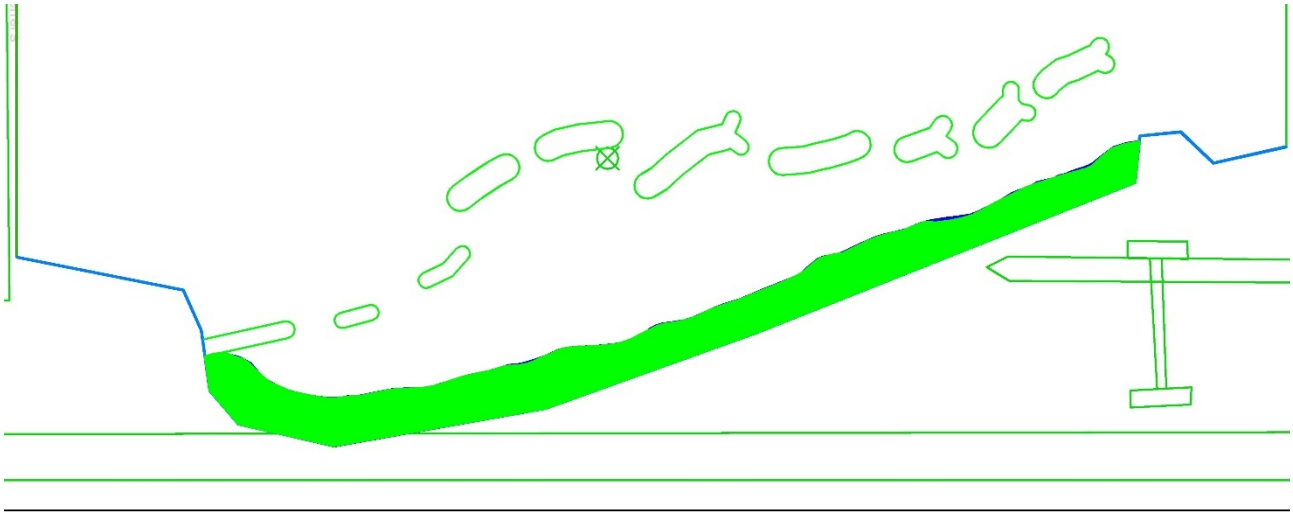

Figure 5.34: Area 1 beach scan data post 6 hr (1 hr model) test of Morph_03, SWL 582.4 ft IGLD 85 (pre-test scan in dark blue, post-test scan in green, structure outline in green)

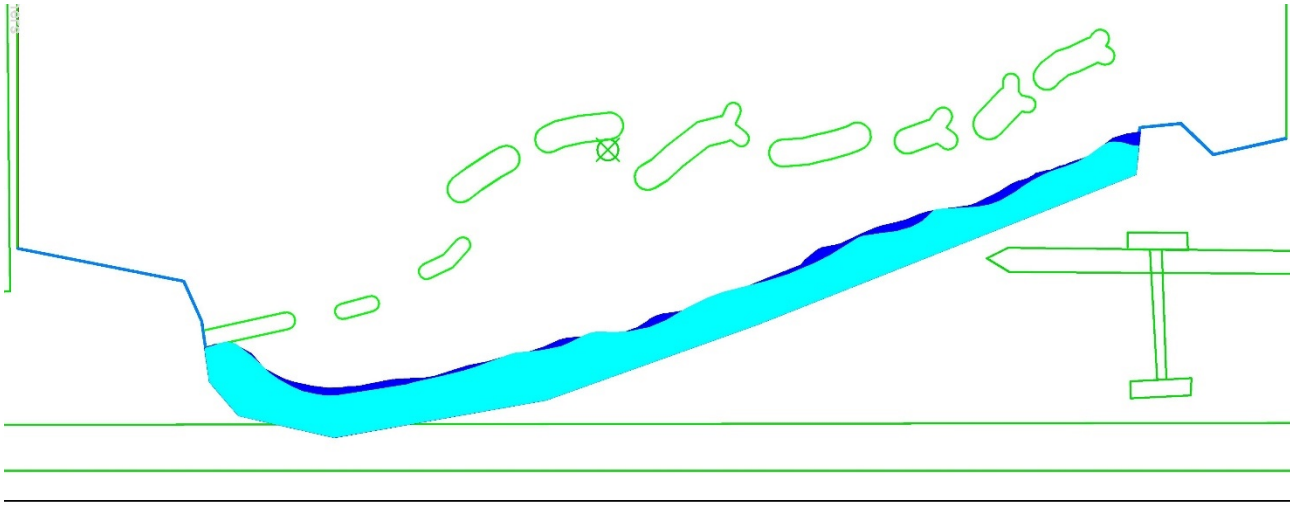

Figure 5.35: Area 1 beach scan data post 59 hr (10 hrs model) test of Morph_03, SWL 582.4 ft IGLD 85 (pre-test scan in dark blue, post-test scan in cyan, structure outline in green)

## 5.7. Stability test results

The stability tests focussed specifically on beach control structures BW1-1, 2, 3, 4, 5, 8 and 10 (Section 5.2.2). Photographs were taken before and after each Test Part and are reproduced in Appendix B.2. Each breakwater of interest has been divided into a series of panels, such as trunk, roundhead and fishtail, seaside and leeside, and where a section is particularly long it has been divided into North and South. The panels are shown in Figure 5.36.

The cumulative number of rocks extracted and the calculated $S_d$ damage parameter for BW1-1, 2, 3, 4, 5, 8 and 10 are presented in Table 5.4 to Table 5.17. For each breakwater there are two tables, the first with the cumulative number of rocks extracted from the armour layer and the second with the calculated $S_d$ damage parameter. The $S_d$ parameter has been calculated using the method described in Section 2.8.

For the majority of structures the damage level was low, with few rocks extracted. Areas of higher damage, $S_d > 8$ (Table 2.3), are the leeside trunk armour of BW1-8, Panel 22 (Appendix B.2.6) and the Western fishtail of BW1-10, Panel 27 (Appendix B.2.7). One structure area was close to the $S_d = 2$ limit, the South seaside trunk armour of BW1-10, Panel 25 (Appendix B.2.7).

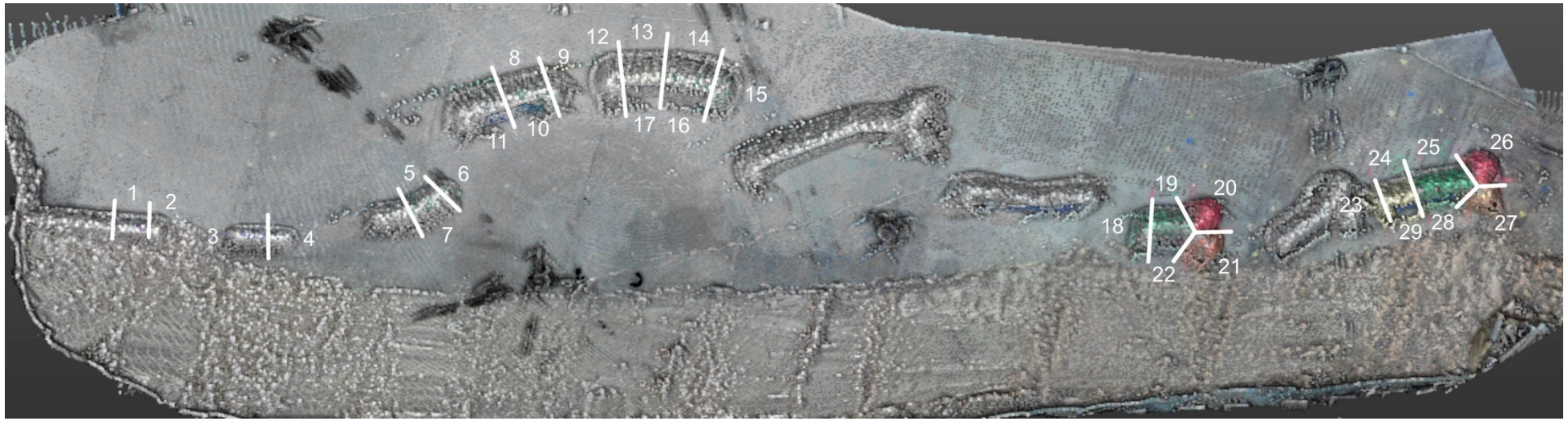


Figure 5.36: Area 1 stability analysis panels

Table 5.4: BW1-1 cumulative number of rocks displaced

| Test Part | Wave condition | Return period | Wave direction (°N) | Trunk (panel 1) | Roundhead (panel 2) |
|---|---|---|---|---|---|
| 1 | WC_LOW_WL | 1:100 | 61 | 0 | 0 |
| 2 | WC_HIGH_WL | 1:100 | 61 | 3 | 1 |
| 3 | WC_EXT_WL_01 | 1:10 | 61 | 3 | 1 |
| 4 | WC_EXT_WL_02 | 1:100 | 61 | 3 | 1 |
| 5 | WC_LOW_WL_SE | 1:100 | 130 | 4 | 1 |
| 6 | WC_HIGH_WL_SE | 1:100 | 130 | 7 | 1 |

Table 5.5: BW1-1 damage parameter $S_d$

| Test Part | Wave condition | Return period | Wave direction (°N) | Trunk (panel 1) | Roundhead (panel 2) |
|---|---|---|---|---|---|
| 1 | WC_LOW_WL | 1:100 | 61 | 0.0 | 0.0 |
| 2 | WC_HIGH_WL | 1:100 | 61 | 0.1 | 0.1 |
| 3 | WC_EXT_WL_01 | 1:10 | 61 | 0.1 | 0.1 |
| 4 | WC_EXT_WL_02 | 1:100 | 61 | 0.1 | 0.1 |
| 5 | WC_LOW_WL_SE | 1:100 | 130 | 0.1 | 0.1 |
| 6 | WC_HIGH_WL_SE | 1:100 | 130 | 0.3 | 0.1 |

Table 5.6: BW1-2 cumulative number of rocks displaced

| Test Part | Wave condition | Return period | Wave direction (°N) | North (panel 3) | South (panel 4) |
|---|---|---|---|---|---|
| 1 | WC_LOW_WL | 1:100 | 61 | 7 | 3 |
| 2 | WC_HIGH_WL | 1:100 | 61 | 8 | 4 |
| 3 | WC_EXT_WL_01 | 1:10 | 61 | 8 | 5 |
| 4 | WC_EXT_WL_02 | 1:100 | 61 | 8 | 6 |
| 5 | WC_LOW_WL_SE | 1:100 | 130 | 8 | 6 |
| 6 | WC_HIGH_WL_SE | 1:100 | 130 | 8 | 6 |

Table 5.7: BW1-2 damage parameter $S_d$

| Test Part | Wave condition | Return period | Wave direction (°N) | North (panel 3) | South (panel 4) |
|---|---|---|---|---|---|
| 1 | WC_LOW_WL | 1:100 | 61 | 0.3 | 0.1 |
| 2 | WC_HIGH_WL | 1:100 | 61 | 0.3 | 0.2 |
| 3 | WC_EXT_WL_01 | 1:10 | 61 | 0.3 | 0.2 |
| 4 | WC_EXT_WL_02 | 1:100 | 61 | 0.3 | 0.3 |
| 5 | WC_LOW_WL_SE | 1:100 | 130 | 0.3 | 0.3 |
| 6 | WC_HIGH_WL_SE | 1:100 | 130 | 0.3 | 0.3 |

Table 5.8: BW1-3 cumulative number of rocks displaced

| Test Part | Wave condition | Return period | Wave direction (°N) | Trunk seaside (panel 5) | Roundhead (panel 6) | Trunk leeside (panel 7) |
|---|---|---|---|---|---|---|
| 1 | WC_LOW_WL | 1:100 | 61 | 0 | 0 | 1 |
| 2 | WC_HIGH_WL | 1:100 | 61 | 0 | 0 | 2 |
| 3 | WC_EXT_WL_01 | 1:10 | 61 | 0 | 0 | 2 |
| 4 | WC_EXT_WL_02 | 1:100 | 61 | 0 | 0 | 3 |
| 5 | WC_LOW_WL_SE | 1:100 | 130 | 0 | 0 | 3 |
| 6 | WC_HIGH_WL_SE | 1:100 | 130 | 0 | 0 | 3 |

Table 5.9: BW1-3 damage parameter $S_d$

| Test Part | Wave condition | Return period | Wave direction (°N) | Trunk seaside (panel 5) | Roundhead (panel 6) | Trunk leeside (panel 7) |
|---|---|---|---|---|---|---|
| 1 | WC_LOW_WL | 1:100 | 61 | 0.0 | 0.0 | 0.1 |
| 2 | WC_HIGH_WL | 1:100 | 61 | 0.0 | 0.0 | 0.1 |
| 3 | WC_EXT_WL_01 | 1:10 | 61 | 0.0 | 0.0 | 0.1 |
| 4 | WC_EXT_WL_02 | 1:100 | 61 | 0.0 | 0.0 | 0.2 |
| 5 | WC_LOW_WL_SE | 1:100 | 130 | 0.0 | 0.0 | 0.2 |
| 6 | WC_HIGH_WL_SE | 1:100 | 130 | 0.0 | 0.0 | 0.2 |

Table 5.10: BW1-4 cumulative number of rocks displaced

| Test Part | Wave condition | Return period | Wave direction (°N) | Trunk seaside (panel 8) | Roundhead (panel 9) | Trunk leeside North (panel 11) | Trunk leeside South (panel 10) |
|---|---|---|---|---|---|---|---|
| 1 | WC_LOW_WL | 1:100 | 61 | 0 | 0 | 0 | 0 |
| 2 | WC_HIGH_WL | 1:100 | 61 | 0 | 0 | 5 | 1 |
| 3 | WC_EXT_WL_01 | 1:10 | 61 | 0 | 0 | 5 | 1 |
| 4 | WC_EXT_WL_02 | 1:100 | 61 | 0 | 0 | 7 | 4 |
| 5 | WC_LOW_WL_SE | 1:100 | 130 | 0 | 0 | 7 | 4 |
| 6 | WC_HIGH_WL_SE | 1:100 | 130 | 0 | 0 | 7 | 4 |

Table 5.11: BW1-4 damage parameter $S_d$

| Test Part | Wave condition | Return period | Wave direction (°N) | Trunk seaside (panel 8) | Roundhead (panel 9) | Trunk leeside North (panel 11) | Trunk leeside South (panel 12) |
|---|---|---|---|---|---|---|---|
| 1 | WC_LOW_WL | 1:100 | 61 | 0.0 | 0.0 | 0.0 | 0.0 |
| 2 | WC_HIGH_WL | 1:100 | 61 | 0.0 | 0.0 | 0.2 | 0.0 |
| 3 | WC_EXT_WL_01 | 1:10 | 61 | 0.0 | 0.0 | 0.2 | 0.0 |
| 4 | WC_EXT_WL_02 | 1:100 | 61 | 0.0 | 0.0 | 0.3 | 0.1 |
| 5 | WC_LOW_WL_SE | 1:100 | 130 | 0.0 | 0.0 | 0.3 | 0.1 |
| 6 | WC_HIGH_WL_SE | 1:100 | 130 | 0.0 | 0.0 | 0.3 | 0.1 |

Table 5.12: BW1-5 cumulative number of rocks displaced

| Test Part | Wave condition | Return period | Wave direction (°N) | Trunk seaside North (panel 13) | Roundhead North (panel 12) | Trunk seaside South (panel 14) | Roundhead South (panel 15) | Trunk leeside North (panel 17) | Trunk leeside South (panel 16) |
|---|---|---|---|---|---|---|---|---|---|
| 1 | WC_LOW_WL | 1:100 | 61 | 0 | 0 | 0 | 0 | 0 | 0 |
| 2 | WC_HIGH_WL | 1:100 | 61 | 0 | 5 | 1 | 2 | 13 | 10 |
| 3 | WC_EXT_WL_01 | 1:10 | 61 | 0 | 6 | 1 | 2 | 13 | 14 |
| 4 | WC_EXT_WL_02 | 1:100 | 61 | 1 | 6 | 2 | 2 | 37 | 14 |
| 5 | WC_LOW_WL_SE | 1:100 | 130 | 1 | 6 | 2 | 2 | 37 | 14 |
| 6 | WC_HIGH_WL_SE | 1:100 | 130 | 1 | 6 | 2 | 2 | 37 | 14 |

Table 5.13: BW1-5 damage parameter $S_d$

| Test Part | Wave condition | Return period | Wave direction (°N) | Trunk seaside North (panel 13) | Roundhead North (panel 12) | Trunk seaside South (panel 14) | Roundhead South (panel 15) | Trunk leeside North (panel 17) | Trunk leeside South (panel 16) |
|---|---|---|---|---|---|---|---|---|---|
| 1 | WC_LOW_WL | 1:100 | 61 | 0.0 | 0.0 | 0.0 | 0.0 | 0.0 | 0.0 |
| 2 | WC_HIGH_WL | 1:100 | 61 | 0.0 | 0.2 | 0.1 | 0.1 | 0.4 | 0.3 |
| 3 | WC_EXT_WL_01 | 1:10 | 61 | 0.0 | 0.3 | 0.1 | 0.1 | 0.4 | 0.4 |
| 4 | WC_EXT_WL_02 | 1:100 | 61 | 0.0 | 0.3 | 0.1 | 0.1 | 1.0 | 0.4 |
| 5 | WC_LOW_WL_SE | 1:100 | 130 | 0.0 | 0.3 | 0.1 | 0.1 | 1.0 | 0.4 |
| 6 | WC_HIGH_WL_SE | 1:100 | 130 | 0.0 | 0.3 | 0.1 | 0.1 | 1.0 | 0.4 |

Table 5.14: BW1-8 cumulative number of rocks displaced

| Test Part | Wave condition | Return period | Wave direction (°N) | Trunk seaside (panel 19) | Roundhead (panel 18) | Fishtail East (panel 20) | Fishtail West (panel 21) | Trunk leeside (panel 22) |
|---|---|---|---|---|---|---|---|---|
| 1 | WC_LOW_WL | 1:100 | 61 | 0 | 0 | 3 | 1 | 0 |
| 2 | WC_HIGH_WL | 1:100 | 61 | 6 | 10 | 5 | 20 | 221 |
| 3 | WC_EXT_WL_01 | 1:10 | 61 | 8 | 11 | 8 | 24 | 221 |
| 4 | WC_EXT_WL_02 | 1:100 | 61 | 8 | 11 | 8 | 27 | 276 |
| 5 | WC_LOW_WL_SE | 1:100 | 130 | 8 | 11 | 8 | 27 | 276 |
| 6 | WC_HIGH_WL_SE | 1:100 | 130 | 8 | 11 | 8 | 27 | 276 |

Table 5.15: BW1-8 damage parameter $S_d$

| Test Part | Wave condition | Return period | Wave direction (°N) | Trunk seaside (panel 19) | Roundhead (panel 18) | Fishtail East (panel 20) | Fishtail West (panel 21) | Trunk leeside (panel 22) |
|---|---|---|---|---|---|---|---|---|
| 1 | WC_LOW_WL | 1:100 | 61 | 0.0 | 0.0 | 0.1 | 0.0 | 0.0 |
| 2 | WC_HIGH_WL | 1:100 | 61 | 0.3 | 0.4 | 0.2 | 0.6 | 6.8 |
| 3 | WC_EXT_WL_01 | 1:10 | 61 | 0.5 | 0.5 | 0.3 | 0.7 | 6.8 |
| 4 | WC_EXT_WL_02 | 1:100 | 61 | 0.5 | 0.5 | 0.3 | 0.8 | 8.5 |
| 5 | WC_LOW_WL_SE | 1:100 | 130 | 0.5 | 0.5 | 0.3 | 0.8 | 8.5 |
| 6 | WC_HIGH_WL_SE | 1:100 | 130 | 0.5 | 0.5 | 0.3 | 0.8 | 8.5 |

Table 5.16: BW1-10 cumulative number of rocks displaced

| Test Part | Wave condition | Return period | Wave direction (°N) | Trunk seaside North (panel 24) | Roundhead North (panel 23) | Trunk seaside South (panel 25) | Fishtail East (panel 26) | Fishtail West (panel 27) | Trunk leeside North (panel 29) | Trunk leeside South (panel 28) |
|---|---|---|---|---|---|---|---|---|---|---|
| 1 | WC_LOW_WL | 1:100 | 61 | 0 | 2 | 0 | 2 | 16 | 0 | 1 |
| 2 | WC_HIGH_WL | 1:100 | 61 | 10 | 9 | 31 | 18 | n/a* | 1 | 2 |
| 3 | WC_EXT_WL_01 | 1:10 | 61 | 12 | 9 | 33 | 20 | n/a* | 1 | 2 |
| 4 | WC_EXT_WL_02 | 1:100 | 61 | 13 | 9 | 33 | 21 | n/a* | 2 | 2 |
| 5 | WC_LOW_WL_SE | 1:100 | 130 | 13 | 9 | 33 | 21 | n/a* | 2 | 2 |
| 6 | WC_HIGH_WL_SE | 1:100 | 130 | 13 | 9 | 33 | 21 | n/a* | 2 | 2 |

*Note: * Due to exposure of the underlayer and subsequent structural failure the West fishtail was covered with foam matting for the remainder of testing.*

Table 5.17: BW1-10 damage parameter $S_d$

| Test Part | Wave condition | Return period | Wave direction (°N) | Trunk seaside North (panel 24) | Roundhead North (panel 23) | Trunk seaside South (panel 25) | Fishtail East (panel 26) | Fishtail West (panel 27) | Trunk leeside North (panel 29) | Trunk leeside South (panel 28) |
|---|---|---|---|---|---|---|---|---|---|---|
| 1 | WC_LOW_WL | 1:100 | 61 | 0.00 | 0.12 | 0.00 | 0.07 | 0.50 | 0.00 | 0.04 |
| 2 | WC_HIGH_WL | 1:100 | 61 | 0.49 | 0.56 | 1.80 | 0.65 | n/a* | 0.04 | 0.07 |
| 3 | WC_EXT_WL_01 | 1:10 | 61 | 0.59 | 0.56 | 1.92 | 0.73 | n/a* | 0.04 | 0.07 |
| 4 | WC_EXT_WL_02 | 1:100 | 61 | 0.64 | 0.56 | 1.92 | 0.76 | n/a* | 0.07 | 0.07 |
| 5 | WC_LOW_WL_SE | 1:100 | 130 | 0.64 | 0.56 | 1.92 | 0.76 | n/a* | 0.07 | 0.07 |
| 6 | WC_HIGH_WL_SE | 1:100 | 130 | 0.64 | 0.56 | 1.92 | 0.76 | n/a* | 0.07 | 0.07 |

*Note: * Due to exposure of the underlayer and subsequent structural failure the West fishtail was covered with foam matting for the remainder of testing.*

## 5.8. Summary

A total of ten beach control structures of various cross-sections and armourstone grades were utilised for the final configuration. In Section 5.4, it was demonstrated that a stable beach could be maintained with a reduced north-south sediment drift using this configuration. The beaches remained static during most of the stability tests, but for the extreme high water 1:10 and 1:100 return period storms, a wide crest at the beach could not be maintained and there was a net transfer of sediment to the immediate hinterland.

Of the beach control structures resistance to wave action during the stability test programme, it is possible to make the following observations:

1. All structures, with the exception of the leeside trunk armour of breakwater BW1-8 (Panel 22) and the fishtail for breakwater BW1-10 (Panel 27), were substantially intact at the end of the testing campaign;
2. All structures were tested for a minimum of 30 hours of storm conditions, and it should be noted that this exceeds any reasonable exposure that might be anticipated during the design life;
3. Where a piled central breakwater section was included (specifically breakwaters BW1-4 to BW1-10), then the potential for crest armour damage was reduced with these configurations.

# 6. Area 2 – Camp Logan

The Area 2 model examined the Camp Logan area of Lake Michigan, situated to the South of Area 1 (Section 5). To the north of this area is Kellogg Creek which creates a small headland into the lake. To the immediate south, there is significant and ongoing beach erosion with a net north to south sediment drift driven predominantly by North East waves, as in Area 1. The first phase of the model included a northern breakwater coming from the small headland to hold the coastline adjacent to Kellogg Creek, followed by a series of shore detached groynes to encourage the development of salients and tombolos to arrest or reduce the north-south sediment drift. As with Area 1, this was done using sandbags to act as proxies for armourstone breakwaters and allowed multiple configurations to be examined using a lightweight modelling sediment. This was tested with a generic Morphological wave condition that was able to mobilise the modelling sediment without affecting the beach response due to wave breaking significantly.

Once a stable configuration had been identified, then the lightweight modelling sediment was replaced with a fine grained modelling sand with the correct density. The final configuration of proxy armourstone structures was replaced with correctly sized and scaled model rock structures, and the whole was then tested with a sequence of six wave and water level conditions from both the North East and South East wave directions. This section describes the model set up, the waves and wave calibrations, the morphological beach testing and the structural stability for Area 2. Some key observations are given in Section 6.9. This section also reports the optimisation of a beach control structure to the North of Kellogg Creek by the SmithGroup on-site representatives.

## 6.1. Wave basin layout

The Area 2 testing was carried out in HR Wallingford's Wave Basin BC which is 50 m long by 32 m wide and has a maximum working depth of 1.0 m (all dimensions in metric model terms). The bathymetry design and construction is described in Section 2.2, with the full basin layout shown in Figure 6.1.

The wave gauge locations for the different phases of testing are presented in Figure 6.1 and Figure 6.2. The locations presented in Figure 6.1 were used for wave calibrations in addition to the morphological testing (anthracite beach). The wave gauge layout for the stability and beach storm response testing was agreed with SmithGroup prior to testing and confirmed in *Area2_Probes.pdf*.

### 6.1.1. Area 2 beach material placement

The anthracite beach material was initially placed according to an idealised profile provided by SmithGroup (*AREA2BEACHSECTIONINCM.dwg*). The profile was used to manufacture beach-normal wooden templates. The templates were arranged along the model with the back placed against the rear wall of the model, then levelled and the initial beach cross-shore profile and plan-shape created using the method outlined for Area 1.

The sand beach material was placed according to an idealised profile with a 1:15 slope from the 570 ft IGLD 85 contour to an elevation of 586 ft IGLD 85 (*4336_001.pdf*). The profile was used to manufacture beach-normal wooden templates. The templates were aligned on the 575 ft IGLD 85 contour to create the main slope and beach crest, and additional modelling material was used to mould the area from 575 ft IGLD 85 down to 570 ft IGLD 85 to better match the final scan data from the end of the morphologic tests.

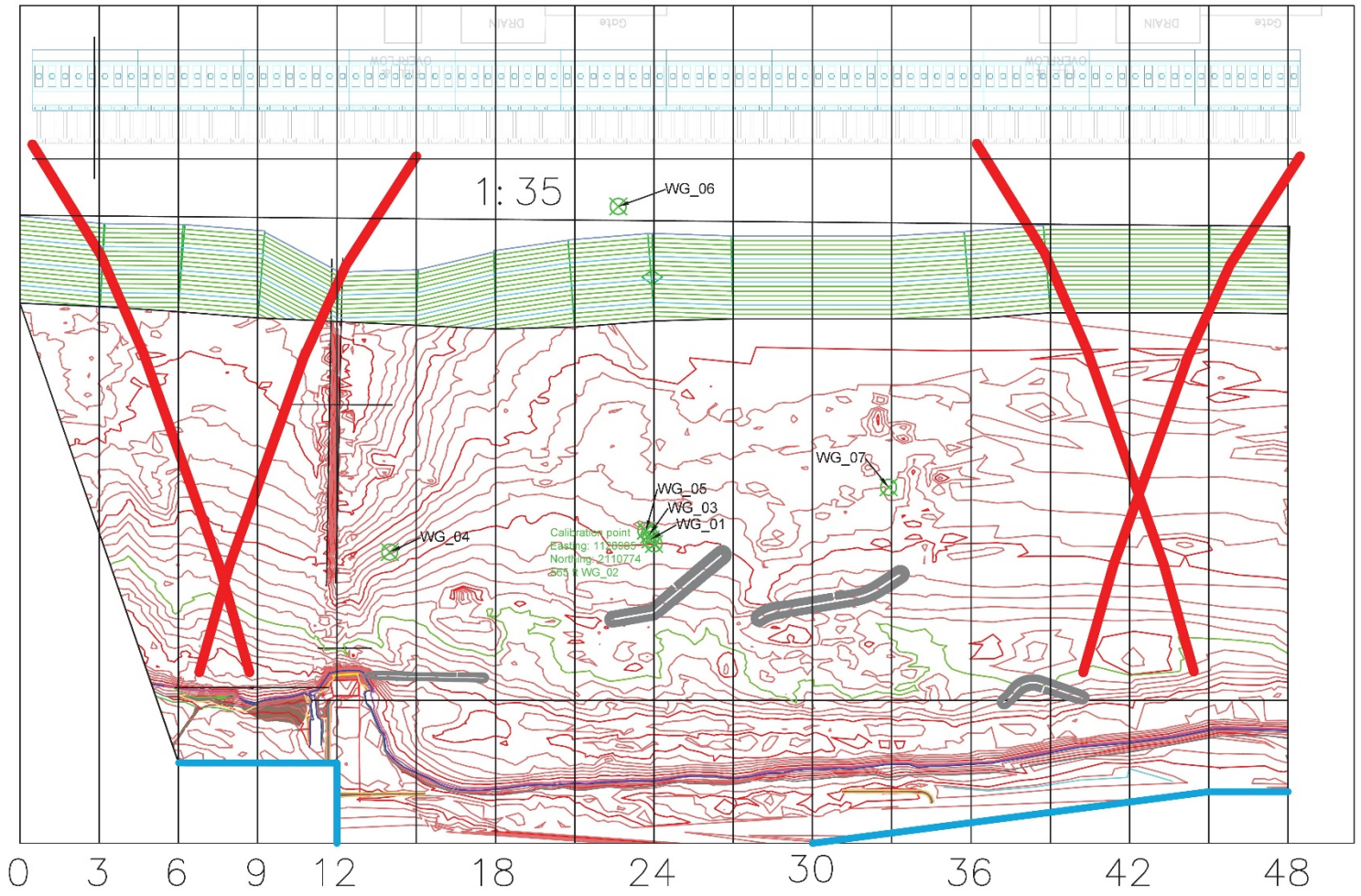


Figure 6.1: Area 2 basin layout showing wave gauge locations for anthracite morphological tests

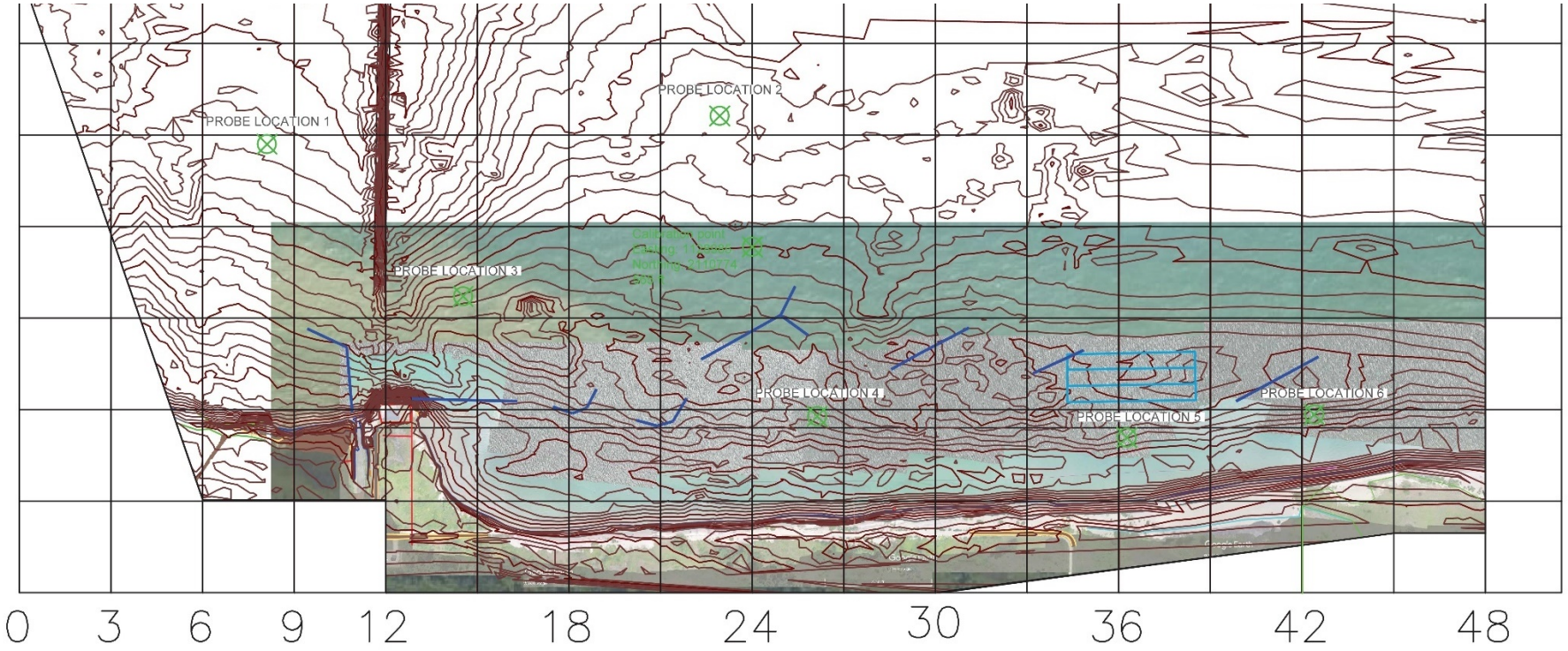


Figure 6.2: Wave gauge locations for Area 2 stability and sand beach storm response tests

*Source: Area2_Probes.pdf*

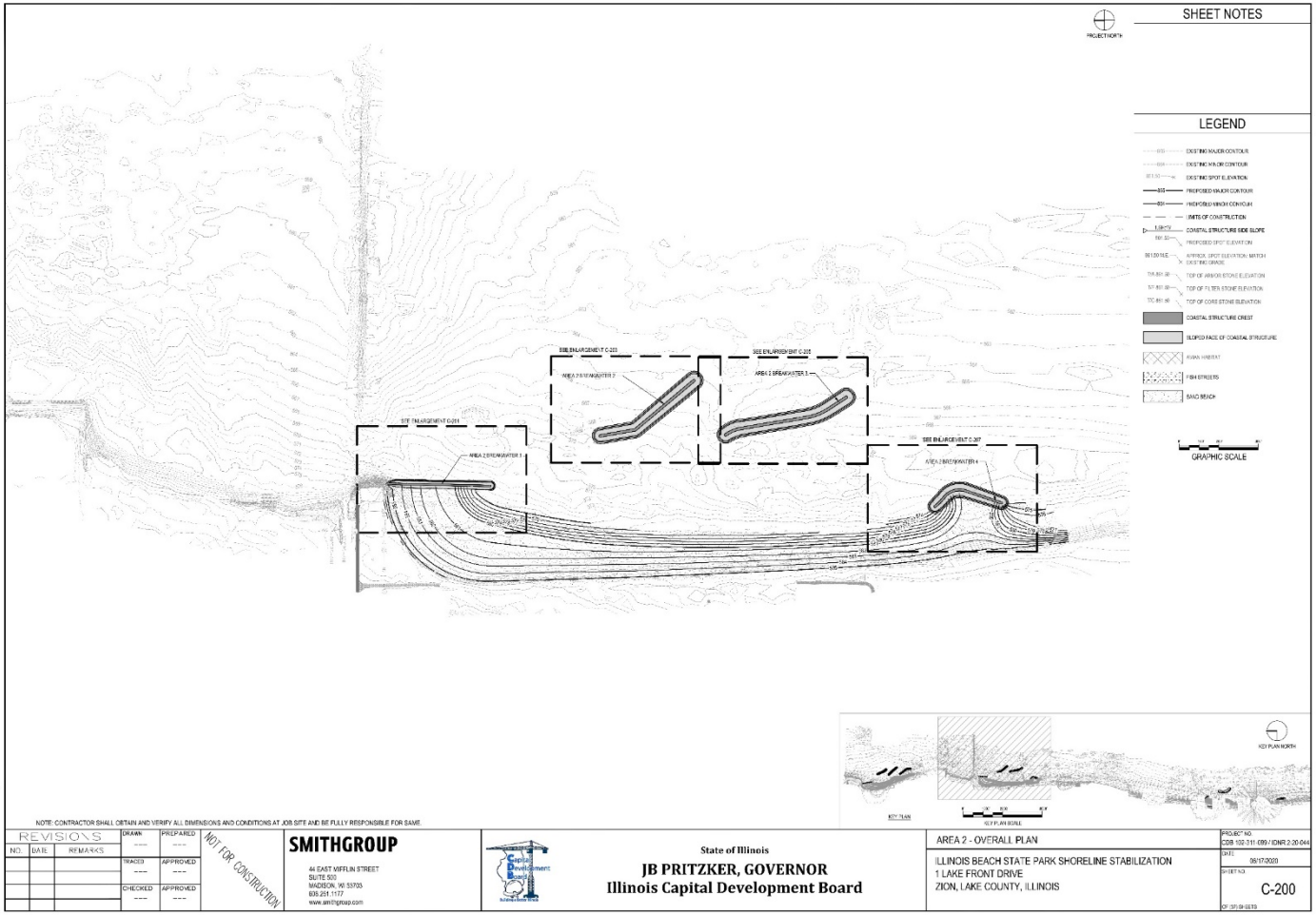


Figure 6.3: Initial layout of Area 2 beach control structures for morphological tests

*Source: 2020-0617 Illinois Beach State Park Shoreline Stabilization.pdf*

## 6.2. Test sections

### 6.2.1. Morphological testing

The beach control structures were optimised during the morphological tests. The initial layout of the beach control structures is shown in Figure 6.3, provided in *2020-0617 Illinois Beach State Park Shoreline Stabilization.pdf*. The intermediate layouts were directed by SmithGroup's on-site representatives based on the results of the preceding tests. The modifications were often small and iterative in nature, and were often only tested for short durations until a layout was showing promising results and subjected to a full morphological test. Photographs and scan records of the significant intermediate structures are given in Appendix C.1, with a summary provided in Section 6.4. There were often no specific drawings for these intermediate structures as they were developed within the physical model. The final layout of the control structures was taken forward for the confirmation (stability) tests. The details of these structures are provided in Section 6.2.2.

During morphological testing, SmithGroup representatives undertook dye tracing and morphological tests around the Kellogg Creek area. This was to assess the sediment transport around the creek mouth and investigate mitigation options to keep the creek mouth open and results are shown in Section 6.5.

### 6.2.2. Stability testing

The beach control structures for the stability tests were provided in *Area2_Stability Test SECTIONS 10 02 2020.dwg*, and are reproduced in Figure 6.4 to Figure 6.22. The plan layout is shown in Figure 6.4 and the cross-sections and long-sections in Figure 6.5 to Figure 6.22. The rock grades used for the stability tests are shownin Table 2.1 along with which grade was used as armour for which structure. Various of the smaller grades were used for under / filter layers where larger armour grades have been used. The grade curves of the prepared model rock classes are given Appendix A. Note: as discussed in Sections 1.2 and 2.4.1, all rock grades use metric tonnes, and so, for example, the primary armour shown in Figure 6.5 as 0.5-1 Ton was modelled as 500-1000kg.

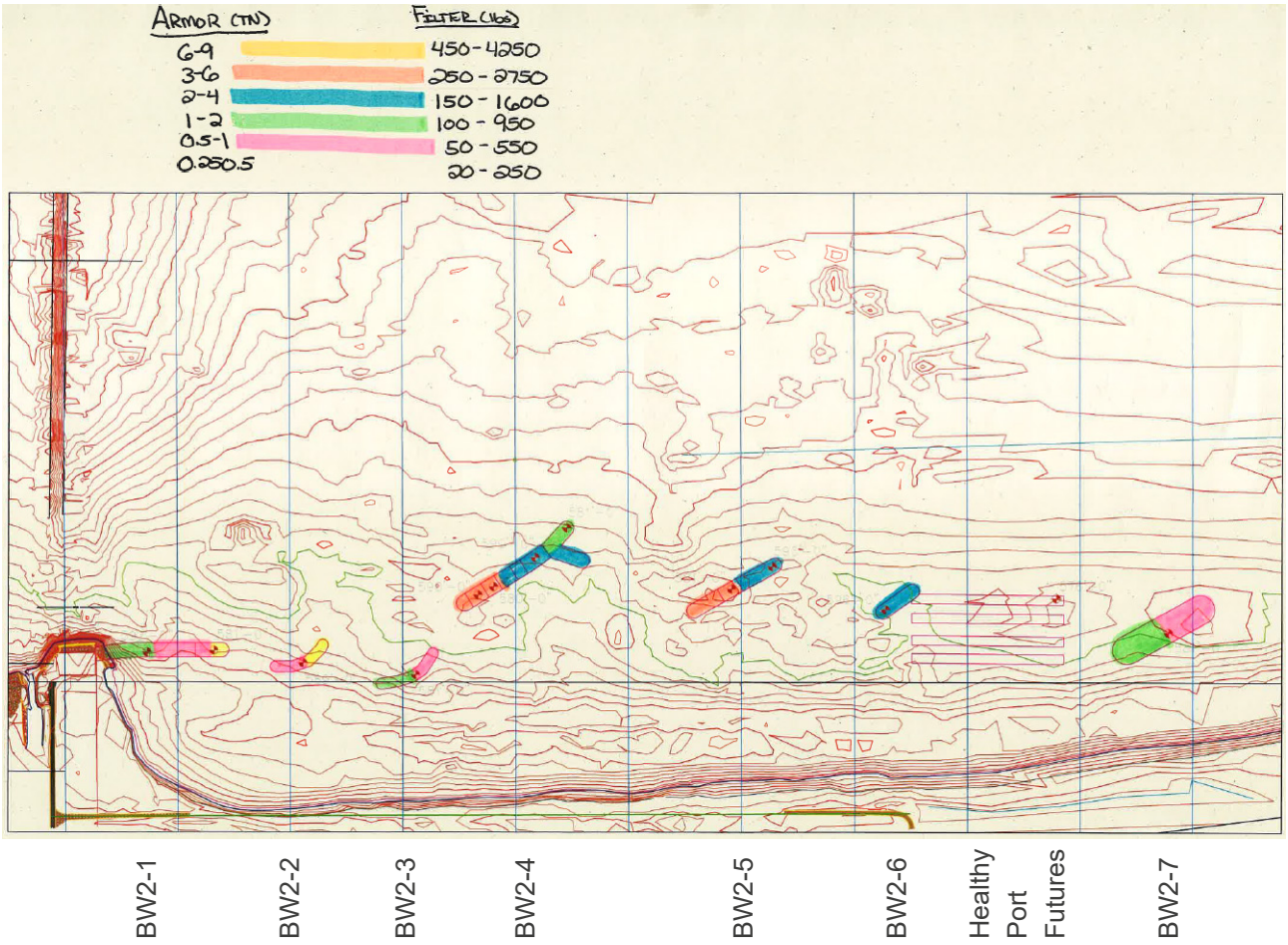


Figure 6.4: Layout drawing of beach control structures for stability tests (armour grades given in key)

*Source: 4335_001.pdf*

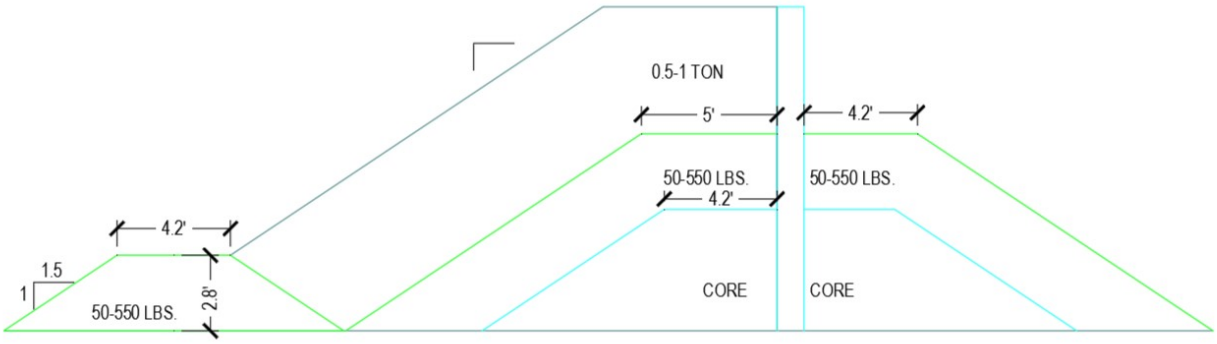


Figure 6.5: BW2-1 trunk cross-section for stability tests

*Source: Area2_Stability Test SECTIONS 10 02 2020.dwg*

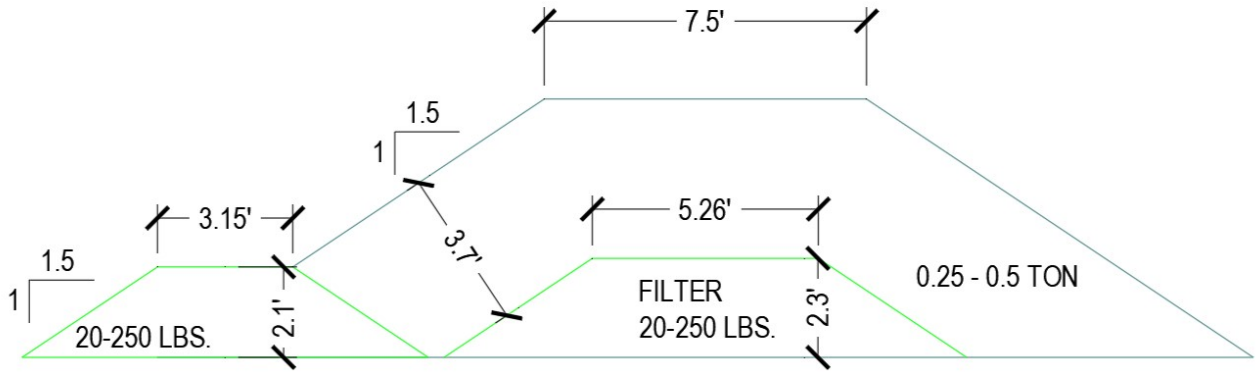


Figure 6.6: BW2-1 seaward end cross-section for stability tests

*Source: Area2_Stability Test SECTIONS 10 02 2020.dwg*

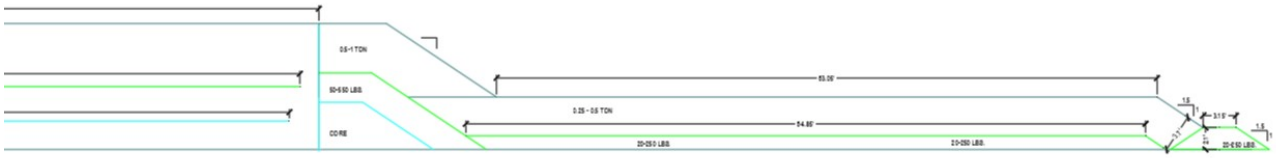

Figure 6.7: BW2-1 long-section for stability tests (seaward end only)

*Source: Area2_Stability Test SECTIONS 10 02 2020.dwg*

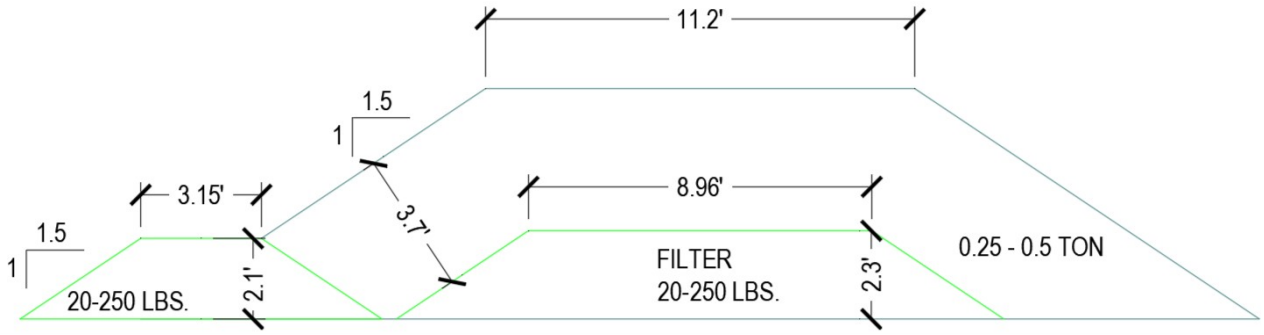


Figure 6.8: BW2-2 trunk cross-section for stability tests

*Source: Area2_Stability Test SECTIONS 10 02 2020.dwg*

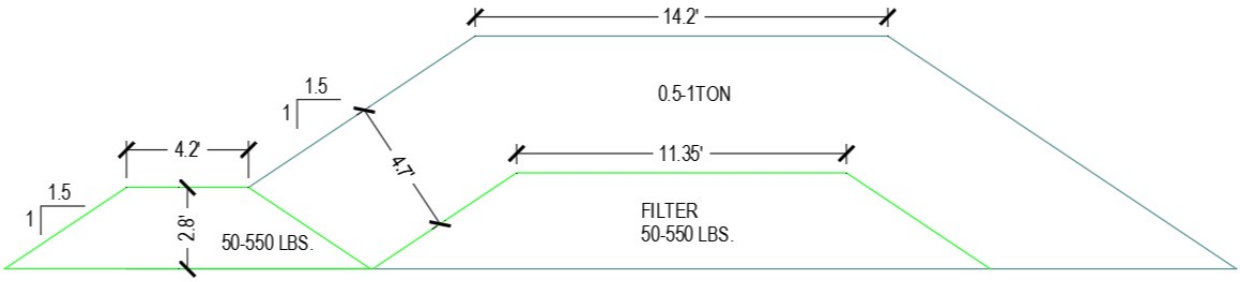


Figure 6.9: BW2-3 trunk cross-section for stability tests

*Source: Area2_Stability Test SECTIONS 10 02 2020.dwg*

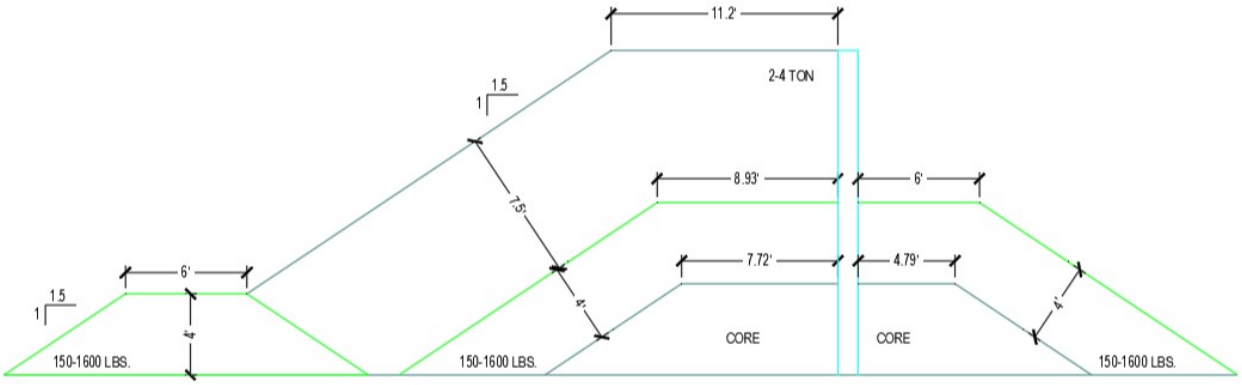


Figure 6.10: BW2-4 trunk cross-section for stability tests

*Source: Area2_Stability Test SECTIONS 10 02 2020.dwg*

Figure 6.11: BW2-4 long-section for stability tests

*Source: Area2_Stability Test SECTIONS 10 02 2020.dwg*

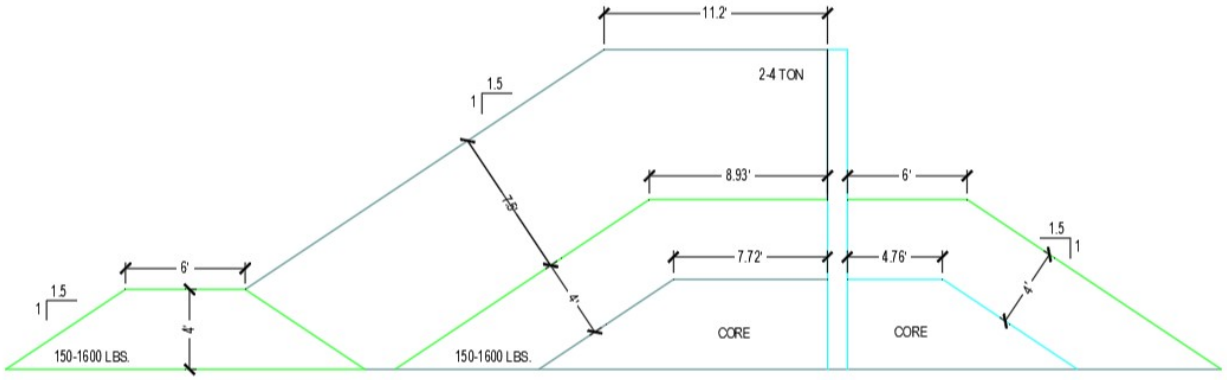


Figure 6.12: BW2-5a trunk cross-section for stability tests

*Source: Area2_Stability Test SECTIONS 10 02 2020.dwg*

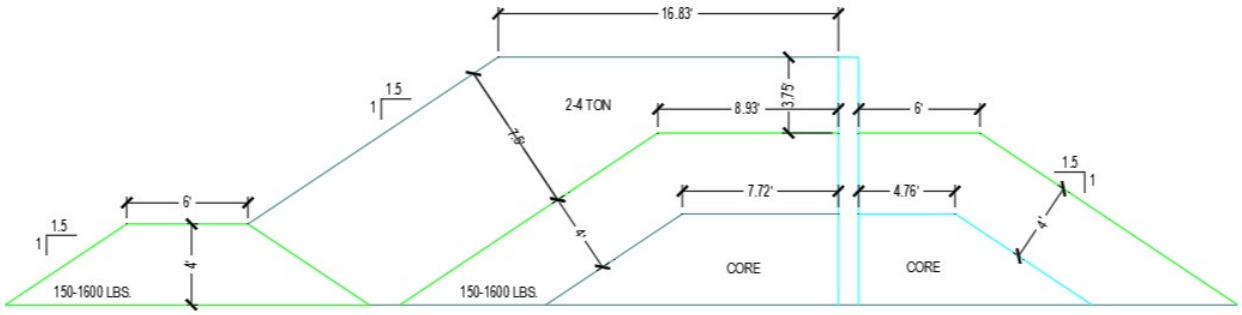


Figure 6.13: BW2-5b trunk cross-section for stability tests

*Source: Area2_Stability Test SECTIONS 10 02 2020.dwg*

Figure 6.14: BW2-5 long-section for stability tests

*Source: Area2_Stability Test SECTIONS 10 02 2020.dwg*

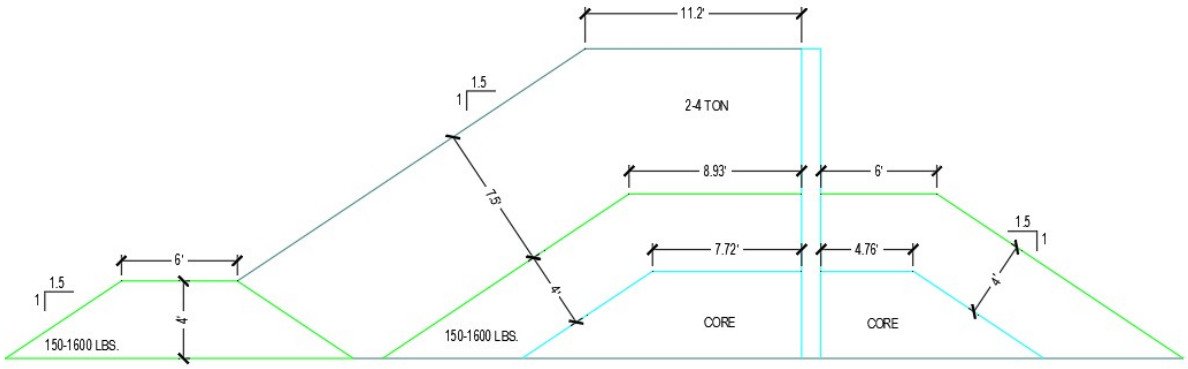


Figure 6.15: BW2-6 trunk cross-section for stability tests

*Source: Area2_Stability Test SECTIONS 10 02 2020.dwg*

Figure 6.16: BW2-6 long-section for stability tests

*Source: Area2_Stability Test SECTIONS 10 02 2020.dwg*

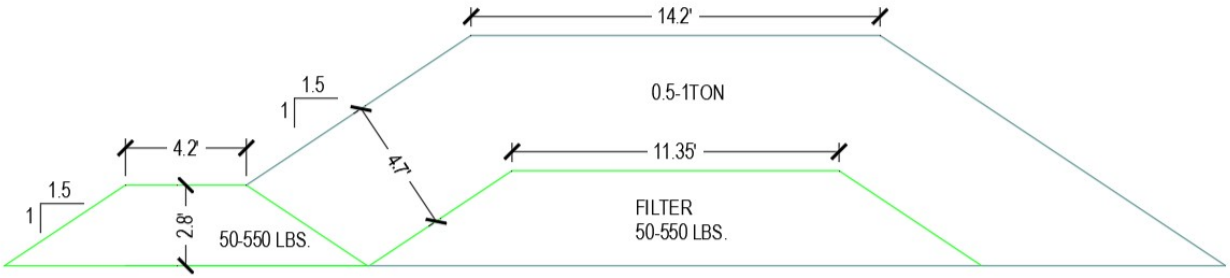


Figure 6.17: BW2-7 trunk cross-section for stability tests

*Source: Area2_Stability Test SECTIONS 10 02 2020.dwg*

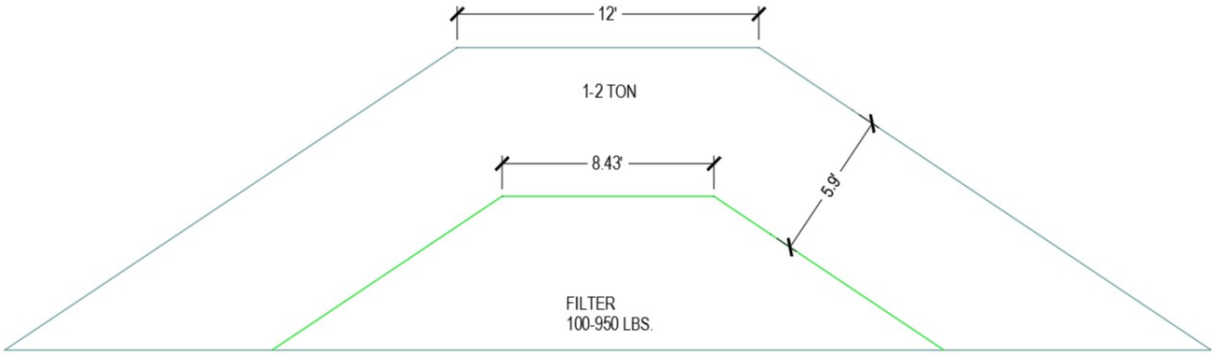


Figure 6.18: Fishtail generic cross-section for stability tests

*Source: Area2_Stability Test SECTIONS 10 02 2020.dwg*

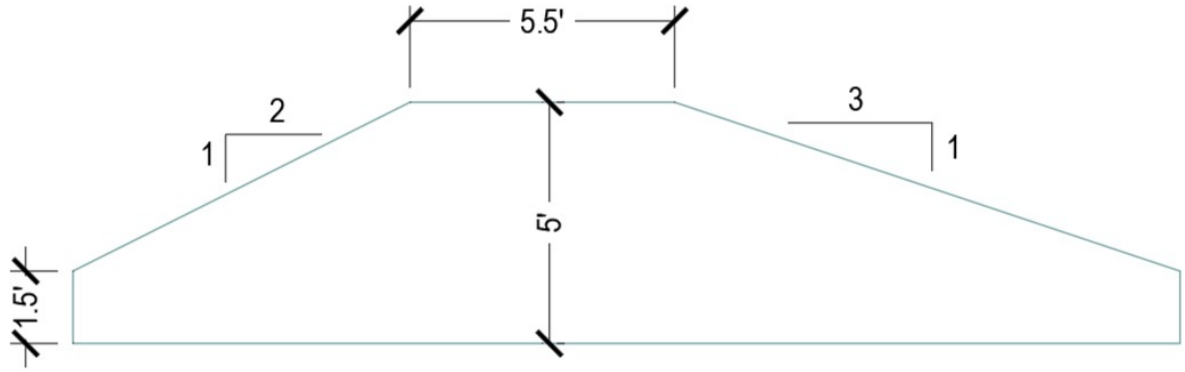


Figure 6.19: Healthy Port Futures fortified ridge (4) trunk cross-section for stability tests

*Source: Area2_Stability Test SECTIONS 10 02 2020.dwg*

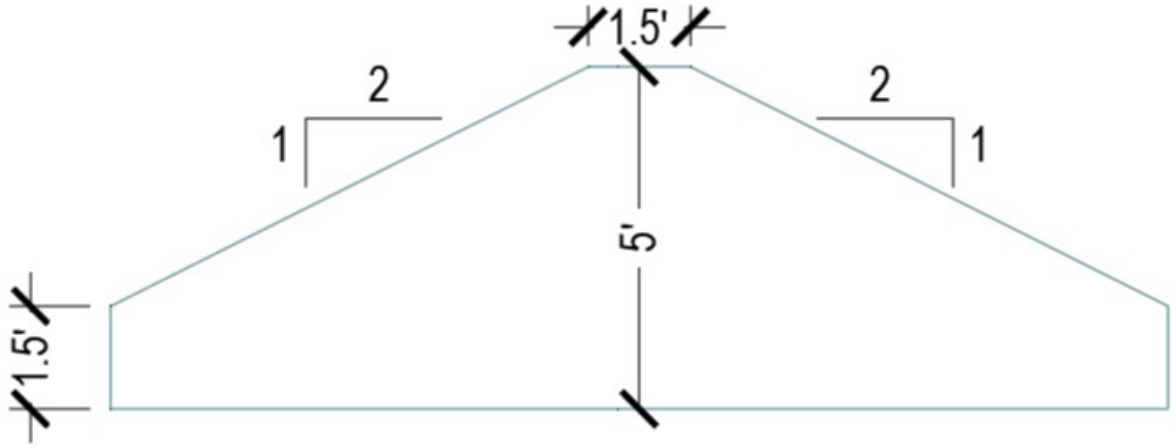


Figure 6.20: Healthy Port Futures basic ridge (5) trunk cross-section for stability tests

*Source: Area2_Stability Test SECTIONS 10 02 2020.dwg*

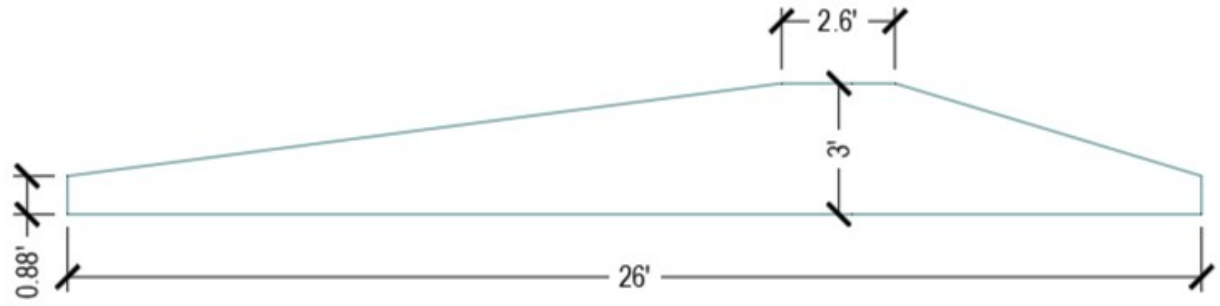


Figure 6.21: Healthy Port Futures habitat ridge, deformed, (6) trunk cross-section for stability tests

*Source: Area2_Stability Test SECTIONS 10 02 2020.dwg*

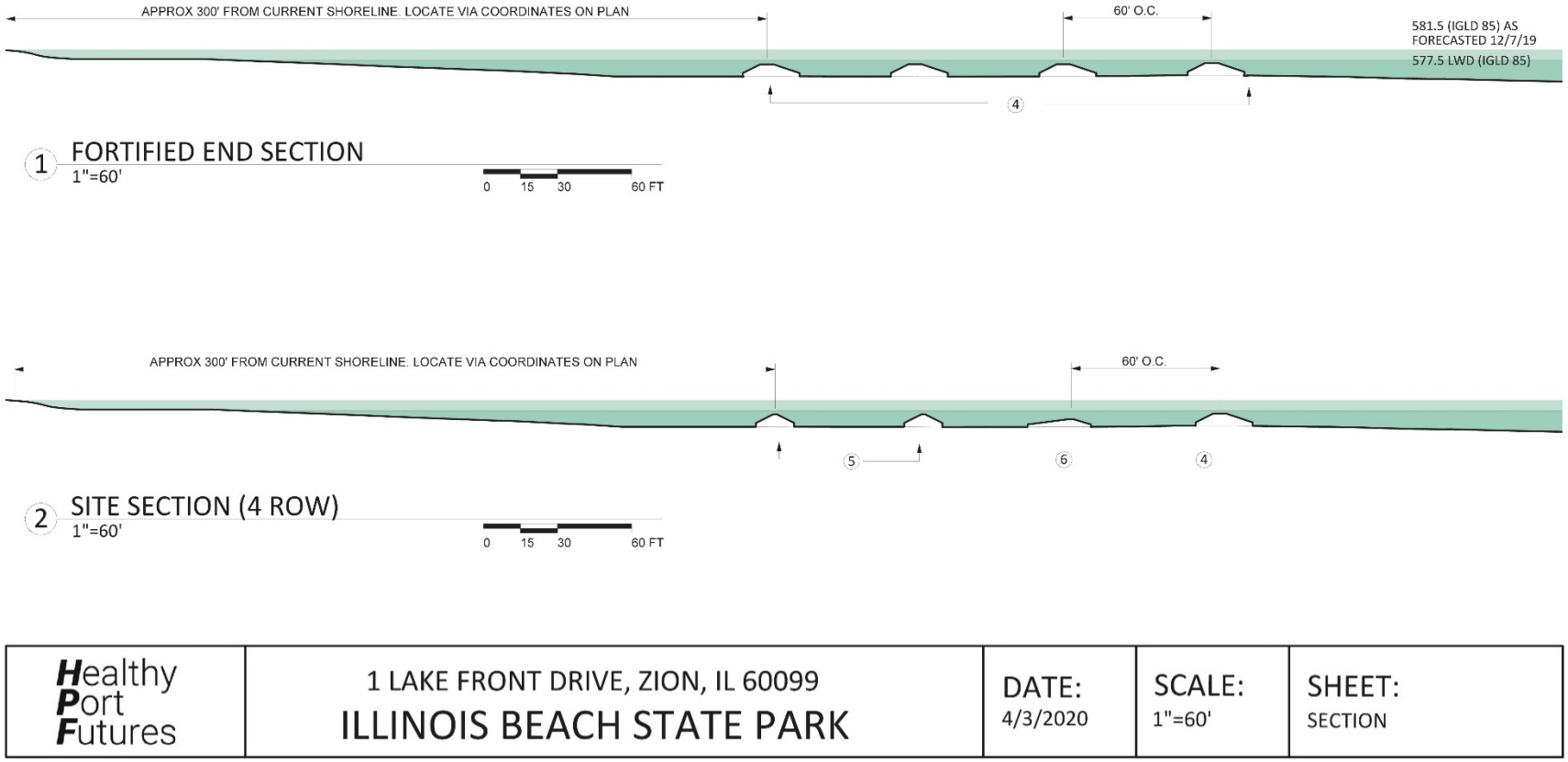


Figure 6.22: Healthy Port Futures layout

*Source: 200403_IBSP_HPF_Plans+Sections.pdf*

## 6.3. Wave calibration results

The results of the wave calibrations are summarised in Table 6.1 for the morphological condition and Table 6.2 for the stability conditions. These were determined at the calibration point (565 ft IGLD 85 contour, see Figure 6.1) using the methods outlined in Section 2.5. The tables present the target wave heights ($H_{m0}$) and periods ($T_p$) at the calibration point, along with the measured $H_{m0}$ (morphological condition) or $H_{1/3}$ (storm conditions) as discussed in Section 2.5. The spectral and Rayleigh plots for the morphological condition are reproduced in Figure 6.23 and Figure 6.24, respectively. The measured morphological condition significant wave height is larger than the target but within the range acceptable for a morphological study where the aim is to mobilise the sediment in a representative manner rather than reproduce a specific wave condition.

The Southeast (130°N) stability test conditions were not calibrated prior to construction of the model structures to accelerate the testing programme. The same paddle settings (gain etc.) were carried over from the Northeast conditions and the conditions were then run for the first time during testing. The wave height reported in Table 6.2 for the Southeast conditions are those measured during testing.

Table 6.1: Results of Area 2 morphological wave calibration at 565 ft IGLD 85 contour

| Wave condition | Target | | Measured |
|---|---|---|---|
| | $H_{m0}$ (ft) | $T_p$ (s) | $H_{m0}$ (ft) |
| Morph_03 | 4.9 | 9.0 | 5.2 |

Table 6.2: Results of Area 2 stability wave calibration at 565 ft IGLD 85 contour

| Wave condition | Direction (°N) | Target | | Measured |
|---|---|---|---|---|
| | | $H_{m0}$ (ft) | $T_p$ (s) | $H_{1/3}$ (ft) |
| WC_EXT_WL_01 | 65 | 11.2 | 10.0 | 11.0 |
| WC_EXT_WL_02 | 65 | 12.1 | 11.5 | 11.3 |
| WC_HIGH_WL | 65 | 11.2 | 11.5 | 10.4 |
| WC_LOW_WL | 65 | 6.6 | 11.5 | 6.3 |
| WC_HIGH_WL_SE | 130 | 6.2 | 7.5 | 5.3* |
| WC_LOW_WL_SE | 130 | 6.2 | 7.5 | 3.7* |

*Note: * Wave height measured during testing.*

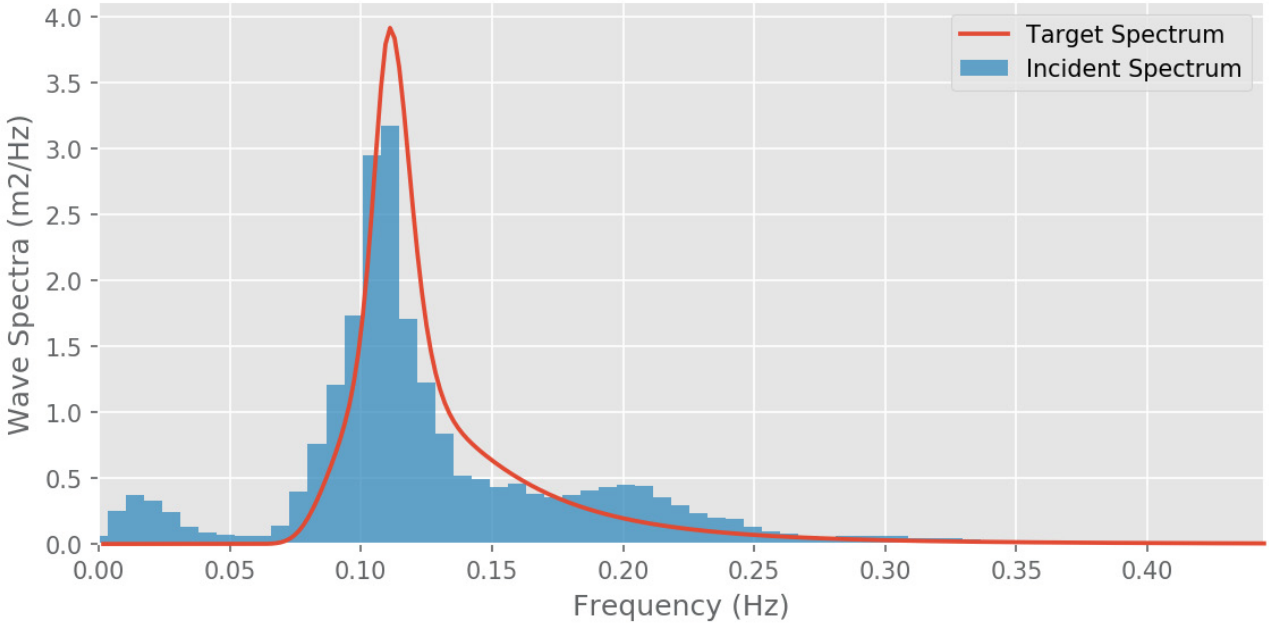


Figure 6.23: Area 2 Morph_03 spectral plot

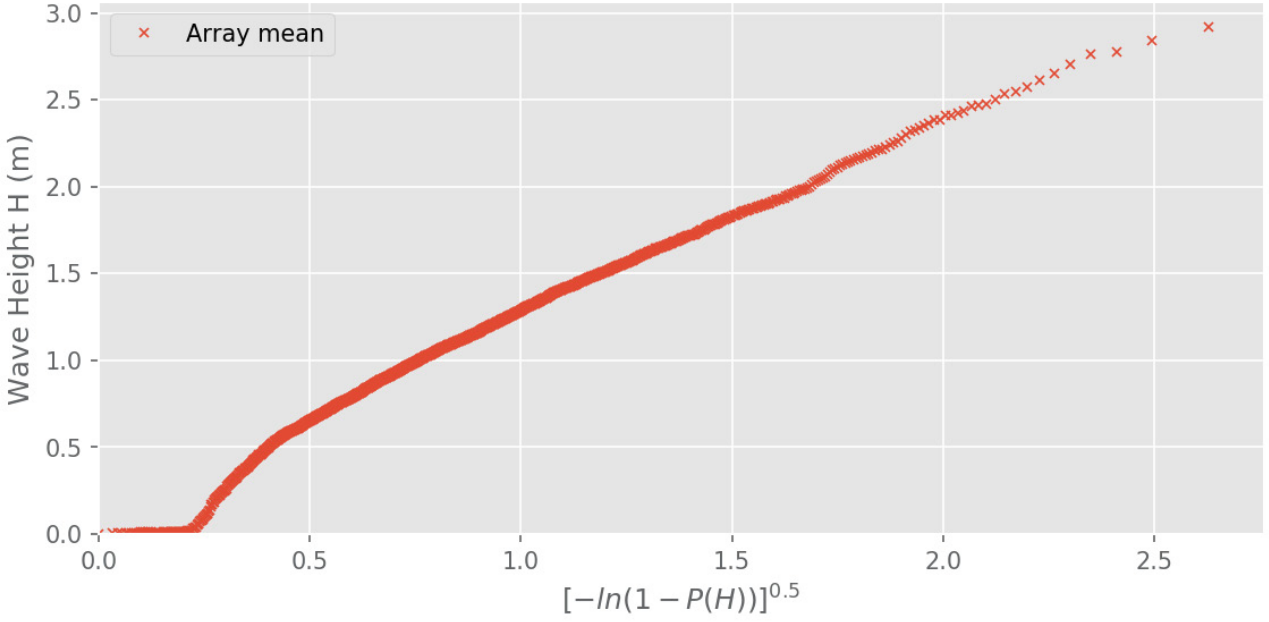


Figure 6.24: Area 2 Morph_03 Rayleigh plot

## 6.4. Morphological tests results – anthracite beach

The starting point for the Area 2 beach control structures optimisation was Configuration 01, and was provided in *2020-0617 Illinois Beach State Park Shoreline Stabilization.pdf* (Figure 6.3). This configuration was tested for 3 hr tests (30 minutes model). The pre and post-test photographs from the 'North' and 'South' time-lapse camera views are shown in Figure 6.26 and Figure 6.27. The layout consisted of two long detached breakwaters with a predominantly Northwest-Southeast alignment, a small third detached breakwater at the Southern end of Area 2 with an almost 90° elbow and a shore connected breakwater at the Northern end of the Area 2 site, adjacent to Kellogg Creek.

The optimisation moved through a further 16 configurations to arrive at the optimised layout, Configuration 17. A complete description of all the configurations leading to the development of the optimised layout are provided in Appendix C.1. Configuration 17 consisted of seven shorter structures, the majority with a Northwest-Southeast alignment, and a series of Healthy Port Futures structures (Figure 6.19 to Figure 6.22) in the Southern third of the site (Figure 6.4). Six of the breakwaters were detached and were a combination of submerged and emergent, with and without fishtails. The original shore connected breakwater was retained with modifications to the seaward extent and roundhead. The pre and post-test photographs from the 'North' and 'South' time-lapse camera views are shown in Figure 6.28 and Figure 6.29. The post-test scan data, including the structure outlines, is shown in Figure 6.25. This configuration was tested for 3 hrs (30 minutes model). All tests were undertaken with the Morph03 wave condition (Table 3.5).

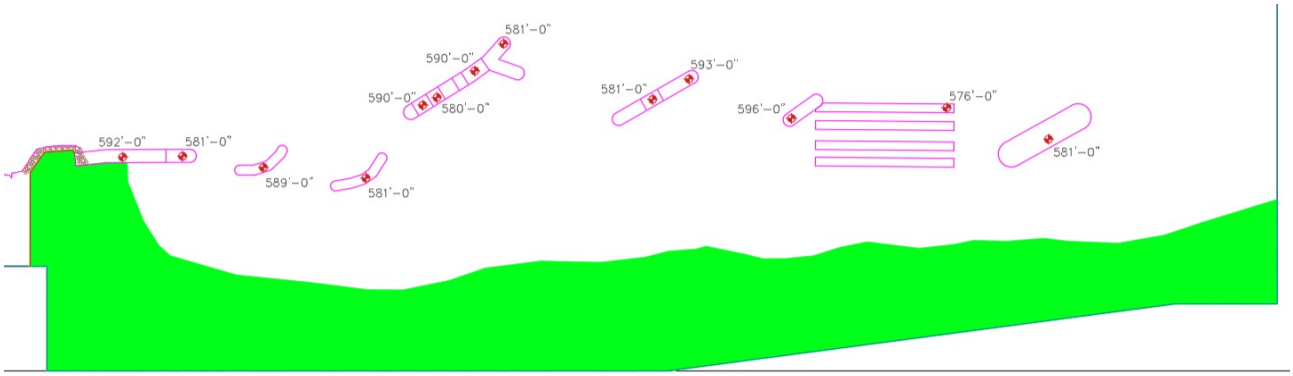


Figure 6.25: Post-test scan data for Area 2 Configuration 17, solid area post-test beach, structures in magenta with spot-heights given for key locations

Figure 6.26: Pre (top) and post-test (bottom) photographs from 'North' view for Area 2 Configuration 01

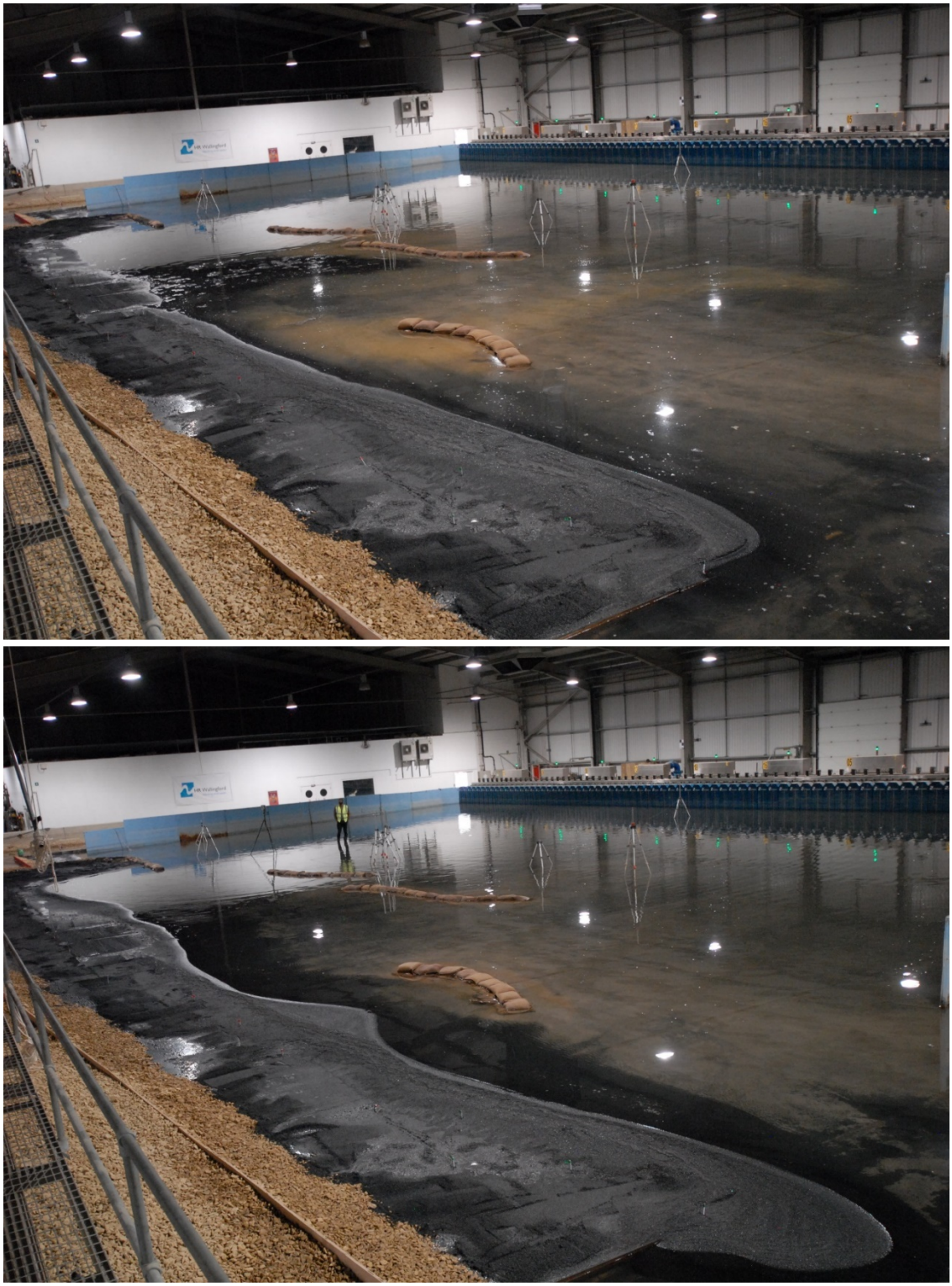

Figure 6.27: Pre (top) and post-test (bottom) photographs from 'South' view for Area 2 Configuration 01

Figure 6.28: Pre (top) and post-test (bottom) photographs from 'North' view for Area 2 Configuration 17

Figure 6.29: Pre (top) and post-test (bottom) photographs from 'South' view for Area 2 Configuration 17

## 6.5. Dye tracing tests

At various points during the anthracite morphological tests the SmithGroup on-site representatives undertook dye tracing tests to observe cross-shore currents and to assess the potential for both high currents and sediment transport around key features (see Section 2.7). The current patterns observed by SmithGroup on-site representatives aided their development and optimisation of the beach control structures. No formal data was recorded by HR Wallingford for these observational dye tracing tests. Dye tracing was used extensively in the development of the control structures around Kellogg Creek, see Section 6.6 below.

## 6.6. Kellogg Creek tests

The Kellogg Creek tests were undertaken by the SmithGroup on-site representative, supported by HR Wallingford staff. The purpose of the tests was to reduce the north-south sediment transport around Kellogg Creek and prevent the creek mouth from silting up and becoming blocked.

To achieve the required wave conditions in the northernmost corner of the physical model, the wave paddles were reconfigured so that only the two northernmost banks of paddles were generating the full wave amplitude, with this progressively ramping down until the last four southernmost banks were not generating any waves. The waves were generated perpendicular to the wave paddles (rather than with the 65°N direction used for the other morphological tests) and the wave guides were used to steer and reflect the waves to give the required angle and longshore current. The wave condition used was based on the Morph_03 condition (Table 3.5) used for the morphological tests (Section 6.4).

The Kellogg Creek tests were split into two phases. Initially different concepts were explored using dye tracing to estimate the likely sediment transport, followed by a second phase of confirmatory tests tracking the anthracite movement.

### 6.6.1. Phase 1 dye tracing optimisation tests

Six different configurations were investigated with one (Configuration 4) tested twice with different levels of sediment build-up to the north of Kellogg Creek. The configurations are shown in Figure 6.30 to Figure 6.36.

Figure 6.30: Kellogg Creek Configuration 1 – showing initial dye placement

Figure 6.31: Kellogg Creek Configuration 2 – showing initial dye placement

Figure 6.32: Kellogg Creek Configuration 3 – showing initial dye placement

Figure 6.33: Kellogg Creek Configuration 4 – showing initial dye placement

Figure 6.34: Kellogg Creek Configuration 4 with additional beach material – showing initial dye placement

Figure 6.35: Kellogg Creek Configuration 5 – showing initial dye placement

Figure 6.36: Kellogg Creek Configuration 6 – showing initial dye placement

### 6.6.2. Phase 2 morphological confirmation tests

Configuration 4 with the additional beach material (Figure 6.34) was taken forward for the confirmatory morphological tests. This configuration was tested for 17 hrs 45 mins (3 hours model). The pre and post-test photographs are shown in Figure 6.37 and Figure 6.38.

Figure 6.37: Kellogg Creek morphological test pre-test photograph

Figure 6.38: Kellogg Creek morphological test post-test photograph

## 6.7. Storm response tests results – sand beach

Following the completion of the Kellogg Creek tests, the anthracite beach was replaced with a sand beach to allow the beach's response to storm conditions to be checked during the stability tests. The test order, including when scans were taken and if the beach was re-profiled is provided in Table 6.3.

Table 6.3: Area 2 sand beach Test Part and scan record

| Activity | Type | Scan |
|---|---|---|
| Initial placement of sand beach | Setup | No |
| Morphological condition from NE used to 'settle' beach – Morph_03 | Setup | Pre-test |
| Stability Test Part 01 - WC_LOW_WL_SE | Test Part | No |
| Stability Test Part 02 - WC_HIGH_WL_SE | Test Part | Post-test |
| Stability Test Part 03 - WC_LOW_WL | Test Part | No |
| Stability Test Part 04 - WC_HIGH_WL | Test Part | Post-test |
| Stability Test Part 05 - WC_EXT_WL_01 | Test Part | No |
| Stability Test Part 06 - WC_EXT_WL_02 | Test Part | Post-test |

### 6.7.1. Storm response from SE conditions

The storm response of the sand beach after both the Southeast storm conditions is shown in Figure 6.39. There is little change in the plan shape of the beach at the SWL (582.2 ft IGLD 85) after the smaller (relative to the Northeast conditions) Southeast storm tests.

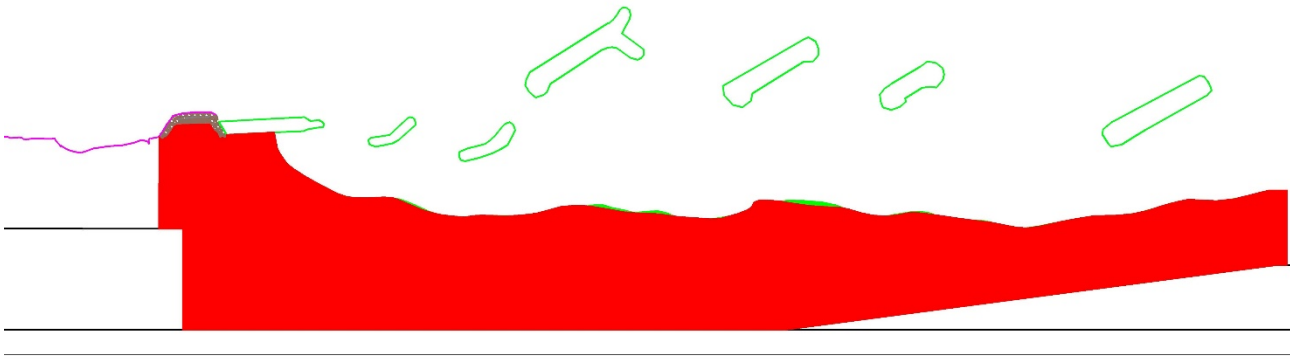

Figure 6.39: Area 2 stability post Test Part 02 beach scan data, SWL 582.2 ft IGLD 85 (pre-test scan in green, post-test scan in red, structure outline in green)

### 6.7.2. Storm response from NE conditions

The storm response of the sand beach to the four Northeast storm conditions is shown in Figure 6.40 and Figure 6.41. Figure 6.40 compares the plan shape of the beach post the Southeast tests with that following both Test Part 03 and 04 (WC_LOW_WL and WC_HIGH_WL). Figure 6.41 compares the plan shape of the beach following the first two Northeast tests with those following all Test Parts. The beach recedes (reduces in width) throughout the progressive storm tests, each storm eroding the beach further at the particular SWL of each Test Part. Following the final Test Part (06), there is still a wide beach above the SWL.

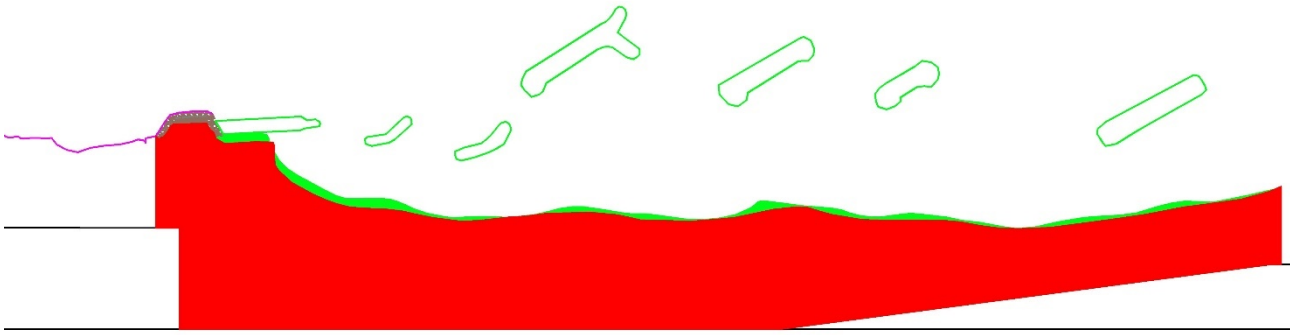

Figure 6.40: Area 2 stability post Test Part 04 beach scan data, SWL 583.3 ft IGLD 85 (pre-test scan in green, post-test scan in red, structure outline in green)

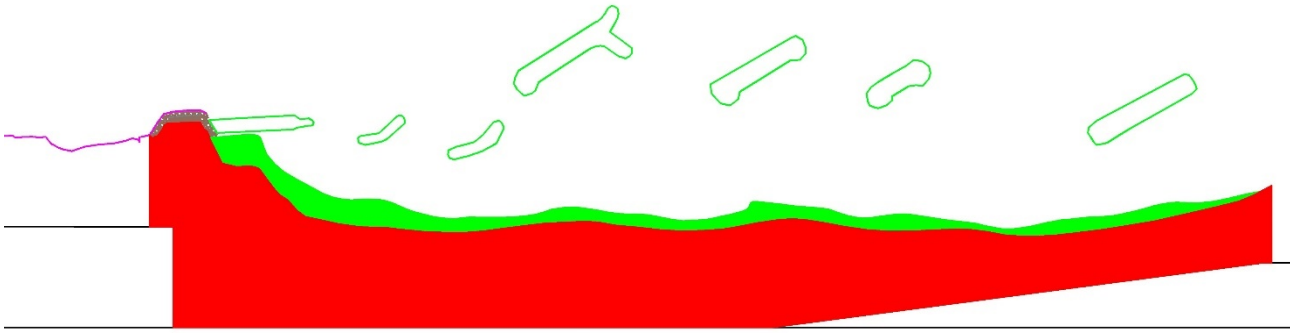

Figure 6.41: Area 2 stability post Test Part 06 beach scan data, SWL 585.2 ft IGLD 85 (pre-test scan in green, post-test scan in red, structure outline in green)

## 6.8. Stability test results

The stability tests focussed on all beach control breakwater structures BW2-1 to BW2-7 (Section 6.2.2). The stability of the Healthy Port Futures structures was not assessed as part of this study. Photographs were taken before and after each Test Part and are reproduced in Appendix C.2. Each breakwater of interest has been divided into a series of panels such as trunk, roundhead and fishtail, seaside and leeside and where a section is particularly long it has been divided into North and South. The panels are shown in Figure 6.42.

The cumulative number of rocks extracted and the calculated $S_d$ damage parameter for each structure are presented in Table 6.4 to Table 6.17. For each breakwater there are two tables, the first with the cumulative number of rocks extracted from the armour layer and the second with the calculated $S_d$ damage parameter. The $S_d$ parameter has been calculated using the method described in Section 2.8.

For the majority of structures the damage level was low, with few rocks extracted. One area of high damage, $S_d > 8$ (Table 2.3), was the leeside armour of BW2-5, Panels 28 and 29 (Appendix C.2.5). One other Structures showed some damage, $2 < S_d < 8$ (Table 2.3), which was the Southern roundhead of BW2-2, Panel 8 (Appendix C.2.2).

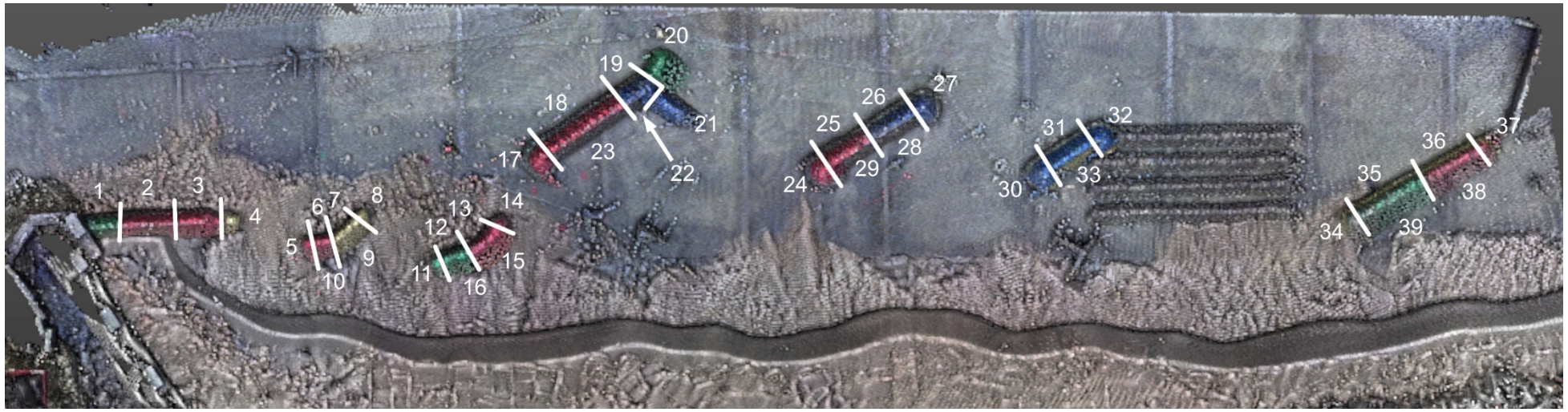


Figure 6.42: Area 2 stability analysis panels

Table 6.4: BW2-1 cumulative number of rocks displaced

| Test Part | Wave condition | Return period | Wave direction (°N) | Trunk North 1-2 t (panel 1) | Trunk North 0.5-1 t (panel 2) | Trunk South (panel 3) | Roundhead (panel 4) |
|---|---|---|---|---|---|---|---|
| 1 | WC_LOW_WL | 1:100 | 130 | 0 | 0 | 1 | 0 |
| 2 | WC_HIGH_WL | 1:100 | 130 | 0 | 0 | 6 | 2 |
| 3 | WC_LOW_WL | 1:100 | 65 | 0 | 0 | 6 | 2 |
| 4 | WC_HIGH_WL | 1:100 | 65 | 3 | 7 | 18 | 2 |
| 5 | WC_EXT_WL_01 | 1:10 | 65 | 4 | 10 | 24 | 4 |
| 6 | WC_EXT_WL_02 | 1:100 | 65 | 4 | 14 | 51 | 20 |

Table 6.5: BW2-1 damage parameter $S_d$

| Test Part | Wave condition | Return period | Wave direction (°N) | Trunk North 1-2 t (panel 1) | Trunk North 0.5-1 t (panel 2) | Trunk South (panel 3) | Roundhead (panel 4) |
|---|---|---|---|---|---|---|---|
| 1 | WC_LOW_WL | 1:100 | 130 | 0.0 | 0.0 | 0.0 | 0.0 |
| 2 | WC_HIGH_WL | 1:100 | 130 | 0.0 | 0.0 | 0.1 | 0.1 |
| 3 | WC_LOW_WL | 1:100 | 65 | 0.0 | 0.0 | 0.1 | 0.1 |
| 4 | WC_HIGH_WL | 1:100 | 65 | 0.2 | 0.2 | 0.4 | 0.1 |
| 5 | WC_EXT_WL_01 | 1:10 | 65 | 0.3 | 0.2 | 0.6 | 0.2 |
| 6 | WC_EXT_WL_02 | 1:100 | 65 | 0.3 | 0.3 | 1.2 | 0.9 |

Table 6.6: BW2-2 cumulative number of rocks displaced

| Test Part | Wave condition | Return period | Wave direction (°N) | Roundhead South (panel 8) | Trunk seaside South (panel 7) | Trunk seaside North (panel 6) | Roundhead North (panel 5) | Trunk leeside South (panel 9) | Trunk seaside North (panel 10) |
|---|---|---|---|---|---|---|---|---|---|
| 1 | WC_LOW_WL | 1:100 | 130 | 10 | 12 | 1 | 0 | 1 | 0 |
| 2 | WC_HIGH_WL | 1:100 | 130 | 11 | 25 | 1 | 0 | 3 | 1 |
| 3 | WC_LOW_WL | 1:100 | 65 | 31 | 25 | 1 | 1 | 3 | 1 |
| 4 | WC_HIGH_WL | 1:100 | 65 | 36 | 29 | 5 | 5 | 15 | 3 |
| 5 | WC_EXT_WL_01 | 1:10 | 65 | 41 | 29 | 5 | 5 | 15 | 3 |
| 6 | WC_EXT_WL_02 | 1:100 | 65 | 41 | 29 | 5 | 5 | 15 | 3 |

Table 6.7: BW2-2 damage parameter $S_d$

| Test Part | Wave condition | Return period | Wave direction (°N) | Roundhead South (panel 8) | Trunk seaside South (panel 7) | Trunk seaside North (panel 6) | Roundhead North (panel 5) | Trunk leeside South (panel 9) | Trunk seaside North (panel 10) |
|---|---|---|---|---|---|---|---|---|---|
| 1 | WC_LOW_WL | 1:100 | 130 | 0.5 | 0.3 | 0.0 | 0.0 | 0.0 | 0.0 |
| 2 | WC_HIGH_WL | 1:100 | 130 | 0.6 | 0.7 | 0.0 | 0.0 | 0.1 | 0.0 |
| 3 | WC_LOW_WL | 1:100 | 65 | 1.6 | 0.7 | 0.0 | 0.1 | 0.1 | 0.0 |
| 4 | WC_HIGH_WL | 1:100 | 65 | 1.9 | 0.8 | 0.2 | 0.3 | 0.4 | 0.1 |
| 5 | WC_EXT_WL_01 | 1:10 | 65 | 2.1 | 0.8 | 0.2 | 0.3 | 0.4 | 0.1 |
| 6 | WC_EXT_WL_02 | 1:100 | 65 | 2.1 | 0.8 | 0.2 | 0.3 | 0.4 | 0.1 |

Table 6.8: BW2-3 cumulative number of rocks displaced

| Test Part | Wave condition | Return period | Wave direction (°N) | Trunk seaside South (panel 13) | Trunk seaside North (panel 12) | Roundhead North (panel 11) | Roundhead South (panel 14) | Trunk leeside South (panel 15) | Trunk seaside North (panel 16) |
|---|---|---|---|---|---|---|---|---|---|
| 1 | WC_LOW_WL | 1:100 | 130 | 0 | 0 | 0 | 0 | 0 | 0 |
| 2 | WC_HIGH_WL | 1:100 | 130 | 0 | 0 | 0 | 0 | 0 | 0 |
| 3 | WC_LOW_WL | 1:100 | 65 | 0 | 0 | 0 | 1 | 0 | 0 |
| 4 | WC_HIGH_WL | 1:100 | 65 | 3 | 0 | 0 | 1 | 1 | 1 |
| 5 | WC_EXT_WL_01 | 1:10 | 65 | 3 | 0 | 0 | 2 | 1 | 1 |
| 6 | WC_EXT_WL_02 | 1:100 | 65 | 5 | 0 | 0 | 2 | 1 | 1 |

Table 6.9: BW2-3 damage parameter $S_d$

| Test Part | Wave condition | Return period | Wave direction (°N) | Trunk seaside South (panel 13) | Trunk seaside North (panel 12) | Roundhead North (panel 11) | Roundhead South (panel 14) | Trunk leeside South (panel 15) | Trunk seaside North (panel 16) |
|---|---|---|---|---|---|---|---|---|---|
| 1 | WC_LOW_WL | 1:100 | 130 | 0.0 | 0.0 | 0.0 | 0.0 | 0.0 | 0.0 |
| 2 | WC_HIGH_WL | 1:100 | 130 | 0.0 | 0.0 | 0.0 | 0.0 | 0.0 | 0.0 |
| 3 | WC_LOW_WL | 1:100 | 65 | 0.0 | 0.0 | 0.0 | 0.1 | 0.0 | 0.0 |
| 4 | WC_HIGH_WL | 1:100 | 65 | 0.1 | 0.0 | 0.0 | 0.1 | 0.0 | 0.0 |
| 5 | WC_EXT_WL_01 | 1:10 | 65 | 0.1 | 0.0 | 0.0 | 0.1 | 0.0 | 0.0 |
| 6 | WC_EXT_WL_02 | 1:100 | 65 | 0.2 | 0.0 | 0.0 | 0.1 | 0.0 | 0.0 |

Table 6.10: BW2-4 cumulative number of rocks displaced

| Test Part | Wave condition | Return period | Wave direction (°N) | Trunk leeside South (panel 22) | Fishtail West (panel 21) | Fishtail East (panel 20) | Trunk seaside South (panel 19) | Trunk seaside North (panel 18) | Roundhead North (panel 17) | Trunk leeside North (panel 23) |
|---|---|---|---|---|---|---|---|---|---|---|
| 1 | WC_LOW_WL | 1:100 | 130 | 0 | 0 | 2 | 0 | 0 | 0 | 0 |
| 2 | WC_HIGH_WL | 1:100 | 130 | 0 | 0 | 2 | 0 | 0 | 0 | 0 |
| 3 | WC_LOW_WL | 1:100 | 65 | 0 | 0 | 5 | 1 | 0 | 0 | 0 |
| 4 | WC_HIGH_WL | 1:100 | 65 | 0 | 1 | 12 | 7 | 6 | 4 | 40 |
| 5 | WC_EXT_WL_01 | 1:10 | 65 | 7 | 1 | 12 | 7 | 6 | 4 | 40 |
| 6 | WC_EXT_WL_02 | 1:100 | 65 | 9 | 3 | 14 | 8 | 7 | 4 | 46 |

Table 6.11: BW2-4 damage parameter $S_d$

| Test Part | Wave condition | Return period | Wave direction (°N) | Trunk leeside South (panel 22) | Fishtail West (panel 21) | Fishtail East (panel 20) | Trunk seaside South (panel 19) | Trunk seaside North (panel 18) | Roundhead North (panel 17) | Trunk leeside North (panel 23) |
|---|---|---|---|---|---|---|---|---|---|---|
| 1 | WC_LOW_WL | 1:100 | 130 | 0.0 | 0.0 | 0.1 | 0.0 | 0.0 | 0.0 | 0.0 |
| 2 | WC_HIGH_WL | 1:100 | 130 | 0.0 | 0.0 | 0.1 | 0.0 | 0.0 | 0.0 | 0.0 |
| 3 | WC_LOW_WL | 1:100 | 65 | 0.0 | 0.0 | 0.2 | 0.0 | 0.0 | 0.0 | 0.0 |
| 4 | WC_HIGH_WL | 1:100 | 65 | 0.0 | 0.0 | 0.4 | 0.3 | 0.1 | 0.2 | 0.8 |
| 5 | WC_EXT_WL_01 | 1:10 | 65 | 0.1 | 0.0 | 0.4 | 0.3 | 0.1 | 0.2 | 0.8 |
| 6 | WC_EXT_WL_02 | 1:100 | 65 | 0.2 | 0.1 | 0.5 | 0.3 | 0.2 | 0.2 | 0.9 |

Table 6.12: BW2-5 cumulative number of rocks displaced

| Test Part | Wave condition | Return period | Wave direction (°N) | Roundhead South (panel 27) | Trunk seaside South (panel 26) | Trunk seaside North (panel 25) | Roundhead North (panel 24) | Trunk leeside North (panel 29) | Trunk leeside South (panel 28) |
|---|---|---|---|---|---|---|---|---|---|
| 1 | WC_LOW_WL | 1:100 | 130 | 1 | 1 | 0 | 0 | 0 | 0 |
| 2 | WC_HIGH_WL | 1:100 | 130 | 1 | 1 | 0 | 0 | 0 | 0 |
| 3 | WC_LOW_WL | 1:100 | 65 | 1 | 1 | 0 | 0 | 0 | 0 |
| 4 | WC_HIGH_WL | 1:100 | 65 | 7 | 16 | 6 | 5 | 232 | 437 |
| 5 | WC_EXT_WL_01 | 1:10 | 65 | 8 | 16 | 8 | 6 | 270 | 510 |
| 6 | WC_EXT_WL_02 | 1:100 | 65 | 8 | 20 | 8 | 7 | 309 | 728 |

Table 6.13: BW2-5 damage parameter $S_d$

| Test Part | Wave condition | Return period | Wave direction (°N) | Roundhead South (panel 27) | Trunk seaside South (panel 26) | Trunk seaside North (panel 25) | Roundhead North (panel 24) | Trunk leeside North (panel 29) | Trunk leeside South (panel 28) |
|---|---|---|---|---|---|---|---|---|---|
| 1 | WC_LOW_WL | 1:100 | 130 | 0.1 | 0.0 | 0.0 | 0.0 | 0.0 | 0.0 |
| 2 | WC_HIGH_WL | 1:100 | 130 | 0.1 | 0.0 | 0.0 | 0.0 | 0.0 | 0.0 |
| 3 | WC_LOW_WL | 1:100 | 65 | 0.1 | 0.0 | 0.0 | 0.0 | 0.0 | 0.0 |
| 4 | WC_HIGH_WL | 1:100 | 65 | 0.4 | 0.5 | 0.3 | 0.3 | 6.7 | 13 |
| 5 | WC_EXT_WL_01 | 1:10 | 65 | 0.4 | 0.5 | 0.3 | 0.4 | 7.9 | 15 |
| 6 | WC_EXT_WL_02 | 1:100 | 65 | 0.4 | 0.6 | 0.3 | 0.4 | 9.0 | 21 |

Table 6.14: BW2-6 cumulative number of rocks displaced

| Test Part | Wave condition | Return period | Wave direction (°N) | Roundhead South (panel 32) | Trunk seaside (panel 31) | Roundhead North (panel 30) | Trunk leeside (panel 33) |
|---|---|---|---|---|---|---|---|
| 1 | WC_LOW_WL | 1:100 | 130 | 1 | 0 | 0 | 0 |
| 2 | WC_HIGH_WL | 1:100 | 130 | 1 | 0 | 0 | 0 |
| 3 | WC_LOW_WL | 1:100 | 65 | 1 | 0 | 0 | 0 |
| 4 | WC_HIGH_WL | 1:100 | 65 | 16 | 5 | 13 | 32 |
| 5 | WC_EXT_WL_01 | 1:10 | 65 | 18 | 6 | 14 | 35 |
| 6 | WC_EXT_WL_02 | 1:100 | 65 | 20 | 6 | 15 | 37 |

Table 6.15: BW2-6 damage parameter $S_d$

| Test Part | Wave condition | Return period | Wave direction (°N) | Roundhead South (panel 32) | Trunk seaside (panel 31) | Roundhead North (panel 30) | Trunk leeside (panel 33) |
|---|---|---|---|---|---|---|---|
| 1 | WC_LOW_WL | 1:100 | 130 | 0.1 | 0.0 | 0.0 | 0.0 |
| 2 | WC_HIGH_WL | 1:100 | 130 | 0.1 | 0.0 | 0.0 | 0.0 |
| 3 | WC_LOW_WL | 1:100 | 65 | 0.1 | 0.0 | 0.0 | 0.0 |
| 4 | WC_HIGH_WL | 1:100 | 65 | 0.8 | 0.2 | 0.7 | 0.8 |
| 5 | WC_EXT_WL_01 | 1:10 | 65 | 0.9 | 0.2 | 0.7 | 0.9 |
| 6 | WC_EXT_WL_02 | 1:100 | 65 | 1.0 | 0.2 | 0.8 | 0.9 |

Table 6.16: BW2-7 cumulative number of rocks displaced

| Test Part | Wave condition | Return period | Wave direction (°N) | Trunk leeside South (panel 38) | Roundhead South (panel 37) | Trunk seaside South (panel 36) | Trunk seaside North (panel 35) | Roundhead North (panel 34) | Trunk leeside North (panel 39) |
|---|---|---|---|---|---|---|---|---|---|
| 1 | WC_LOW_WL | 1:100 | 130 | 0 | 0 | 0 | 0 | 0 | 0 |
| 2 | WC_HIGH_WL | 1:100 | 130 | 0 | 0 | 0 | 0 | 0 | 0 |
| 3 | WC_LOW_WL | 1:100 | 65 | 0 | 3 | 4 | 0 | 0 | 0 |
| 4 | WC_HIGH_WL | 1:100 | 65 | 0 | 3 | 8 | 0 | 0 | 0 |
| 5 | WC_EXT_WL_01 | 1:10 | 65 | 0 | 3 | 8 | 0 | 0 | 0 |
| 6 | WC_EXT_WL_02 | 1:100 | 65 | 1 | 3 | 8 | 0 | 0 | 0 |

Table 6.17: BW2-7 damage parameter $S_d$

| Test Part | Wave condition | Return period | Wave direction (°N) | Trunk leeside South (panel 38) | Roundhead South (panel 37) | Trunk seaside South (panel 36) | Trunk seaside North (panel 35) | Roundhead North (panel 34) | Trunk leeside North (panel 39) |
|---|---|---|---|---|---|---|---|---|---|
| 1 | WC_LOW_WL | 1:100 | 130 | 0.0 | 0.0 | 0.0 | 0.0 | 0.0 | 0.0 |
| 2 | WC_HIGH_WL | 1:100 | 130 | 0.0 | 0.0 | 0.0 | 0.0 | 0.0 | 0.0 |
| 3 | WC_LOW_WL | 1:100 | 65 | 0.0 | 0.2 | 0.1 | 0.0 | 0.0 | 0.0 |
| 4 | WC_HIGH_WL | 1:100 | 65 | 0.0 | 0.2 | 0.1 | 0.0 | 0.0 | 0.0 |
| 5 | WC_EXT_WL_01 | 1:10 | 65 | 0.0 | 0.2 | 0.1 | 0.0 | 0.0 | 0.0 |
| 6 | WC_EXT_WL_02 | 1:100 | 65 | 0.0 | 0.2 | 0.1 | 0.0 | 0.0 | 0.0 |

## 6.9. Summary

A total of seven beach control structures of various cross-sections and armourstone grades were utilised for the final configuration. In Section 6.4, it was demonstrated that a stable beach could be maintained with a reduced north-south sediment drift using this configuration. The beaches remained static during the stability tests (Section 6.7), with a wide crest at the beach maintained throughout.

The SmithGroup on-site representatives utilised the Area 2 model to optimise an additional beach control structure to the North of Kellogg Creek which further reduced north-south sediment drift and allowed the creek mouth to remain open (Section 6.6).

Of the beach control structures resistance to wave action during the stability test programme, it is possible to make the following observations:

1. All structures, with the exception of the leeside trunk armour of breakwater BW2-5 (Panels 28 and 29), were substantially intact at the end of the testing campaign;
2. All structures were tested for a minimum of 30 hours of storm conditions, and it should be noted that this exceeds any reasonable exposure that might be anticipated during the design life;
3. Where a piled central breakwater section was included (specifically breakwaters BW2-4 to BW2-6), then the potential for crest armour damage was reduced with these configurations.

# 7. Area 3 – Swimming Beach

The Area 3 model examined the Swimming Beach area of Lake Michigan, situated some distance to the South of Area 2 (Section 6). In the North of this area is the swimming beach and to the South is a hotel and wedding venue complex currently protected by hard engineered structures. To the area immediately south of the modelled area, there is significant and ongoing beach erosion with a net north to south sediment drift driven predominantly by North East waves, as in Area 1 and 2. The first phase of the model included a series of shore detached groynes to encourage the development of salients and tombolos to arrest or reduce the north-south sediment drift. As with Area 1 and 2, this was done using sandbags to act as proxies for armourstone breakwaters and allowed multiple configurations to be examined using a lightweight modelling sediment. This was tested with a generic Morphological wave condition that was able to mobilise the modelling sediment without affecting the beach response due to wave breaking significantly.

As for both Areas 1 and 2, once a stable configuration had been identified, then the lightweight modelling sediment was replaced with a fine grained modelling sand with the correct density. The final configuration of proxy armourstone structures was replaced with correctly sized and scaled model rock structures, and the whole was then tested with a sequence of six wave and water level conditions from both the North East and South East wave directions. This section describes the model set up, the waves and wave calibrations, the morphological beach testing and the structural stability for Area 3. Some key observations are given in Section 7.8.

## 7.1. Wave basin layout

The Area 3 testing was carried out in HR Wallingford's Wave Basin ABC which is 75 m long by 32 m wide and has a maximum working depth of 1.0 m (all dimensions in metric model terms). The bathymetry design and construction is described in Section 2.2, with the full basin layout shown in Figure 7.1.

The wave gauge locations for the different phases of testing are presented in Figure 7.1 and Figure 7.2. The locations presented in Figure 7.1 were used for wave calibrations in addition to the morphological testing (anthracite beach). The wave gauge layout for the stability and beach storm response testing was agreed with SmithGroup prior to testing and confirmed verbally on the model.

### 7.1.1. Area 3 beach material placement

The anthracite beach material was initially placed according to an idealised profile consisting of a 1:15 slope to from 570ft IGLD 85 to 586 ft IGLD 85 contour. The levelled backshore to existing structures was 115 ft wide and 70 ft wide along the recreational beach respectively. The profile was used to manufacture beach-normal wooden templates. The templates were arranged along the model with the tow aligned to the 570 ft IGLD 85 contour and then levelled into position using an optical dumpy level, and the gaps between them bulk-filled with ground anthracite.

The sand beach material was placed according to an idealised profile with a 1:15 slope from the 570 ft IGLD 85 contour to an elevation of 586 ft IGLD 85 (based on *scan 34* from the anthracite morphological tests). The profile was used to manufacture beach-normal wooden templates. The templates were aligned based on the *scan 34* beach plan shape and then levelled into position using an optical dumpy level, and the gaps between them bulk-filled with fine modelling sand.

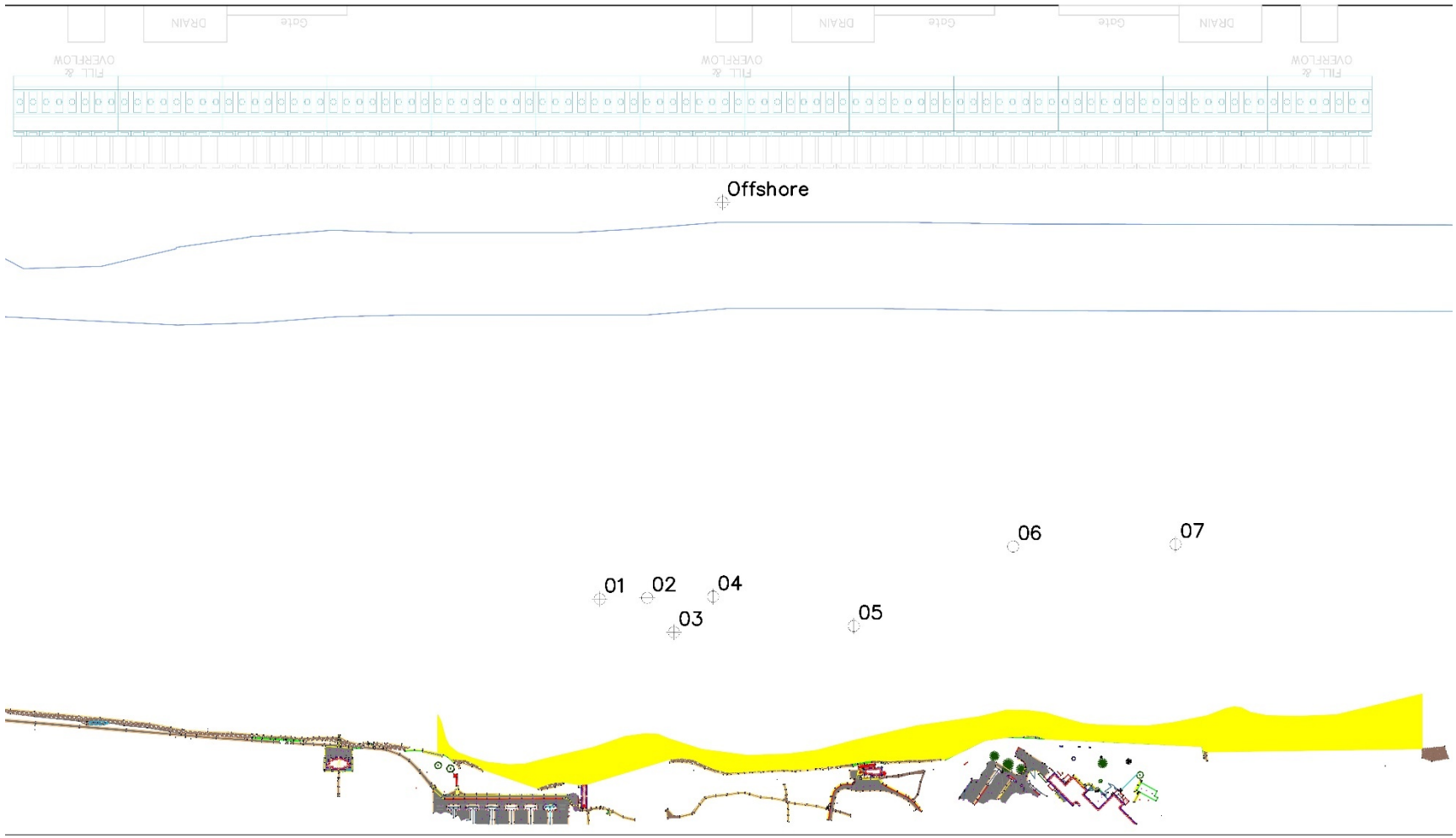


Figure 7.1: Area 3 basin layout showing wave gauge locations for anthracite morphological tests

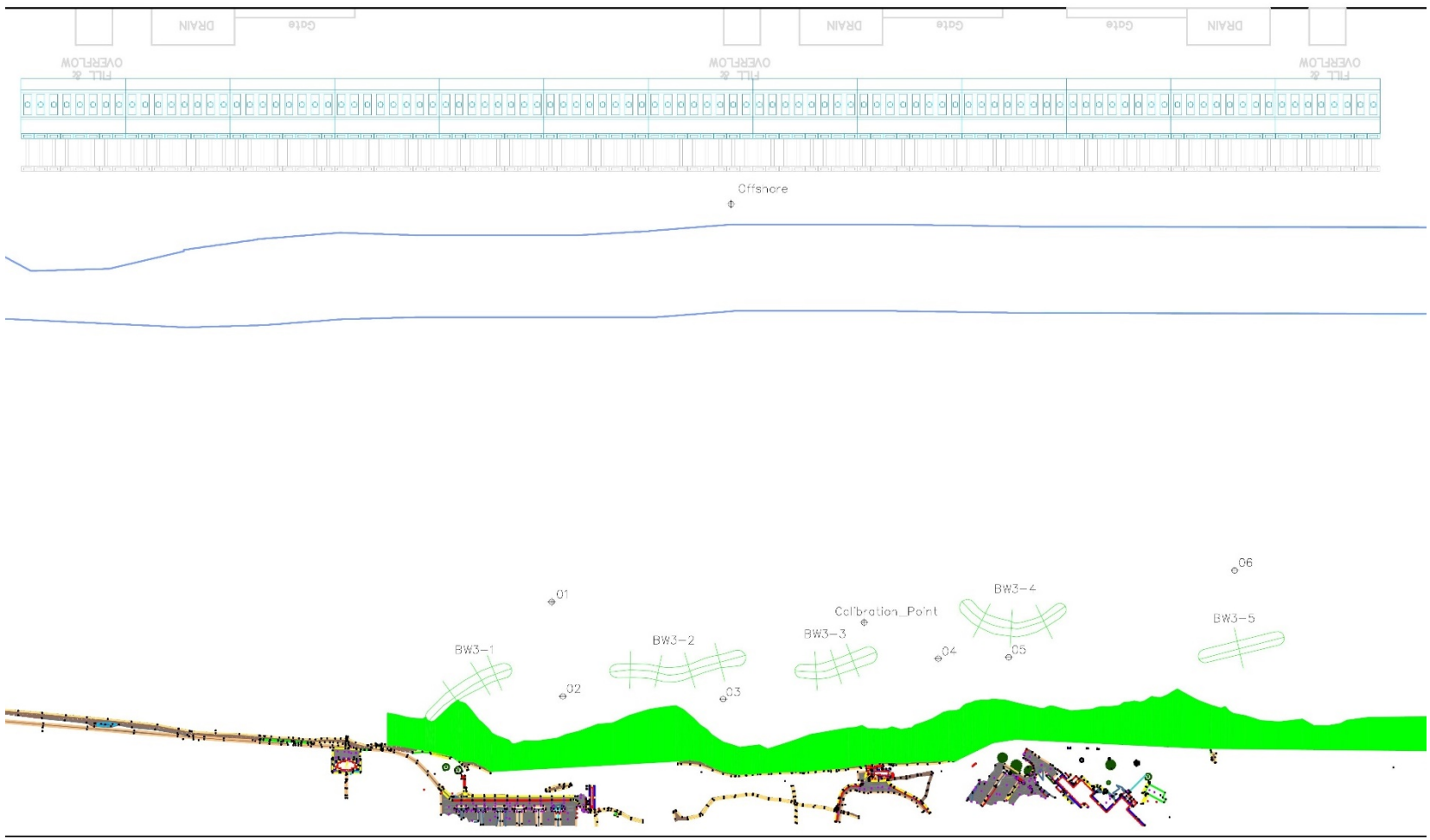


Figure 7.2: Wave gauge locations for Area 3 stability and sand beach storm response tests

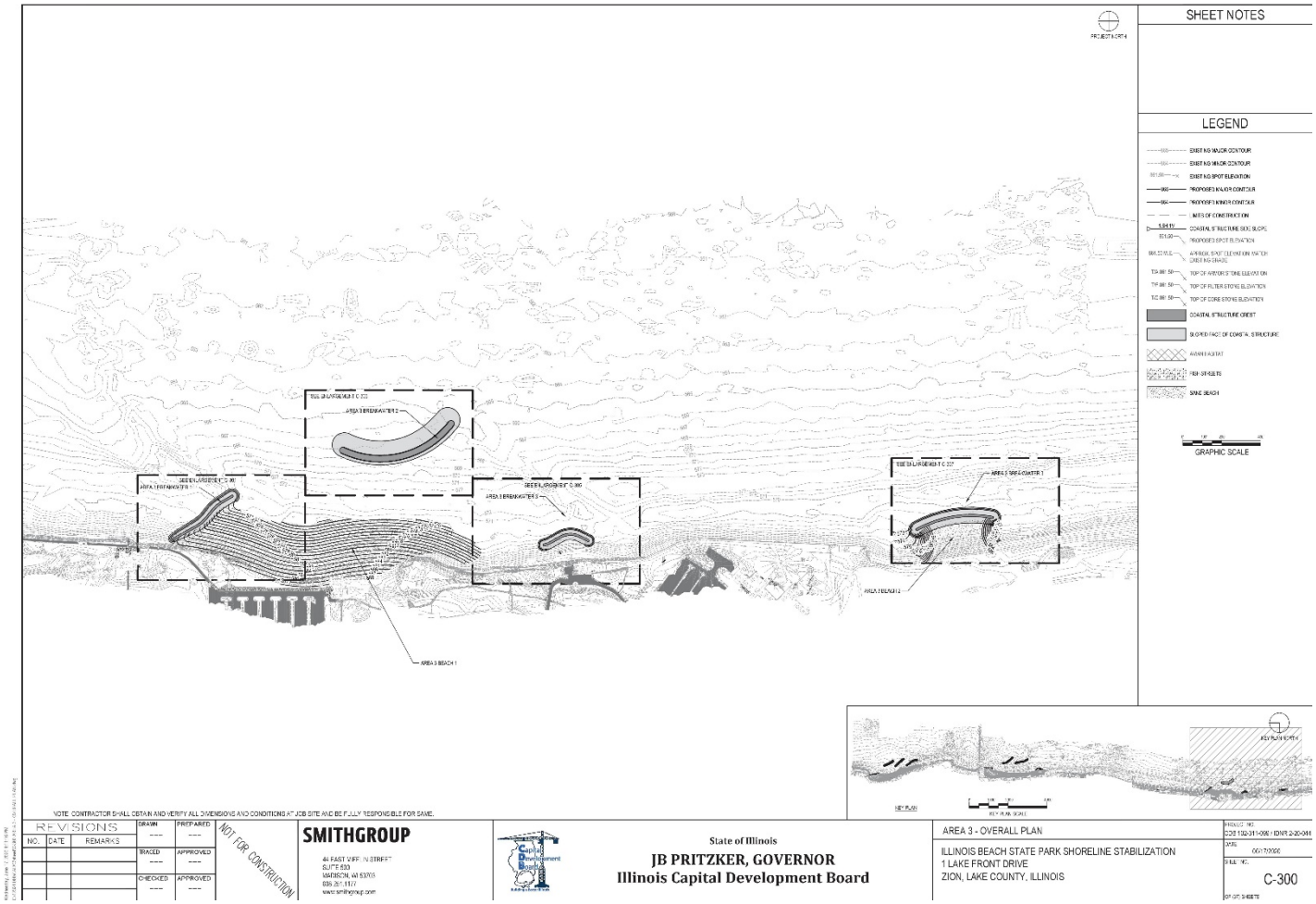


Figure 7.3: Initial layout of Area 3 beach control structures for morphological tests

*Source: 2020-0617 Illinois Beach State Park Shoreline Stabilization.pdf*

## 7.2. Test sections

### 7.2.1. Morphological testing

The beach control structures were optimised during the morphological tests. The initial layout of the beach control structures is shown in Figure 7.3, provided in *2020-0617 Illinois Beach State Park Shoreline Stabilization.pdf*. The intermediate layouts were directed by SmithGroup's on-site representatives based on the results of the preceding tests. The modifications were often small and iterative in nature, and were often only tested for short durations until a layout was showing promising results and subjected to a full morphological test. Photographs and scan records of the significant intermediate structures are given in Appendix D.1, with a summary provided in Section 7.4. There were often no specific drawings for these intermediate structures as they were developed within the physical model. The final layout of the control structures was taken forward for the confirmation (stability) tests. The details of these structures are provided in Section 7.2.2.

### 7.2.2. Stability testing

The beach control structures for the stability tests were provided in *2020-1203 Cross Sections-Area3 - FOR LAB.dwg*, and are reproduced in Figure 7.4 to Figure 7.12. The plan layout is shown in Figure 7.4 and the cross-sections and long-sections in Figure 7.5 to Figure 7.12. The rock grades used for the stability tests are given in Table 2.1 along with which grade was used as armour for which structure. Various of the smaller grades were used for under / filter layers where larger armour grades have been used. The grade curves of the prepared model rock classes are given Appendix A. Note: as discussed in Sections 1.2 and 2.4.1, all rock grades use metric tonnes, and so, for example, the primary armour shown in Figure 7.5 as 2-4 tn was modelled as 2000-4000kg.

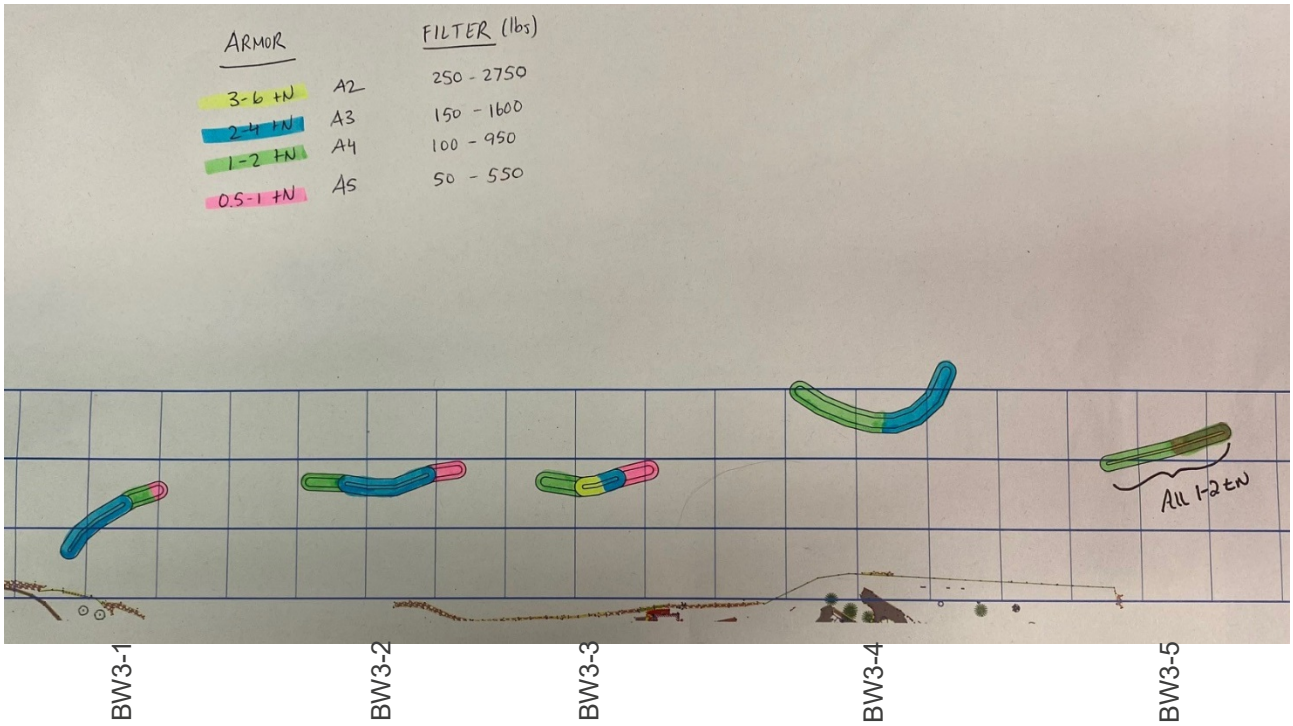


Figure 7.4: Layout drawing of beach control structures for stability tests (armour grades given in key)

*Source: Final Structure Layout.jpg*

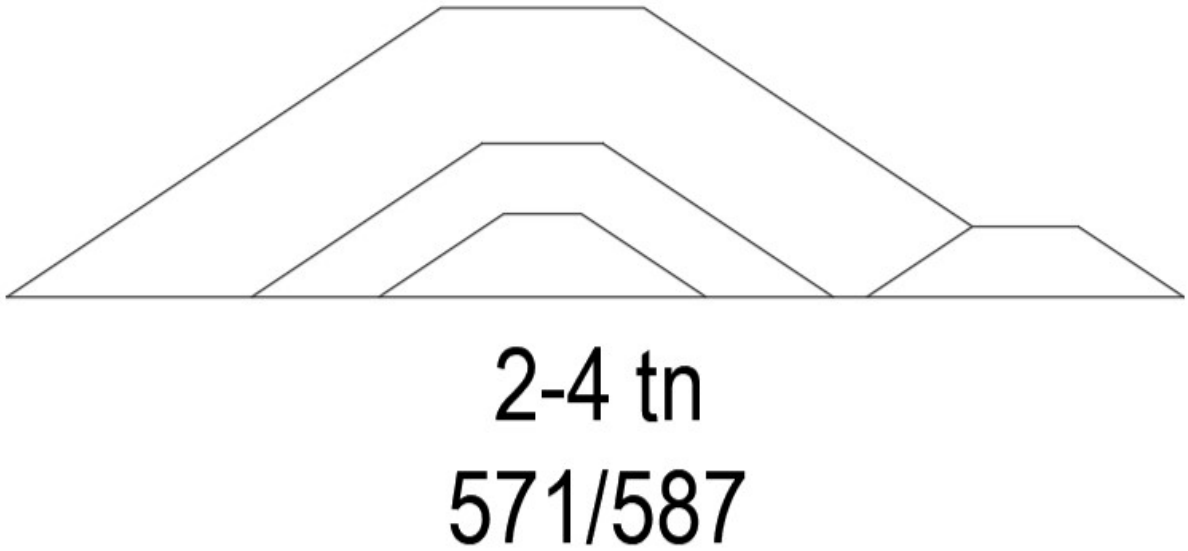


Figure 7.5: BW3-1 2-4 t armour cross-section

*Source: 2020-1203 Cross Sections-Area3 - FOR LAB.dwg*

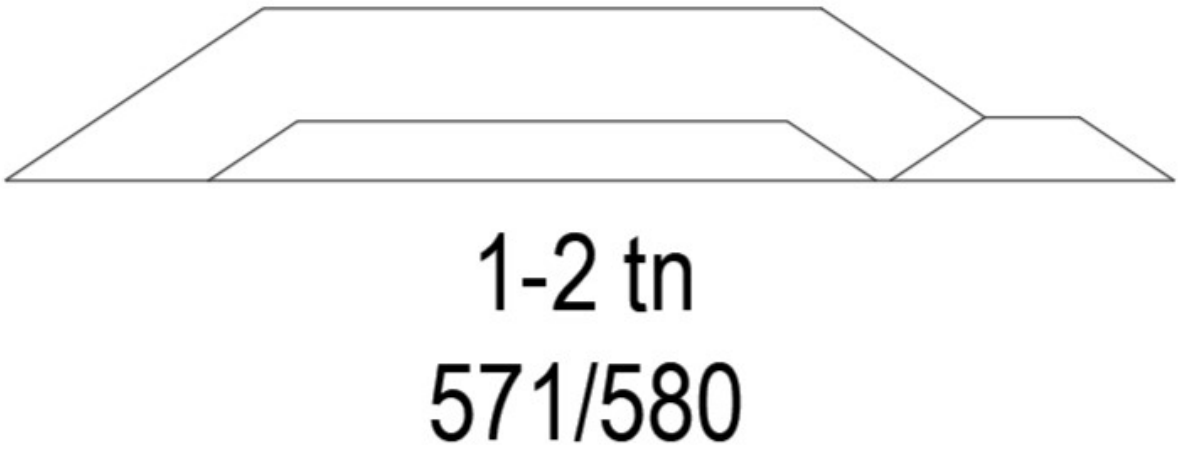


Figure 7.6: BW3-1 1-2 t armour cross-section (also section for BW3-2 and BW3-3)

*Source: 2020-1203 Cross Sections-Area3 - FOR LAB.dwg*

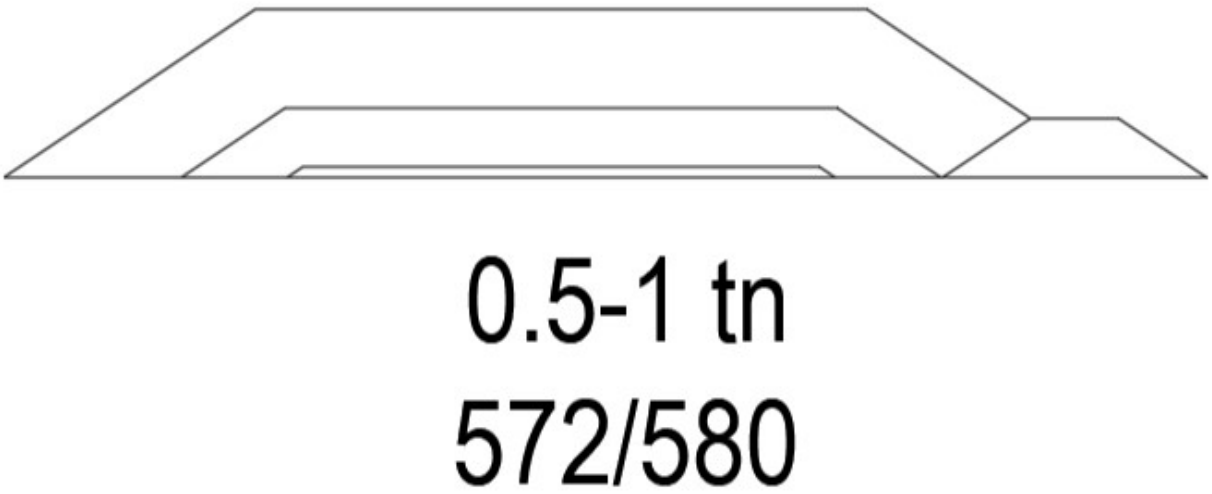


Figure 7.7: BW3-1 0.5-1 t armour cross-section (also section for BW3-2 and BW3-3)

*Source: 2020-1203 Cross Sections-Area3 - FOR LAB.dwg*

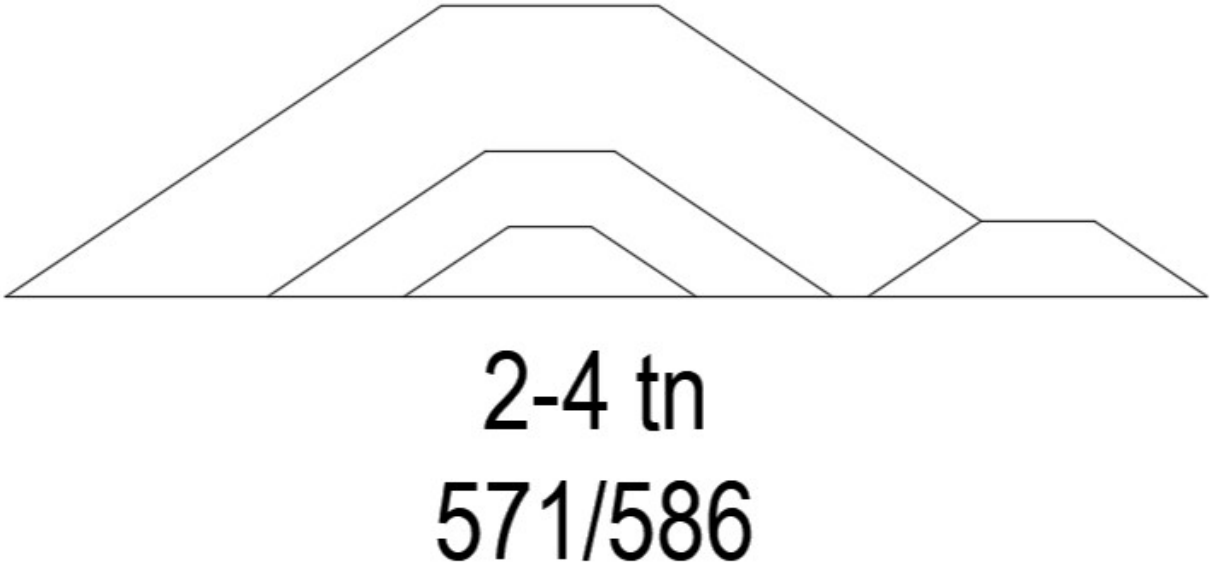


Figure 7.8: BW3-2 2-4 t armour cross-section (also section for BW3-3)

*Source: 2020-1203 Cross Sections-Area3 - FOR LAB.dwg*

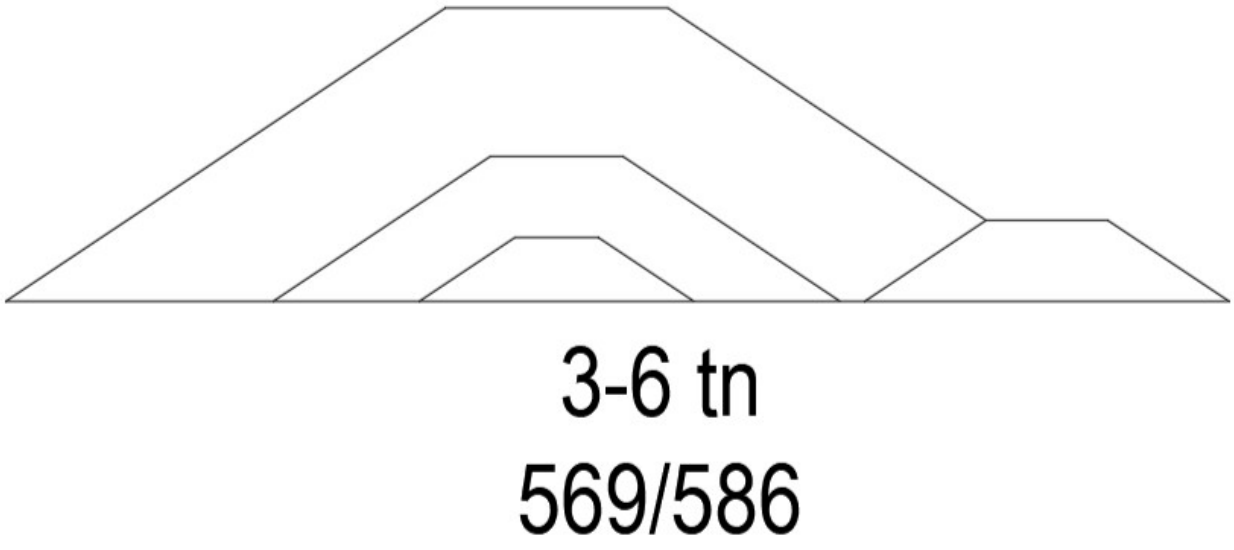


Figure 7.9: BW3-3 3-6 t armour cross-section

*Source: 2020-1203 Cross Sections-Area3 - FOR LAB.dwg*

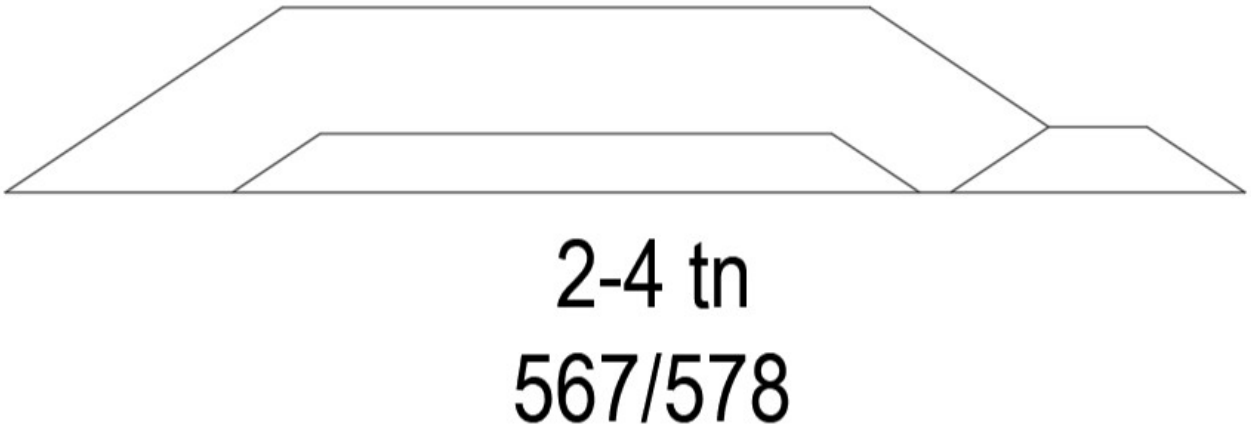


Figure 7.10: BW3-4 2-4 t armour cross-section

*Source: 2020-1203 Cross Sections-Area3 - FOR LAB.dwg*

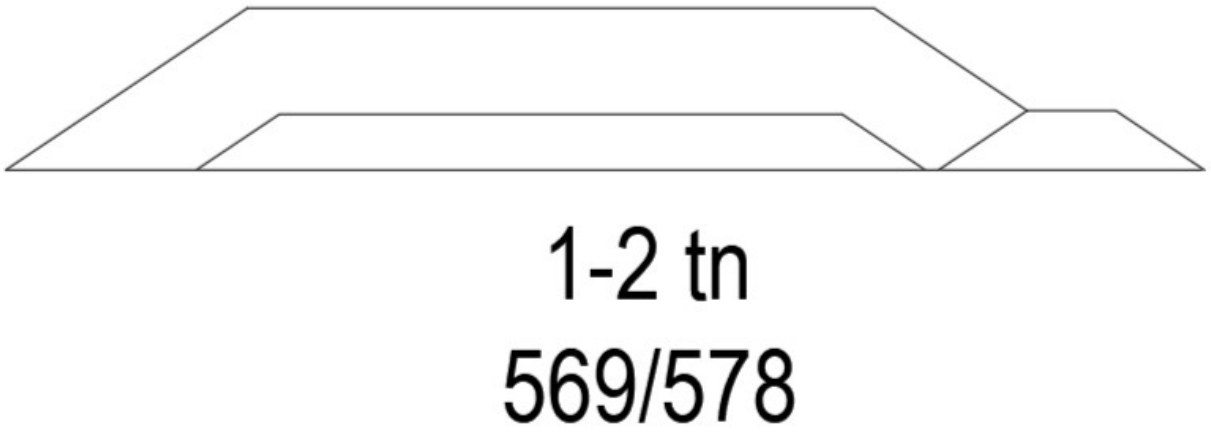


Figure 7.11: BW3-1 1-2 t armour cross-section

*Source: 2020-1203 Cross Sections-Area3 - FOR LAB.dwg*

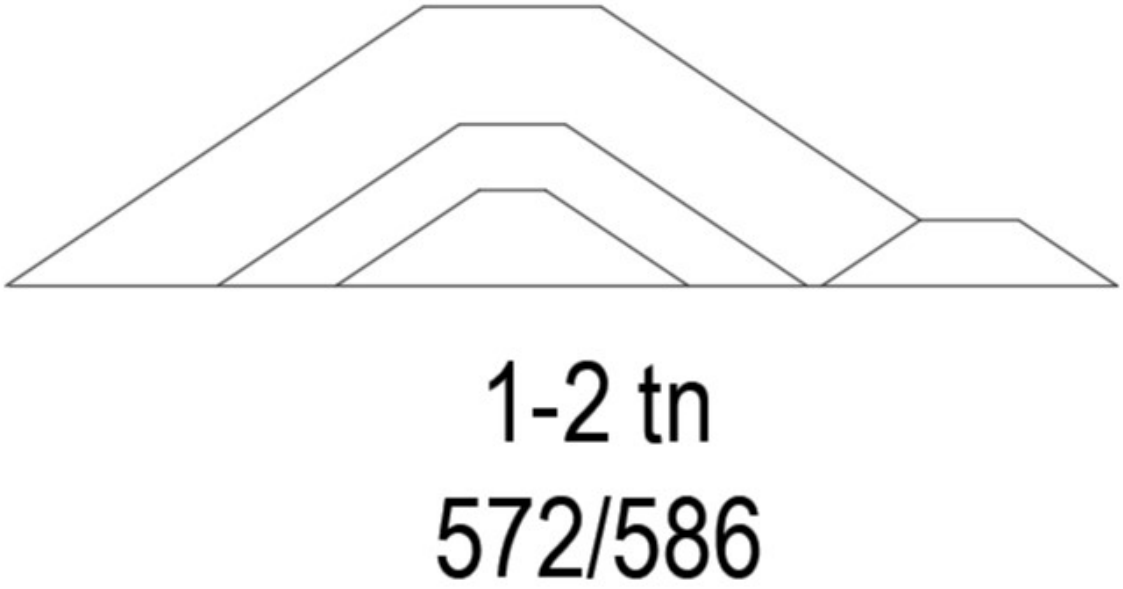


Figure 7.12: BW3-5 1-2 t armour cross-section

*Source: 2020-1203 Cross Sections-Area3 - FOR LAB.dwg*

## 7.3. Wave calibration results

The results of the wave calibrations are summarised in Table 7.1 for the morphological condition. This was determined at the calibration point (565 ft IGLD 85 contour, see Figure 7.1) using the method outlined in Section 2.5.1. Table 7.1 presents the target wave heights ($H_{m0}$) and periods ($T_p$) at the calibration point, along with the measured $H_{m0}$. The spectral and Rayleigh plots for the morphological condition are reproduced in Figure 7.13 and Figure 7.14, respectively.

The calibration of the Morph_03 condition acted as confirmation that there was no significant change required in the wave paddle settings between Area 2 and Area 3 models. This was anticipated and was due to the majority of the bathymetry from the Area 2 model being retained and extended with a similar slope etc. for the Area 3 model. This meant there was no difference in the way waves generated at the wave paddles propagated across the model to the beach and beach control structures.

With the agreement of the SmithGroup on-site representatives, the stability wave conditions, which were the same as those used in Area 2, were not re-calibrated for the Area 3 model, speeding the transition from anthracite morphological tests to stability confirmation tests. The results from the Area 2 wave calibrations can be found in Section 6.3.

Table 7.1: Results of Area 3 morphological wave calibration at 565 ft IGLD 85 contour

| Wave condition | Target | | Measured |
|---|---|---|---|
| | $H_{m0}$ (ft) | $T_p$ (s) | $H_{m0}$ (ft) |
| Morph_03 | 4.9 | 9.0 | 4.9 |

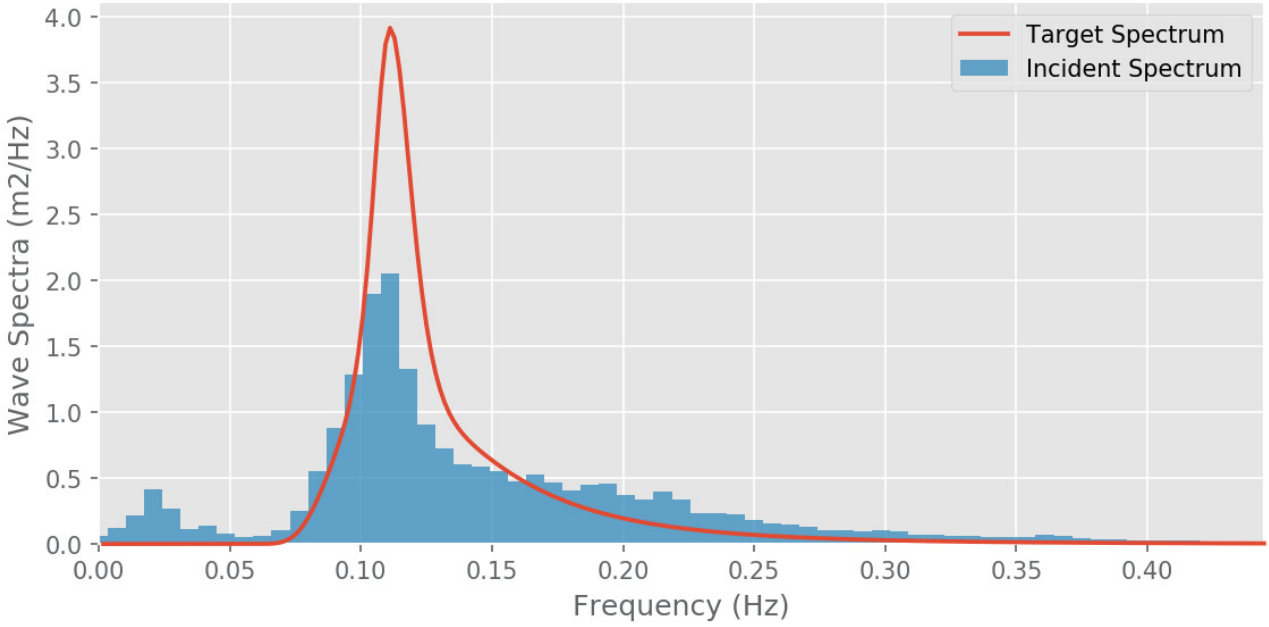


Figure 7.13: Area 3 Morph_03 spectral plot

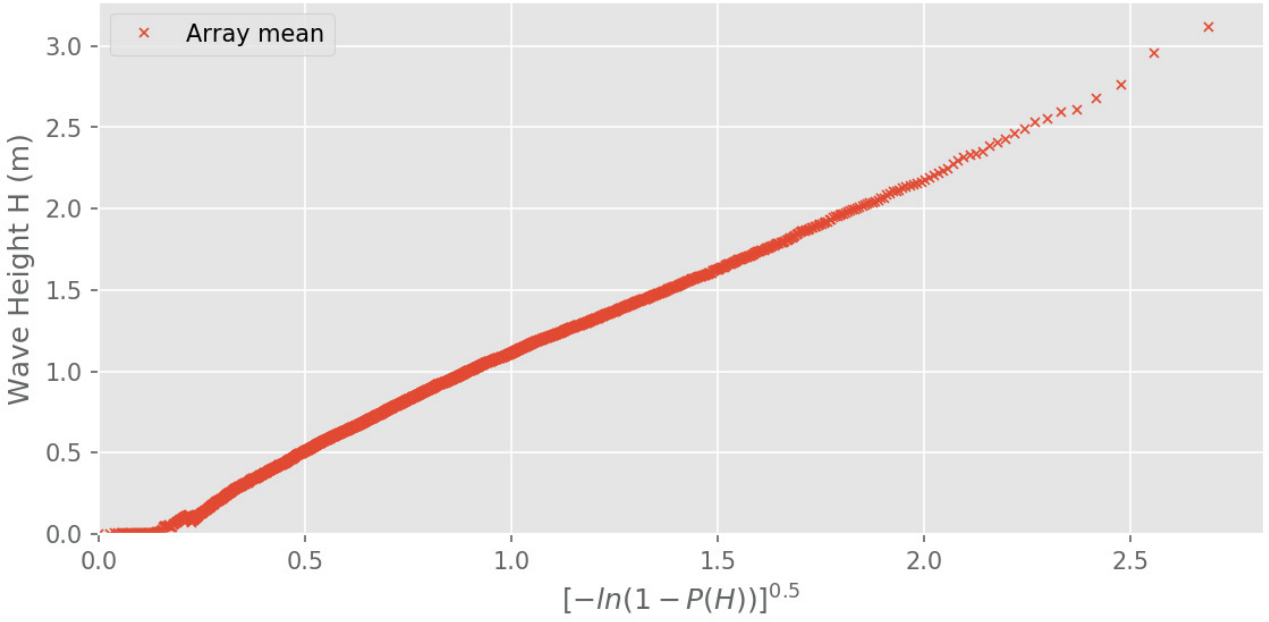


Figure 7.14: Area 3 Morph_03 Rayleigh plot

## 7.4. Morphological tests results – anthracite beach

The starting point for the Area 3 beach control structures optimisation was Configuration 01, and was provided in *2020-0617 Illinois Beach State Park Shoreline Stabilization.pdf* (Figure 7.3). This configuration was tested for 18 hr tests (3 hrs model). The pre and post-test photographs from the 'North' and 'South' time-lapse camera views are shown in Figure 7.16 and Figure 7.17. The layout consisted of four detached breakwaters, three shore parallel and one at approximately 45° to the shore, aligned Northwest to Southeast. The Northernmost shore parallel structure had a concave plan shape and was situated farthest from the shoreline. The other two shore parallel structures had a slight convex shape and were closer to the shore.

The optimisation moved through a further 33 configurations to arrive at the optimised layout, Configuration 34. A complete description of all the configurations leading to the development of the optimised layout are provided in Appendix D.1. Configuration 34 consisted of five detached breakwaters, four shore parallel and one at approximately 45° to the shore, aligned Northwest to Southeast, similar to Configuration 01. The central three breakwaters had a concave plan shape, with the Southernmost of the three having the greatest curved plan shape. The Southernmost of all the structures, had a straight plan shape and a slight Northwest to Southeast alignment relative to the shoreline. The pre and post-test photographs from the 'North' and 'South' time-lapse camera views are shown in Figure 7.18 and Figure 7.19. The post-test scan data, including the structure outlines, is shown in Figure 7.15. This configuration was tested for 9 hrs (1.5 hrs model). All tests were undertaken with the Morph03 wave condition (Table 3.5).

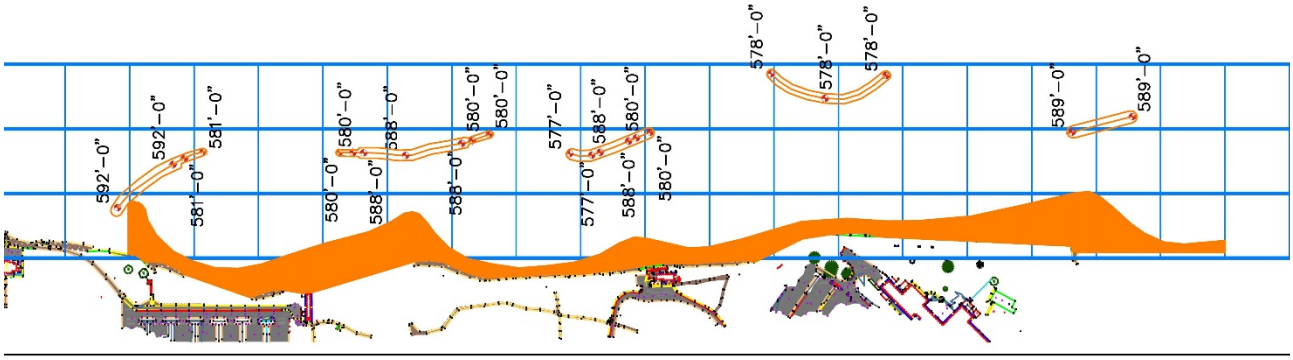


Figure 7.15: Post-test scan data for Area 3 Configuration 34, solid area post-test beach, structures in orange with spot-heights given for key locations

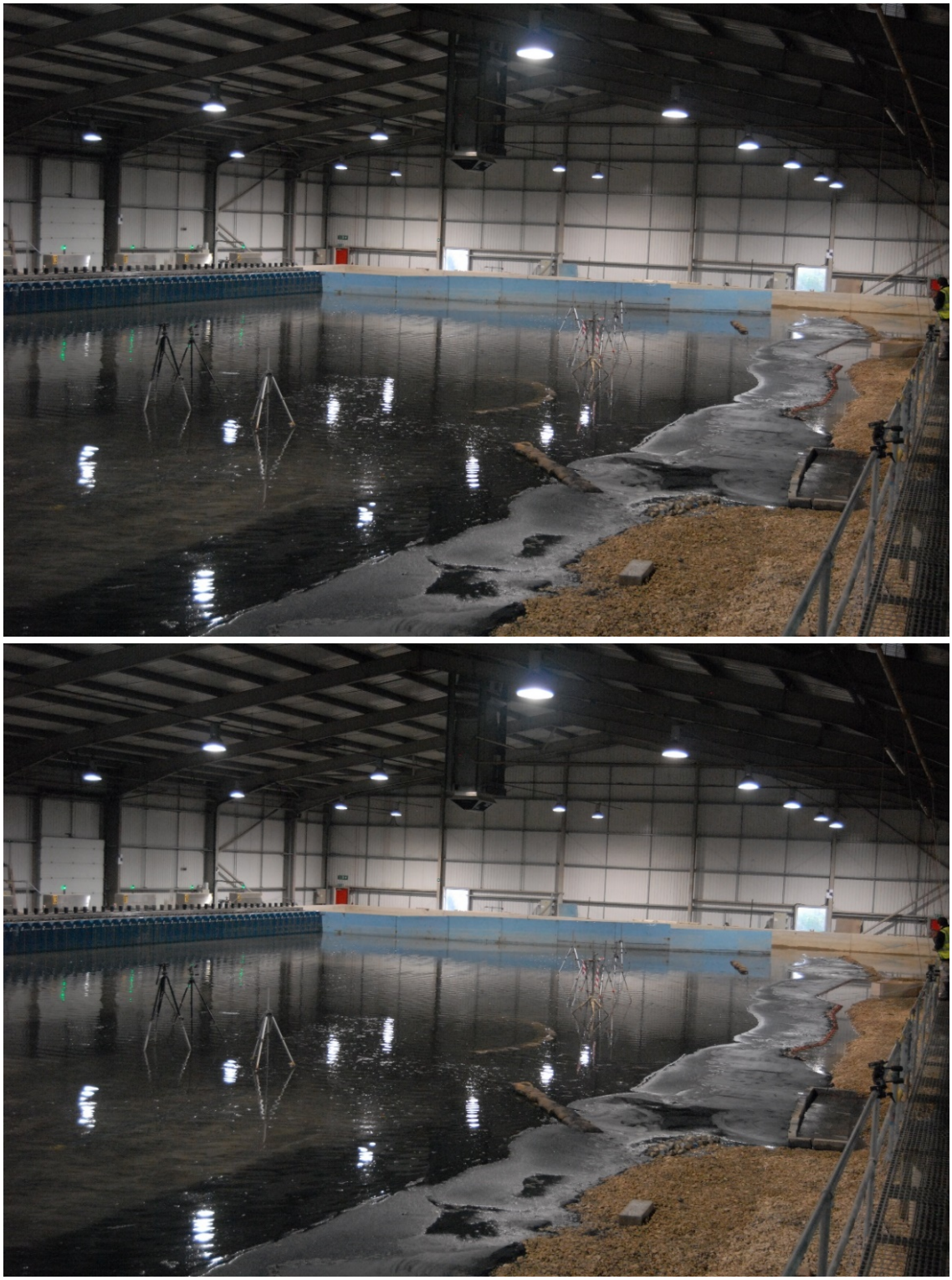

Figure 7.16: Pre (top) and post-test (bottom) photographs from ‘North’ view for Area 3 Configuration 01

Figure 7.17: Pre (top) and post-test (bottom) photographs from ‘South’ view for Area 3 Configuration 01

Figure 7.18: Pre (top) and post-test (bottom) photographs from ‘North’ view for Area 3 Configuration 34

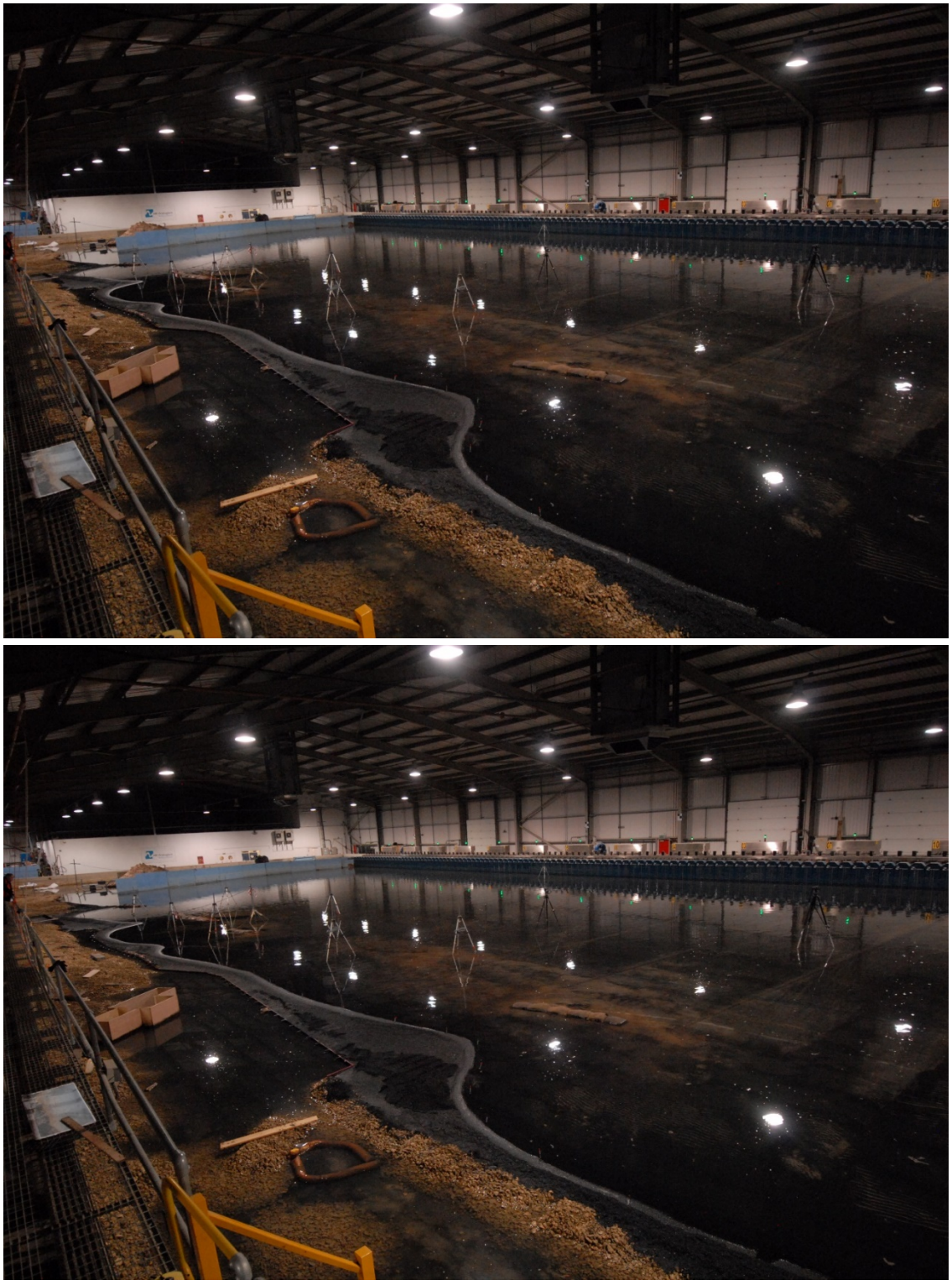

Figure 7.19: Pre (top) and post-test (bottom) photographs from ‘South’ view for Area 3 Configuration 34

## 7.5. Dye tracing tests

At various points during the anthracite morphological tests, the SmithGroup on-site representatives undertook dye tracing tests to observe cross-shore currents and to assess the potential for both high currents and sediment transport around key features (see Section 2.7). The current patterns observed by SmithGroup's on-site representatives aided the development and optimisation of the beach control structures. No formal data was recorded by HR Wallingford for these observational dye tracing tests.

## 7.6. Storm response tests results – sand beach

Following the completion of the anthracite morphological tests, the anthracite beach was replaced with a sand beach to allow the beach's response to storm conditions to be checked during the stability tests. The test order, including when scans were taken and if the beach was re-profiled is provided in Table 7.2.

Table 7.2: Area 3 sand beach Test Part and scan record

| Activity | Type | Scan |
|---|---|---|
| Initial placement of sand beach | Setup | Pre-test |
| Stability Test Part 01 - WC_LOW_WL_SE | Test Part | Post-test |
| Stability Test Part 02 - WC_HIGH_WL_SE | Test Part | Post-test |
| Stability Test Part 03 - WC_LOW_WL | Test Part | Post-test |
| Stability Test Part 04 - WC_HIGH_WL | Test Part | Post-test |
| Stability Test Part 05 - WC_EXT_WL_01 | Test Part | Post-test |
| Stability Test Part 06 - WC_EXT_WL_02 | Test Part | Post-test |

### 7.6.1. Storm response from SE conditions

The storm response of the sand beach to the two Southeast storm conditions is shown in Figure 7.20 and Figure 7.21. The beach recedes at the SWL of the first Test Part (579.2 ft IGLD 85) as expected during storm conditions, Figure 7.20. During the second higher water level, Test Part (SWL 582.2 ft IGLD 85), the plan shape of the beach increases (moves seaward) at that elevation, Figure 7.21. This is probably due to the change in water level and the initial shape of the beach at this elevation which is unlikely to have been modified during the first Test Part.

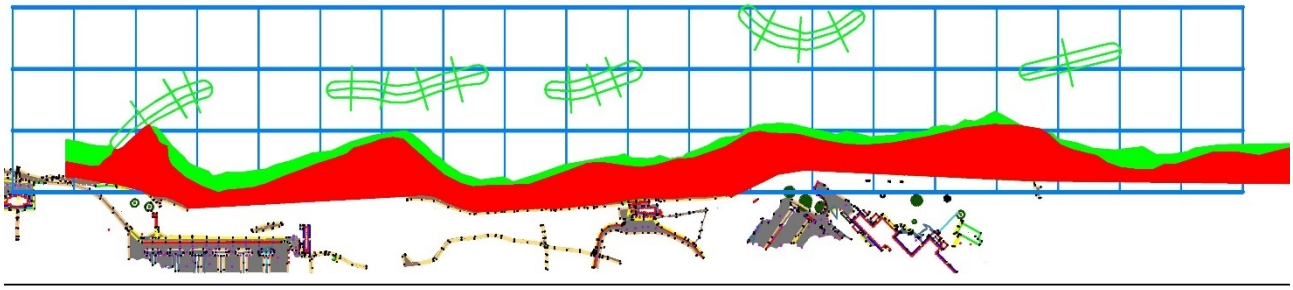

Figure 7.20: Area 3 stability Test Part 01 beach scan data, SWL 579.2 ft IGLD 85 (pre-test scan in green, post-test scan in red, structure outline in green)

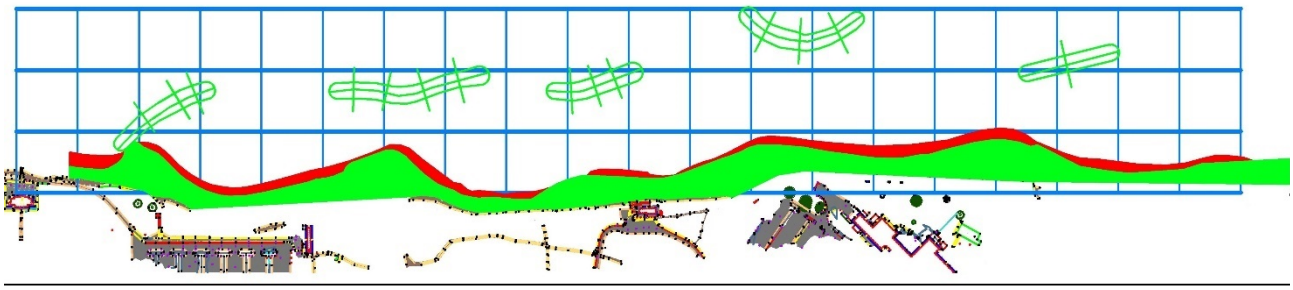

Figure 7.21: Area 3 stability Test Part 02 beach scan data, SWL 582.2 ft IGLD 85 (pre-test scan in green, post-test scan in red, structure outline in green)

### 7.6.2. Storm response from NE conditions

The storm response of the sand beach to the four Northeast storm conditions is shown in Figure 7.22 to Figure 7.25. The beach recedes (reduces in width) throughout the progressive storm tests, each storm eroding the beach farther at the particular SWL of each Test Part. Following the final Test Part (06), there is little beach above the SWL, with none present in the southern end of the model. This represents an extreme case as six full storm conditions have been tested by this point, replicating something that is unlikely to occur in prototype.

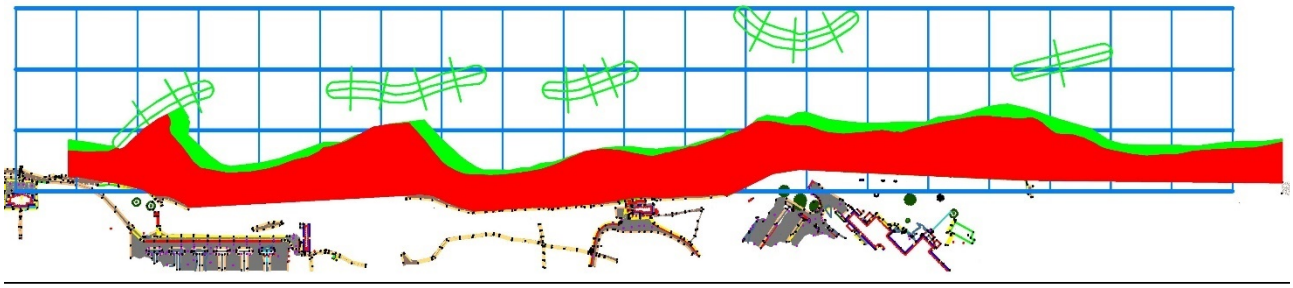

Figure 7.22: Area 3 stability Test Part 03 beach scan data, SWL 576.0 ft IGLD 85 (pre-test scan in green, post-test scan in red, structure outline in green)

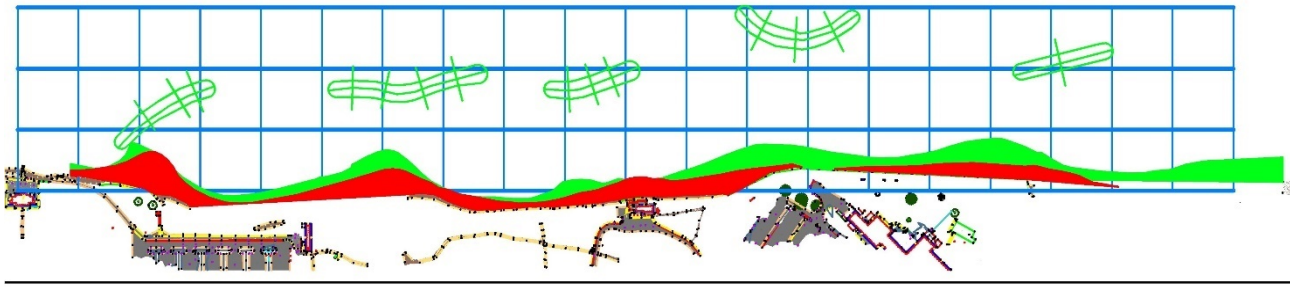

Figure 7.23: Area 3 stability Test Part 04 beach scan data, SWL 583.3 ft IGLD 85 (pre-test scan in green, post-test scan in red, structure outline in green)

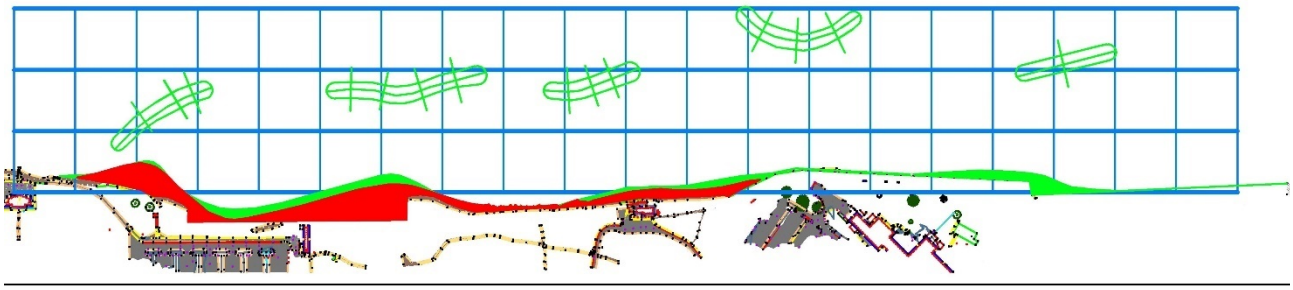

Figure 7.24: Area 3 stability Test Part 05 beach scan data, SWL 585.2 ft IGLD 85 (pre-test scan in green, post-test scan in red, structure outline in green)

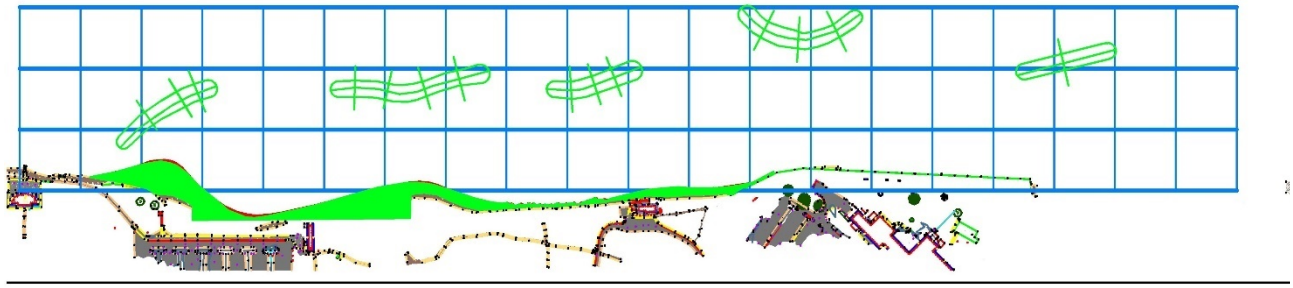

Figure 7.25: Area 3 stability Test Part 06 beach scan data, SWL 585.2 ft IGLD 85 (pre-test scan in green, post-test scan in red, structure outline in green)

## 7.7. Stability test results

The stability tests focussed specifically on all beach control breakwater structures BW3-1 to BW3-5 (Section 7.2.2). Photographs were taken before and after each Test Part and are reproduced in Appendix D.2. Each breakwater of interest has been divided into a series of panels such as trunk, roundhead and fishtail, seaside and leeside and where a section is particularly long it has been divided into North and South. The panels are shown in Figure 7.26.

The cumulative number of rocks extracted and the calculated $S_d$ damage parameter for each structure are presented in Table 7.3 to Table 7.12. For each breakwater there are two tables, the first with the cumulative number of rocks extracted from the armour layer and the second with the calculated $S_d$ damage parameter. The $S_d$ parameter has been calculated using the method described in Section 2.8.

For the majority of structures the damage level is low, with few rocks extracted. There were no areas of higher damage, $S_d > 8$ (Table 2.3). Structures with some damage, $2 < S_d < 8$ (Table 2.3), are the BW3-5, particularly the Southern seaside trunk (Appendix D.2.5). Here the rock on the crest was not sufficiently supported by the smaller underlayer size rock used on the leeward face for this section. This allowed the waves overtopping the structure to push the crest rocks over the back of the crest and down the leeward face of the breakwater. The displaced crest armour effectively covered the leeward face preventing damage or erosion of the smaller leeward armour.

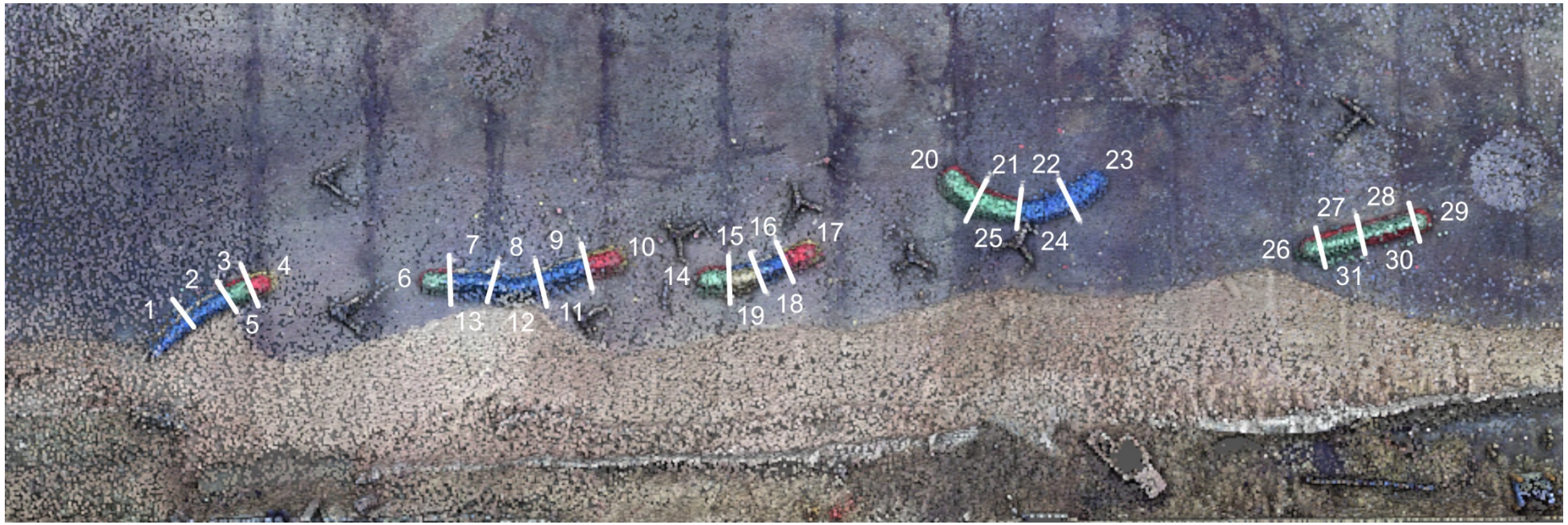


Figure 7.26: Area 3 stability analysis panels

Table 7.3: BW3-1 cumulative number of rocks displaced

| Test Part | Wave condition | Return period | Wave direction (°N) | Trunk seaside 2-4t North (panel 1) | Trunk seaside 2-4t South (panel 2) | Trunk seaside 1-2t (panel 3) | Roundhead South (panel 4) | Trunk leeside 1-2t (panel 5) |
|---|---|---|---|---|---|---|---|---|
| 1 | WC_LOW_WL | 1:100 | 130 | 0 | 0 | 0 | 2 | 0 |
| 2 | WC_HIGH_WL | 1:100 | 130 | 0 | 0 | 0 | 2 | 0 |
| 3 | WC_LOW_WL | 1:100 | 65 | 0 | 0 | 0 | 3 | 0 |
| 4 | WC_HIGH_WL | 1:100 | 65 | 0 | 0 | 0 | 5 | 2 |
| 5 | WC_EXT_WL_01 | 1:10 | 65 | 0 | 0 | 0 | 5 | 2 |
| 6 | WC_EXT_WL_02 | 1:100 | 65 | 0 | 0 | 0 | 6 | 2 |

Table 7.4: BW3-1 damage parameter $S_d$

| Test Part | Wave condition | Return period | Wave direction (°N) | Trunk seaside 2-4t North (panel 1) | Trunk seaside 2-4t South (panel 2) | Trunk seaside 1-2t (panel 3) | Roundhead South (panel 4) | Trunk leeside 1-2t (panel 5) |
|---|---|---|---|---|---|---|---|---|
| 1 | WC_LOW_WL | 1:100 | 130 | 0.0 | 0.0 | 0.0 | 0.1 | 0.0 |
| 2 | WC_HIGH_WL | 1:100 | 130 | 0.0 | 0.0 | 0.0 | 0.1 | 0.0 |
| 3 | WC_LOW_WL | 1:100 | 65 | 0.0 | 0.0 | 0.0 | 0.1 | 0.0 |
| 4 | WC_HIGH_WL | 1:100 | 65 | 0.0 | 0.0 | 0.0 | 0.1 | 0.1 |
| 5 | WC_EXT_WL_01 | 1:10 | 65 | 0.0 | 0.0 | 0.0 | 0.1 | 0.1 |
| 6 | WC_EXT_WL_02 | 1:100 | 65 | 0.0 | 0.0 | 0.0 | 0.2 | 0.1 |

Table 7.5: BW3-2 cumulative number of rocks displaced

| Test Part | Wave condition | Return period | Wave direction (°N) | Round-head North (panel 6) | Trunk seaside North (panel 7) | Trunk seaside mid (panel 8) | Trunk seaside South (panel 9) | Round-head South (panel 10) | Trunk leeside South (panel 11) | Trunk leeside Mid (panel 12) | Trunk leeside North (panel 13) |
|---|---|---|---|---|---|---|---|---|---|---|---|
| 1 | WC_LOW_WL | 1:100 | 130 | 0 | 0 | 0 | 0 | 3 | 0 | 0 | 0 |
| 2 | WC_HIGH_WL | 1:100 | 130 | 0 | 1 | 0 | 0 | 3 | 2 | 1 | 0 |
| 3 | WC_LOW_WL | 1:100 | 65 | 1 | 2 | 0 | 0 | 10 | 2 | 1 | 0 |
| 4 | WC_HIGH_WL | 1:100 | 65 | 3 | 2 | 0 | 1 | 12 | 10 | 8 | 4 |
| 5 | WC_EXT_WL_01 | 1:10 | 65 | 3 | 2 | 0 | 1 | 14 | 10 | 8 | 4 |
| 6 | WC_EXT_WL_02 | 1:100 | 65 | 3 | 3 | 1 | 3 | 15 | 11 | 8 | 4 |

Table 7.6: BW3-2 damage parameter $S_d$

| Test Part | Wave condition | Return period | Wave direction (°N) | Round-head North (panel 6) | Trunk seaside North (panel 7) | Trunk seaside mid (panel 8) | Trunk seaside South (panel 9) | Round-head South (panel 10) | Trunk leeside South (panel 11) | Trunk leeside Mid (panel 12) | Trunk leeside North (panel 13) |
|---|---|---|---|---|---|---|---|---|---|---|---|
| 1 | WC_LOW_WL | 1:100 | 130 | 0.0 | 0.0 | 0.0 | 0.0 | 0.1 | 0.0 | 0.0 | 0.0 |
| 2 | WC_HIGH_WL | 1:100 | 130 | 0.0 | 0.0 | 0.0 | 0.0 | 0.1 | 0.1 | 0.0 | 0.0 |
| 3 | WC_LOW_WL | 1:100 | 65 | 0.0 | 0.1 | 0.0 | 0.0 | 0.2 | 0.1 | 0.0 | 0.0 |
| 4 | WC_HIGH_WL | 1:100 | 65 | 0.1 | 0.1 | 0.0 | 0.0 | 0.2 | 0.3 | 0.2 | 0.2 |
| 5 | WC_EXT_WL_01 | 1:10 | 65 | 0.1 | 0.1 | 0.0 | 0.0 | 0.3 | 0.3 | 0.2 | 0.2 |
| 6 | WC_EXT_WL_02 | 1:100 | 65 | 0.1 | 0.1 | 0.0 | 0.1 | 0.3 | 0.4 | 0.2 | 0.2 |

Table 7.7: BW3-3 cumulative number of rocks displaced

| Test Part | Wave condition | Return period | Wave direction (°N) | Roundhead North (panel 14) | Trunk seaside 3-6t (panel 15) | Trunk seaside 2-4t (panel 16) | Roundhead South (panel 17) | Trunk leeside 2-4t (panel 18) | Trunk leeside 3-6t (panel 19) |
|---|---|---|---|---|---|---|---|---|---|
| 1 | WC_LOW_WL | 1:100 | 130 | 0 | 0 | 0 | 1 | 0 | 0 |
| 2 | WC_HIGH_WL | 1:100 | 130 | 0 | 0 | 0 | 2 | 0 | 0 |
| 3 | WC_LOW_WL | 1:100 | 65 | 0 | 0 | 0 | 5 | 0 | 0 |
| 4 | WC_HIGH_WL | 1:100 | 65 | 4 | 0 | 0 | 19 | 6 | 5 |
| 5 | WC_EXT_WL_01 | 1:10 | 65 | 4 | 0 | 0 | 19 | 6 | 5 |
| 6 | WC_EXT_WL_02 | 1:100 | 65 | 5 | 0 | 0 | 19 | 7 | 6 |

Table 7.8: BW3-3 damage parameter $S_d$

| Test Part | Wave condition | Return period | Wave direction (°N) | Roundhead North (panel 14) | Trunk seaside 3-6t (panel 15) | Trunk seaside 2-4t (panel 16) | Roundhead South (panel 17) | Trunk leeside 2-4t (panel 18) | Trunk leeside 3-6t (panel 19) |
|---|---|---|---|---|---|---|---|---|---|
| 1 | WC_LOW_WL | 1:100 | 130 | 0.0 | 0.0 | 0.0 | 0.0 | 0.0 | 0.0 |
| 2 | WC_HIGH_WL | 1:100 | 130 | 0.0 | 0.0 | 0.0 | 0.0 | 0.0 | 0.0 |
| 3 | WC_LOW_WL | 1:100 | 65 | 0.0 | 0.0 | 0.0 | 0.1 | 0.0 | 0.0 |
| 4 | WC_HIGH_WL | 1:100 | 65 | 0.1 | 0.0 | 0.0 | 0.4 | 0.4 | 0.3 |
| 5 | WC_EXT_WL_01 | 1:10 | 65 | 0.1 | 0.0 | 0.0 | 0.4 | 0.4 | 0.3 |
| 6 | WC_EXT_WL_02 | 1:100 | 65 | 0.1 | 0.0 | 0.0 | 0.4 | 0.4 | 0.3 |

Table 7.9: BW3-4 cumulative number of rocks displaced

| Test Part | Wave condition | Return period | Wave direction (°N) | Roundhead North (panel 20) | Trunk seaside 1-2t (panel 21) | Trunk seaside 2-4t (panel 22) | Roundhead South (panel 23) | Trunk leeside 2-4t (panel 24) | Trunk leeside 1-2t (panel 25) |
|---|---|---|---|---|---|---|---|---|---|
| 1 | WC_LOW_WL | 1:100 | 130 | 0 | 0 | 0 | 0 | 0 | 0 |
| 2 | WC_HIGH_WL | 1:100 | 130 | 0 | 0 | 0 | 0 | 0 | 0 |
| 3 | WC_LOW_WL | 1:100 | 65 | 7 | 1 | 2 | 3 | 4 | 0 |
| 4 | WC_HIGH_WL | 1:100 | 65 | 14 | 3 | 4 | 3 | 4 | 0 |
| 5 | WC_EXT_WL_01 | 1:10 | 65 | 14 | 3 | 4 | 3 | 4 | 1 |
| 6 | WC_EXT_WL_02 | 1:100 | 65 | 14 | 4 | 4 | 3 | 4 | 1 |

Table 7.10: BW3-4 damage parameter $S_d$

| Test Part | Wave condition | Return period | Wave direction (°N) | Roundhead North (panel 20) | Trunk seaside 1-2t (panel 21) | Trunk seaside 2-4t (panel 22) | Roundhead South (panel 23) | Trunk leeside 2-4t (panel 24) | Trunk leeside 1-2t (panel 25) |
|---|---|---|---|---|---|---|---|---|---|
| 1 | WC_LOW_WL | 1:100 | 130 | 0.0 | 0.0 | 0.0 | 0.0 | 0.0 | 0.0 |
| 2 | WC_HIGH_WL | 1:100 | 130 | 0.0 | 0.0 | 0.0 | 0.0 | 0.0 | 0.0 |
| 3 | WC_LOW_WL | 1:100 | 65 | 0.2 | 0.0 | 0.0 | 0.1 | 0.1 | 0.0 |
| 4 | WC_HIGH_WL | 1:100 | 65 | 0.3 | 0.1 | 0.1 | 0.1 | 0.1 | 0.0 |
| 5 | WC_EXT_WL_01 | 1:10 | 65 | 0.3 | 0.1 | 0.1 | 0.1 | 0.1 | 0.0 |
| 6 | WC_EXT_WL_02 | 1:100 | 65 | 0.3 | 0.1 | 0.1 | 0.1 | 0.1 | 0.0 |

Table 7.11: BW3-5 cumulative number of rocks displaced

| Test Part | Wave condition | Return period | Wave direction (°N) | Roundhead North (panel 26) | Truck seaside North (panel 27) | Trunk seaside South (panel 28) | Roundhead South (panel 29) | Trunk leeside South (panel 30) | Trunk leeside North (panel 31) |
|---|---|---|---|---|---|---|---|---|---|
| 1 | WC_LOW_WL | 1:100 | 130 | 1 | 0 | 2 | 5 | 0 | 0 |
| 2 | WC_HIGH_WL | 1:100 | 130 | 4 | 0 | 52 | 6 | 1 | 2 |
| 3 | WC_LOW_WL | 1:100 | 65 | 5 | 1 | 55 | 8 | 3 | 2 |
| 4 | WC_HIGH_WL | 1:100 | 65 | 12 | 13 | 195 | 17 | 3 | 65 |
| 5 | WC_EXT_WL_01 | 1:10 | 65 | 13 | 13 | 199 | 18 | 3 | 65 |
| 6 | WC_EXT_WL_02 | 1:100 | 65 | 15 | 14 | 212 | 20 | 3 | 70 |

Table 7.12: BW3-5 damage parameter $S_d$

| Test Part | Wave condition | Return period | Wave direction (°N) | Roundhead North (panel 26) | Truck seaside North (panel 27) | Trunk seaside South (panel 28) | Roundhead South (panel 29) | Trunk leeside South (panel 30) | Trunk leeside North (panel 31) |
|---|---|---|---|---|---|---|---|---|---|
| 1 | WC_LOW_WL | 1:100 | 130 | 0.1 | 0.0 | 0.0 | 0.3 | 0.0 | 0.0 |
| 2 | WC_HIGH_WL | 1:100 | 130 | 0.2 | 0.0 | 1.1 | 0.4 | 0.0 | 0.0 |
| 3 | WC_LOW_WL | 1:100 | 65 | 0.3 | 0.0 | 1.2 | 0.5 | 0.0 | 0.0 |
| 4 | WC_HIGH_WL | 1:100 | 65 | 0.7 | 0.3 | 4.2 | 1.0 | 0.0 | 1.6 |
| 5 | WC_EXT_WL_01 | 1:10 | 65 | 0.8 | 0.3 | 4.3 | 1.1 | 0.0 | 1.6 |
| 6 | WC_EXT_WL_02 | 1:100 | 65 | 0.9 | 0.3 | 4.6 | 1.2 | 0.0 | 1.7 |

## 7.8. Summary

A total of five beach control structures of various cross-sections and armourstone grades were utilised for the final configuration. In Section 7.4, it was demonstrated that a stable beach could be maintained with a reduced north-south sediment drift using this configuration. The beaches remained static during the stability tests (Section 7.6), with a wide crest at the beach maintained throughout.

Of the beach control structures resistance to wave action during the stability test programme, it is possible to make the following observations:

1. All structures were substantially intact at the end of the testing campaign;
2. All structures were tested for a minimum of 30 hours of storm conditions, and it should be noted that this exceeds any reasonable exposure that might be anticipated during the design life;
3. The unsupported crest armour on the Southern half of breakwater BW3-5 was displaced by the wave overtopping and pushed down the leeside of the structure, resulting in the highest level of damage seen on any of the Area 3 structures.

# 8. Summary

The 3D physical modelling campaign described in this report for Illinois Beach State Park, Lake Michigan covers Area 1 (North Beach), then Area 2 (Camp Logan) and Area 3 (Swimming Beach). Each Area model began with the optimisation of the beach control structures using proxies for armoured rubble mounds and lightweight anthracite sediment. Following optimisation of the beach control structure layout, the proxy armoured structures and the anthracite beaches were removed from the model. Fully scaled model armour breakwaters were then constructed and the beach material was replaced with modelling sand. A full suite of armour stability and beach storm response tests were then run from two directions using a series of storm conditions. At the conclusion of each Area model, the armour performance of each beach control structure was assessed.

The optimised layout for Area 1 consisted of ten beach control structures of various cross-sections and armourstone grades. It was demonstrated that a stable beach could be maintained with a reduced north-south sediment drift using this configuration. The beaches remained static during most of the stability tests, but for the extreme high water 1:10 and 1:100 return period storms, a wide crest at the beach could not be maintained and there was a net transfer of sediment to the immediate hinterland. All structures, with the exception of the leeside trunk armour of breakwater BW1-8 (Panel 22) and the fishtail for breakwater BW1-10 (Panel 27), were substantially intact at the end of the stability testing campaign. Where a piled central breakwater section was included (specifically breakwaters BW1-4 to BW1-10), then the potential for crest armour damage was reduced with these configurations.

For Area 2, the optimised layout consisted of seven beach control structures of various cross-sections and armourstone grades. The beaches remained static during the stability tests, with a wide crest at the beach maintained throughout. The SmithGroup on-site representatives utilised the Area 2 model to optimise an additional beach control structure to the North of Kellogg Creek, which further reduced north-south sediment drift and allowed the creek mouth to remain open. All beach control structures, with the exception of the leeside trunk armour of breakwater BW2-5 (Panels 28 and 29), were substantially intact at the end of the stability testing campaign. As with Area 1, where a piled central breakwater section was included (specifically breakwaters BW2-4 to BW2-6), then the potential for crest armour damage was reduced with these configurations.

The optimised layout for Area 3 consisted of five beach control structures of various cross-sections and armourstone grades. Again, it was demonstrated that a stable beach could be maintained with a reduced north-south sediment drift using this configuration. The beaches remained static during the stability tests, with a wide crest at the beach maintained throughout. All structures were substantially intact at the end of the testing campaign.

# 9. References

CEM (2002), Coastal Engineering Manual (CEM), Engineer Manual 1110-2-1100, U.S. Army Corps of Engineers, Washington, D.C. (6 volumes).

CERC, (1984) Coastal Engineering Research Centre, "Shore Protection Manual." CERC, US Government Printing Office, Washington, Vols 1 & 2.COSMOS-2D Nearshore sediment transport model. Description of model structure and input. HR Wallingford Internal Report, HR, 1994.

CIRIA, CUR, CETMEF (2007). The Rock Manual. The use of rock in hydraulic engineering (2nd edition). C683, CIRIA, London.

Dean, R.G. (1985), "Physical Modelling of Littoral Processes," In: R.A. Dalrymple, Physical Modelling in Coastal Eng., 1985.

Engelund F., (1953) 'The Laminar and Turbulent Flows of Ground Water through Homogeneous Sand', Trans. Danish Acad Tech Sci, 3(4), 1953.

Haliermeier, R. J. (1978). “Uses for a calculated limit depth to beach erosion.” Proceedings, 16th Coastal Engineering Conference, American Society of Civil Engineers, 1493-15 12.

Haliermeier, R. J. (1981). “A profile zonation for seasonal sand beaches from wave climate,” Coastal Engineering 4,253-277.

HR Wallingford. (2021), Lake Michigan beach protection – 2D physical modelling final report, DKR6353-RT001-R01-00.

HYDRALAB III, 2007 Guidelines for physical model testing of breakwaters: rubble mound breakwaters, HYDRALAB III Deliverable NA3.1, Version 1.3.

Jensen O J and Klinting P., (1983), 'Evaluation of Scale Effects in Hydraulic Models by Analysis of Laminar and Turbulent Flows', Coastal Engineering, pp 319-329, 1983.

Kamphuis J W (1983):"Preliminary Discussion of Scale Effects Tests on Large Coastal Mobile Bed Models"; Proc. Canadian Coastal Conference 1983, Vancouver, BC, pp.237-251, May.

Noda E K (1971):"Coastal Movable-bed Scale-model Relationship"; Tetra Tech Inc., Final Report No.P-71-191-1, March.

Soulsby, R. (1997). Dynamics of marine sands a manual for practical applications. Thomas Telford Services Limited, London.

Soulsby, R. & Whitehouse, R. J. S. (1997) Threshold of sediment motion in coastal environments. Proc. Pacific Coasta and Ports 97 Conf., Christchurch, 1, pp. 149-154, University of Canterbury, NZ.

Via-Estrem, Lluis & Pullen, Tim & Stewart, Terry & Allsop, William. (2013). Damage to Rubble Mound Breakwaters – Extracting Design Guidance from 'Old' Test Data. 10.1680/fsts.59757.015.

# Appendices

## A. Rock grading curves

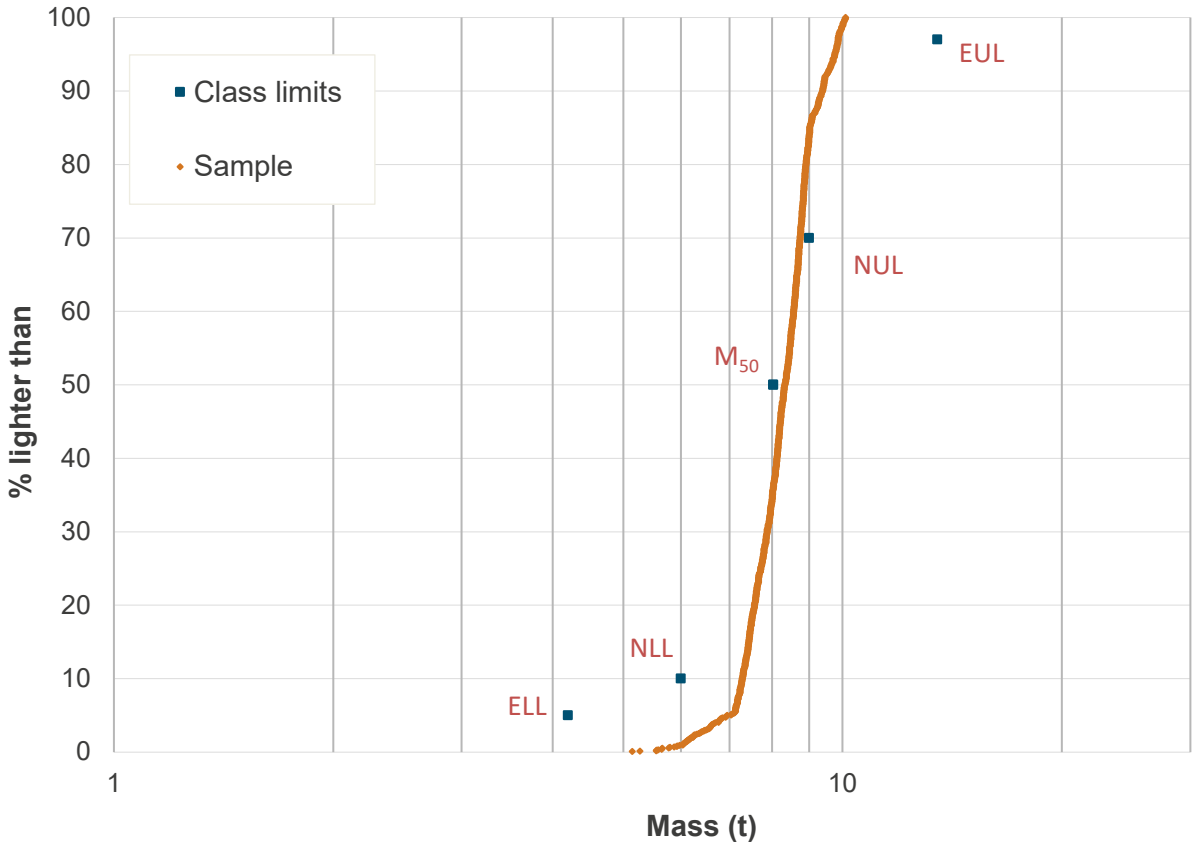


Figure A.1: Model material grading curve for 6-9 t rock

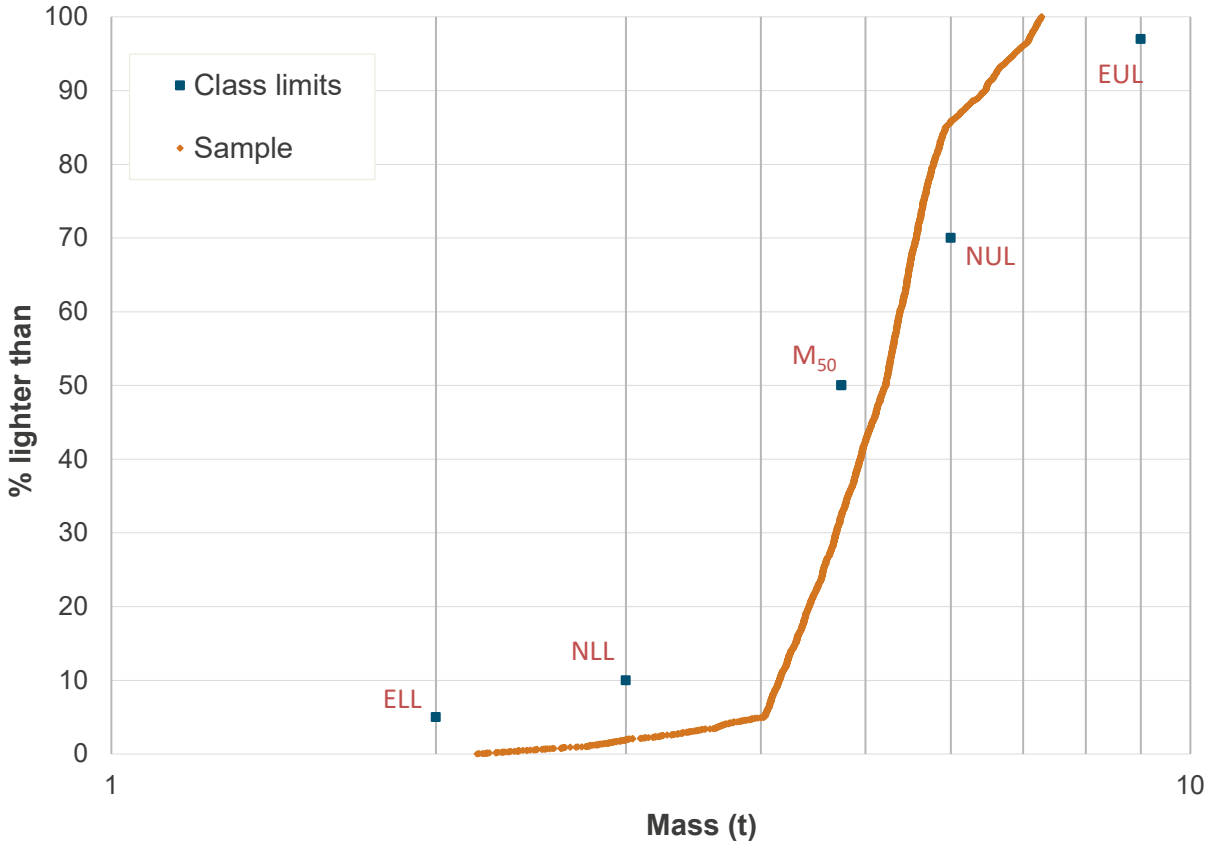


Figure A.2: Model material grading curve for 3-6 t rock

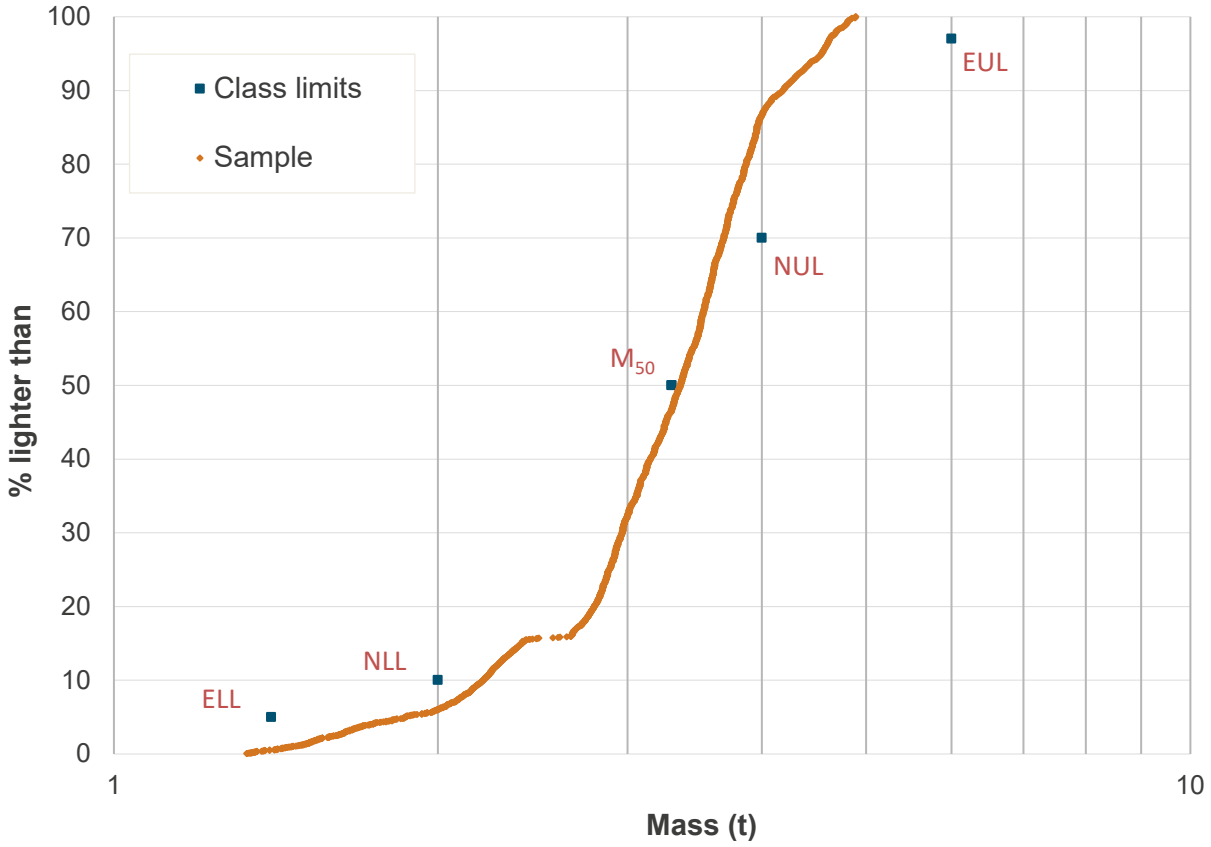


Figure A.3: Model material grading curve for 2-4 t rock

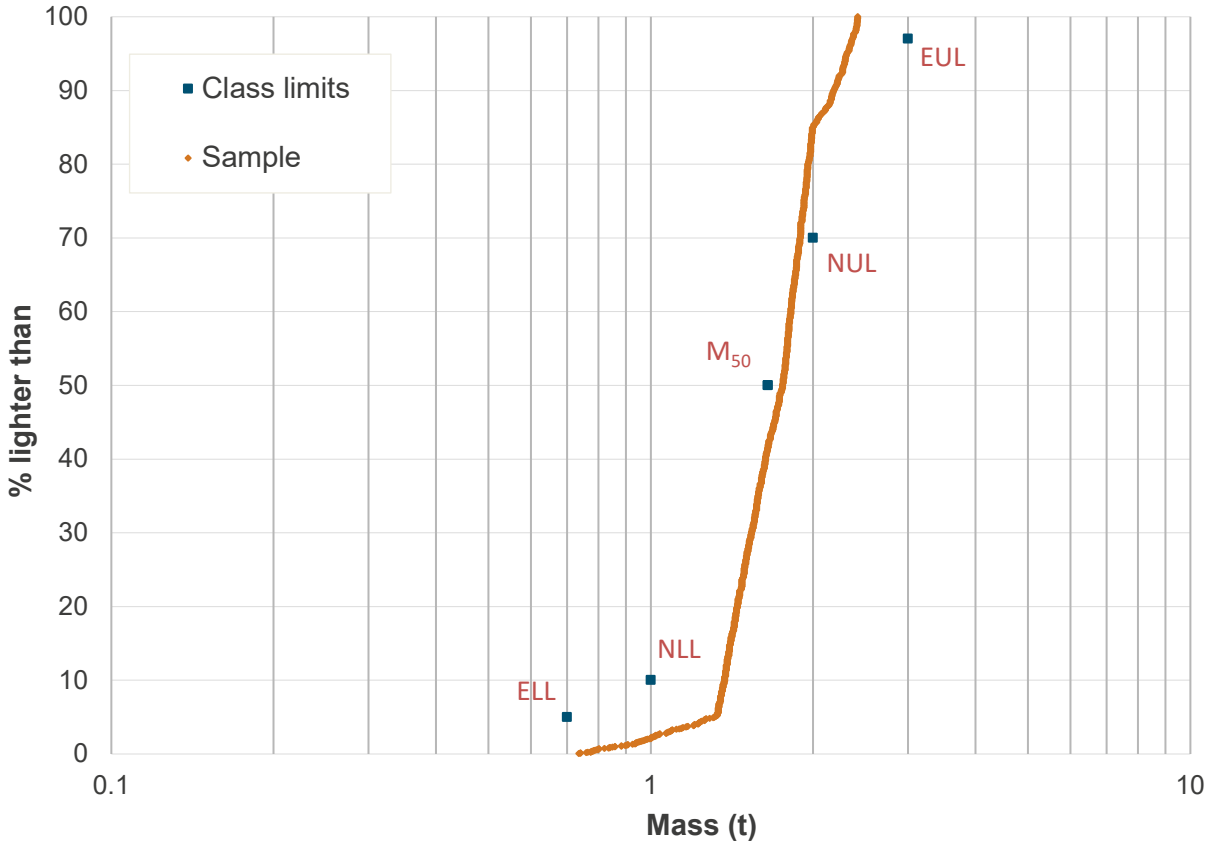


Figure A.4: Model material grading curve for 1-2 t rock

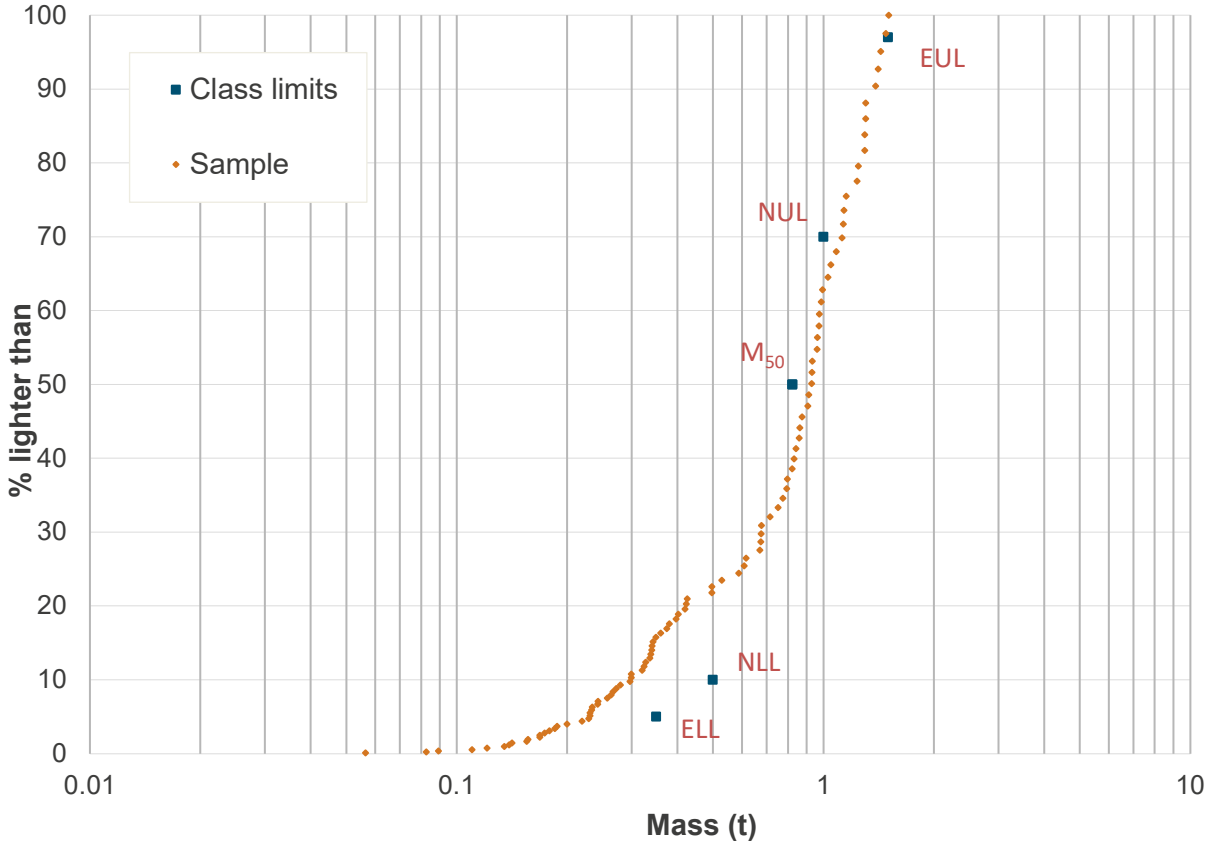


Figure A.5: Model material grading curve for 0.5-1 t rock

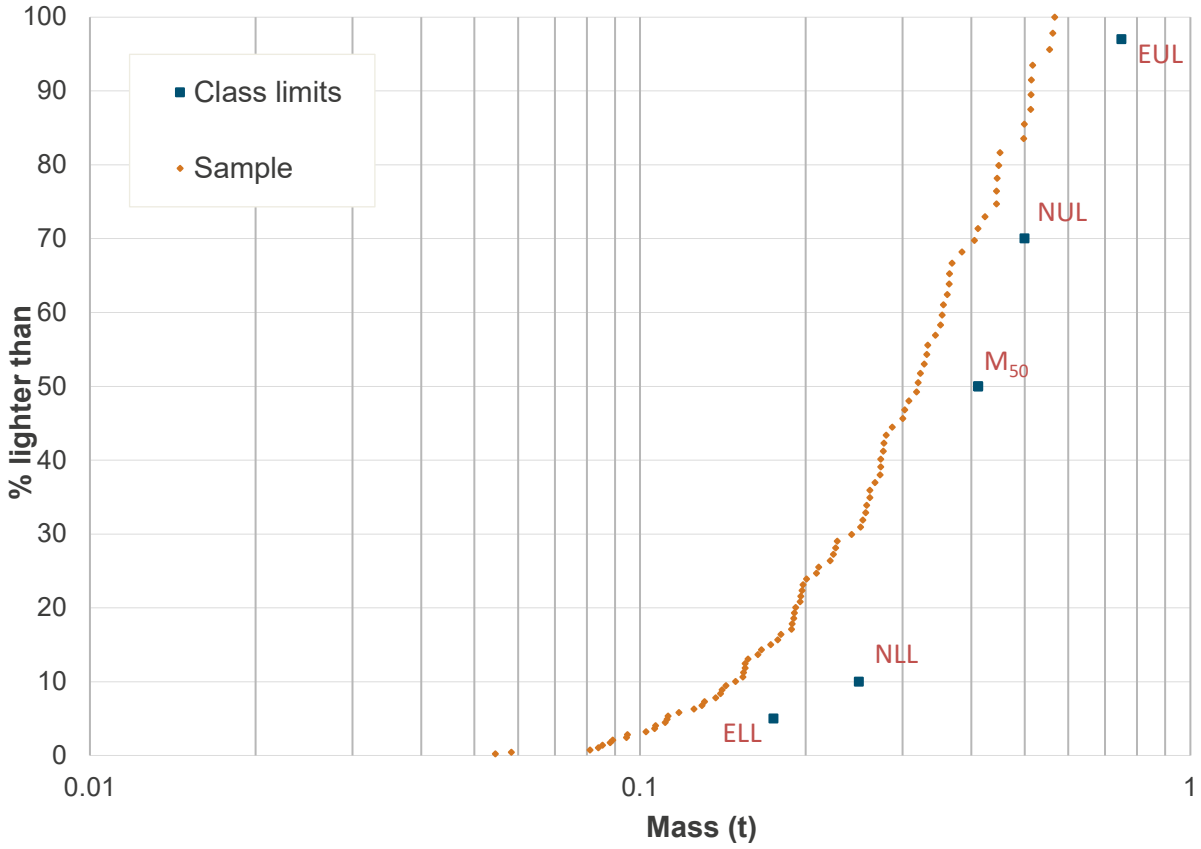


Figure A.6: Model material grading curve for 0.25-0.5 t rock

# B. Area 1 – North Beach: morphological and stability photographs and scan data

## B.1. Morphological photographs

### B.1.1. Configuration 01 – Initial configuration

Configuration 01 was the starting point for the optimisation of the beach control structures, and was provided in *2020-0617 Illinois Beach State Park Shoreline Stabilization.pdf* (Figure 5.4). This configuration was tested for 1.5 hrs then two 3 hr tests (15 minutes then 2 x 30 minutes model). The pre and post-test photographs from the 'North' and 'South' time-lapse camera views are shown in Figure B.1 and Figure B.2.

Figure B.1: Pre (top) and post-test (bottom) photographs from 'North' view for Configuration 01

Figure B.2: Pre (top) and post-test (bottom) photographs from ‘South’ view for Configuration 01

### B.1.2. Configuration 02

Configuration 02 differed from Configuration 01 with the removal of three sandbags from the 'dog leg' in the southernmost breakwater, making the central section submerged. This configuration was tested for two 3 hr tests (2 x 30 minutes model). The pre and post-test photographs from the 'North' and 'South' time-lapse camera views are shown in Figure B.4 and Figure B.5. The post-test scan data is shown in Figure B.3.

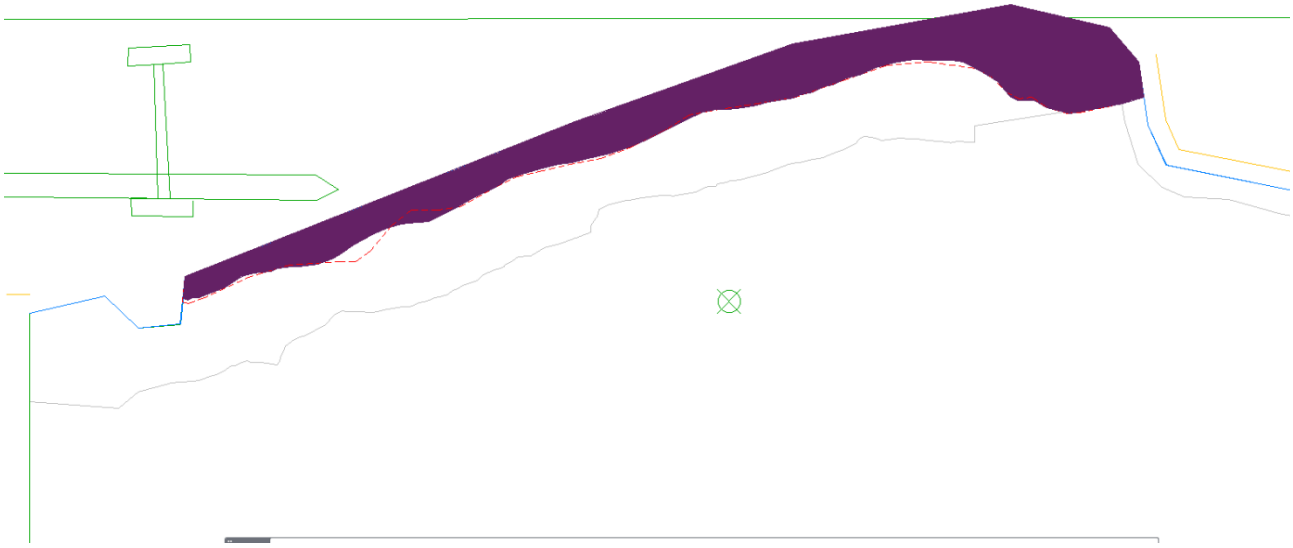

Figure B.3: Post-test scan data for Configuration 02 (Scan04), dotted line pre-test, solid area post-test

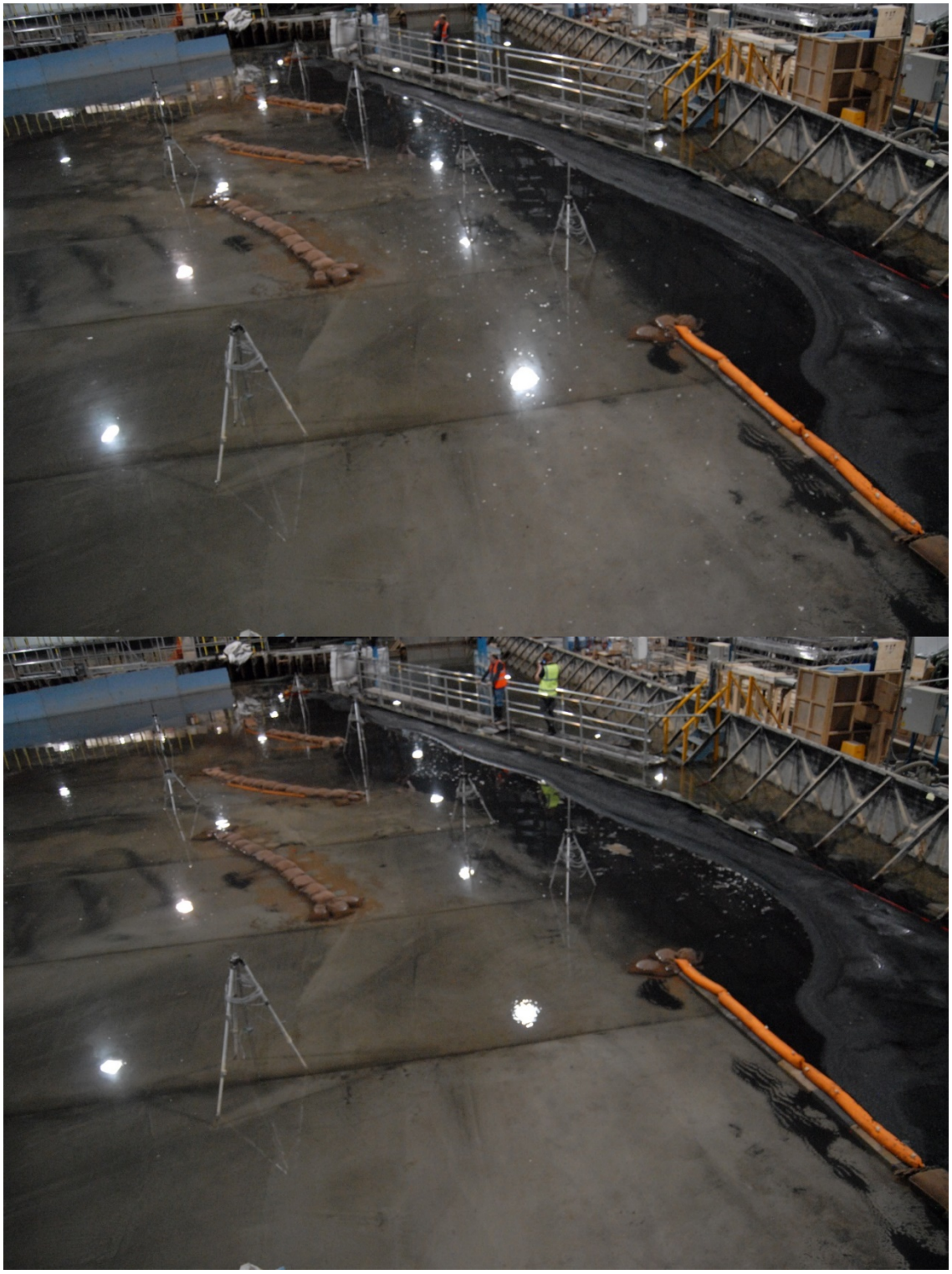

Figure B.4: Pre (top) and post-test (bottom) photographs from 'North' view for Configuration 02

Figure B.5: Pre (top) and post-test (bottom) photographs from 'South' view for Configuration 02

### B.1.3. Configuration 03

Configuration 03 differed from Configuration 02 with the removal of the central submerged section of the southern breakwater to create two breakwaters, and the extension of the southernmost new breakwater with a submerged section of three concrete blocks. This configuration was tested once for 3 hr (30 minutes model). The pre and post-test photographs from the 'North' and 'South' time-lapse camera views are shown in Figure B.7 and Figure B.8. The post-test scan data is shown in Figure B.6.

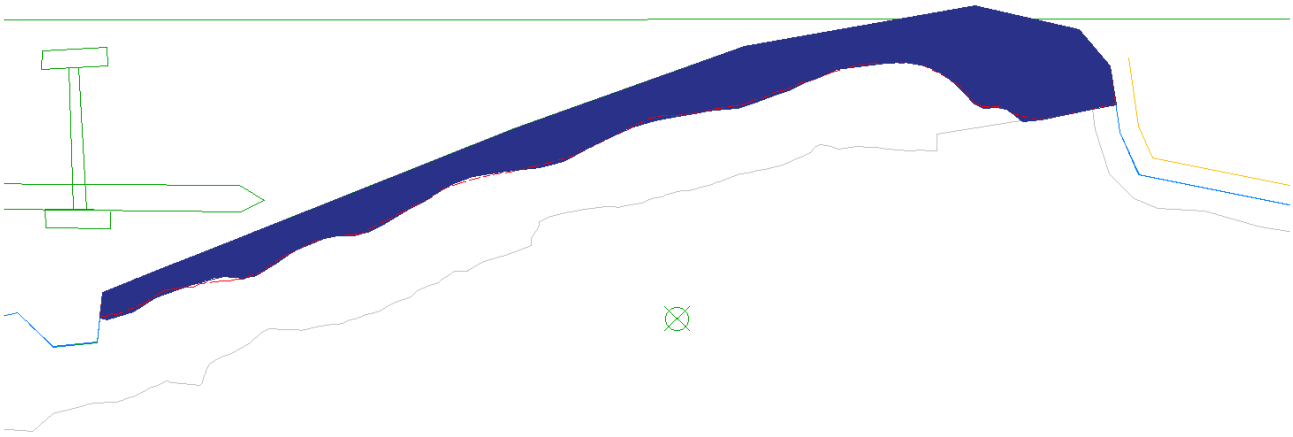

Figure B.6: Post-test scan data for Configuration 03 (Scan05), dotted line pre-test, solid area post-test

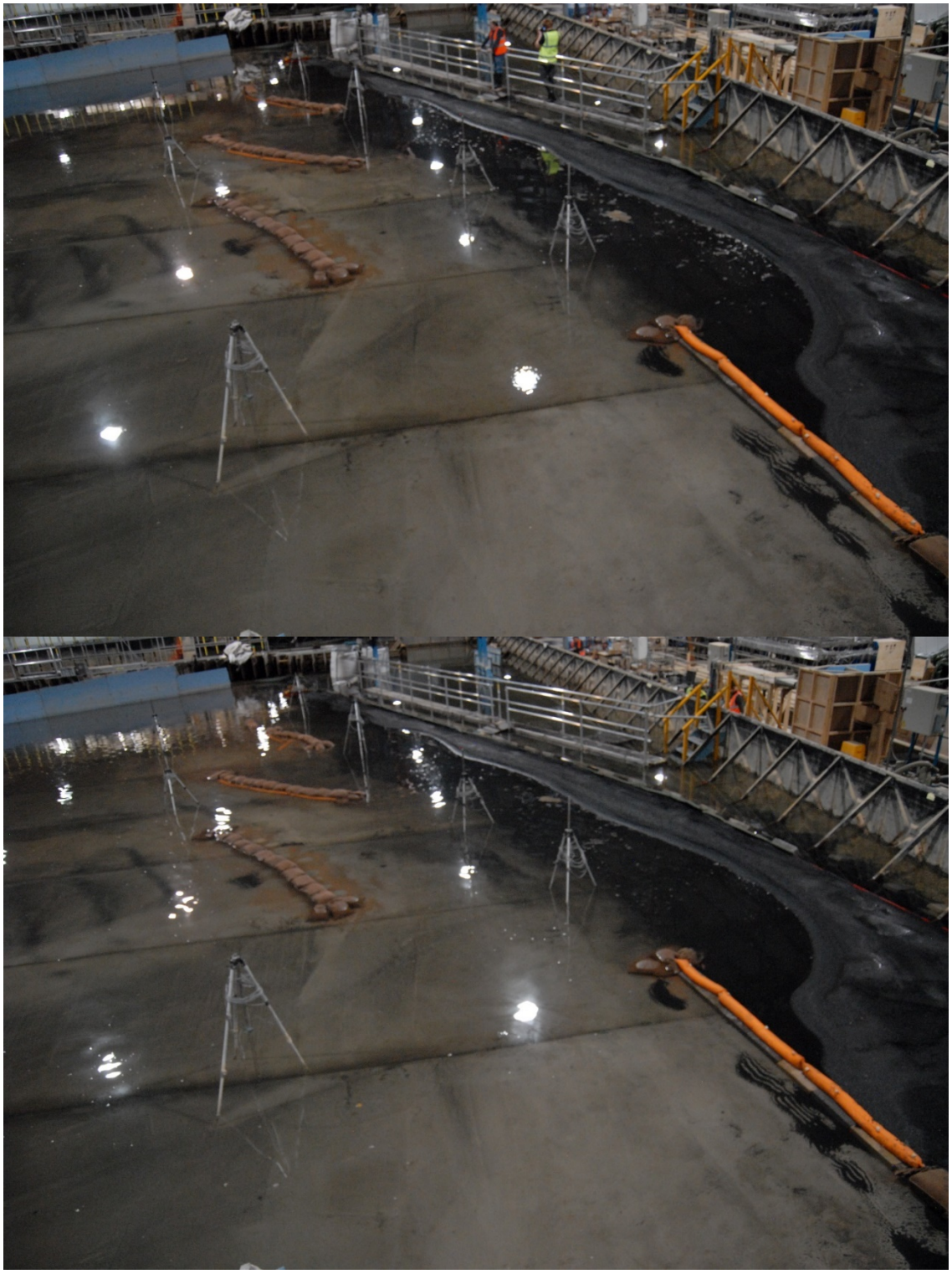

Figure B.7: Pre (top) and post-test (bottom) photographs from 'North' view for Configuration 03

Figure B.8: Pre (top) and post-test (bottom) photographs from ‘South’ view for Configuration 03

### B.1.4. Configuration 04

Configuration 04 differed from Configuration 03 with the removal of the submerged extension on the southernmost breakwater, straightening of the northern half of the second most southern breakwater, rotation of the northern end of the 'middle' breakwater to be more shore parallel, and the fish tail removed from the southern end of shore connected breakwater and a 45° extension added (pointing away from shore). This configuration was tested once for 3 hr (30 minutes model). The pre and post-test photographs from the 'North' and 'South' time-lapse camera views are shown in Figure B.10 and Figure B.11. The post-test scan data is shown in Figure B.9.

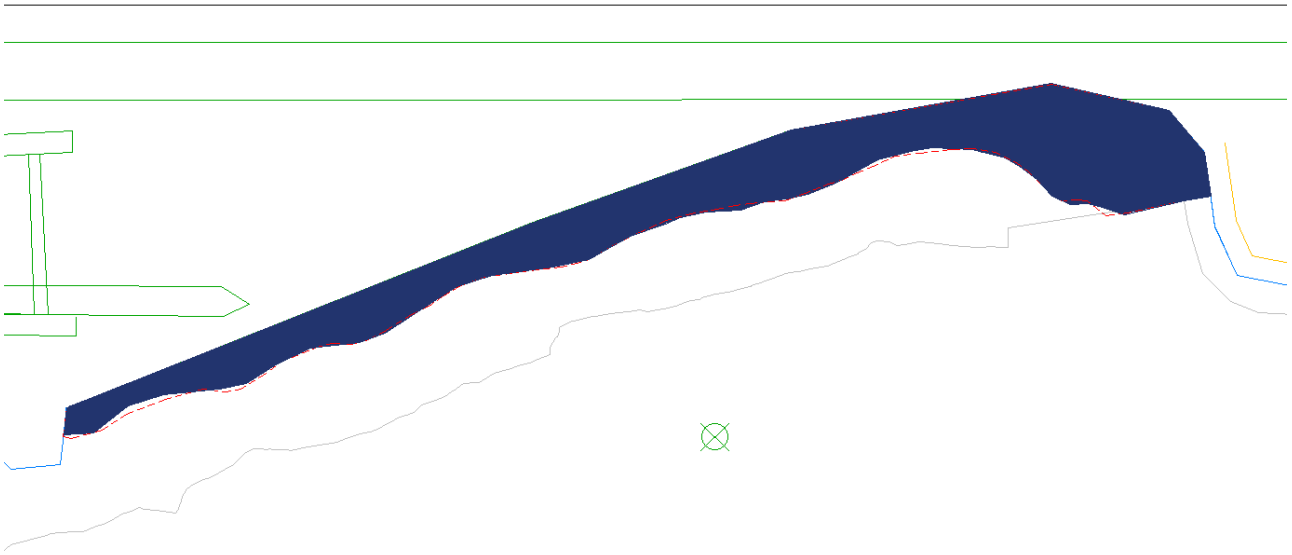

Figure B.9: Post-test scan data for Configuration 04 (Scan06), dotted line pre-test, solid area post-test

Figure B.10: Pre (top) and post-test (bottom) photographs from ‘North’ view for Configuration 04

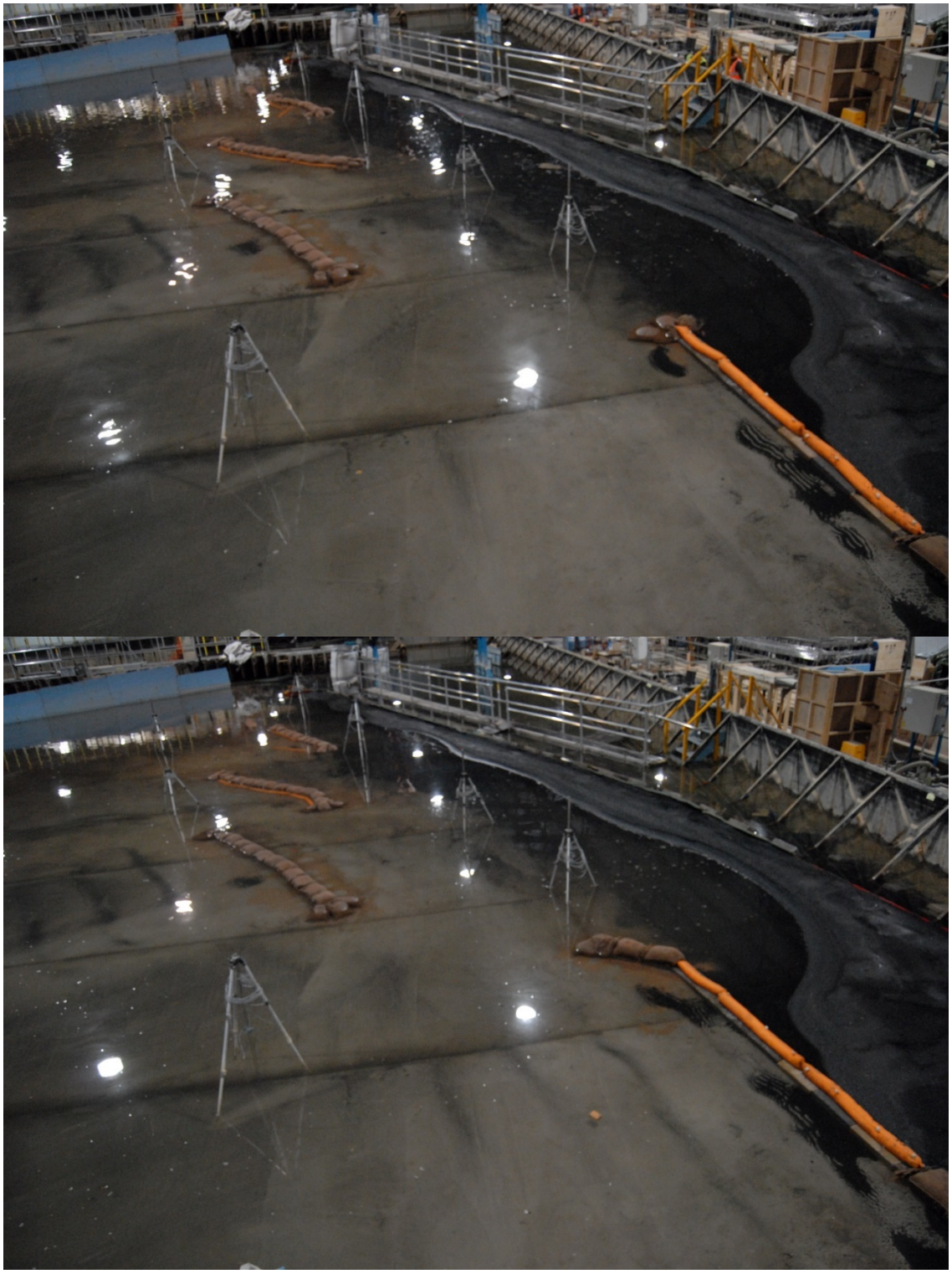

Figure B.11: Pre (top) and post-test (bottom) photographs from 'South' view for Configuration 04

## B.1.5. Configuration 05

Configuration 05 differed from Configuration 04 with the addition of a small (two concrete block) submerged breakwater close to shore on the lee of the northern end of the northernmost detached breakwater. The penultimate southern breakwater was split into two with a small shore perpendicular 'dog leg' added to the southern end of the northern most of the new breakwaters. This configuration was tested once for 3 hr (30 minutes model). The pre and post-test photographs from the 'North' and 'South' time-lapse camera views are shown in Figure B.13 and Figure B.14. The post-test scan data is shown in Figure B.12.

Figure B.12: Post-test scan data for Configuration 05 (Scan07), dotted line pre-test, solid area post-test

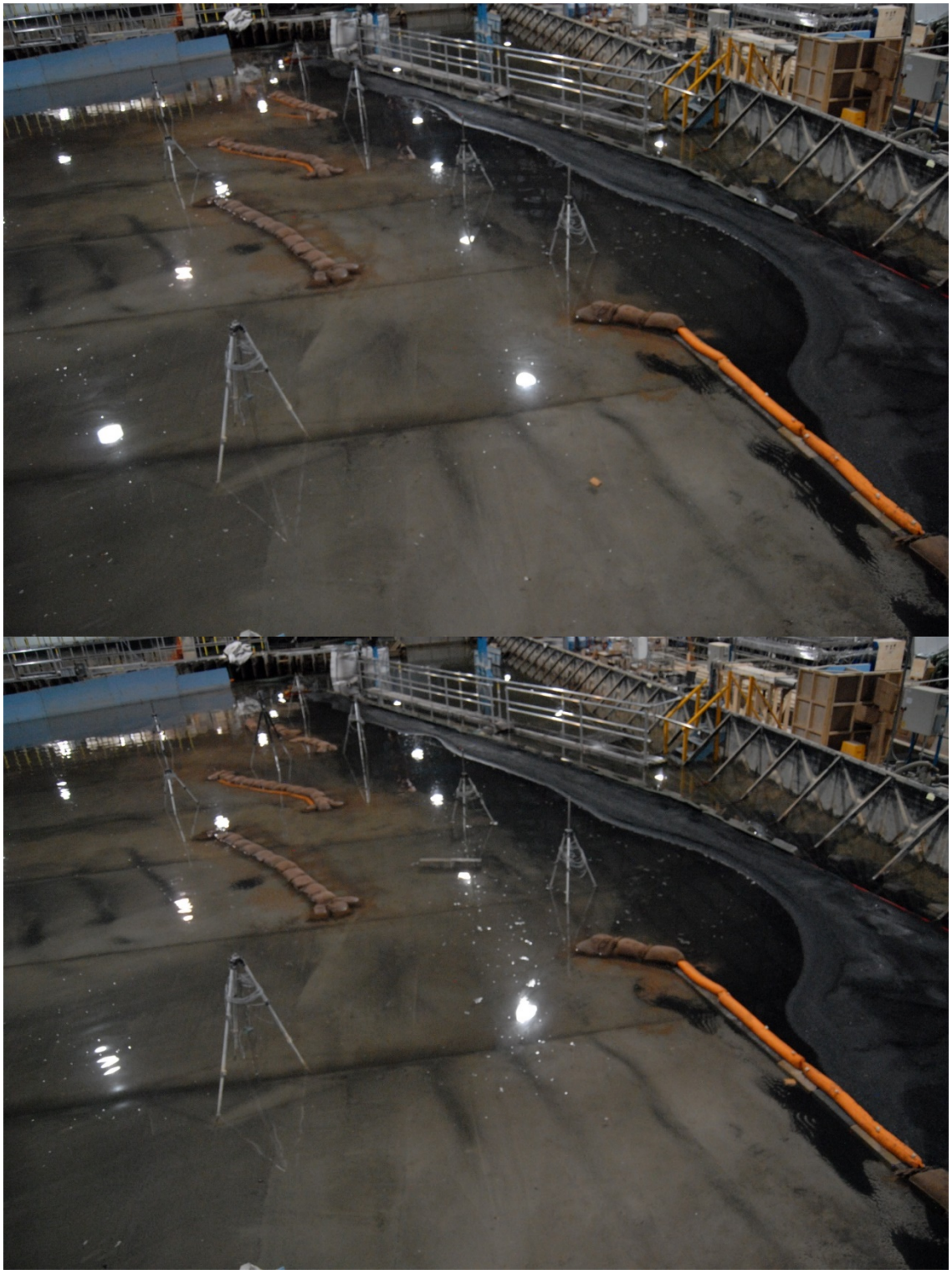

Figure B.13: Pre (top) and post-test (bottom) photographs from ‘North’ view for Configuration 05

Figure B.14: Pre (top) and post-test (bottom) photographs from ‘South’ view for Configuration 05

## B.1.6. Configuration 06

Configuration 06 differed from Configuration 05 with the removal of the extension to the shore connected breakwater, splitting the 'middle' detached breakwater into two and extending the northern part to overlap the now detached southern part. The small near-shore breakwater was extended to three concrete blocks, made emergent and moved northwards to between the northernmost detached breakwater and the shore connected breakwater. The beach was also re-set (re-screeded) between Configuration 05 and 06. Configuration 06 was tested twice for 3 hrs (2 x 30 minutes model). The pre and post-test photographs from the 'North' and 'South' time-lapse camera views are shown in Figure B.16 and Figure B.17. The post-test scan data is shown in Figure B.15.

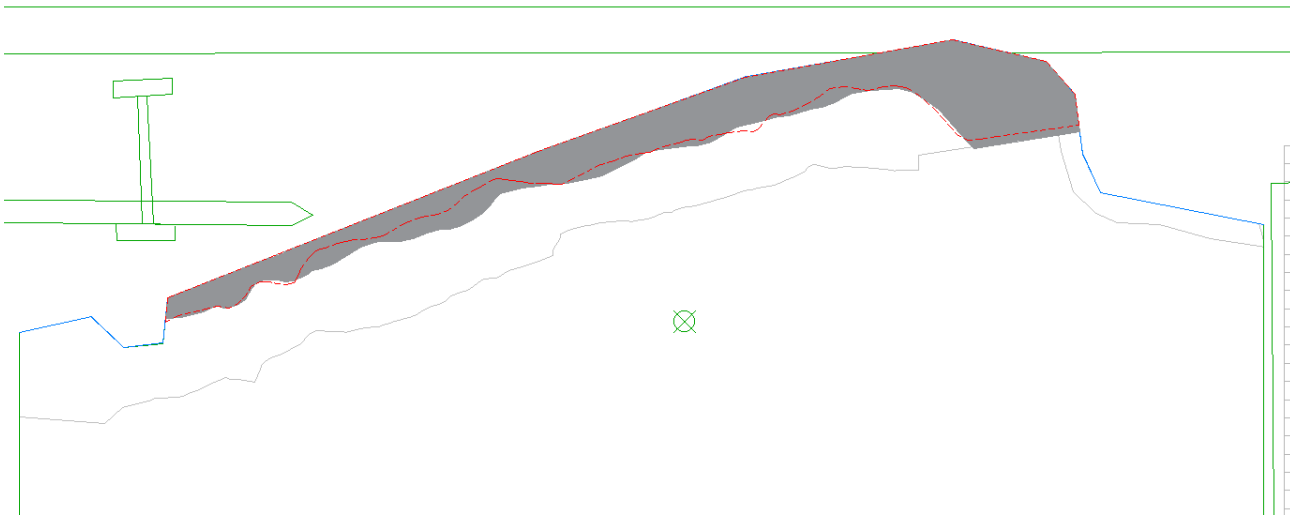

Figure B.15: Post-test scan data for Configuration 06 (Scan09), dotted line pre-test, solid area post-test

Figure B.16: Pre (top) and post-test (bottom) photographs from ‘North’ view for Configuration 06

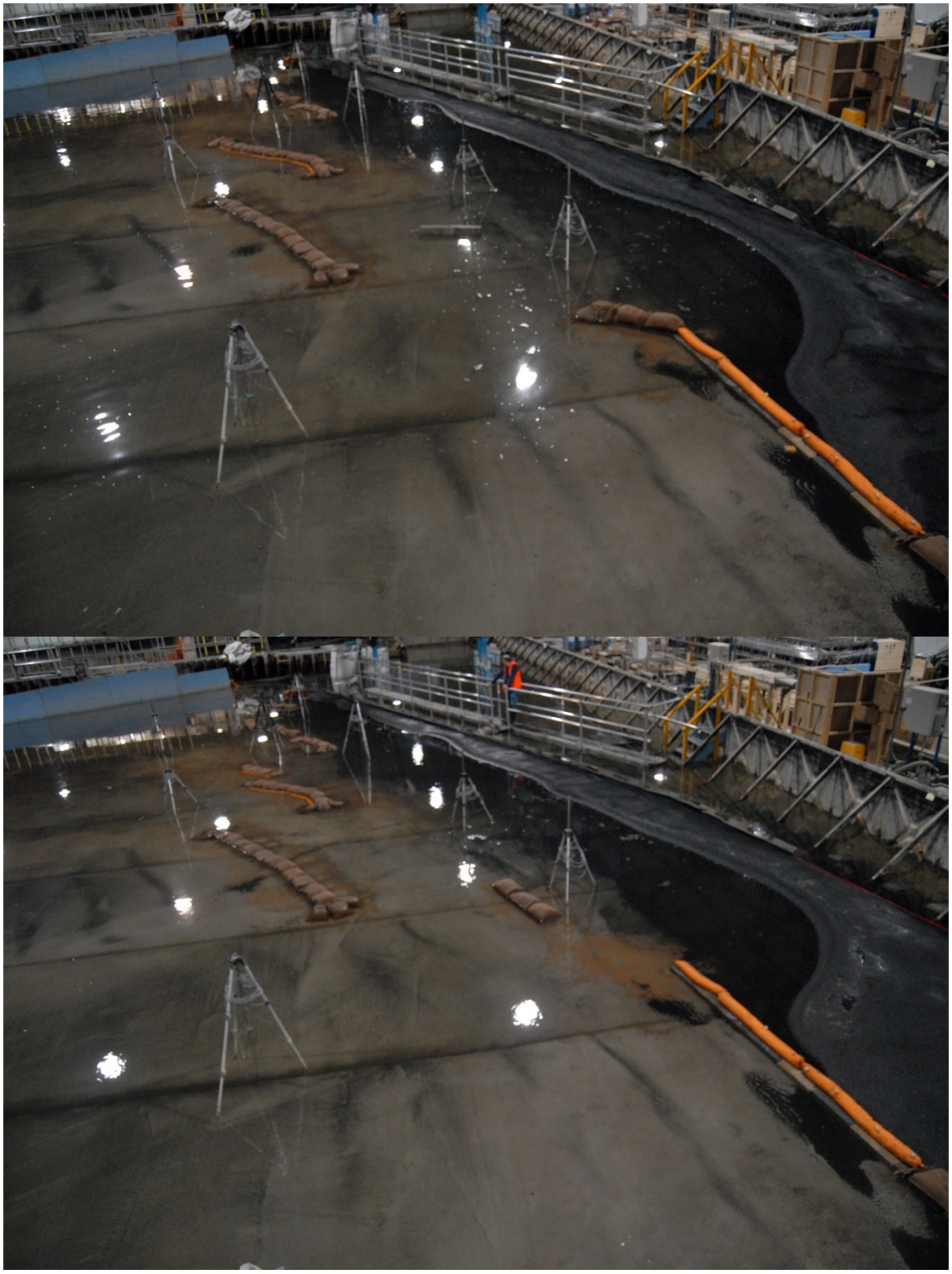

Figure B.17: Pre (top) and post-test (bottom) photographs from 'South' view for Configuration 06

### B.1.7. Configuration 07

Configuration 07 differed from Configuration 06 with the re-connecting of the 'middle' breakwater, a widening and extending of the fishtail on the southern end of the penultimate southernmost breakwater and the 'dog legged' extension to the north end of the northernmost breakwater in the southern group of three. This configuration was tested once for 3 hr (30 minutes model). The pre and post-test photographs from the 'North' and 'South' time-lapse camera views are shown in Figure B.18 and Figure B.19.

Figure B.18: Pre (top) and post-test (bottom) photographs from ‘North’ view for Configuration 07

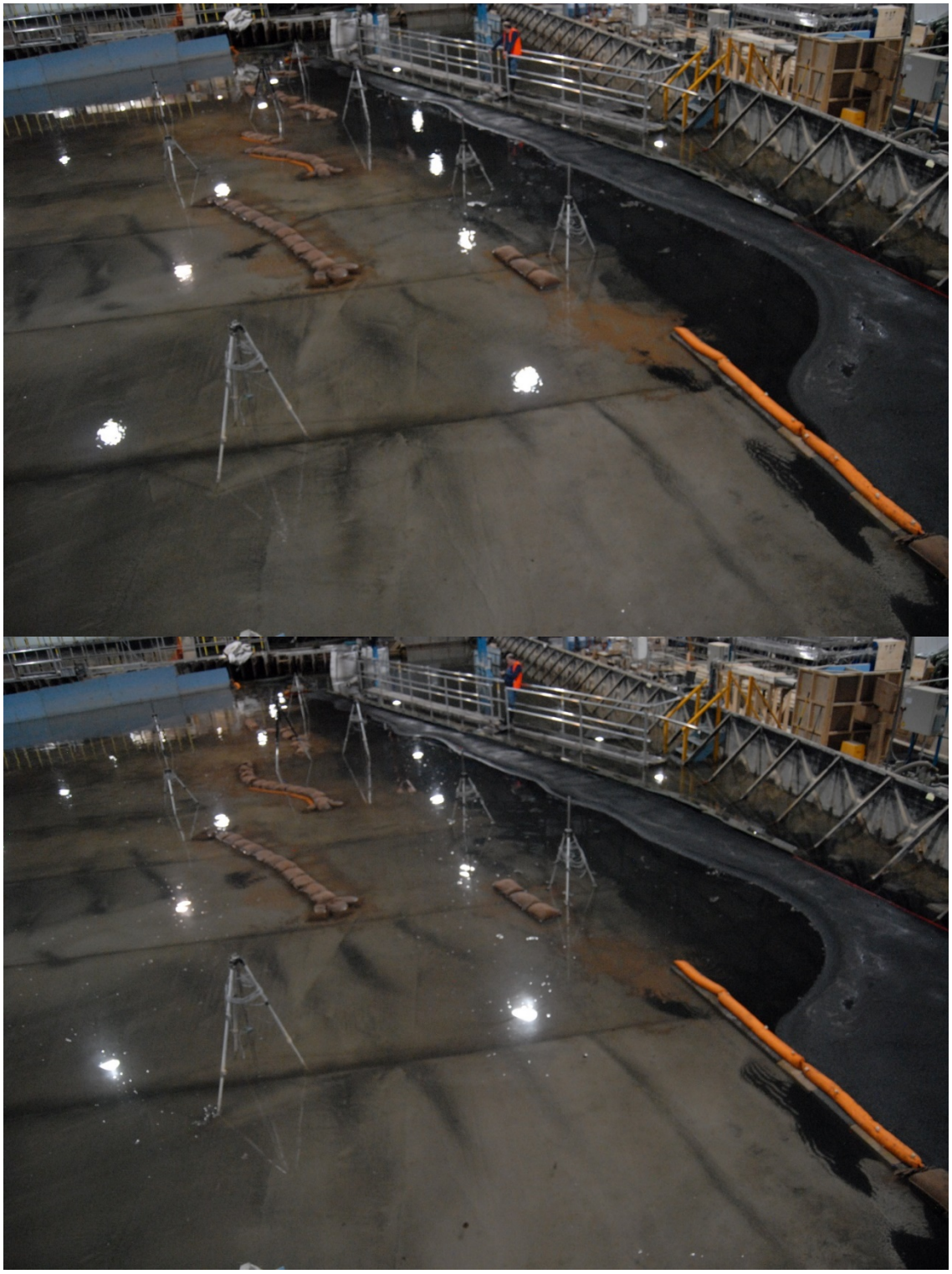

Figure B.19: Pre (top) and post-test (bottom) photographs from ‘South’ view for Configuration 07

### B.1.8. Configuration 08

Configuration 08 differed from Configuration 07 with the extension to the north of the middle of the three southern breakwaters and the shortening (from the south) of the northernmost of the three. This configuration was tested once for 3 hr (30 minutes model). The pre and post-test photographs from the 'North' and 'South' time-lapse camera views are shown in Figure B.20 and Figure B.21.

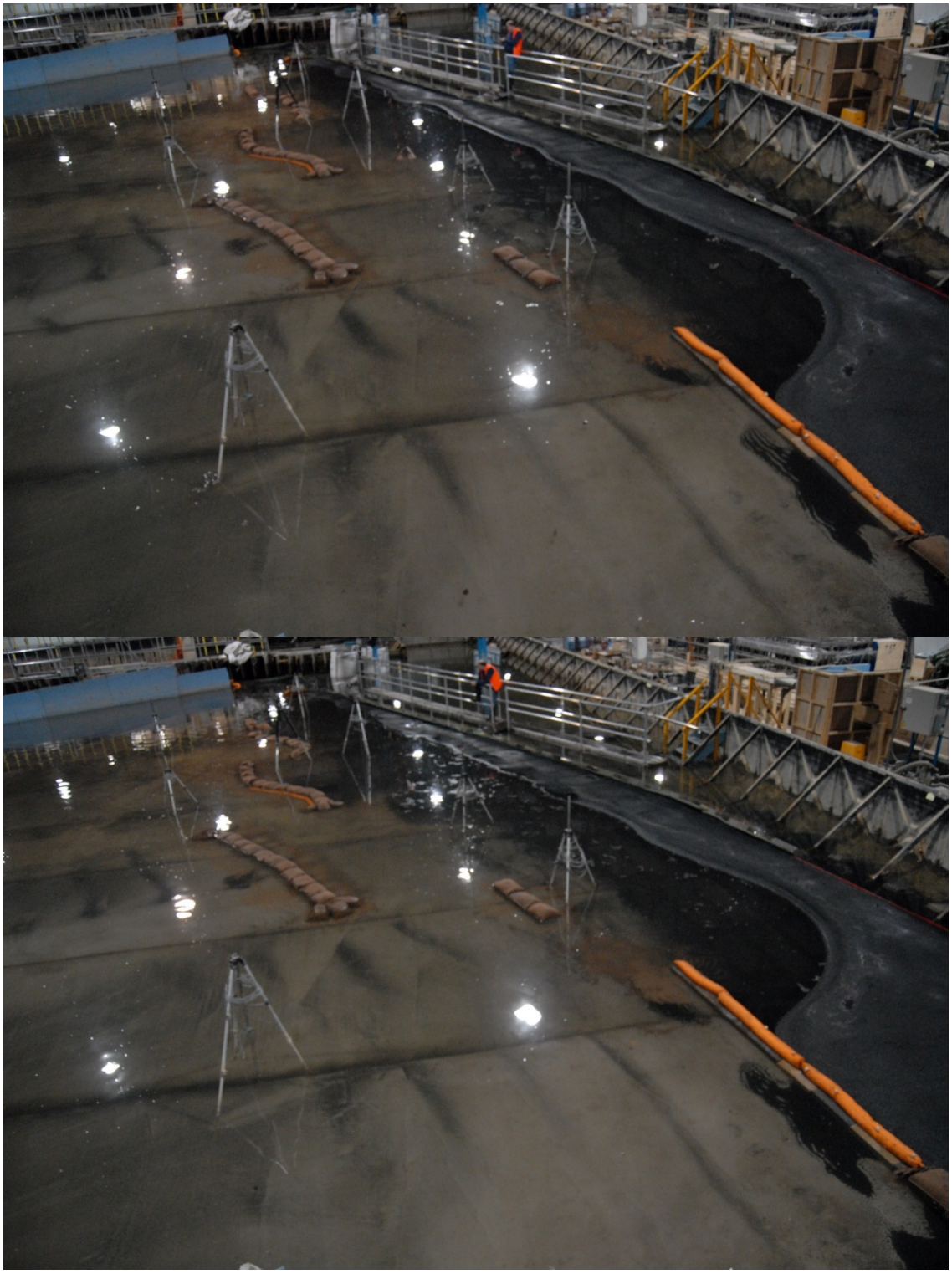

Figure B.20: Pre (top) and post-test (bottom) photographs from ‘North’ view for Configuration 08

Figure B.21: Pre (top) and post-test (bottom) photographs from ‘South’ view for Configuration 08

### B.1.9. Configuration 09

Configuration 09 differed from Configuration 08 with the combining of the two northernmost breakwaters in the southern group of three, the removal of the fishtails and the extension of the southernmost breakwater to the north to finish parallel with the southern end of the newly combined breakwater. This configuration was tested once for 3 hr (30 minutes model). The pre and post-test photographs from the 'North' and 'South' time-lapse camera views are shown in Figure B.22 and Figure B.23.

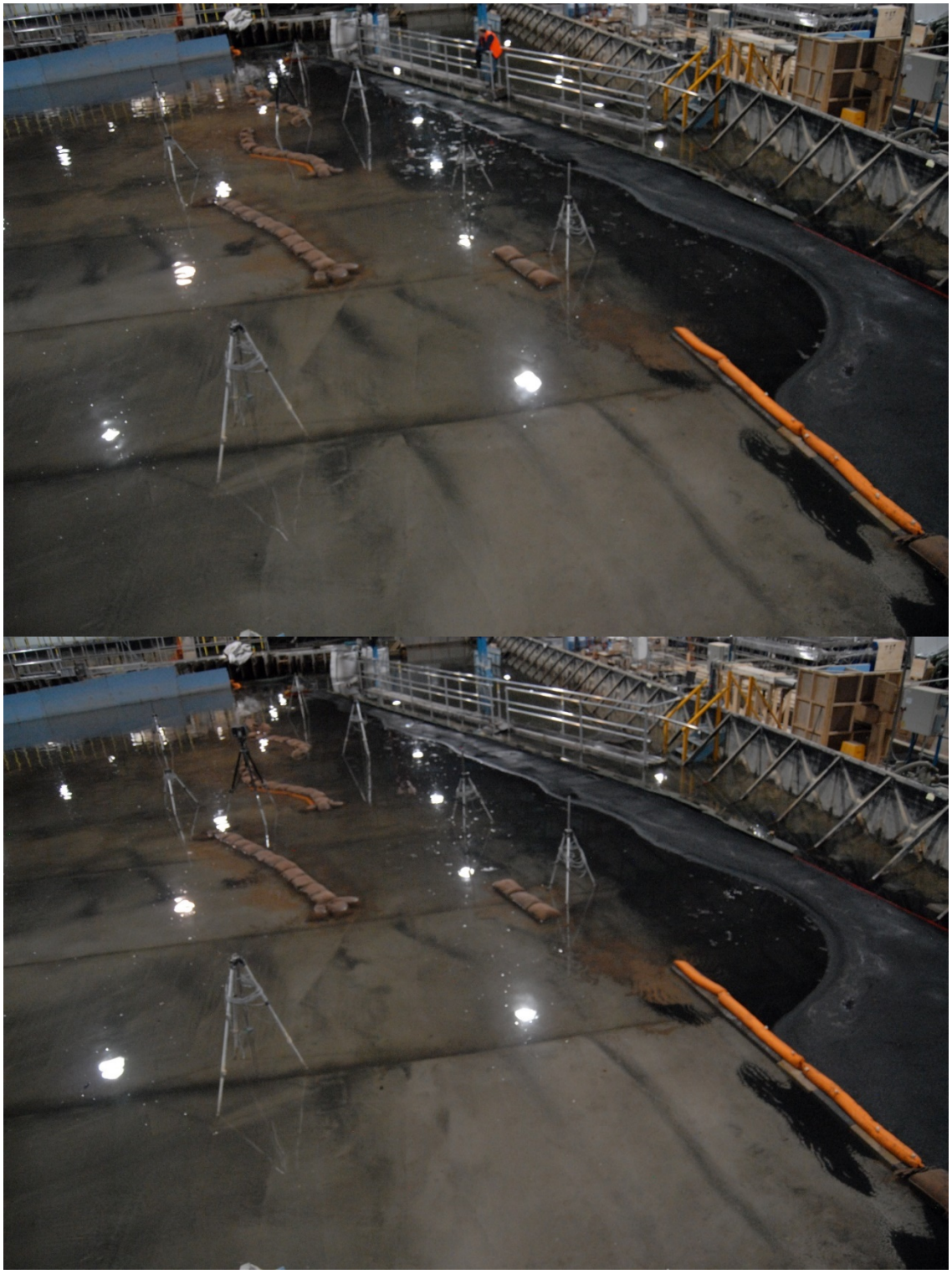

Figure B.22: Pre (top) and post-test (bottom) photographs from ‘North’ view for Configuration 09

Figure B.23: Pre (top) and post-test (bottom) photographs from ‘South’ view for Configuration 09

## B.1.10. Configuration 10

Configuration 10 differed from Configuration 09 with the removal of three sandbags from the dog leg in the southernmost breakwater, making the centre submerged. The beach was also re-set (re-screeded) between Configuration 09 and 10. This configuration was tested for five 3 hr tests (5 x 30 minutes model). The pre and post-test photographs from the 'North' and 'South' time-lapse camera views are shown in Figure B.26 and Figure B.27. The post-test scan data is shown in Figure B.24 and Figure B.25 showing the post-test beach shape and the structure layout respectively.

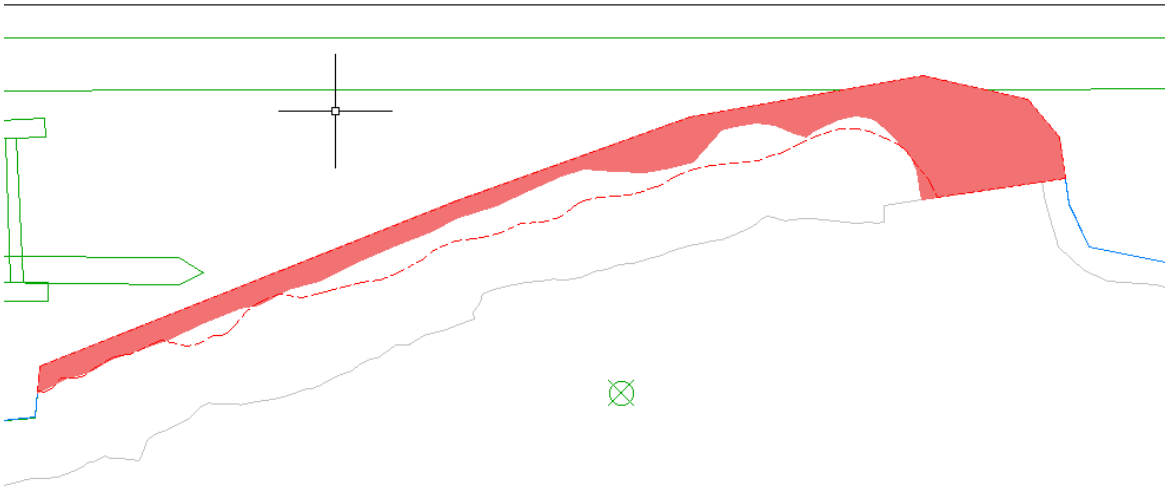

Figure B.24: Post-test scan data for Configuration 10 (Scan12), dotted line pre-test, solid area post-test

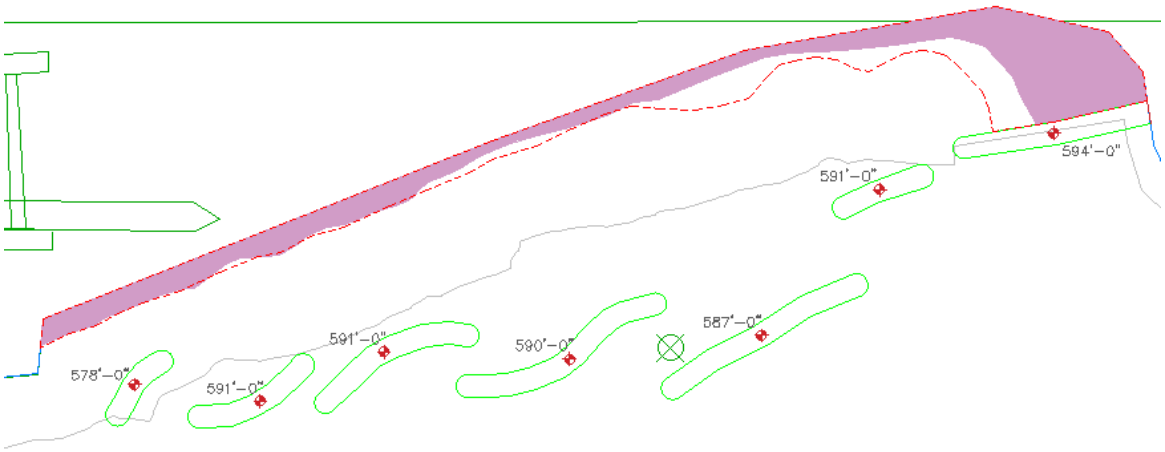


Figure B.25: Post-test scan data for Configuration 10 (Scan13), basin drained to allow structures to be identified (outlined in green)

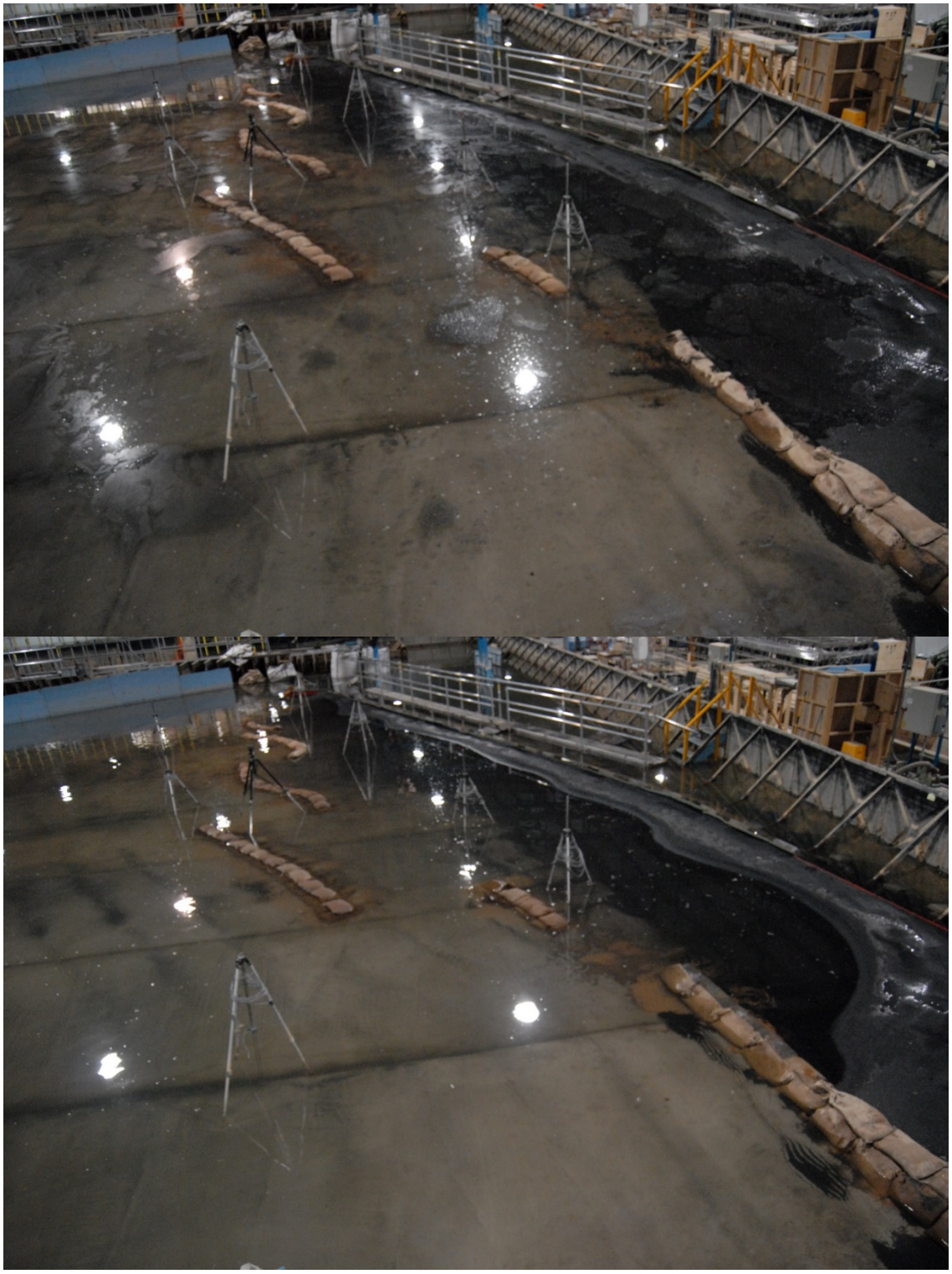

Figure B.26: Pre (top) and post-test (bottom) photographs from ‘North’ view for Configuration 10

Figure B.27: Pre (top) and post-test (bottom) photographs from ‘South’ view for Configuration 10

### B.1.11. Configuration 11

Configuration 11 differed from Configuration 10 with the removal part of the shore connected breakwater, leaving the farthest offshore two concrete blocks in place, a gap of two concrete blocks was made. This configuration was tested for four 3 hr tests (4 x 30 minutes model). The pre and post-test photographs from the 'North' and 'South' time-lapse camera views are shown in Figure B.28 and Figure B.29.

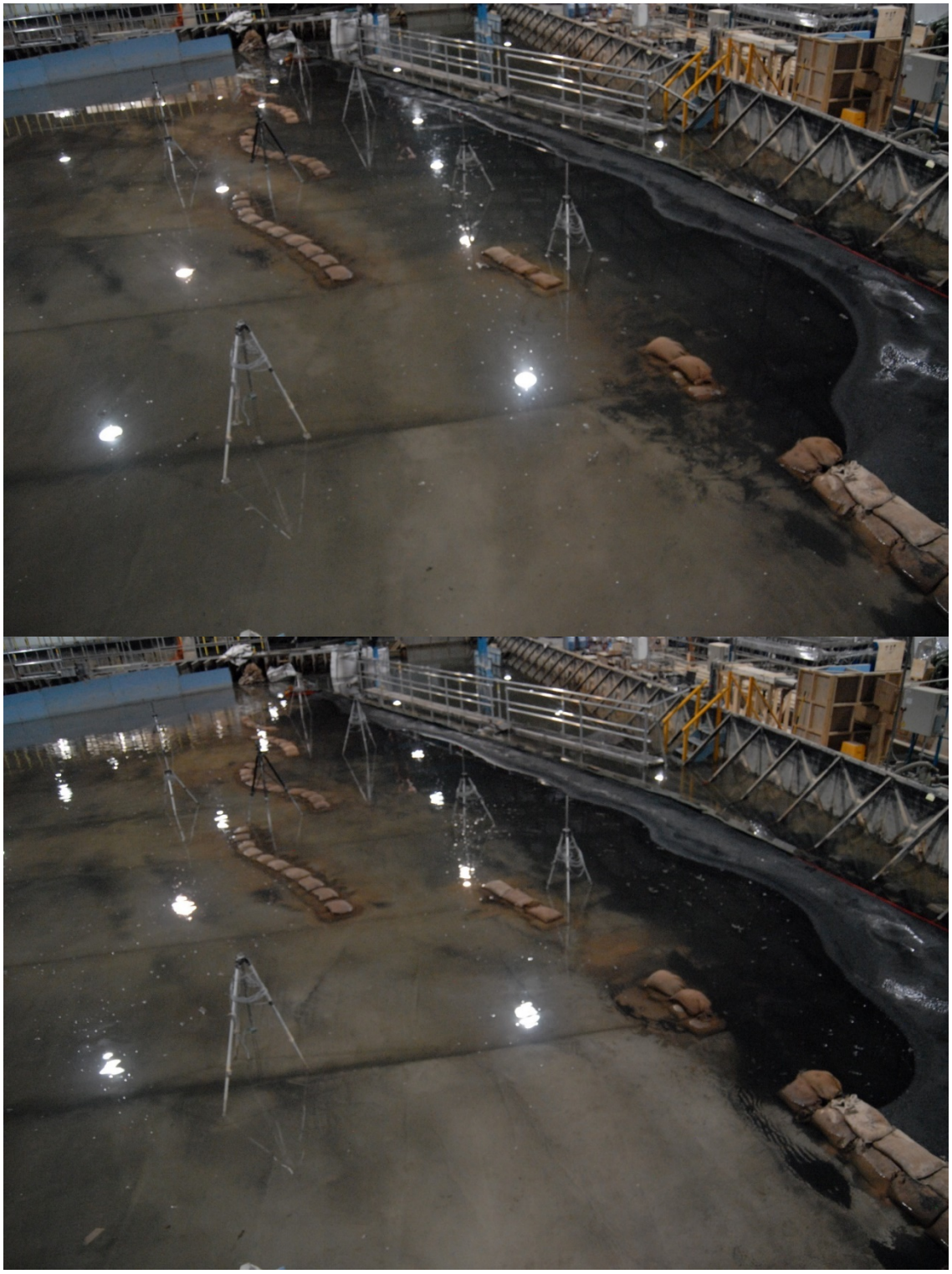

Figure B.28: Pre (top) and post-test (bottom) photographs from ‘North’ view for Configuration 11

Figure B.29: Pre (top) and post-test (bottom) photographs from ‘South’ view for Configuration 11

### B.1.12. Configuration 12

Configuration 12 differed from Configuration 11 in making the two small northernmost detached breakwaters submerged. This configuration was tested once for 3 hr (30 minutes model). The pre and post-test photographs from the 'North' and 'South' time-lapse camera views are shown in Figure B.30 and Figure B.31.

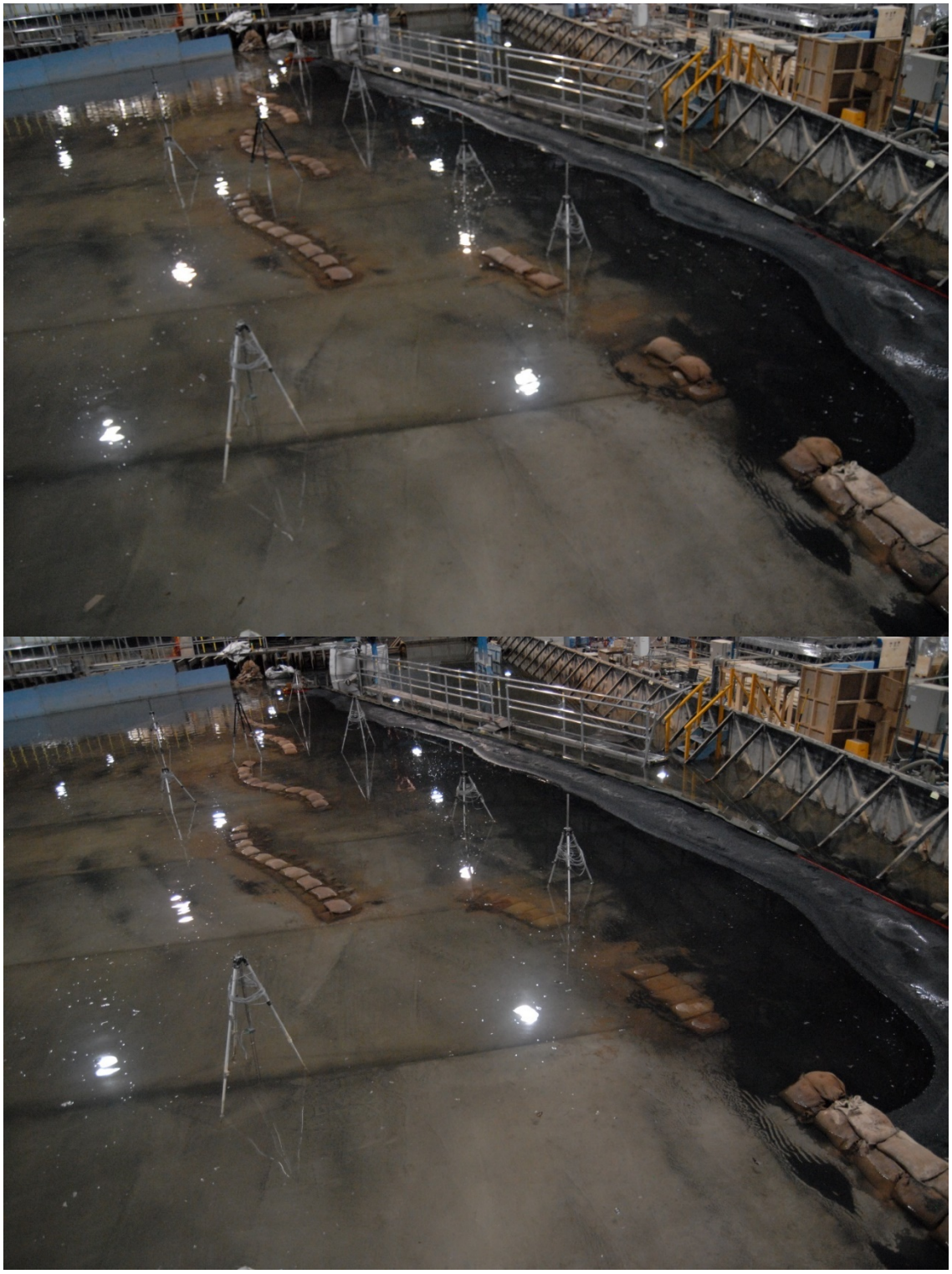

Figure B.30: Pre (top) and post-test (bottom) photographs from ‘North’ view for Configuration 12

Figure B.31: Pre (top) and post-test (bottom) photographs from ‘South’ view for Configuration 12

## B.1.13. Configuration 13

Configuration 13 differed from Configuration 12 with the dividing of the farthest seaward breakwater into two, with a gap in the middle of one concrete block. The beach was also re-set (re-screeded) between Configuration 12 and 13. This configuration was tested for six 3 hr tests (6 x 30 minutes model). The pre and post-test photographs from the 'North' and 'South' time-lapse camera views are shown in Figure B.33 and Figure B.34. The post-test scan data is shown in Figure B.32.

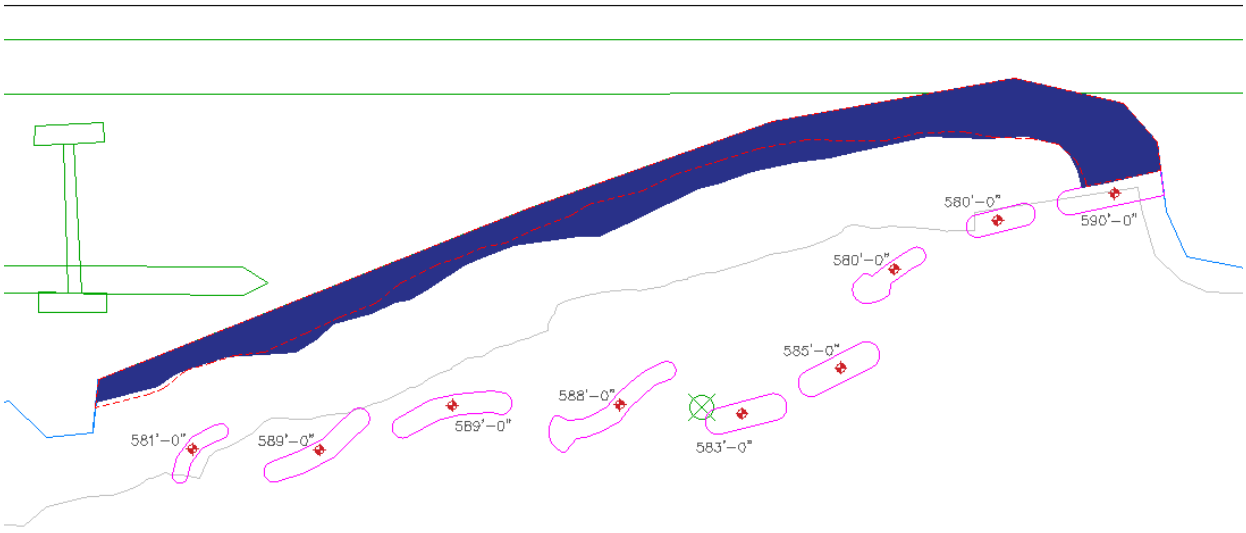


Figure B.32: Post-test scan data for Configuration 13 (Scan19), dotted line pre-test, solid area post-test, structures in magenta

Figure B.33: Pre (top) and post-test (bottom) photographs from 'North' view for Configuration 13

Figure B.34: Pre (top) and post-test (bottom) photographs from ‘South’ view for Configuration 13

### B.1.14. Configuration 14

Configuration 14 differed from Configuration 13 with the addition of a fishtail to the southern end of the southernmost breakwater. This configuration was tested once for 3 hr (30 minutes model). The pre and post-test photographs from the 'North' and 'South' time-lapse camera views are shown in Figure B.35 and Figure B.36.

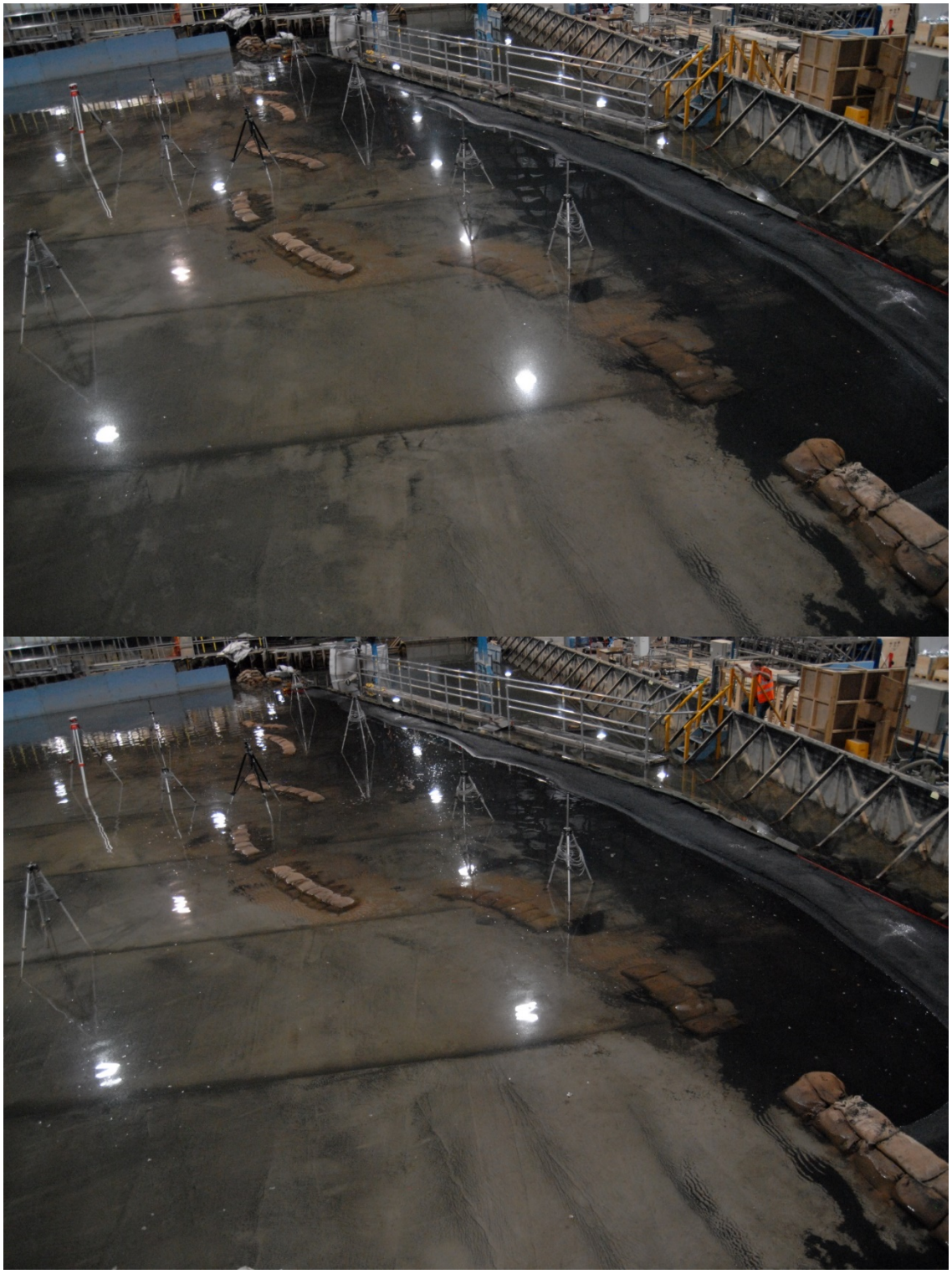

Figure B.35: Pre (top) and post-test (bottom) photographs from ‘North’ view for Configuration 14

Figure B.36: Pre (top) and post-test (bottom) photographs from ‘South’ view for Configuration 14

## B.1.15. Configuration 15

Configuration 15 differed from Configuration 14 with the addition of a new submerged breakwater to the south of those in Configuration 14. The beach was also re-set (re-screeded) between Configuration 14 and 15. This configuration was tested for five 3 hr tests (5 x 30 minutes model). The pre and post-test photographs from the 'North' and 'South' time-lapse camera views are shown in Figure B.38 and Figure B.39. The post-test scan data is shown in Figure B.37.

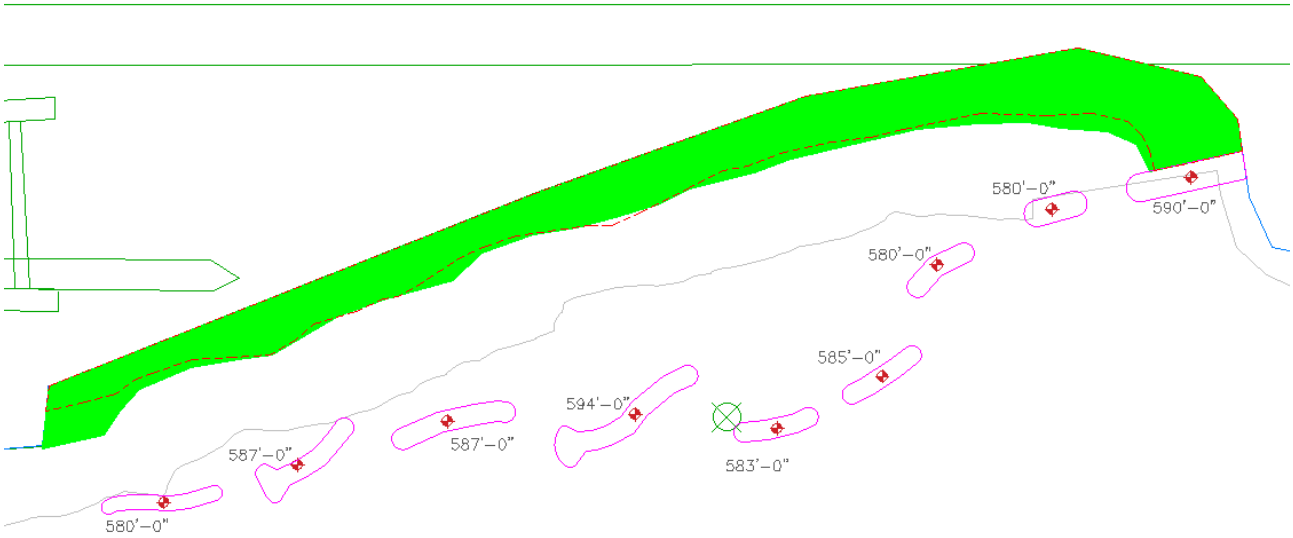


Figure B.37: Post-test scan data for Configuration 15 (Scan20), dotted line pre-test, solid area post-test, structures in magenta

Figure B.38: Pre (top) and post-test (bottom) photographs from ‘North’ view for Configuration 15

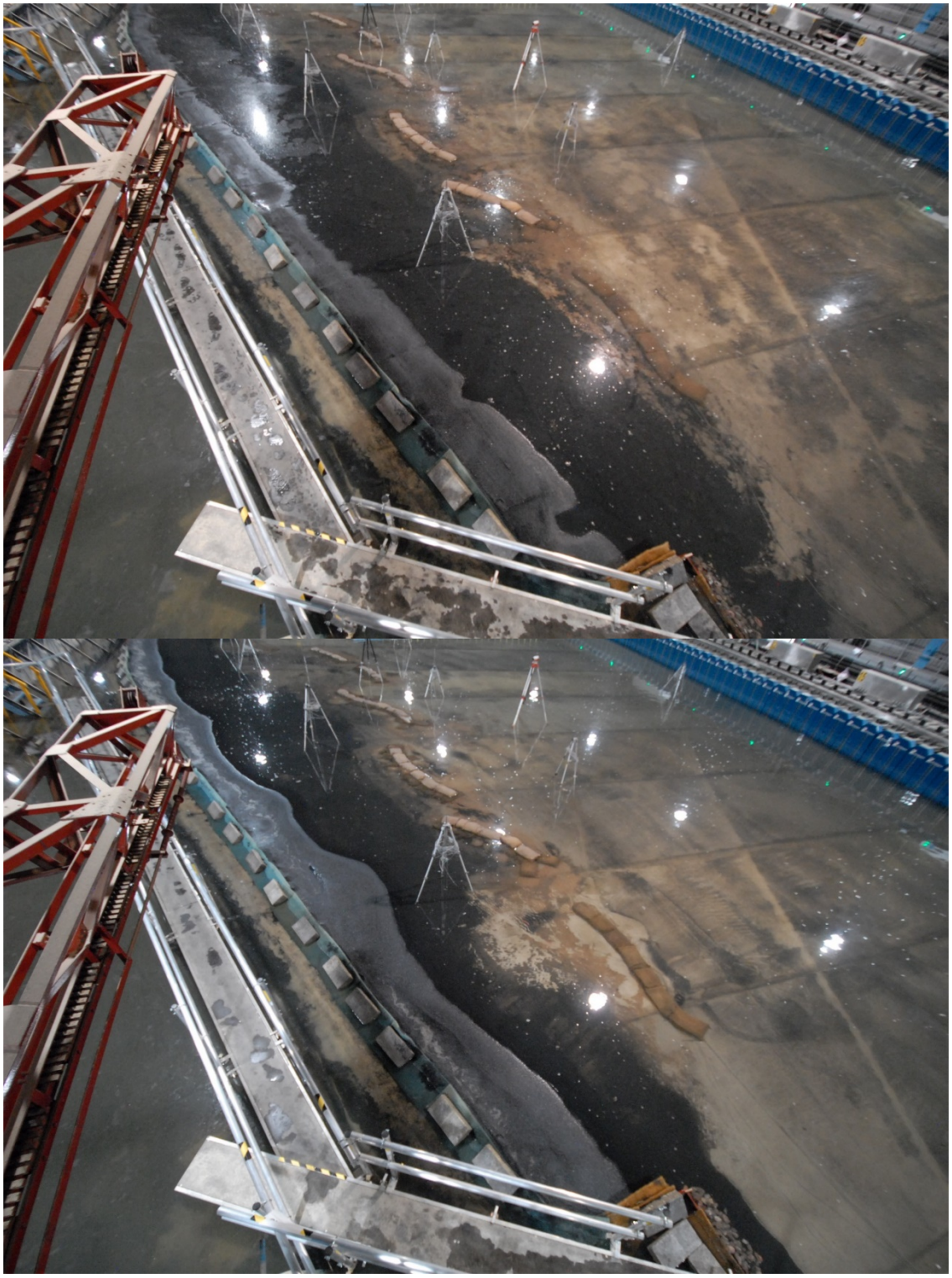

Figure B.39: Pre (top) and post-test (bottom) photographs from ‘South’ view for Configuration 15

### B.1.16. Configuration 16

Configuration 16 differed from Configuration 15 with the removal of two sandbags from the north end of the southernmost emergent breakwater. This configuration was tested twice for 3 hr tests (2 x 30 minutes model). The pre and post-test photographs from the 'North' and 'South' time-lapse camera views are shown in Figure B.40 and Figure B.41.

Figure B.40: Pre (top) and post-test (bottom) photographs from ‘North’ view for Configuration 16

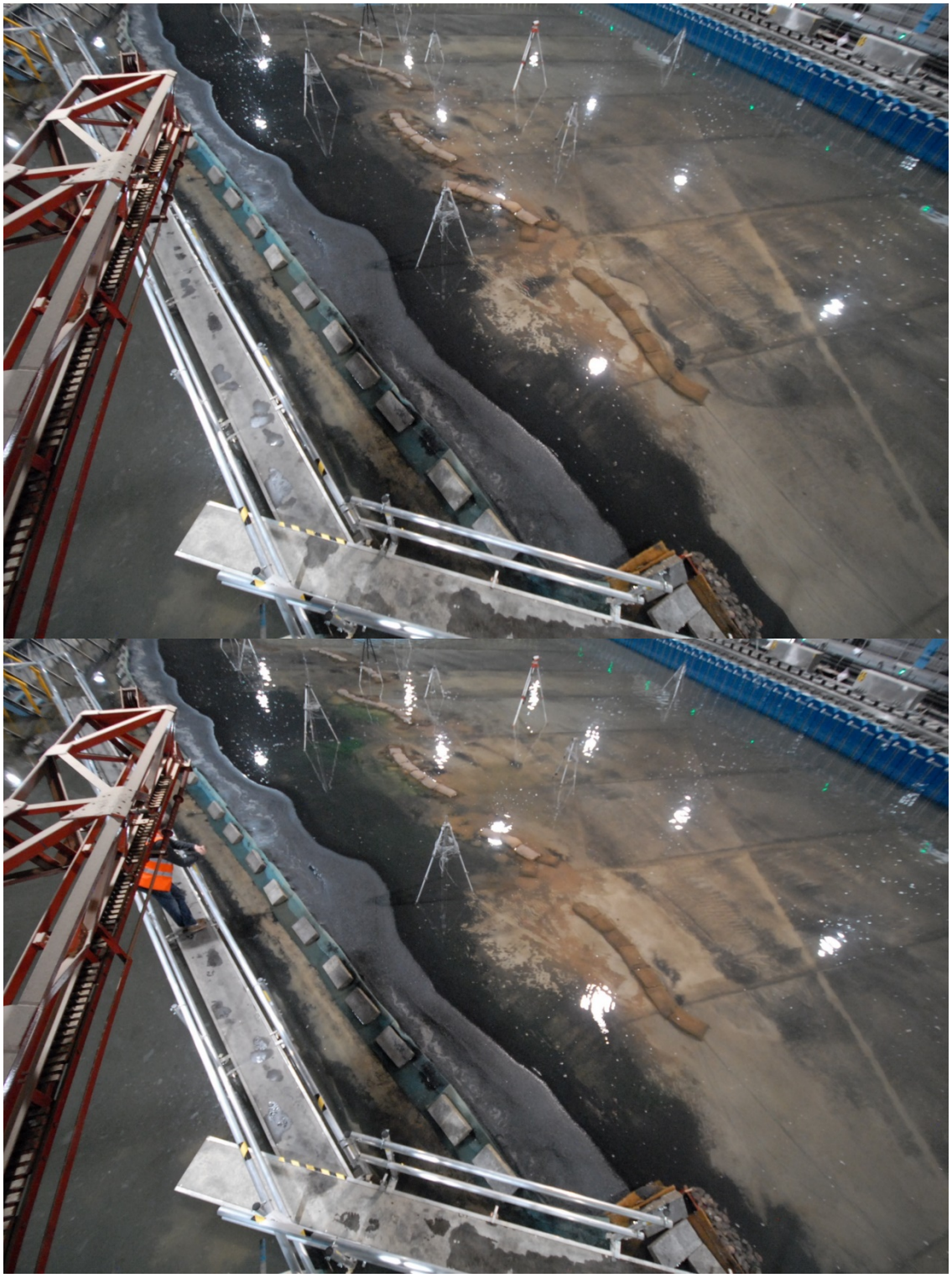

Figure B.41: Pre (top) and post-test (bottom) photographs from ‘South’ view for Configuration 16

### B.1.17. Configuration 17

Configuration 17 differed from Configuration 16 with the removal of the southernmost emergent breakwater and the addition of fishtails to the breakwater just north of the one removed during second test on this configuration. This configuration was tested twice for 3 hr tests (2 x 30 minutes model). The pre and post-test photographs from the 'North' and 'South' time-lapse camera views are shown in Figure 6.28 and Figure 6.29.

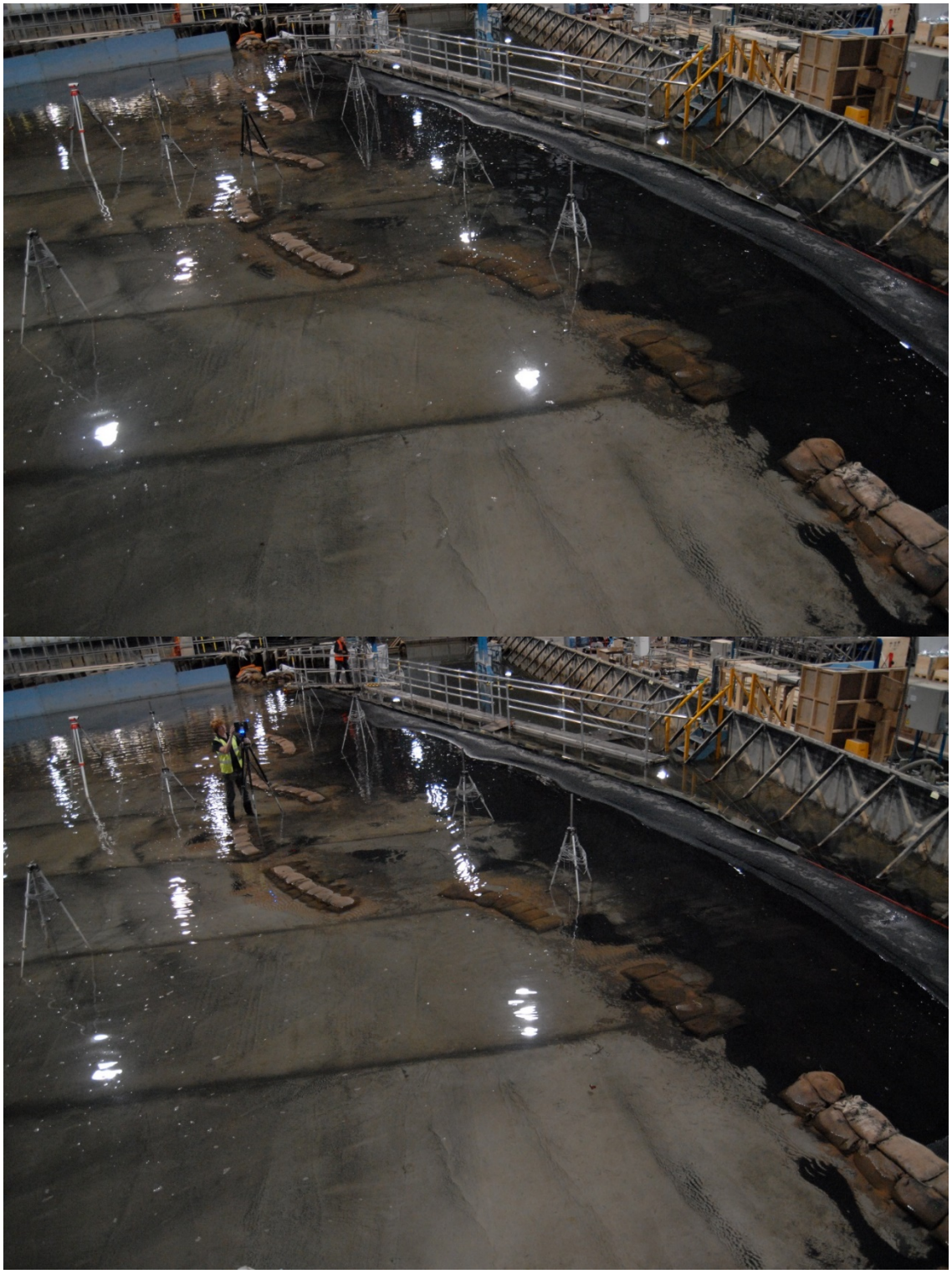

Figure B.42: Pre (top) and post-test (bottom) photographs from 'North' view for Configuration 17

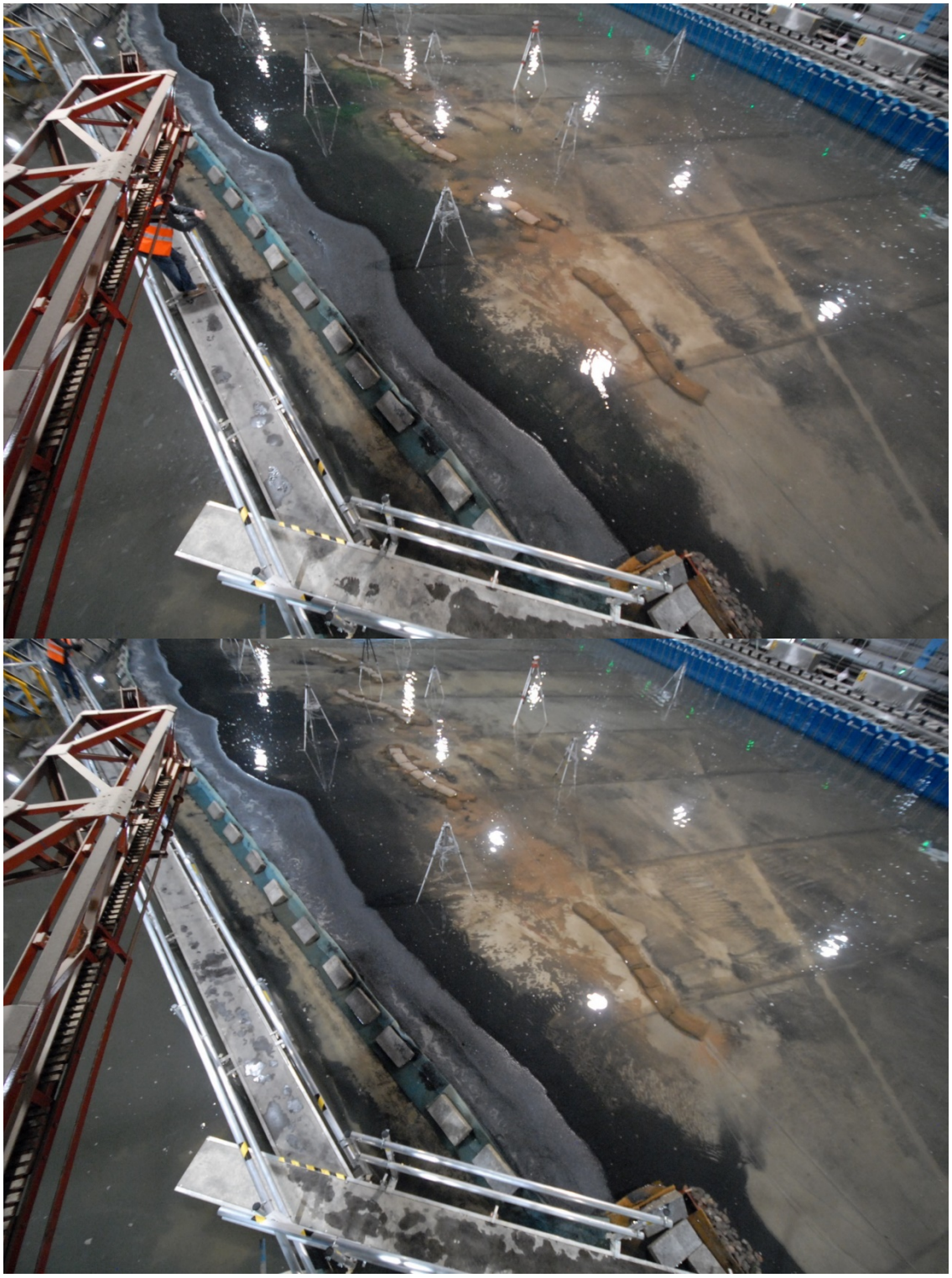

Figure B.43: Pre (top) and post-test (bottom) photographs from ‘South’ view for Configuration 17

## B.1.18. Configuration 18

Configuration 18 differed from Configuration 17 with the removal of the southernmost submerged breakwater and the addition of a collection of small submerged reef and fishtail structures in its place. This configuration was tested once for 3 hr tests (30 minutes model). The pre and post-test photographs from the 'North' and 'South' time-lapse camera views are shown in Figure B.45 and Figure B.46. The post-test scan data is shown in Figure B.44.

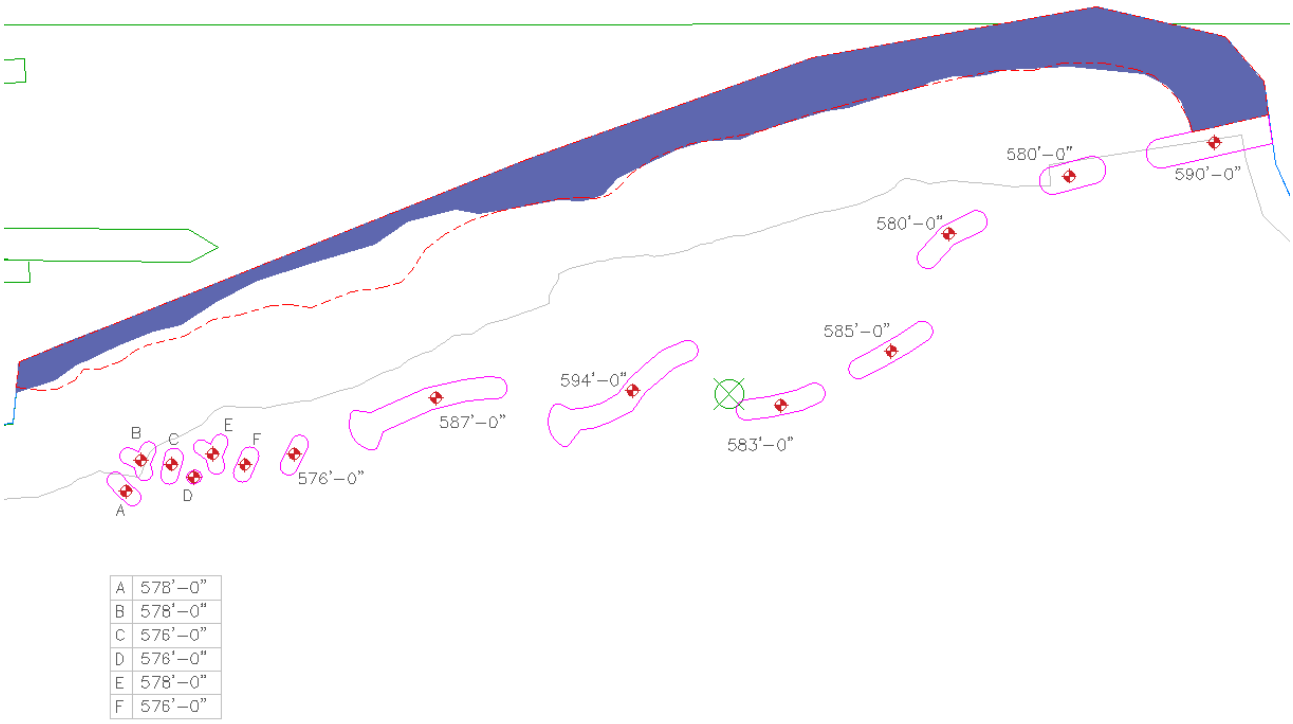


| | |
|---|---|
| A | 578'–0" |
| B | 578'–0" |
| C | 576'–0" |
| D | 576'–0" |
| E | 578'–0" |
| F | 576'–0" |

Figure B.44: Post-test scan data for Configuration 18 (Scan23), dotted line pre-test, solid area post-test, structures in magenta

Figure B.45: Pre (top) and post-test (bottom) photographs from ‘North’ view for Configuration 18

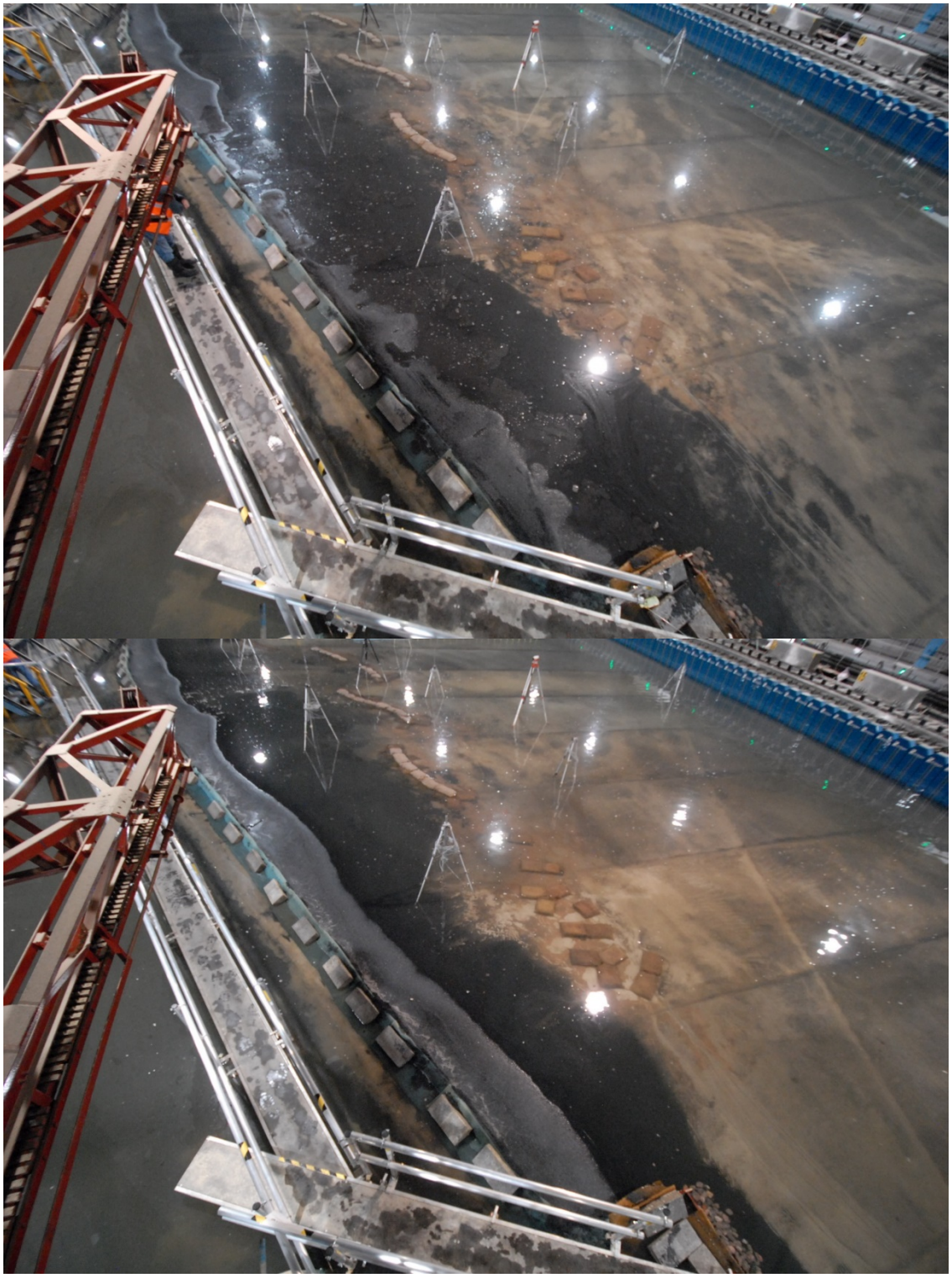

Figure B.46: Pre (top) and post-test (bottom) photographs from ‘South’ view for Configuration 18

## B.1.19. Configuration 19

Configuration 19 differed from Configuration 18 with the rearrangement of the southern submerged reefs and fishtail structures. This configuration was tested twice for 3 hr tests (2 x 30 minutes model). The pre and post-test photographs from the 'North' and 'South' time-lapse camera views are shown in Figure B.48 and Figure B.49. The post-test scan data is shown in Figure B.47.

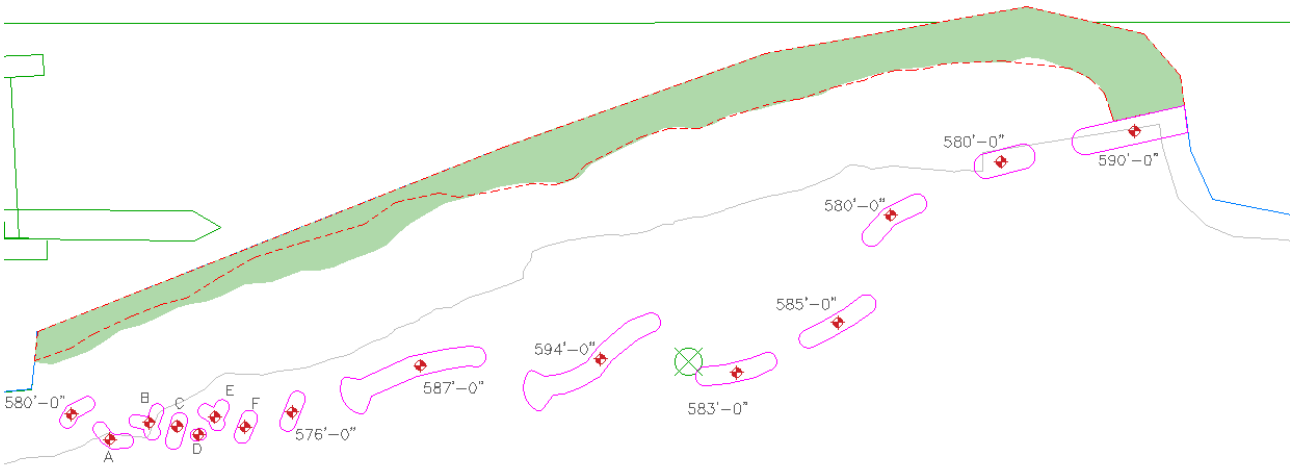


| | |
|---|---|
| A | 580'–0" |
| B | 578'–0" |
| C | 576'–0" |
| D | 576'–0" |
| E | 578'–0" |
| F | 576'–0" |

Figure B.47: Post-test scan data for Configuration 19 (Scan24), dotted line pre-test, solid area post-test, structures in magenta

Figure B.48: Pre (top) and post-test (bottom) photographs from ‘North’ view for Configuration 19

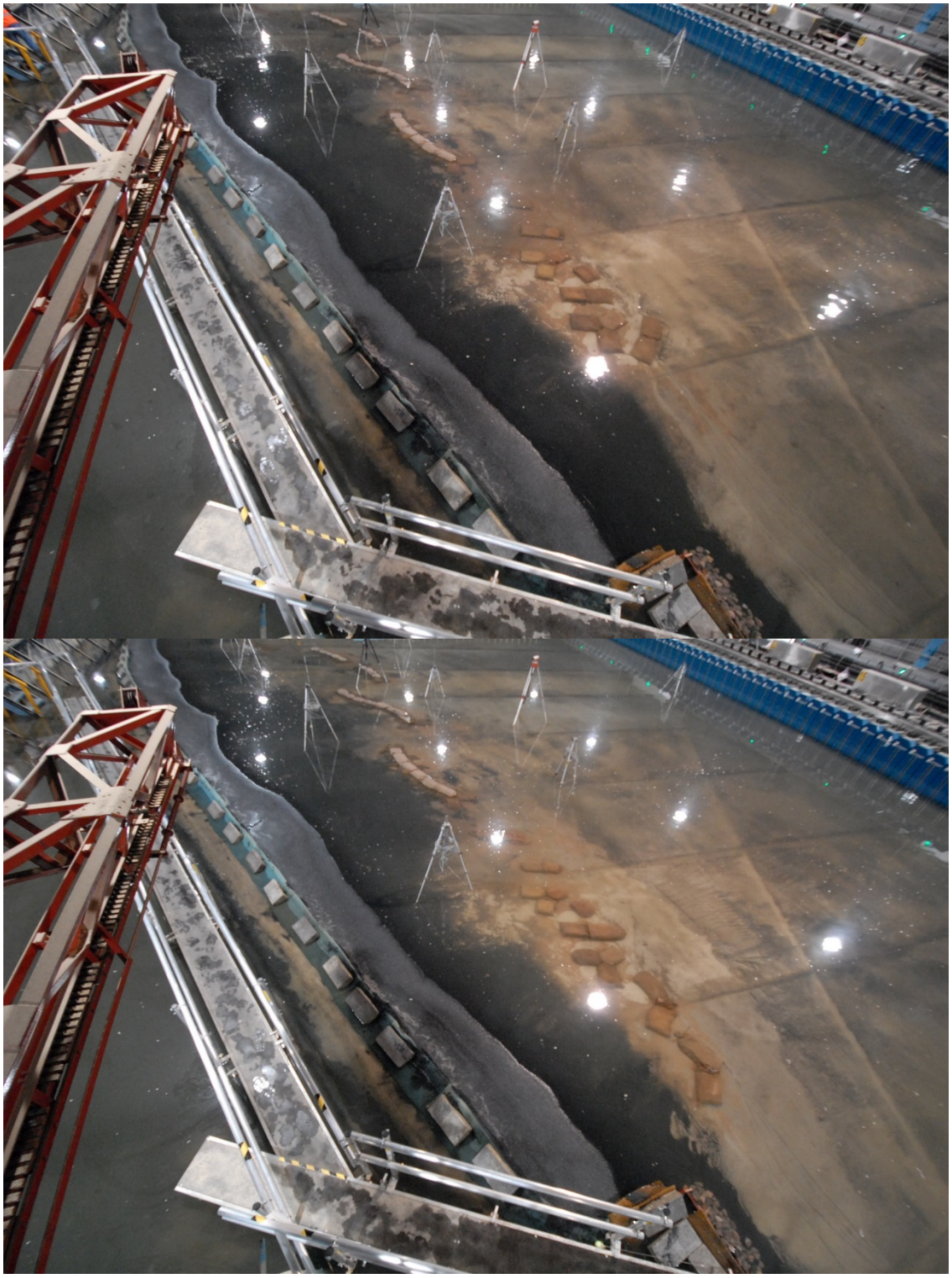

Figure B.49: Pre (top) and post-test (bottom) photographs from ‘South’ view for Configuration19

## B.1.20. Configuration 20

Configuration 20 differed from Configuration 19 with the removal of the southern submerged reef and fishtail structures and the reinstatement of three partially emergent breakwater in their place with submerged fishtails on the southern ends of the southern and northernmost. The southernmost emergent breakwater in Configuration 19 was shortened, removing the fishtails on the southern end, and the central section lowered to make it submerged. The beach was also re-set (re-screeded) between Configuration 19 and 20. This configuration was tested once for 3 hr tests (30 minutes model). The pre and post-test photographs from the 'North' and 'South' time-lapse camera views are shown in Figure B.50 and Figure B.51.

Figure B.50: Pre (top) and post-test (bottom) photographs from 'North' view for Configuration 20 (Configuration 21 shown in post-test photograph)

Figure B.51: Pre (top) and post-test (bottom) photographs from 'South' view for Configuration 20 (Configuration 21 shown in post-test photograph)

### B.1.21. Configuration 21

Configuration 21 differed from Configuration 20 with the removal of the fishtail on the southern end of the southernmost breakwater and replacing it with a one sandbag emergent extension. This configuration was tested once for 3 hr tests (30 minutes model). The pre and post-test photographs from the 'North' and 'South' time-lapse camera views are shown in Figure B.52 and Figure B.53.

Figure B.52: Pre (top) and post-test (bottom) photographs from 'North' view for Configuration 21 (Configuration 22 shown in post-test photograph)

Figure B.53: Pre (top) and post-test (bottom) photographs from 'South' view for Configuration 21 (Configuration 22 shown in post-test photograph)

## B.1.22. Configuration 22

Configuration 22 differed from Configuration 21 with the addition of fishtails to the southern ends of the two southernmost breakwaters with additional emergent sections. This configuration was tested once for 3 hr tests (30 minutes model). The pre and post-test photographs from the 'North' and 'South' time-lapse camera views are shown in Figure B.55 and Figure B.56. The post-test scan data is shown in Figure B.54.

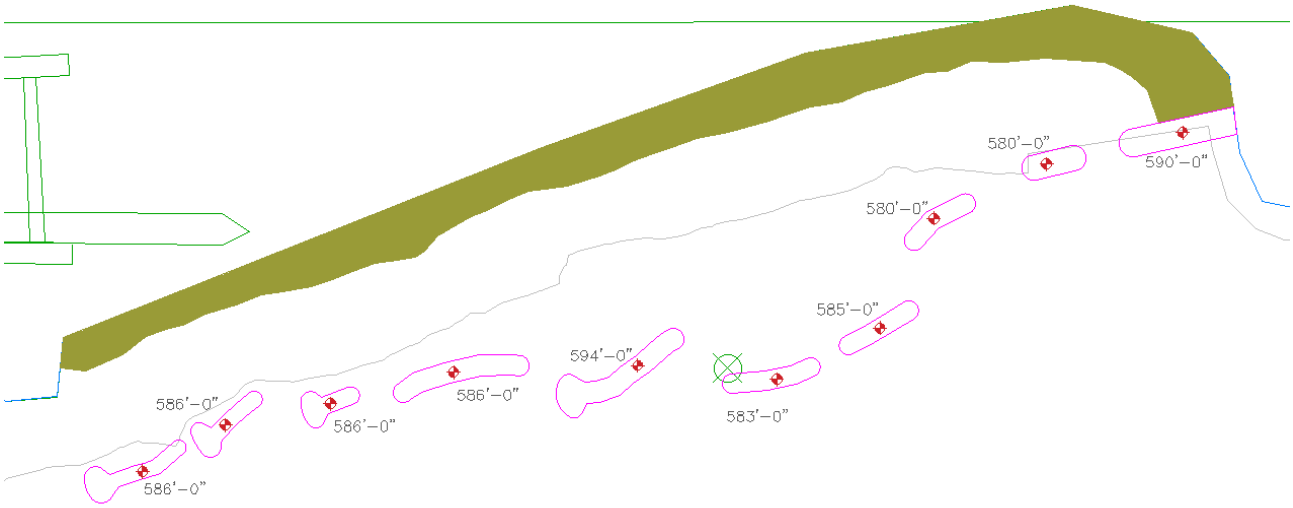


Figure B.54: Post-test scan data for Configuration 22 (Scan26), solid area post-test beach, structures in magenta

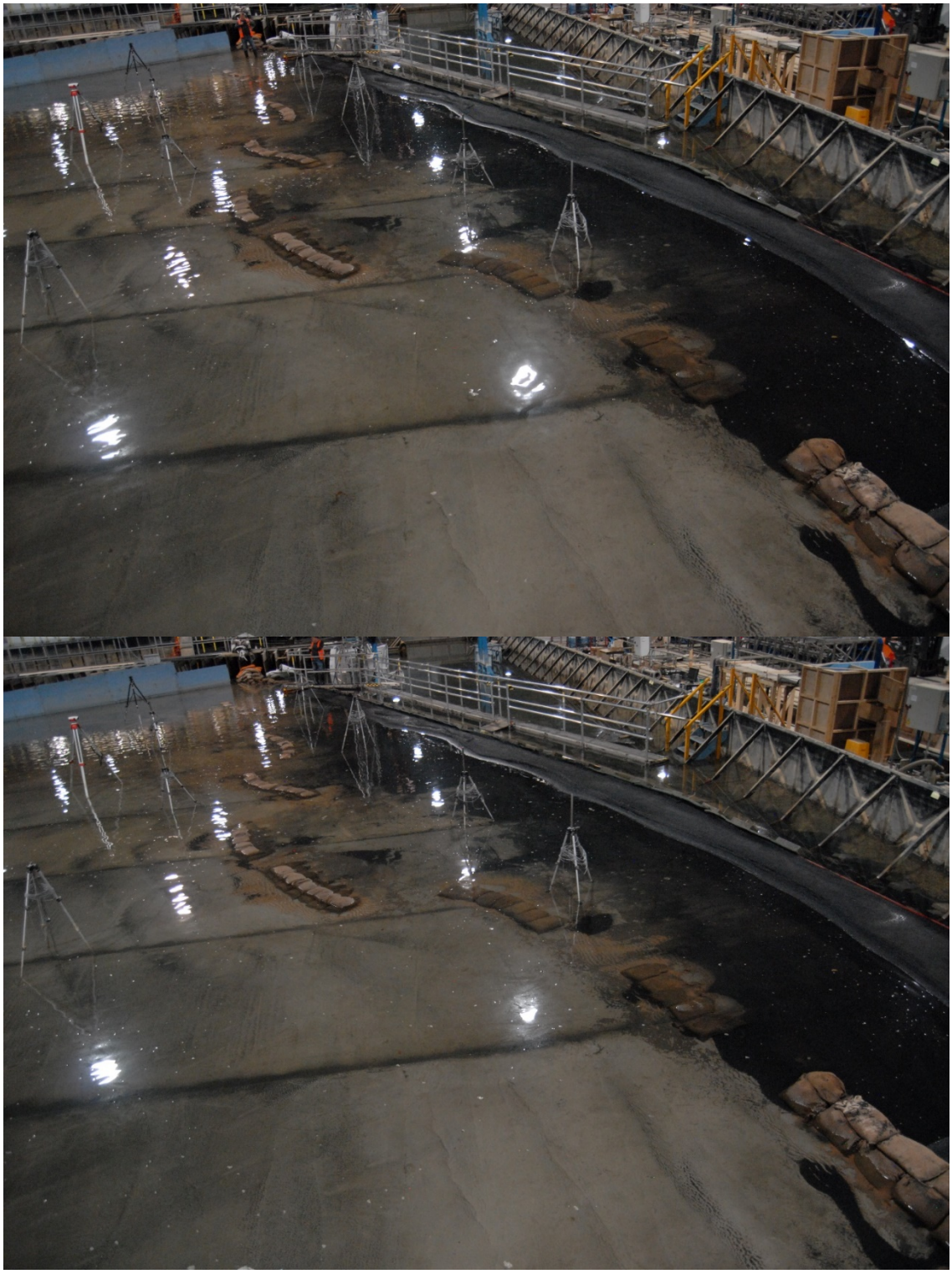

Figure B.55: Pre (top) and post-test (bottom) photographs from 'North' view for Configuration 22

Figure B.56: Pre (top) and post-test (bottom) photographs from ‘South’ view for Configuration 22

# B.2. Stability photographs

## B.2.1. BW1-1

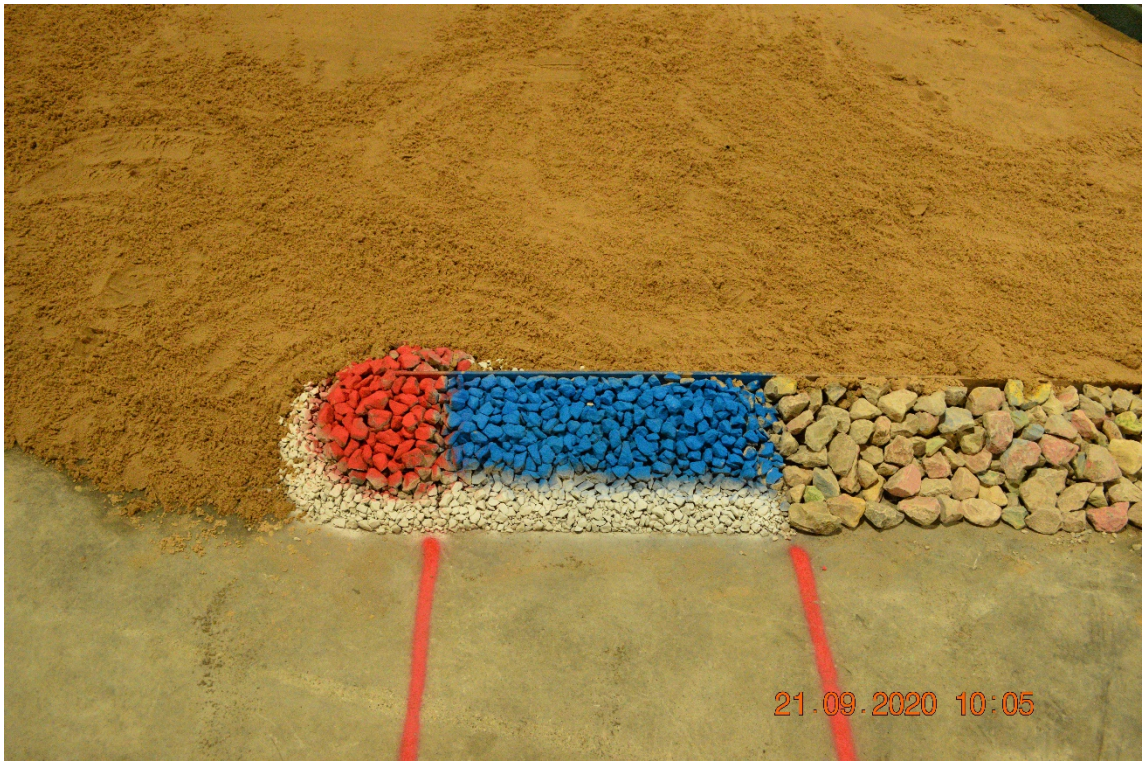


Figure B.57: Pre-test stability photograph for BW1-1, position 1

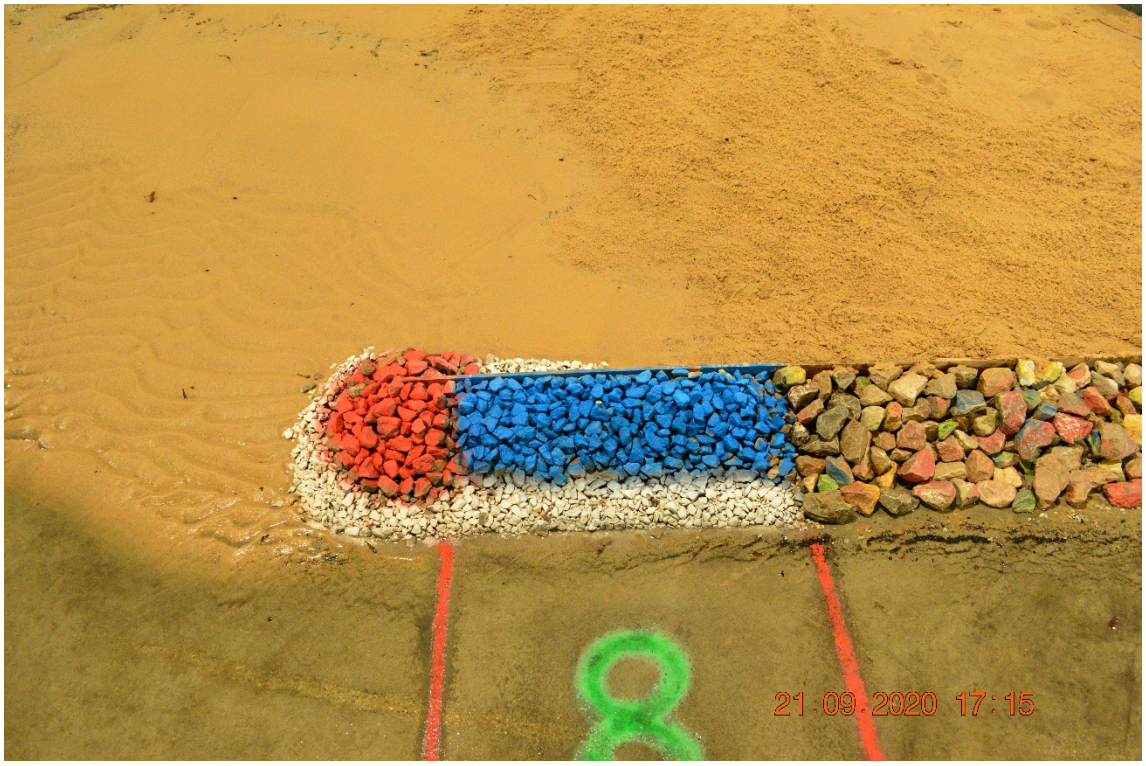


Figure B.58: Post Test Part 01 (WC_LOW_WL) stability photograph for BW1-1, position 1

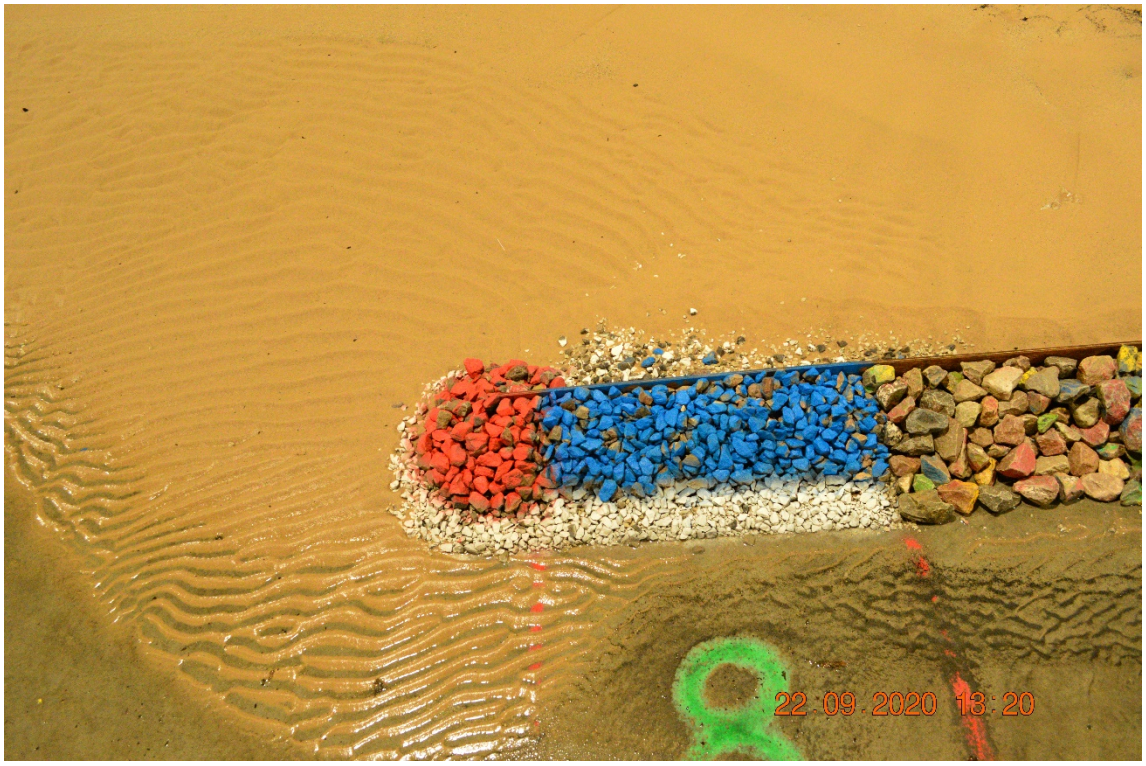


Figure B.59: Post Test Part 02 (WC_HIGH_WL) stability photograph for BW1-1, position 1

Figure B.60: Post Test Part 03 (WC_EXT_WL_01) stability photograph for BW1-1, position 1

Figure B.61: Post Test Part 04 (WC_EXT_WL_02) stability photograph for BW1-1, position 1

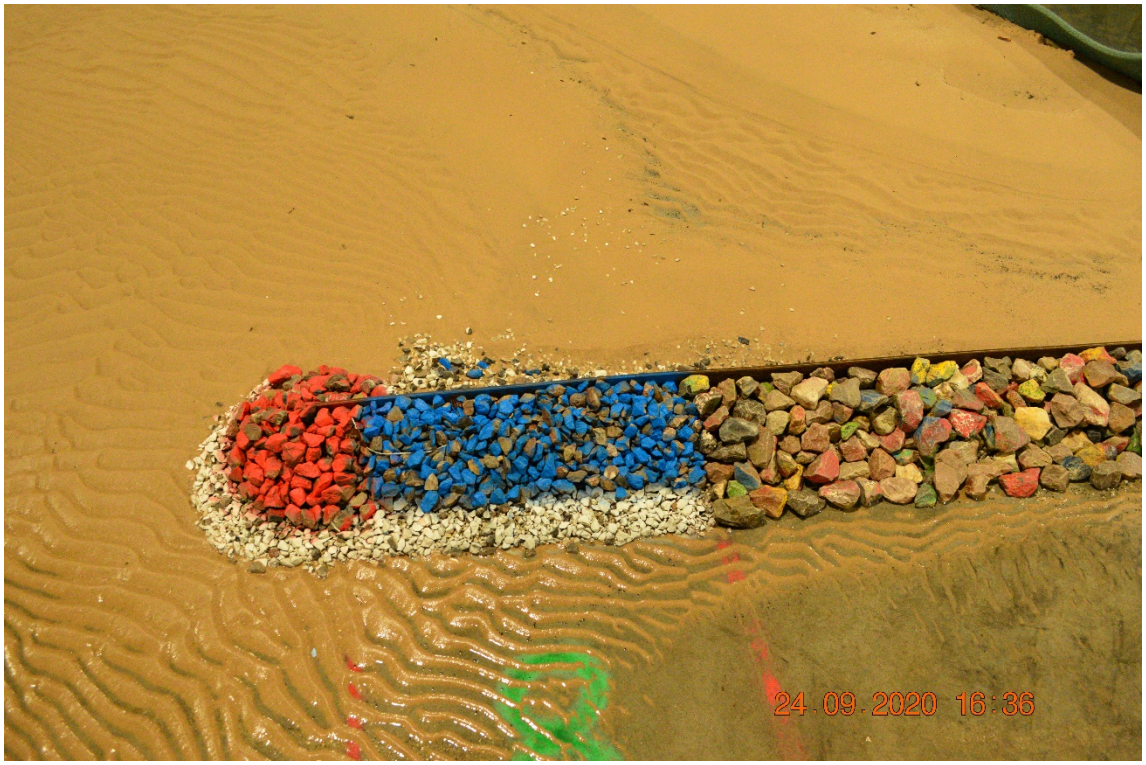


Figure B.62: Post Test Part 05 (WC_LOW_WL, SE) stability photograph for BW1-1, position 1

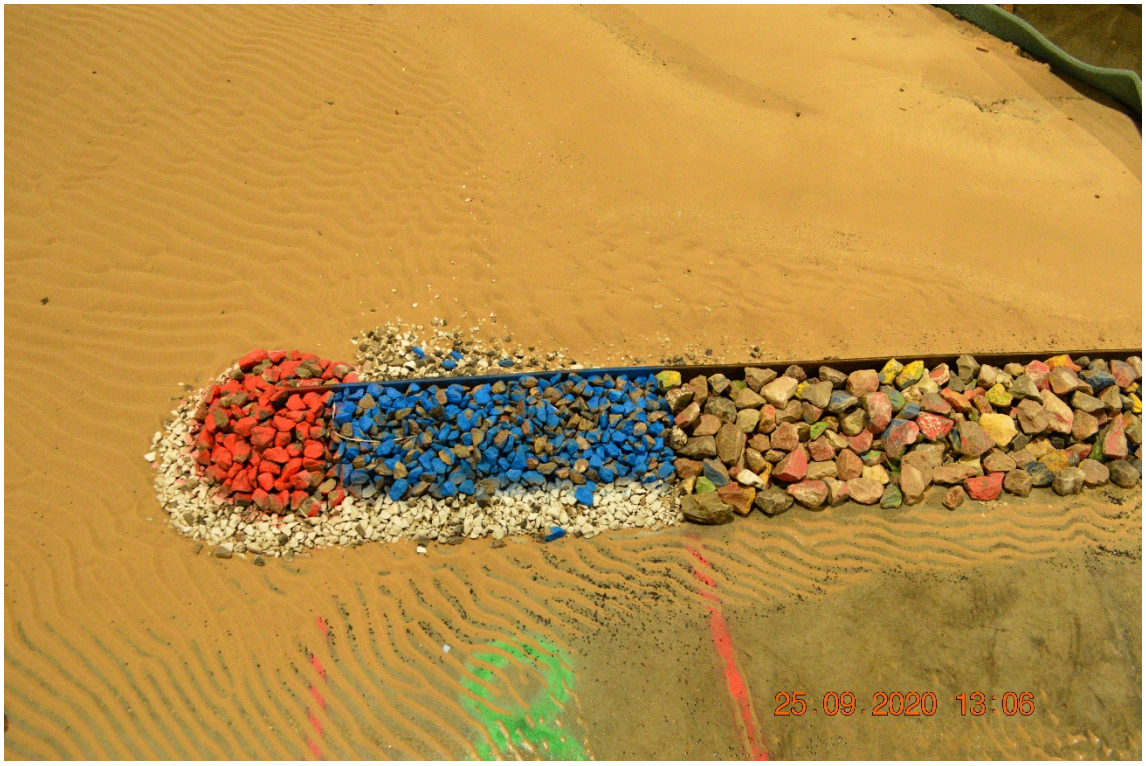


Figure B.63: Post Test Part 06 (WC_HIGH_WL, SE) stability photograph for BW1-1, position 1

## B.2.2. BW1-2

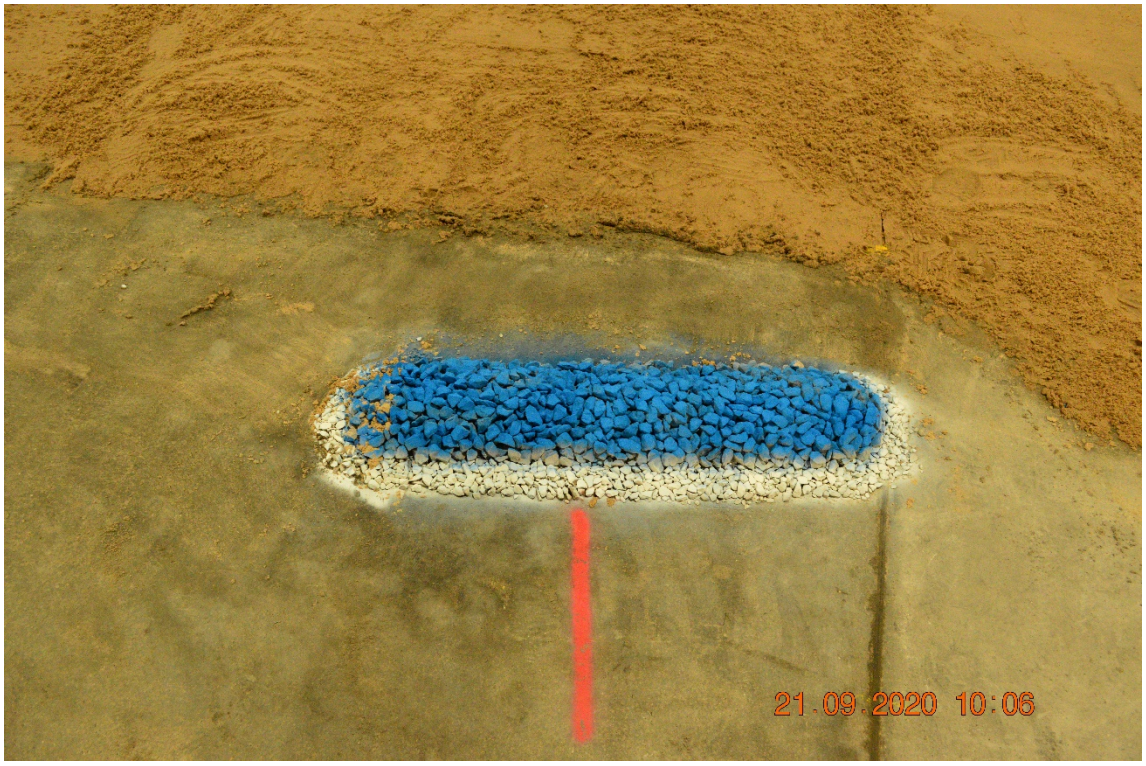


Figure B.64: Pre-test stability photograph for BW1-2, position 2

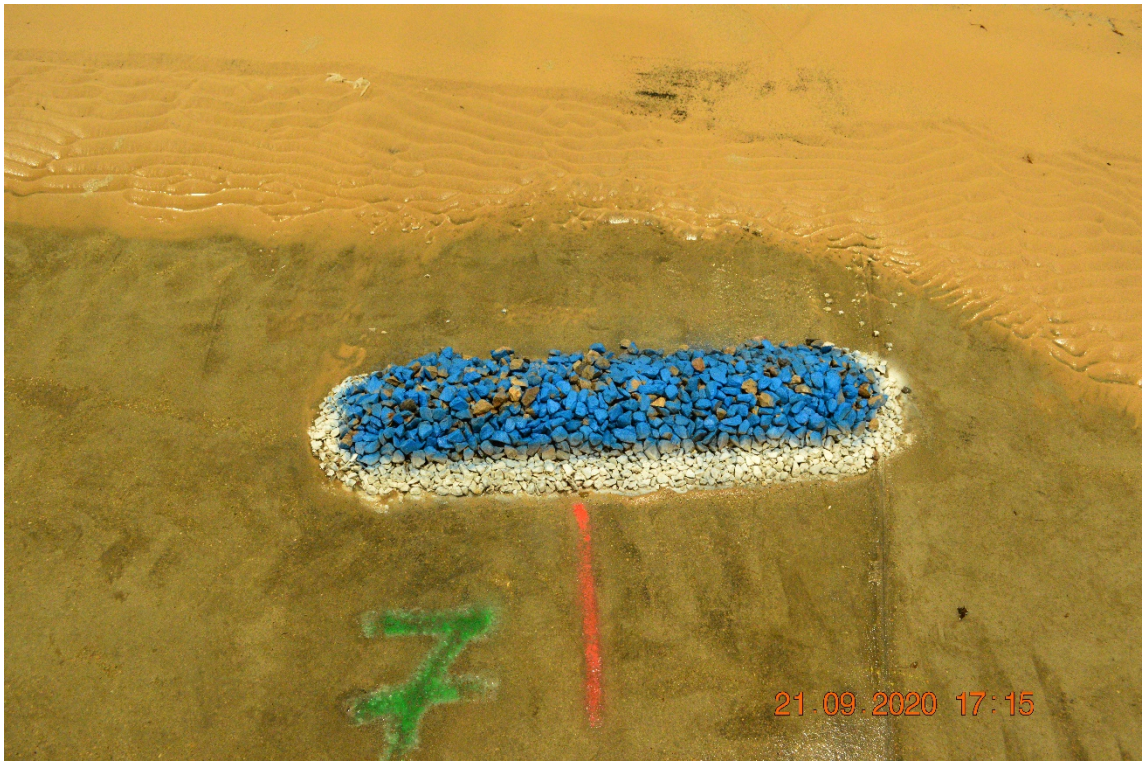


Figure B.65: Post Test Part 01 (WC_LOW_WL) stability photograph for BW1-2, position 2

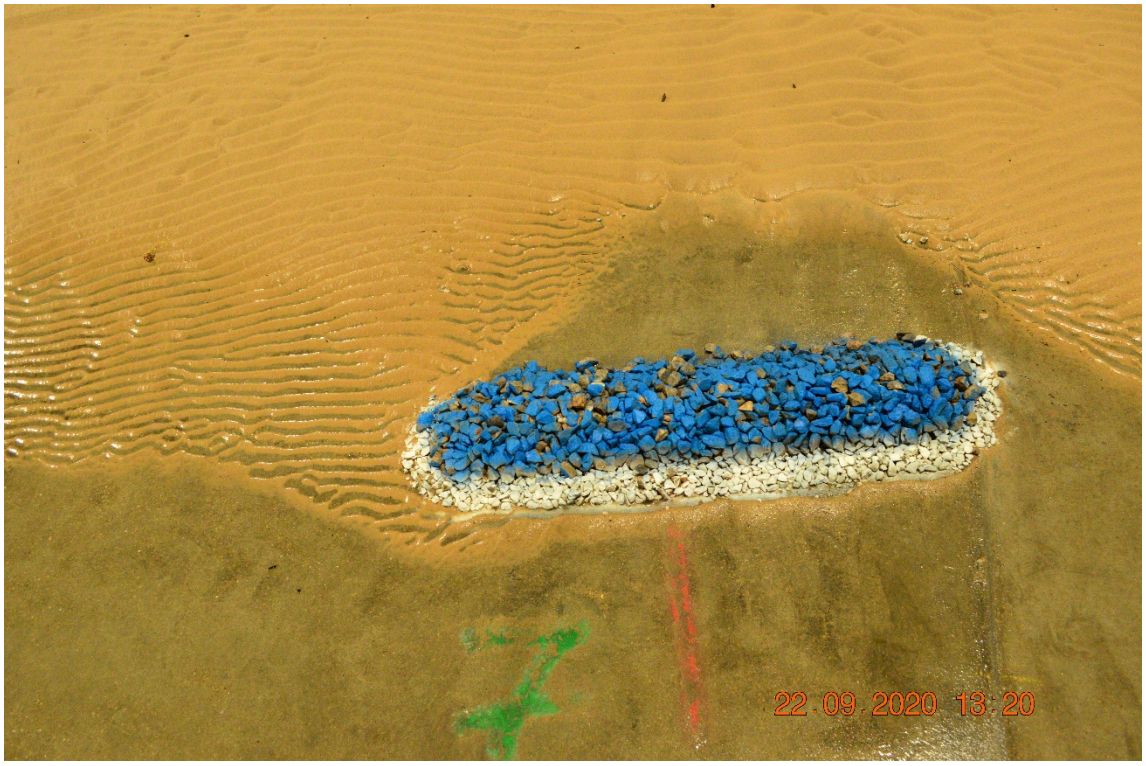


Figure B.66: Post Test Part 02 (WC_HIGH_WL) stability photograph for BW1-2, position 2

Figure B.67: Post Test Part 03 (WC_EXT_WL_01) stability photograph for BW1-2, position 2

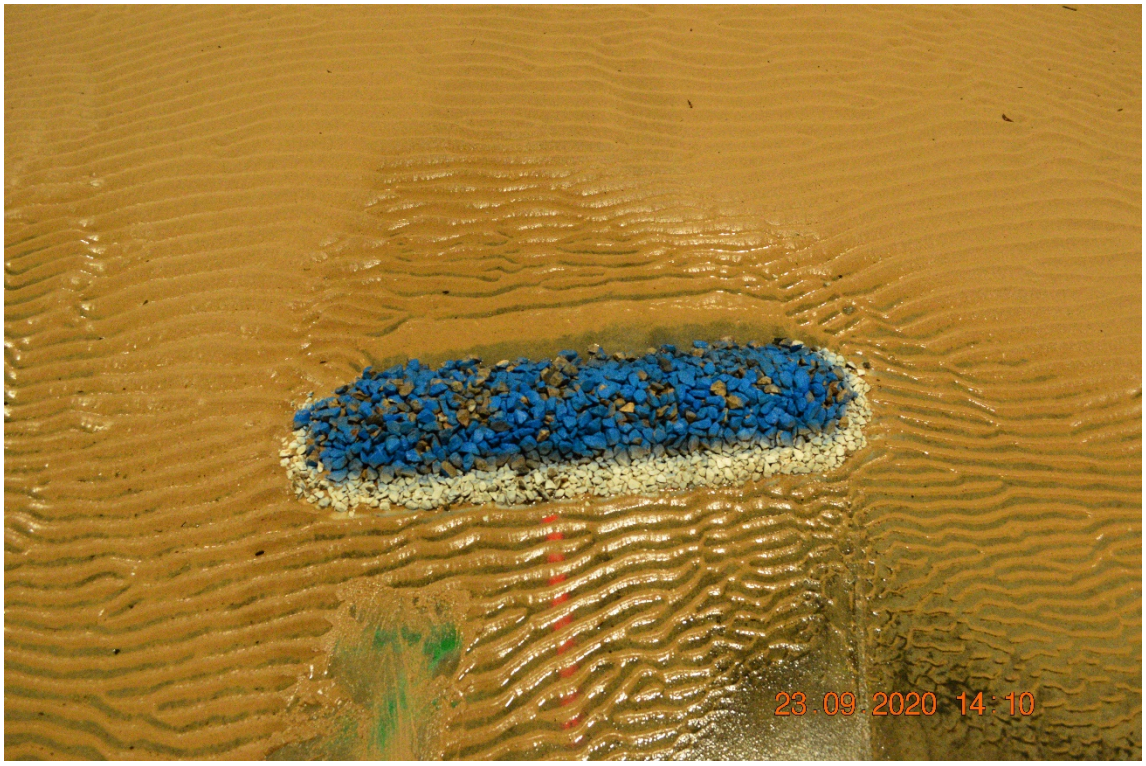


Figure B.68: Post Test Part 04 (WC_EXT_WL_02) stability photograph for BW1-2, position 2

Figure B.69: Post Test Part 05 (WC_LOW_WL, SE) stability photograph for BW1-2, position 2

Figure B.70: Post Test Part 06 (WC_HIGH_WL, SE) stability photograph for BW1-2, position 2

## B.2.3. BW1-3

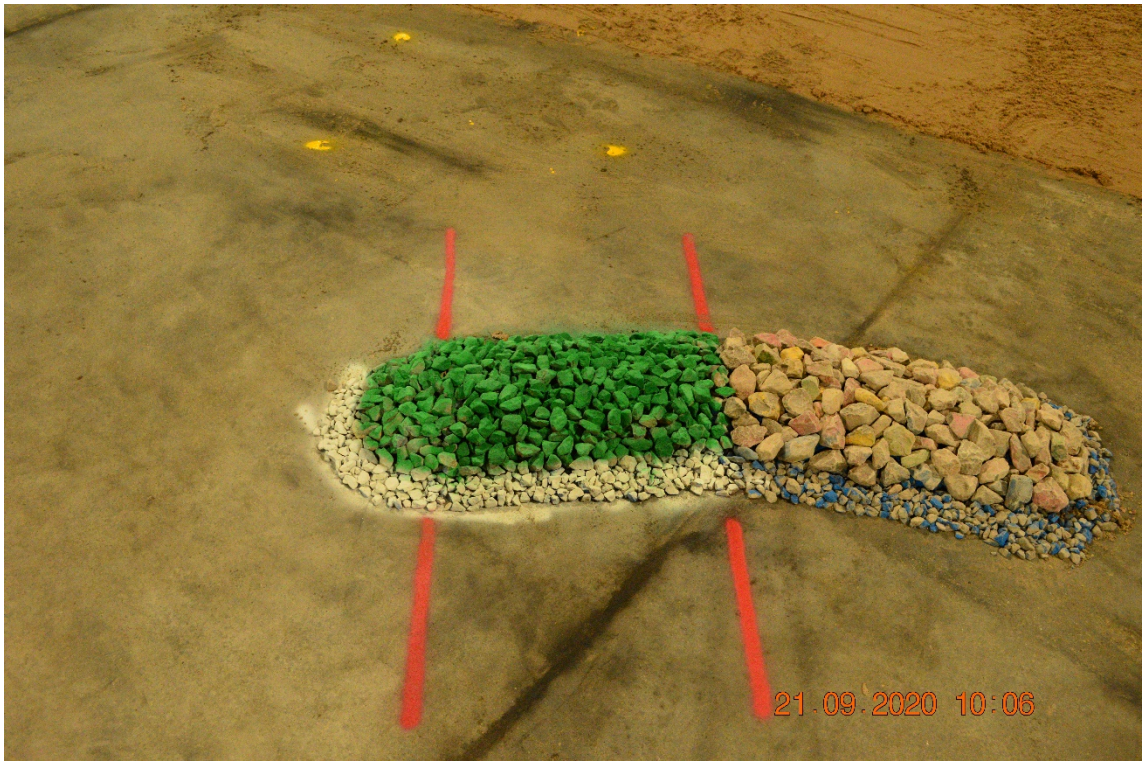


Figure B.71: Pre-test stability photograph for BW1-3, position 3

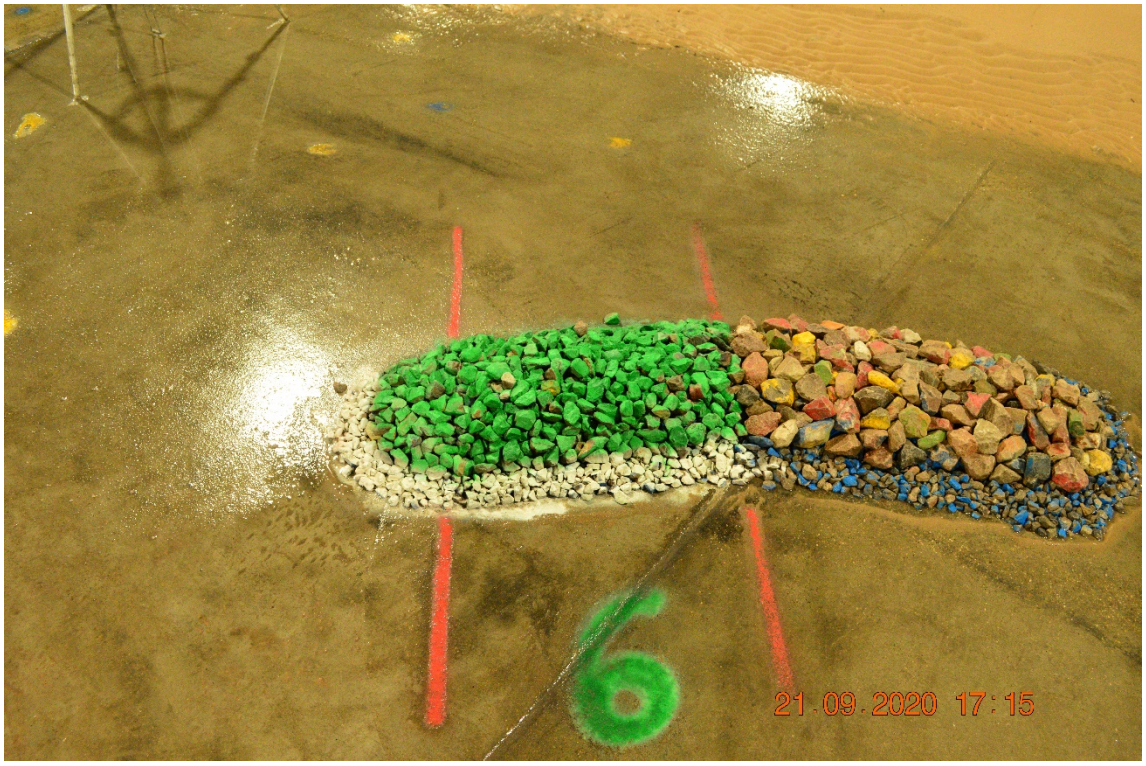


Figure B.72: Post Test Part 01 (WC_LOW_WL) stability photograph for BW1-3, position 3

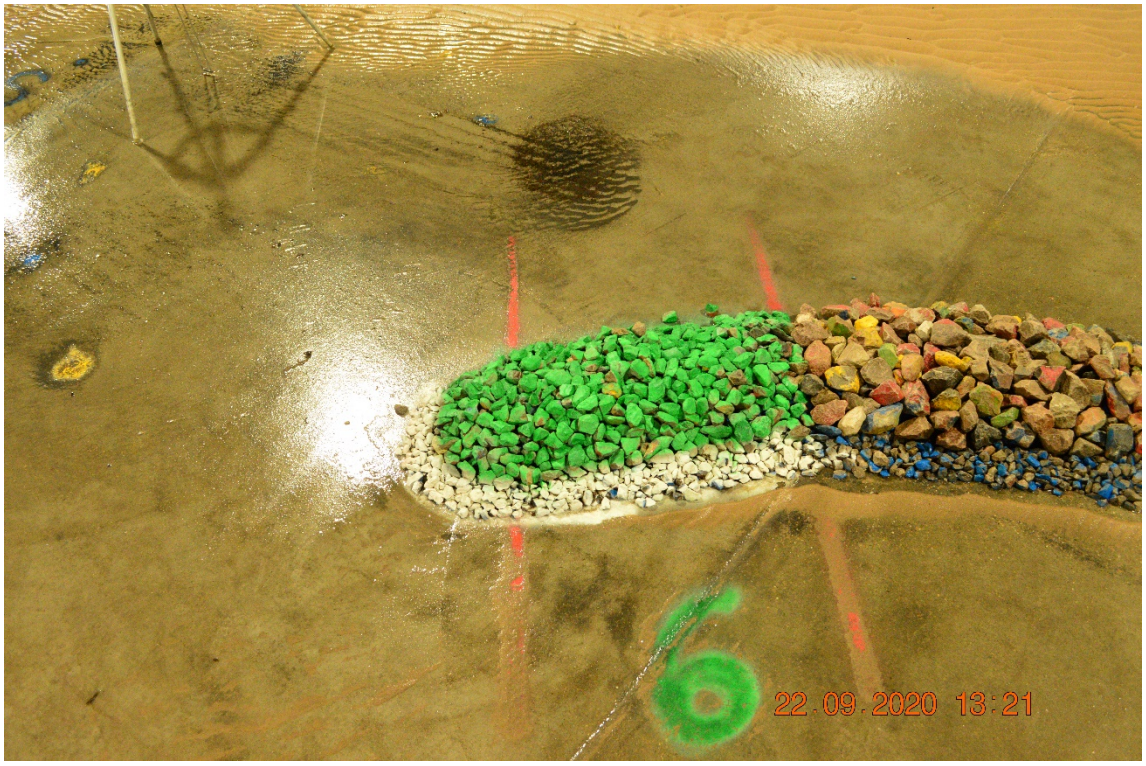


Figure B.73: Post Test Part 02 (WC_HIGH_WL) stability photograph for BW1-3, position 3

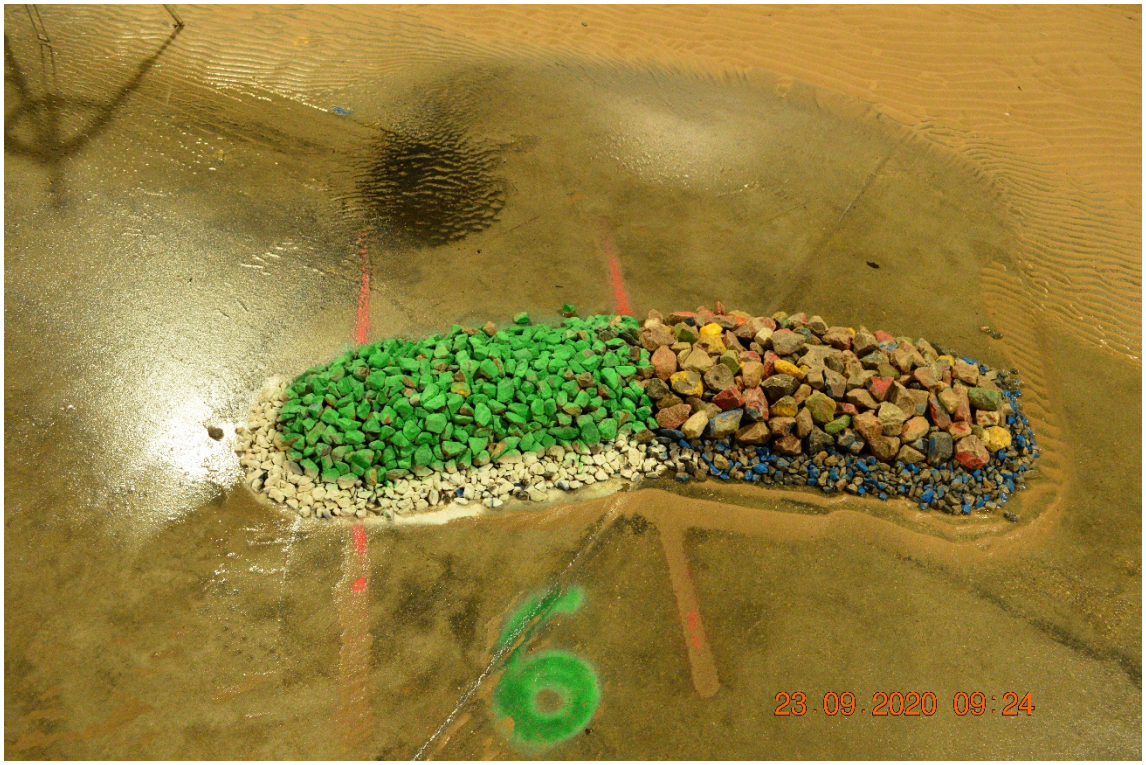


Figure B.74: Post Test Part 03 (WC_EXT_WL_01) stability photograph for BW1-3, position 3

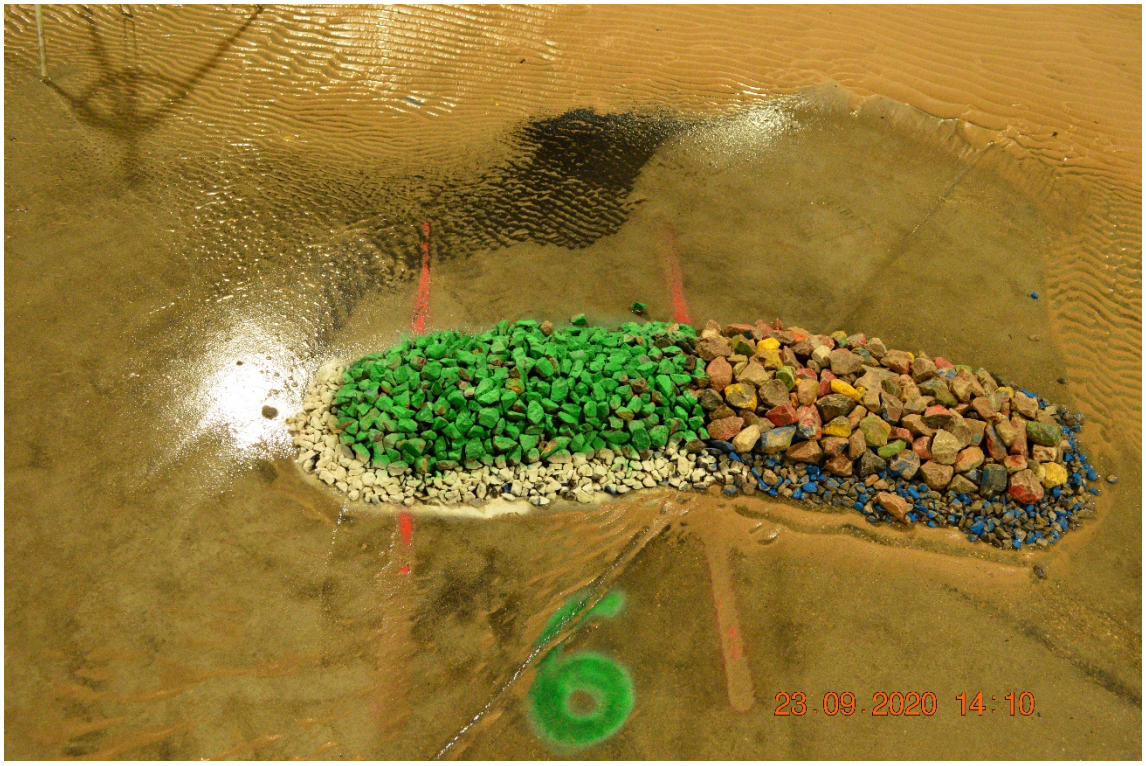


Figure B.75: Post Test Part 04 (WC_EXT_WL_02) stability photograph for BW1-3, position 3

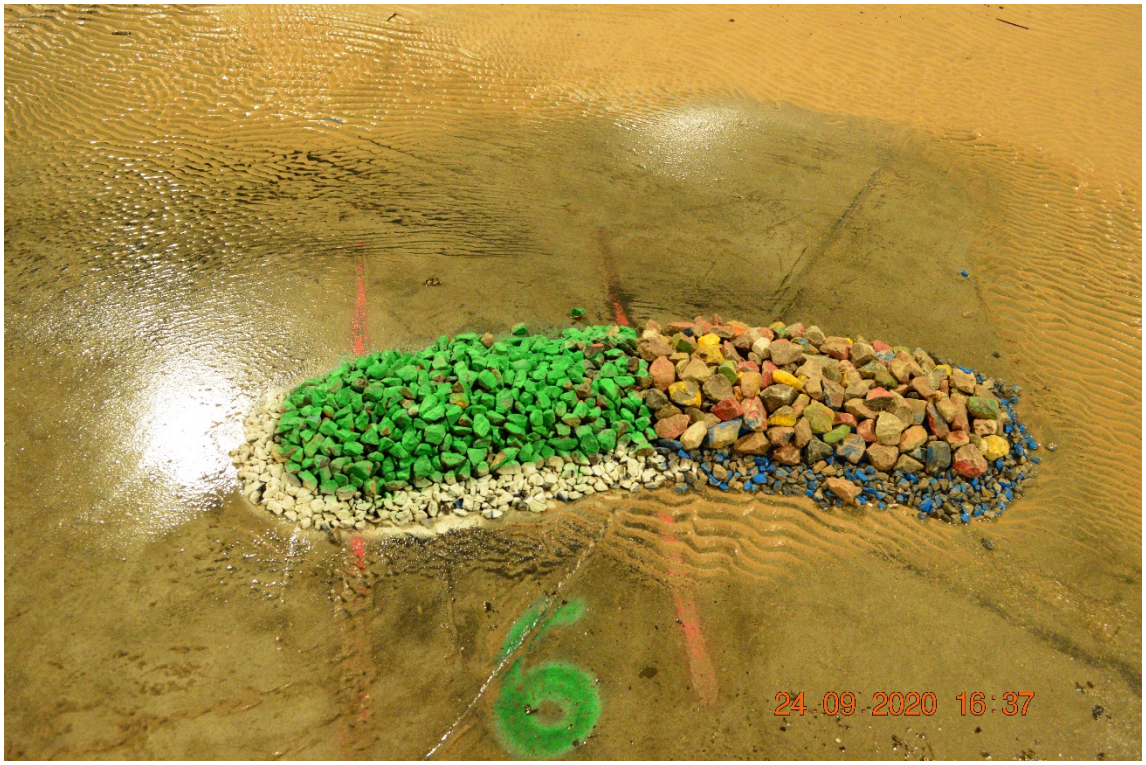


Figure B.76: Post Test Part 05 (WC_LOW_WL, SE) stability photograph for BW1-3, position 3

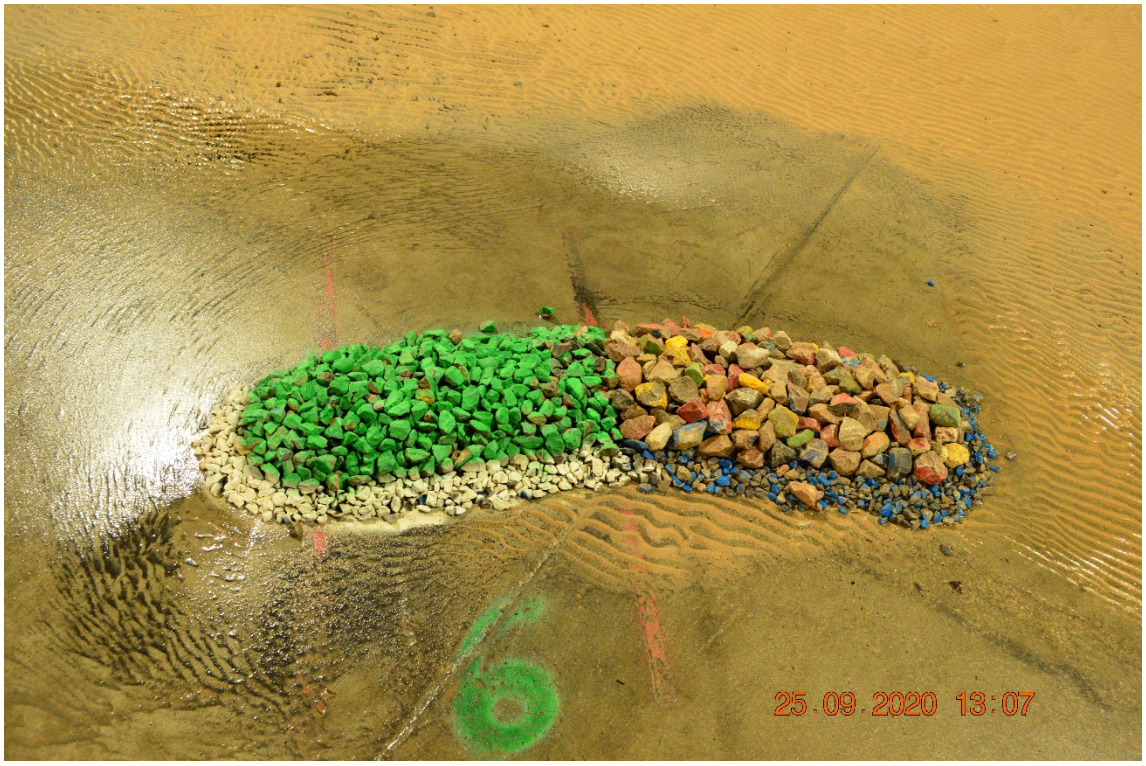


Figure B.77: Post Test Part 06 (WC_HIGH_WL, SE) stability photograph for BW1-3, position 3

Figure B.78: Pre-test stability photograph for BW1-3, position 4

Figure B.79: Post Test Part 01 (WC_LOW_WL) stability photograph for BW1-3, position 4

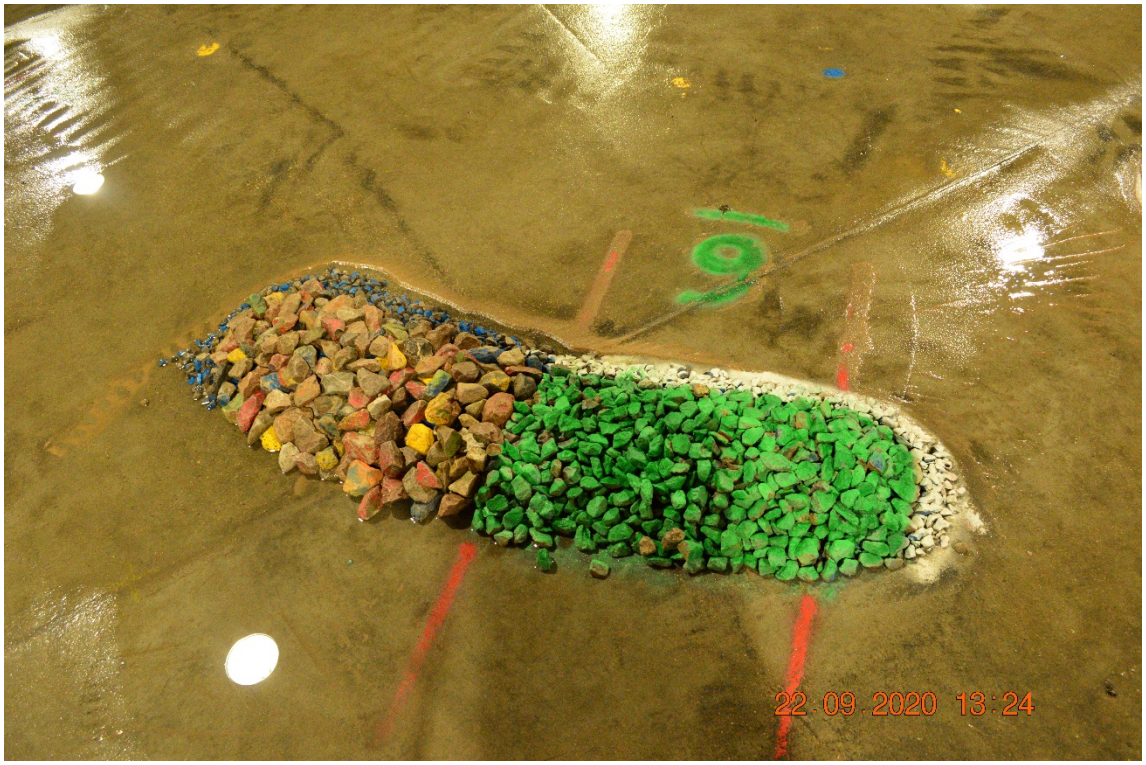


Figure B.80: Post Test Part 02 (WC_HIGH_WL) stability photograph for BW1-3, position 4

Figure B.81: Post Test Part 03 (WC_EXT_WL_01) stability photograph for BW1-3, position 4

Figure B.82: Post Test Part 04 (WC_EXT_WL_02) stability photograph for BW1-3, position 4

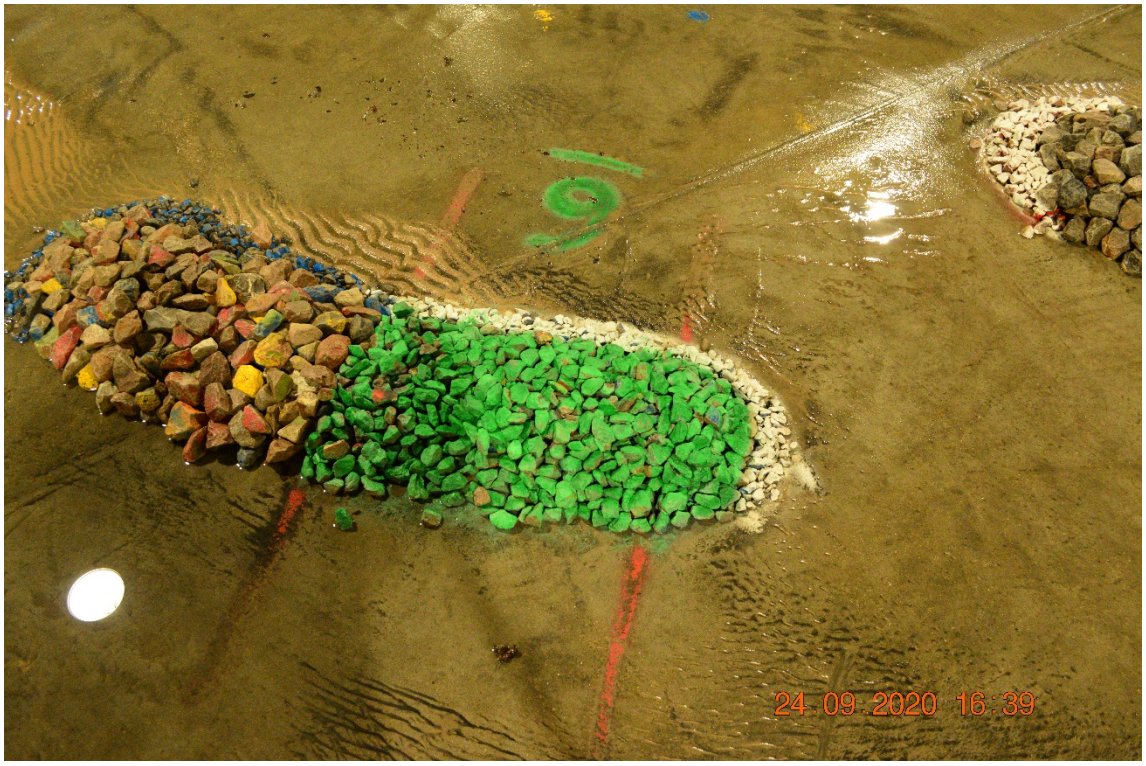


Figure B.83: Post Test Part 05 (WC_LOW_WL, SE) stability photograph for BW1-3, position 4

Figure B.84: Post Test Part 06 (WC_HIGH_WL, SE) stability photograph for BW1-3, position 4

## B.2.4. BW1-4

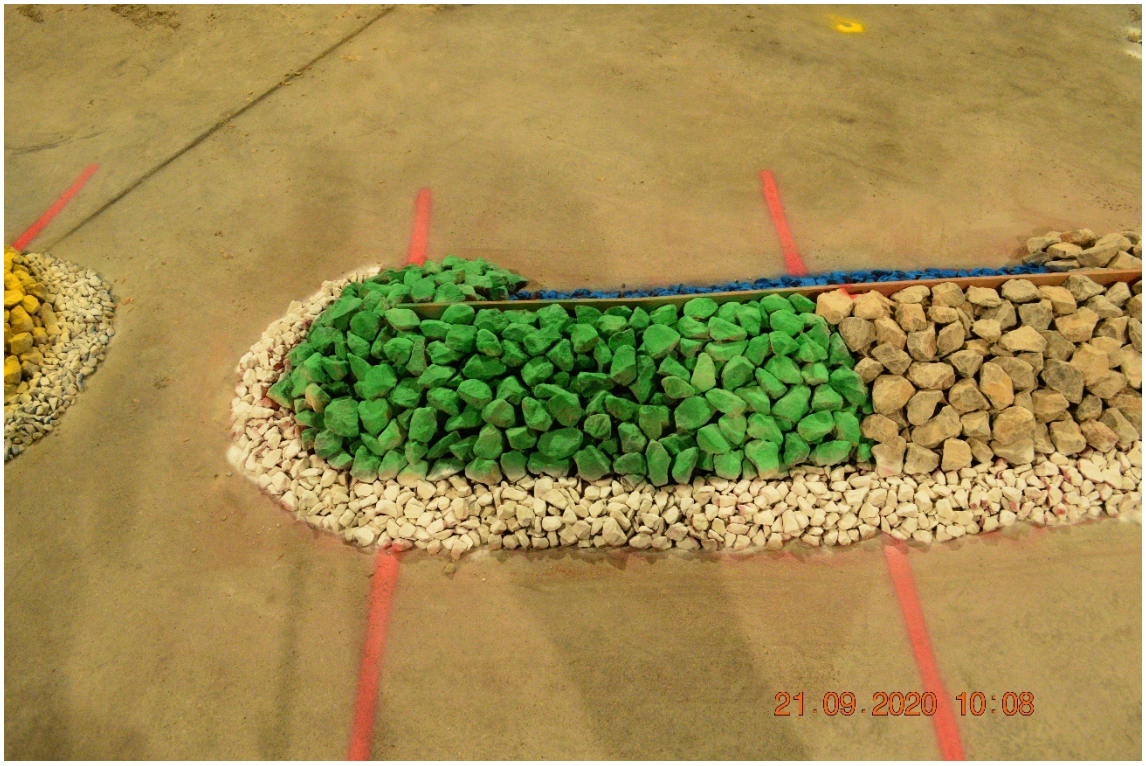


Figure B.85: Pre-test stability photograph for BW1-4, position 5

Figure B.86: Post Test Part 01 (WC_LOW_WL) stability photograph for BW1-4, position 5

Figure B.87: Post Test Part 02 (WC_HIGH_WL) stability photograph for BW1-4, position 5

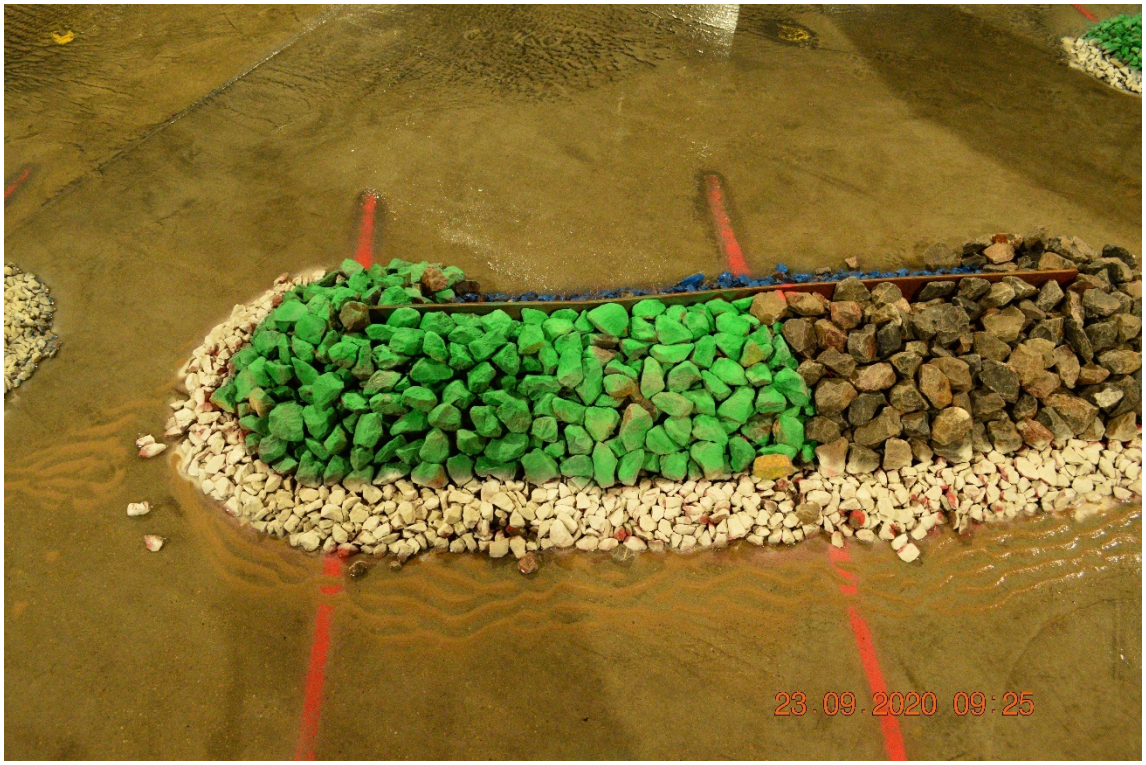


Figure B.88: Post Test Part 03 (WC_EXT_WL_01) stability photograph for BW1-4, position 5

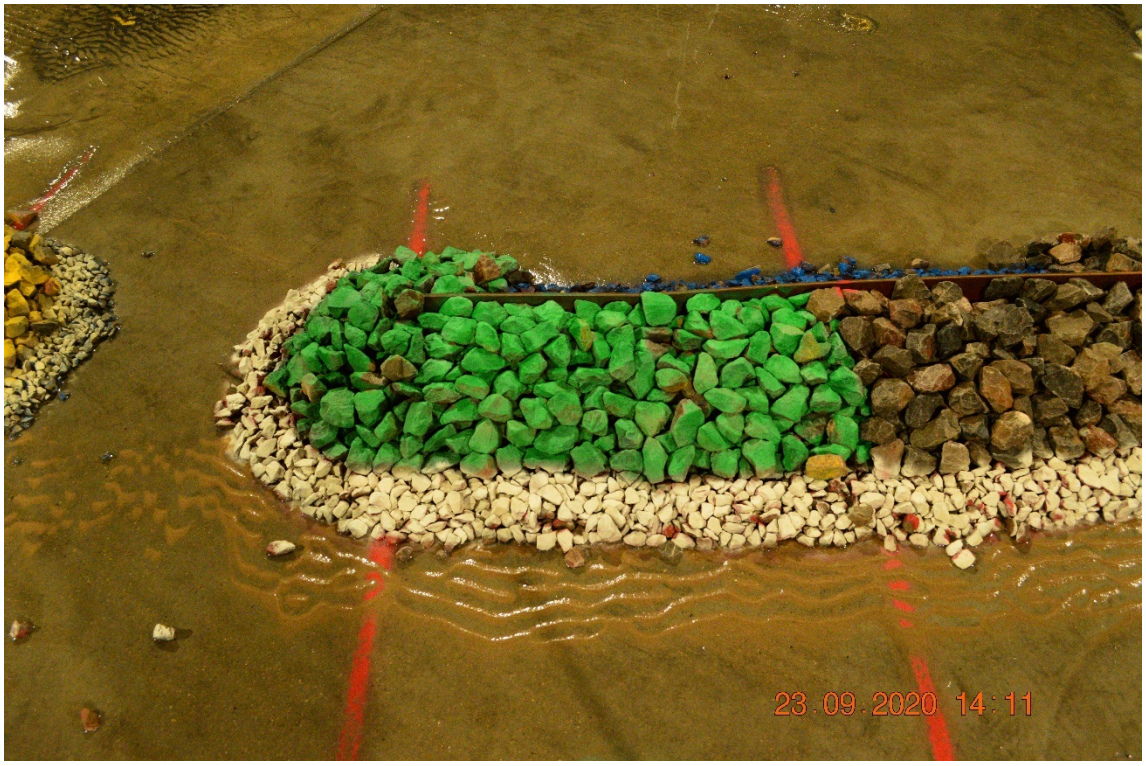


Figure B.89: Post Test Part 04 (WC_EXT_WL_02) stability photograph for BW1-4, position 5

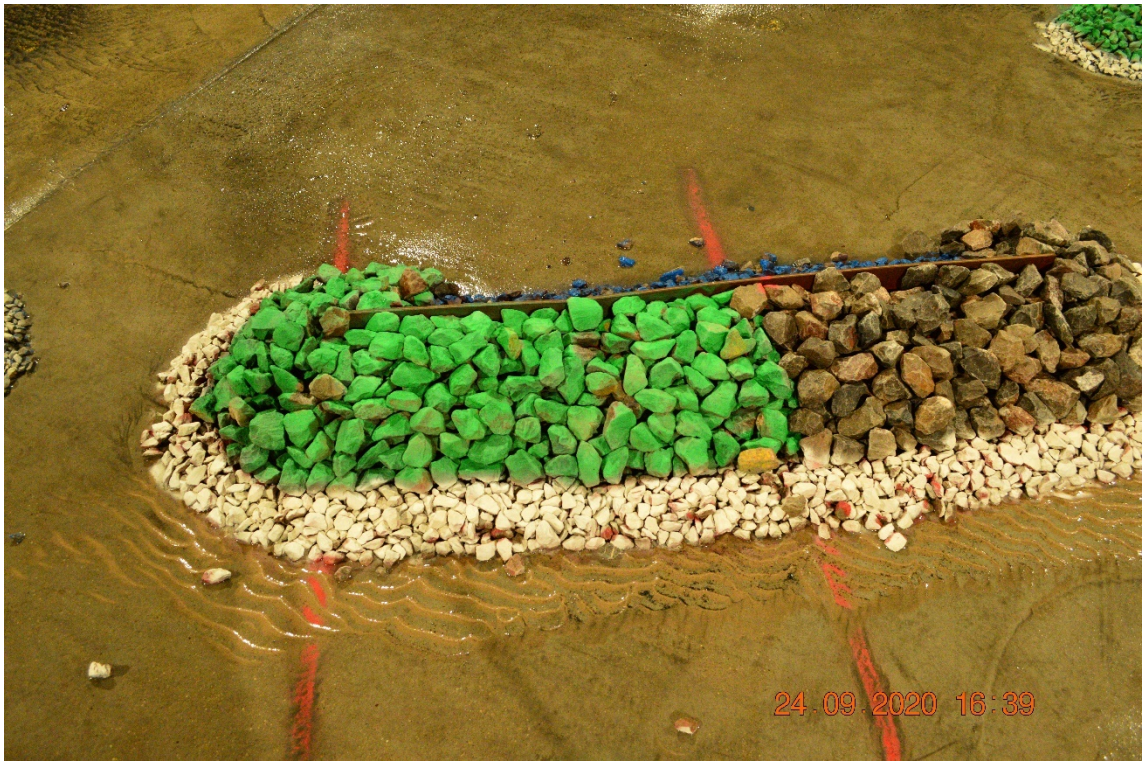


Figure B.90: Post Test Part 05 (WC_LOW_WL, SE) stability photograph for BW1-4, position 5

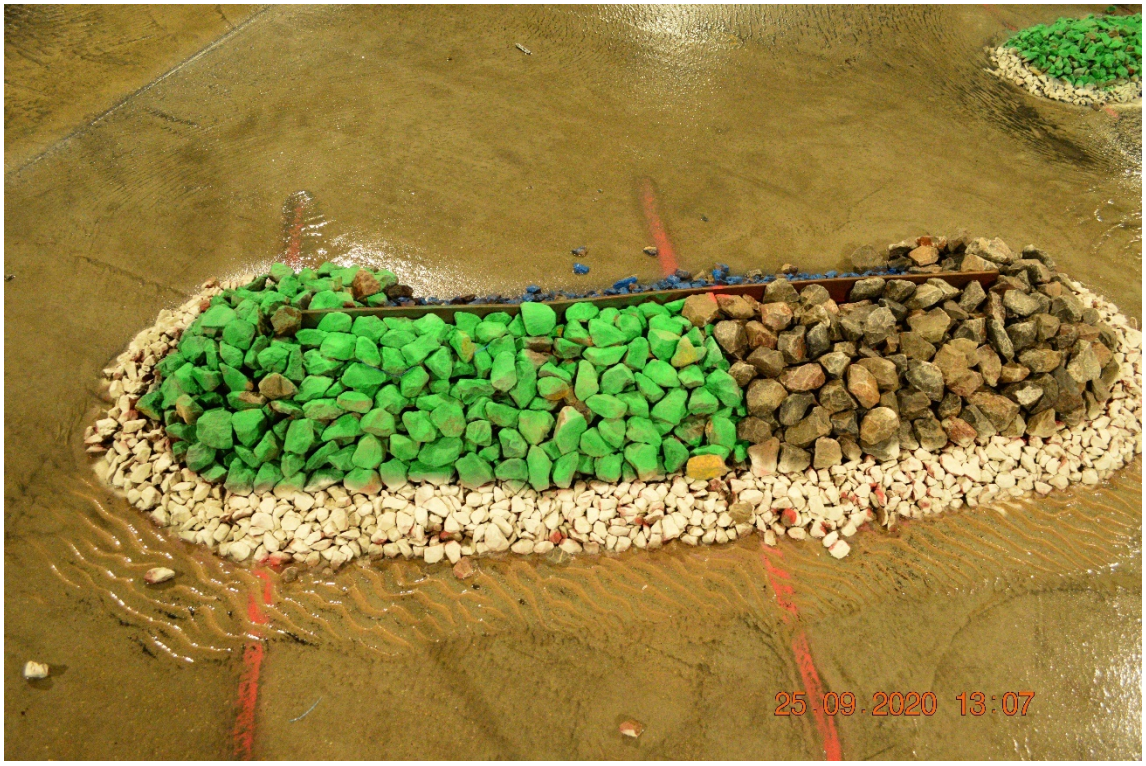


Figure B.91: Post Test Part 06 (WC_HIGH_WL, SE) stability photograph for BW1-4, position 5

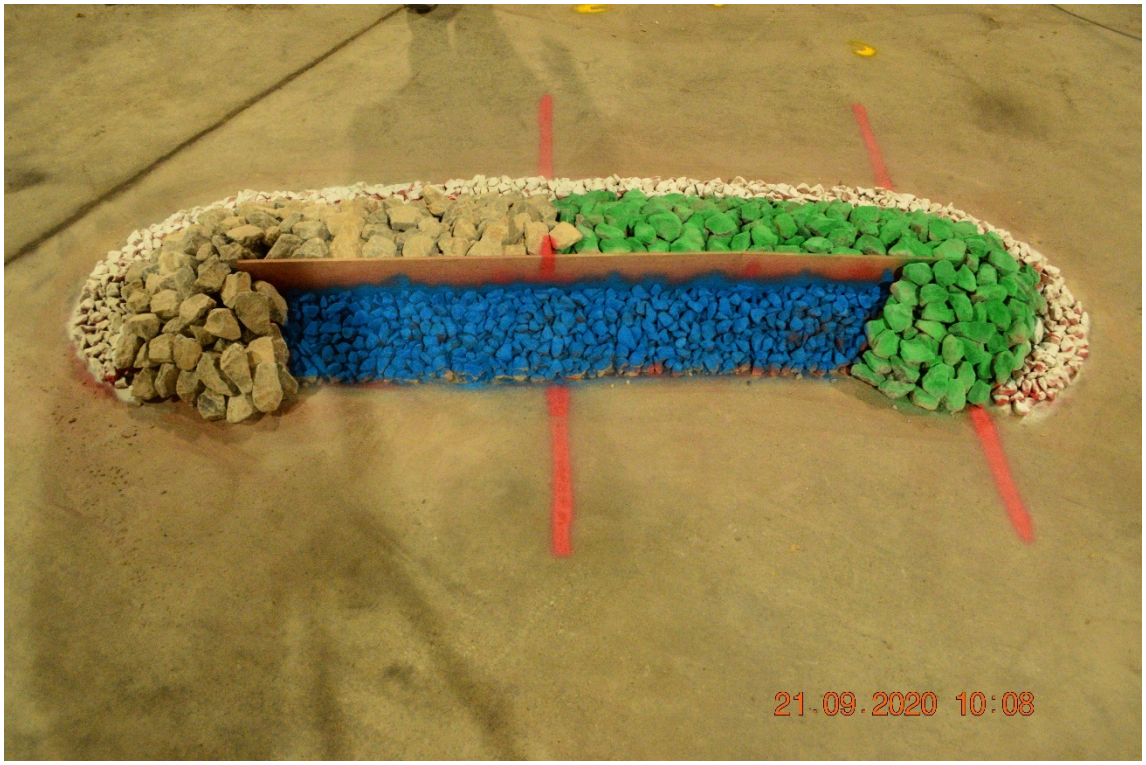


Figure B.92: Pre-test stability photograph for BW1-4, position 6

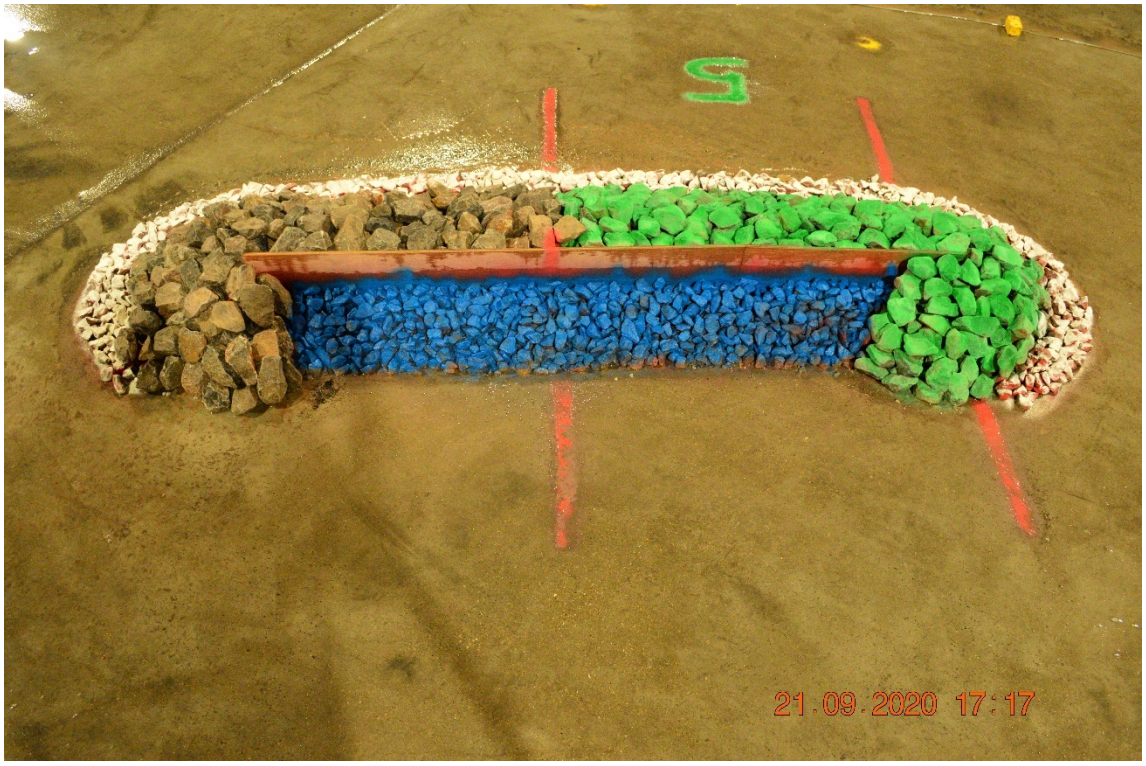


Figure B.93: Post Test Part 01 (WC_LOW_WL) stability photograph for BW1-4, position 6

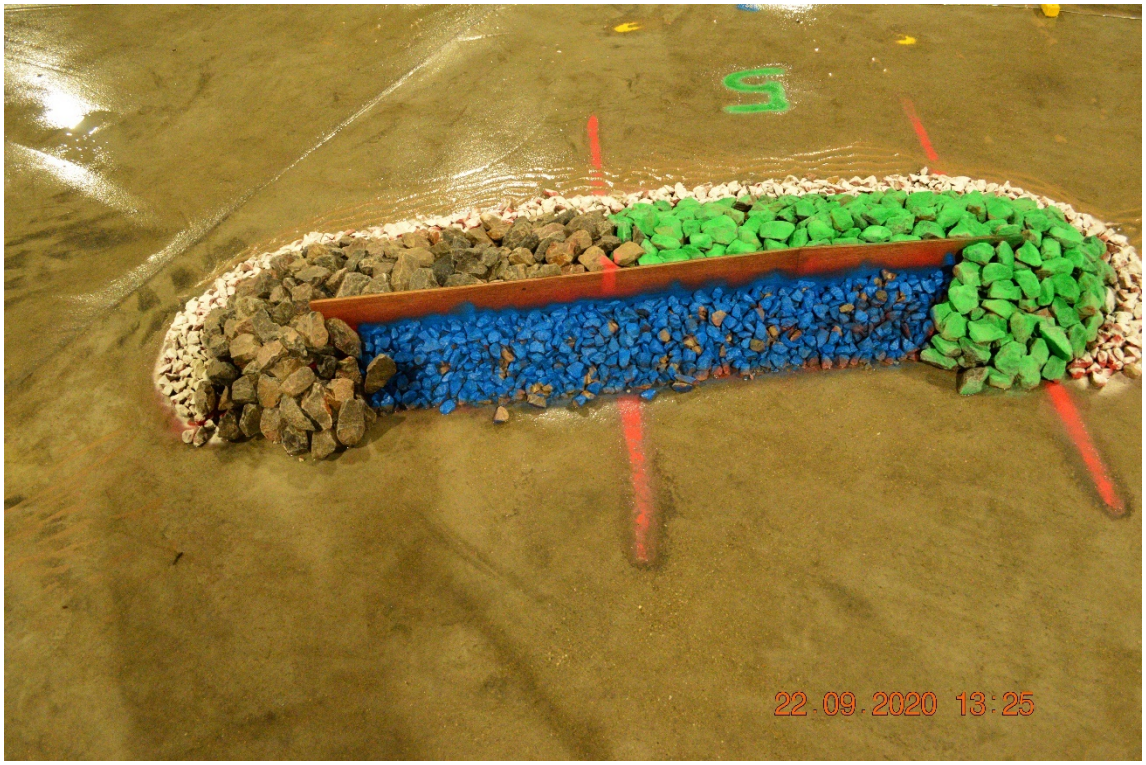


Figure B.94: Post Test Part 02 (WC_HIGH_WL) stability photograph for BW1-4, position 6

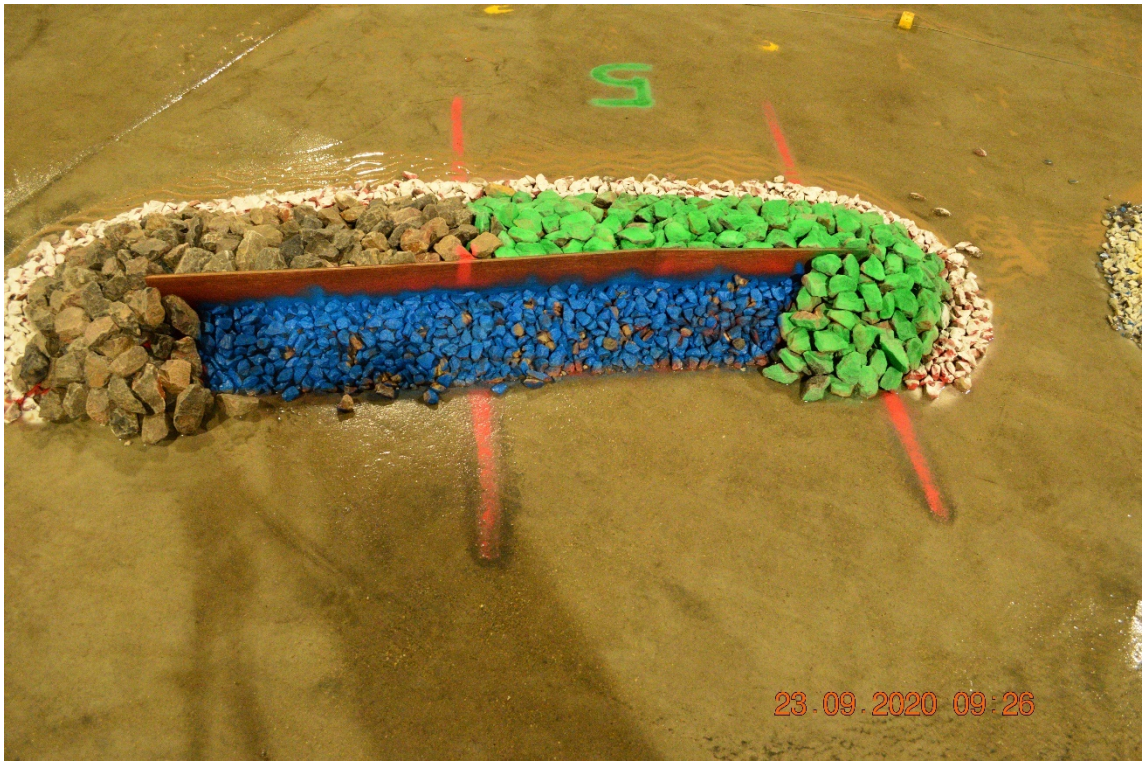


Figure B.95: Post Test Part 03 (WC_EXT_WL_01) stability photograph for BW1-4, position 6

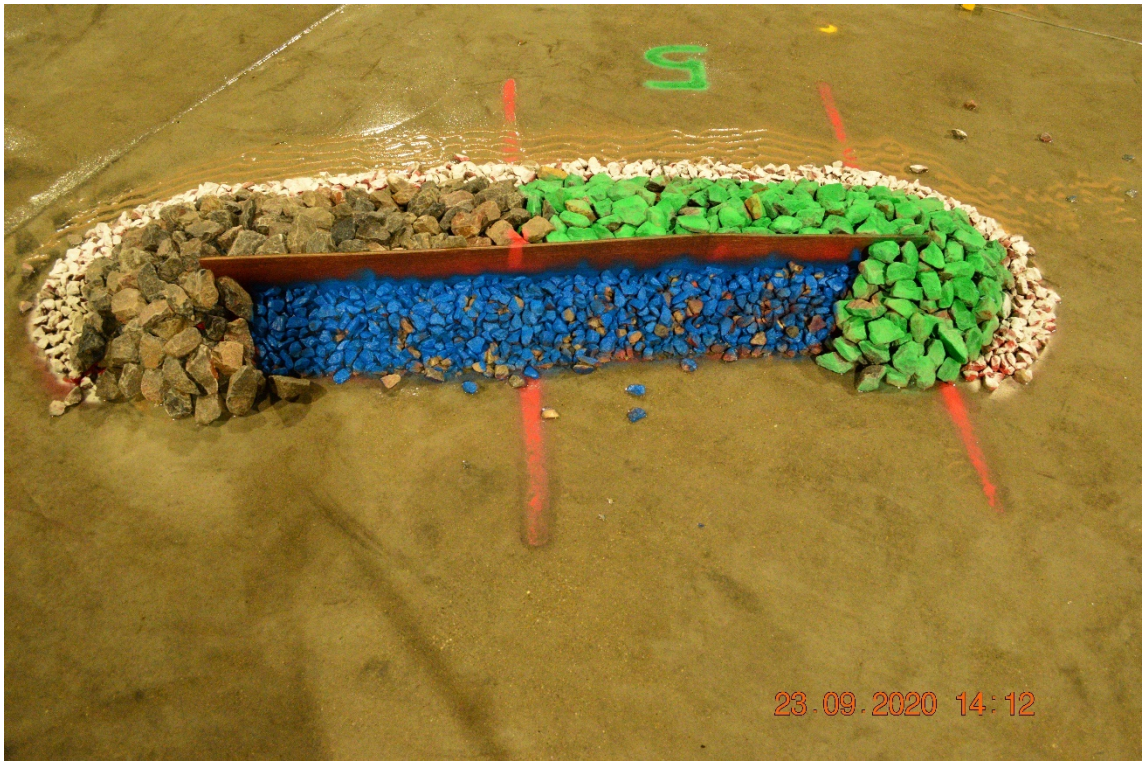


Figure B.96: Post Test Part 04 (WC_EXT_WL_02) stability photograph for BW1-4, position 6

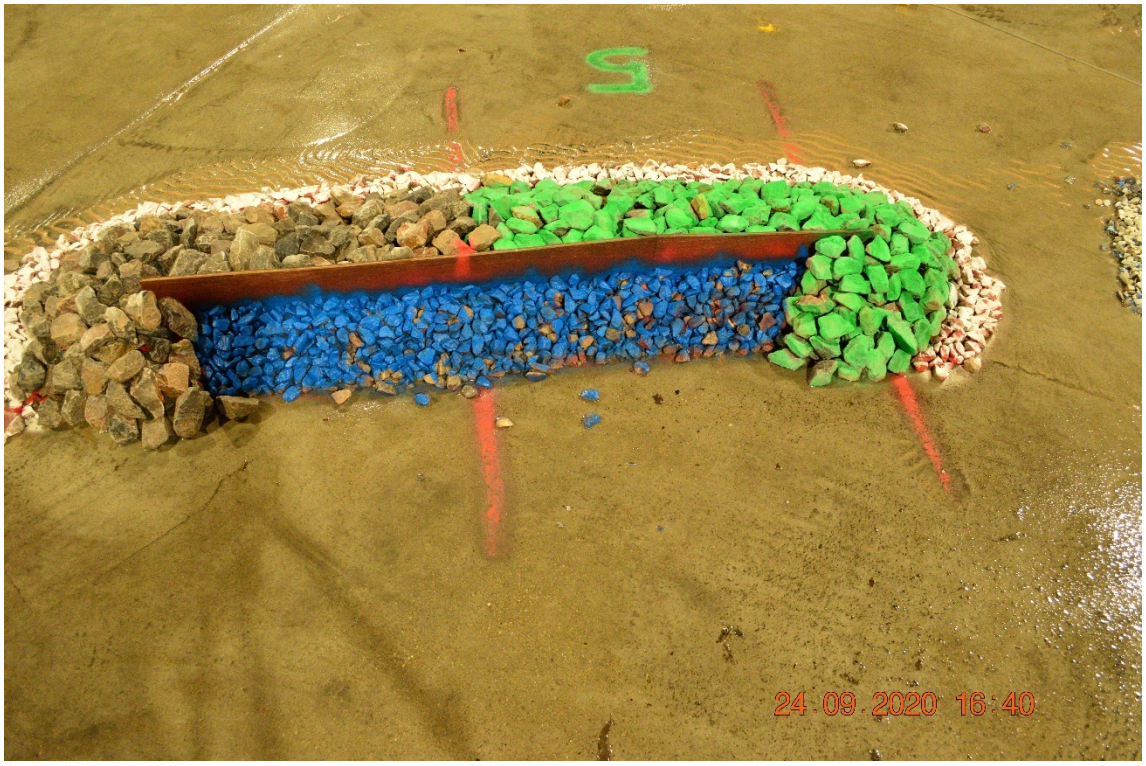


Figure B.97: Post Test Part 05 (WC_LOW_WL, SE) stability photograph for BW1-4, position 6

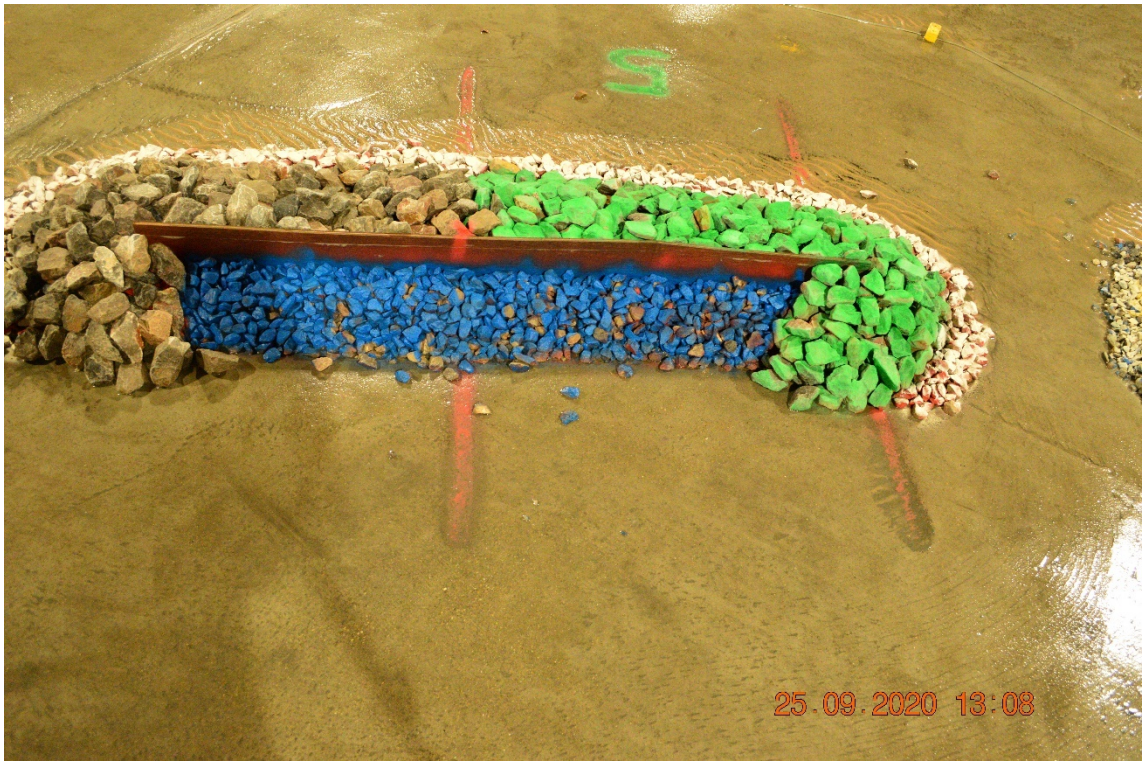


Figure B.98: Post Test Part 06 (WC_HIGH_WL, SE) stability photograph for BW1-4, position 6

## B.2.5. BW1-5

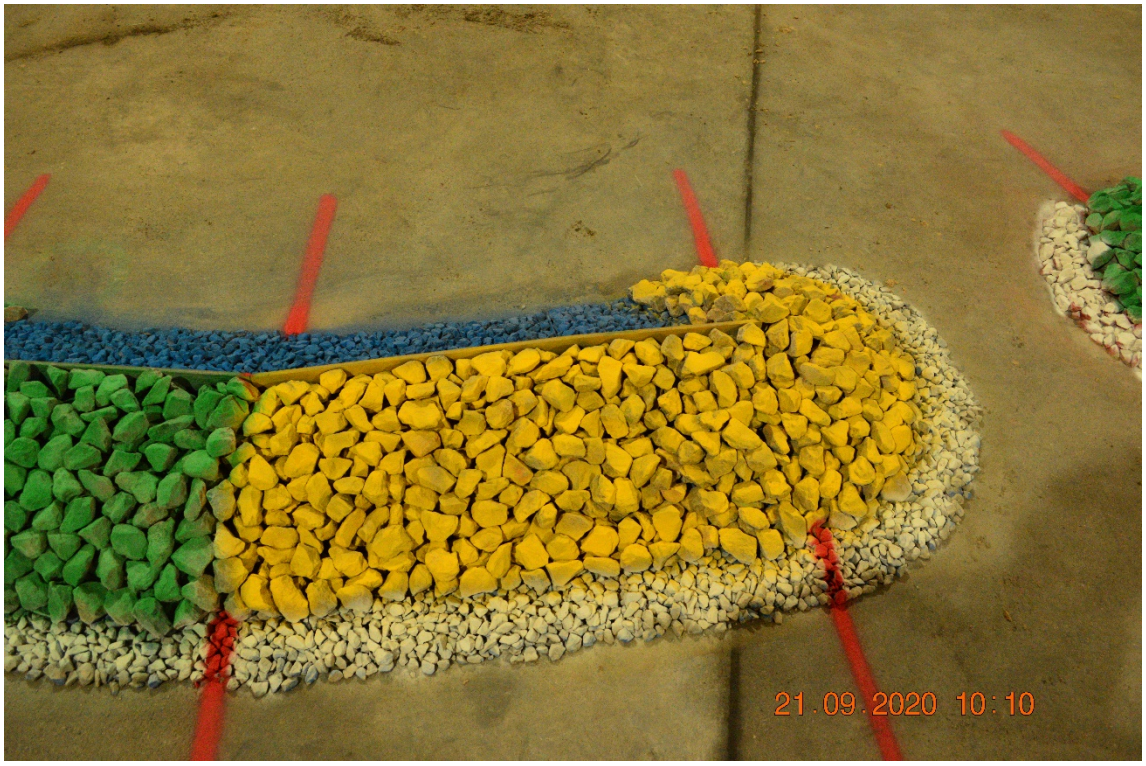


Figure B.99: Pre-test stability photograph for BW1-5, position 7

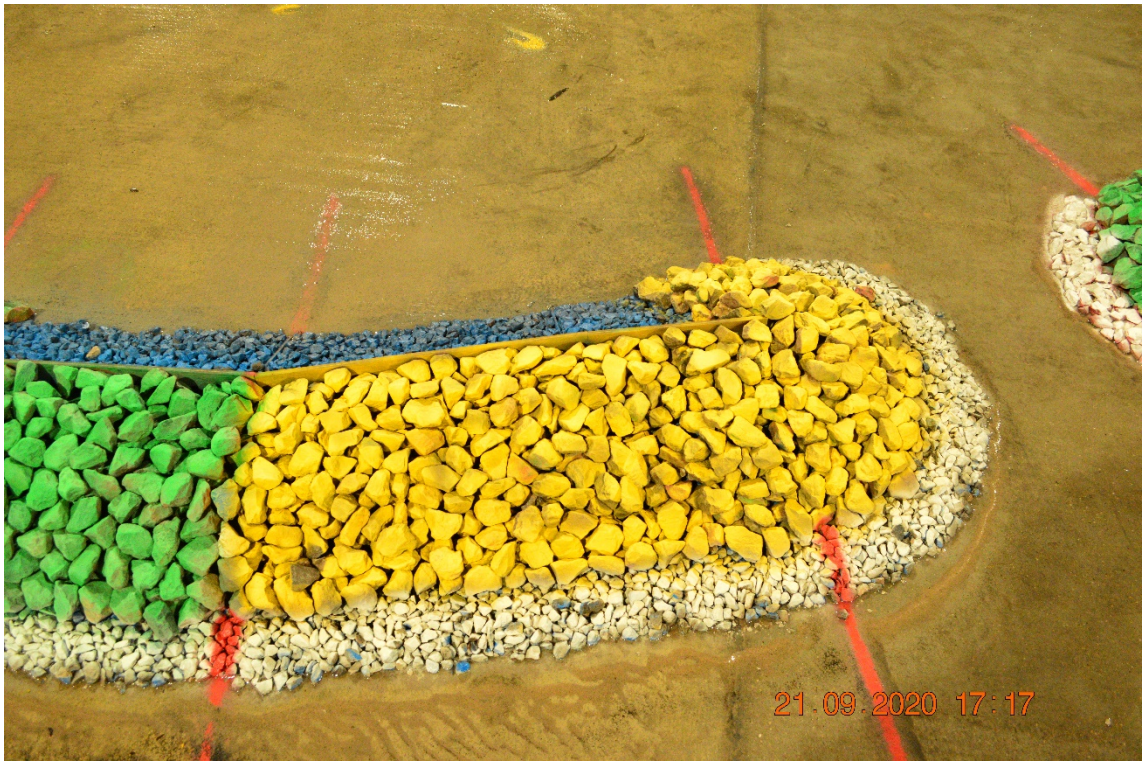


Figure B.100: Post Test Part 01 (WC_LOW_WL) stability photograph for BW1-5, position 7

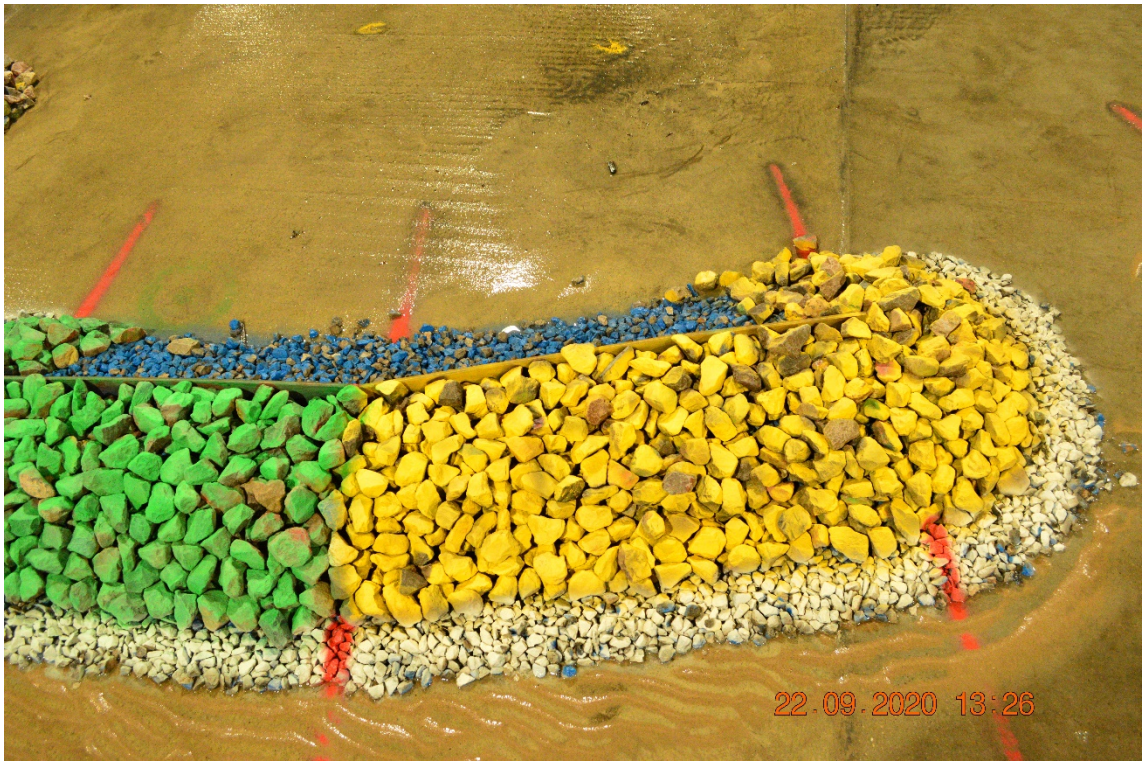


Figure B.101: Post Test Part 02 (WC_HIGH_WL) stability photograph for BW1-5, position 7

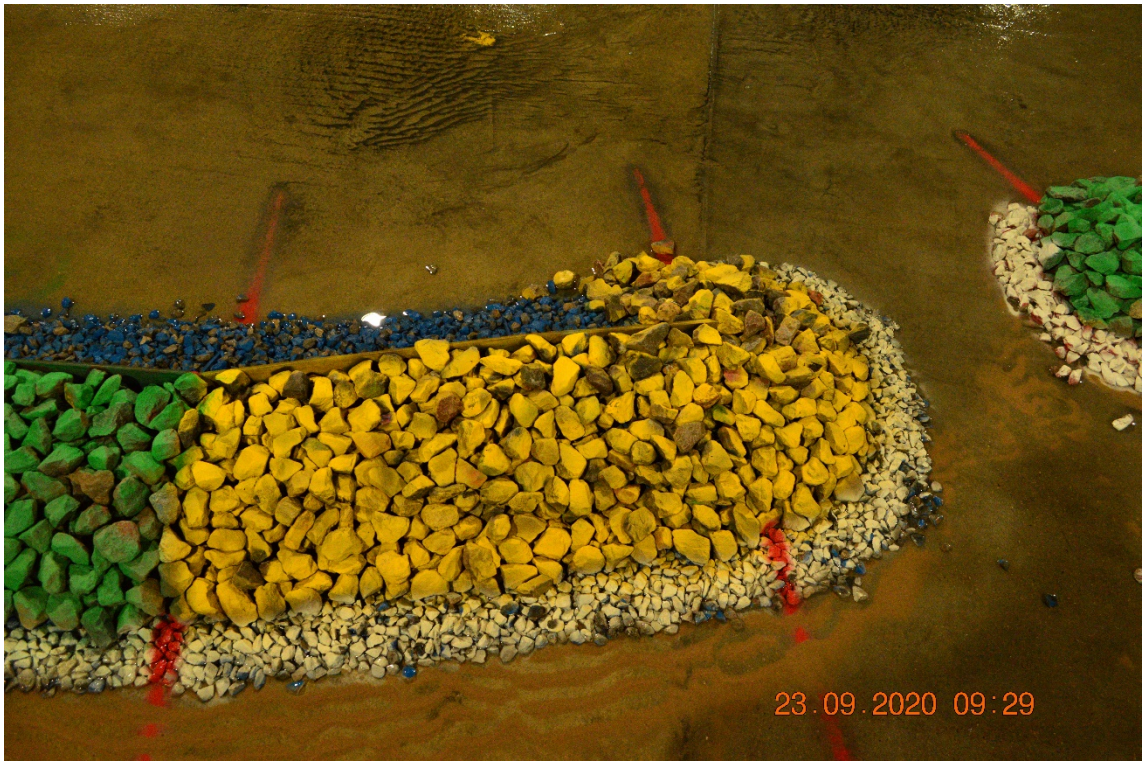


Figure B.102: Post Test Part 03 (WC_EXT_WL_01) stability photograph for BW1-5, position 7

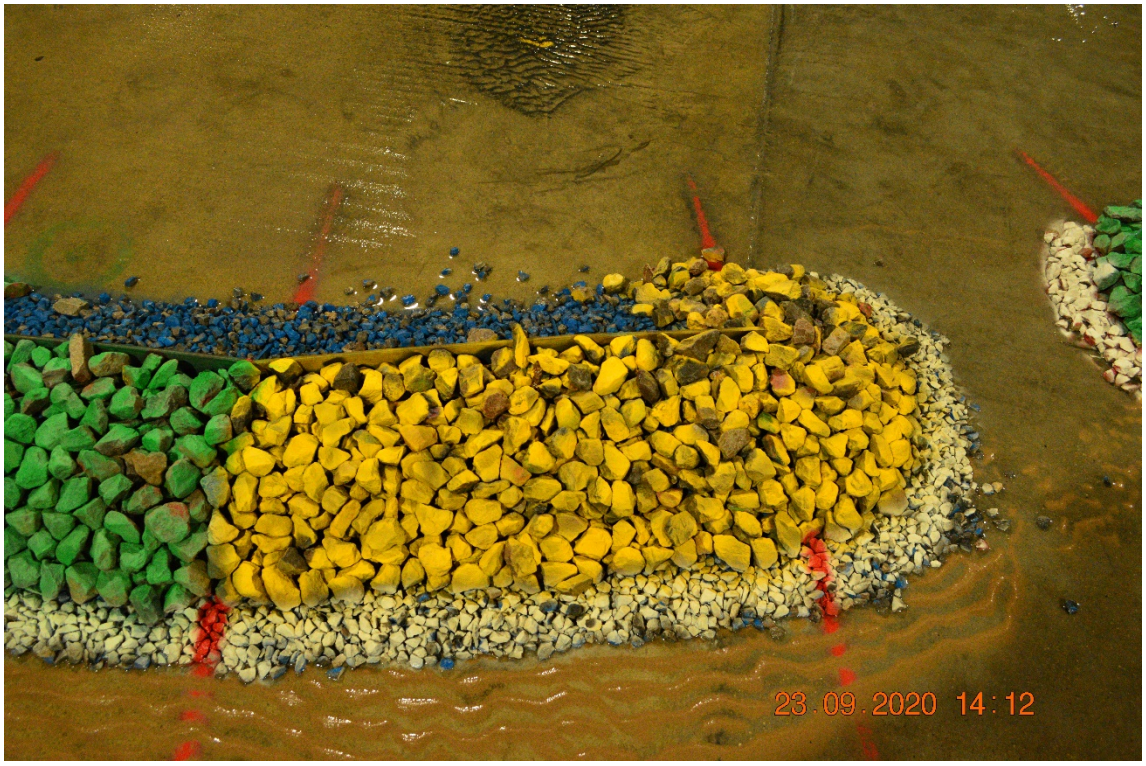


Figure B.103: Post Test Part 04 (WC_EXT_WL_02) stability photograph for BW1-5, position 7

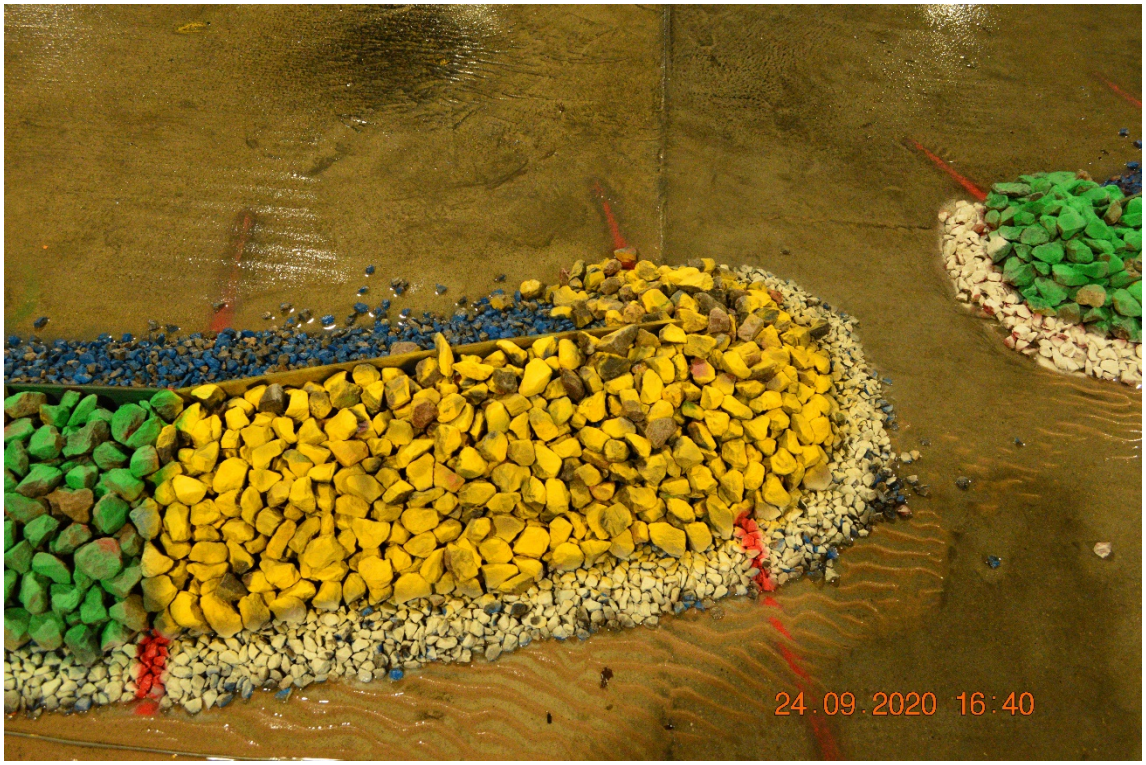


Figure B.104: Post Test Part 05 (WC_LOW_WL, SE) stability photograph for BW1-5, position 7

Figure B.105: Post Test Part 06 (WC_HIGH_WL, SE) stability photograph for BW1-5, position 7

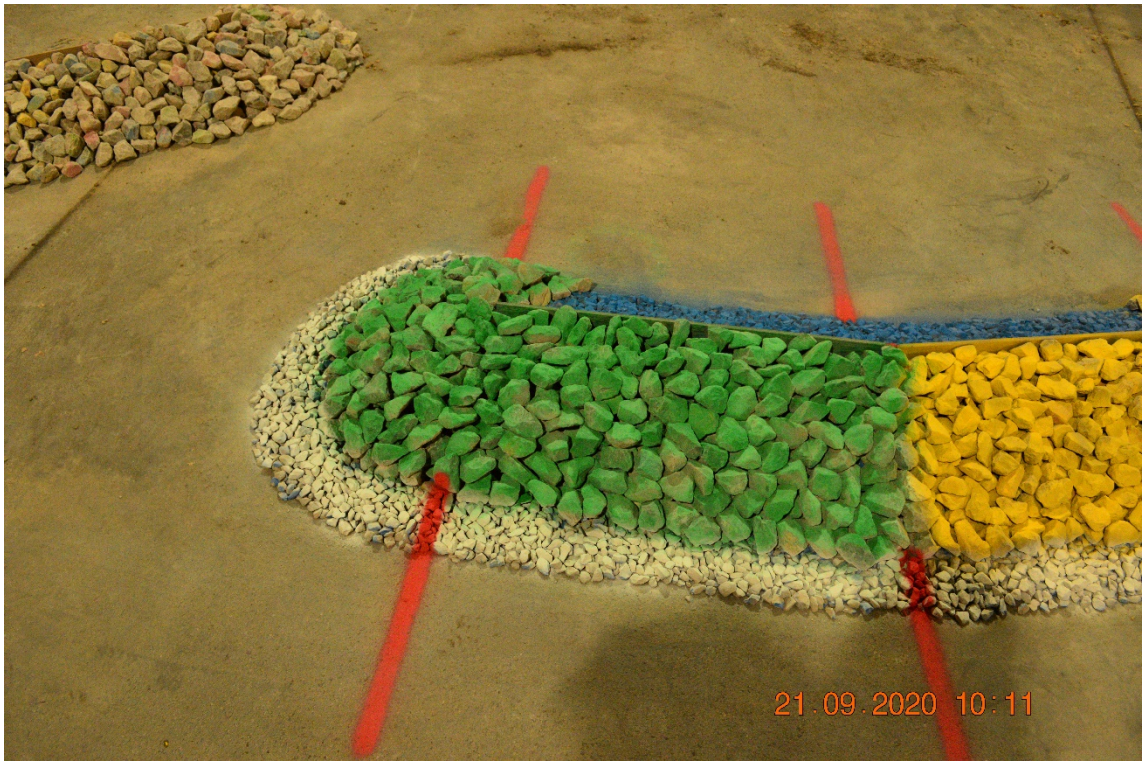


Figure B.106: Pre-test stability photograph for BW1-5, position 8

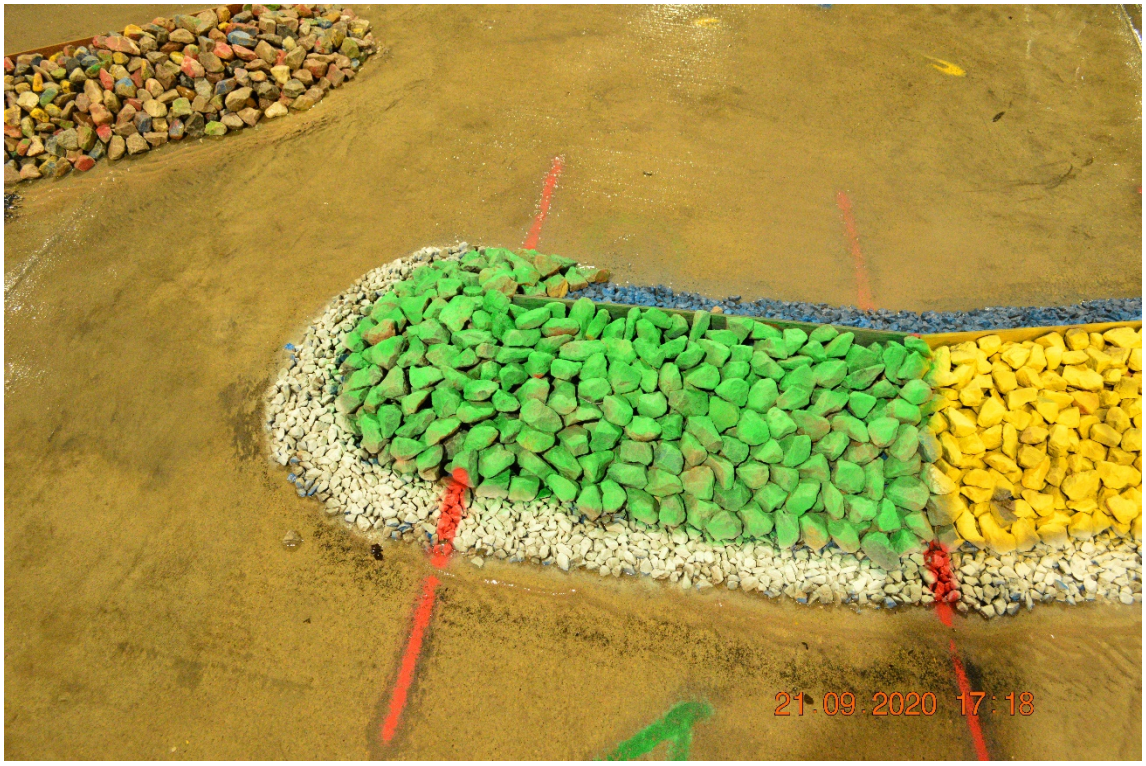


Figure B.107: Post Test Part 01 (WC_LOW_WL) stability photograph for BW1-5, position 8

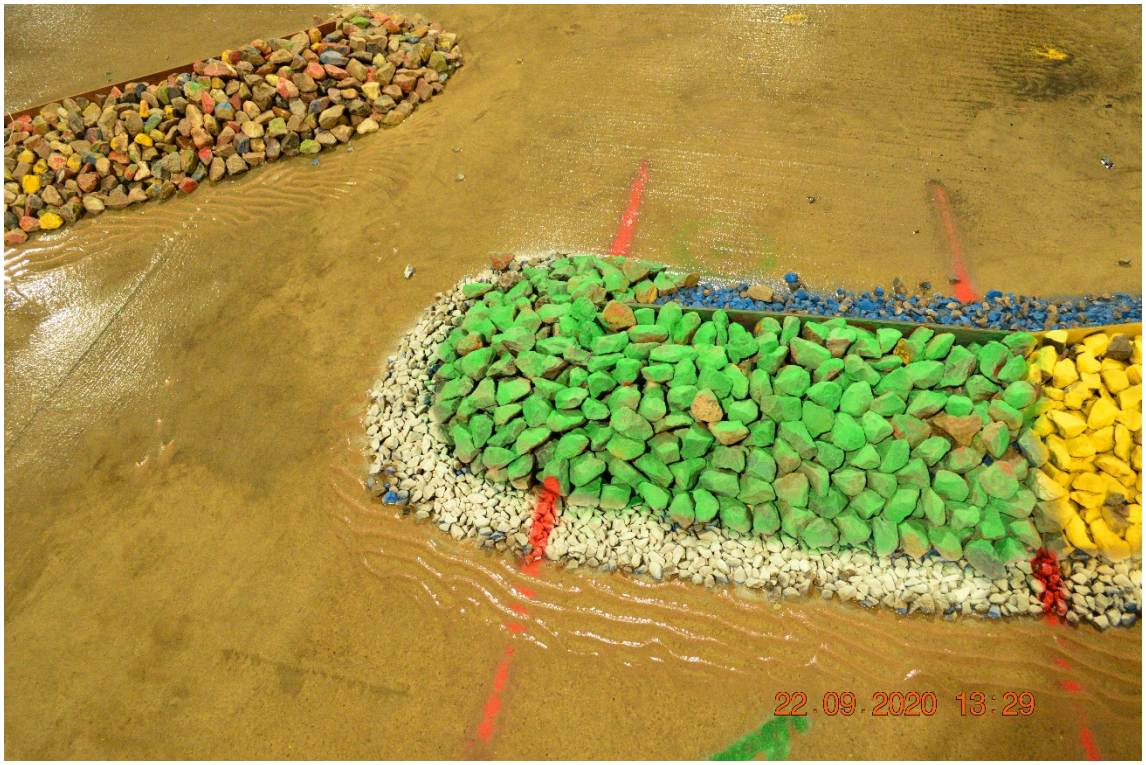


Figure B.108: Post Test Part 02 (WC_HIGH_WL) stability photograph for BW1-5, position 8

Figure B.109: Post Test Part 03 (WC_EXT_WL_01) stability photograph for BW1-5, position 8

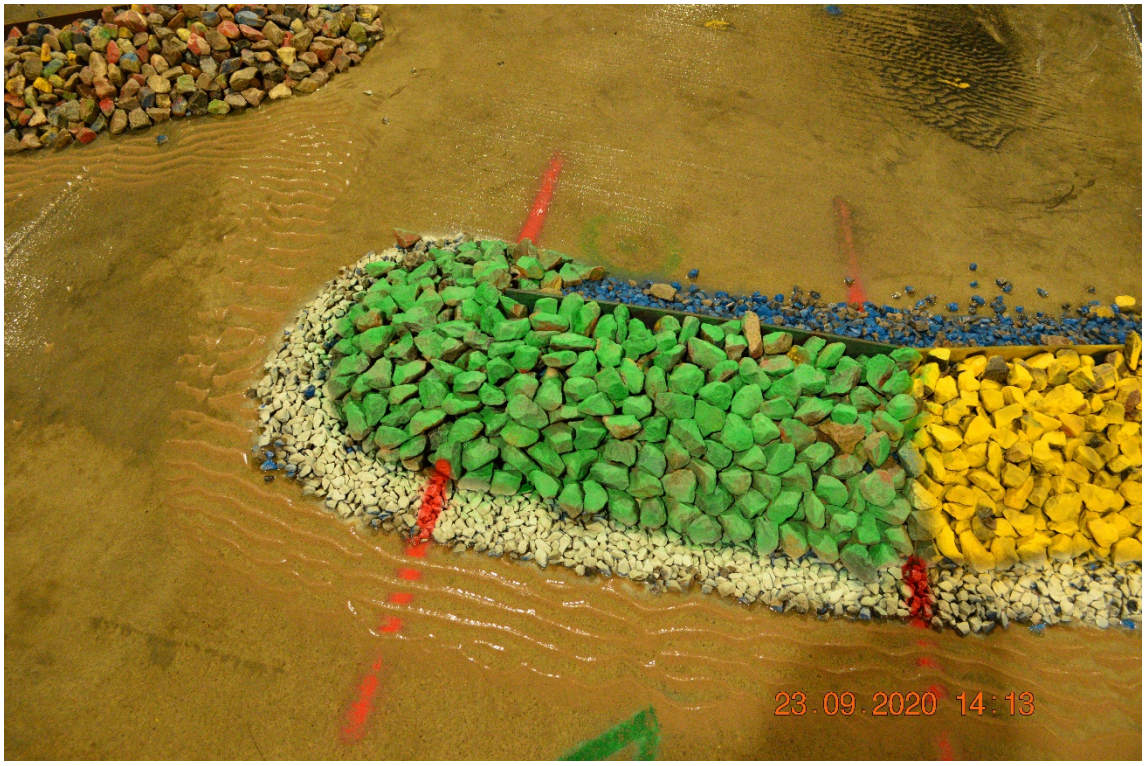


Figure B.110: Post Test Part 04 (WC_EXT_WL_02) stability photograph for BW1-5, position 8

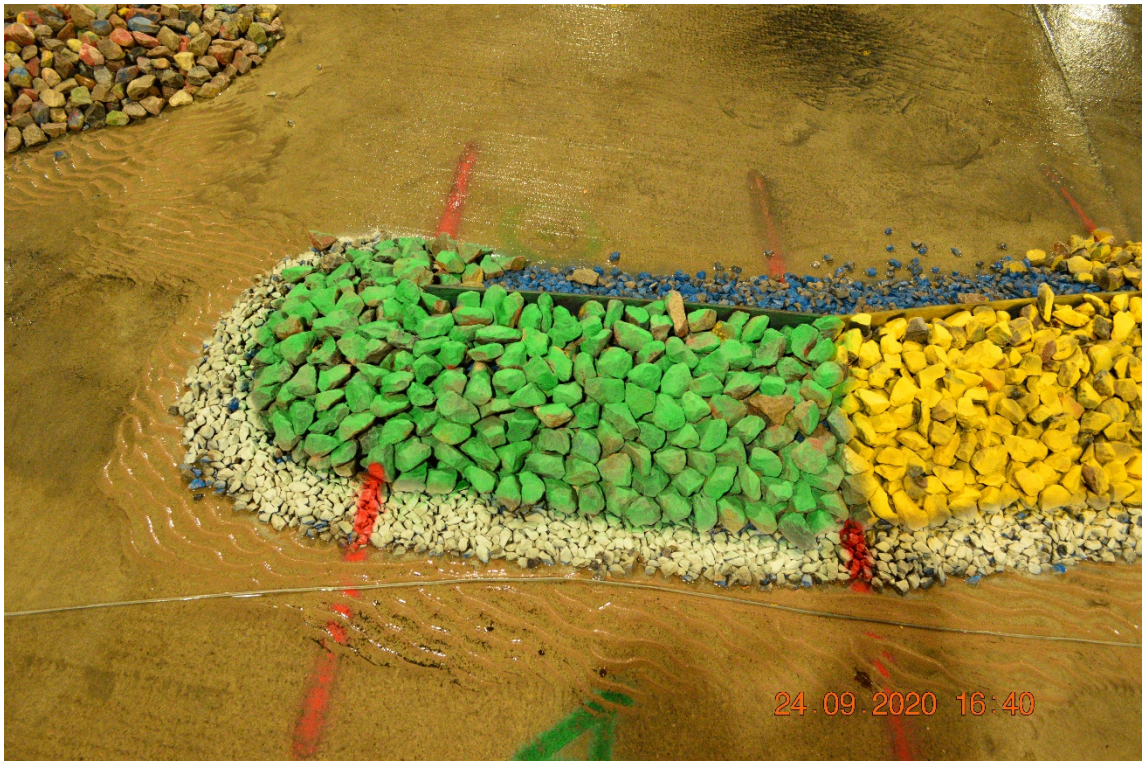


Figure B.111: Post Test Part 05 (WC_LOW_WL, SE) stability photograph for BW1-5, position 8

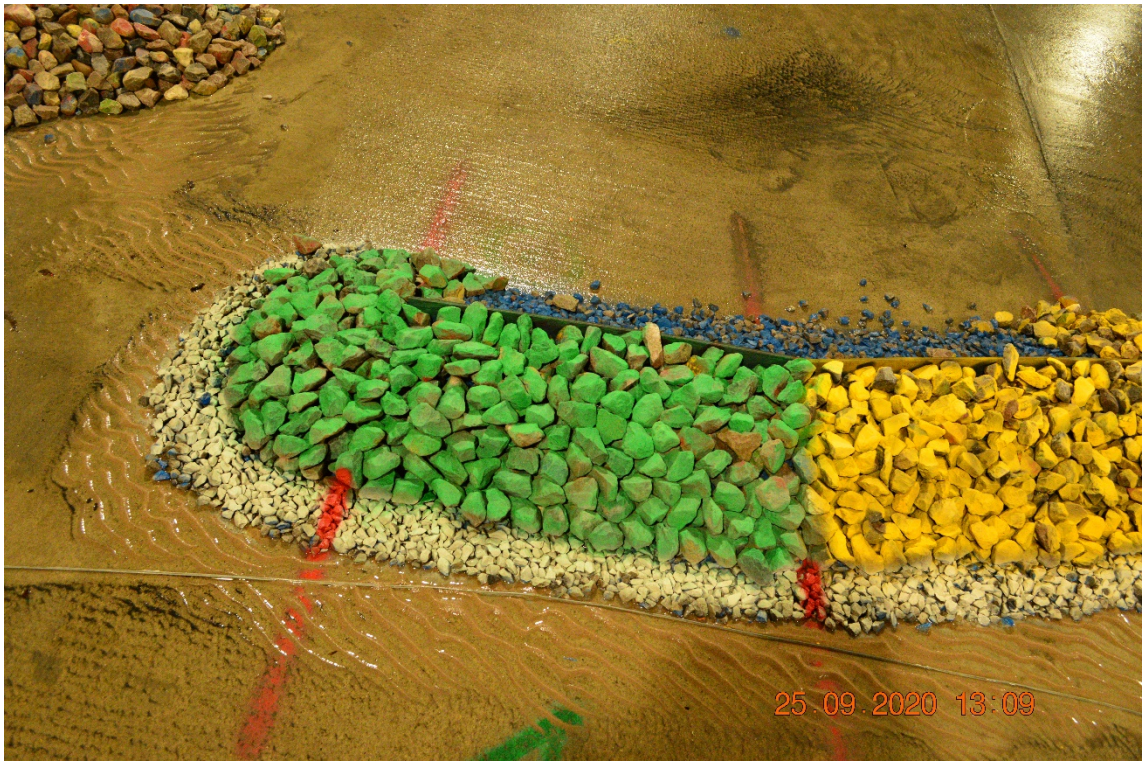


Figure B.112: Post Test Part 06 (WC_HIGH_WL, SE) stability photograph for BW1-5, position 8

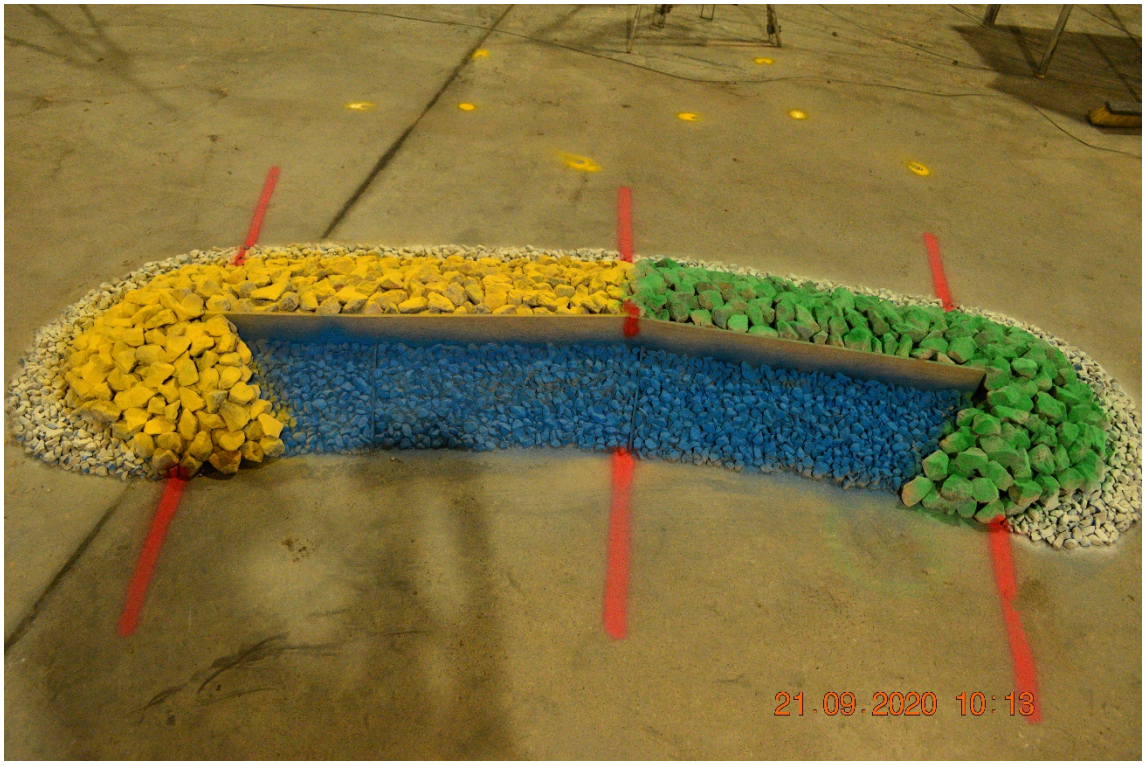


Figure B.113: Pre-test stability photograph for BW1-5, position 9

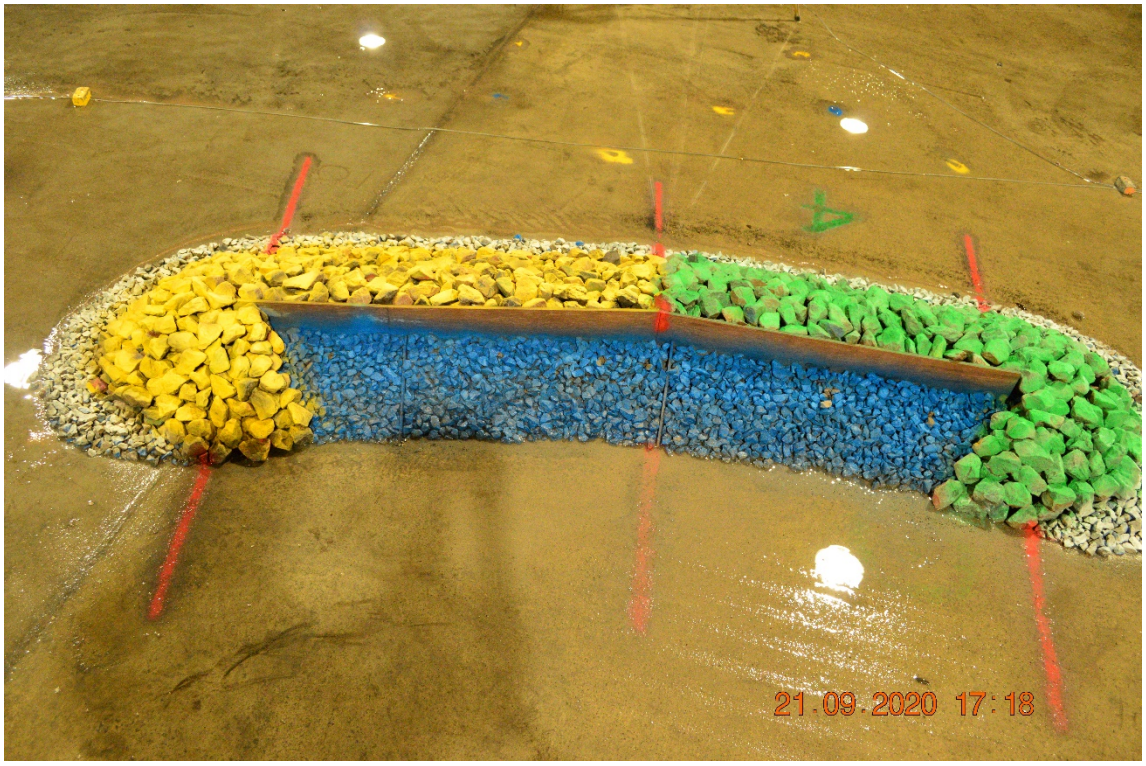


Figure B.114: Post Test Part 01 (WC_LOW_WL) stability photograph for BW1-5, position 9

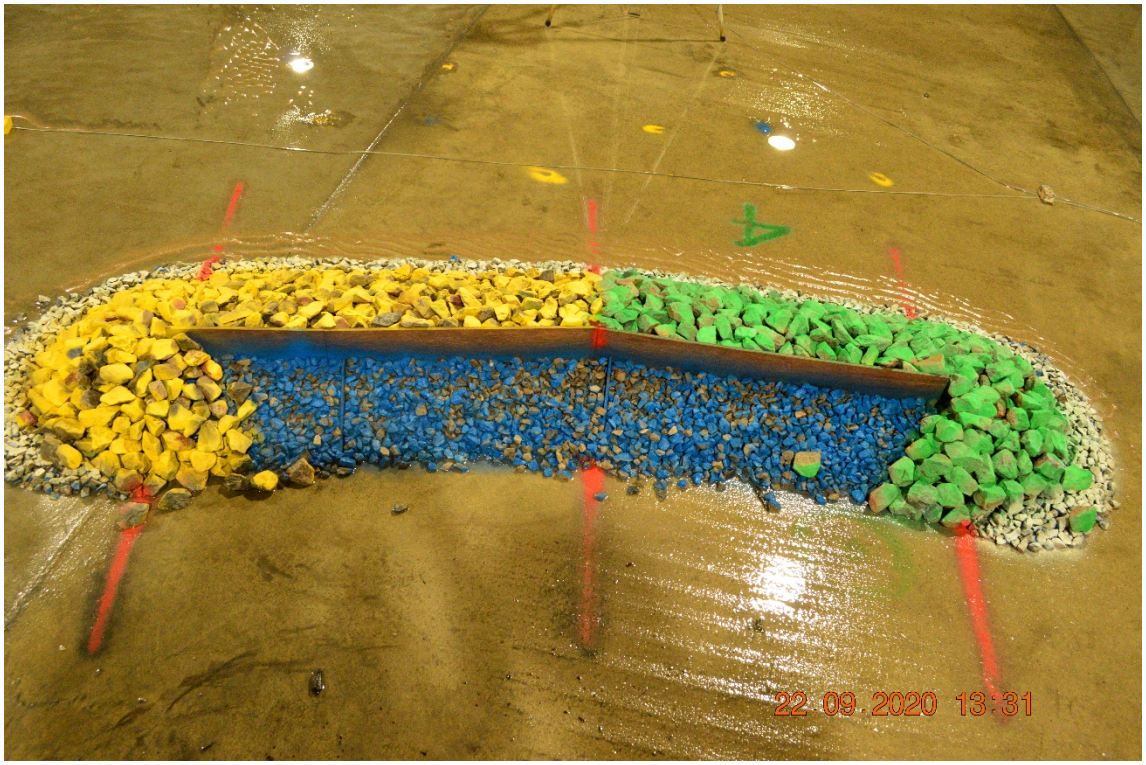


Figure B.115: Post Test Part 02 (WC_HIGH_WL) stability photograph for BW1-5, position 9

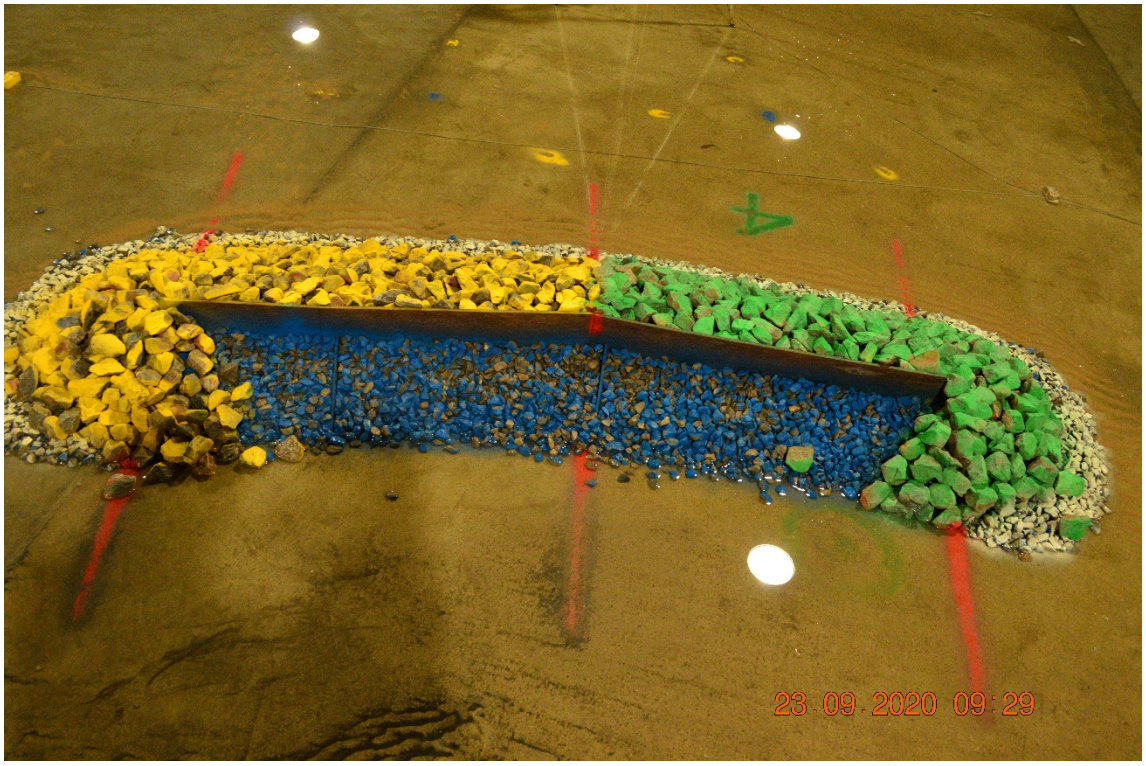


Figure B.116: Post Test Part 03 (WC_EXT_WL_01) stability photograph for BW1-5, position 9

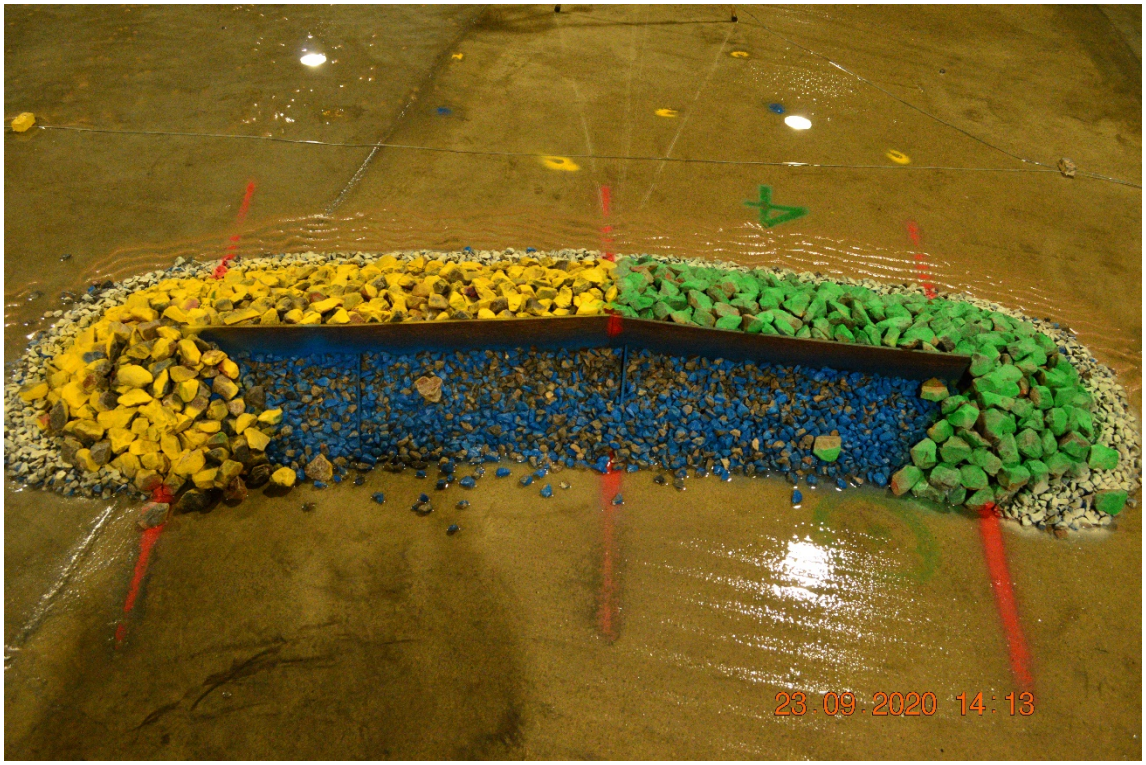


Figure B.117: Post Test Part 04 (WC_EXT_WL_02) stability photograph for BW1-5, position 9

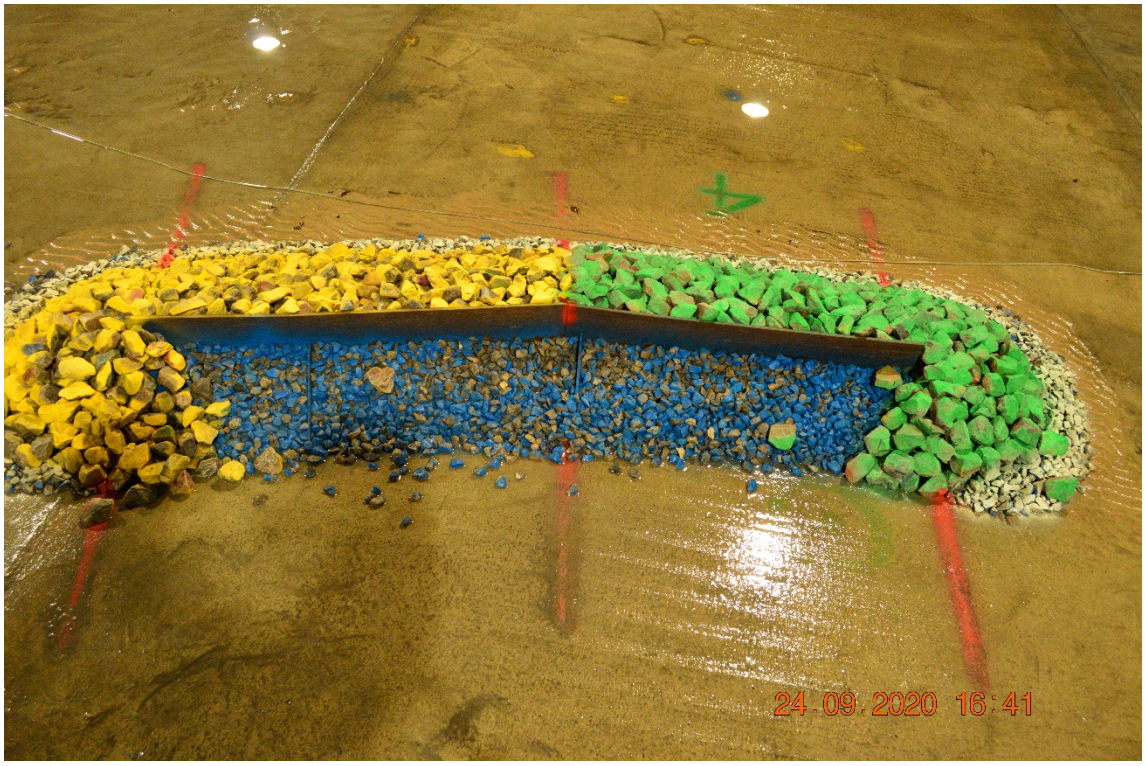


Figure B.118: Post Test Part 05 (WC_LOW_WL, SE) stability photograph for BW1-5, position 9

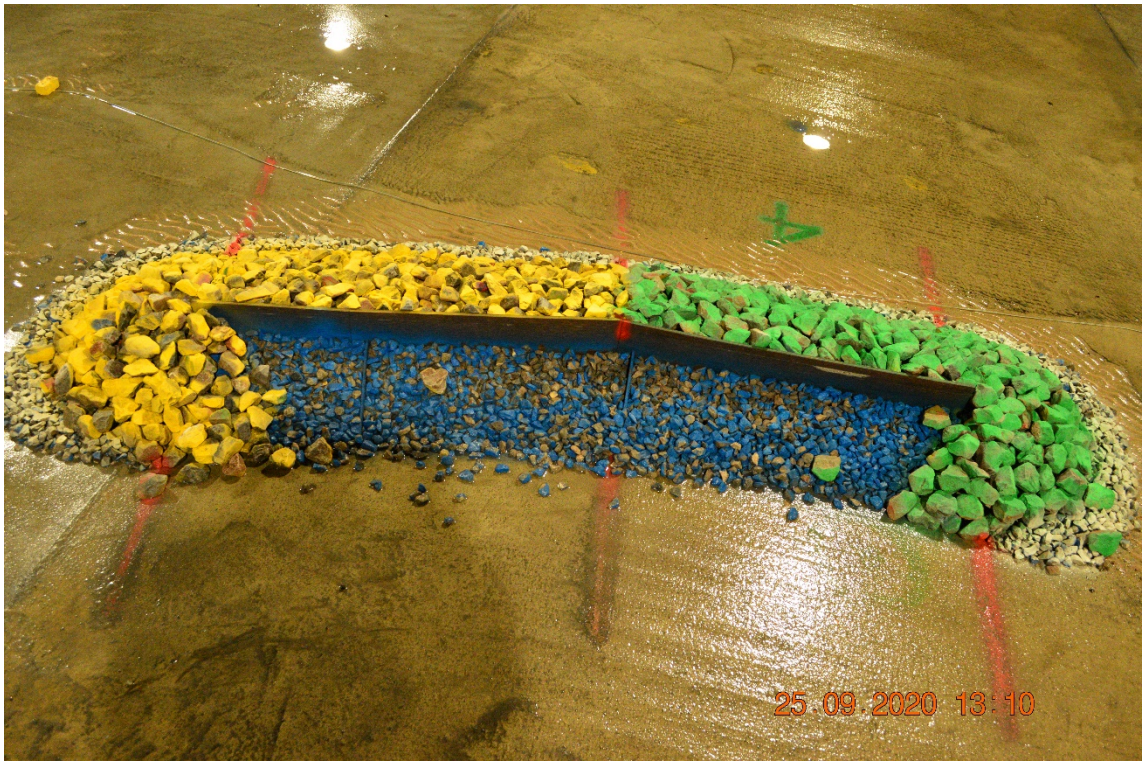


Figure B.119: Post Test Part 06 (WC_HIGH_WL, SE) stability photograph for BW1-5, position 9

## B.2.6. BW1-8

Figure B.120: Pre-test stability photograph for BW1-8, position 10

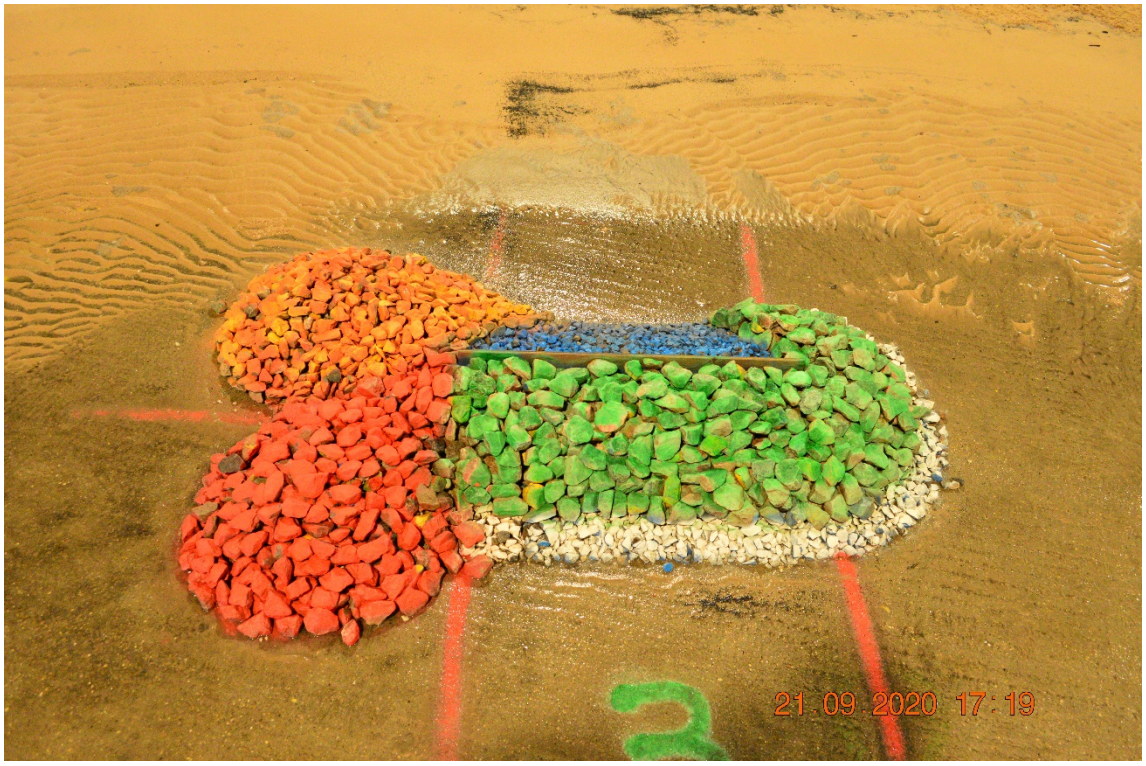


Figure B.121: Post Test Part 01 (WC_LOW_WL) stability photograph for BW1-8, position 10

Figure B.122: Post Test Part 02 (WC_HIGH_WL) stability photograph for BW1-8, position 10

Figure B.123: Post Test Part 03 (WC_EXT_WL_01) stability photograph for BW1-8, position 10

Figure B.124: Post Test Part 04 (WC_EXT_WL_02) stability photograph for BW1-8, position 10

Figure B.125: Post Test Part 05 (WC_LOW_WL, SE) stability photograph for BW1-8, position 10

Figure B.126: Post Test Part 06 (WC_HIGH_WL, SE) stability photograph for BW1-8, position 10

Figure B.127: Pre-test stability photograph for BW1-8, position 11

Figure B.128: Post Test Part 01 (WC_LOW_WL) stability photograph for BW1-8, position 11

Figure B.129: Post Test Part 02 (WC_HIGH_WL) stability photograph for BW1-8, position 11

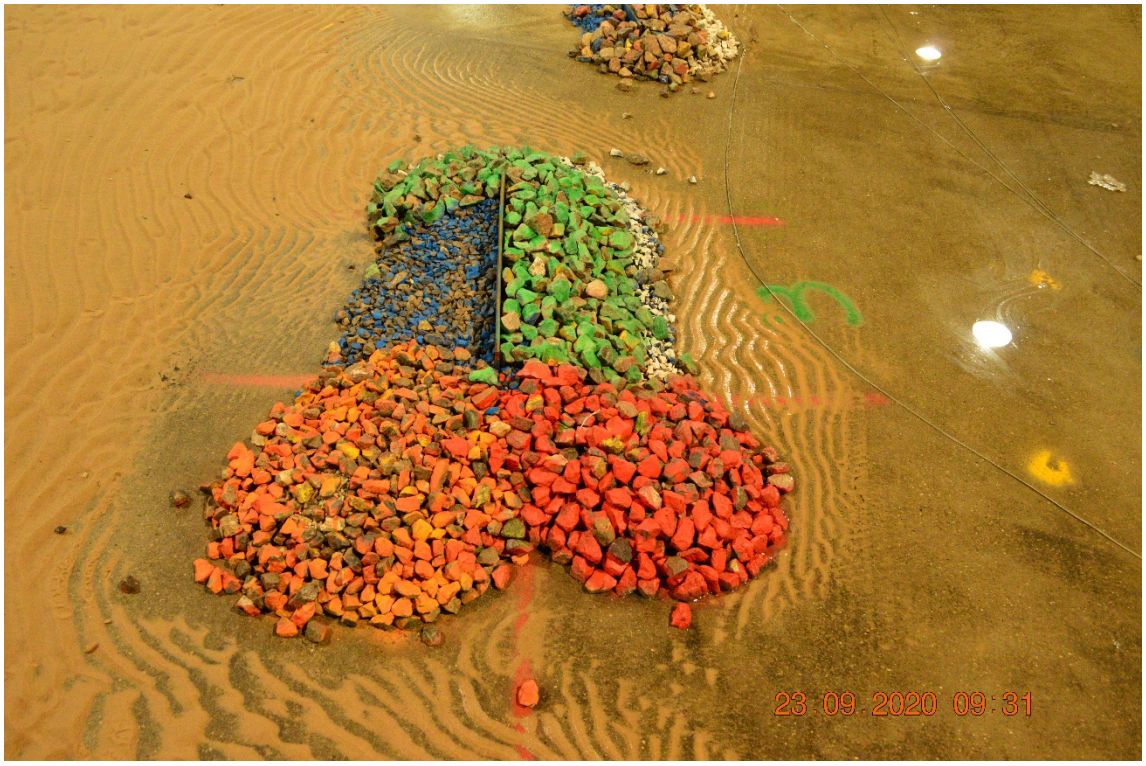


Figure B.130: Post Test Part 03 (WC_EXT_WL_01) stability photograph for BW1-8, position 11

Figure B.131: Post Test Part 04 (WC_EXT_WL_02) stability photograph for BW1-8, position 11

Figure B.132: Post Test Part 05 (WC_LOW_WL, SE) stability photograph for BW1-8, position 11

Figure B.133: Post Test Part 06 (WC_HIGH_WL, SE) stability photograph for BW1-8, position 11

Figure B.134: Pre-test stability photograph for BW1-8, position 12

Figure B.135: Post Test Part 01 (WC_LOW_WL) stability photograph for BW1-8, position 12

No image available

Figure B.136: Post Test Part 02 (WC_HIGH_WL) stability photograph for BW1-8, position 12

Figure B.137: Post Test Part 03 (WC_EXT_WL_01) stability photograph for BW1-8, position 12

Figure B.138: Post Test Part 04 (WC_EXT_WL_02) stability photograph for BW1-8, position 12

Figure B.139: Post Test Part 05 (WC_LOW_WL, SE) stability photograph for BW1-8, position 12

Figure B.140: Post Test Part 06 (WC_HIGH_WL, SE) stability photograph for BW1-8, position 12

## B.2.7. BW1-10

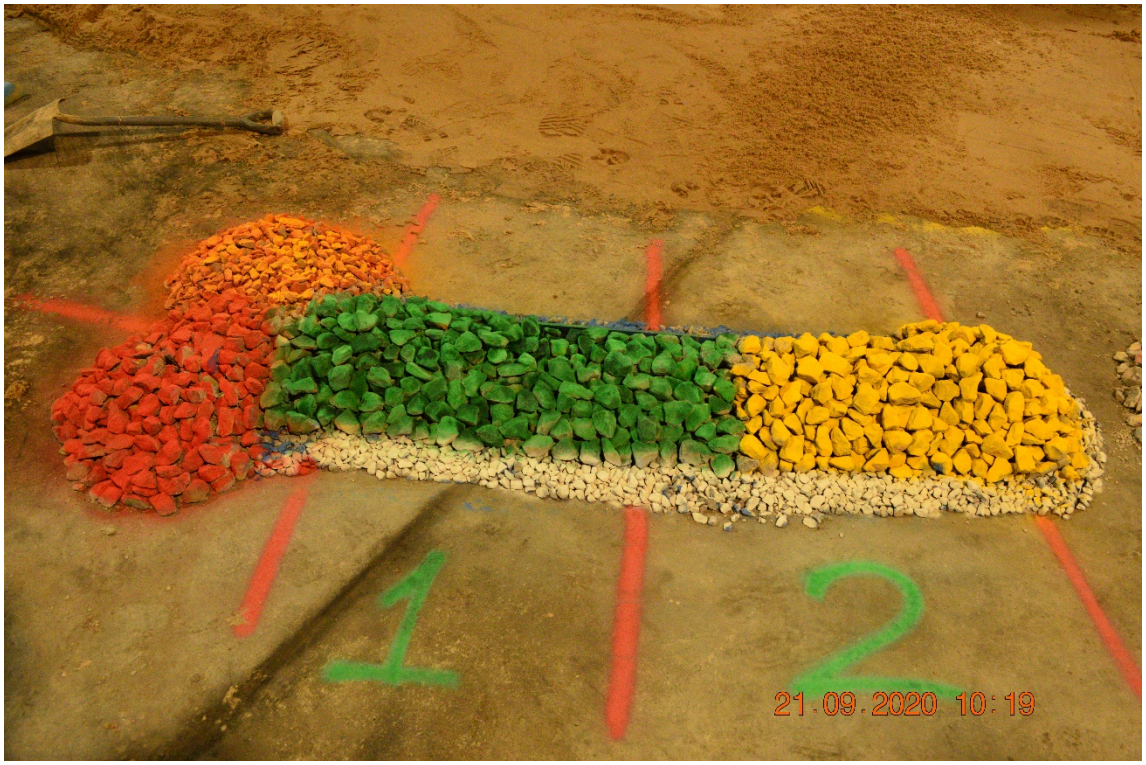


Figure B.141: Pre-test stability photograph for BW1-10, position 13

Figure B.142: Post Test Part 01 (WC_LOW_WL) stability photograph for BW1-10, position 13

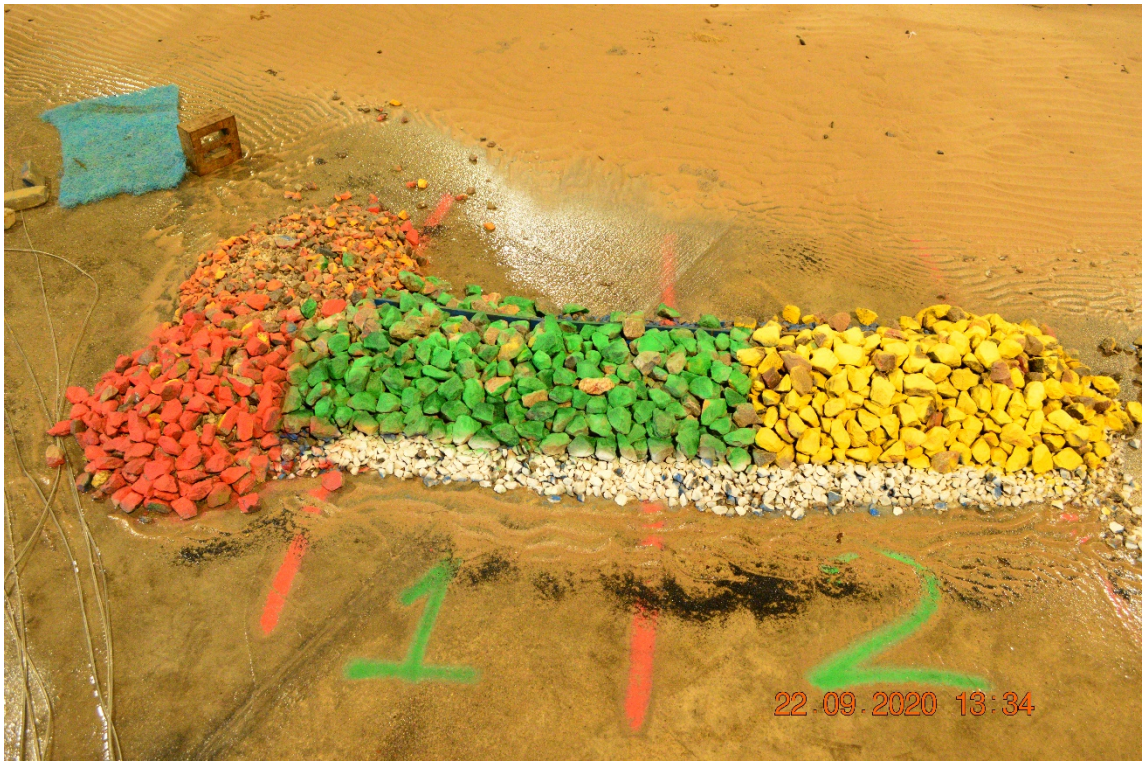


Figure B.143: Post Test Part 02 (WC_HIGH_WL) stability photograph for BW1-10, position 13

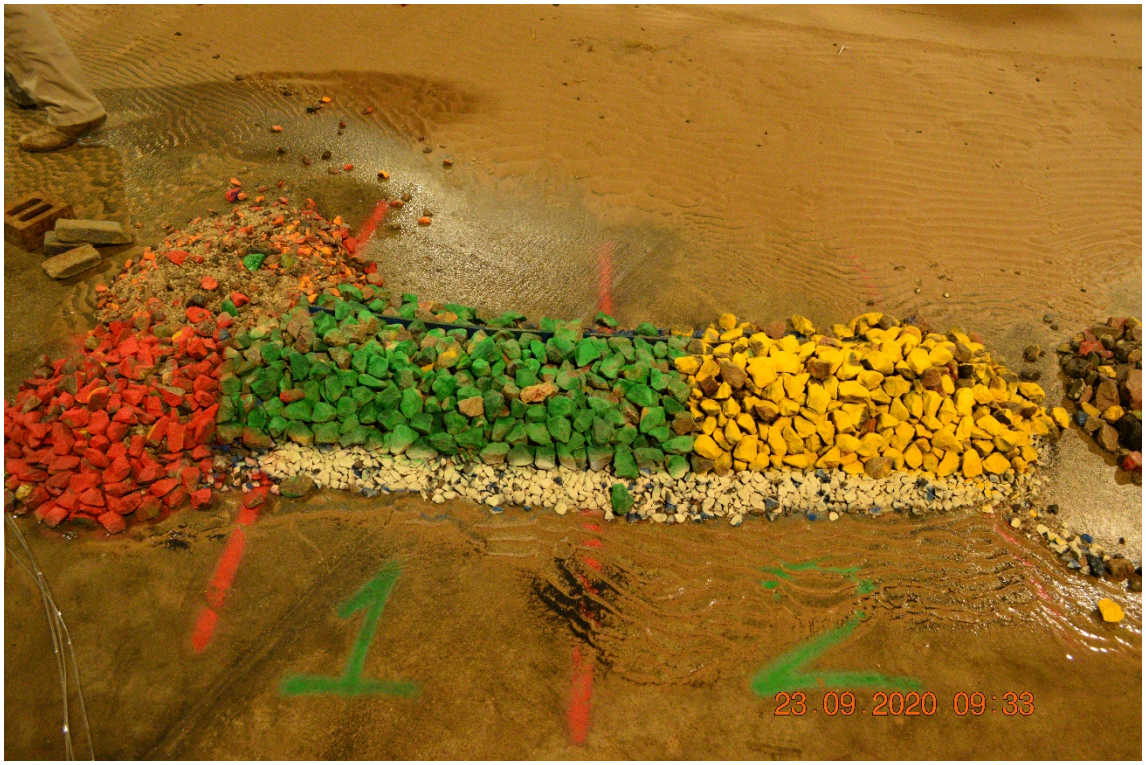


Figure B.144: Post Test Part 03 (WC_EXT_WL_01) stability photograph for BW1-10, position 13

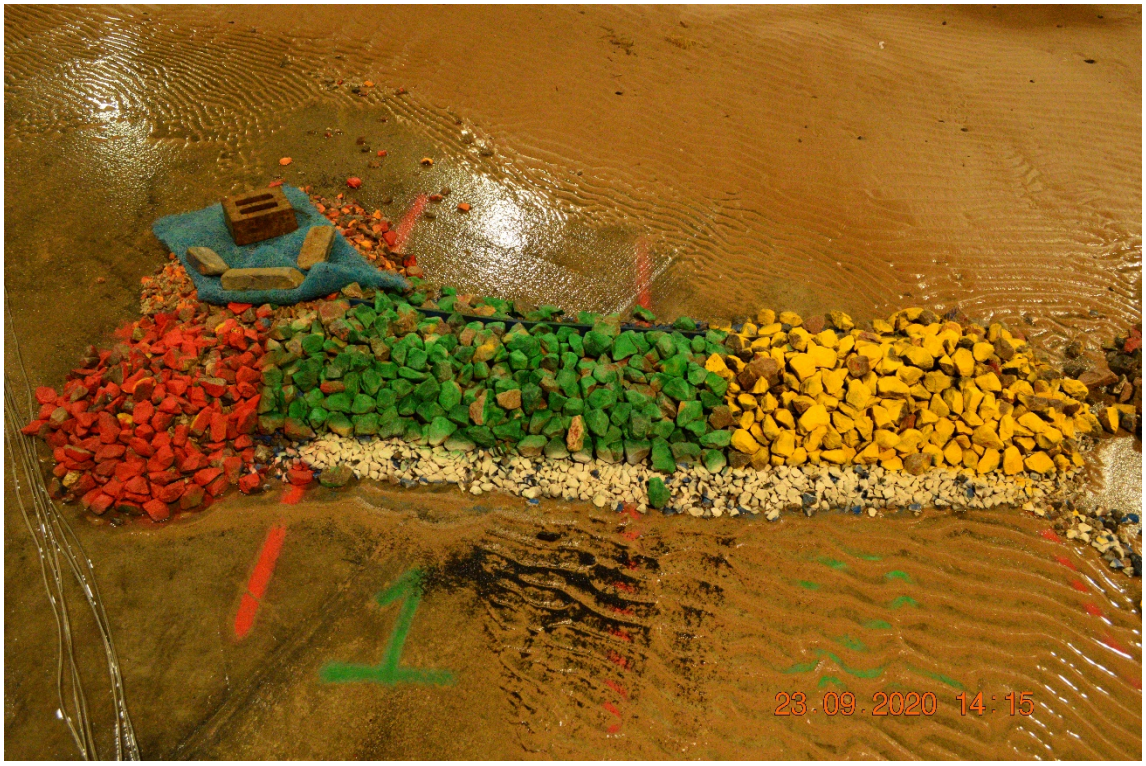


Figure B.145: Post Test Part 04 (WC_EXT_WL_02) stability photograph for BW1-10, position 13

Figure B.146: Post Test Part 05 (WC_LOW_WL, SE) stability photograph for BW1-10, position 13

Figure B.147: Post Test Part 06 (WC_HIGH_WL, SE) stability photograph for BW1-10, position 13

Figure B.148: Pre-test stability photograph for BW1-10, position 14

Figure B.149: Post Test Part 01 (WC_LOW_WL) stability photograph for BW1-10, position 14

Figure B.150: Post Test Part 02 (WC_HIGH_WL) stability photograph for BW1-10, position 14

Figure B.151: Post Test Part 03 (WC_EXT_WL_01) stability photograph for BW1-10, position 14

Figure B.152: Post Test Part 04 (WC_EXT_WL_02) stability photograph for BW1-10, position 14

Figure B.153: Post Test Part 05 (WC_LOW_WL, SE) stability photograph for BW1-10, position 14

Figure B.154: Post Test Part 06 (WC_HIGH_WL, SE) stability photograph for BW1-10, position 14

Figure B.155: Pre-test stability photograph for BW1-10, position 15

Figure B.156: Post Test Part 01 (WC_LOW_WL) stability photograph for BW1-10, position 15

No image available

Figure B.157: Post Test Part 02 (WC_HIGH_WL) stability photograph for BW1-10, position 15

Figure B.158: Post Test Part 03 (WC_EXT_WL_01) stability photograph for BW1-10, position 15

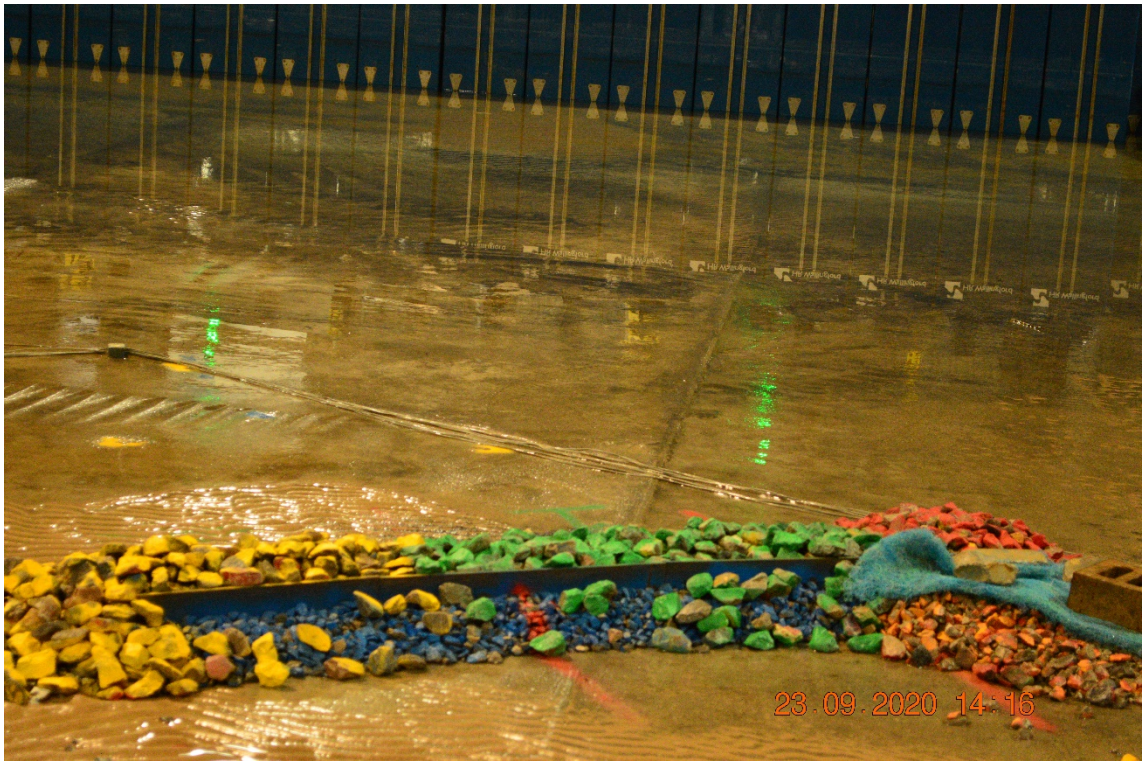


Figure B.159: Post Test Part 04 (WC_EXT_WL_02) stability photograph for BW1-10, position 15

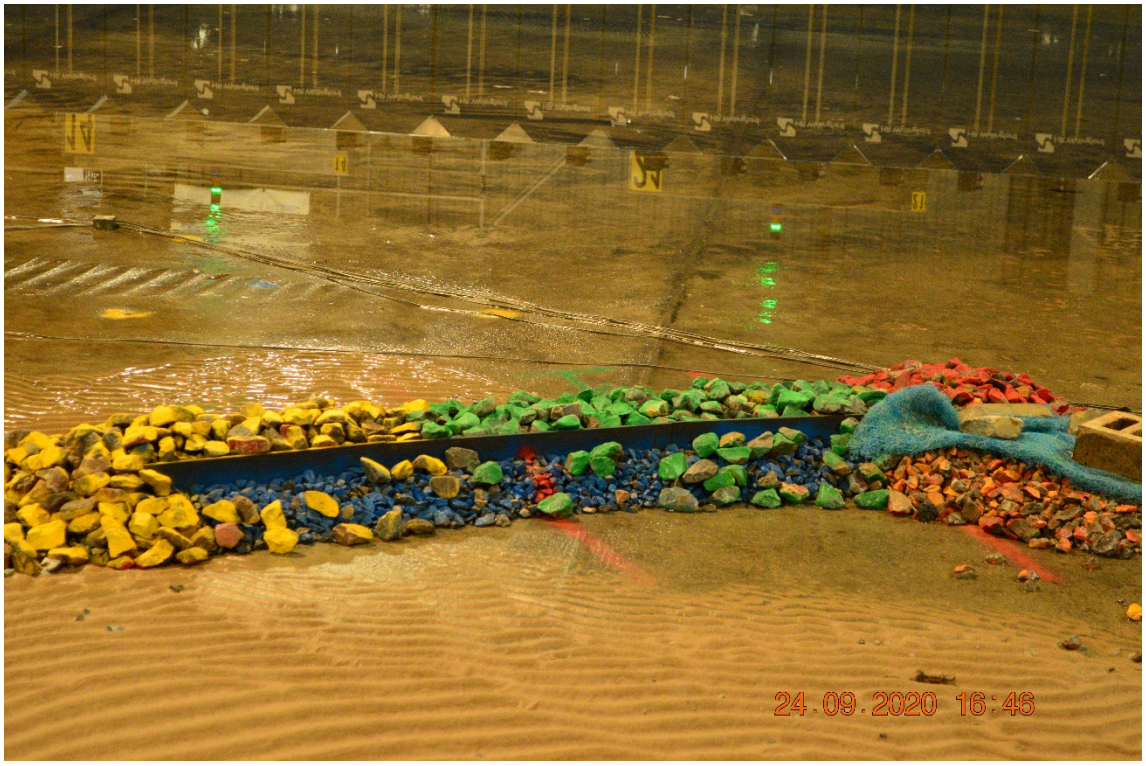


Figure B.160: Post Test Part 05 (WC_LOW_WL, SE) stability photograph for BW1-10, position 15

Figure B.161: Post Test Part 06 (WC_HIGH_WL, SE) stability photograph for BW1-10, position 15

# C. Area 2 – Camp Logan: morphological and stability photographs and scan data

## C.1. Morphological photographs

### C.1.1. Configuration 01 – Initial configuration

Configuration 01 was the starting point for the optimisation of the beach control structures, and was provided in *2020-0617 Illinois Beach State Park Shoreline Stabilization.pdf* (Figure 6.3). This configuration was tested for 3 hr tests (30 minutes model). The pre and post-test photographs from the 'North' and 'South' time-lapse camera views are shown in Figure C.2 and Figure C.3. The post-test scan data, including the structure outlines, is shown in Figure C.1.

Figure C.1: Post-test scan data for Area 2 Configuration 01, solid area post-test beach

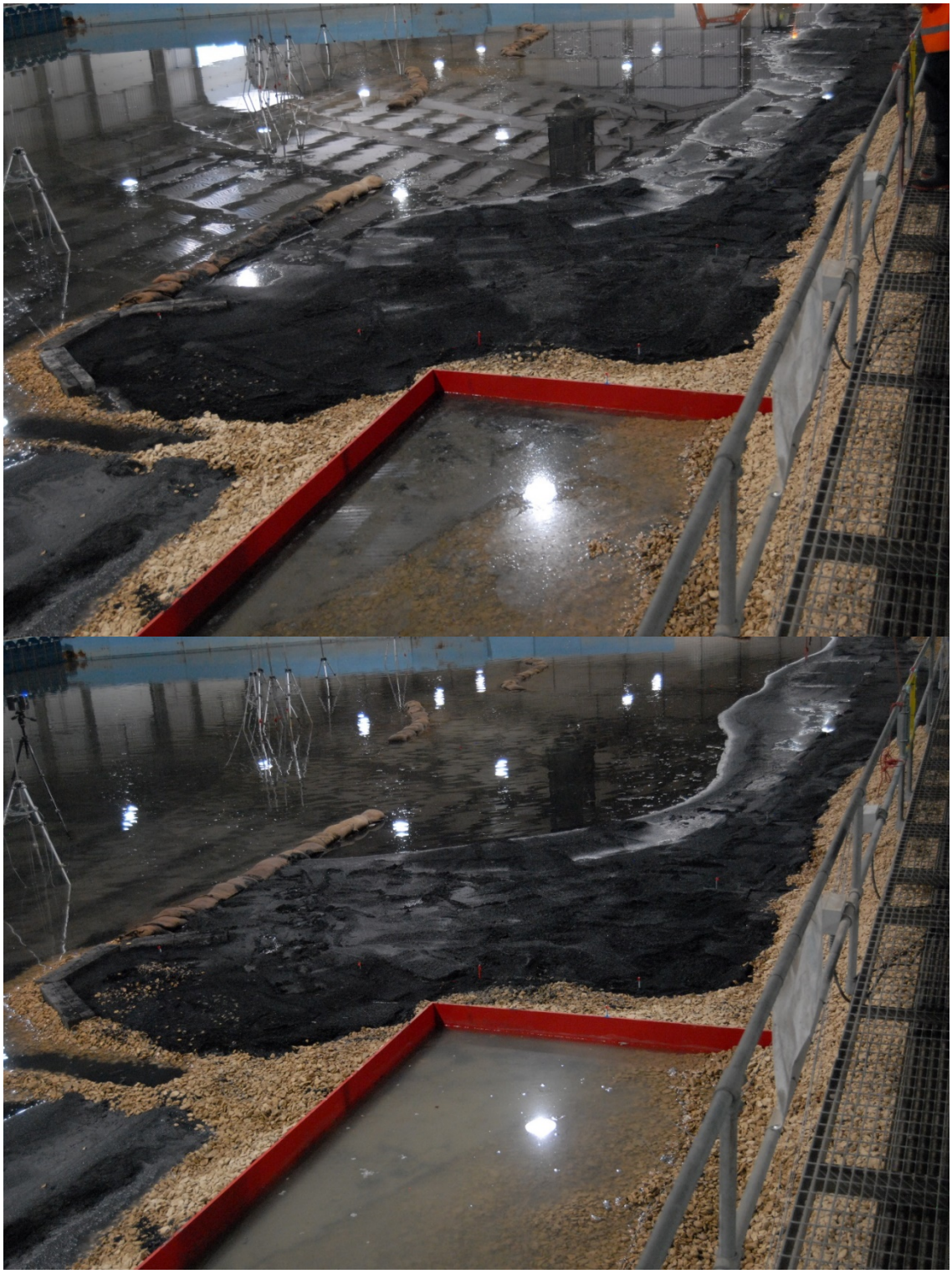

Figure C.2: Pre (top) and post-test (bottom) photographs from 'North' view for Configuration 01

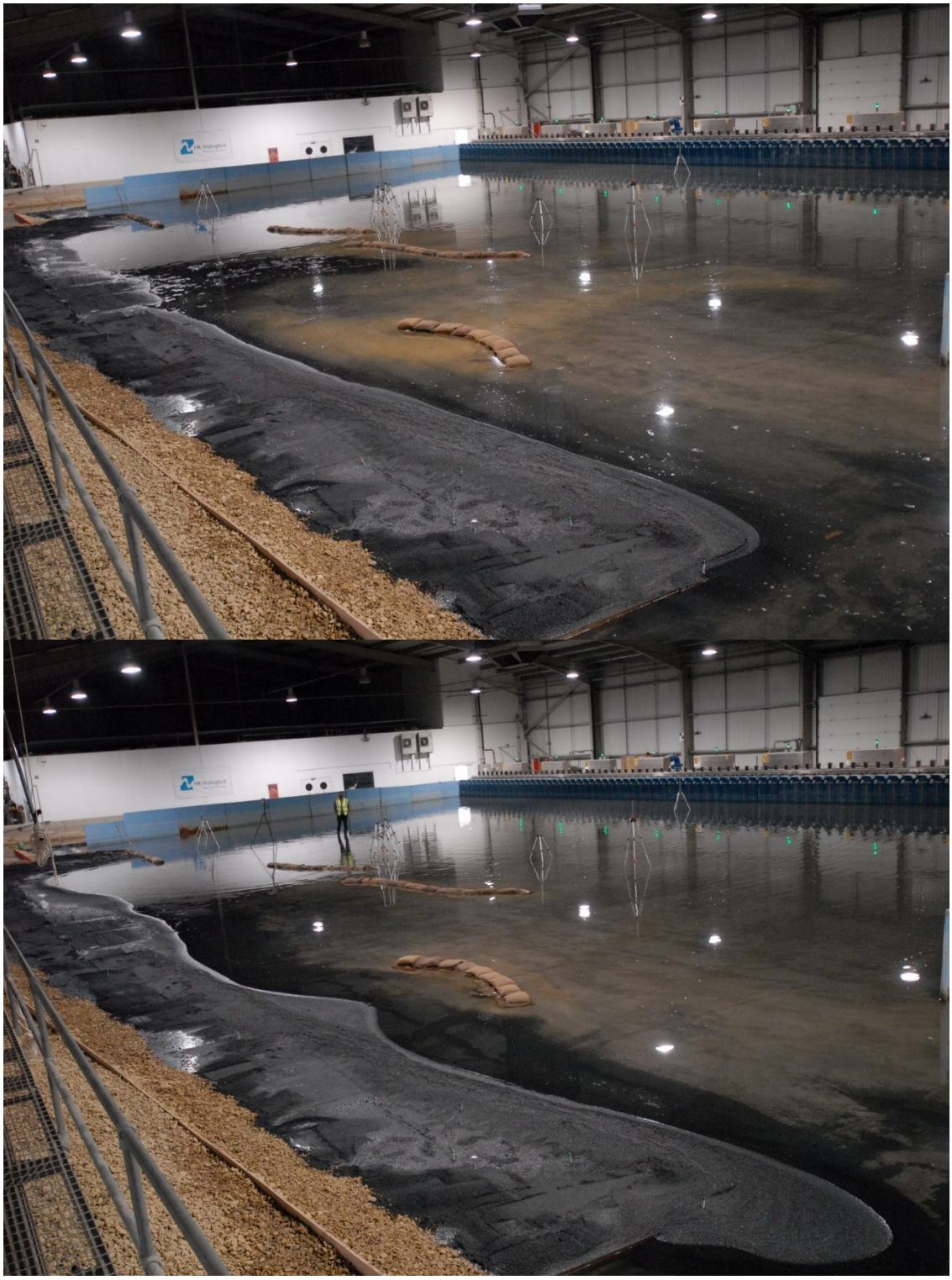

Figure C.3: Pre (top) and post-test (bottom) photographs from 'South' view for Configuration 01

### C.1.2. Configuration 02

Configuration 02 differed from Configuration 01 with the shortening of the shore connected breakwater by five sandbags and the addition of two small submerged breakwaters between the shore connected breakwater and the northernmost emergent detached breakwater (each 5 sandbags long). The centre of the northernmost emergent detached breakwater was lowered, creating a saddle, the northern end of the 'middle' breakwater was removed and a submerged breakwater seven sandbags long was added between the 'middle' breakwater and the southernmost breakwater. This configuration was tested for 6 hrs (1 hour model). The pre and post-test photographs from the 'North' and 'South' time-lapse camera views are shown in Figure C.4 and Figure C.5.

Figure C.4: Pre (top) and post-test (bottom) photographs from 'North' view for Configuration 02

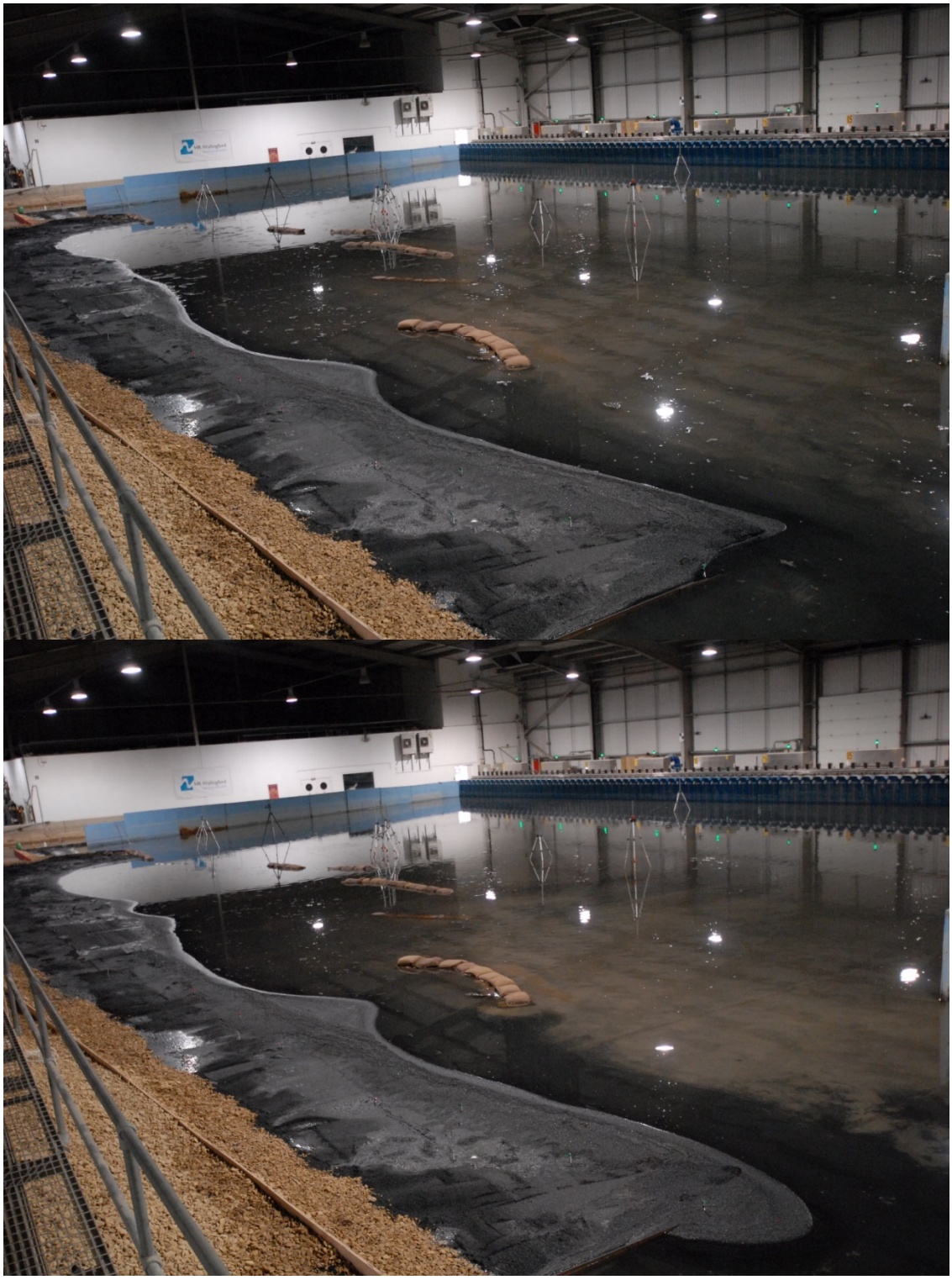

Figure C.5: Pre (top) and post-test (bottom) photographs from 'South' view for Configuration 02

### C.1.3. Configuration 03

Configuration 03 differed from Configuration 02 with the removal of a further two sandbags from the shore connected breakwater and four sandbags removed from the northern end of the northernmost emergent breakwater (with saddle). The s-shape in the 'middle' emergent breakwater was changed to give a constant shallow curve so the breakwater sat more shore parallel than in configuration 02. This configuration was tested for 21 hr (3.5 hours model). The pre and post-test photographs from the 'North' and 'South' time-lapse camera views are shown in Figure C.6 and Figure C.7.

Figure C.6: Pre (top) and post-test (bottom) photographs from 'North' view for Configuration 03

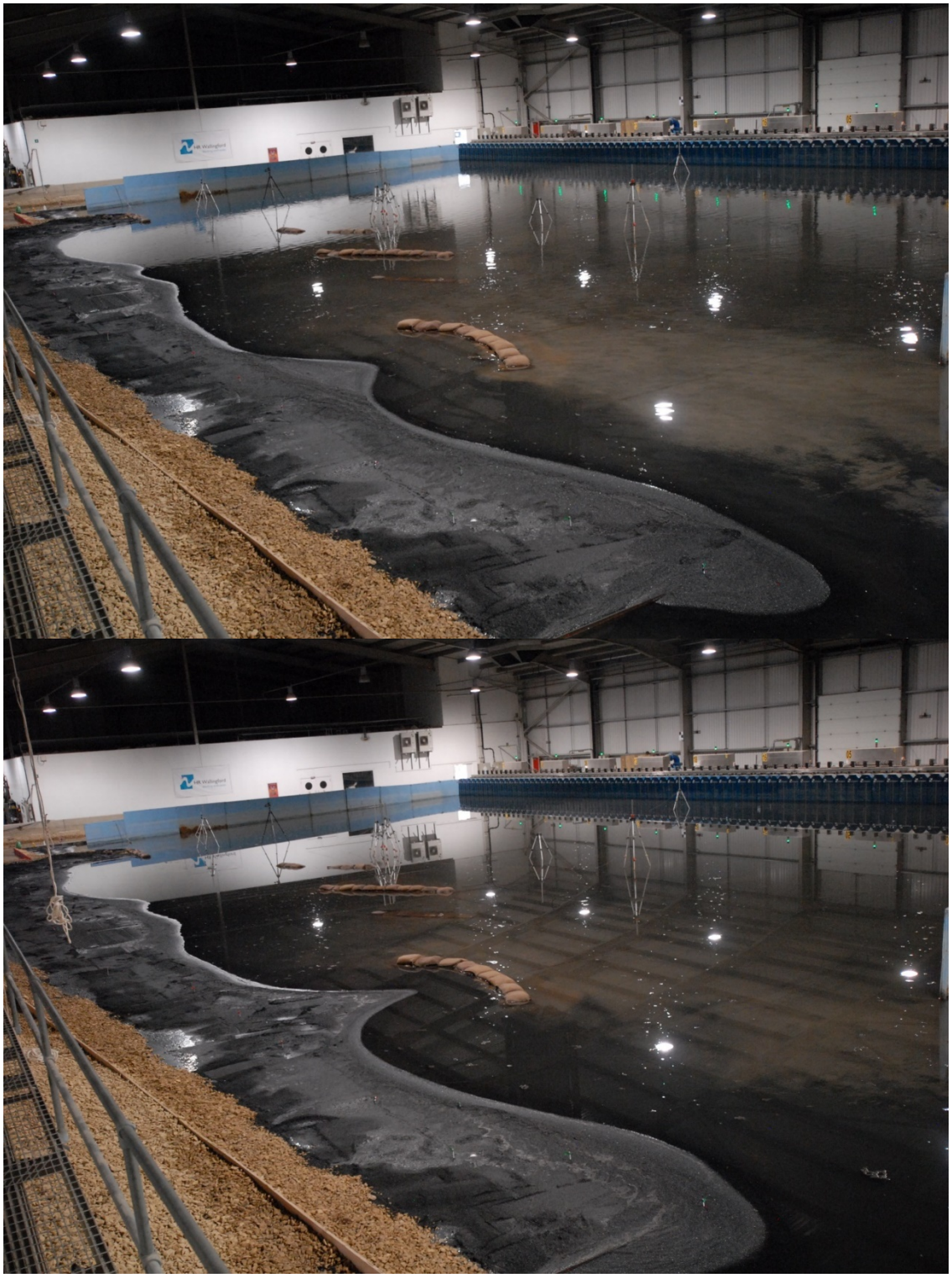

Figure C.7: Pre (top) and post-test (bottom) photographs from 'South' view for Configuration 03

## C.1.4. Configuration 04

Configuration 04 differed from Configuration 03 in the movement of the southernmost breakwater closer to the shore and making the angle of the arms more acute. This configuration was tested for 14 hrs 45 mins (2.5 hours model). The pre and post-test photographs from the 'North' and 'South' time-lapse camera views are shown in Figure C.9 and Figure C.10. The post-test scan data, including the structure outlines, is shown in Figure C.8.

Figure C.8: Post-test scan data for Area 2 Configuration 04, solid area post-test beach

Figure C.9: Pre (top) and post-test (bottom) photographs from 'North' view for Configuration 04

Figure C.10: Pre (top) and post-test (bottom) photographs from ‘South’ view for Configuration 04

## C.1.5. Configuration 05

Configuration 05 differed from Configuration 04 with the southernmost breakwater moved offshore and straightened (at a slight angle to the shoreline, southern end furthest from shore). This process of straightening was repeated for the other two southern breakwaters and all were made emergent. The two northern submerged breakwaters were extended and curved (northernmost concave relative to the shoreline and the southern convex relative to the shoreline). The northern end of the 'middle' breakwater (that had a saddle) was lowered to make it submerged and was extended and curved towards the shore. This configuration was tested for 17 hrs 45 mins (3 hours model). The pre and post-test photographs from the 'North' and 'South' time-lapse camera views are shown in Figure C.12 and Figure C.13. The post-test scan data, including the structure outlines, is shown in Figure C.11.

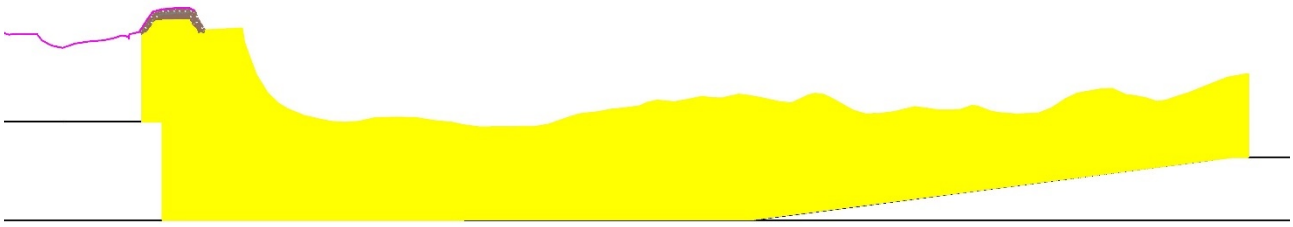

Figure C.11: Post-test scan data for Area 2 Configuration 05, solid area post-test beach

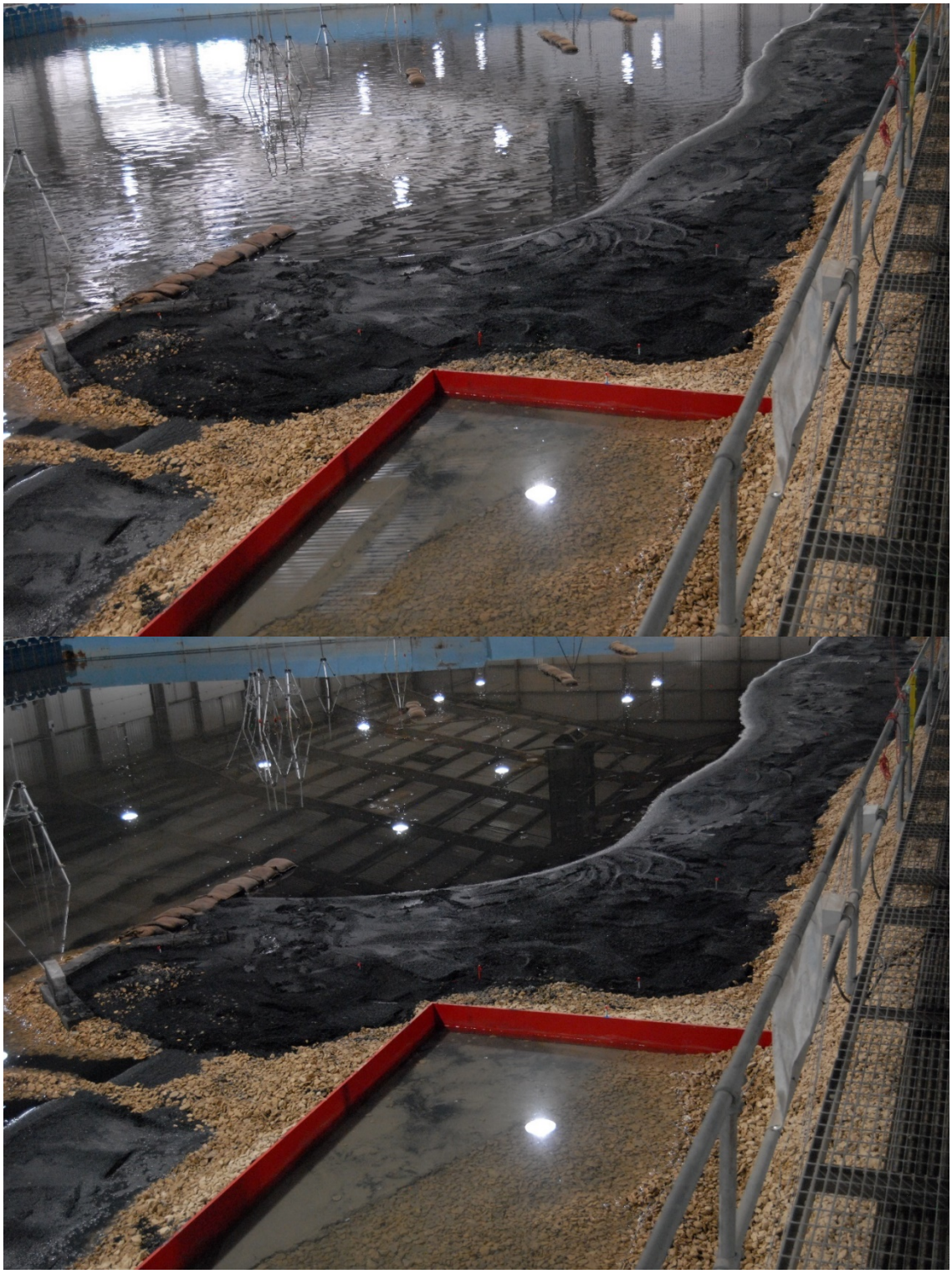

Figure C.12: Pre (top) and post-test (bottom) photographs from 'North' view for Configuration 05

Figure C.13: Pre (top) and post-test (bottom) photographs from ‘South’ view for Configuration 05

## C.1.6. Configuration 06

Configuration 06 differed from Configuration 05 with the removal of the two southernmost breakwaters and the addition of wooden planks to represent the Healthy Port Futures structures at the southern end of the model. This configuration was tested for 17 hrs 45 mins (3 hours model). The pre and post-test photographs from the 'North' and 'South' time-lapse camera views are shown in Figure C.15 and Figure C.16. The post-test scan data, including the structure outlines, is shown in Figure C.14.

Figure C.14: Post-test scan data for Area 2 Configuration 06, solid area post-test beach

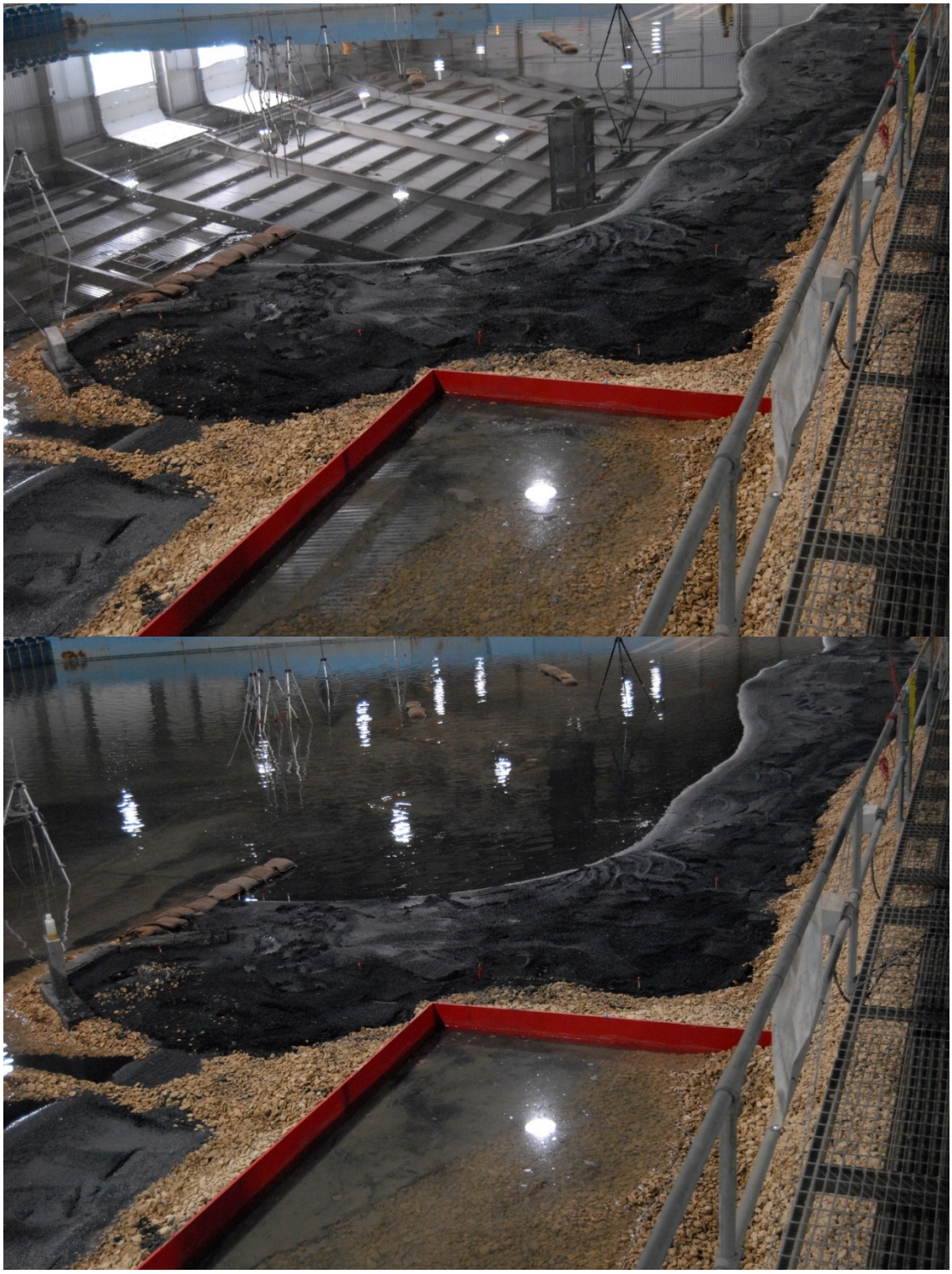

Figure C.15: Pre (top) and post-test (bottom) photographs from 'North' view for Configuration 06

Figure C.16: Pre (top) and post-test (bottom) photographs from 'South' view for Configuration 06

## C.1.7. Configuration 07

Configuration 07 differed from Configuration 06 with the addition of a small emergent breakwater on the norther end of the Healthy Ports Futures structures and a submerged one on the southern end. The shore connected breakwater was also extended seawards by two submerged sandbags and one emergent. This configuration was tested for 14 hrs 45 mins (2.5 hours model). The pre and post-test photographs from the 'North' and 'South' time-lapse camera views are shown in Figure C.18 and Figure C.19. The post-test scan data, including the structure outlines, is shown in Figure C.17.

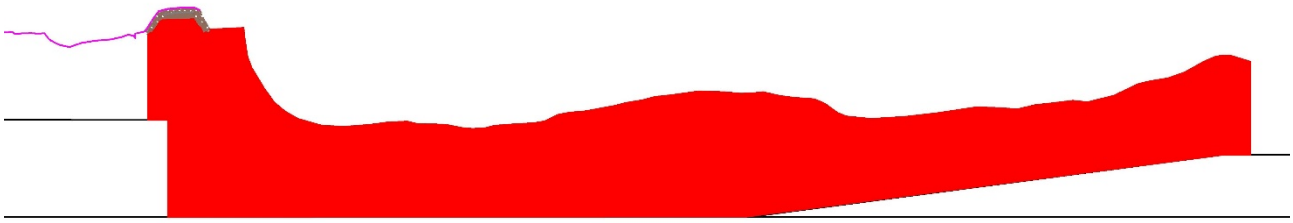

Figure C.17: Post-test scan data for Area 2 Configuration 07, solid area post-test beach

Figure C.18: Pre (top) and post-test (bottom) photographs from ‘North’ view for Configuration 07

Figure C.19: Pre (top) and post-test (bottom) photographs from 'South' view for Configuration 07

## C.1.8. Configuration 08

Configuration 08 differed from Configuration 07 with the submerging of the seaward end of the shore connected breakwater, the rotation by 180° of the northernmost submerged breakwater and making the northernmost emergent breakwater ('middle' breakwater) submerged. The southernmost submerged breakwater was also moved southwards away from the Healthy Port Futures structures. This configuration was tested for approximately 12 hrs (2 hours model). The pre and post-test photographs from the 'North' and 'South' time-lapse camera views are shown in Figure C.21 and Figure C.22. The post-test scan data, including the structure outlines, is shown in Figure C.20.

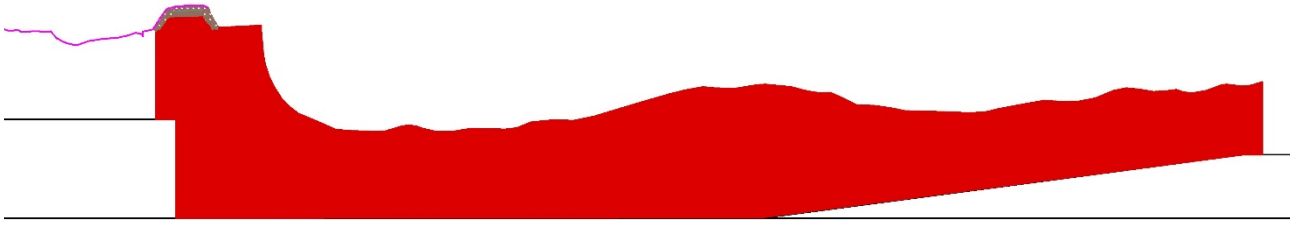

Figure C.20: Post-test scan data for Area 2 Configuration 08, solid area post-test beach

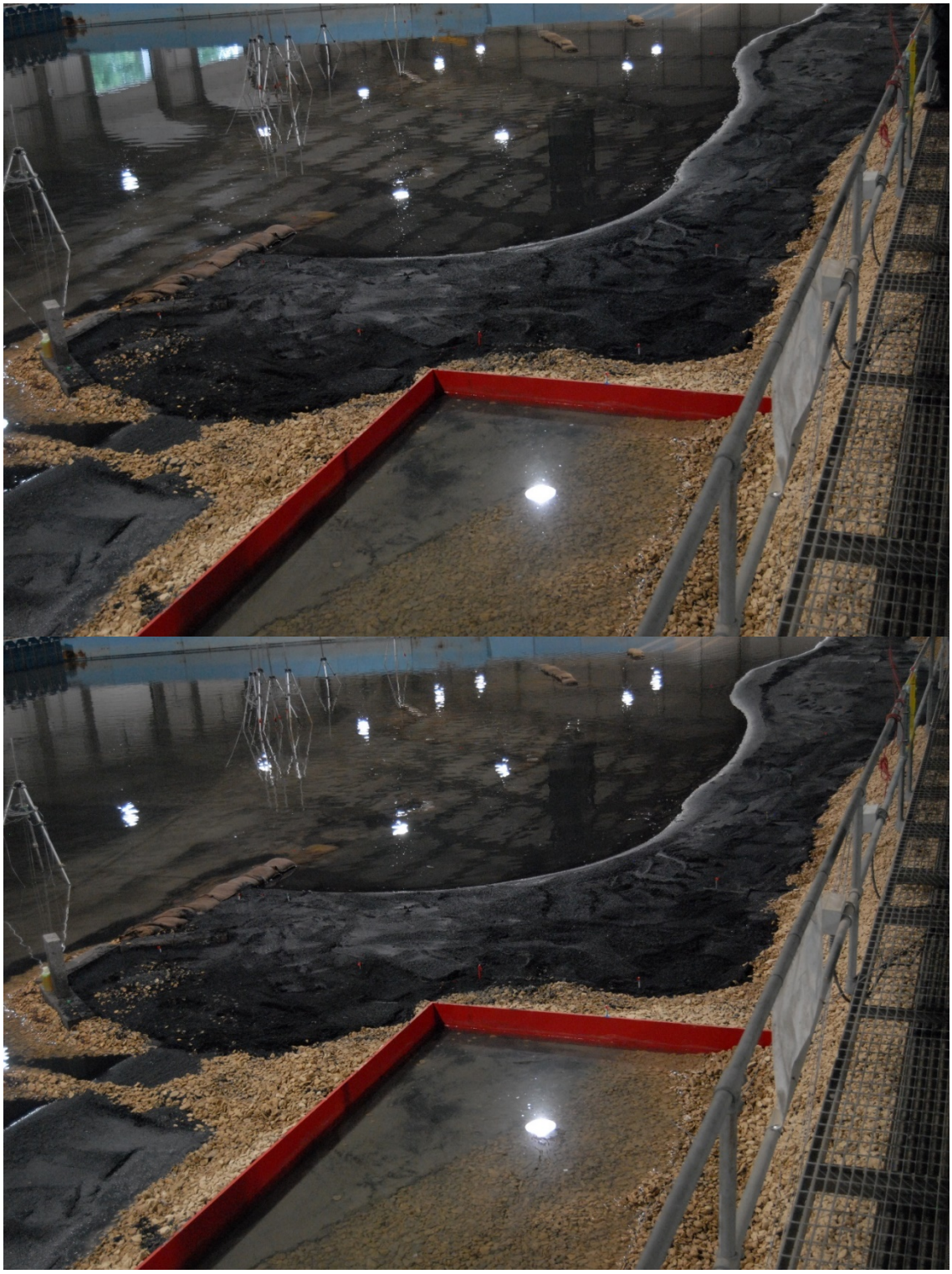

Figure C.21: Pre (top) and post-test (bottom) photographs from ‘North’ view for Configuration 08

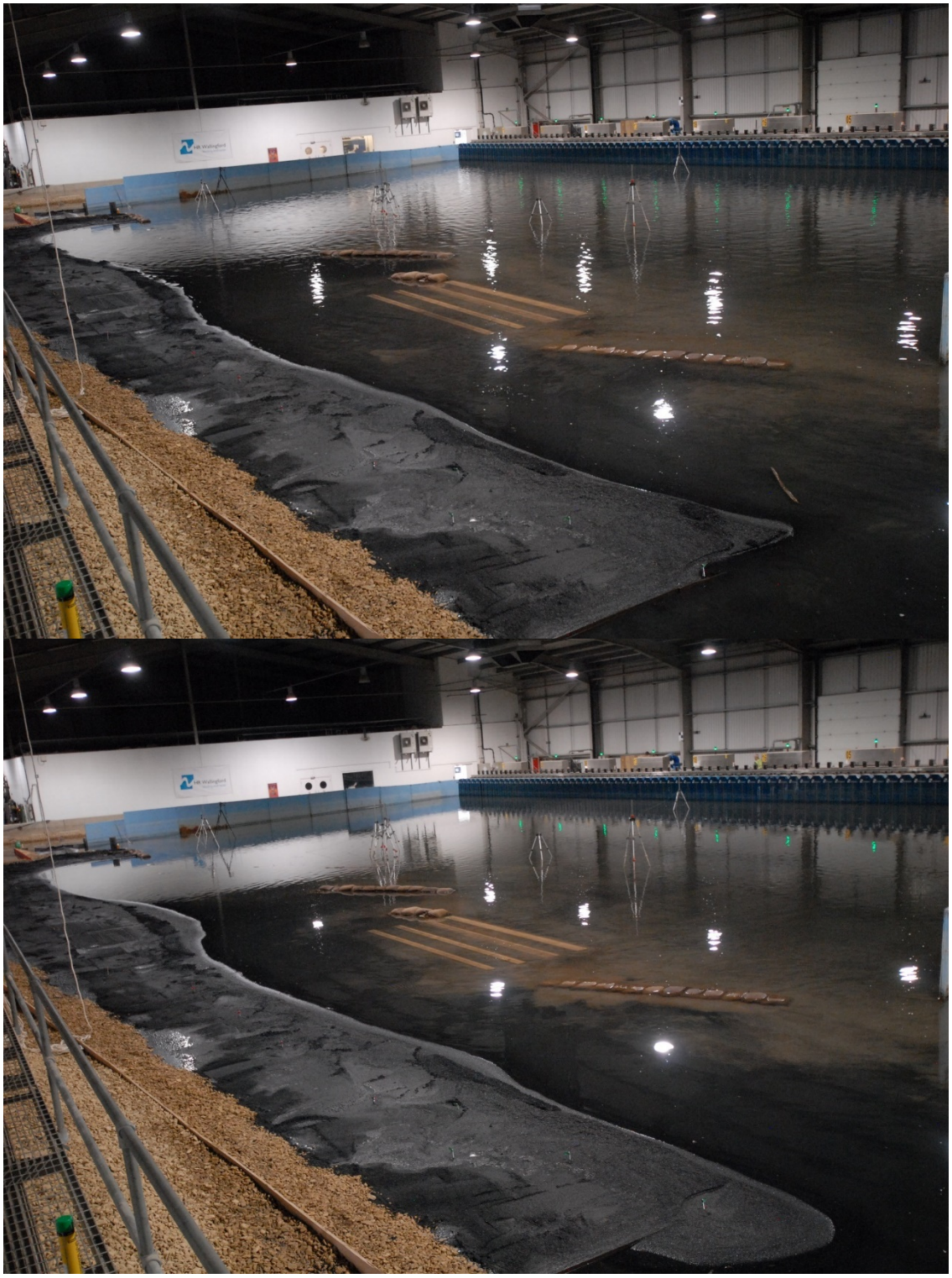

Figure C.22: Pre (top) and post-test (bottom) photographs from ‘South’ view for Configuration 08

### C.1.9. Configuration 09

Configuration 09 differed from Configuration 08 with the straightening of the curved section on the 'middle' breakwater and making it emergent. This configuration was tested for 3 hr (30 minutes model). The pre and post-test photographs from the 'North' and 'South' time-lapse camera views are shown in Figure C.23 and Figure C.24.

Figure C.23: Pre (top) and post-test (bottom) photographs from ‘North’ view for Configuration 09

Figure C.24: Pre (top) and post-test (bottom) photographs from ‘South’ view for Configuration 09

## C.1.10. Configuration 10

Configuration 10 differed from Configuration 09 with the addition of a fishtail to the southern end (furthest from shore) of the 'middle' breakwater (northernmost emergent breakwater). This configuration was tested for 9 hr (1.5 hours model). The pre and post-test photographs from the 'North' and 'South' time-lapse camera views are shown in Figure C.25 and Figure C.26.

Figure C.25: Pre (top) and post-test (bottom) photographs from 'North' view for Configuration 10

Figure C.26: Pre (top) and post-test (bottom) photographs from ‘South’ view for Configuration 10

### C.1.11. Configuration 11

Configuration 11 differed from Configuration 10 with the submerged breakwater on the north side of Healthy Port Futures structures moved to the southeast 'in front' of the northeast corner of the Healthy Port Futures structures. The two ends of the southernmost structure were made emergent and the overall structure shortened. This configuration was tested for 26.5 hr (4.5 hours model). The pre and post-test photographs from the 'North' and 'South' time-lapse camera views are shown in Figure C.27 and Figure C.28.

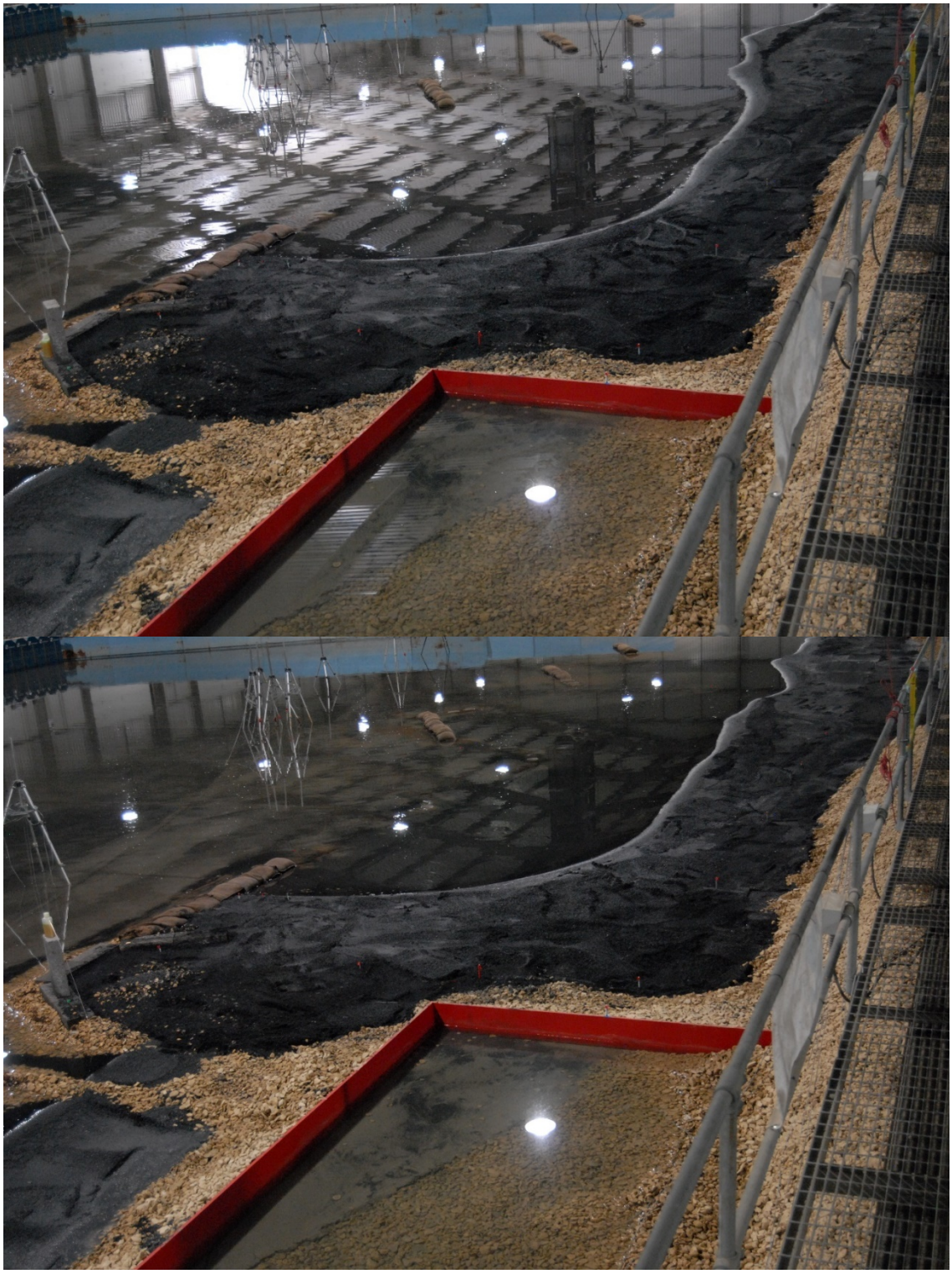

Figure C.27: Pre (top) and post-test (bottom) photographs from 'North' view for Configuration 11

Figure C.28: Pre (top) and post-test (bottom) photographs from 'South' view for Configuration 11

## C.1.12. Configuration 12

Configuration 12 differed from Configuration 11 with the southern of the two middle emergent breakwaters shortened by two sandbags from south end and lengthened by five submerged sandbags on the north end. This configuration was tested for 3 hr (30 minutes model). The pre and post-test photographs from the 'North' and 'South' time-lapse camera views are shown in Figure C.29 and Figure C.30.

Post-test image unavailable

Figure C.29: Pre (top) and post-test (bottom) photographs from 'North' view for Configuration 12

Post-test image unavailable

Figure C.30: Pre (top) and post-test (bottom) photographs from ‘South’ view for Configuration 12

### C.1.13. Configuration 13

Configuration 13 differed from Configuration 12 in the northernmost submerged breakwater being made emergent. This configuration was tested for 6 hrs (1 hour model). The pre and post-test photographs from the 'North' and 'South' time-lapse camera views are shown in Figure C.31 and Figure C.32.

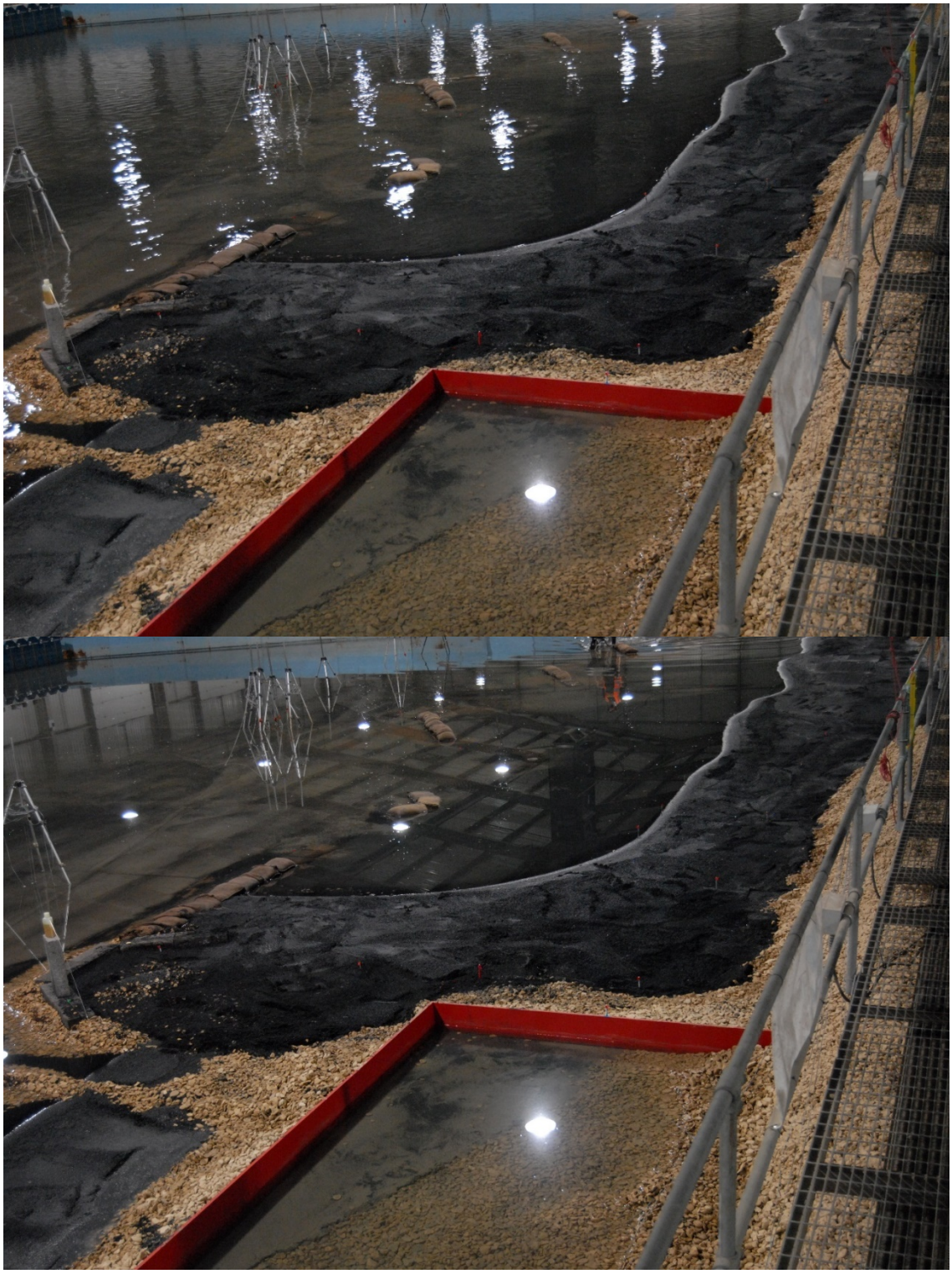

Figure C.31: Pre (top) and post-test (bottom) photographs from 'North' view for Configuration 13

Figure C.32: Pre (top) and post-test (bottom) photographs from ‘South’ view for Configuration 13

### C.1.14. Configuration 14

Configuration 14 differed from Configuration 13 in making sections of the two middle emergent breakwaters submerged. In the northern of the two a double saddle was created, and in the southern, both the ends were made submerged with the finished profile three submerged sandbags, three emergent and then three submerged. This configuration was tested for 3 hrs (30 minutes model). The pre and post-test photographs from the 'North' and 'South' time-lapse camera views are shown in Figure C.33 and Figure C.34.

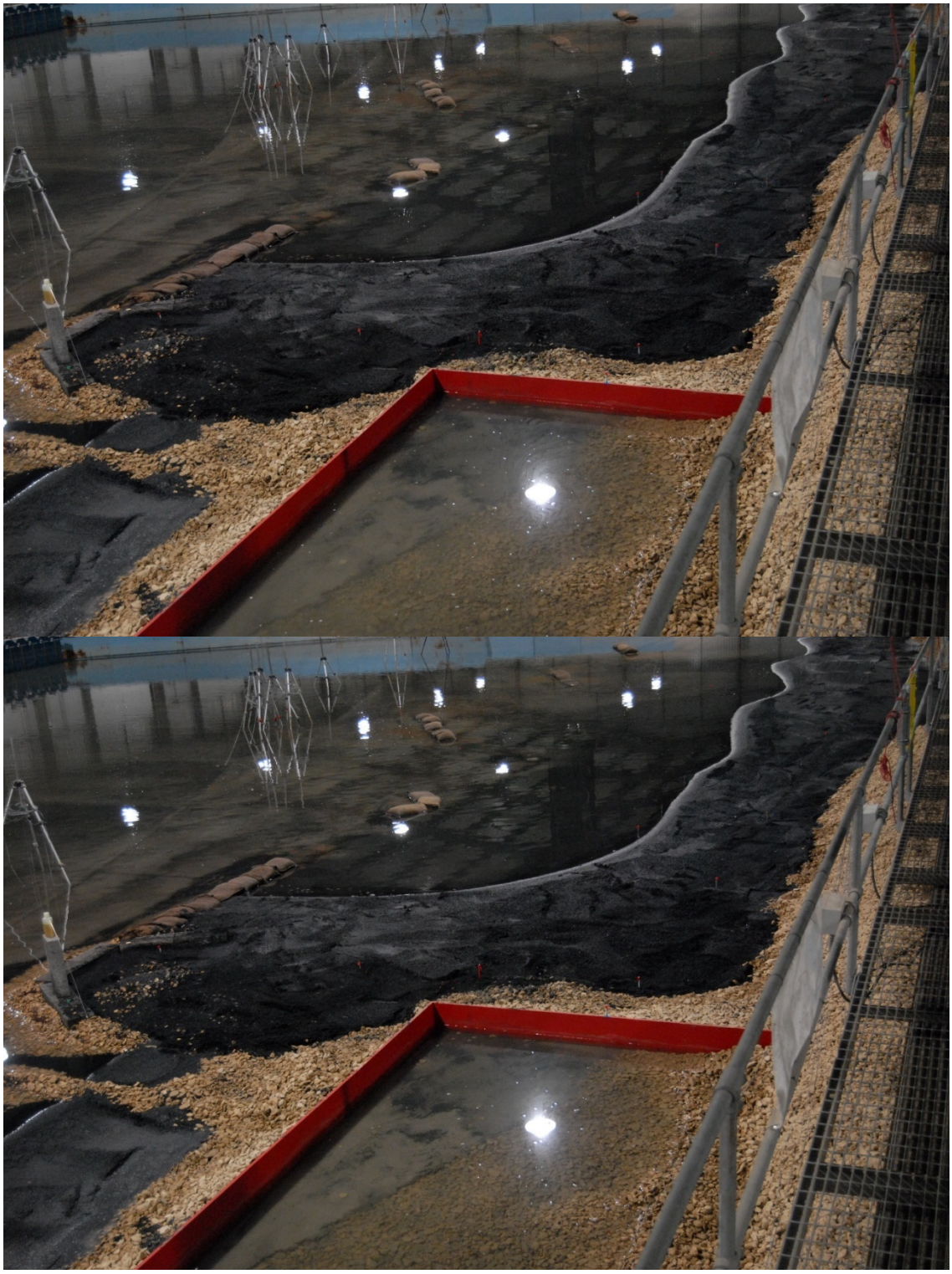

Figure C.33: Pre (top) and post-test (bottom) photographs from 'North' view for Configuration 14

Figure C.34: Pre (top) and post-test (bottom) photographs from 'South' view for Configuration 14

### C.1.15. Configuration 15

Configuration 15 differed from Configuration 14 with the removal of the fishtail on the southern end of the 'middle' breakwater and replacing it with a three sandbag long submerged 'dogleg' curving to be more shore parallel. A submerged 'dogleg' was also added to the southern end of the breakwater immediately to the south. This configuration was tested for 9 hrs (1.5 hours model). The pre and post-test photographs from the 'North' and 'South' time-lapse camera views are shown in Figure C.35 and Figure C.36.

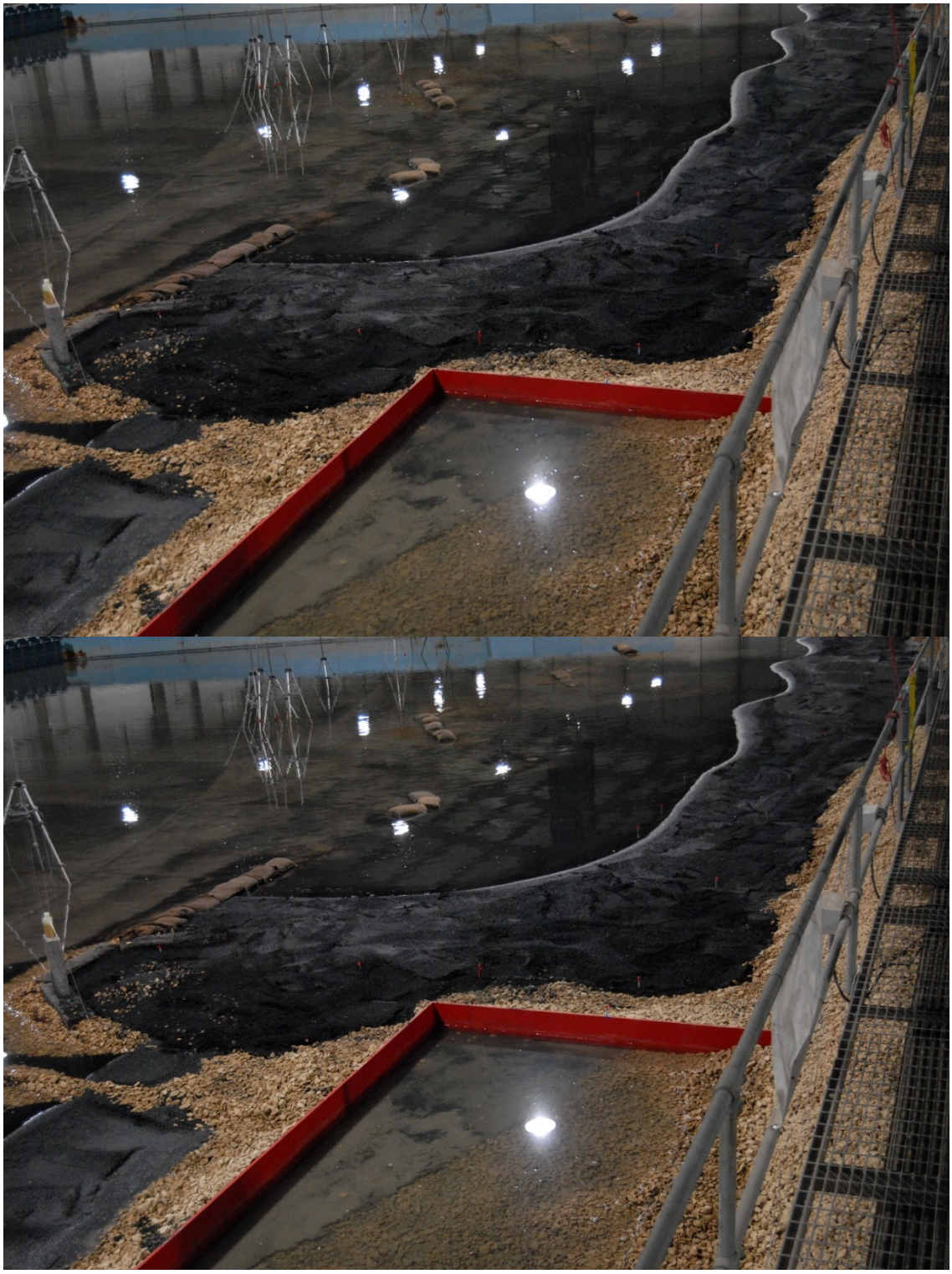

Figure C.35: Pre (top) and post-test (bottom) photographs from 'North' view for Configuration 15

Figure C.36: Pre (top) and post-test (bottom) photographs from 'South' view for Configuration 15

## C.1.16. Configuration 16

Configuration 16 differed from Configuration 15 with the lengthening of the southernmost breakwater by one sandbag on wither end, moving the breakwater on the northeast corner of Health Port Futures to the position from Configurations 7 to 9 and removing the 'doglegs' from the middle pair of breakwaters. The northern end of the southern breakwater in the pair was made emergent and the fishtails reinstated on the southern end of the northern breakwater in the pair (similar to Configurations 12 to 14). This configuration was tested for 6 hrs (1 hour model). The pre and post-test photographs from the 'North' and 'South' time-lapse camera views are shown in Figure C.37 and Figure C.38.

Figure C.37: Pre (top) and post-test (bottom) photographs from 'North' view for Configuration 16

Figure C.38: Pre (top) and post-test (bottom) photographs from 'South' view for Configuration 16

## C.1.17. Configuration 17

Configuration 17 differed from Configuration 16 in making the southernmost breakwater submerged along the entire length, removing the emergent ends. This configuration was tested for 3 hrs (30 minutes model). The pre and post-test photographs from the 'North' and 'South' time-lapse camera views are shown in Figure C.40 and Figure C.41. The post-test scan data, including the structure outlines, is shown in Figure C.39.

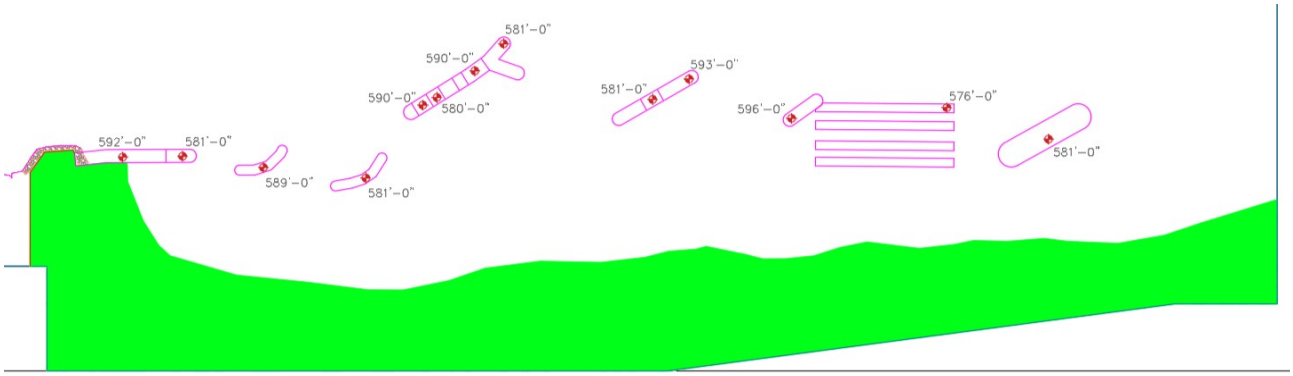


Figure C.39: Post-test scan data for Area 2 Configuration 17, solid area post-test beach, structures in magenta with spot-heights given for key locations

Figure C.40: Pre (top) and post-test (bottom) photographs from 'North' view for Configuration 17

Figure C.41: Pre (top) and post-test (bottom) photographs from 'South' view for Configuration 17

# C.2. Stability photographs

## C.2.1. BW2-1

Figure C.42: Pre-test stability photograph for BW2-1, position 1

Figure C.43: Post Test Part 01 (WC_LOW_WL_SE) stability photograph for BW2-1, position 1

Figure C.44: Post Test Part 02 (WC_HIGH_WL_SE) stability photograph for BW2-1, position 1

Figure C.45: Post Test Part 03 (WC_LOW_WL) stability photograph for BW2-1, position 1

Figure C.46: Post Test Part 04 (WC_HIGH_WL) stability photograph for BW2-1, position 1

Figure C.47: Post Test Part 05 (WC_EXT_WL_01) stability photograph for BW2-1, position 1

Figure C.48: Post Test Part 06 (WC_EXT_WL_02) stability photograph for BW2-1, position 1

Figure C.49: Pre-test stability photograph for BW2-1, position 2

Figure C.50: Post Test Part 01 (WC_LOW_WL_SE) stability photograph for BW2-1, position 2

Figure C.51: Post Test Part 02 (WC_HIGH_WL_SE) stability photograph for BW2-1, position 2

Figure C.52: Post Test Part 03 (WC_LOW_WL) stability photograph for BW2-1, position 2

Figure C.53: Post Test Part 04 (WC_HIGH_WL) stability photograph for BW2-1, position 2

Figure C.54: Post Test Part 05 (WC_EXT_WL_01) stability photograph for BW2-1, position 2

Figure C.55: Post Test Part 06 (WC_EXT_WL_02) stability photograph for BW2-1, position 2

## C.2.2. BW2-2

Figure C.56: Pre-test stability photograph for BW2-2, position 3

Figure C.57: Post Test Part 01 (WC_LOW_WL_SE) stability photograph for BW2-2, position 3

Figure C.58: Post Test Part 02 (WC_HIGH_WL_SE) stability photograph for BW2-2, position 3

Figure C.59: Post Test Part 03 (WC_LOW_WL) stability photograph for BW2-2, position 3

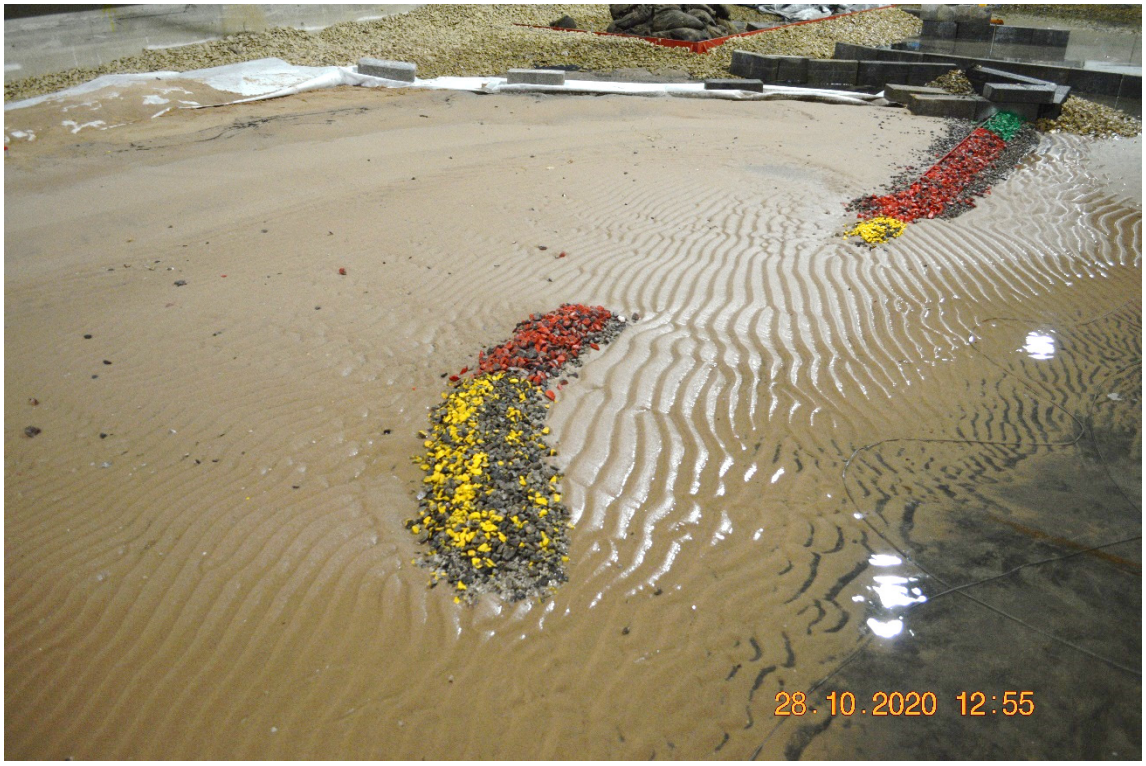


Figure C.60: Post Test Part 04 (WC_HIGH_WL) stability photograph for BW2-2, position 3

Figure C.61: Post Test Part 05 (WC_EXT_WL_01) stability photograph for BW2-2, position 3

Figure C.62: Post Test Part 06 (WC_EXT_WL_02) stability photograph for BW2-2, position 3

Figure C.63: Pre-test stability photograph for BW2-2, position 4

Figure C.64: Post Test Part 01 (WC_LOW_WL_SE) stability photograph for BW2-2, position 4

Figure C.65: Post Test Part 02 (WC_HIGH_WL_SE) stability photograph for BW2-2, position 4

Figure C.66: Post Test Part 03 (WC_LOW_WL) stability photograph for BW2-2, position 4

Figure C.67: Post Test Part 04 (WC_HIGH_WL) stability photograph for BW2-2, position 4

Figure C.68: Post Test Part 05 (WC_EXT_WL_01) stability photograph for BW2-2, position 4

Figure C.69: Post Test Part 06 (WC_EXT_WL_02) stability photograph for BW2-2, position 4

Figure C.70: Pre-test stability photograph for BW2-2, position 5

Figure C.71: Post Test Part 01 (WC_LOW_WL_SE) stability photograph for BW2-2, position 5

Figure C.72: Post Test Part 02 (WC_HIGH_WL_SE) stability photograph for BW2-2, position 5

Figure C.73: Post Test Part 03 (WC_LOW_WL) stability photograph for BW2-2, position 5

Figure C.74: Post Test Part 04 (WC_HIGH_WL) stability photograph for BW2-2, position 5

Figure C.75: Post Test Part 05 (WC_EXT_WL_01) stability photograph for BW2-2, position 5

Figure C.76: Post Test Part 06 (WC_EXT_WL_02) stability photograph for BW2-2, position 5

## C.2.3. BW2-3

Figure C.77: Pre-test stability photograph for BW2-3, position 6

Figure C.78: Post Test Part 01 (WC_LOW_WL_SE) stability photograph for BW2-3, position 6

Figure C.79: Post Test Part 02 (WC_HIGH_WL_SE) stability photograph for BW2-3, position 6

Figure C.80: Post Test Part 03 (WC_LOW_WL) stability photograph for BW2-3, position 6

Figure C.81: Post Test Part 04 (WC_HIGH_WL) stability photograph for BW2-3, position 6

Figure C.82: Post Test Part 05 (WC_EXT_WL_01) stability photograph for BW2-3, position 6

Figure C.83: Post Test Part 06 (WC_EXT_WL_02) stability photograph for BW2-3, position 6

Figure C.84: Pre-test stability photograph for BW2-3, position 7

Figure C.85: Post Test Part 01 (WC_LOW_WL_SE) stability photograph for BW2-3, position 7

Figure C.86: Post Test Part 02 (WC_HIGH_WL_SE) stability photograph for BW2-3, position 7

Figure C.87: Post Test Part 03 (WC_LOW_WL) stability photograph for BW2-3, position 7

Figure C.88: Post Test Part 04 (WC_HIGH_WL) stability photograph for BW2-3, position 7

No image available

Figure C.89: Post Test Part 05 (WC_EXT_WL_01) stability photograph for BW2-3, position 7

Figure C.90: Post Test Part 06 (WC_EXT_WL_02) stability photograph for BW2-3, position 7

Figure C.91: Pre-test stability photograph for BW2-3, position 8

Figure C.92: Post Test Part 01 (WC_LOW_WL_SE) stability photograph for BW2-3, position 8

Figure C.93: Post Test Part 02 (WC_HIGH_WL_SE) stability photograph for BW2-3, position 8

Figure C.94: Post Test Part 03 (WC_LOW_WL) stability photograph for BW2-3, position 8

Figure C.95: Post Test Part 04 (WC_HIGH_WL) stability photograph for BW2-3, position 8

Figure C.96: Post Test Part 05 (WC_EXT_WL_01) stability photograph for BW2-3, position 8

Figure C.97: Post Test Part 06 (WC_EXT_WL_02) stability photograph for BW2-3, position 8

## C.2.4. BW2-4

Figure C.98: Pre-test stability photograph for BW2-4, position 9

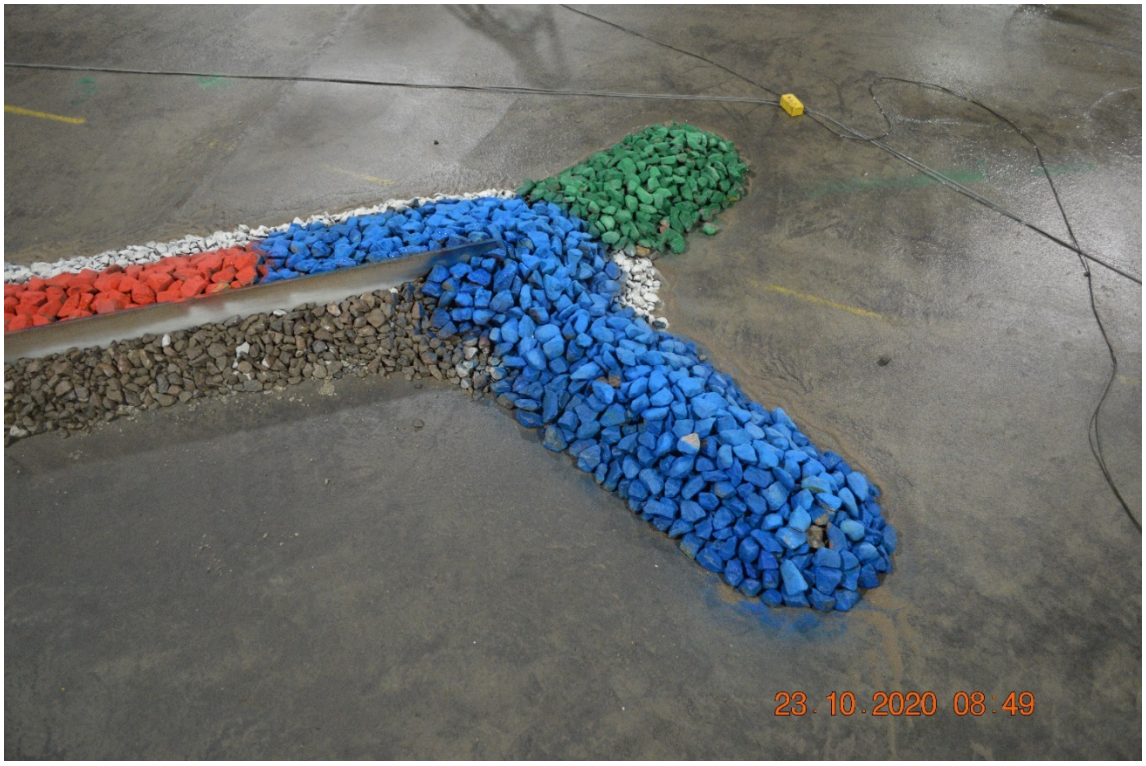


Figure C.99: Post Test Part 01 (WC_LOW_WL_SE) stability photograph for BW2-4, position 9

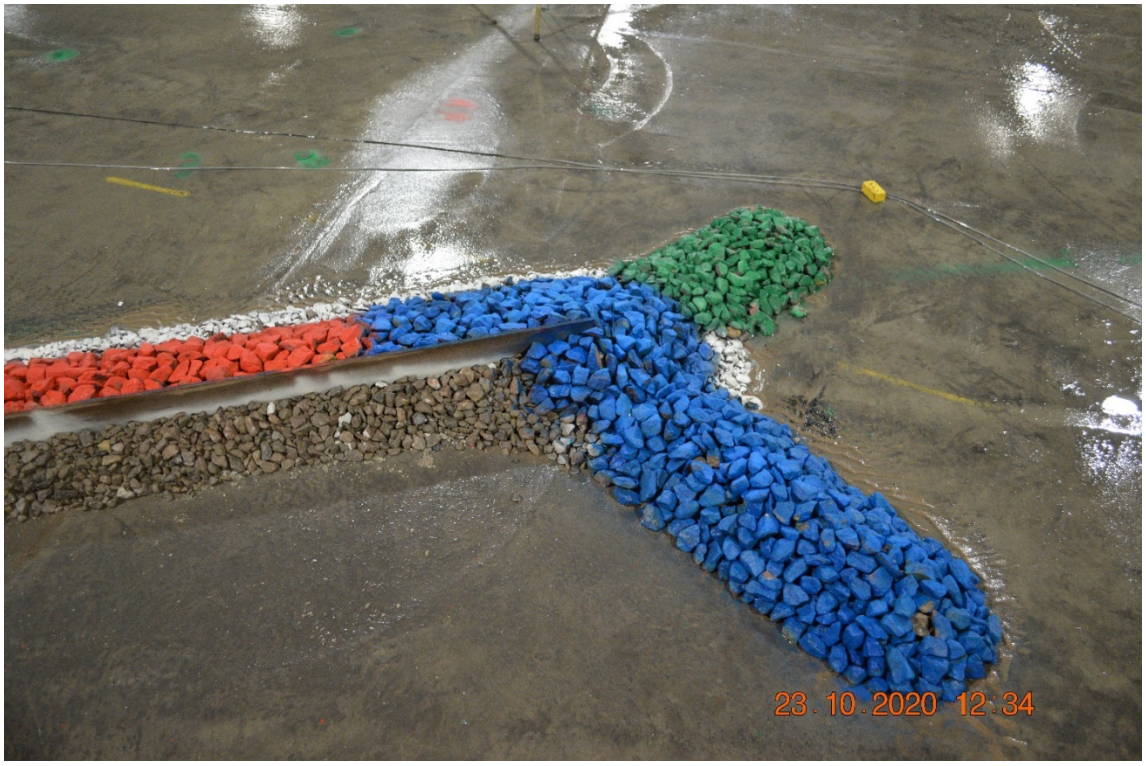


Figure C.100: Post Test Part 02 (WC_HIGH_WL_SE) stability photograph for BW2-4, position 9

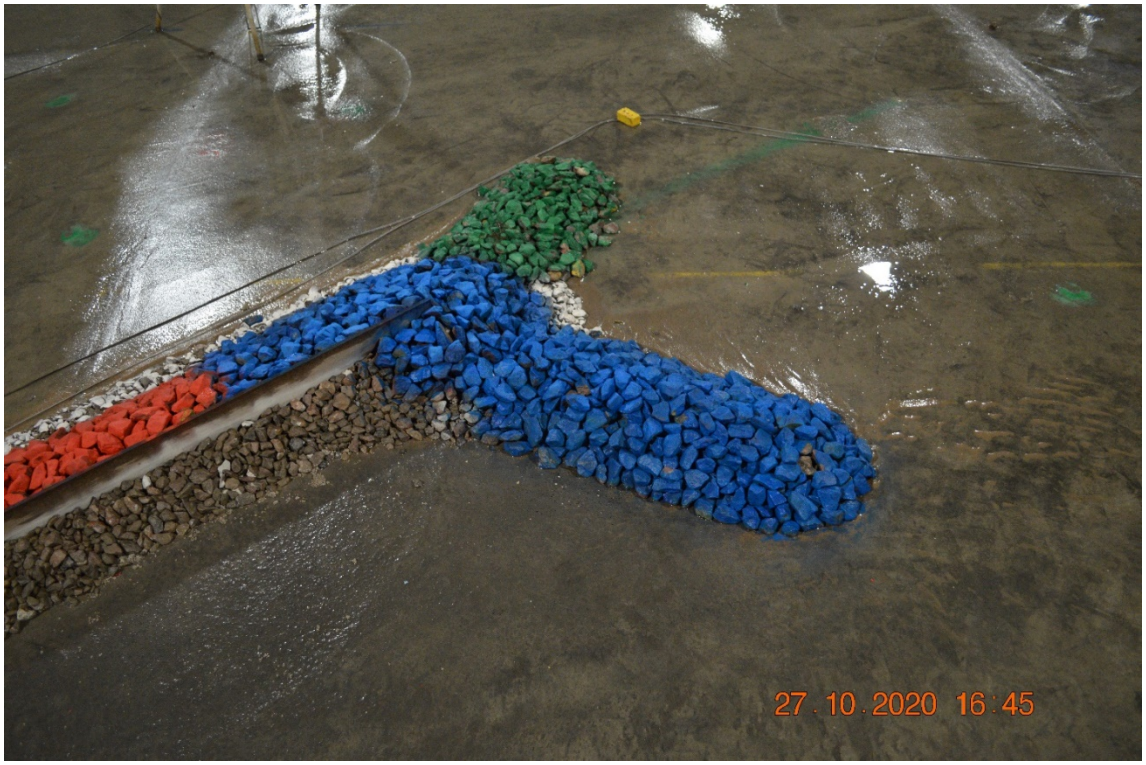


Figure C.101: Post Test Part 03 (WC_LOW_WL) stability photograph for BW2-4, position 9

Figure C.102: Post Test Part 04 (WC_HIGH_WL) stability photograph for BW2-4, position 9

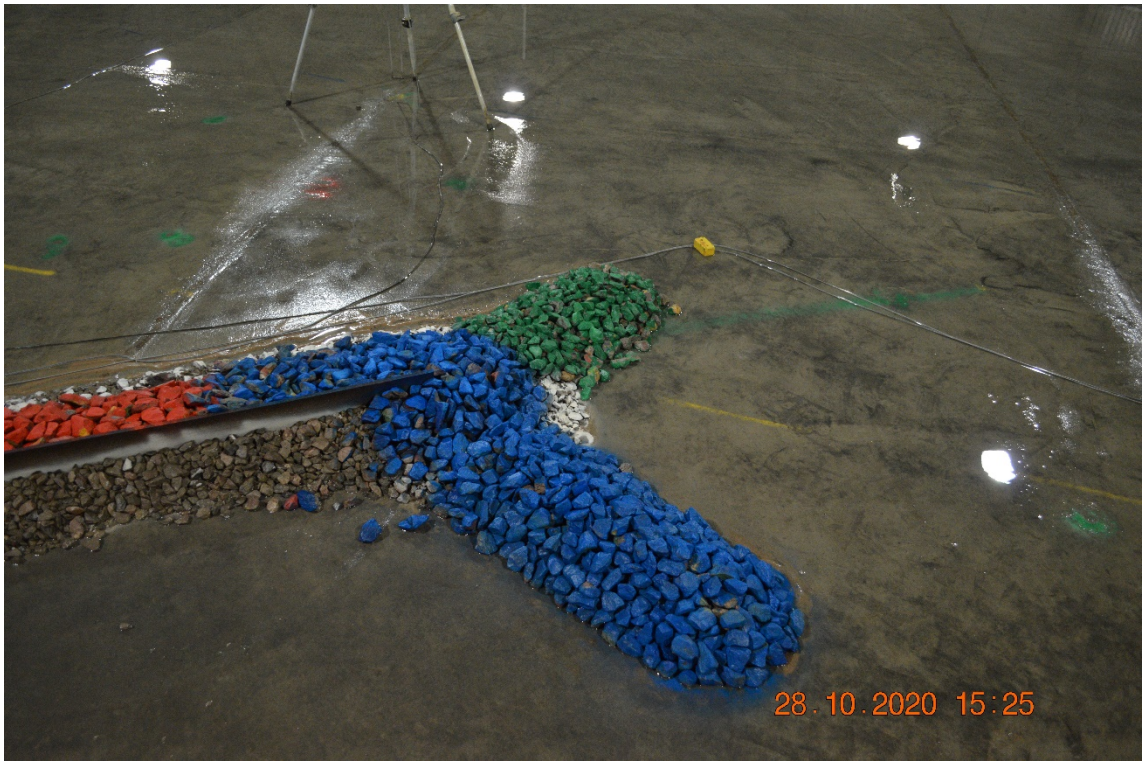


Figure C.103: Post Test Part 05 (WC_EXT_WL_01) stability photograph for BW2-4, position 9

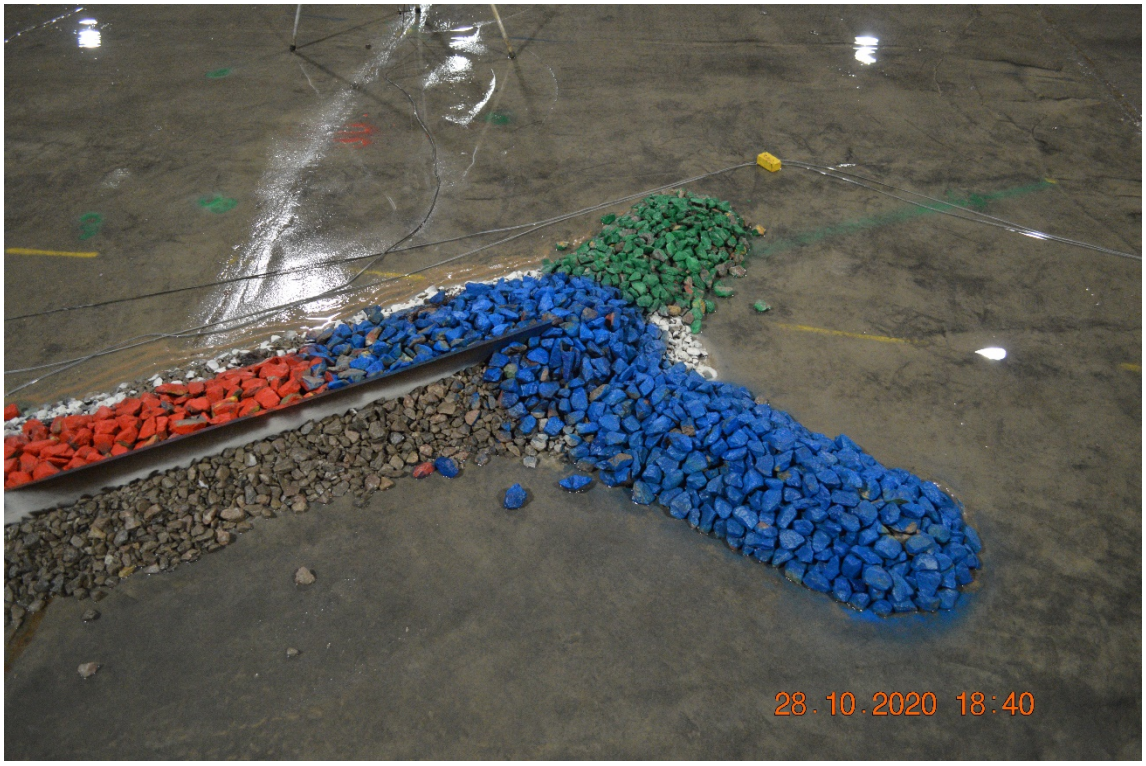


Figure C.104: Post Test Part 06 (WC_EXT_WL_02) stability photograph for BW2-4, position 9

Figure C.105: Pre-test stability photograph for BW2-4, position 10

Figure C.106: Post Test Part 01 (WC_LOW_WL_SE) stability photograph for BW2-4, position 10

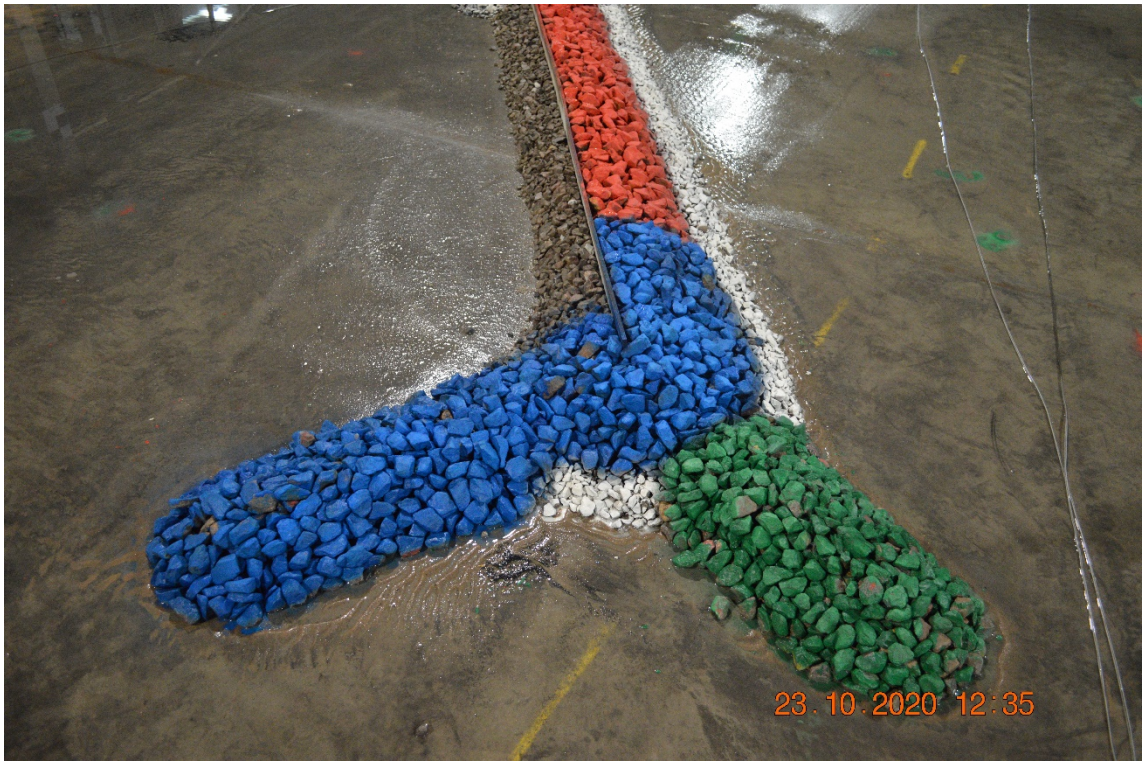


Figure C.107: Post Test Part 02 (WC_HIGH_WL_SE) stability photograph for BW2-4, position 10

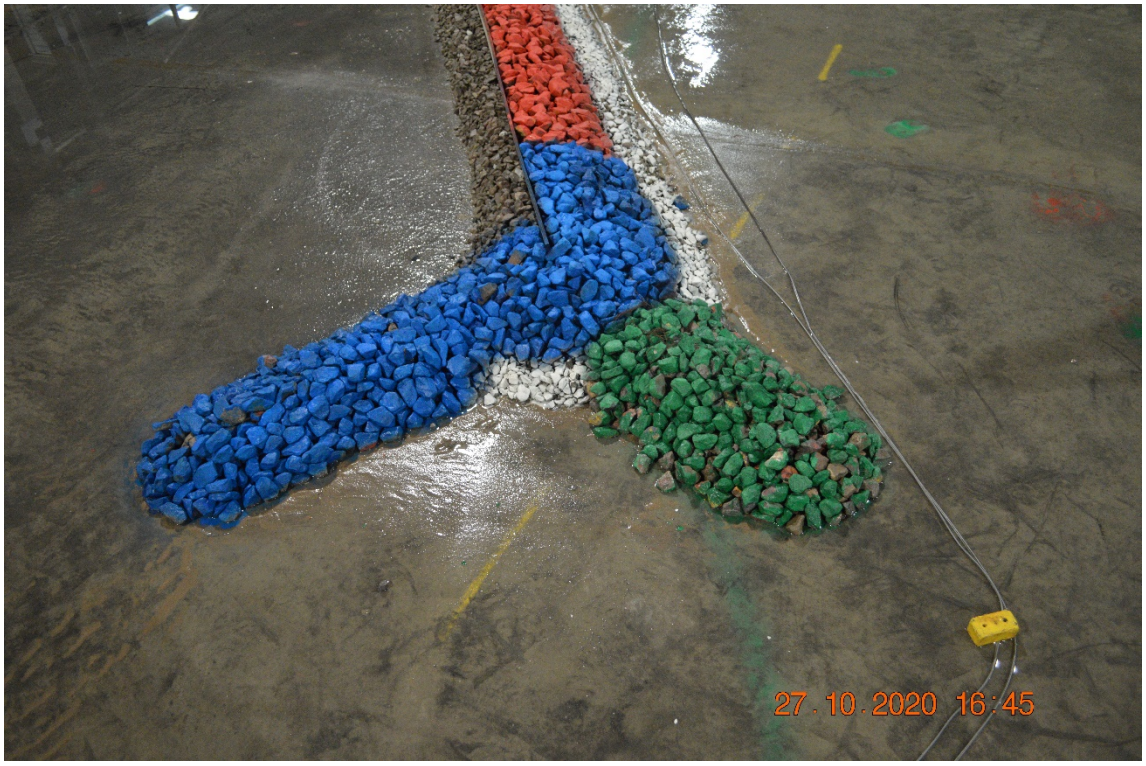


Figure C.108: Post Test Part 03 (WC_LOW_WL) stability photograph for BW2-4, position 10

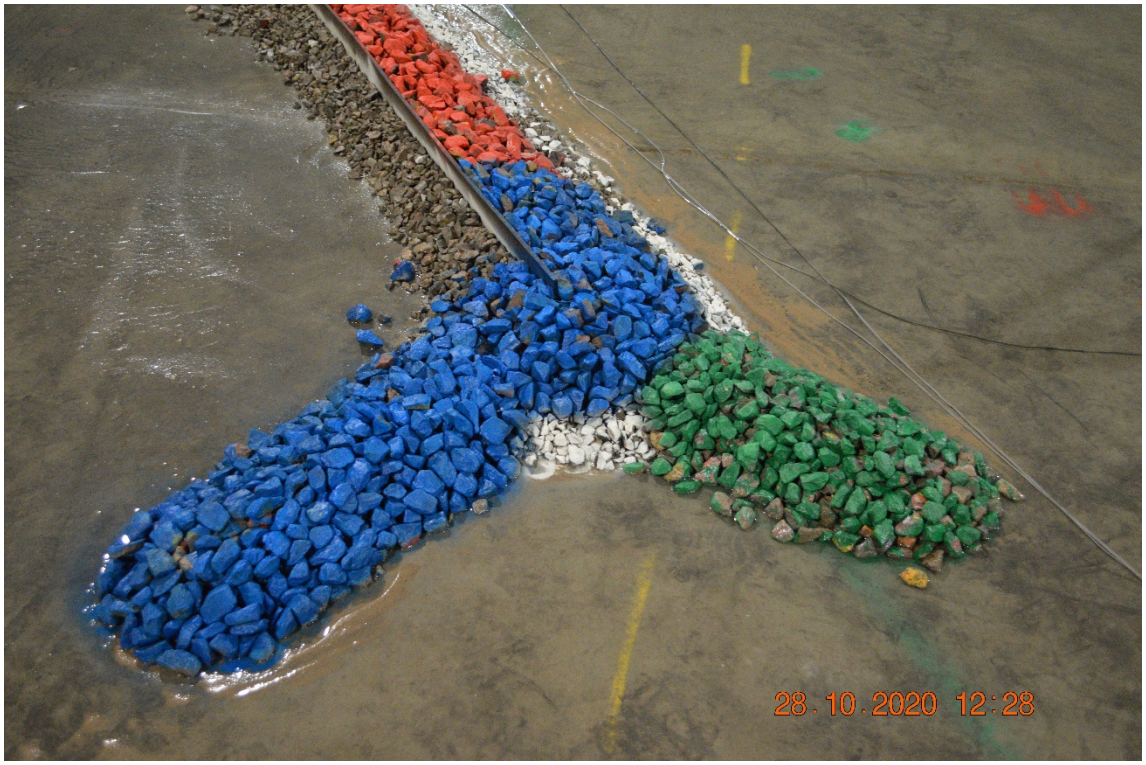


Figure C.109: Post Test Part 04 (WC_HIGH_WL) stability photograph for BW2-4, position 10

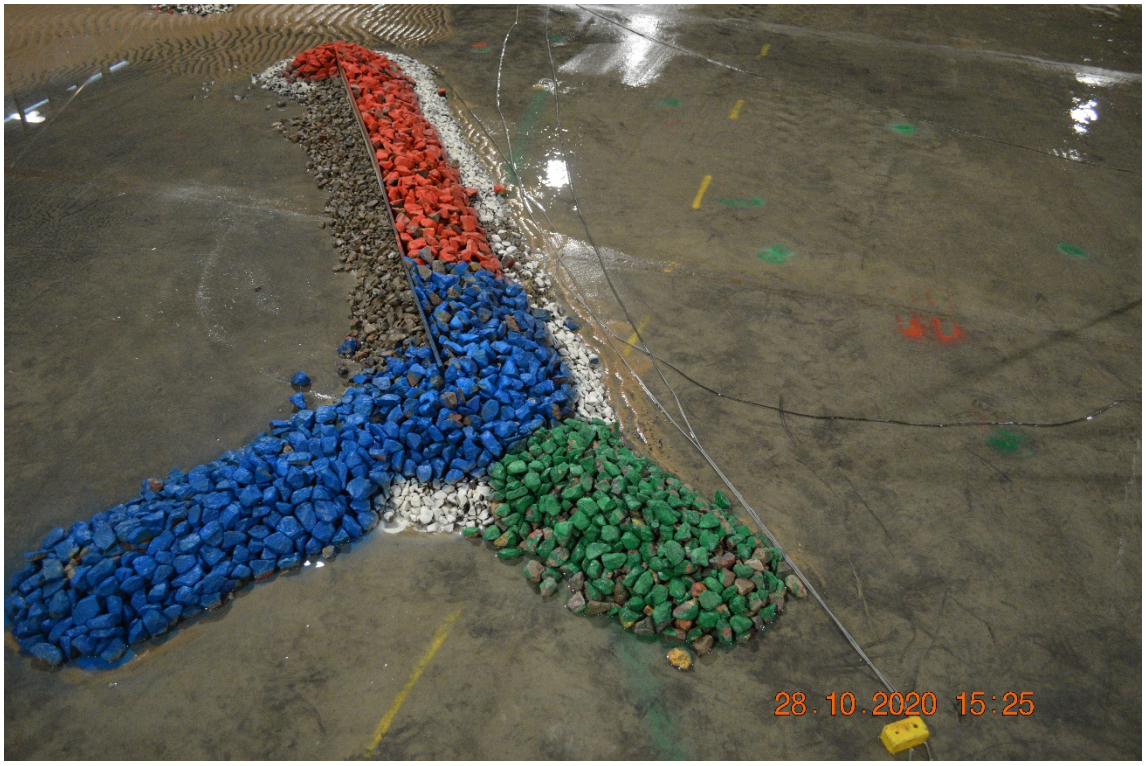


Figure C.110: Post Test Part 05 (WC_EXT_WL_01) stability photograph for BW2-4, position 10

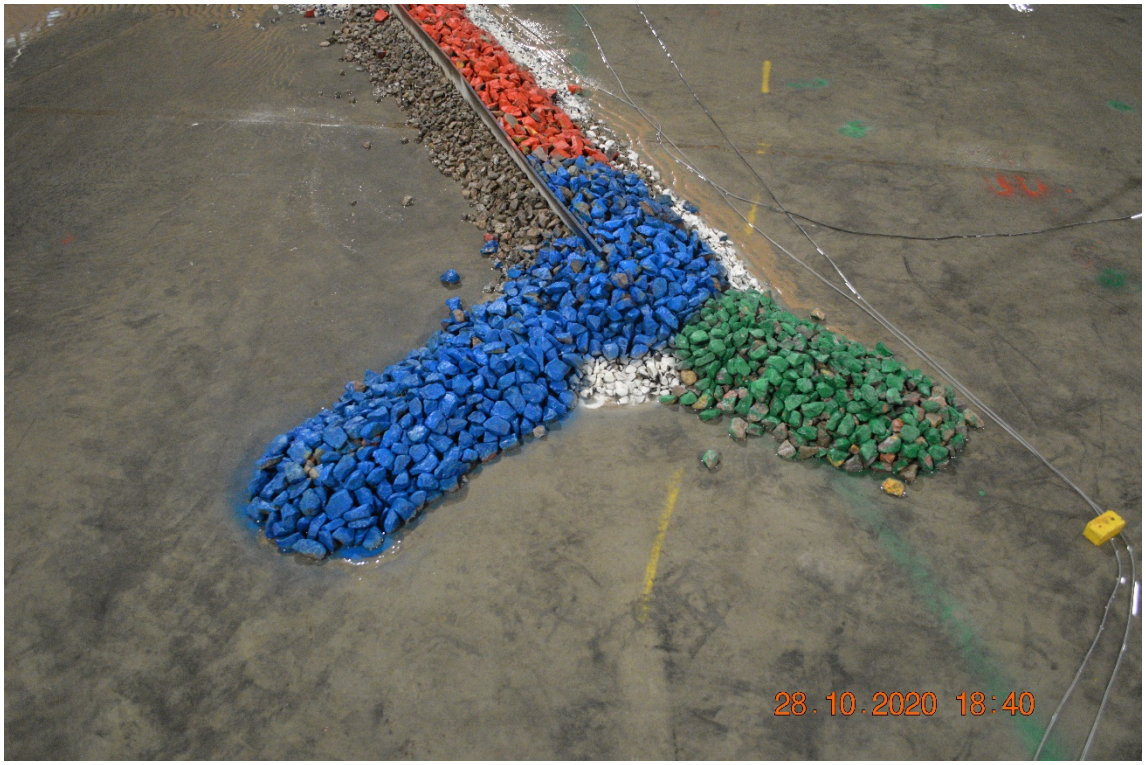


Figure C.111: Post Test Part 06 (WC_EXT_WL_02) stability photograph for BW2-4, position 10

Figure C.112: Pre-test stability photograph for BW2-4, position 11

Figure C.113: Post Test Part 01 (WC_LOW_WL_SE) stability photograph for BW2-4, position 11

Figure C.114: Post Test Part 02 (WC_HIGH_WL_SE) stability photograph for BW2-4, position 11

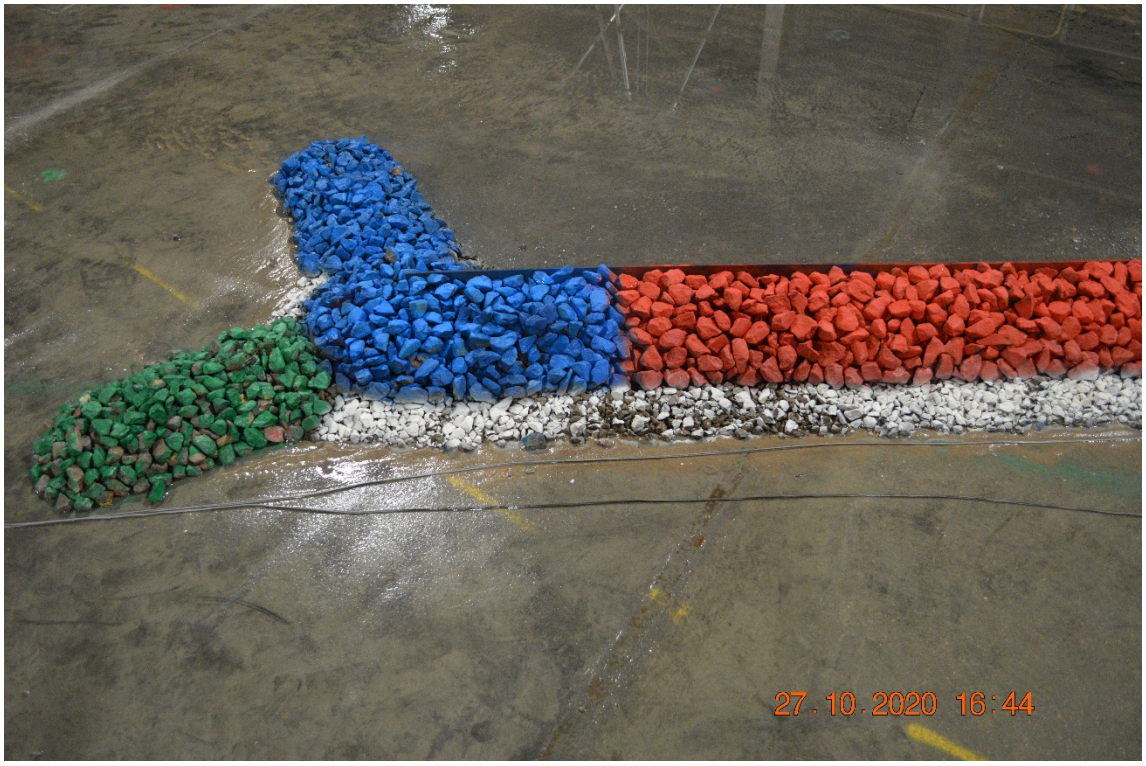


Figure C.115: Post Test Part 03 (WC_LOW_WL) stability photograph for BW2-4, position 11

Figure C.116: Post Test Part 04 (WC_HIGH_WL) stability photograph for BW2-4, position 11

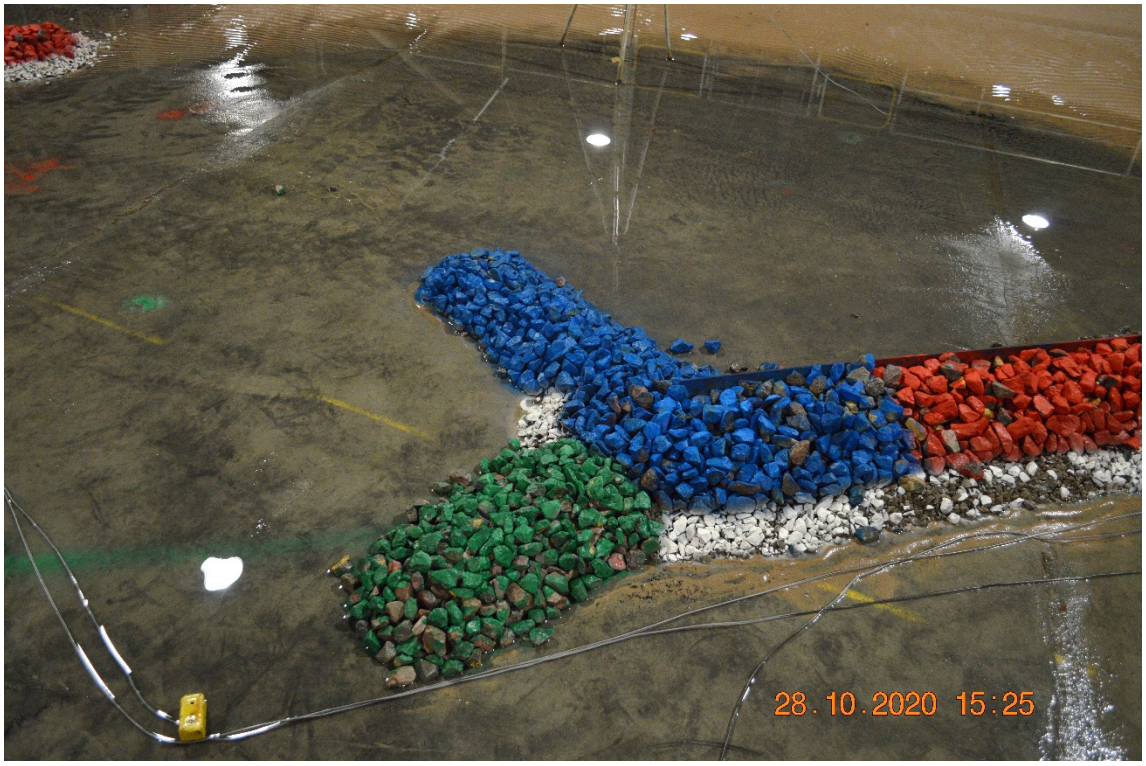


Figure C.117: Post Test Part 05 (WC_EXT_WL_01) stability photograph for BW2-4, position 11

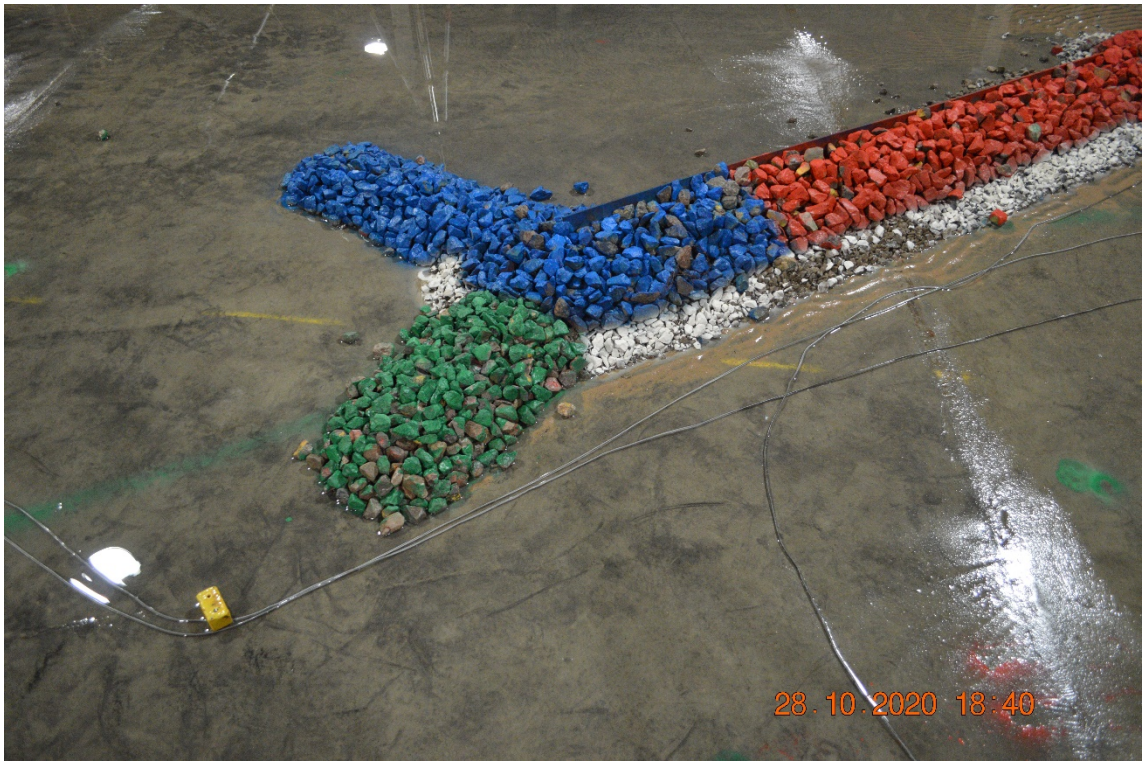


Figure C.118: Post Test Part 06 (WC_EXT_WL_02) stability photograph for BW2-4, position 11

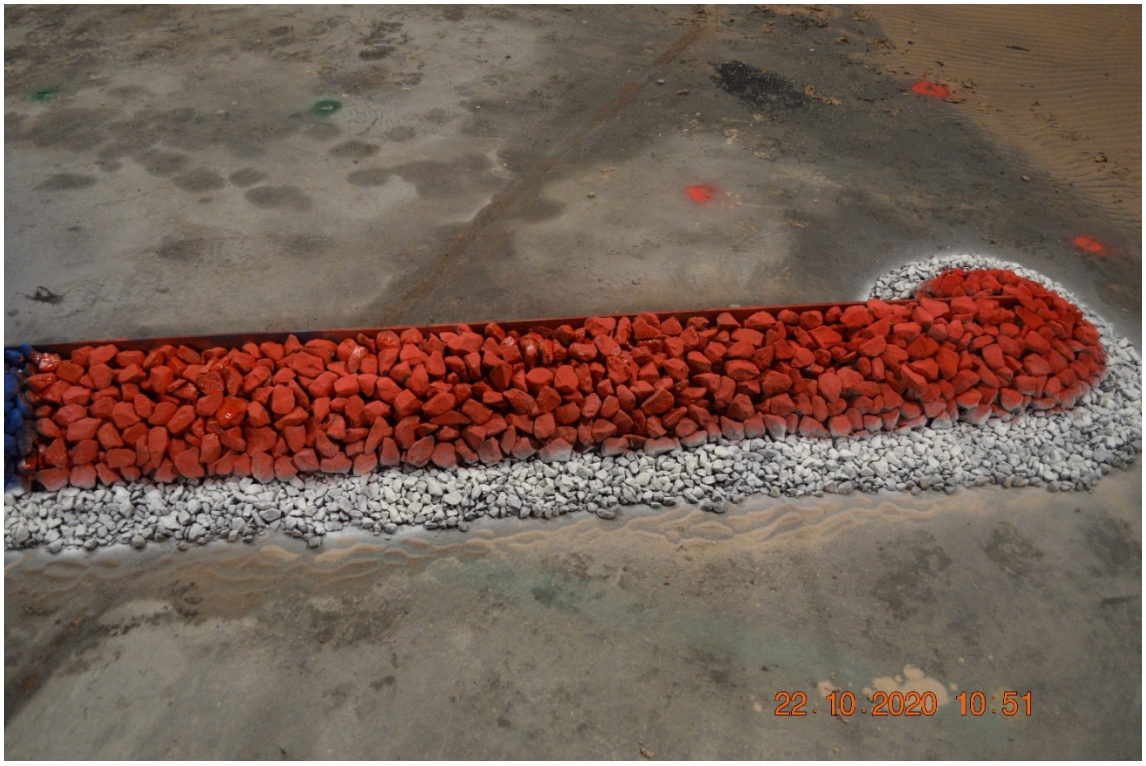


Figure C.119: Pre-test stability photograph for BW2-4, position 12

Figure C.120: Post Test Part 01 (WC_LOW_WL_SE) stability photograph for BW2-4, position 12

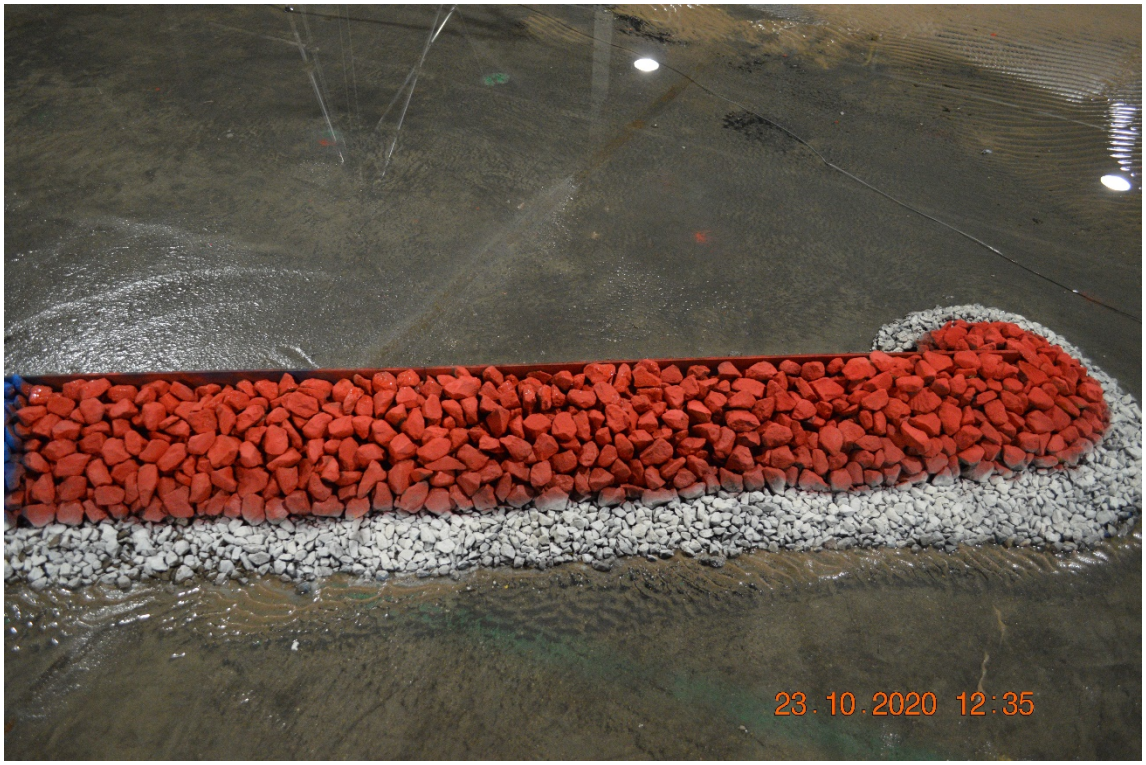


Figure C.121: Post Test Part 02 (WC_HIGH_WL_SE) stability photograph for BW2-4, position 12

Figure C.122: Post Test Part 03 (WC_LOW_WL) stability photograph for BW2-4, position 12

Figure C.123: Post Test Part 04 (WC_HIGH_WL) stability photograph for BW2-4, position 12

Figure C.124: Post Test Part 05 (WC_EXT_WL_01) stability photograph for BW2-4, position 12

Figure C.125: Post Test Part 06 (WC_EXT_WL_02) stability photograph for BW2-4, position 12

No image available

Figure C.126: Pre-test stability photograph for BW2-4, position 13

Figure C.127: Post Test Part 01 (WC_LOW_WL_SE) stability photograph for BW2-4, position 13

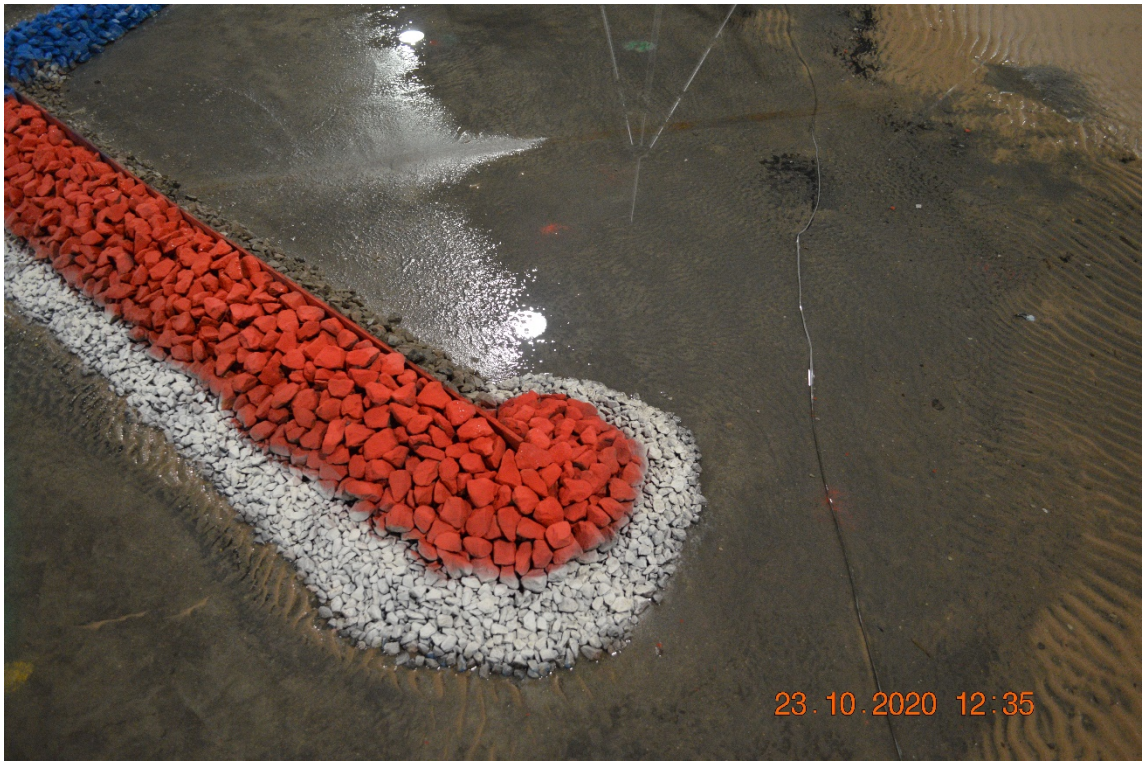


Figure C.128: Post Test Part 02 (WC_HIGH_WL_SE) stability photograph for BW2-4, position 13

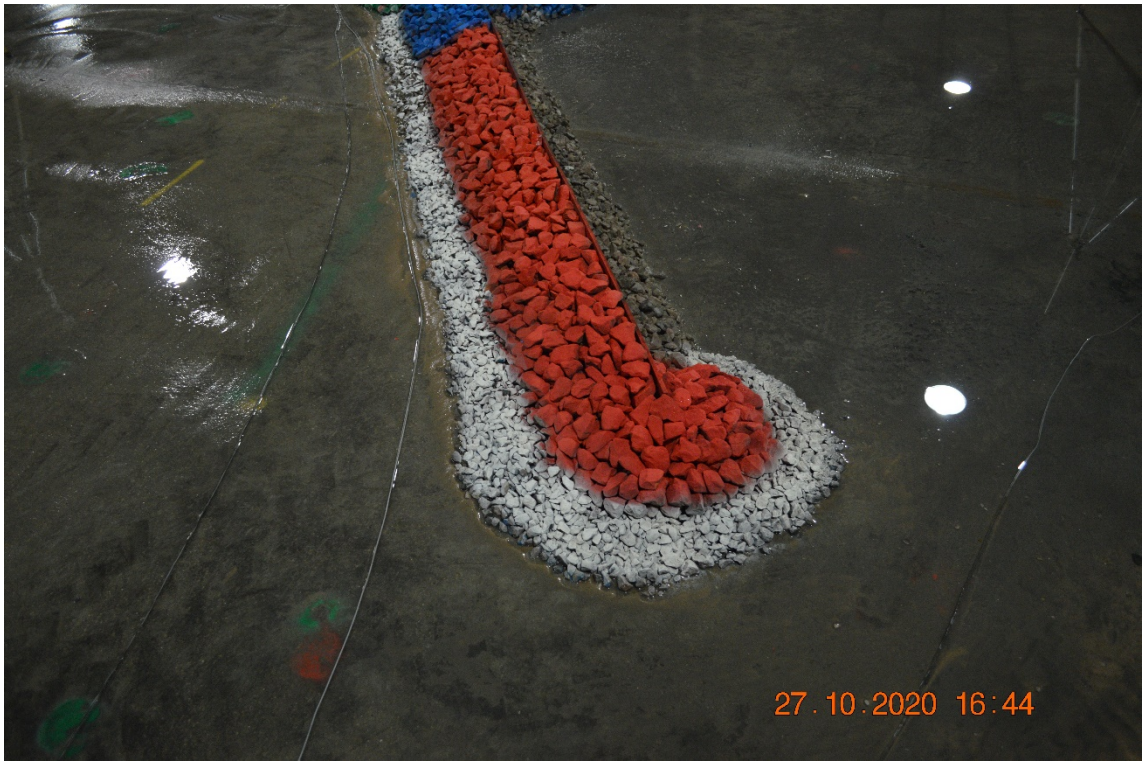


Figure C.129: Post Test Part 03 (WC_LOW_WL) stability photograph for BW2-4, position 13

Figure C.130: Post Test Part 04 (WC_HIGH_WL) stability photograph for BW2-4, position 13

Figure C.131: Post Test Part 05 (WC_EXT_WL_01) stability photograph for BW2-4, position 13

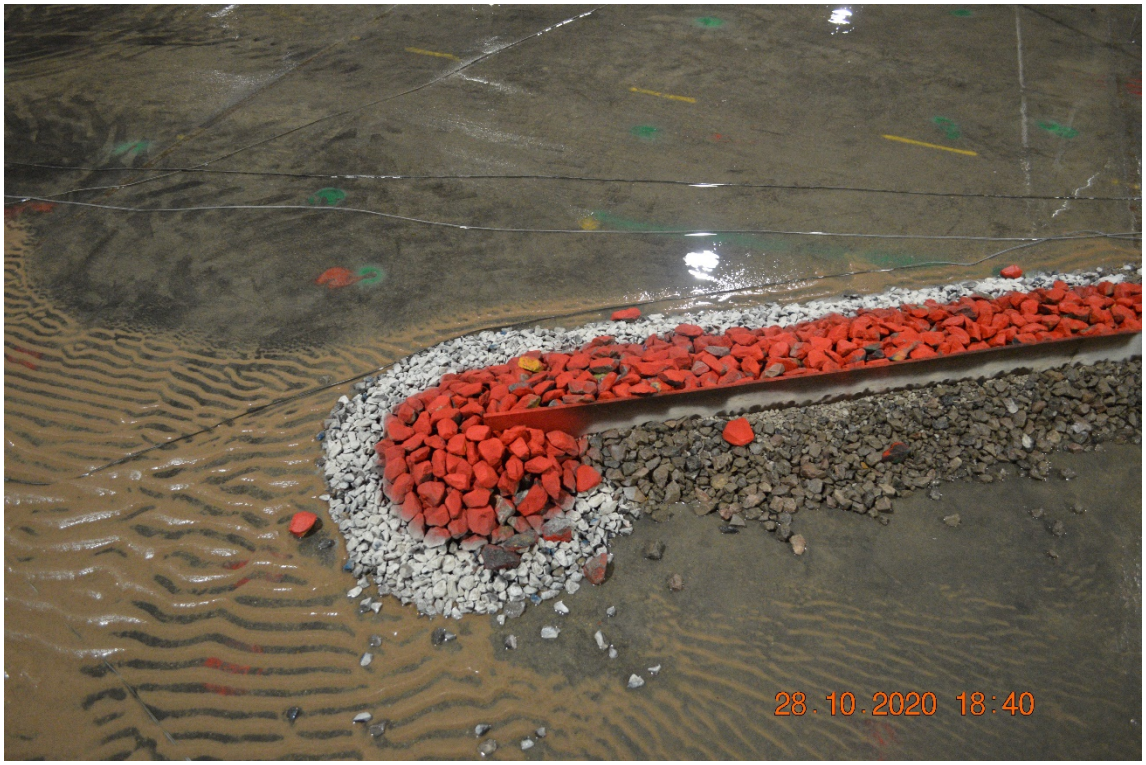


Figure C.132: Post Test Part 06 (WC_EXT_WL_02) stability photograph for BW2-4, position 13

## C.2.5. BW2-5

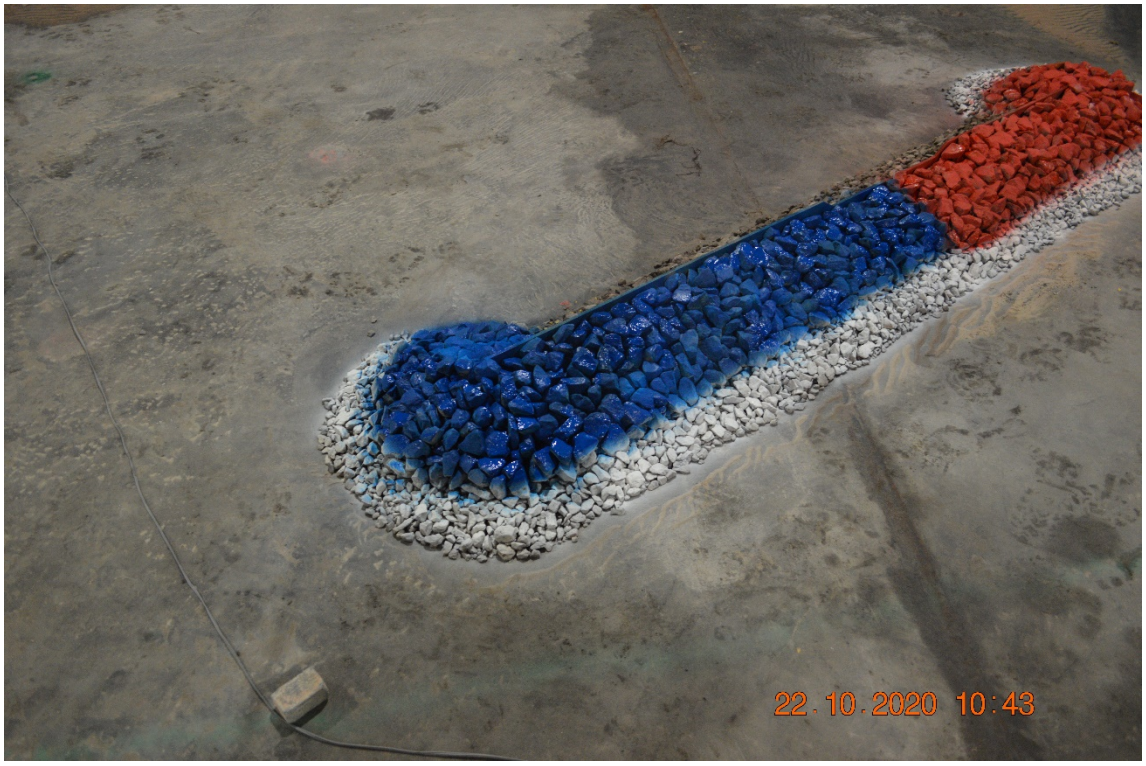


Figure C.133: Pre-test stability photograph for BW2-5, position 14

Figure C.134: Post Test Part 01 (WC_LOW_WL_SE) stability photograph for BW2-5, position 14

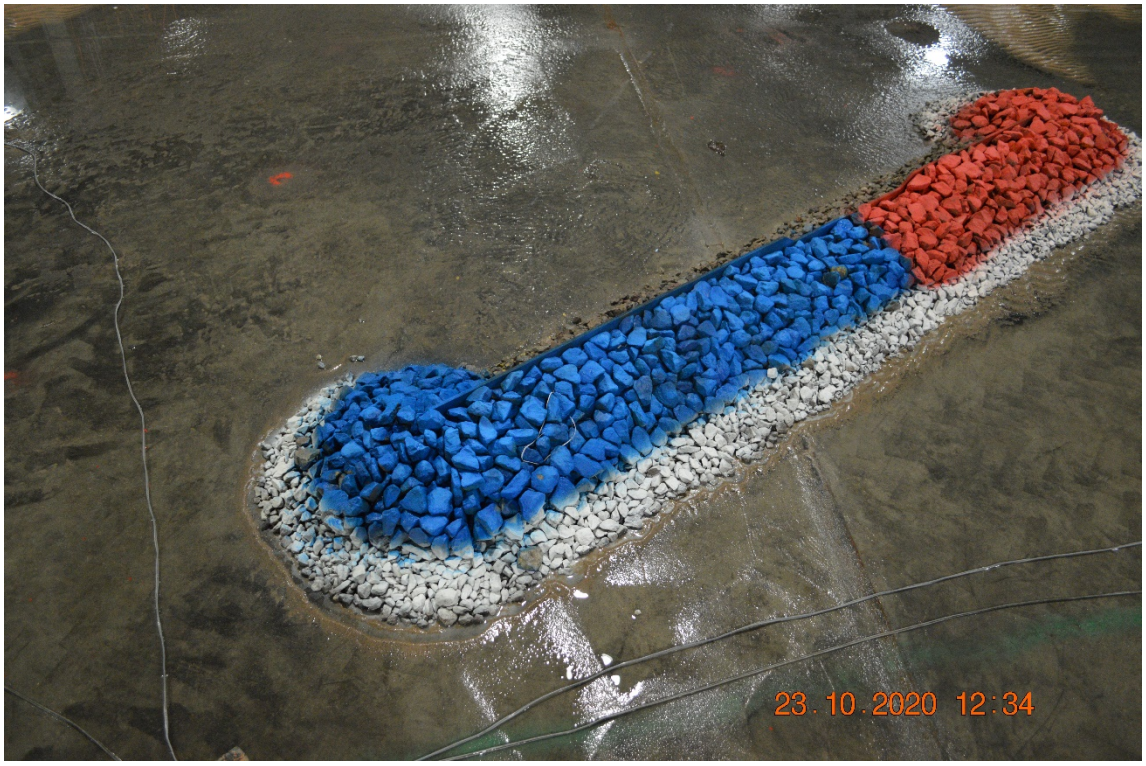


Figure C.135: Post Test Part 02 (WC_HIGH_WL_SE) stability photograph for BW2-5, position 14

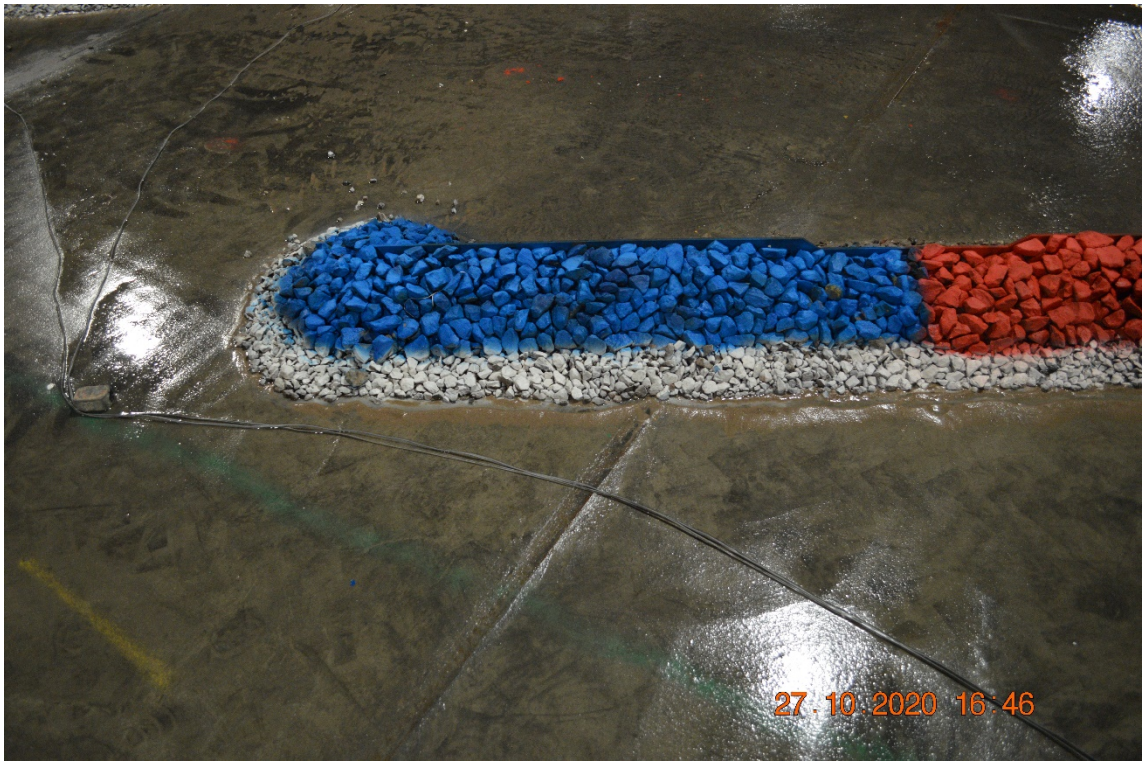


Figure C.136: Post Test Part 03 (WC_LOW_WL) stability photograph for BW2-5, position 14

Figure C.137: Post Test Part 04 (WC_HIGH_WL) stability photograph for BW2-5, position 14

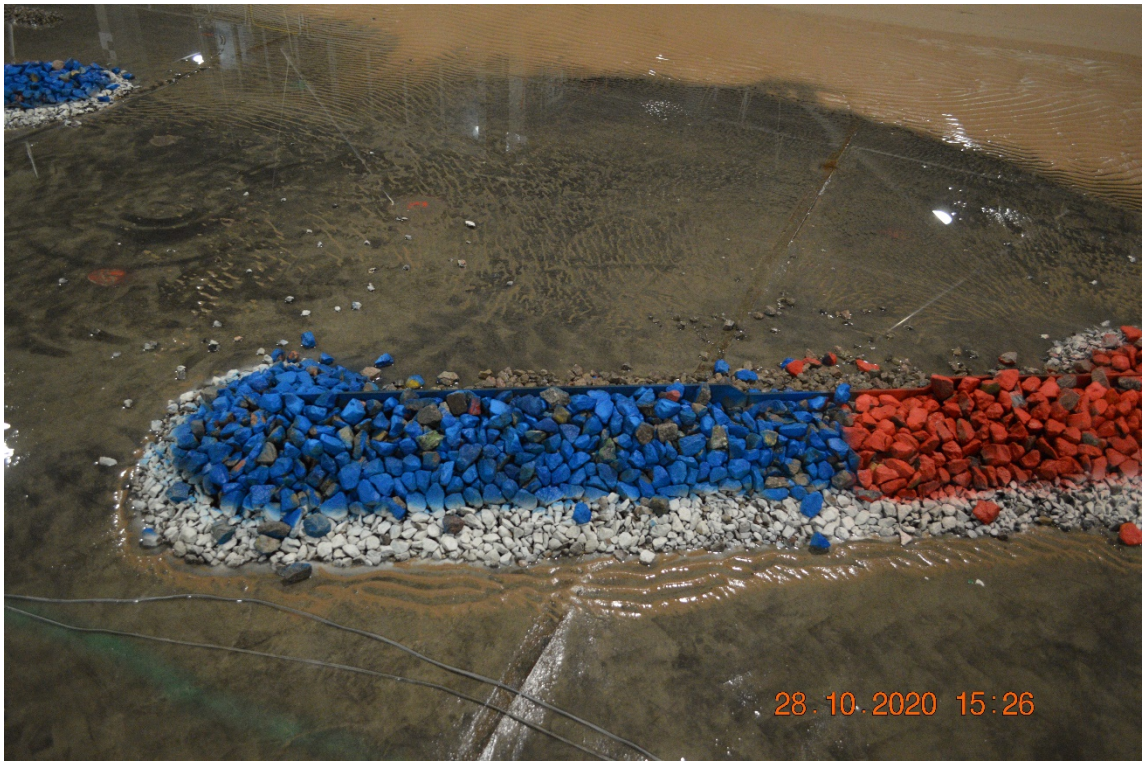


Figure C.138: Post Test Part 05 (WC_EXT_WL_01) stability photograph for BW2-5, position 14

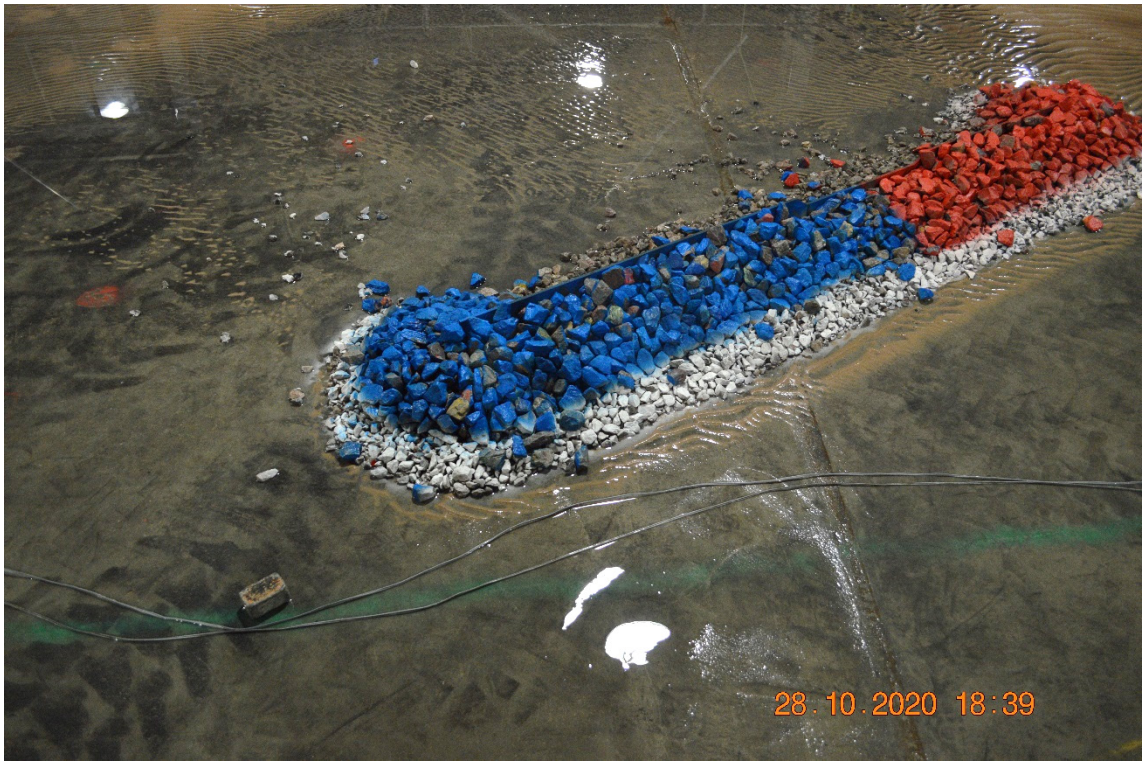


Figure C.139: Post Test Part 06 (WC_EXT_WL_02) stability photograph for BW2-5, position 14

Figure C.140: Pre-test stability photograph for BW2-5, position 15

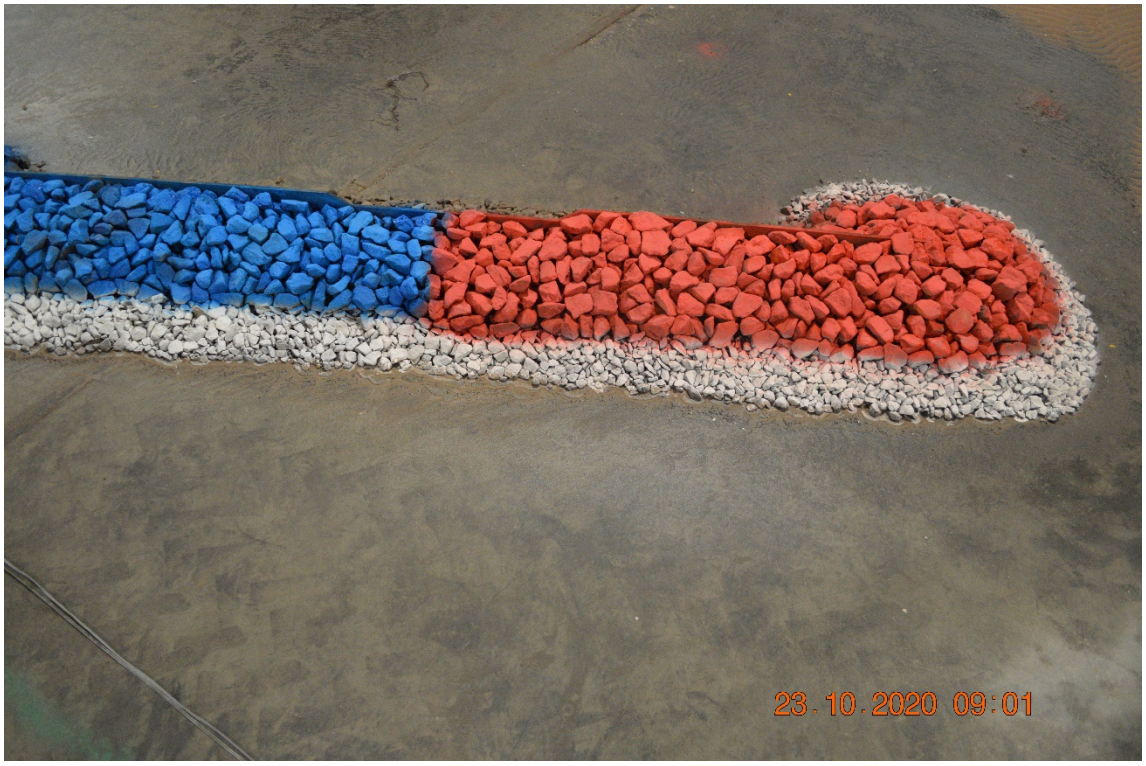


Figure C.141: Post Test Part 01 (WC_LOW_WL_SE) stability photograph for BW2-5, position 15

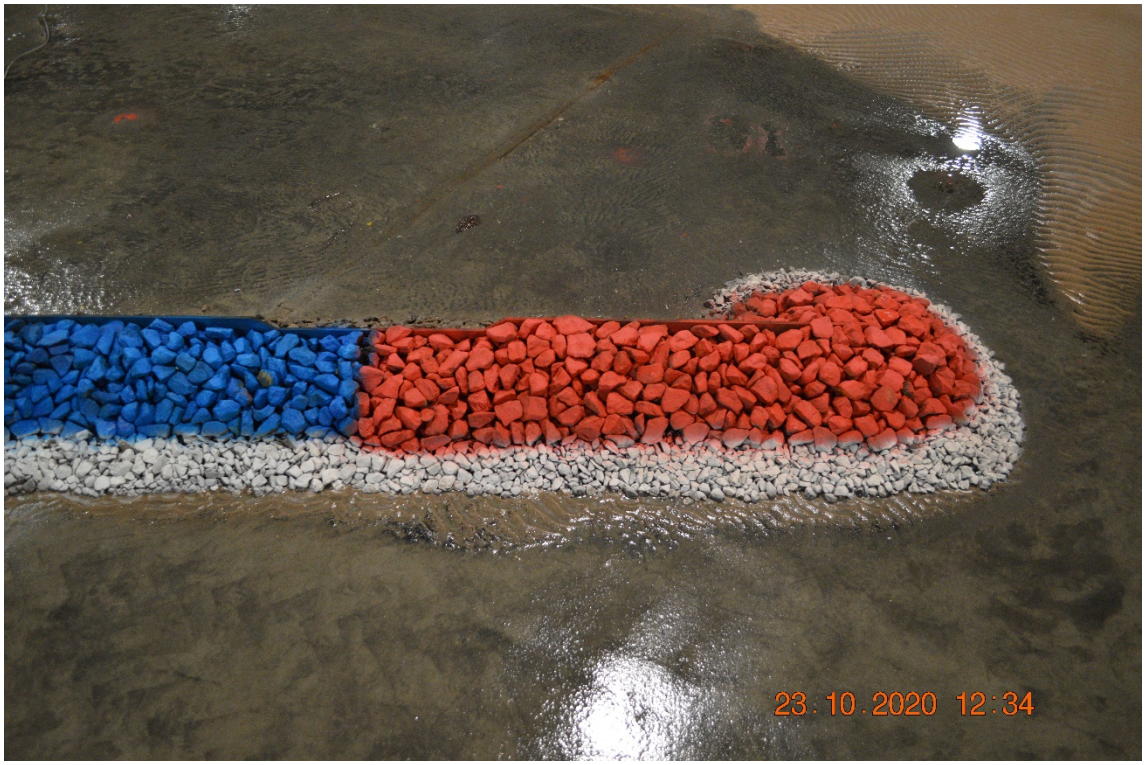


Figure C.142: Post Test Part 02 (WC_HIGH_WL_SE) stability photograph for BW2-5, position 15

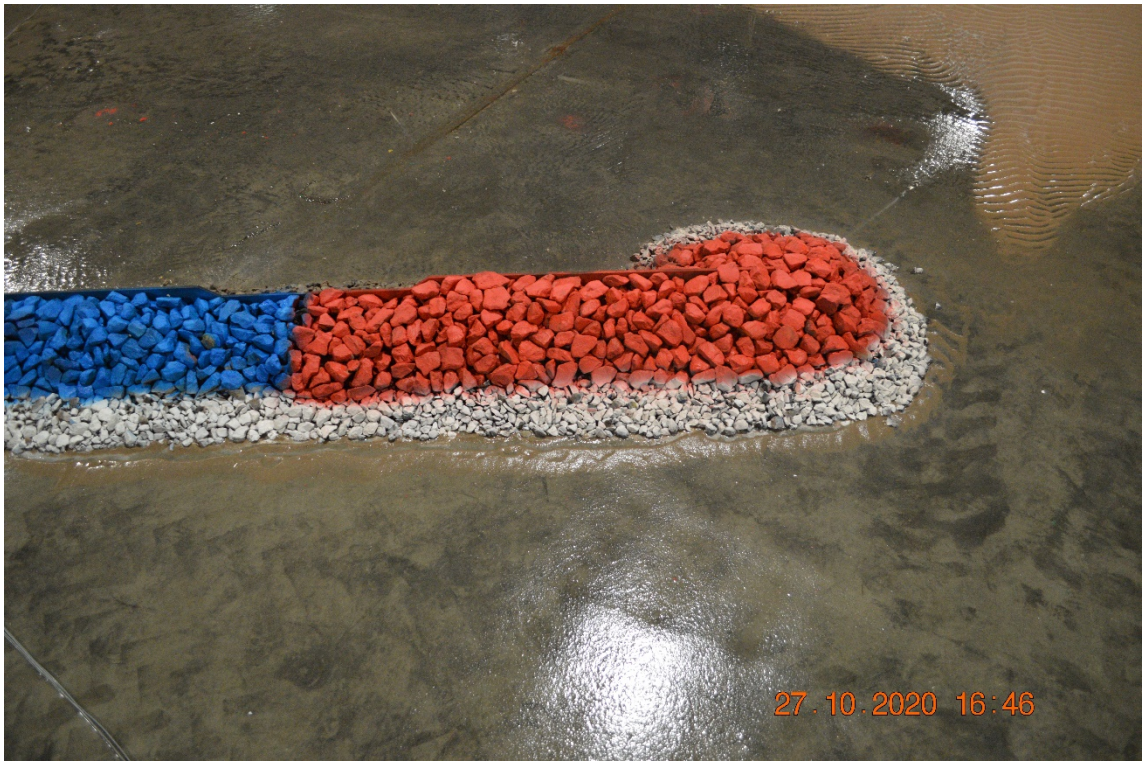


Figure C.143: Post Test Part 03 (WC_LOW_WL) stability photograph for BW2-5, position 15

Figure C.144: Post Test Part 04 (WC_HIGH_WL) stability photograph for BW2-5, position 15

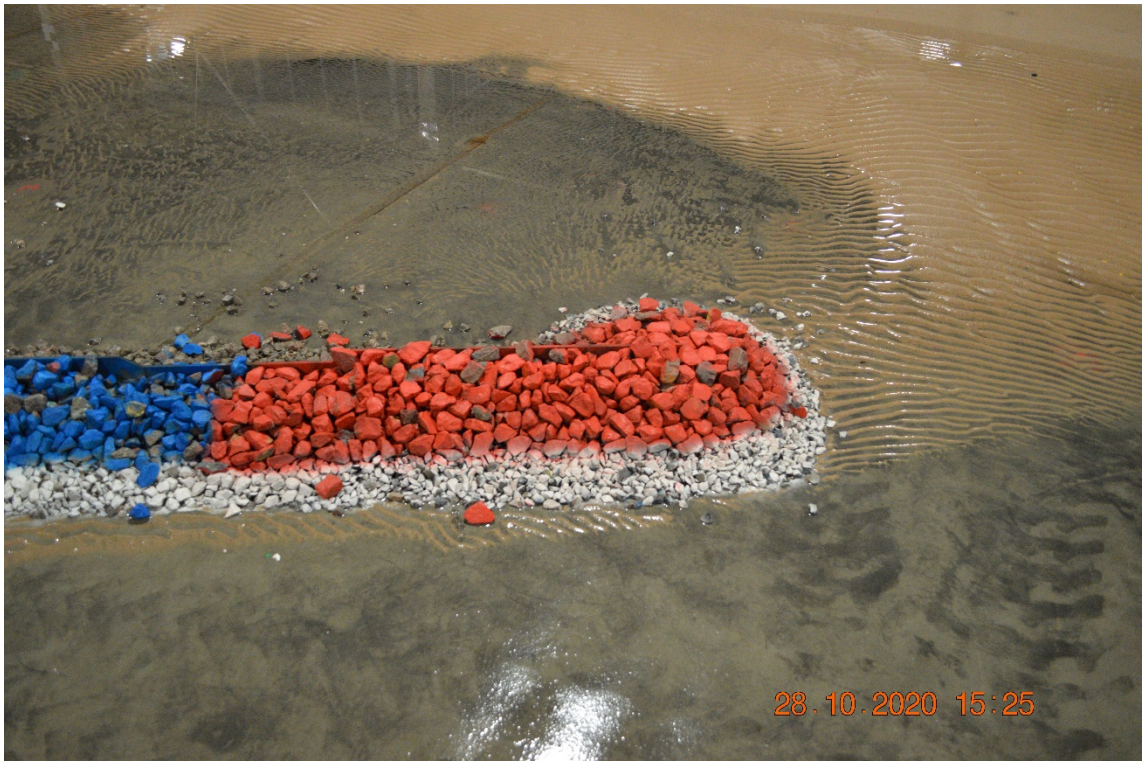


Figure C.145: Post Test Part 05 (WC_EXT_WL_01) stability photograph for BW2-5, position 15

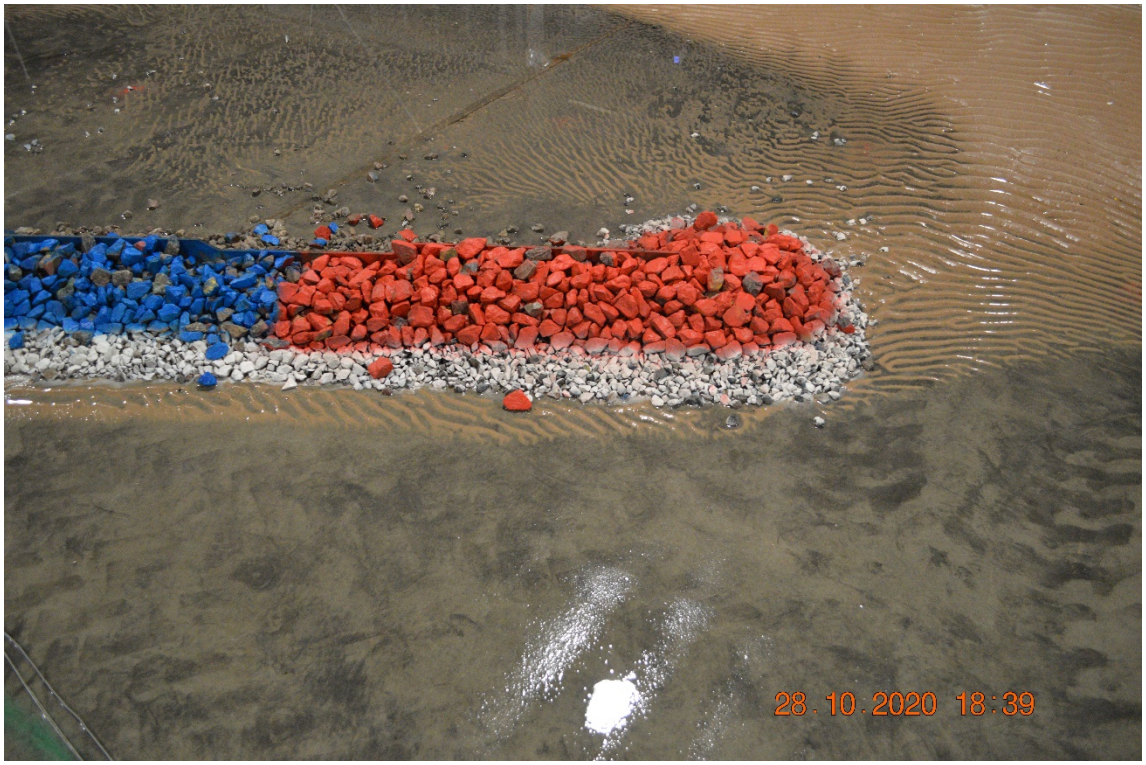


Figure C.146: Post Test Part 06 (WC_EXT_WL_02) stability photograph for BW2-5, position 15

Figure C.147: Pre-test stability photograph for BW2-5, position 16

Figure C.148: Post Test Part 01 (WC_LOW_WL_SE) stability photograph for BW2-5, position 16

Figure C.149: Post Test Part 02 (WC_HIGH_WL_SE) stability photograph for BW2-5, position 16

Figure C.150: Post Test Part 03 (WC_LOW_WL) stability photograph for BW2-5, position 16

Figure C.151: Post Test Part 04 (WC_HIGH_WL) stability photograph for BW2-5, position 16

Figure C.152: Post Test Part 05 (WC_EXT_WL_01) stability photograph for BW2-5, position 16

Figure C.153: Post Test Part 06 (WC_EXT_WL_02) stability photograph for BW2-5, position 16

Figure C.154: Pre-test stability photograph for BW2-5, position 17

Figure C.155: Post Test Part 01 (WC_LOW_WL_SE) stability photograph for BW2-5, position 17

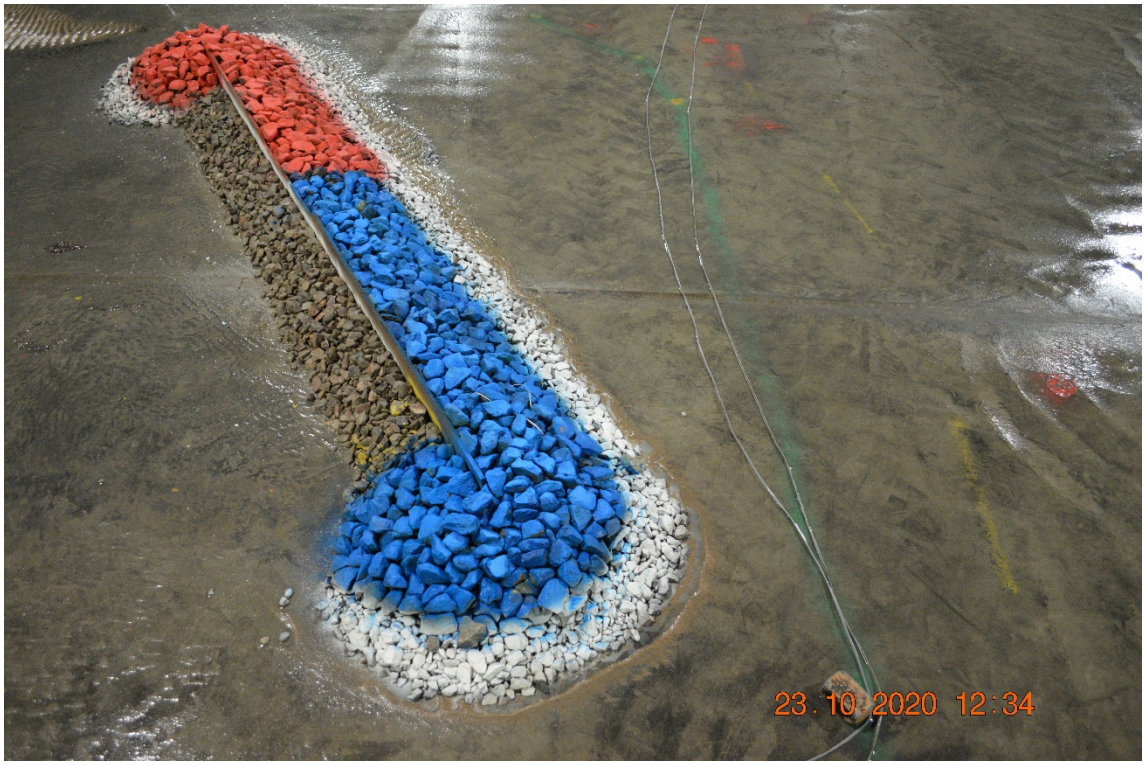


Figure C.156: Post Test Part 02 (WC_HIGH_WL_SE) stability photograph for BW2-5, position 17

Figure C.157: Post Test Part 03 (WC_LOW_WL) stability photograph for BW2-5, position 17

No image available

Figure C.158: Post Test Part 04 (WC_HIGH_WL) stability photograph for BW2-5, position 17

Figure C.159: Post Test Part 05 (WC_EXT_WL_01) stability photograph for BW2-5, position 17

Figure C.160: Post Test Part 06 (WC_EXT_WL_02) stability photograph for BW2-5, position 17

Figure C.161: Pre-test stability photograph for BW2-5, position 18

Figure C.162: Post Test Part 01 (WC_LOW_WL_SE) stability photograph for BW2-5, position 18

Figure C.163: Post Test Part 02 (WC_HIGH_WL_SE) stability photograph for BW2-5, position 18

Figure C.164: Post Test Part 03 (WC_LOW_WL) stability photograph for BW2-5, position 18

No image available

Figure C.165: Post Test Part 04 (WC_HIGH_WL) stability photograph for BW2-5, position 18

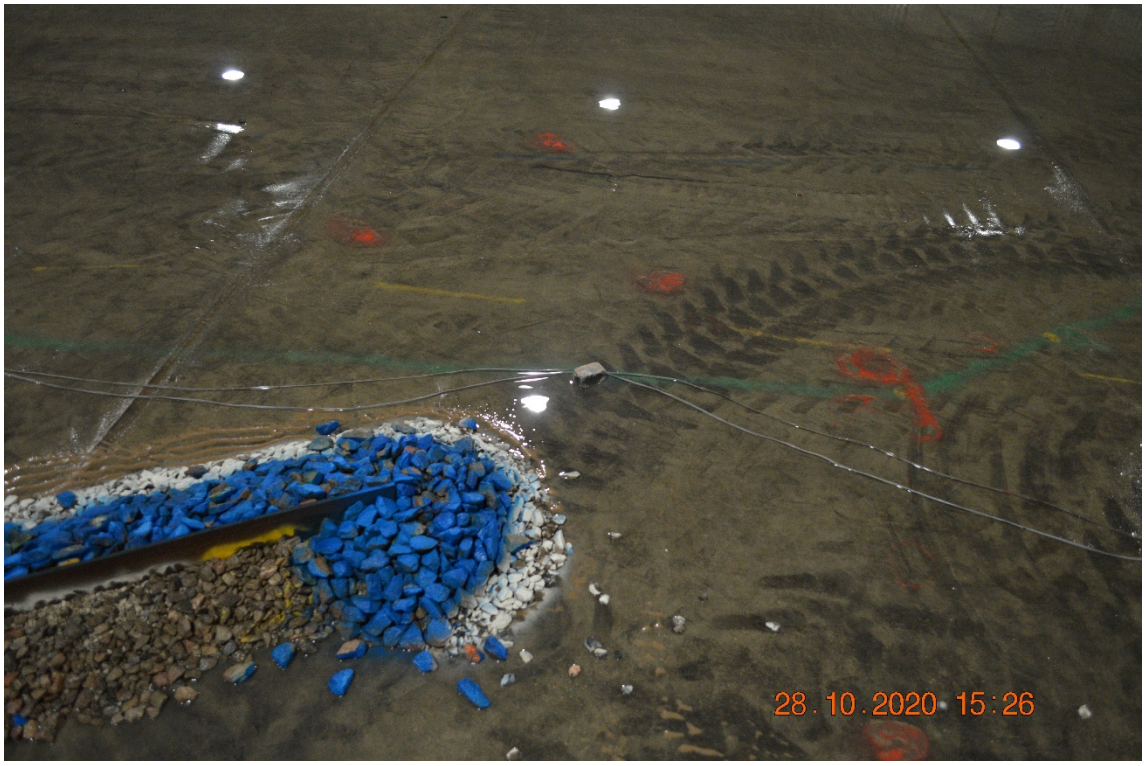


Figure C.166: Post Test Part 05 (WC_EXT_WL_01) stability photograph for BW2-5, position 18

Figure C.167: Post Test Part 06 (WC_EXT_WL_02) stability photograph for BW2-5, position 18

## C.2.6. BW2-6

Figure C.168: Pre-test stability photograph for BW2-6, position 19

Figure C.169: Post Test Part 01 (WC_LOW_WL_SE) stability photograph for BW2-6, position 19

Figure C.170: Post Test Part 02 (WC_HIGH_WL_SE) stability photograph for BW2-6, position 19

Figure C.171: Post Test Part 03 (WC_LOW_WL) stability photograph for BW2-6, position 19

Figure C.172: Post Test Part 04 (WC_HIGH_WL) stability photograph for BW2-6, position 19

Figure C.173: Post Test Part 05 (WC_EXT_WL_01) stability photograph for BW2-6, position 19

Figure C.174: Post Test Part 06 (WC_EXT_WL_02) stability photograph for BW2-6, position 19

Figure C.175: Pre-test stability photograph for BW2-6, position 20

Figure C.176: Post Test Part 01 (WC_LOW_WL_SE) stability photograph for BW2-6, position 20

Figure C.177: Post Test Part 02 (WC_HIGH_WL_SE) stability photograph for BW2-6, position 20

Figure C.178: Post Test Part 03 (WC_LOW_WL) stability photograph for BW2-6, position 20

Figure C.179: Post Test Part 04 (WC_HIGH_WL) stability photograph for BW2-6, position 20

Figure C.180: Post Test Part 05 (WC_EXT_WL_01) stability photograph for BW2-6, position 20

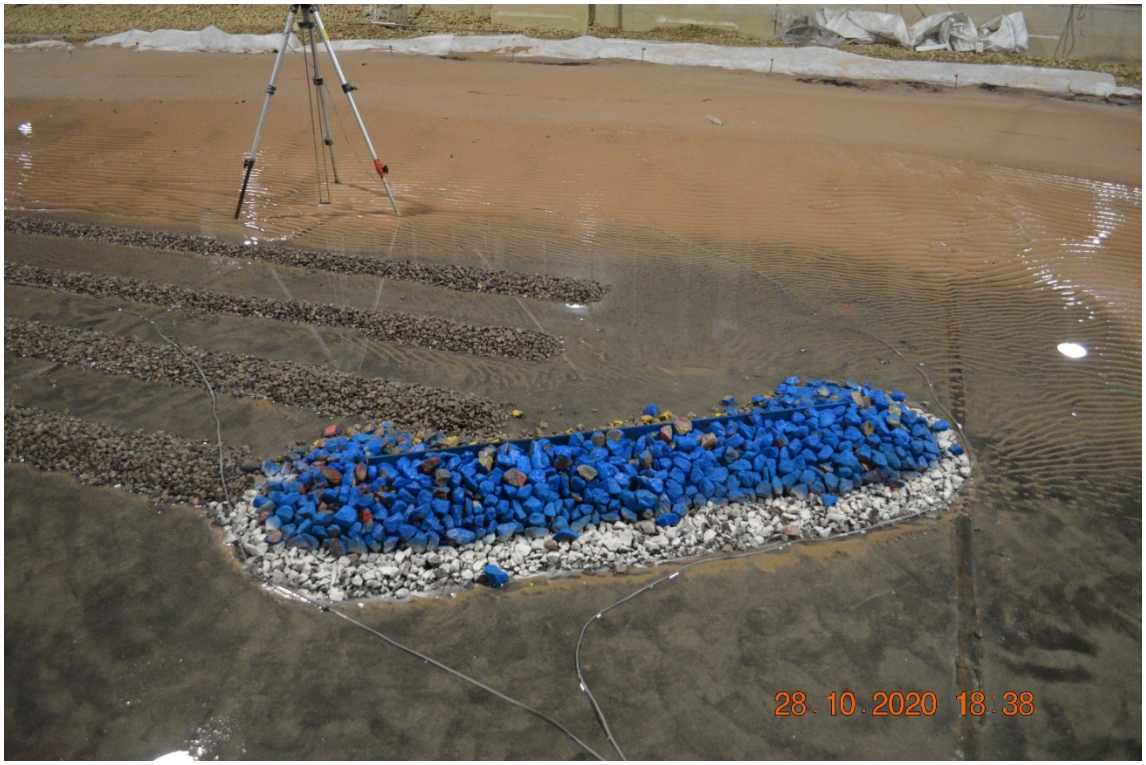


Figure C.181: Post Test Part 06 (WC_EXT_WL_02) stability photograph for BW2-6, position 20

Figure C.182: Pre-test stability photograph for BW2-6, position 21

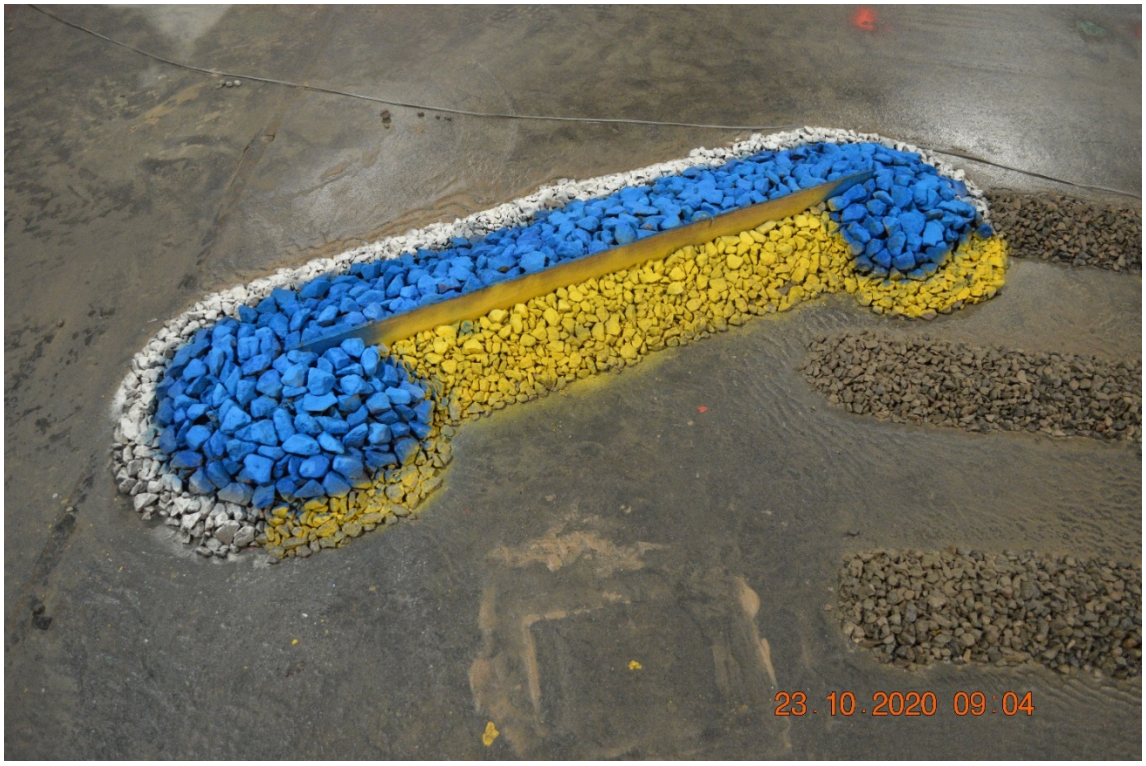


Figure C.183: Post Test Part 01 (WC_LOW_WL_SE) stability photograph for BW2-6, position 21

Figure C.184: Post Test Part 02 (WC_HIGH_WL_SE) stability photograph for BW2-6, position 21

Figure C.185: Post Test Part 03 (WC_LOW_WL) stability photograph for BW2-6, position 21

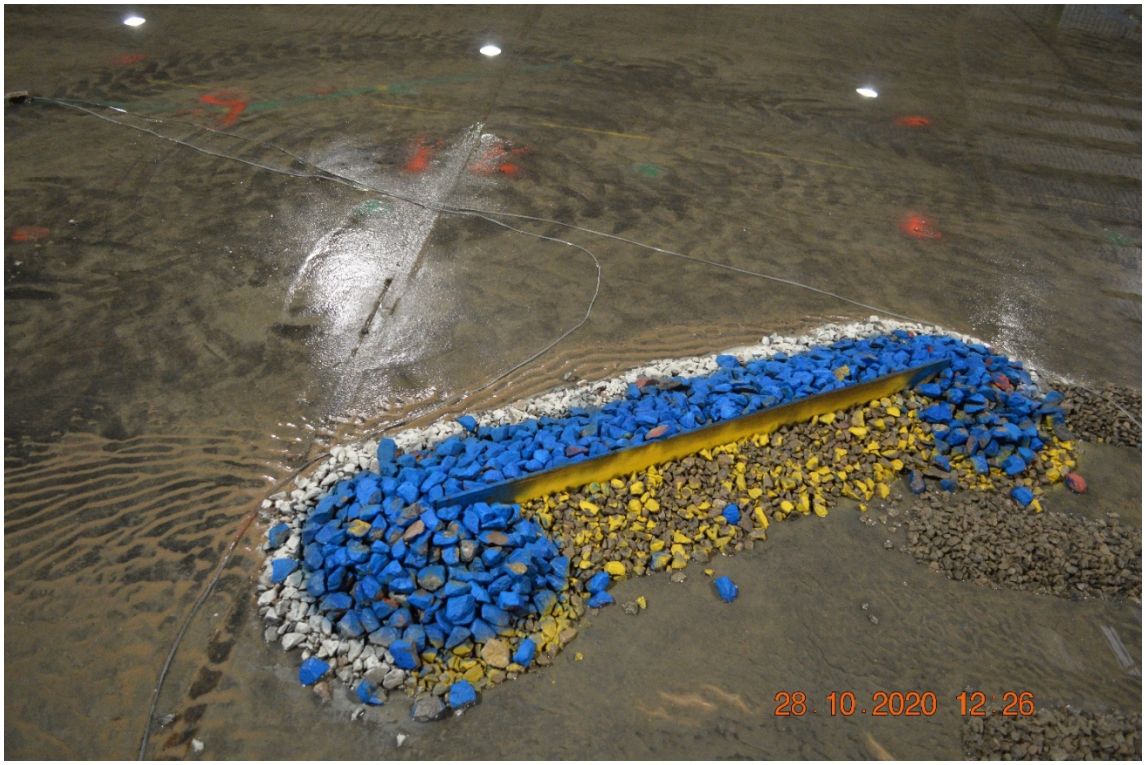


Figure C.186: Post Test Part 04 (WC_HIGH_WL) stability photograph for BW2-6, position 21

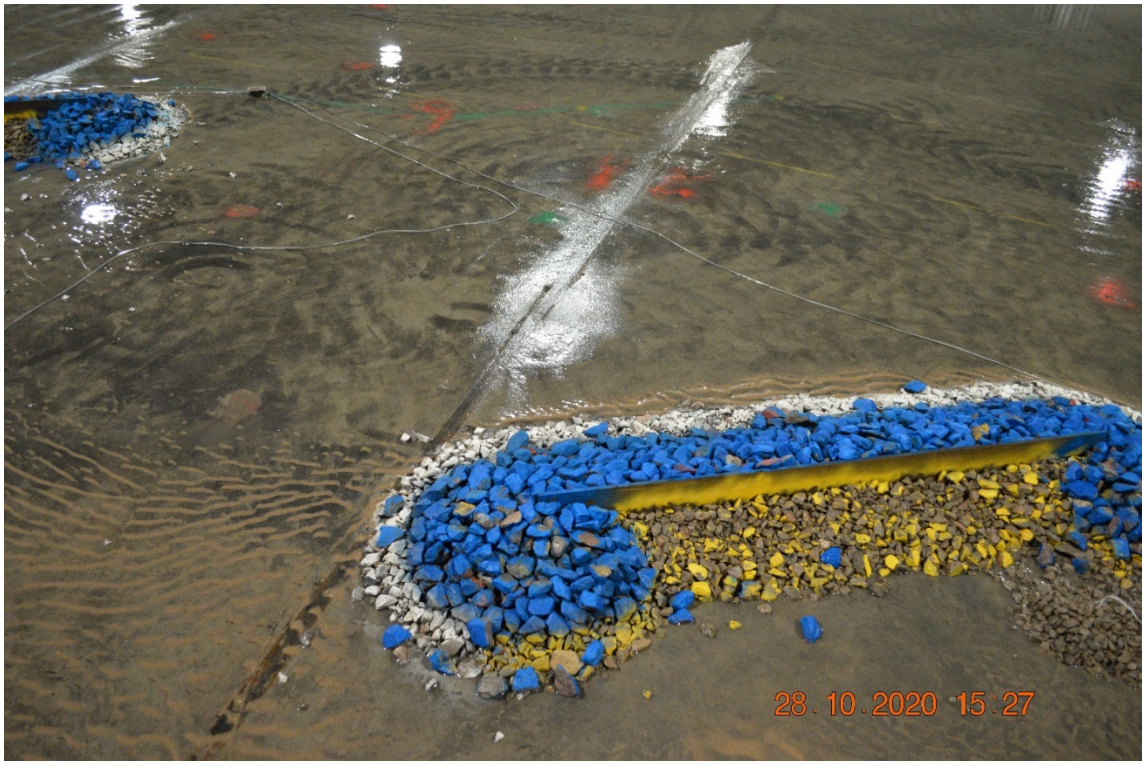


Figure C.187: Post Test Part 05 (WC_EXT_WL_01) stability photograph for BW2-6, position 21

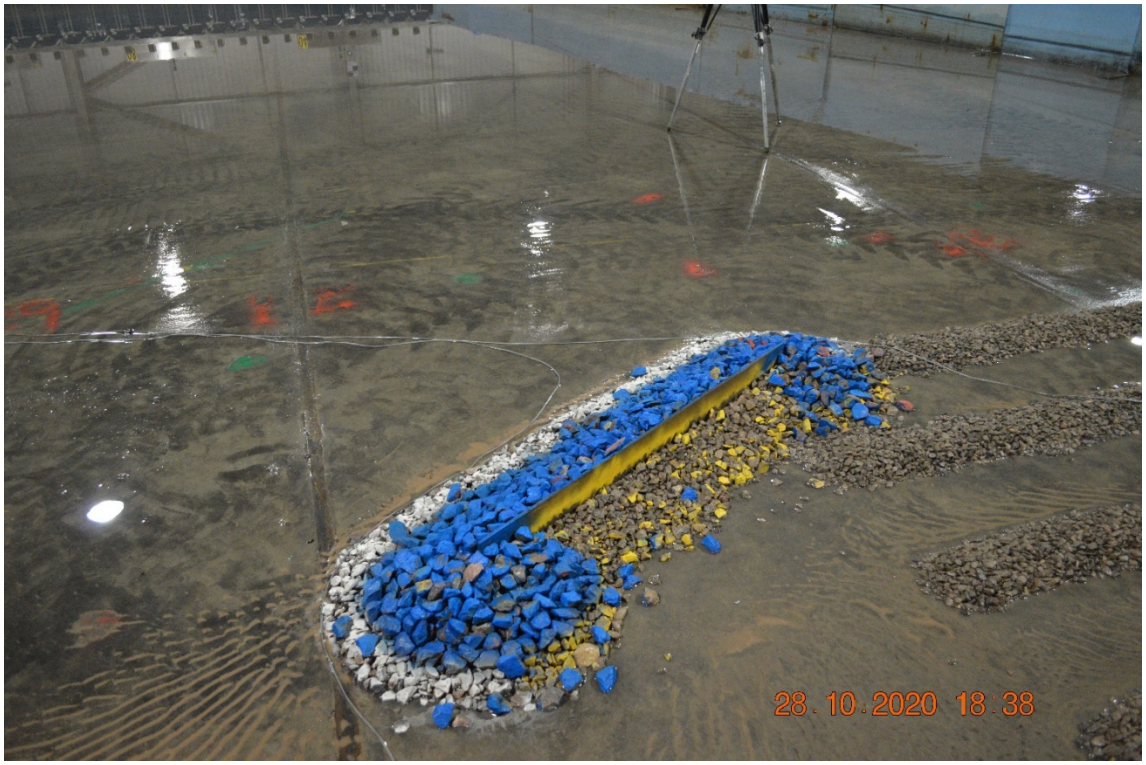


Figure C.188: Post Test Part 06 (WC_EXT_WL_02) stability photograph for BW2-6, position 21

## C.2.7. BW2-7

Figure C.189: Pre-test stability photograph for BW2-7, position 22

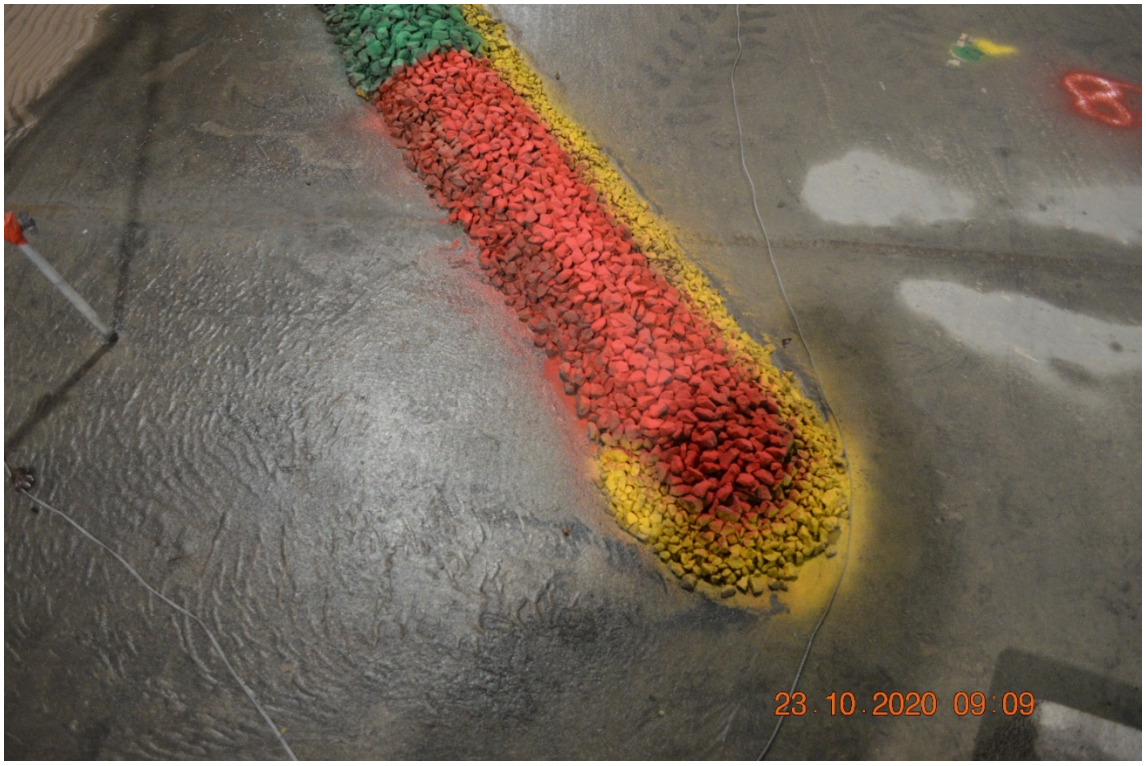


Figure C.190: Post Test Part 01 (WC_LOW_WL_SE) stability photograph for BW2-7, position 22

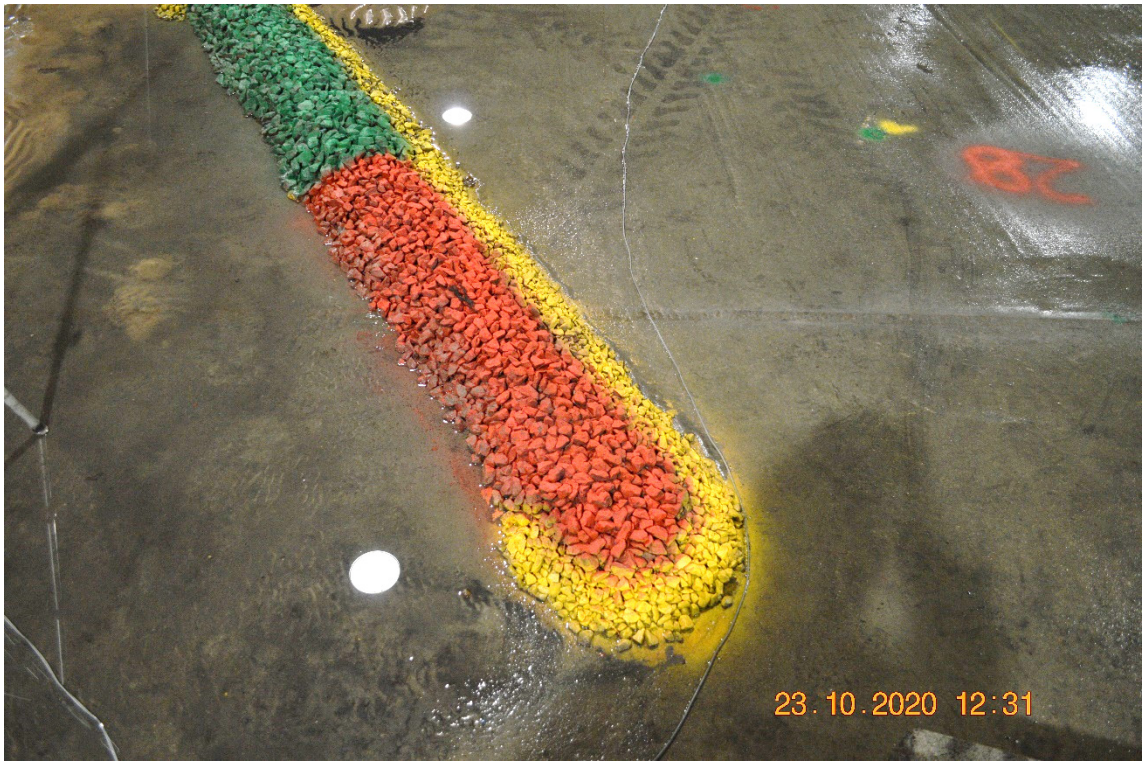


Figure C.191: Post Test Part 02 (WC_HIGH_WL_SE) stability photograph for BW2-7, position 22

No image available

Figure C.192: Post Test Part 03 (WC_LOW_WL) stability photograph for BW2-7, position 22

No image available

Figure C.193: Post Test Part 04 (WC_HIGH_WL) stability photograph for BW2-7, position 22

Figure C.194: Post Test Part 05 (WC_EXT_WL_01) stability photograph for BW2-7, position 22

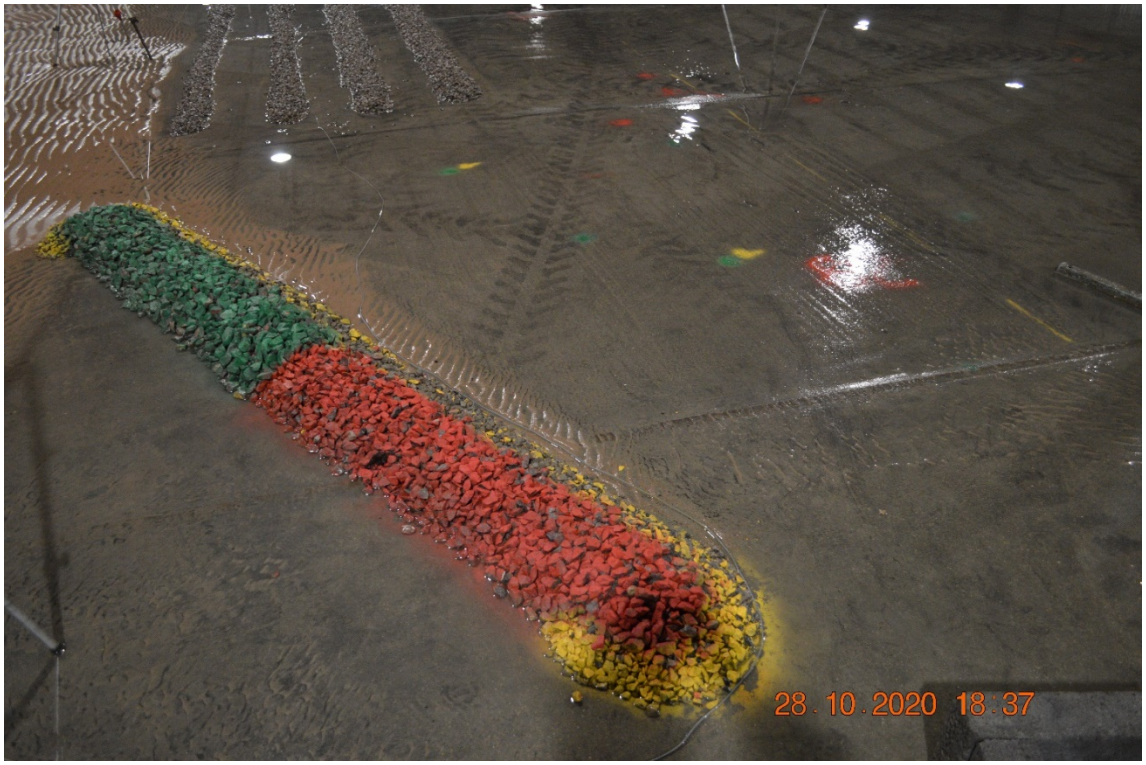


Figure C.195: Post Test Part 06 (WC_EXT_WL_02) stability photograph for BW2-7, position 22

Figure C.196: Pre-test stability photograph for BW2-7, position 23

Figure C.197: Post Test Part 01 (WC_LOW_WL_SE) stability photograph for BW2-7, position 23

Figure C.198: Post Test Part 02 (WC_HIGH_WL_SE) stability photograph for BW2-7, position 23

Figure C.199: Post Test Part 03 (WC_LOW_WL) stability photograph for BW2-7, position 23

Figure C.200: Post Test Part 04 (WC_HIGH_WL) stability photograph for BW2-7, position 23

Figure C.201: Post Test Part 05 (WC_EXT_WL_01) stability photograph for BW2-7, position 23

Figure C.202: Post Test Part 06 (WC_EXT_WL_02) stability photograph for BW2-7, position 23

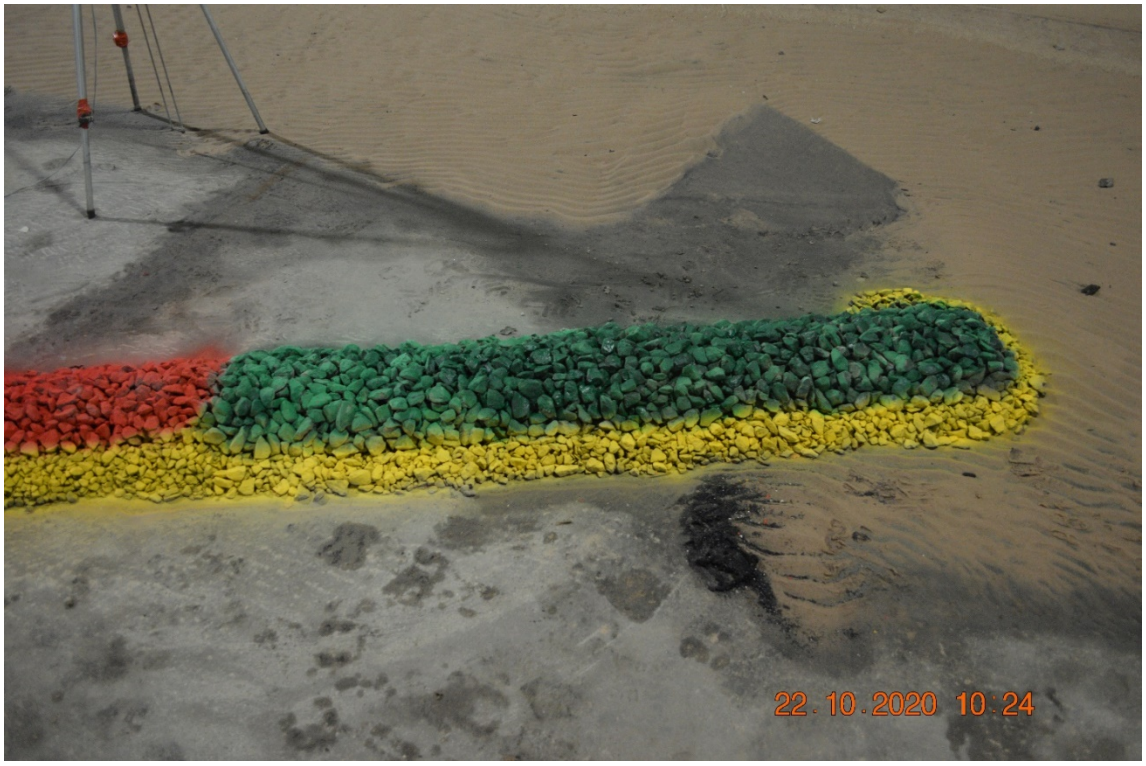


Figure C.203: Pre-test stability photograph for BW2-7, position 24

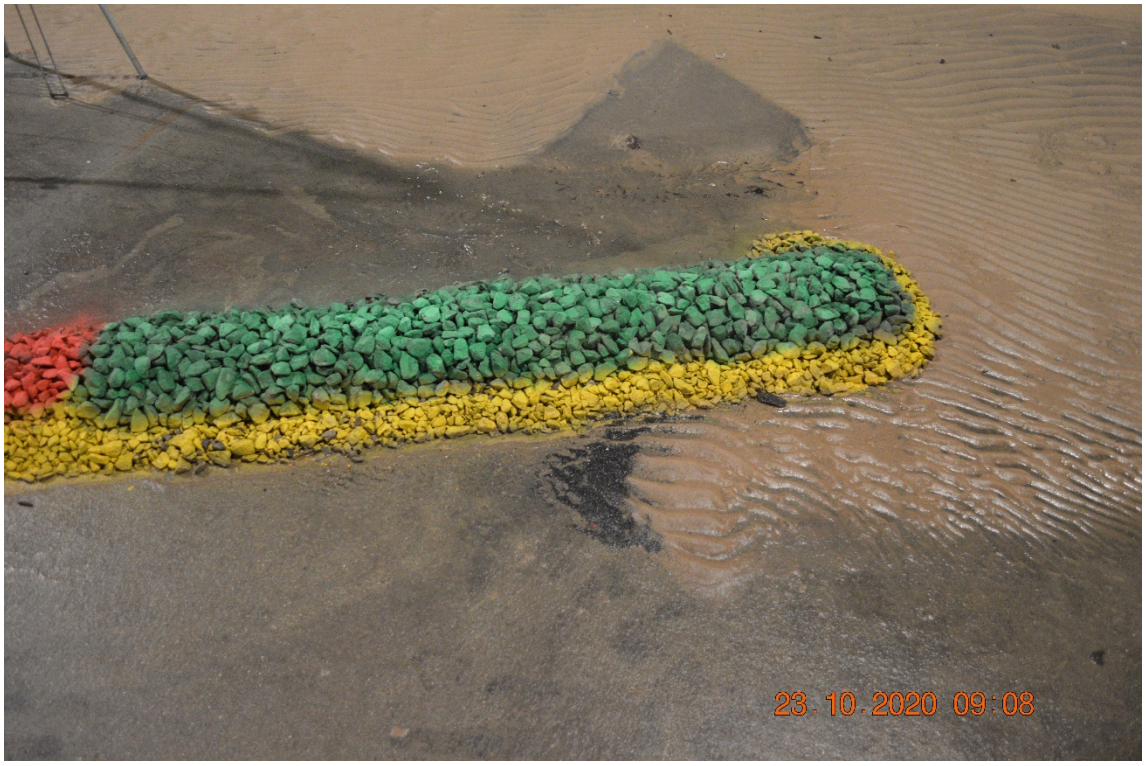


Figure C.204: Post Test Part 01 (WC_LOW_WL_SE) stability photograph for BW2-7, position 24

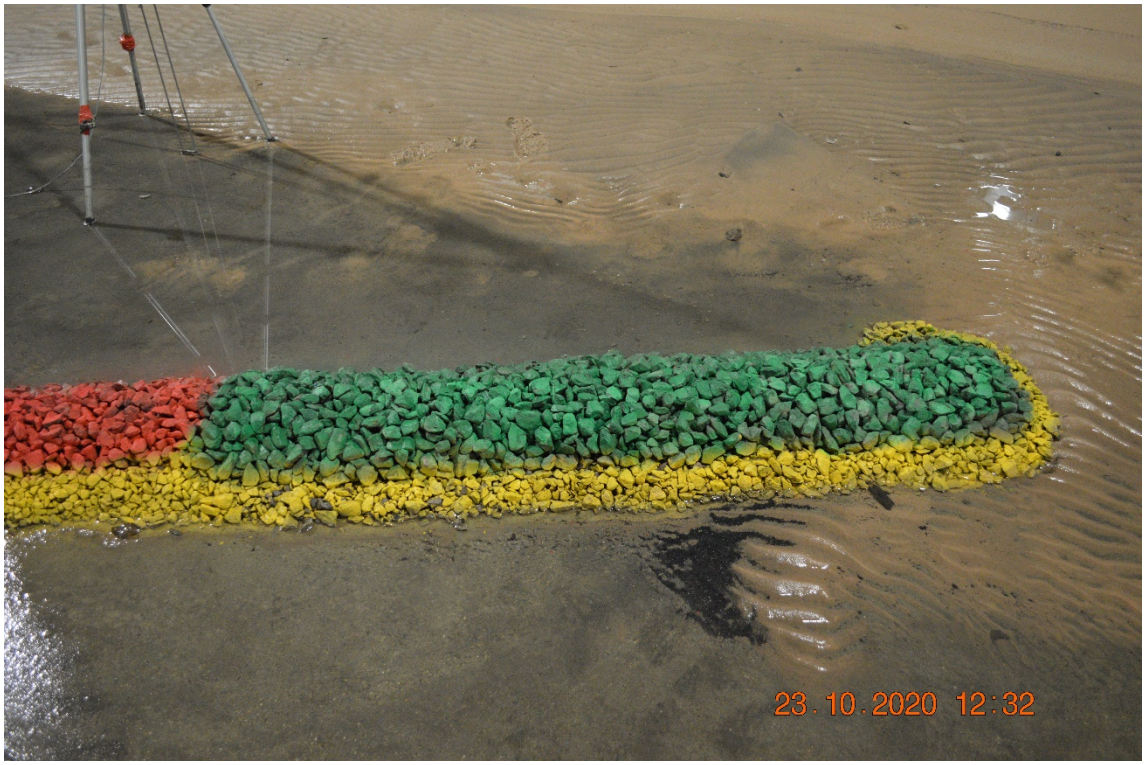


Figure C.205: Post Test Part 02 (WC_HIGH_WL_SE) stability photograph for BW2-7, position 24

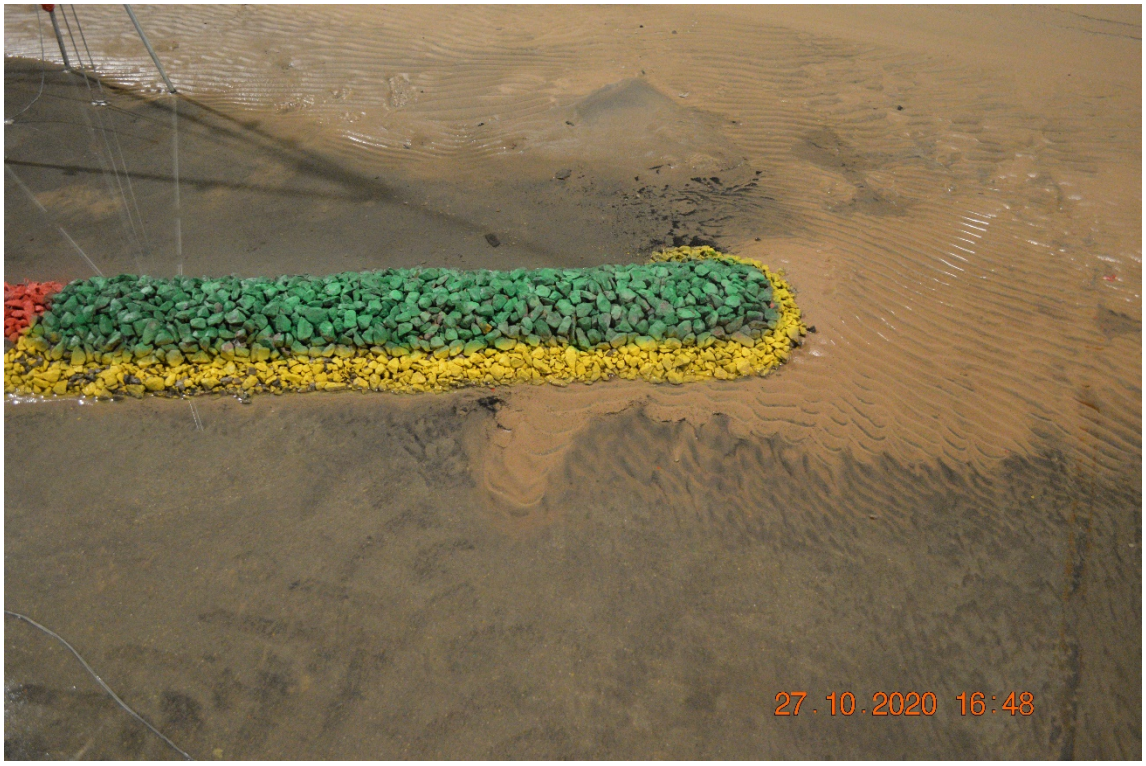


Figure C.206: Post Test Part 03 (WC_LOW_WL) stability photograph for BW2-7, position 24

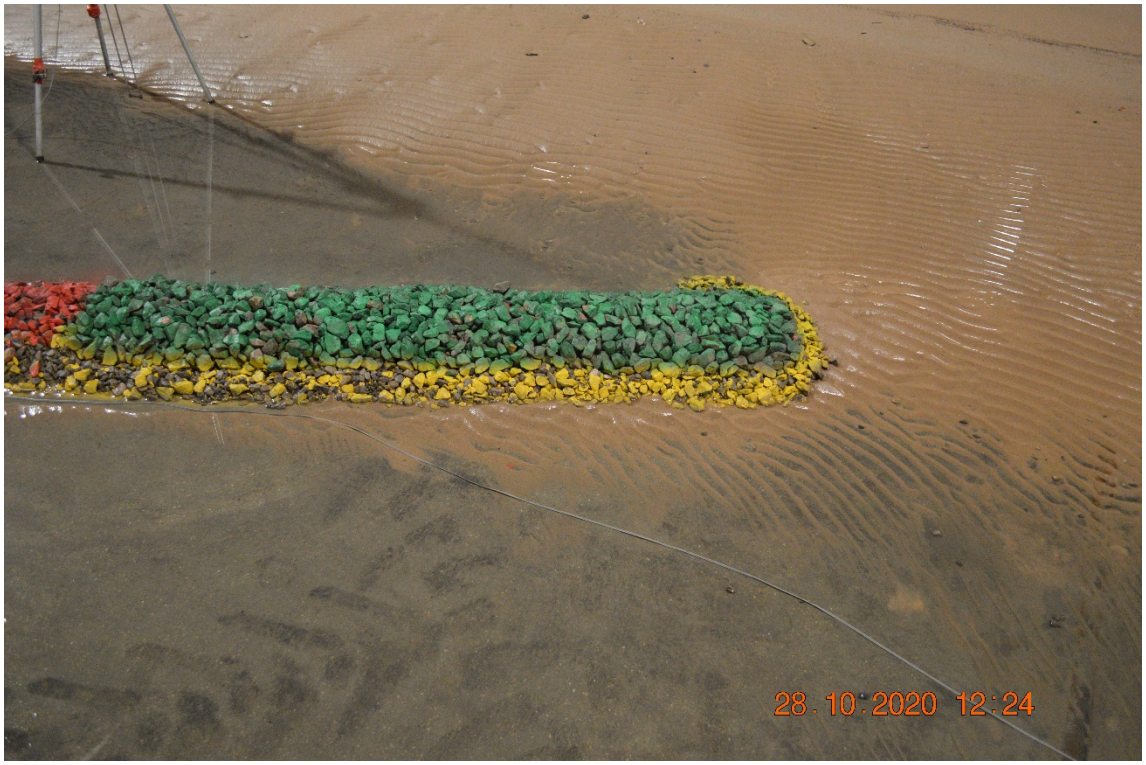


Figure C.207: Post Test Part 04 (WC_HIGH_WL) stability photograph for BW2-7, position 24

Figure C.208: Post Test Part 05 (WC_EXT_WL_01) stability photograph for BW2-7, position 24

Figure C.209: Post Test Part 06 (WC_EXT_WL_02) stability photograph for BW2-7, position 24

Figure C.210: Pre-test stability photograph for BW2-7, position 25

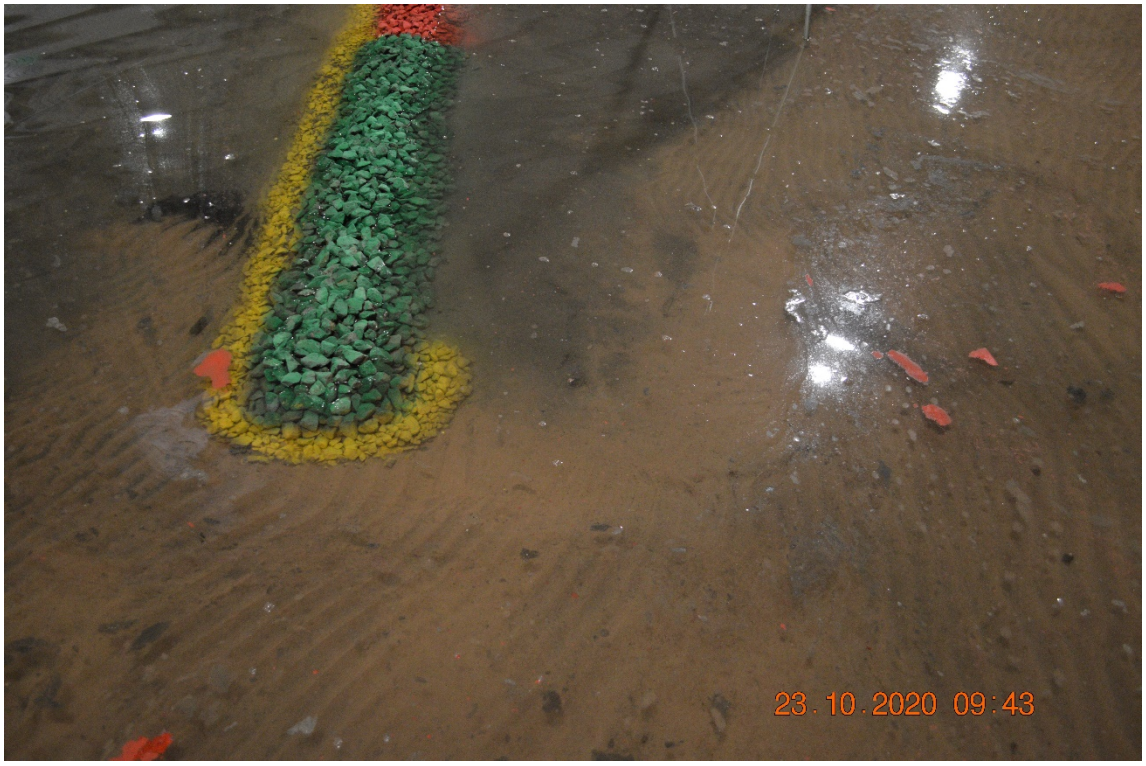


Figure C.211: Post Test Part 01 (WC_LOW_WL_SE) stability photograph for BW2-7, position 25

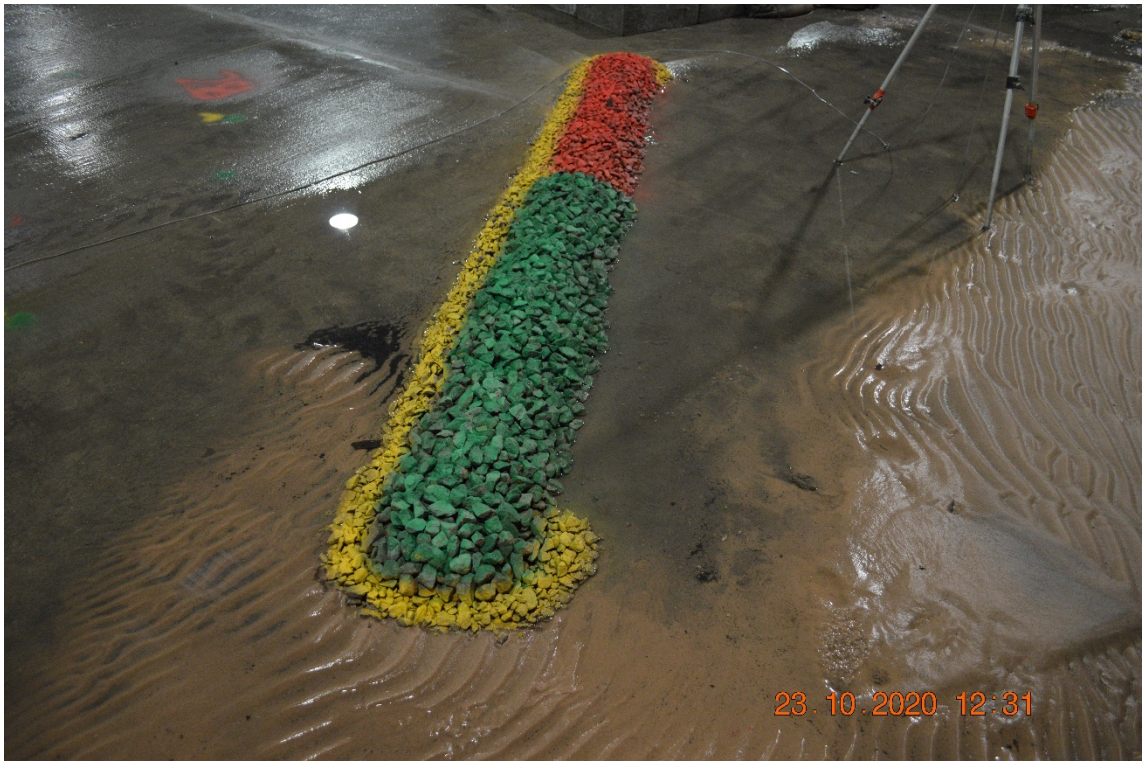


Figure C.212: Post Test Part 02 (WC_HIGH_WL_SE) stability photograph for BW2-7, position 25

Figure C.213: Post Test Part 03 (WC_LOW_WL) stability photograph for BW2-7, position 25

Figure C.214: Post Test Part 04 (WC_HIGH_WL) stability photograph for BW2-7, position 25

Figure C.215: Post Test Part 05 (WC_EXT_WL_01) stability photograph for BW2-7, position 25

Figure C.216: Post Test Part 06 (WC_EXT_WL_02) stability photograph for BW2-7, position 25

# D. Area 3 – Swimming Beach: morphological and stability photographs and scan data

## D.1. Morphological photographs

### D.1.1. Configuration 01 – Initial configuration

Configuration 01 was the starting point for the optimisation of the beach control structures, and was provided in *2020-0617 Illinois Beach State Park Shoreline Stabilization.pdf* (Figure 7.3). This configuration was tested for 18 hr (3 hrs model). The pre and post-test photographs from the 'North' and 'South' time-lapse camera views are shown in Figure D.1 and Figure D.2.

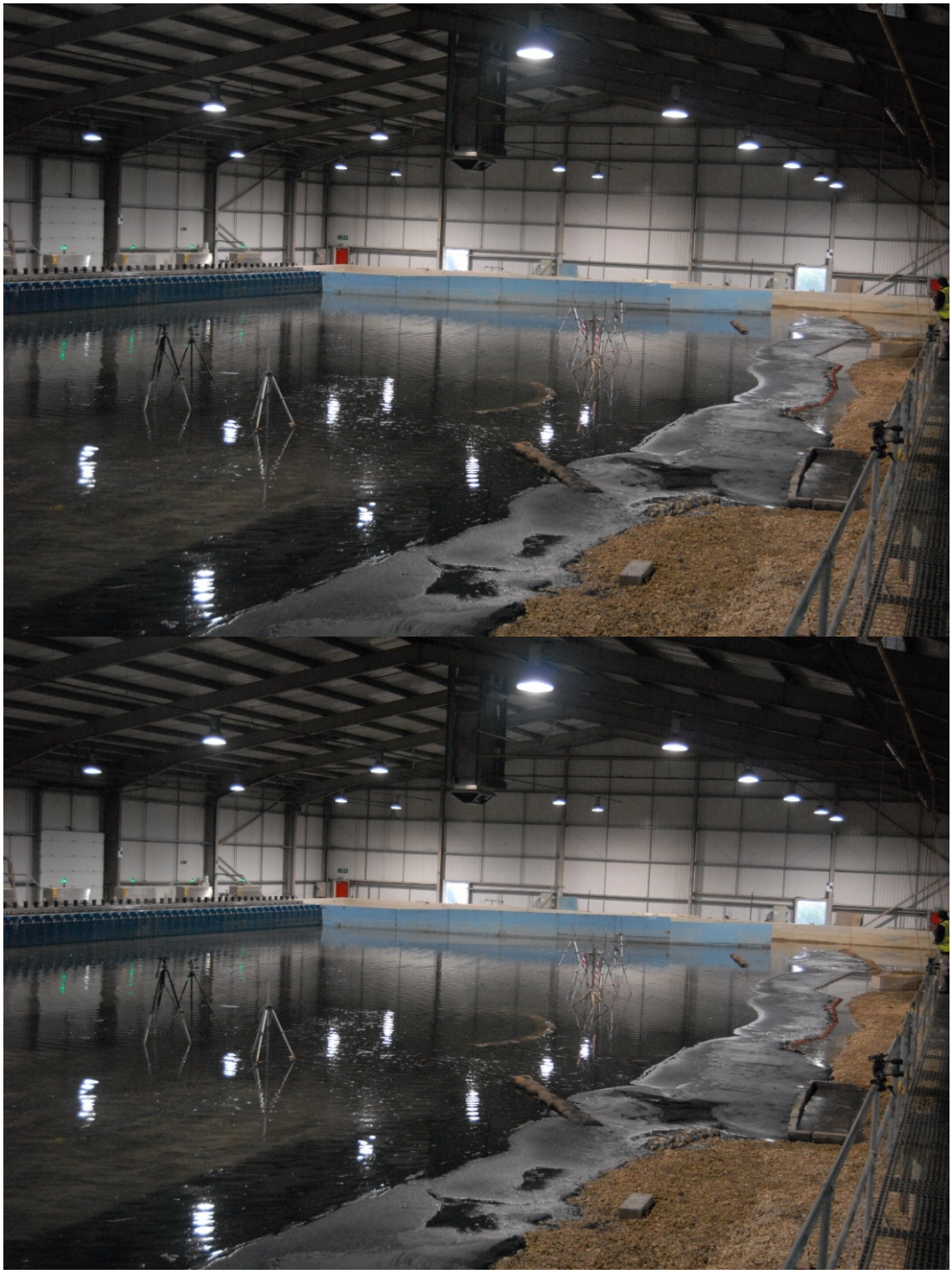

Figure D.1: Pre (top) and post-test (bottom) photographs from 'North' view for Configuration 01

Figure D.2: Pre (top) and post-test (bottom) photographs from 'South' view for Configuration 01

## D.1.2. Configuration 02

Configuration 02 differed from Configuration 01 with the extension of the Northernmost breakwater to the Southeast, the shortening (4 sandbags each) on the Southern end of the middle two breakwaters and the shortening of the Southernmost breakwater (5 sandbags) from the southern end. This configuration was tested for 12 hrs (2 hours model). The pre and post-test photographs from the 'North' and 'South' time-lapse camera views are shown in Figure D.4 and Figure D.5. The post-test scan data is shown in Figure D.3.

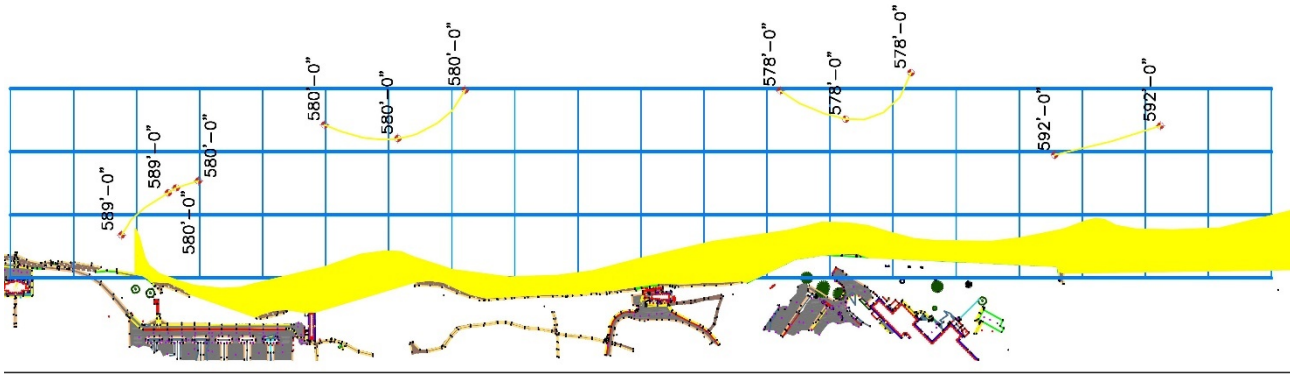


Figure D.3: Post-test scan data for Area 3 Configuration 02, solid area post-test beach, structures in yellow with spot-heights given for key locations

Figure D.4: Pre (top) and post-test (bottom) photographs from 'North' view for Configuration 02

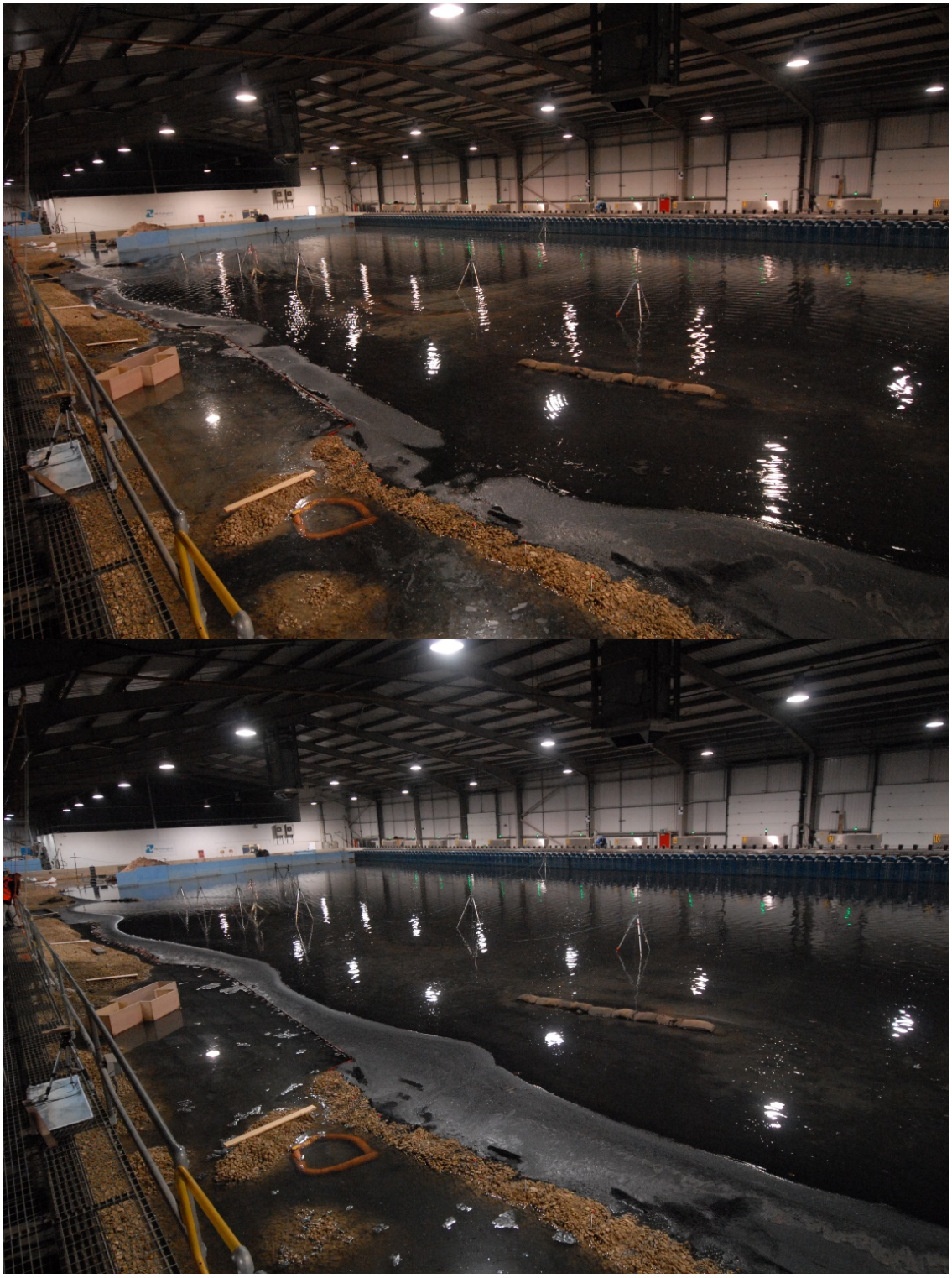

Figure D.5: Pre (top) and post-test (bottom) photographs from 'South' view for Configuration 02

### D.1.3. Configuration 03

Configuration 03 differed from Configuration 02 with the removal of the Northern of the middle breakwaters and curving the Southernmost breakwater so the ends are turned lakewards. This configuration was tested for 6 hrs (1 hour model). The pre and post-test photographs from the 'North' and 'South' time-lapse camera views are shown in Figure D.6 and Figure D.7.

Figure D.6: Pre (top) and post-test (bottom) photographs from 'North' view for Configuration 03

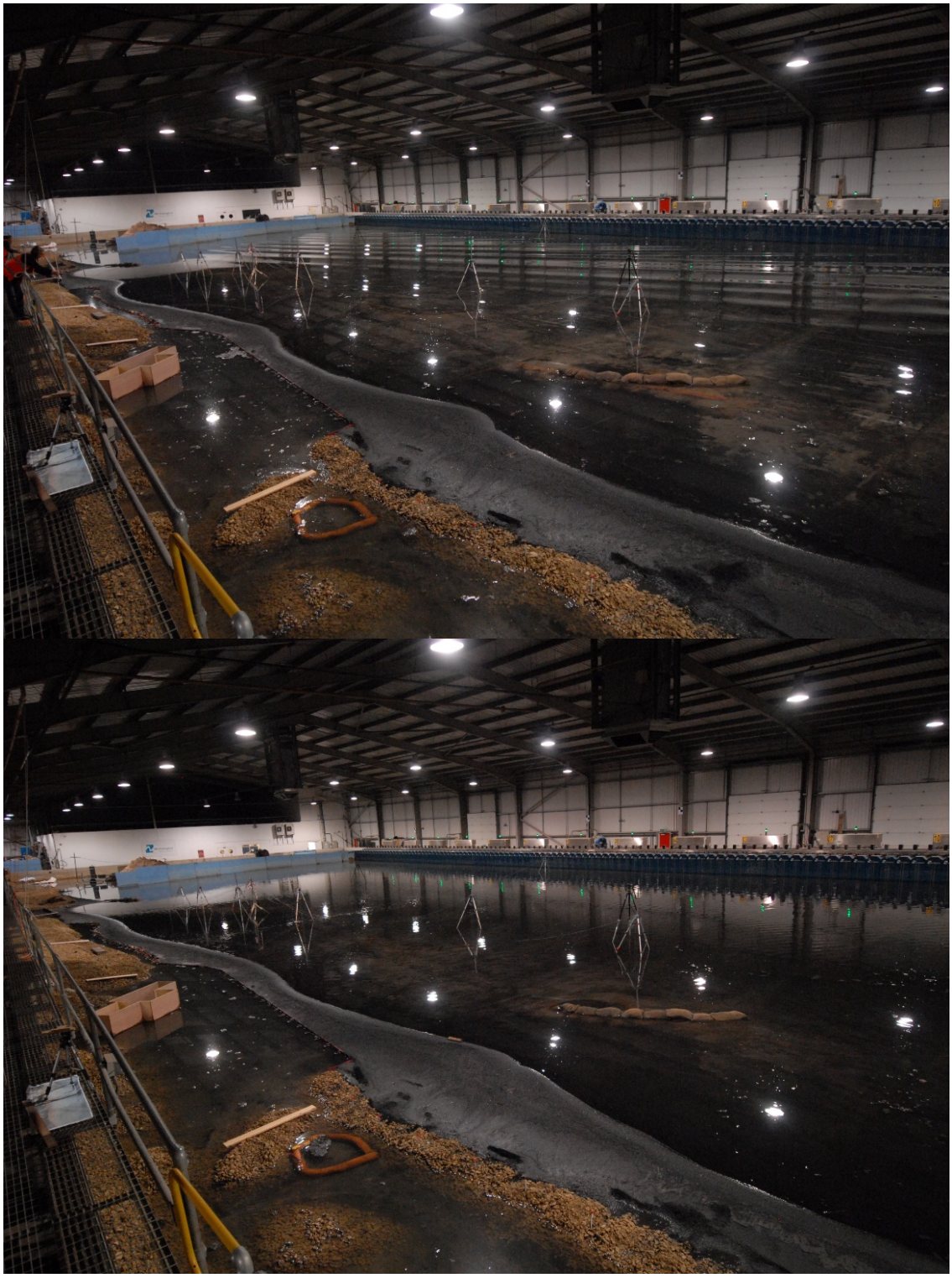

Figure D.7: Pre (top) and post-test (bottom) photographs from 'South' view for Configuration 03

### D.1.4. Configuration 04

Configuration 04 differed from Configuration 03 with the introduction of two breakwaters to the South of the Northernmost breakwater, the shortening on the Southern end (6 sandbags) of the penultimate Southern breakwater and the shortening and moving further offshore of the Southernmost breakwater. This configuration was tested for 12 hrs (2 hours model). The pre and post-test photographs from the 'North' and 'South' time-lapse camera views are shown in Figure D.8 and Figure D.9.

Figure D.8: Pre (top) and post-test (bottom) photographs from 'North' view for Configuration 04

Figure D.9: Pre (top) and post-test (bottom) photographs from 'South' view for Configuration 04

### D.1.5. Configuration 05

Configuration 05 differed from Configuration 04 with the addition of two fishtails to the Southern end of the second breakwater from the North of the model, the removal of the top layer of sandbags on the Southernmost breakwater and the moving of four sandbags from the Northern end to the Southern end of the penultimate Southernmost breakwater. The beach was replenished and re-profiled between the second and third Northern breakwaters prior to the test. This configuration was tested for 9 hrs (1.5 hours model). The pre and post-test photographs from the 'North' and 'South' time-lapse camera views are shown in Figure D.10 and Figure D.11.

Figure D.10: Pre (top) and post-test (bottom) photographs from 'North' view for Configuration 05

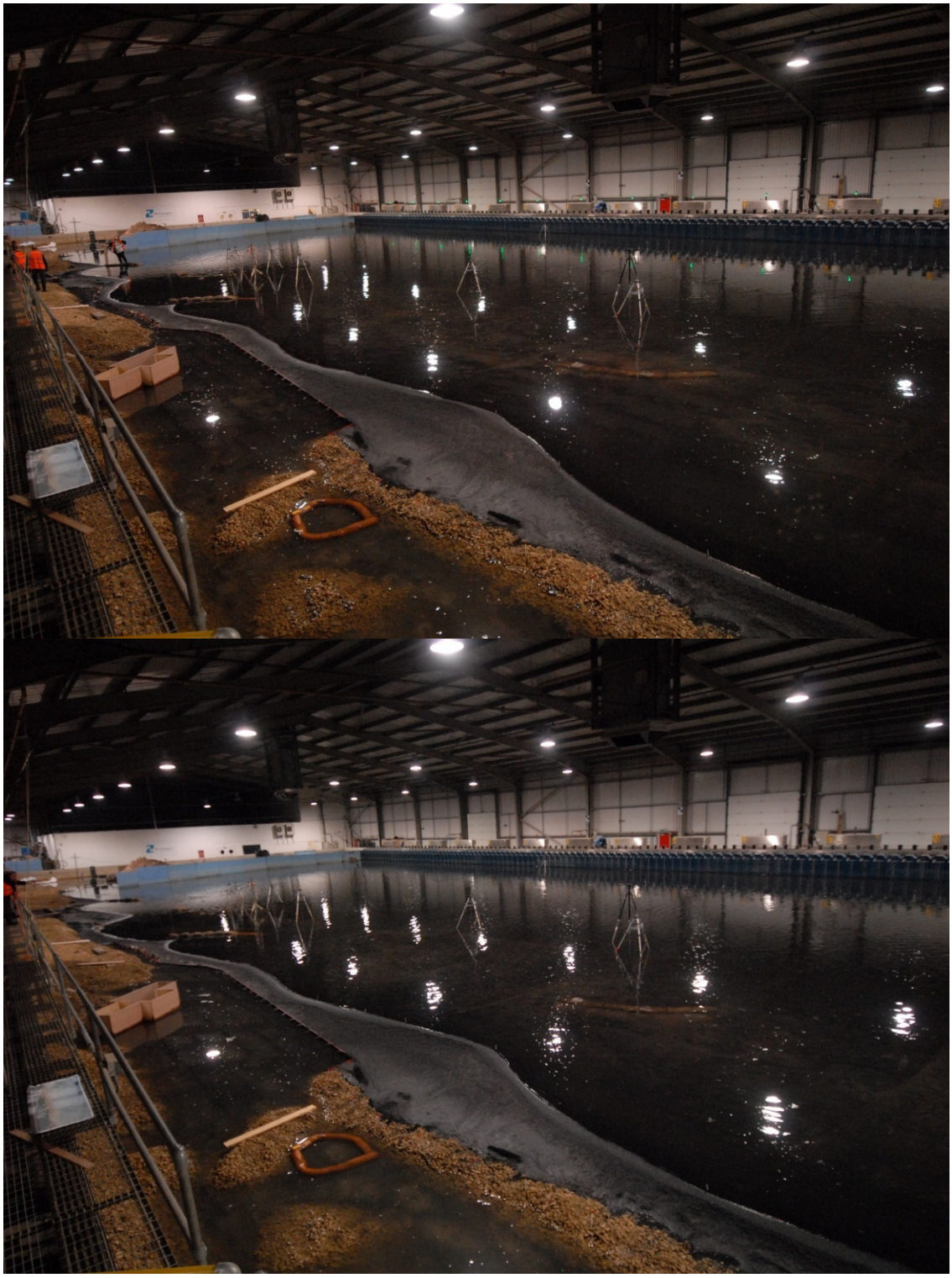

Figure D.11: Pre (top) and post-test (bottom) photographs from 'South' view for Configuration 05

### D.1.6. Configuration 06

Configuration 06 differed from Configuration 05 with the addition of four sandbags (three to the South and one to the North) of the second breakwater from the Southern end of the model, the removal of the fishtail from the second Northernmost breakwater and the addition of three small breakwaters between this and the breakwater to the South (middle breakwater) consisting of two, three and three sandbags respectively. The Norther end of the middle breakwater was also turned lakeward. The beach was re-set to its initial profile prior to testing this configuration. This configuration was tested for 12 hrs (2 hours model). The pre and post-test photographs from the 'North' and 'South' time-lapse camera views are shown in Figure D.12 and Figure D.13.

Figure D.12: Pre (top) and post-test (bottom) photographs from 'North' view for Configuration 06

Figure D.13: Pre (top) and post-test (bottom) photographs from ‘South’ view for Configuration 06

### D.1.7. Configuration 07

Configuration 07 differed from Configuration 06 by making the southern end of the second Northernmost breakwater emergent, combining the two Northernmost of the three small breakwaters and removing the third (Southernmost). Two submerged sandbags were added to the Northern end of 'middle' breakwater and the second Southernmost breakwater was split into two separate submerged breakwaters (six and eight sandbags respectively). This configuration was tested for 6 hrs (1 hour model). The pre and post-test photographs from the 'North' and 'South' time-lapse camera views are shown in Figure D.14 and Figure D.15.

Figure D.14: Pre (top) and post-test (bottom) photographs from ‘North’ view for Configuration 07

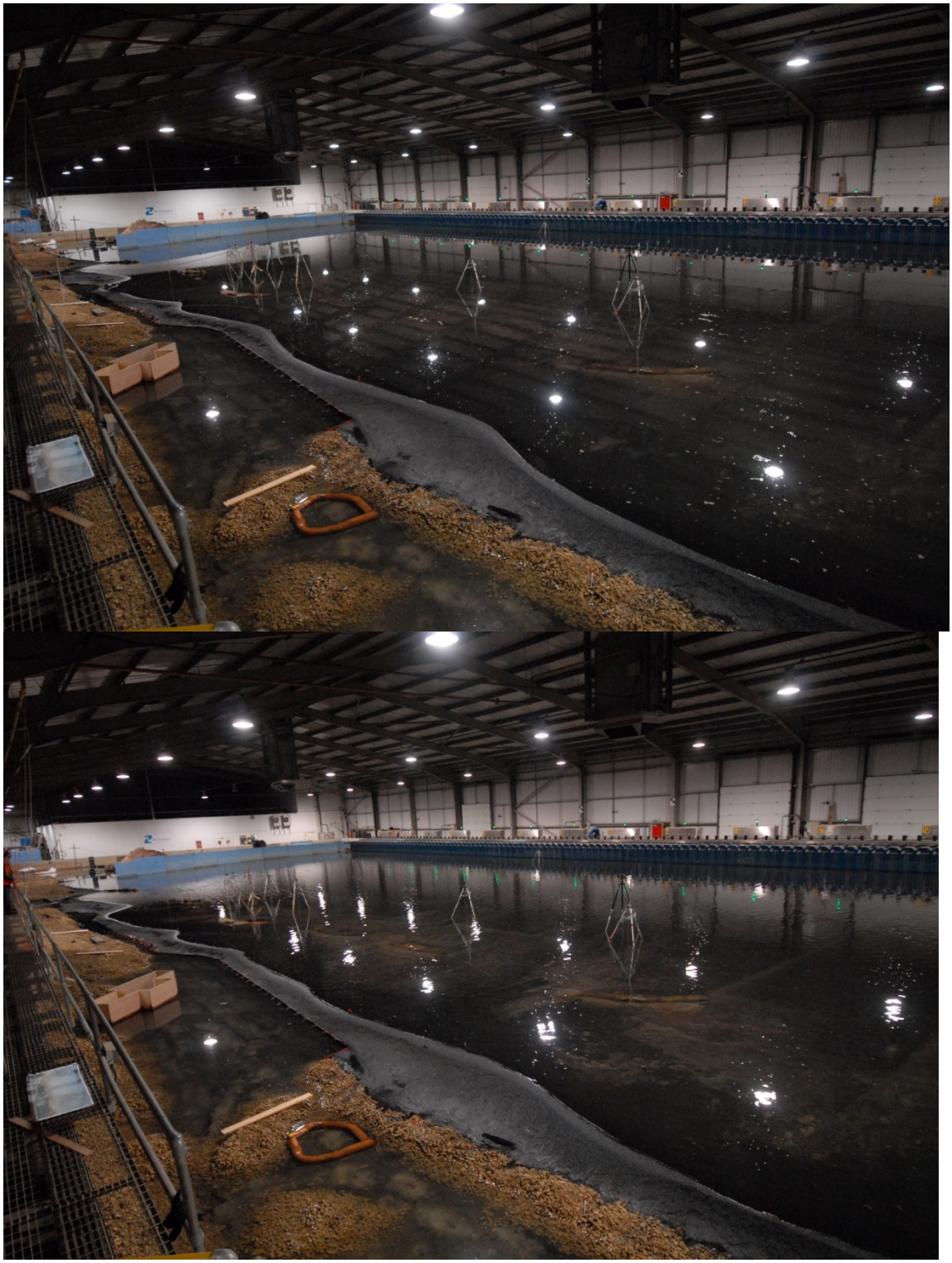

Figure D.15: Pre (top) and post-test (bottom) photographs from 'South' view for Configuration 07

### D.1.8. Configuration 08

Configuration 08 differed from Configuration 07 with small changes of alignment for the Southern breakwaters and the move of two sandbags and one sandbag on the 'middle' breakwater and the third Southernmost respectively. This configuration was tested for 9 hrs (1.5 hours model). The pre and post-test photographs from the 'North' and 'South' time-lapse camera views are shown in Figure D.16 and Figure D.17.

Figure D.16: Pre (top) and post-test (bottom) photographs from ‘North’ view for Configuration 08

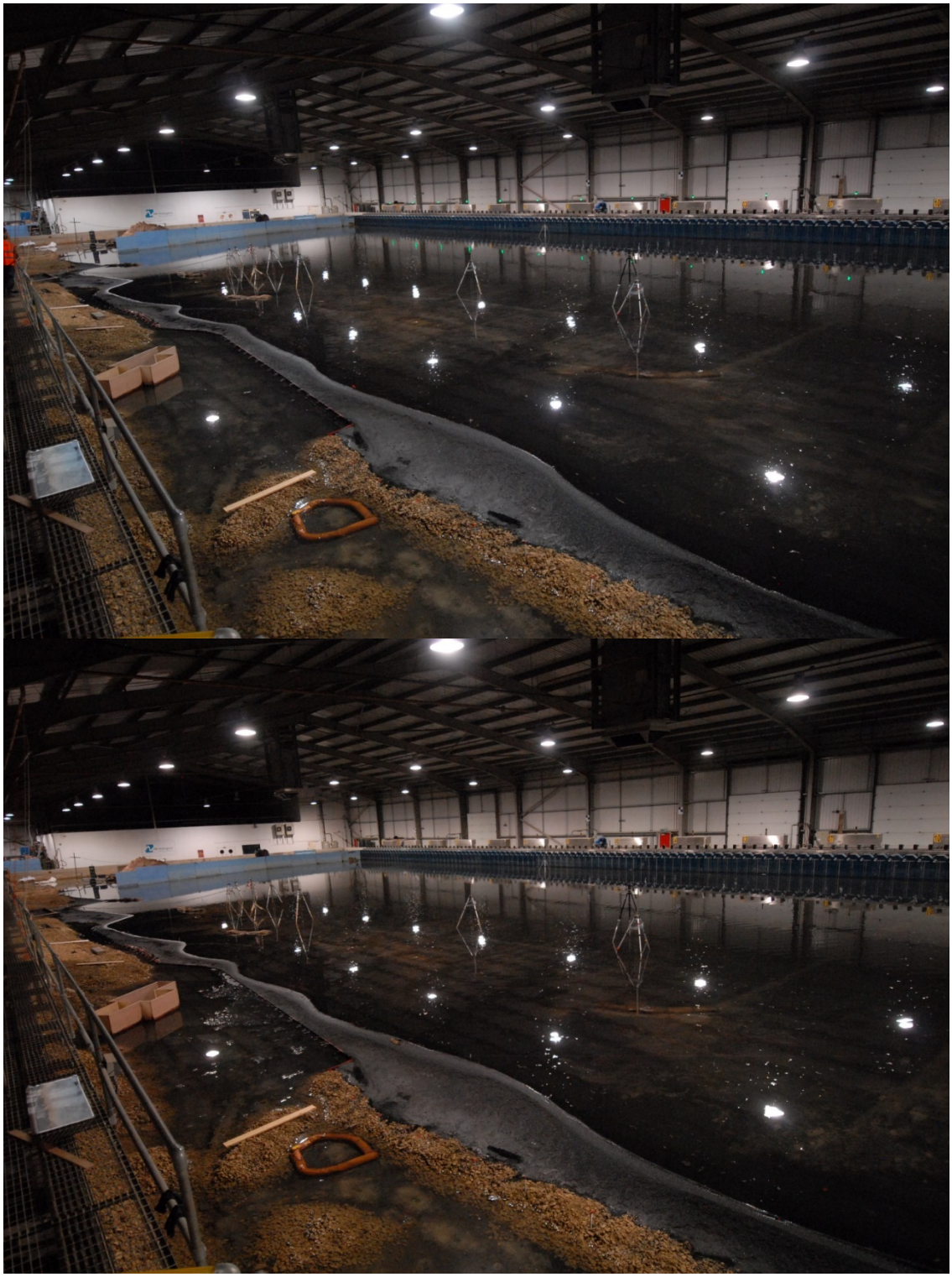

Figure D.17: Pre (top) and post-test (bottom) photographs from 'South' view for Configuration 08

### D.1.9. Configuration 09

Configuration 09 differed from Configuration 08 with the construction of the Northernmost structure from Configuration 02 (Section ) as the ‘middle’ breakwater (replacing the previous ‘middle’ and third Southernmost breakwaters. The eroded areas of the beach were replenished before testing this configuration. This configuration was tested for 9 hrs (1.5 hours model). The pre and post-test photographs from the ‘North’ and ‘South’ time-lapse camera views are shown in Figure D.18 and Figure D.19.

Figure D.18: Pre (top) and post-test (bottom) photographs from ‘North’ view for Configuration 09

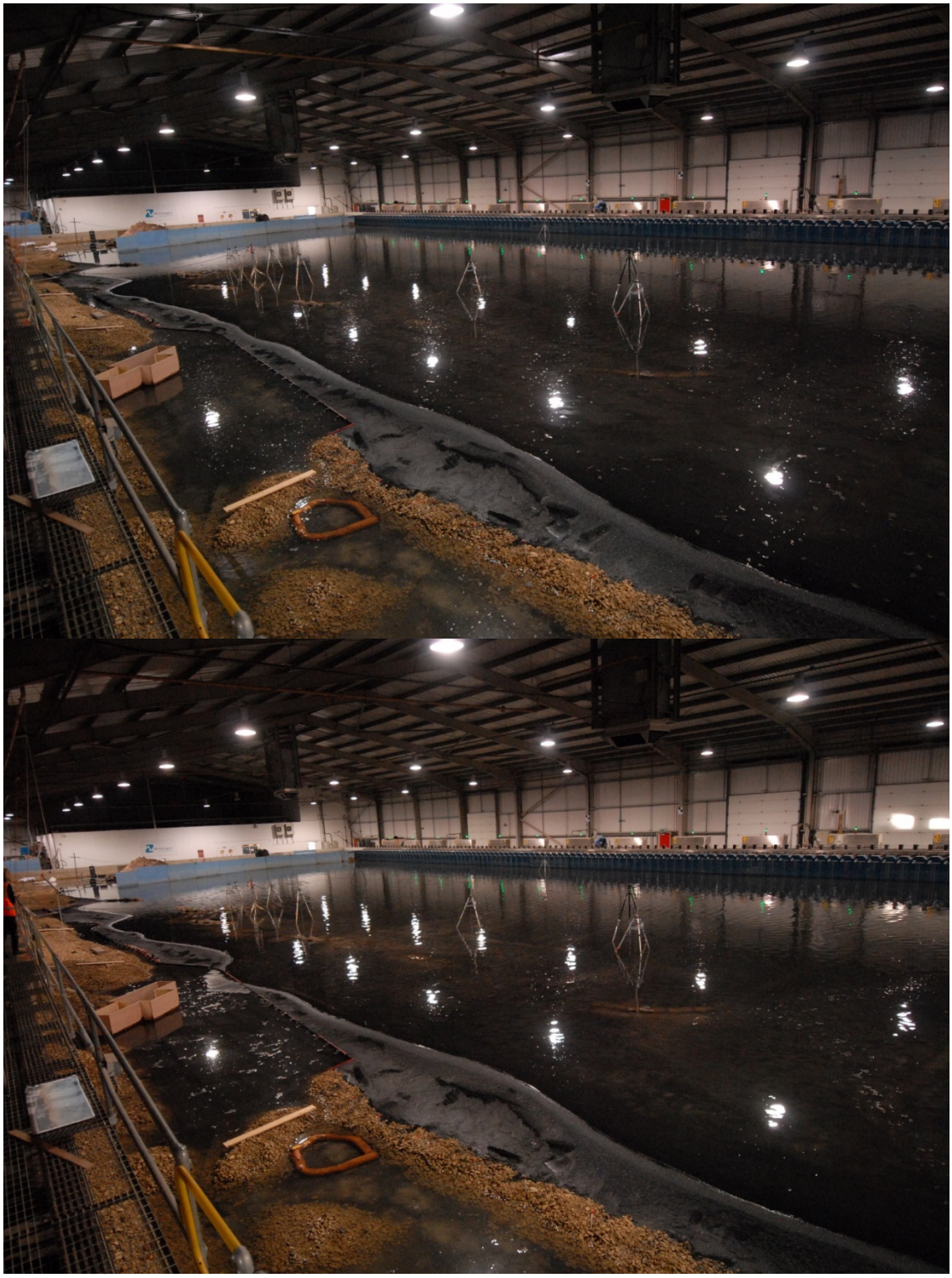

Figure D.19: Pre (top) and post-test (bottom) photographs from 'South' view for Configuration 09

### D.1.10. Configuration 10

Configuration 10 differed from Configuration 09 with the separation of the 'middle' breakwater into two, the Northern half being submerged. The beach was replenished and reprofiled to the initial layout before testing this configuration. This configuration was tested for 9 hrs (1.5 hours model). The pre and post-test photographs from the 'North' and 'South' time-lapse camera views are shown in Figure D.20 and Figure D.21.

Figure D.20: Pre (top) and post-test (bottom) photographs from 'North' view for Configuration 10

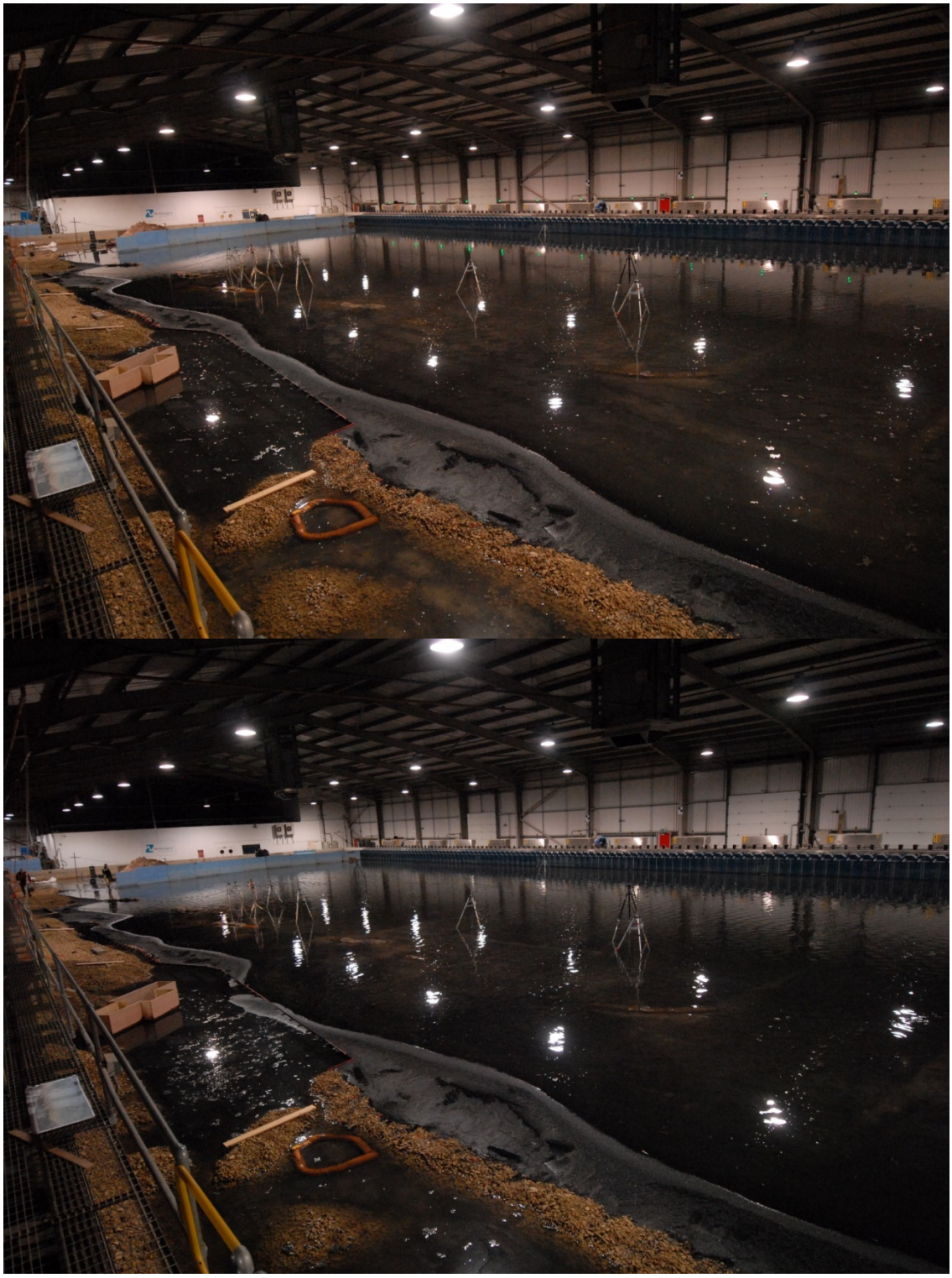

Figure D.21: Pre (top) and post-test (bottom) photographs from ‘South’ view for Configuration 10

### D.1.11. Configuration 11

Configuration 11 differed from Configuration 10 with the joining of the two Southernmost breakwaters with a submerged section approximately 7 sandbags long. This configuration was tested for 6 hrs (1 hour model). The pre and post-test photographs from the 'North' and 'South' time-lapse camera views are shown in Figure D.22 and Figure D.23.

Figure D.22: Pre (top) and post-test (bottom) photographs from 'North' view for Configuration 11

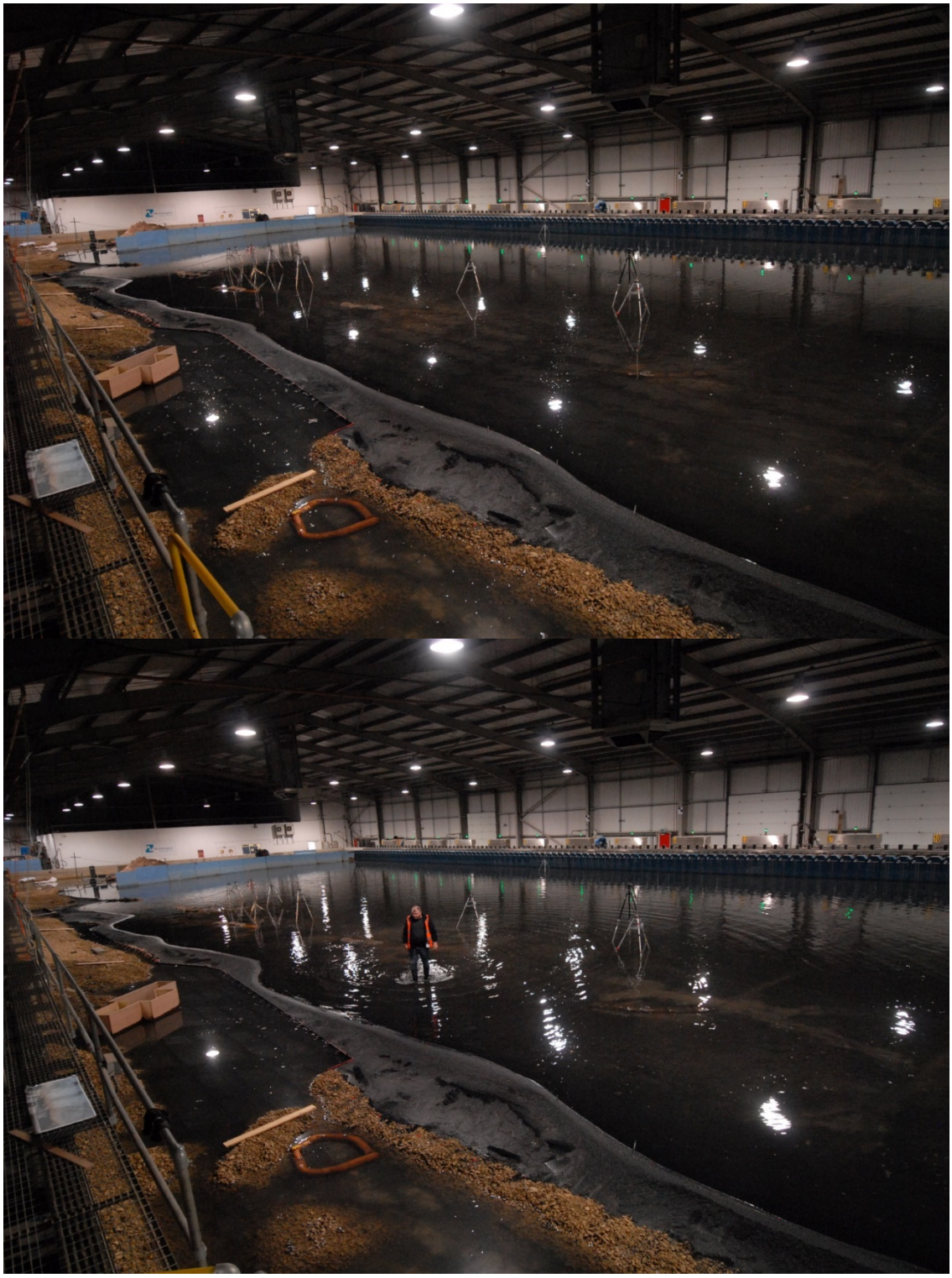

Figure D.23: Pre (top) and post-test (bottom) photographs from 'South' view for Configuration 11

### D.1.12. Configuration 12

Configuration 12 differed from Configuration 11 with only minor alignment changes. This configuration was tested for 3 hrs (0.5 hours model). The pre and post-test photographs from the 'North' and 'South' time-lapse camera views are shown in Figure D.24 and Figure D.25.

Figure D.24: Pre (top) and post-test (bottom) photographs from ‘North’ view for Configuration 12

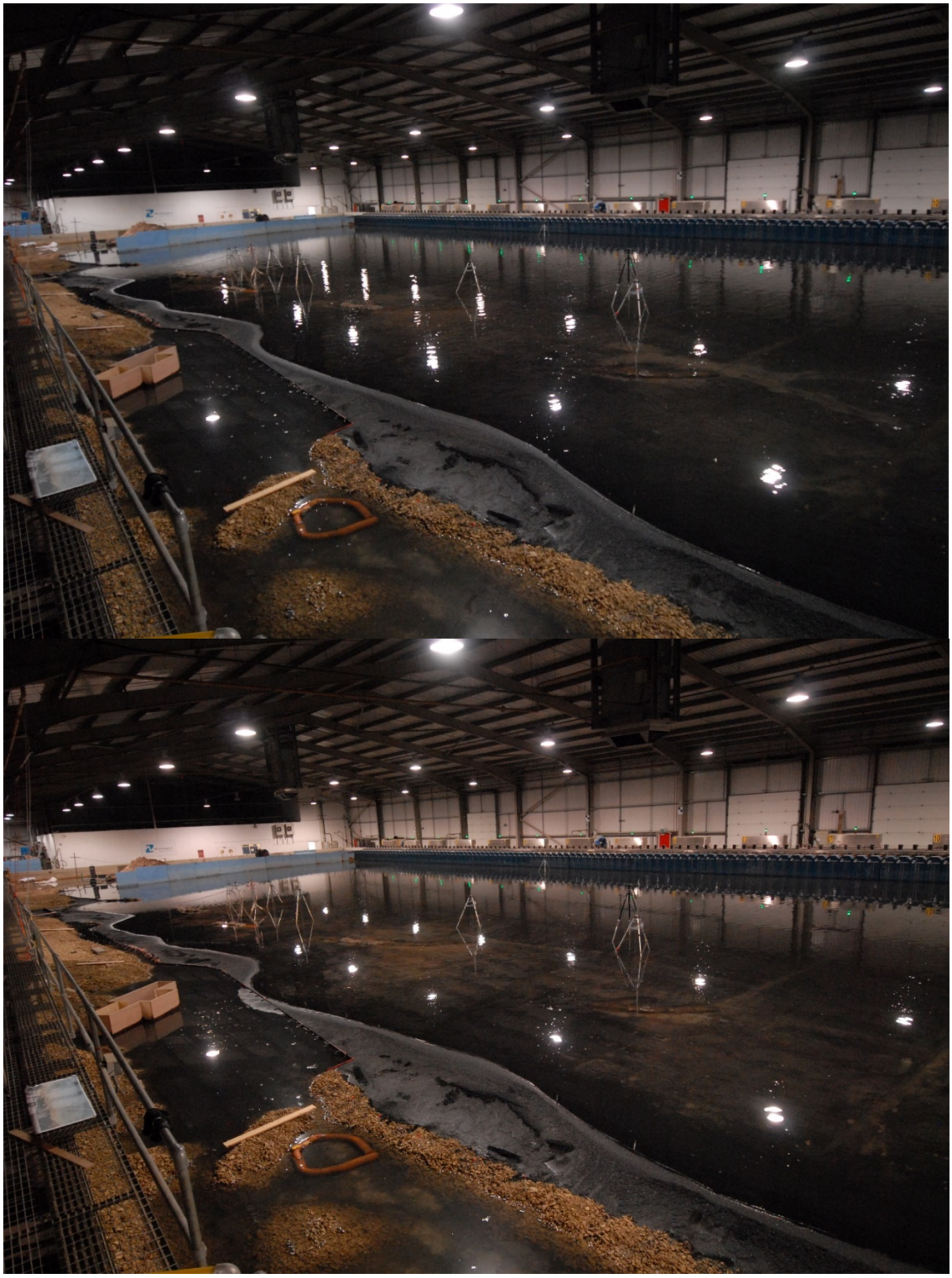

Figure D.25: Pre (top) and post-test (bottom) photographs from 'South' view for Configuration 12

## D.1.13. Configuration 13

Configuration 13 differed from Configuration 12 with the removal of the third Northernmost breakwater, the extension to the South of the second Northernmost breakwater and straightening to make it more shore parallel. The 'middle' breakwater was extended Northwards by two submerged sandbags and moved lakeward. A double submerged reef was also added to the South of the second Southernmost breakwater. This configuration was tested for 12 hrs (2 hours model). The pre and post-test photographs from the 'North' and 'South' time-lapse camera views are shown in Figure D.27 and Figure D.28. The post-test scan data is shown in Figure D.26.

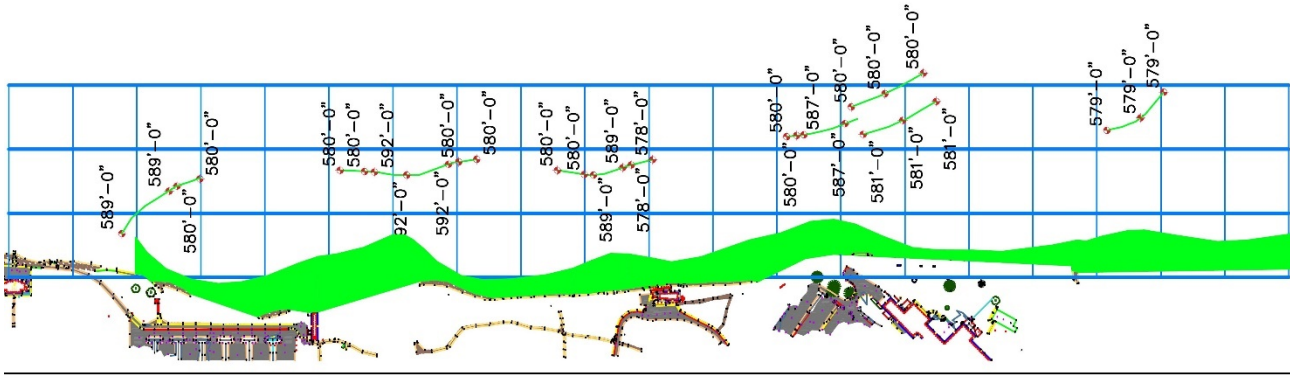


Figure D.26: Post-test scan data for Area 3 Configuration 13, solid area post-test beach, structures in green with spot-heights given for key locations

Figure D.27: Pre (top) and post-test (bottom) photographs from ‘North’ view for Configuration 13

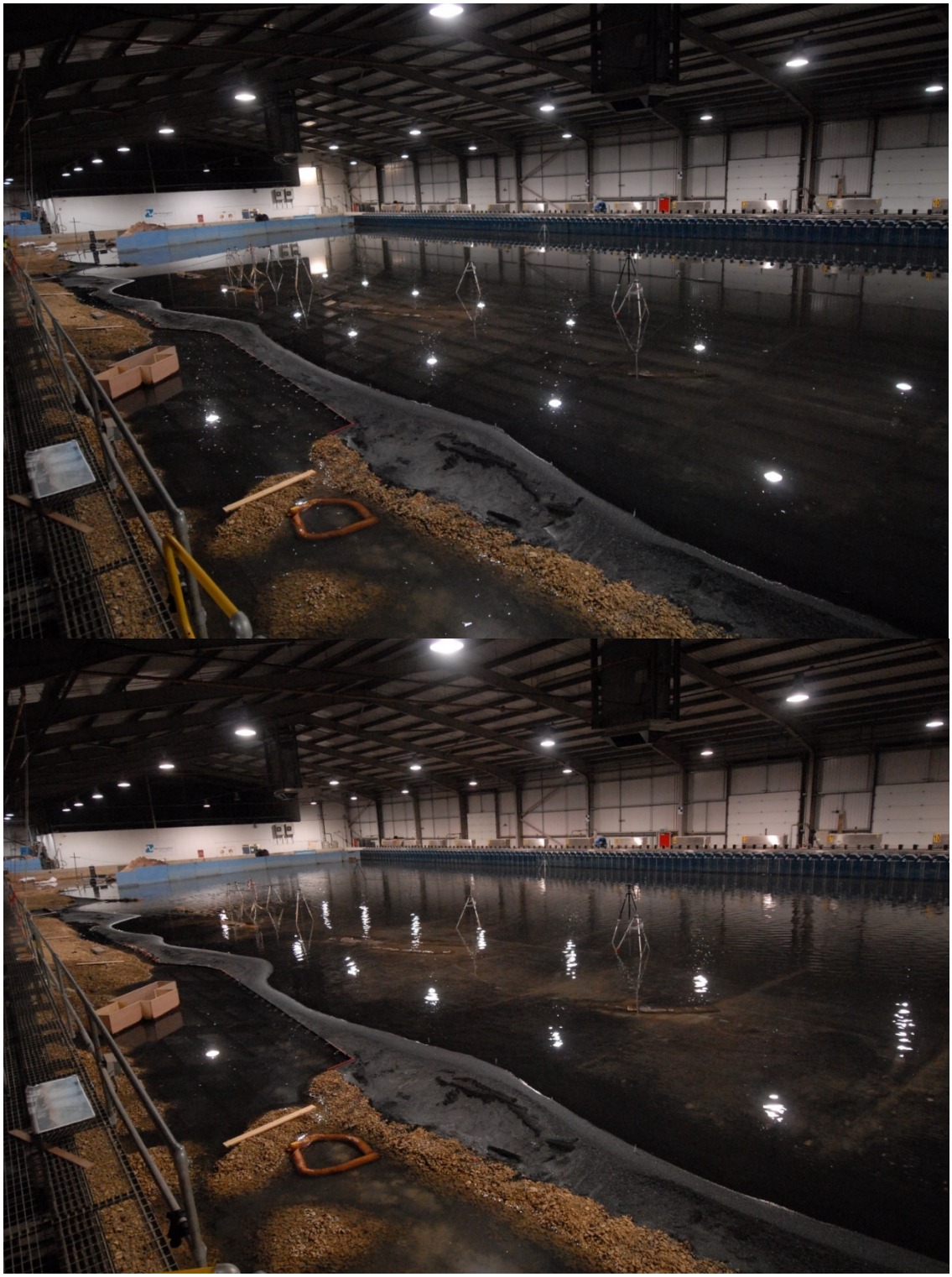

Figure D.28: Pre (top) and post-test (bottom) photographs from 'South' view for Configuration 13

### D.1.14. Configuration 14

Configuration 14 differed from Configuration 13 with the moving of two sandbags from the 'middle' breakwater to the second Northernmost breakwater, the removal of the double submerged reef and the extension to the South of the second Southernmost breakwater in place of the reefs and the extension and move Northwards of the Southernmost breakwater. This configuration was tested for 12 hrs (2 hours model). The pre and post-test photographs from the 'North' and 'South' time-lapse camera views are shown in Figure D.29 and Figure D.30.

Figure D.29: Pre (top) and post-test (bottom) photographs from ‘North’ view for Configuration 14

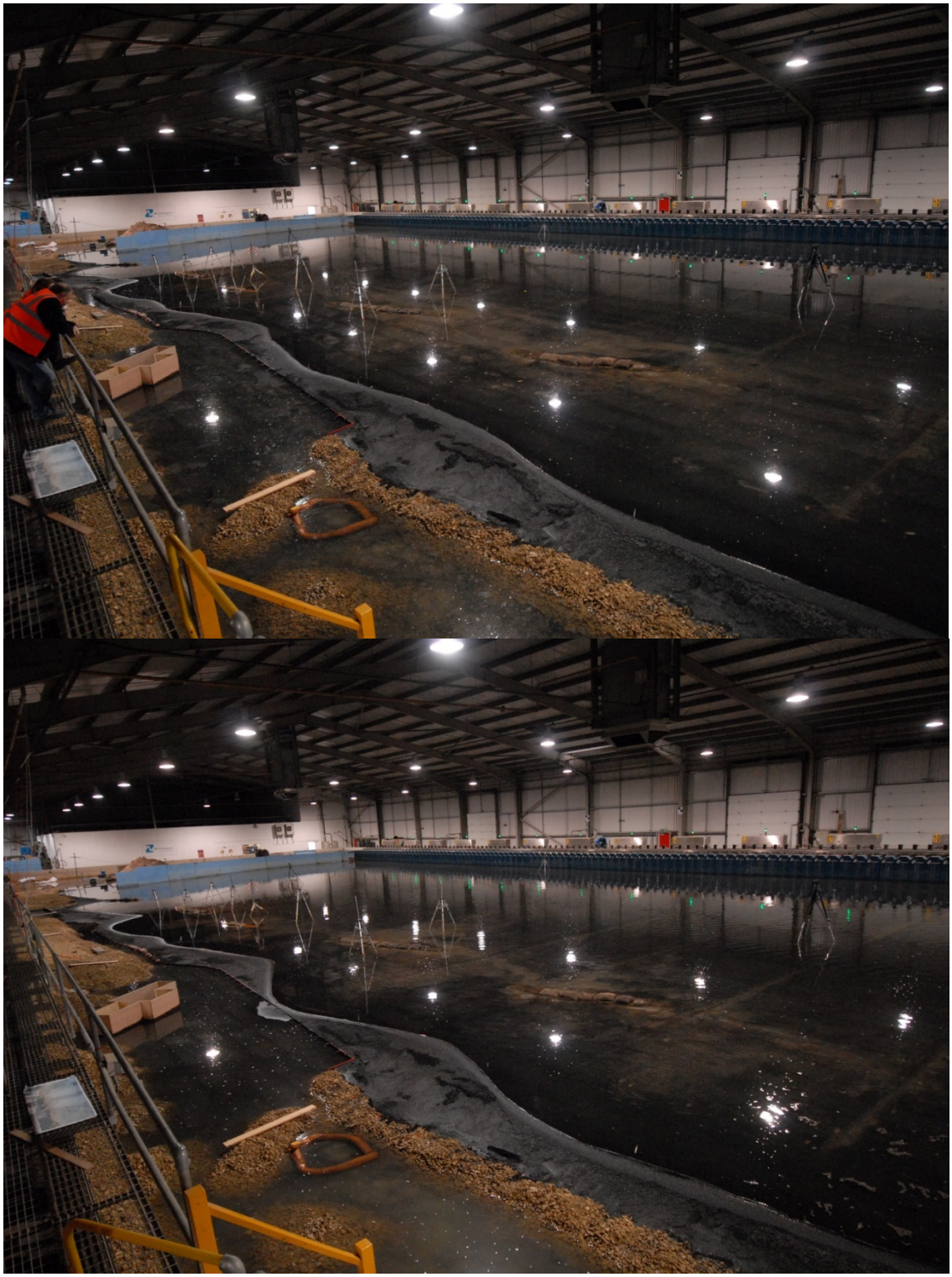

Figure D.30: Pre (top) and post-test (bottom) photographs from 'South' view for Configuration 14

## D.1.15. Configuration 15

Configuration 15 differed from Configuration 14 with the repositioning of the two Southern breakwaters. The Southernmost was moved Northwards and the North end curved lakeward. The Second Southernmost breakwater was moved lakeward. This configuration was tested for 12 hrs (2 hours model). The pre and post-test photographs from the 'North' and 'South' time-lapse camera views are shown in Figure D.32 and Figure D.33. The post-test scan data is shown in Figure D.31.

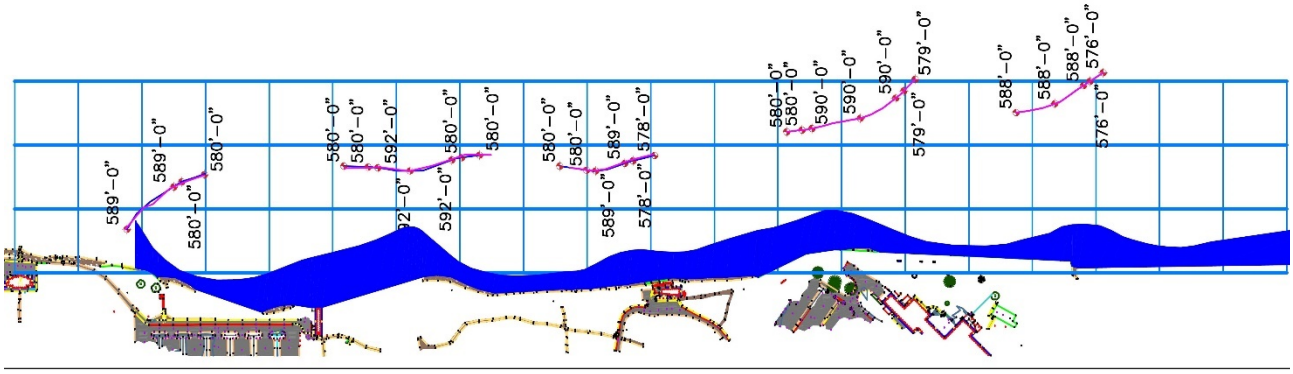


Figure D.31: Post-test scan data for Area 3 Configuration 15, solid area post-test beach, structures in magenta with spot-heights given for key locations

Figure D.32: Pre (top) and post-test (bottom) photographs from ‘North’ view for Configuration 15

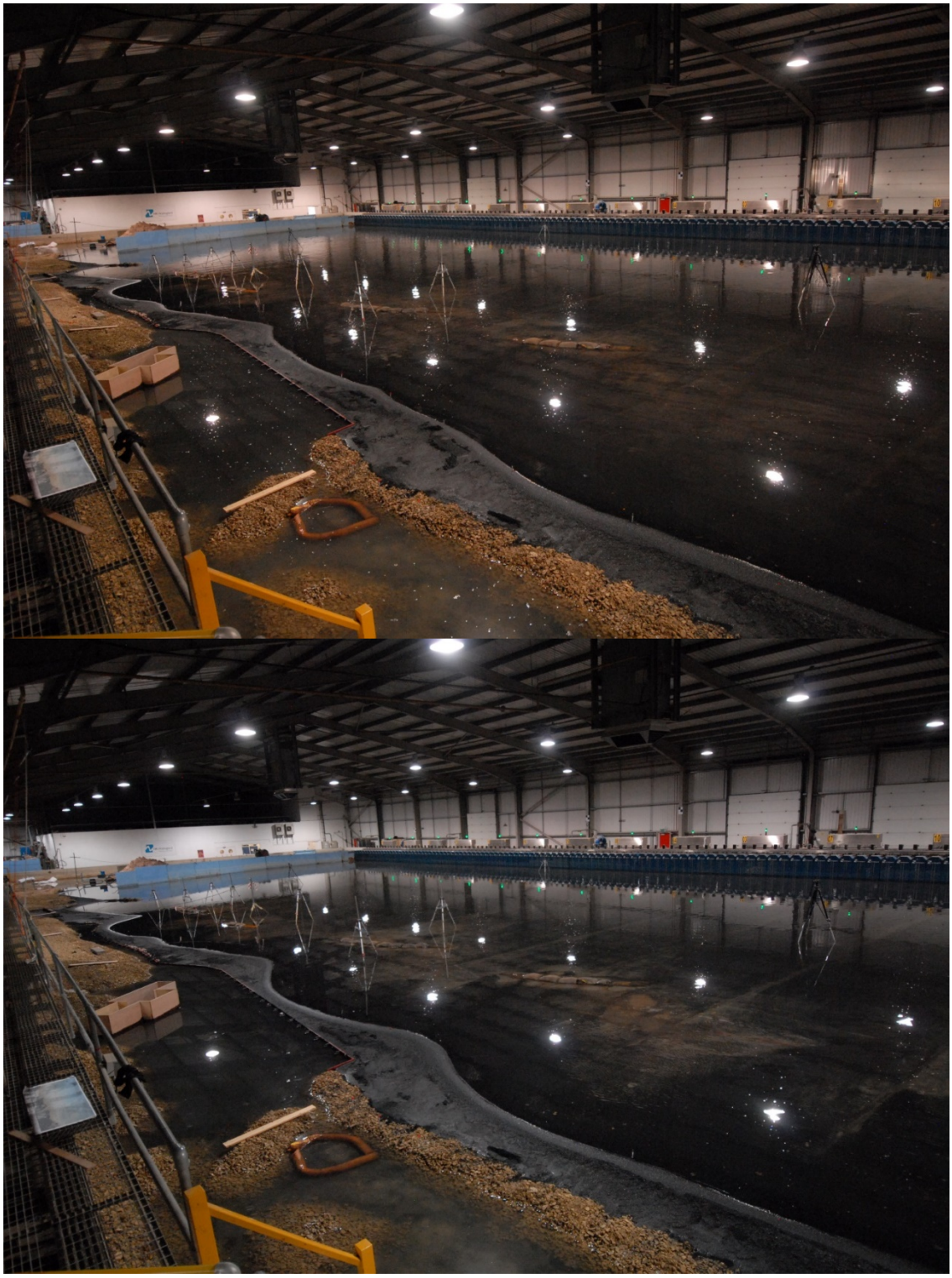

Figure D.33: Pre (top) and post-test (bottom) photographs from 'South' view for Configuration 15

## D.1.16. Configuration 16

Configuration 16 differed from Configuration 15 with the move of two sandbags from the Southern end of the second Southernmost breakwater to the Northern end and shifting the Southern end of the same breakwater towards the shore. This configuration was tested for 12 hrs (2 hours model). The pre and post-test photographs from the 'North' and 'South' time-lapse camera views are shown in Figure D.34 and Figure D.35.

Figure D.34: Pre (top) and post-test (bottom) photographs from ‘North’ view for Configuration 16

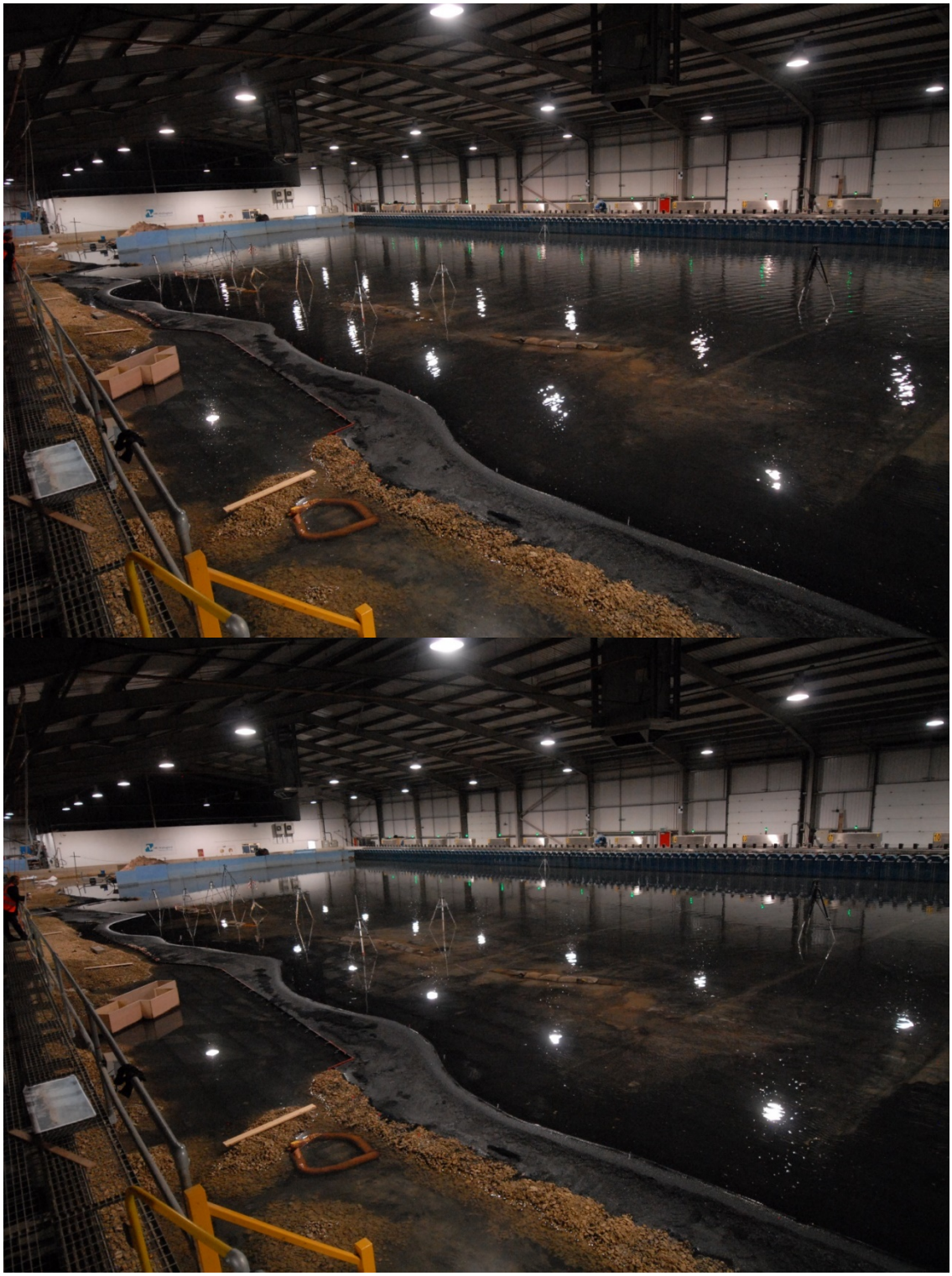

Figure D.35: Pre (top) and post-test (bottom) photographs from 'South' view for Configuration 16

## D.1.17. Configuration 17

Configuration 17 differed from Configuration 16 with the removal of all submerged outer end sections of breakwater. This configuration was tested for 6 hrs (1 hour model). The pre and post-test photographs from the 'North' and 'South' time-lapse camera views are shown in Figure D.36 and Figure D.37.

Figure D.36: Pre (top) and post-test (bottom) photographs from ‘North’ view for Configuration 17

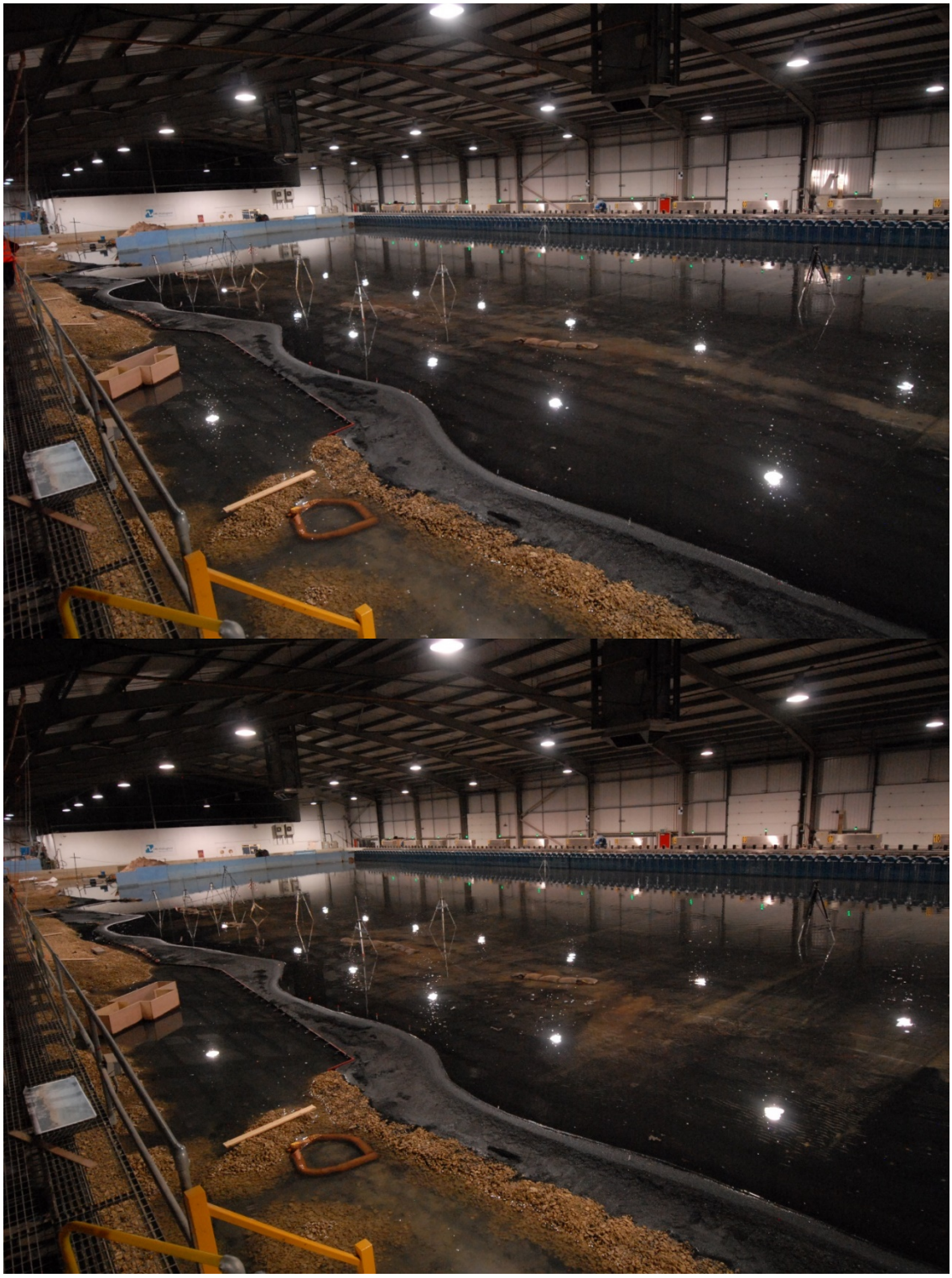

Figure D.37: Pre (top) and post-test (bottom) photographs from ‘South’ view for Configuration 17

## D.1.18. Configuration 18

Configuration 18 differed from Configuration 17 with the centre of the second southernmost breakwater made emergent. This configuration was tested for 6 hrs (1 hour model). The pre and post-test photographs from the 'North' and 'South' time-lapse camera views are shown in Figure D.38 and Figure D.39.

Figure D.38: Pre (top) and post-test (bottom) photographs from ‘North’ view for Configuration 18

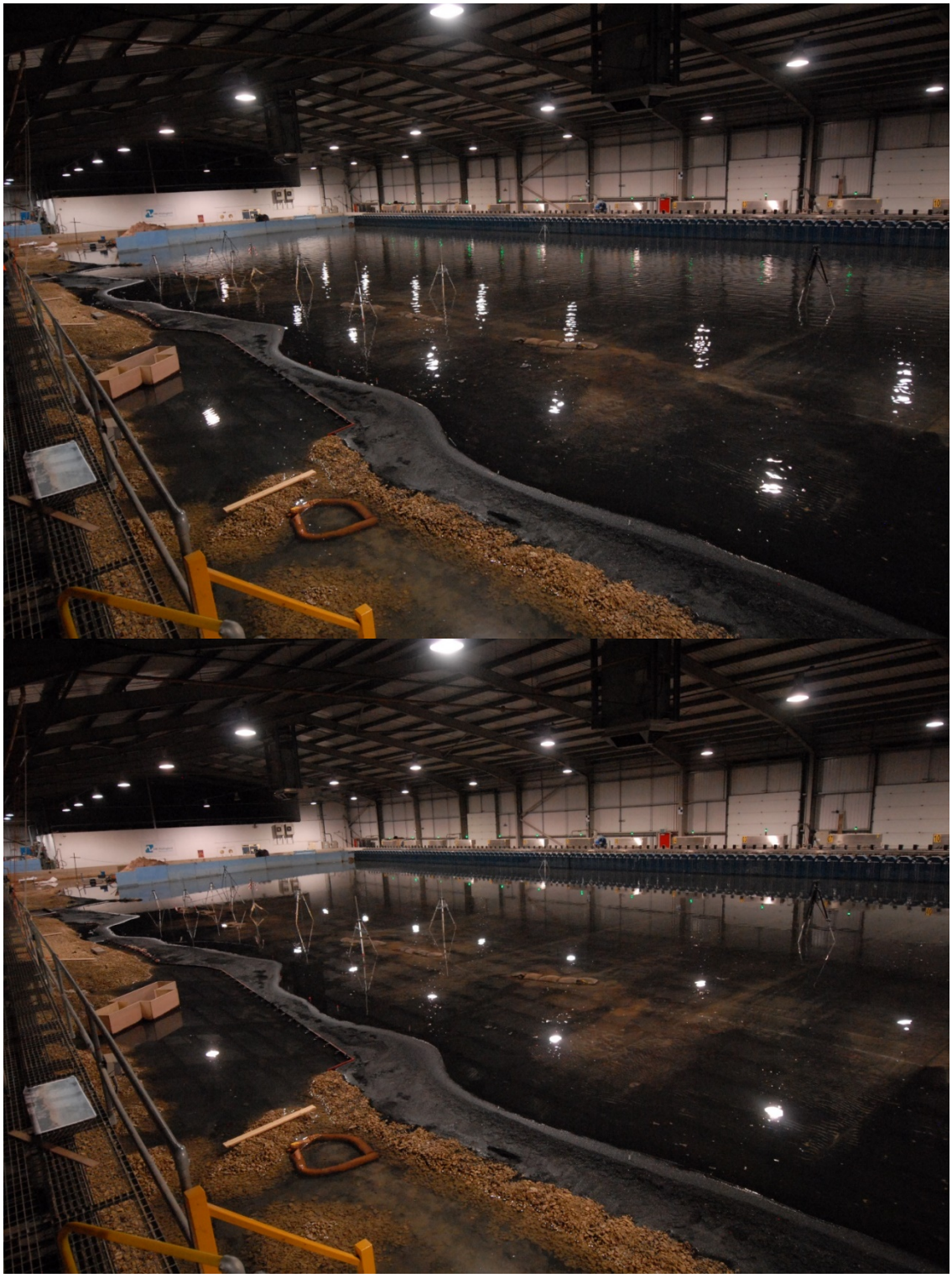

Figure D.39: Pre (top) and post-test (bottom) photographs from 'South' view for Configuration 18

## D.1.19. Configuration 19

Configuration 19 differed from Configuration 18 with the ‘middle’ breakwater moved shoreward. This configuration was tested for 6 hrs (1 hour model). The pre and post-test photographs from the ‘North’ and ‘South’ time-lapse camera views are shown in Figure D.40 and Figure D.41.

Figure D.40: Pre (top) and post-test (bottom) photographs from ‘North’ view for Configuration 19

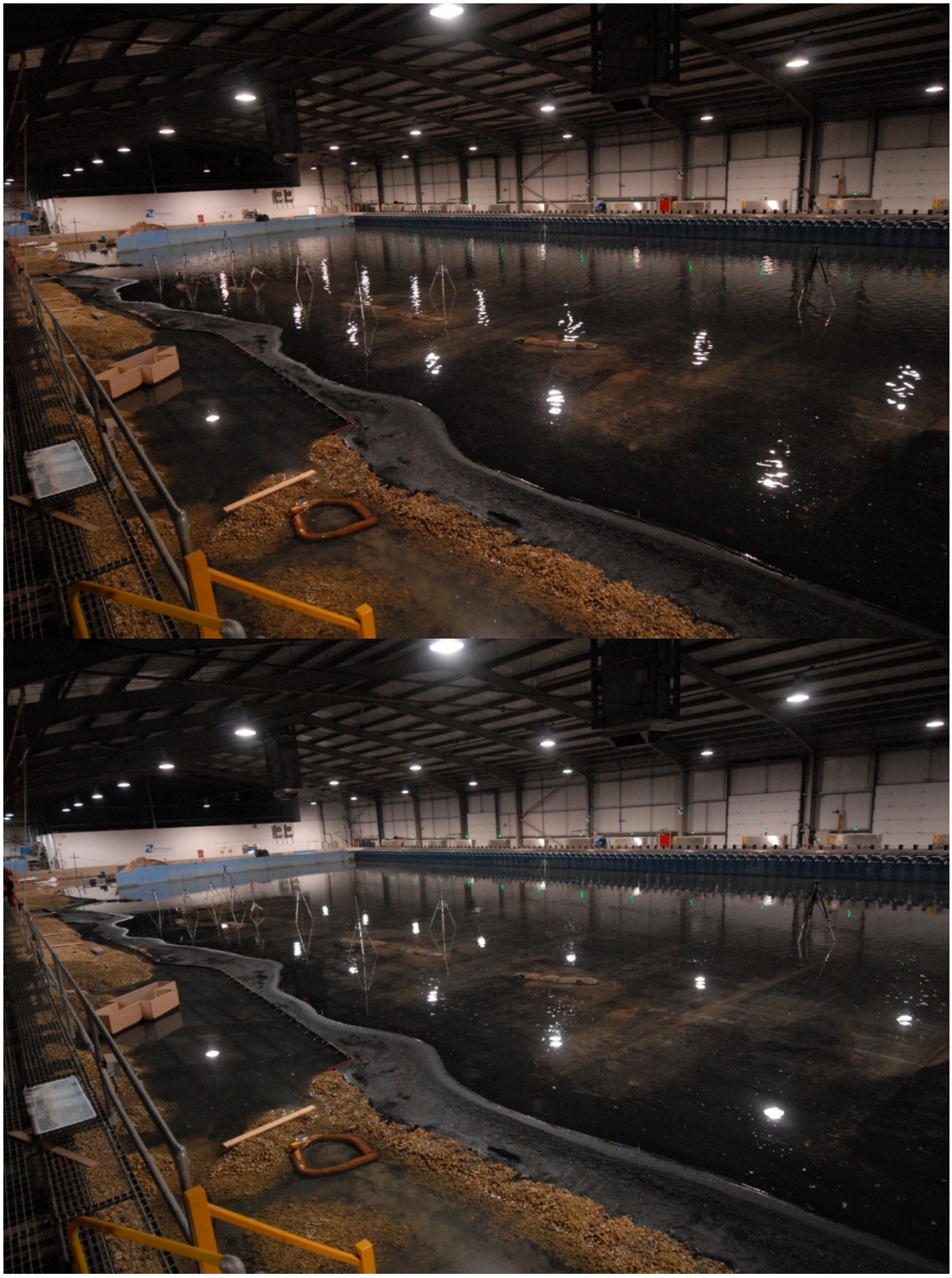

Figure D.41: Pre (top) and post-test (bottom) photographs from 'South' view for Configuration 19

## D.1.20. Configuration 20

Configuration 20 differed from Configuration 19 with the move lakeward of the 'middle' breakwater and the rotation of the Southern end lakeward. The second Southernmost breakwater was also made submerged. This configuration was tested for 6 hrs (1 hour model). The pre and post-test photographs from the 'North' and 'South' time-lapse camera views are shown in Figure D.42 and Figure D.43.

Figure D.42: Pre (top) and post-test (bottom) photographs from ‘North’ view for Configuration 20

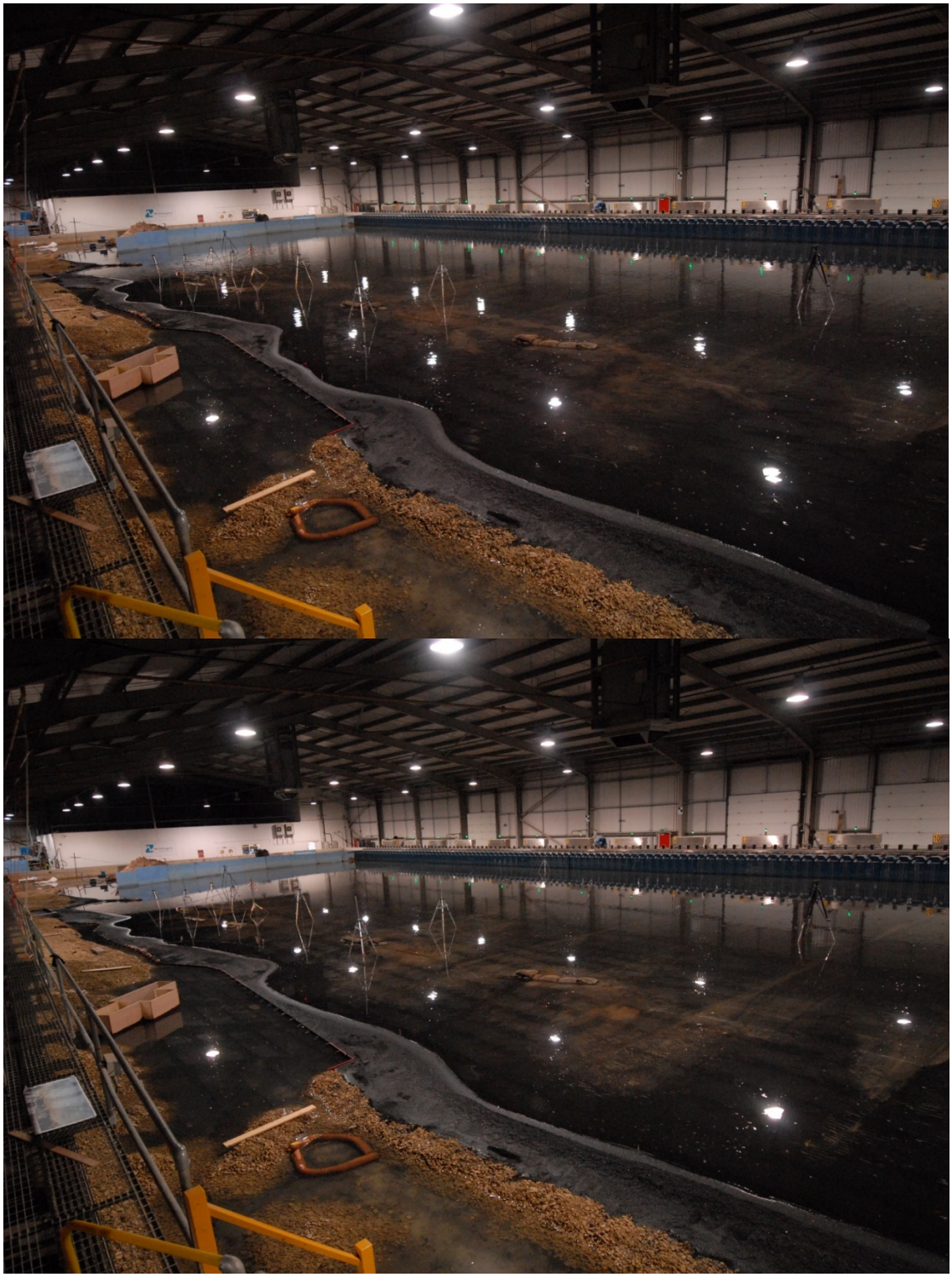

Figure D.43: Pre (top) and post-test (bottom) photographs from 'South' view for Configuration 20

## D.1.21. Configuration 21

Configuration 21 differed from Configuration 20 with the second Southernmost breakwater was made emergent, the next breakwater Northwards was moved shoreward and half a sandbag was moved from the North end of the third Northernmost breakwater to the South end of the second Northernmost breakwater. This configuration was tested for 6 hrs (1 hour model). The pre and post-test photographs from the 'North' and 'South' time-lapse camera views are shown in Figure D.44 and Figure D.45. During this test a salient formed behind third Northernmost breakwater and the beach receded just near the second Northernmost breakwater.

Figure D.44: Pre (top) and post-test (bottom) photographs from ‘North’ view for Configuration 21

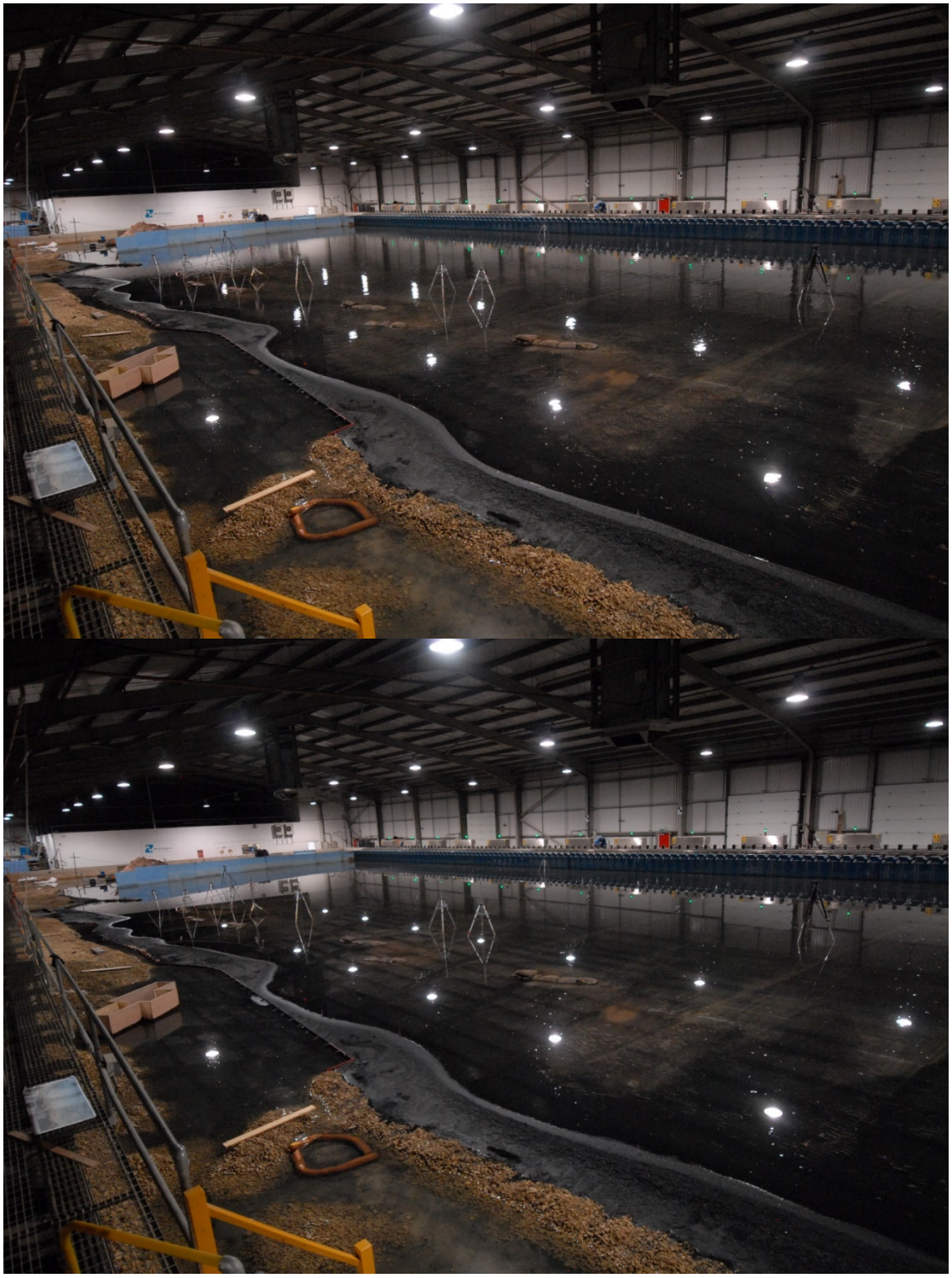

Figure D.45: Pre (top) and post-test (bottom) photographs from 'South' view for Configuration 21

## D.1.22. Configuration 22

Configuration 22 differed from Configuration 21 with the addition of submerged sections to the Southern ends of the Northernmost and second Northernmost breakwaters, the merging of the second and third Southernmost breakwaters and a slight realignment of the Southernmost breakwater. This configuration was tested for 3 hrs (0.5 hours model). The pre and post-test photographs from the 'North' and 'South' time-lapse camera views are shown in Figure D.46 and Figure D.47.

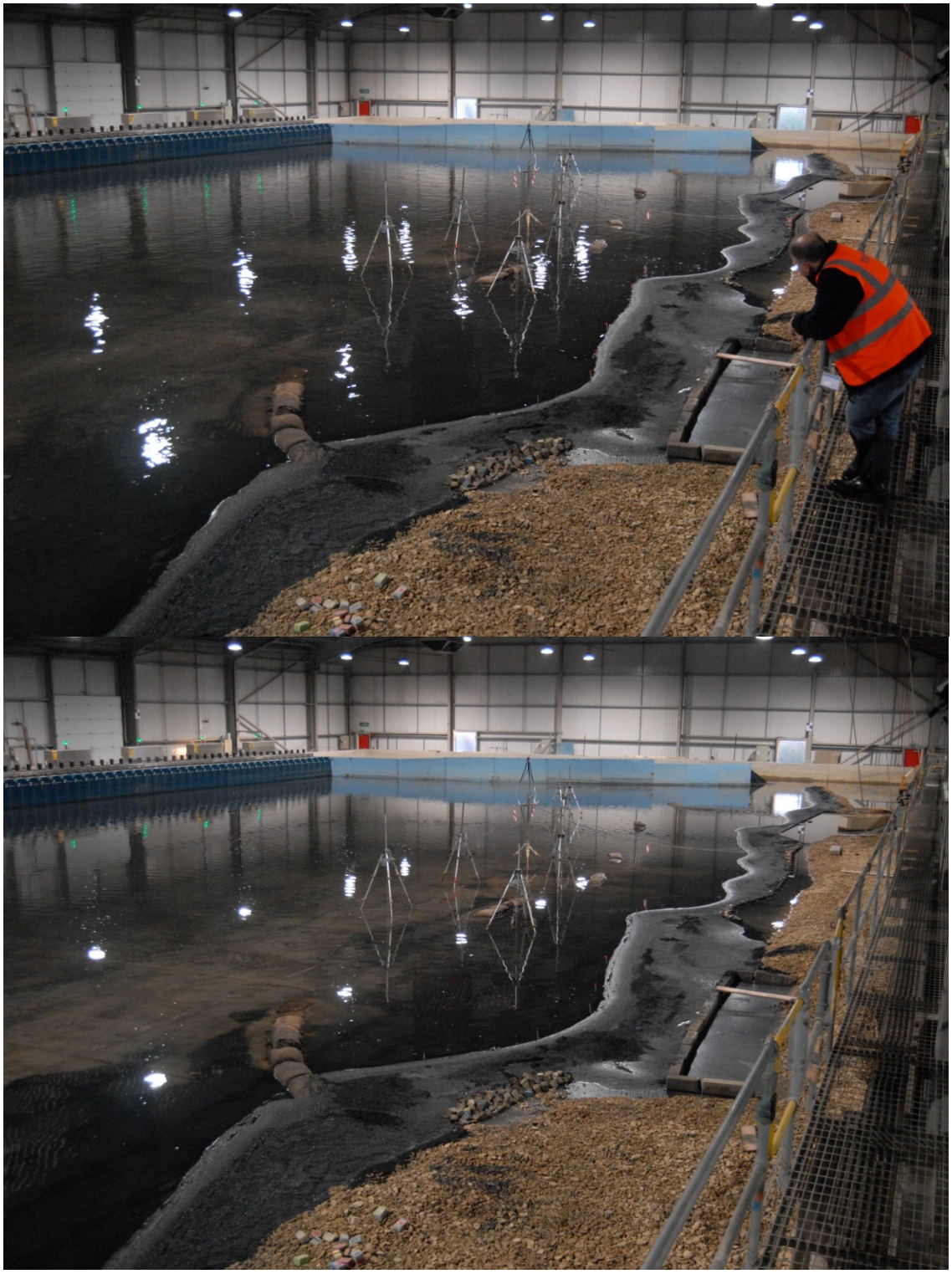

Figure D.46: Pre (top) and post-test (bottom) photographs from ‘North’ view for Configuration 22

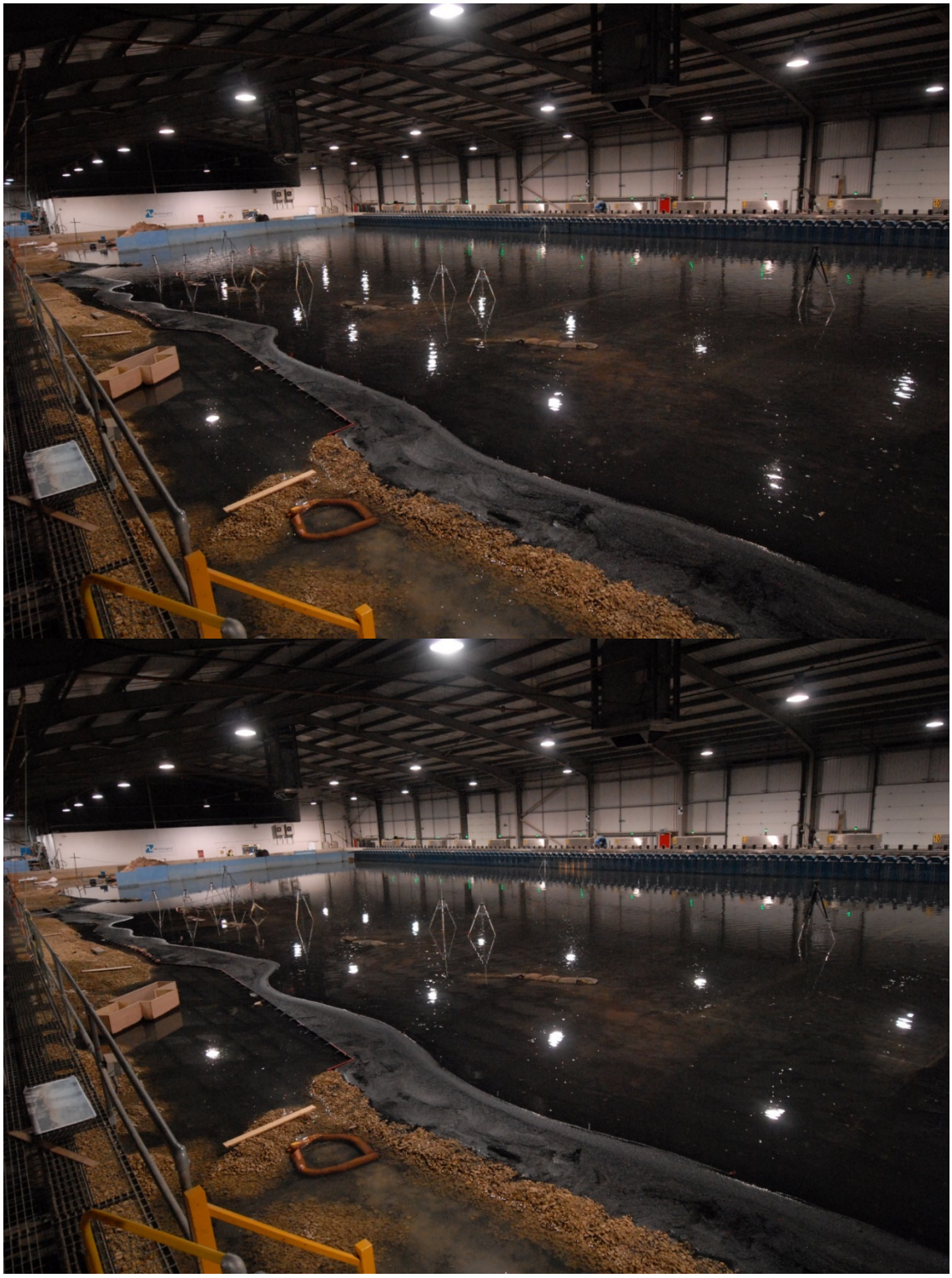

Figure D.47: Pre (top) and post-test (bottom) photographs from ‘South’ view for Configuration 22

## D.1.23. Configuration 23

Configuration 23 differed from Configuration 22 with the reverting of the Southernmost breakwater to that of Configuration 18 and 19 and the move shoreward of the Southern end of the second Southernmost breakwater to create an ‘S’ shape. The beach was replenished and re-profiled before this configuration was tested. This configuration was tested for 6 hrs (1 hour model). The pre and post-test photographs from the ‘North’ and ‘South’ time-lapse camera views are shown in Figure D.48 and Figure D.49.

Figure D.48: Pre (top) and post-test (bottom) photographs from ‘North’ view for Configuration 23

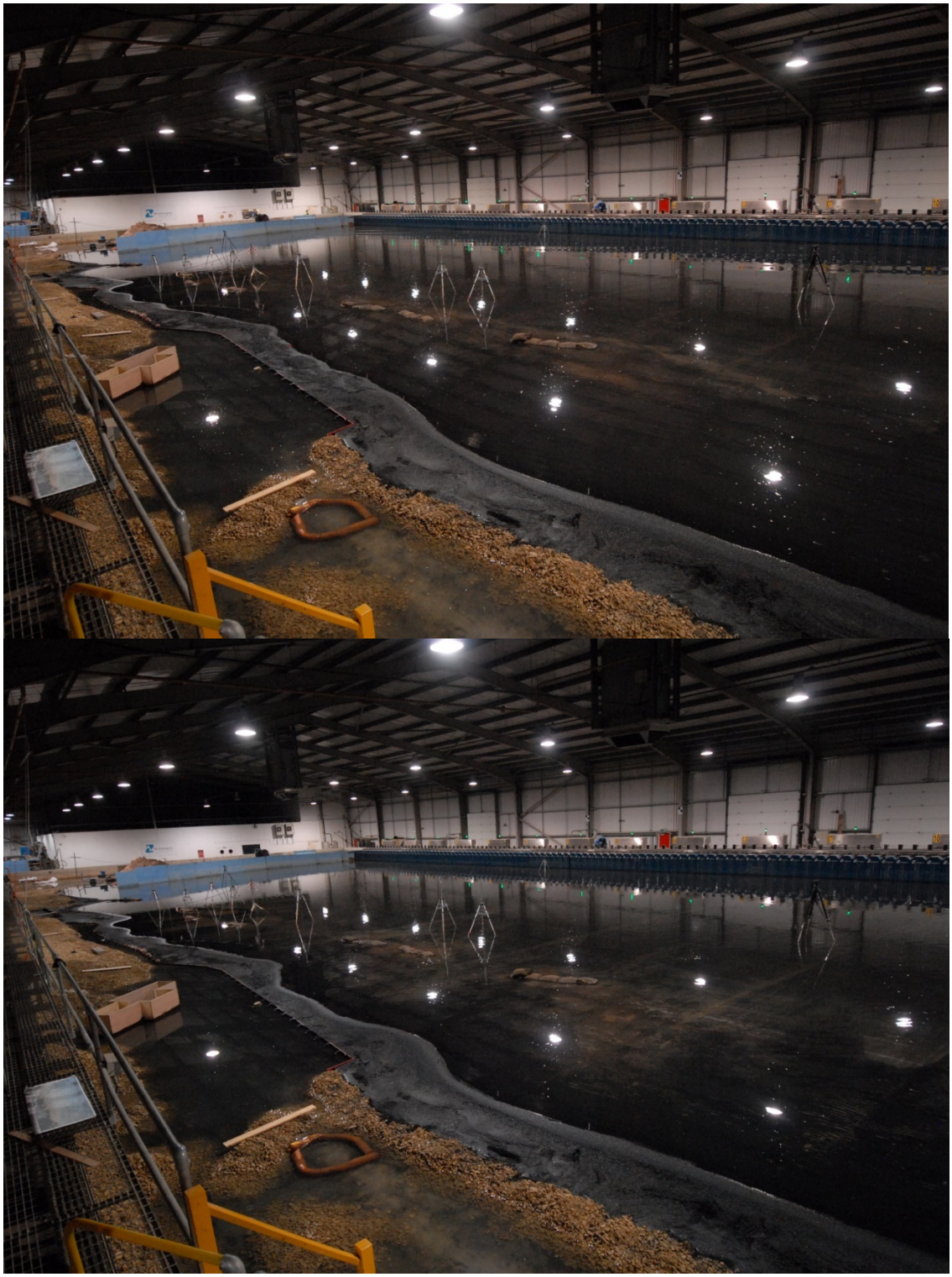

Figure D.49: Pre (top) and post-test (bottom) photographs from 'South' view for Configuration 23

## D.1.24. Configuration 24

Configuration 24 differed from Configuration 23 by making all of the second Northernmost breakwater emergent and moving the third Northernmost breakwater Southwards. This configuration was tested for 15 hrs (2.5 hours model). The pre and post-test photographs from the 'North' and 'South' time-lapse camera views are shown in Figure D.51 and Figure D.52. The post-test scan data is shown in Figure D.50.

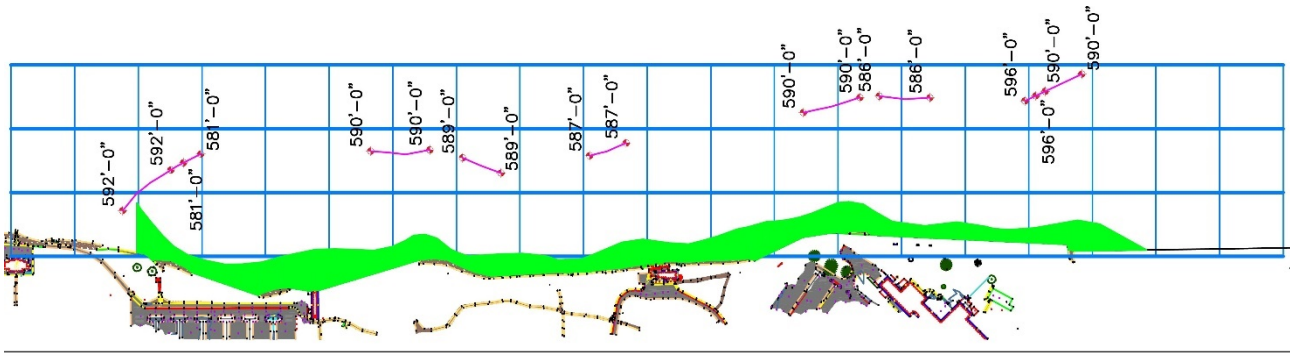


Figure D.50: Post-test scan data for Area 3 Configuration 24, solid area post-test beach, structures in green with spot-heights given for key locations

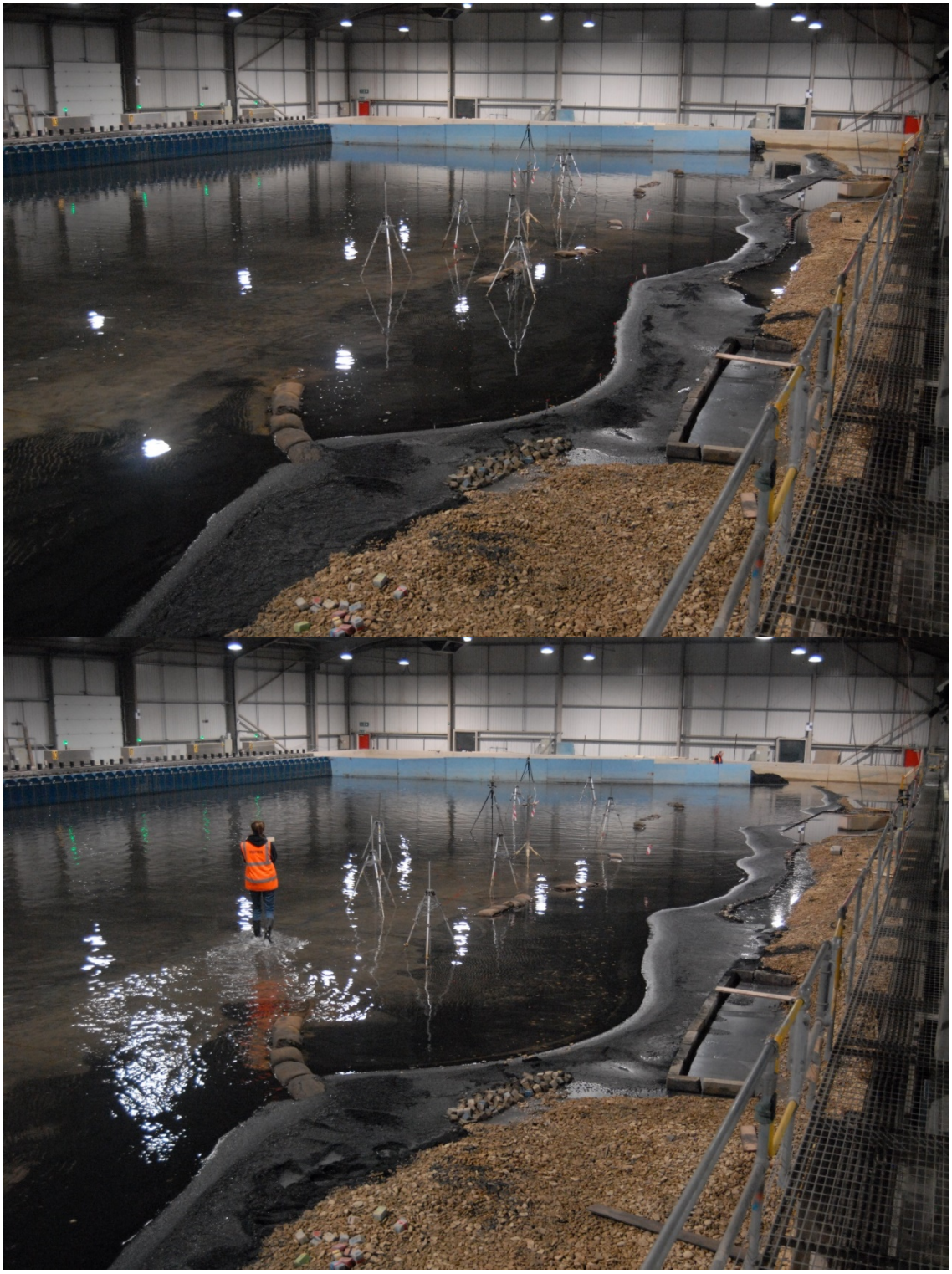

Figure D.51: Pre (top) and post-test (bottom) photographs from ‘North’ view for Configuration 24

Figure D.52: Pre (top) and post-test (bottom) photographs from ‘South’ view for Configuration 24

## D.1.25. Configuration 25

Configuration 25 differed from Configuration 24 with the addition of a submerged seawall in front of the 'wedding venue' (Southern end of the model between the Southernmost and second Southernmost breakwaters). This configuration was tested for 3 hrs (0.5 hours model). The pre and post-test photographs from the 'North' and 'South' time-lapse camera views are shown in Figure D.53 and Figure D.54.

Figure D.53: Pre (top) and post-test (bottom) photographs from 'North' view for Configuration 25

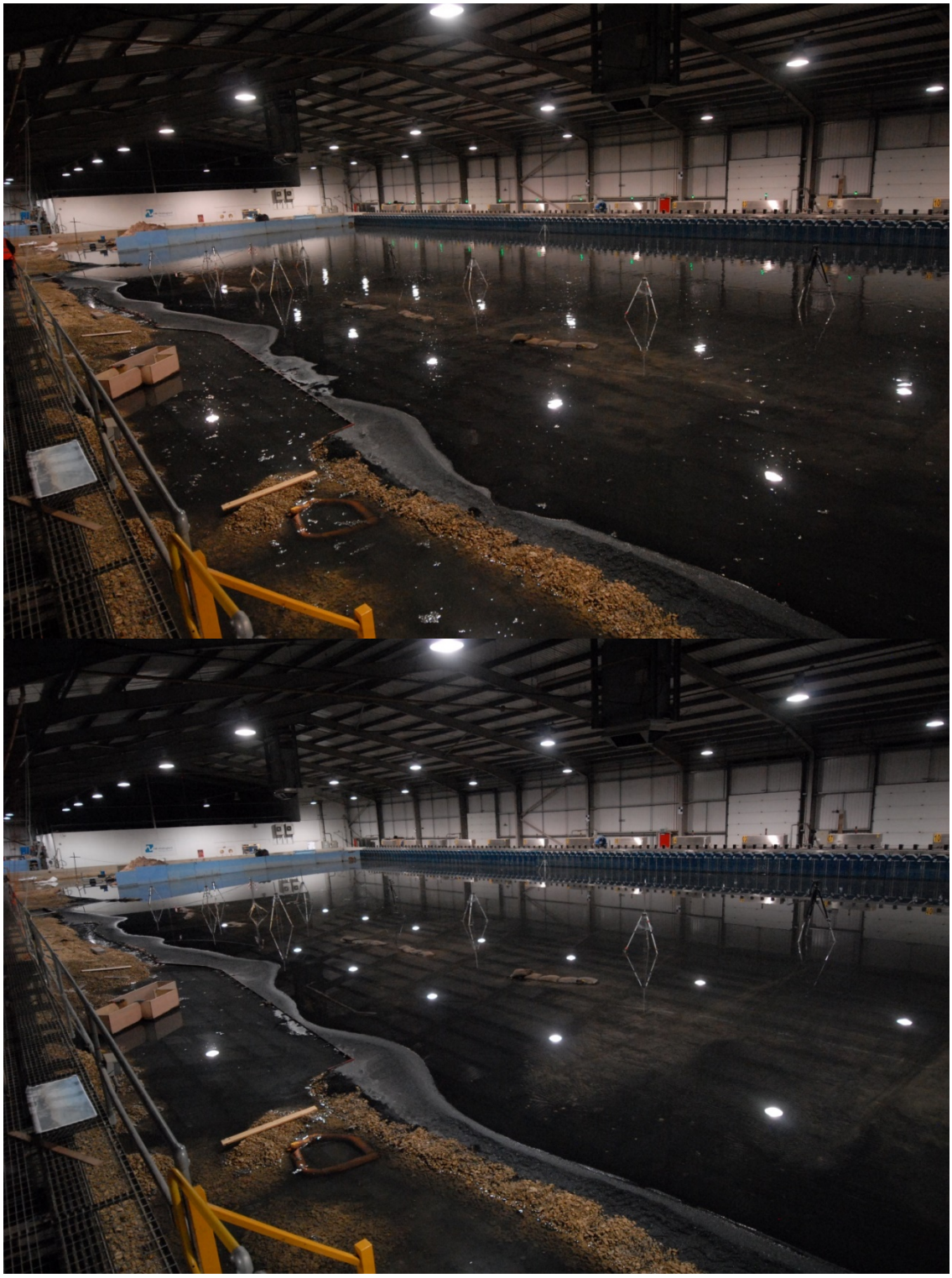

Figure D.54: Pre (top) and post-test (bottom) photographs from ‘South’ view for Configuration 25

## D.1.26. Configuration 26

Configuration 26 differed from Configuration 25 with the removal of one sandbag from the Southern end of the third Southernmost breakwater, a submerged section added to the Southern end of the second Southernmost breakwater, the addition of submerged 'wings' on both ends of the Southernmost breakwater and the rotation shoreward of the Southern end of the Southernmost breakwater. This configuration was tested for 20 hrs 45 mins (3.5 hours model). The pre and post-test photographs from the 'North' and 'South' time-lapse camera views are shown in Figure D.55 and Figure D.56.

Figure D.55: Pre (top) and post-test (bottom) photographs from 'North' view for Configuration 26

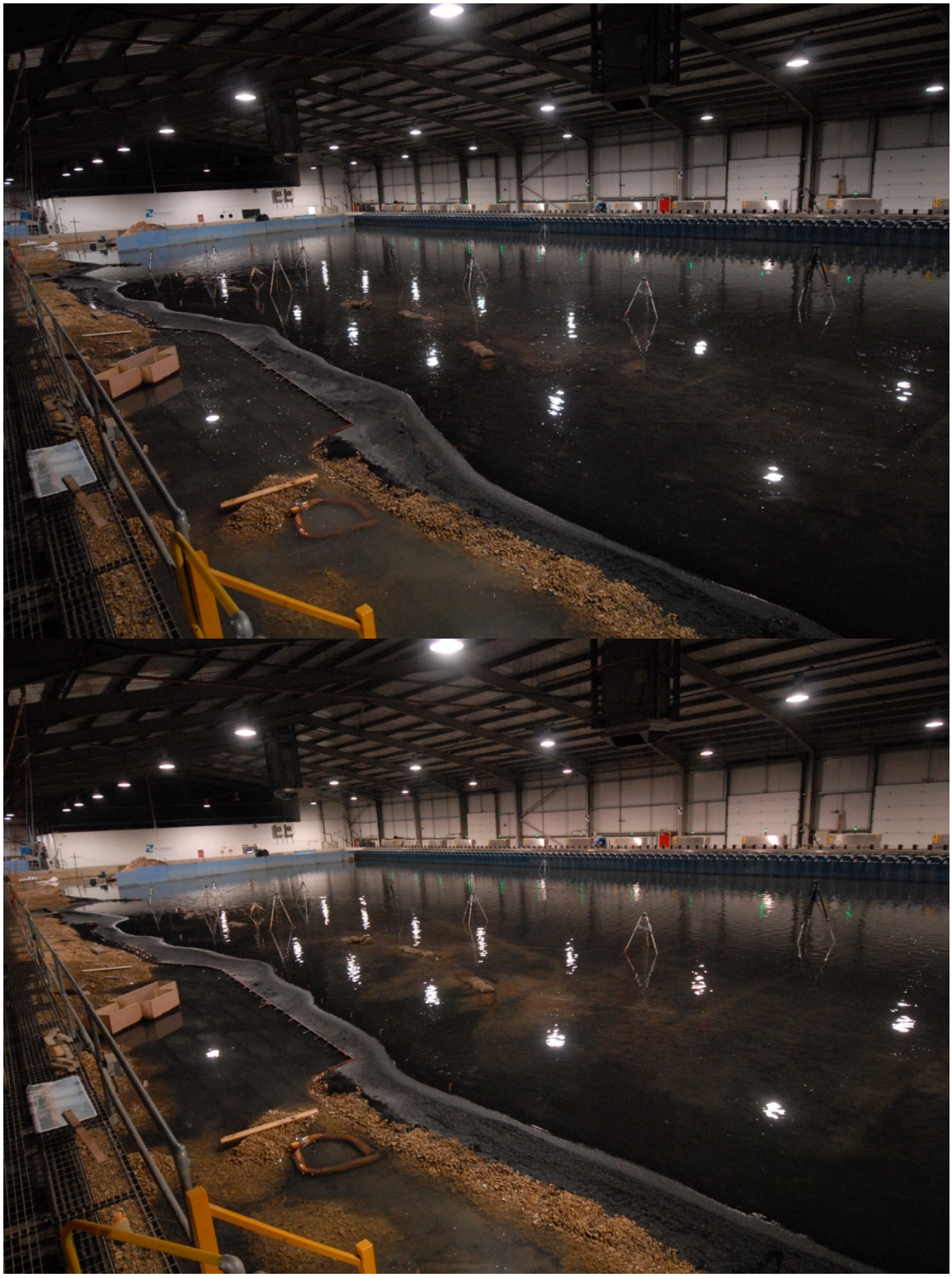

Figure D.56: Pre (top) and post-test (bottom) photographs from 'South' view for Configuration 26

## D.1.27. Configuration 27

Configuration 27 differed from Configuration 26 with the move lakeward of the Southernmost breakwater (reverting to Configuration 24 position) and the two sandbag submerged Southern end converted into one emergent sandbag section. This configuration was tested for 9 hrs (1.5 hours model). The pre and post-test photographs from the 'North' and 'South' time-lapse camera views are shown in Figure D.58 and Figure D.59. The post-test scan data is shown in Figure D.57.

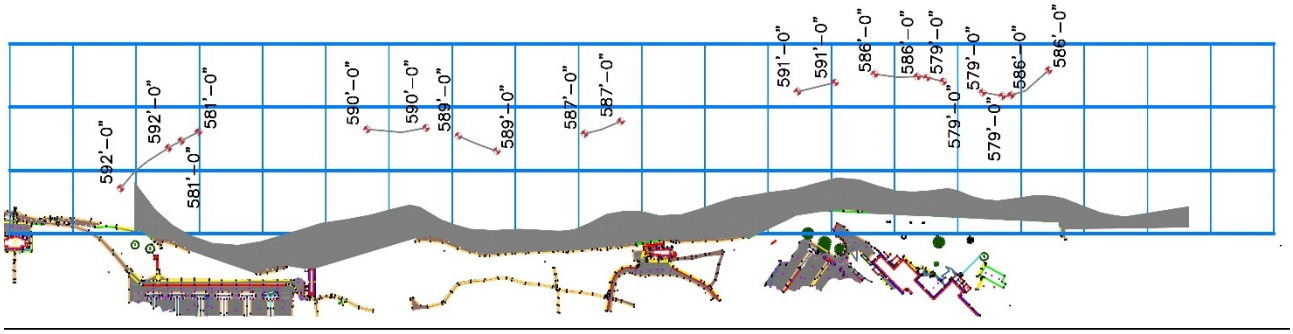


Figure D.57: Post-test scan data for Area 3 Configuration 27, solid area post-test beach, structures in grey with spot-heights given for key locations

Figure D.58: Pre (top) and post-test (bottom) photographs from 'North' view for Configuration 27

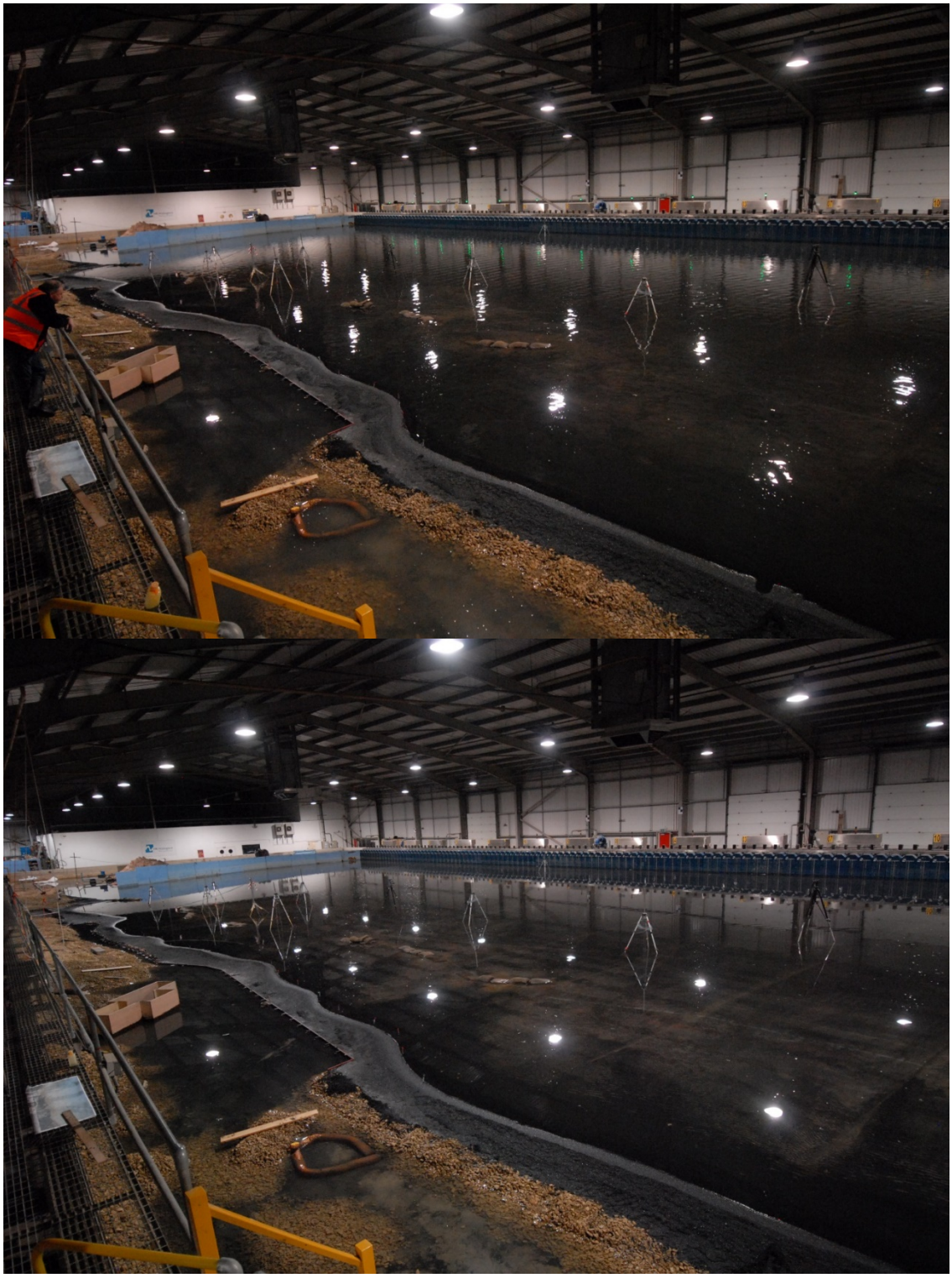

Figure D.59: Pre (top) and post-test (bottom) photographs from 'South' view for Configuration 27

## D.1.28. Configuration 28

Configuration 28 differed from Configuration 27 with the addition of two sandbags (one emergent and one submerged) to the South end of the Northernmost breakwater and the straightening and addition of two submerged sandbags to the Southern end of the Southernmost breakwater. This configuration was tested for 15 hrs (2.5 hours model). The pre and post-test photographs from the 'North' and 'South' time-lapse camera views are shown in Figure D.60 and Figure D.61.

Figure D.60: Pre (top) and post-test (bottom) photographs from 'North' view for Configuration 28

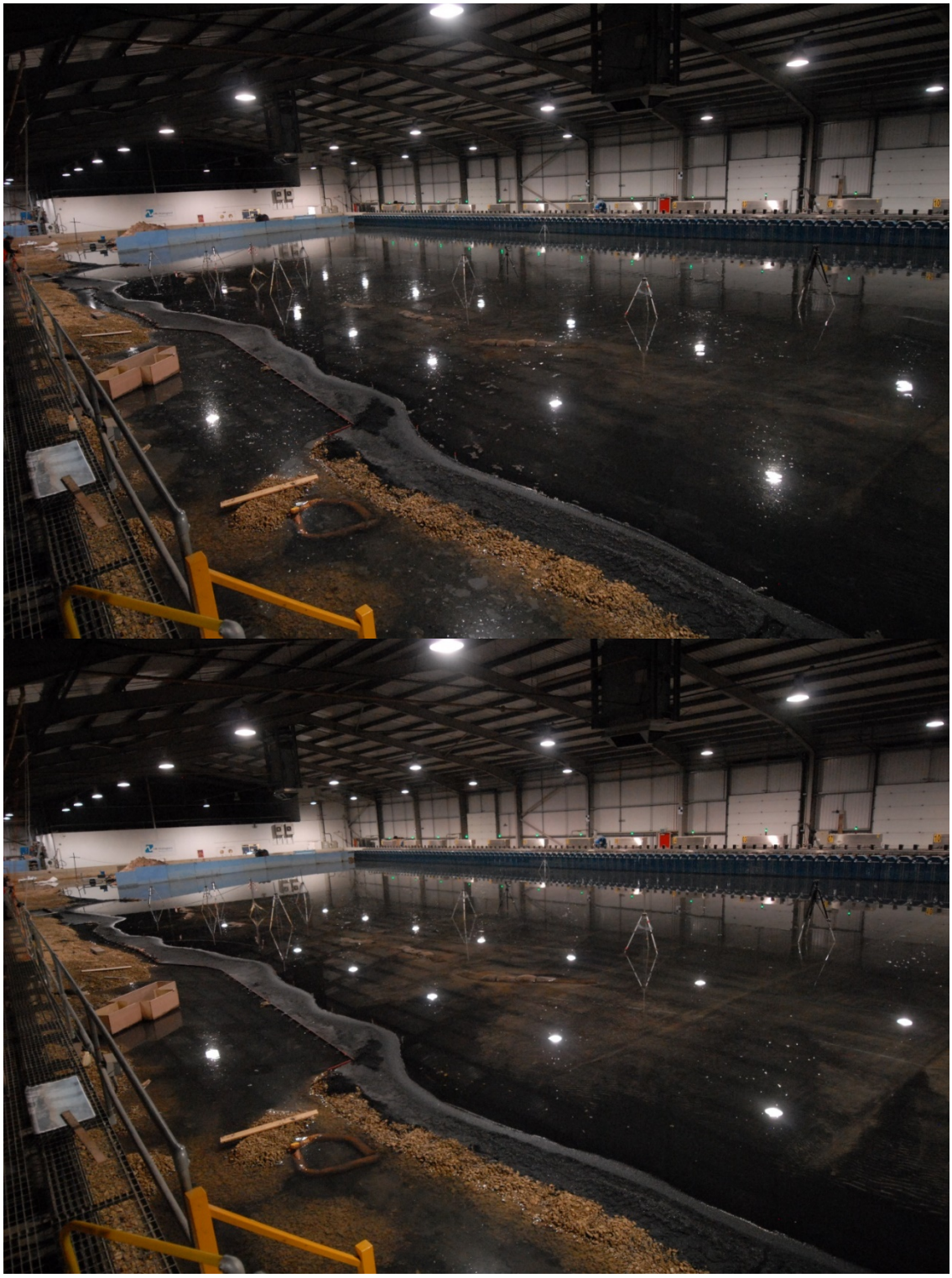

Figure D.61: Pre (top) and post-test (bottom) photographs from 'South' view for Configuration 28

## D.1.29. Configuration 29

Configuration 29 differed from Configuration 28 with the dividing of the Southernmost breakwater into two breakwaters. The beach was replenished and re-profiled at the Southern end of the model in front of the hotel. This configuration was tested for 18 hrs (3 hours model). The pre and post-test photographs from the 'North' and 'South' time-lapse camera views are shown in Figure D.63 and Figure D.64. The post-test scan data is shown in Figure D.62.

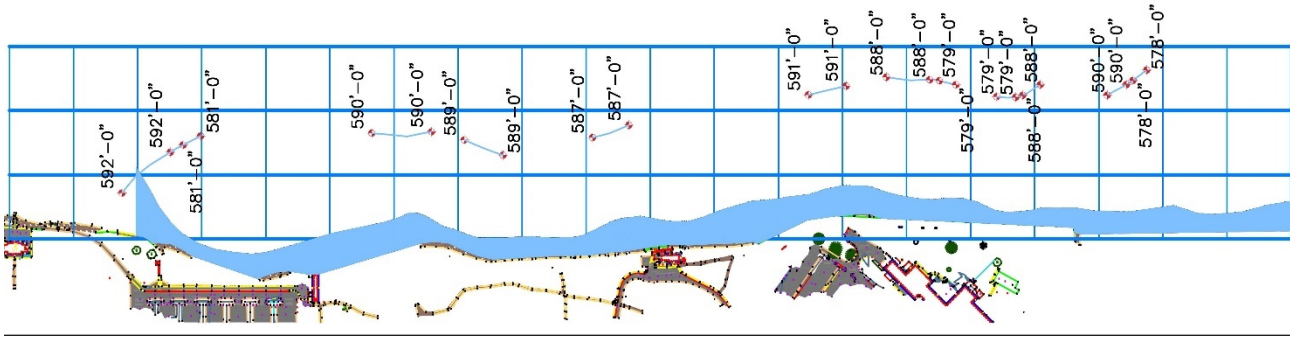


Figure D.62: Post-test scan data for Area 3 Configuration 29, solid area post-test beach, structures in blue with spot-heights given for key locations

Figure D.63: Pre (top) and post-test (bottom) photographs from ‘North’ view for Configuration 29

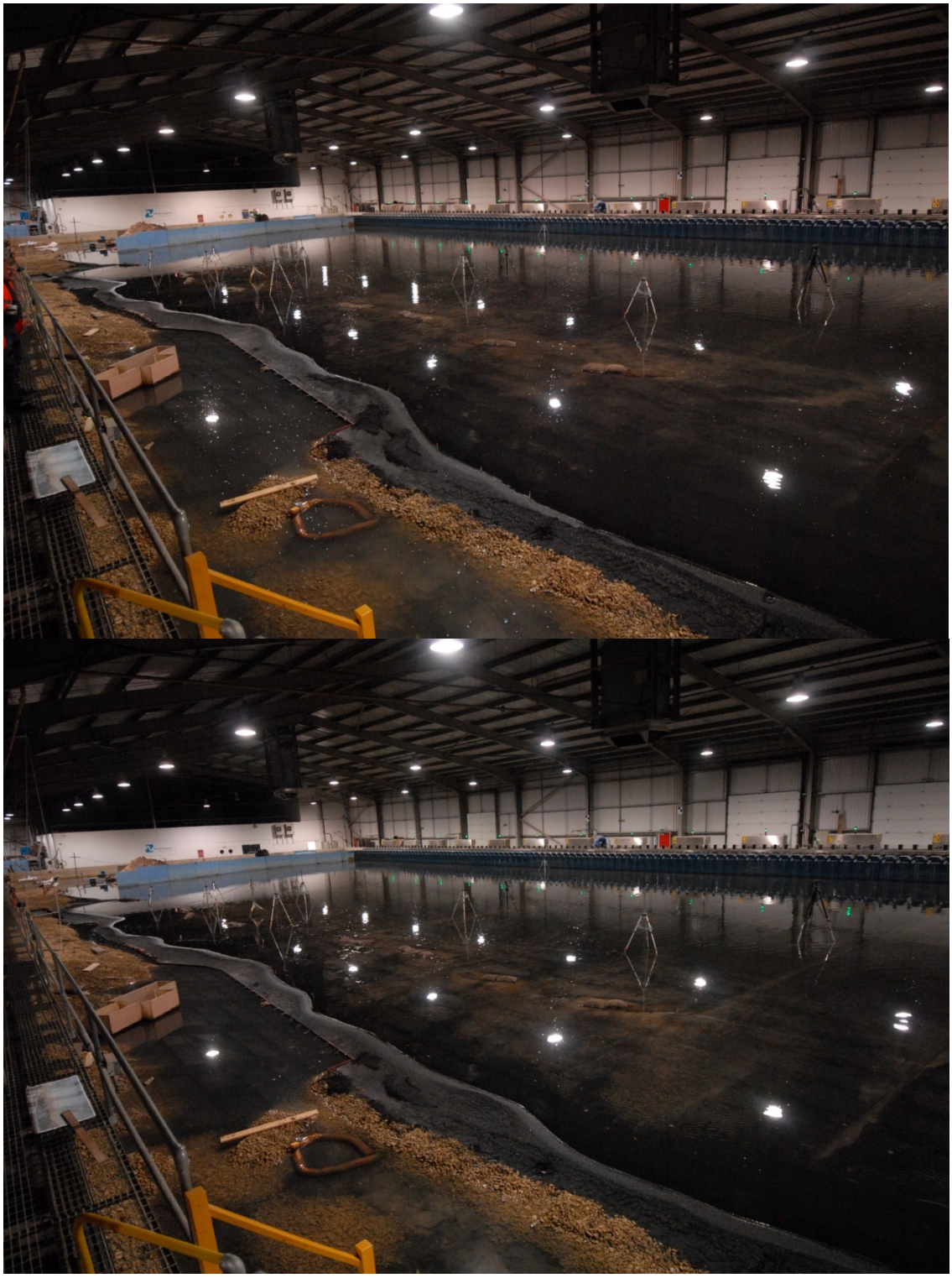

Figure D.64: Pre (top) and post-test (bottom) photographs from ‘South’ view for Configuration 29

## D.1.30. Configuration 30

Configuration 30 differed from Configuration 29 by changing all the structures so the three Northern breakwaters matched Configuration 15 and the two Southern breakwaters matched Configuration 02, resulting in five breakwater in total. This configuration was tested for 20 hrs 45 mins (3.5 hours model). The pre and post-test photographs from the 'North' and 'South' time-lapse camera views are shown in Figure D.65 and Figure D.66.

Figure D.65: Pre (top) and post-test (bottom) photographs from ‘North’ view for Configuration 30

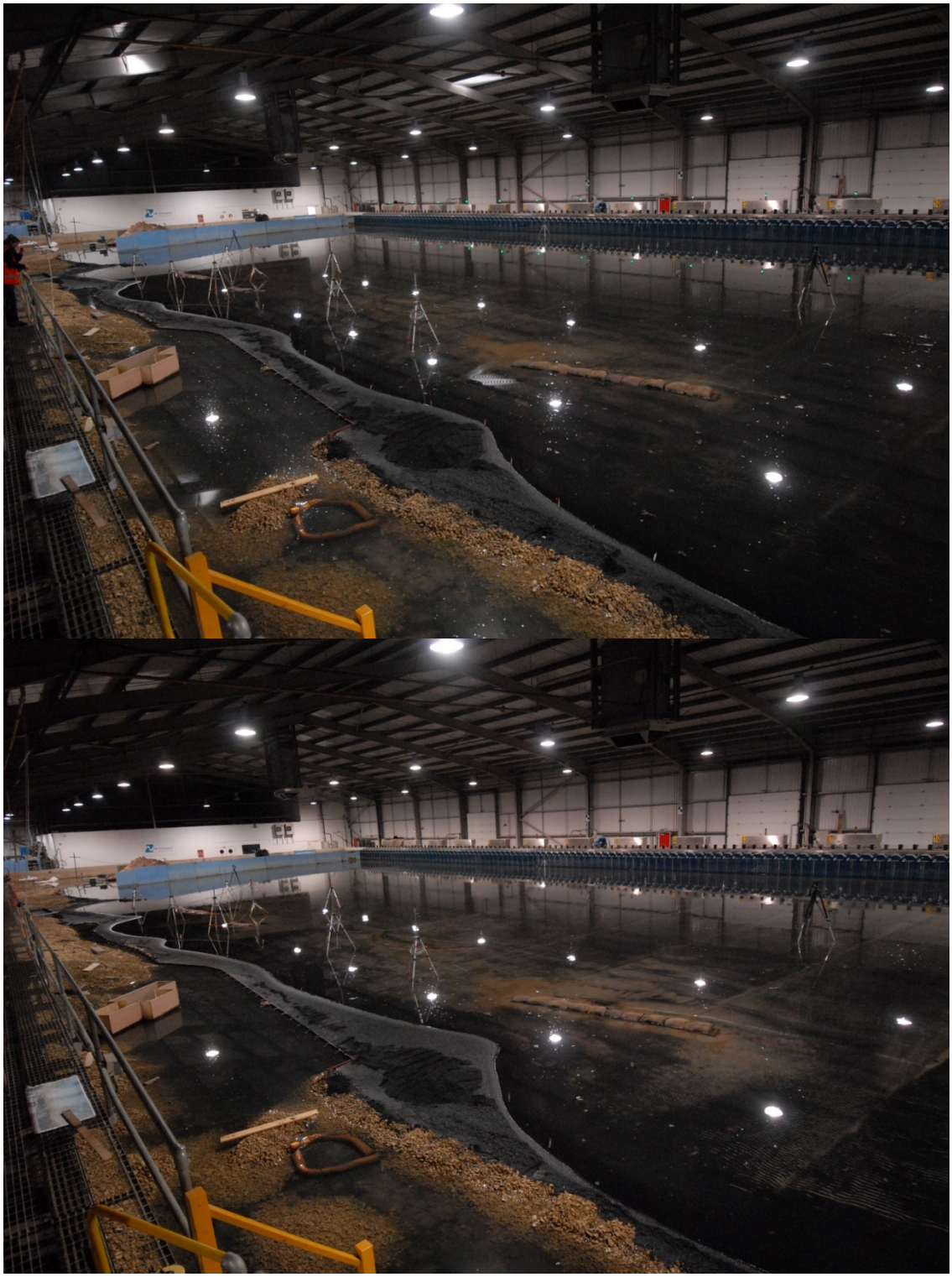

Figure D.66: Pre (top) and post-test (bottom) photographs from 'South' view for Configuration 30

## D.1.31. Configuration 31

Configuration 31 differed from Configuration 30 with the shortening and dividing into two of the second Southernmost breakwater, the resulting Northern breakwater consisted of five sandbags and the Southern of seven. This configuration was tested for 6 hrs (1 hour model). The pre and post-test photographs from the 'North' and 'South' time-lapse camera views are shown in Figure D.67 and Figure D.68.

Figure D.67: Pre (top) and post-test (bottom) photographs from 'North' view for Configuration 31

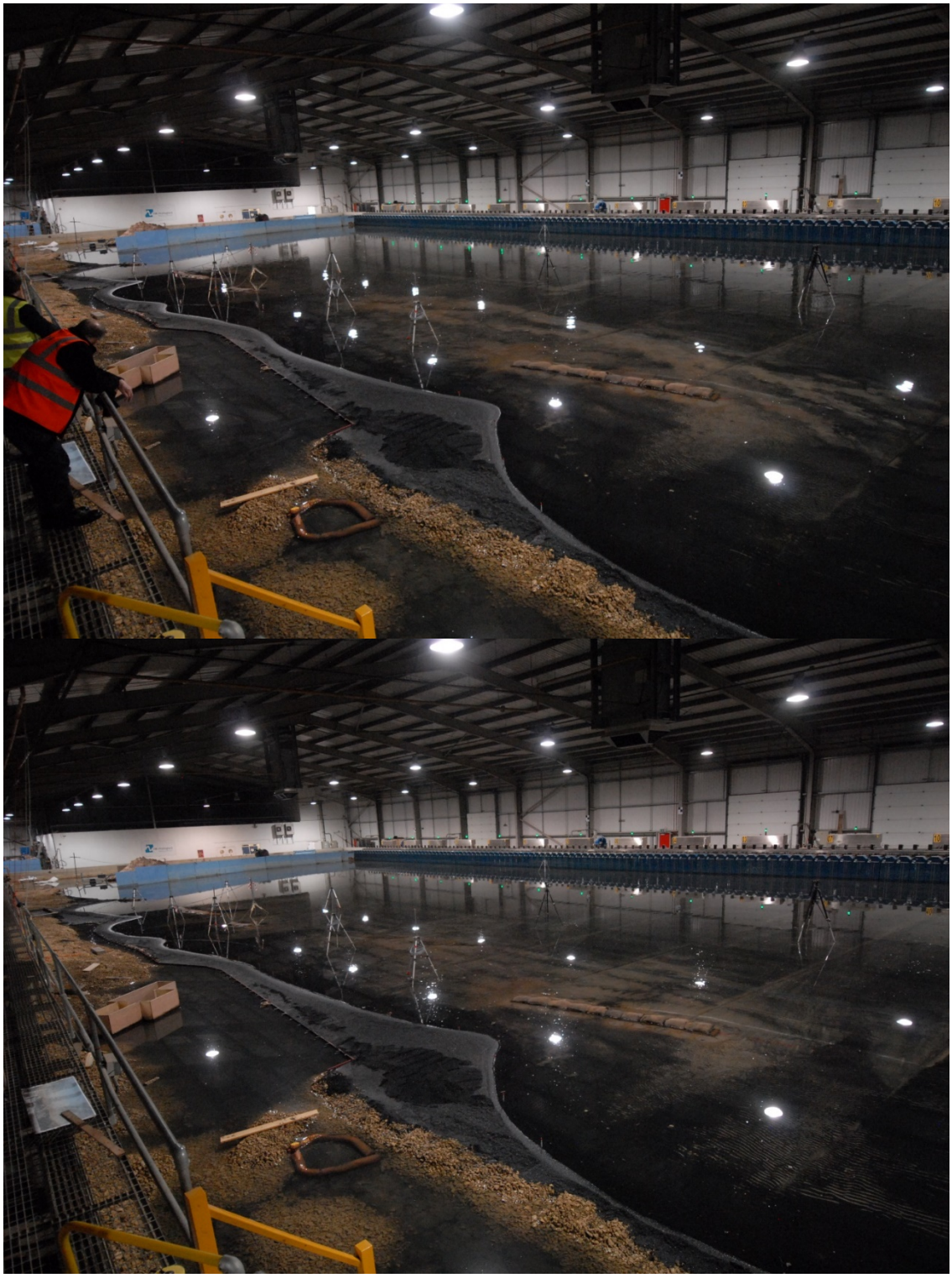

Figure D.68: Pre (top) and post-test (bottom) photographs from 'South' view for Configuration 31

## D.1.32. Configuration 32

Configuration 32 differed from Configuration 31 with the removal of four sandbags from the second Southernmost breakwater and the restoration of the ‘smile’ from Configuration 30. This configuration was tested for 6 hrs (1 hour model). The pre and post-test photographs from the ‘North’ and ‘South’ time-lapse camera views are shown in Figure D.69 and Figure D.70.

Figure D.69: Pre (top) and post-test (bottom) photographs from ‘North’ view for Configuration 32

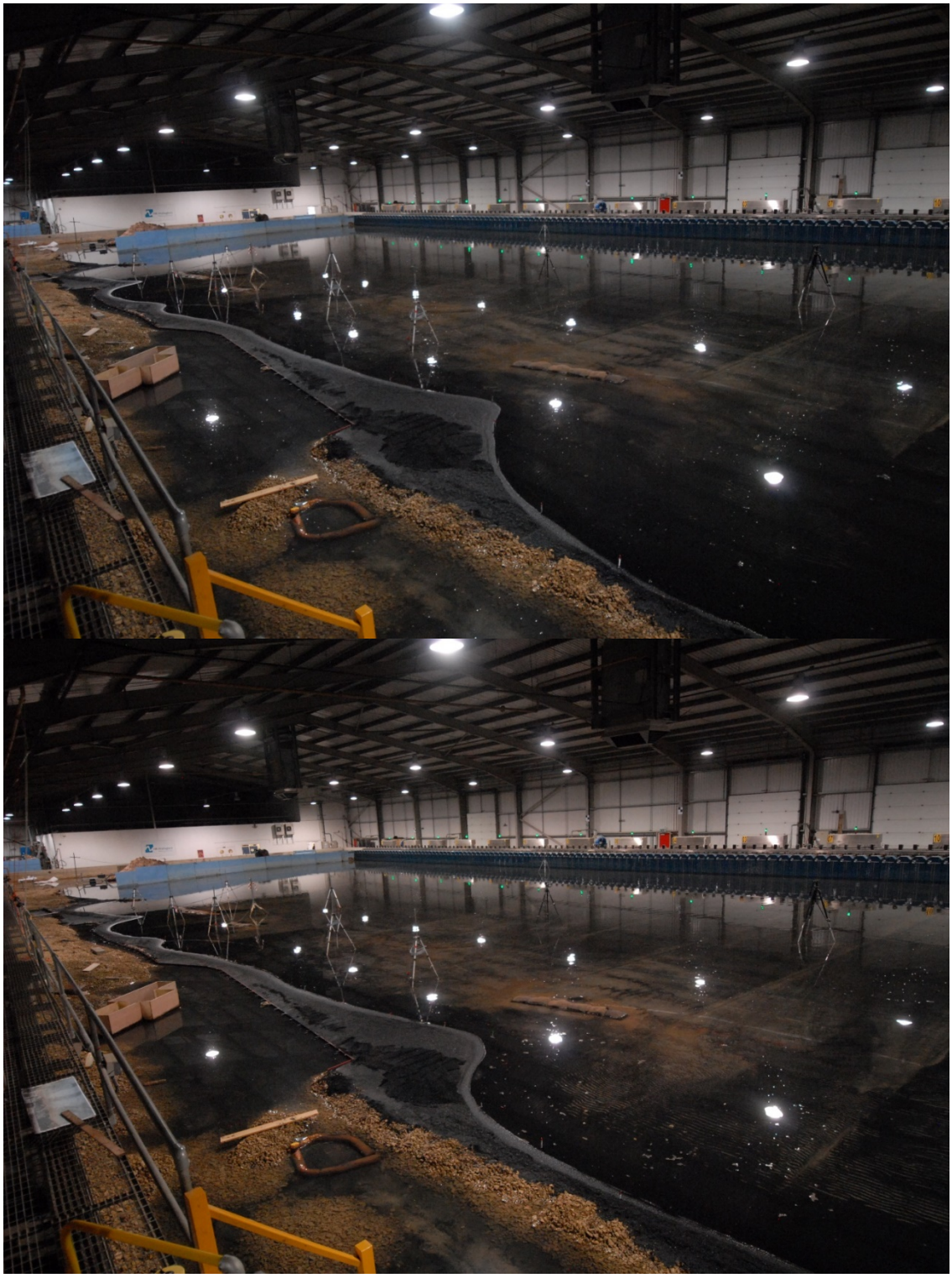

Figure D.70: Pre (top) and post-test (bottom) photographs from ‘South’ view for Configuration 32

## D.1.33. Configuration 33

Configuration 33 differed from Configuration 32 with the move Northwards of the second Southernmost breakwater by 70 ft. This configuration was tested for 6 hrs (1 hour model). The pre and post-test photographs from the 'North' and 'South' time-lapse camera views are shown in Figure D.71 and Figure D.72.

Figure D.71: Pre (top) and post-test (bottom) photographs from ‘North’ view for Configuration 33

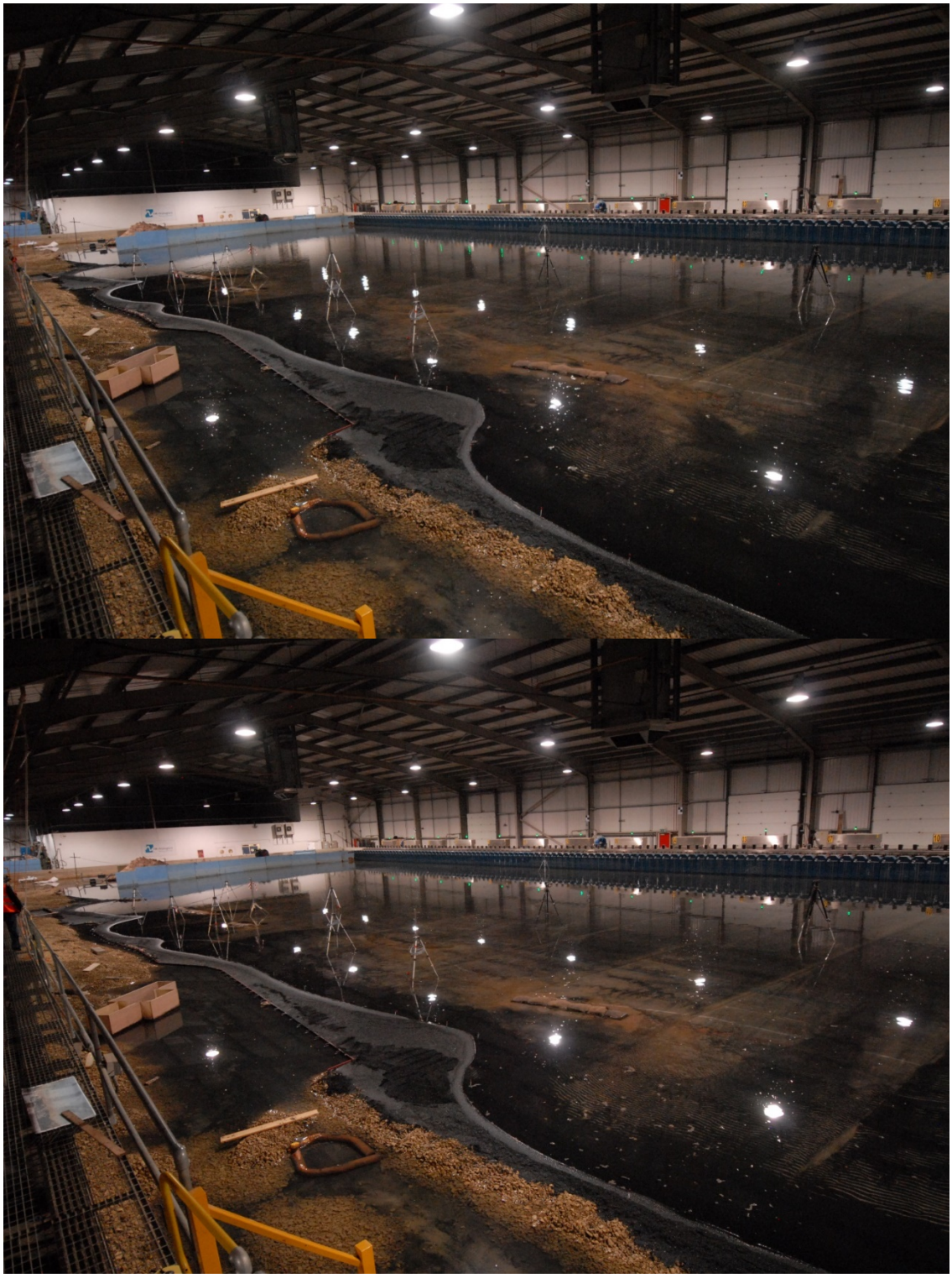

Figure D.72: Pre (top) and post-test (bottom) photographs from 'South' view for Configuration 33

## D.1.34. Configuration 34

Configuration 34 differed from Configuration 33 with the penultimate Southern breakwater moved 70 ft to the North. This configuration was tested for 9 hrs (1.5 hrs model). The pre and post-test photographs from the 'North' and 'South' time-lapse camera views are shown in Figure C.40 and Figure C.41. The post-test scan data is shown in Figure D.73.

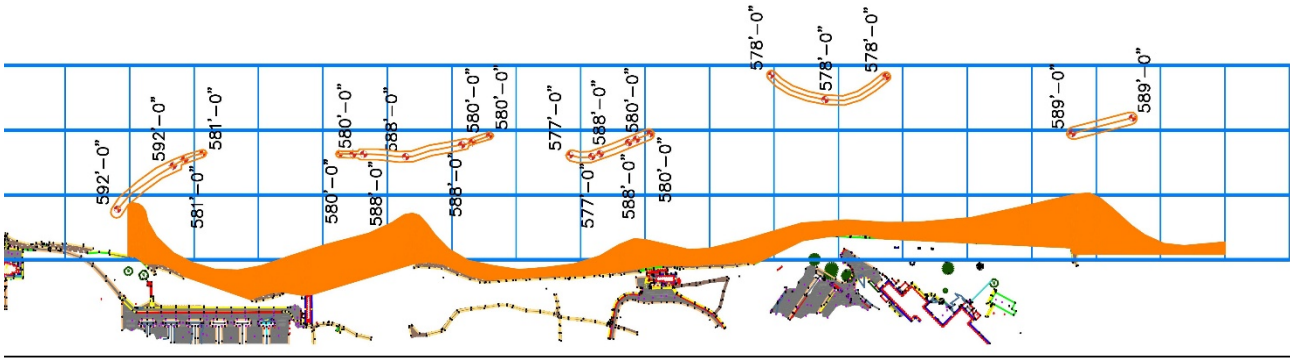


Figure D.73: Post-test scan data for Area 3 Configuration 34, solid area post-test beach, structures in orange with spot-heights given for key locations

Figure D.74: Pre (top) and post-test (bottom) photographs from ‘North’ view for Configuration 34

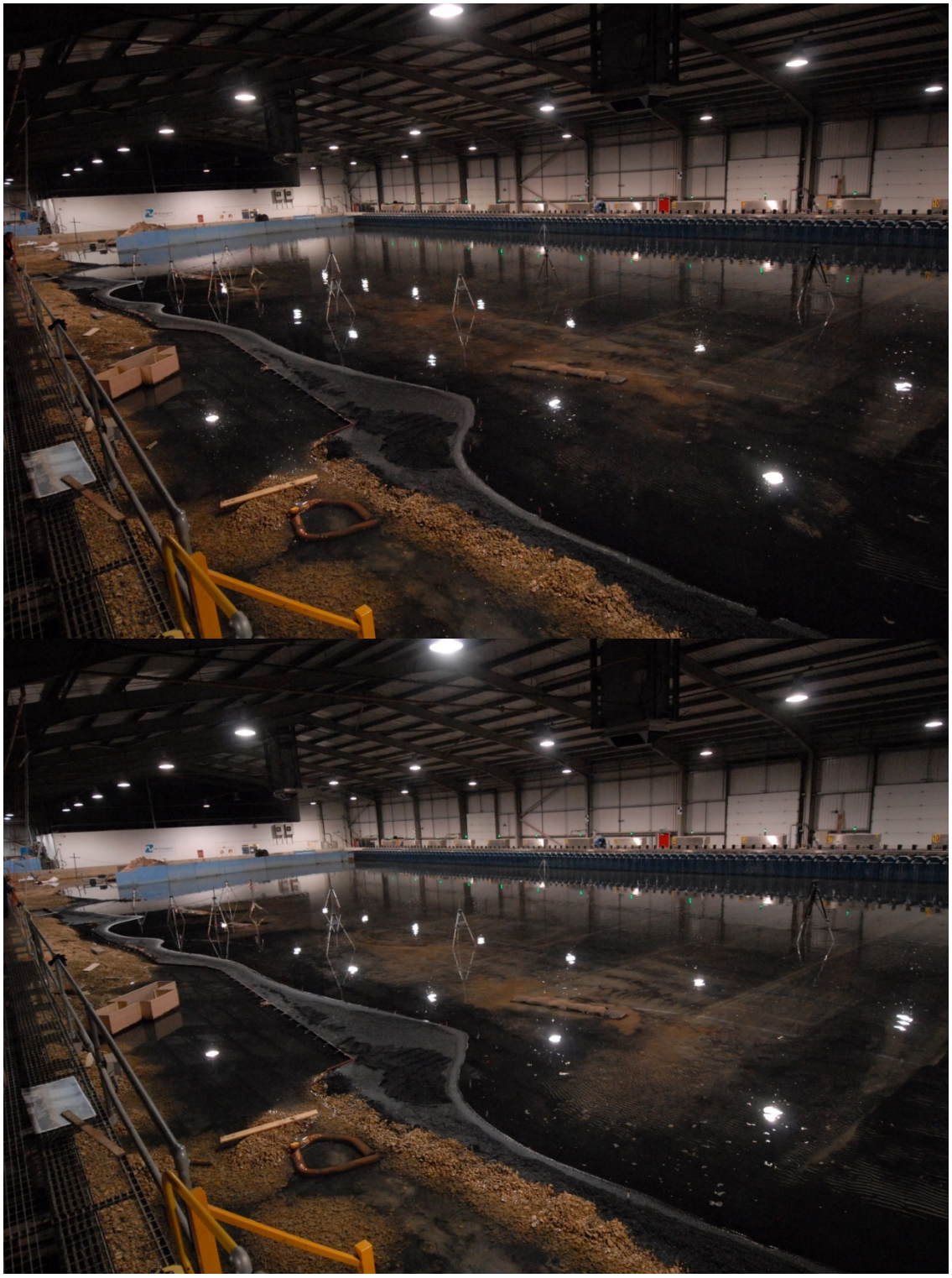

Figure D.75: Pre (top) and post-test (bottom) photographs from ‘South’ view for Configuration 34

# D.2. Stability photographs

## D.2.1. BW3-1

Figure D.76: Pre-test stability photograph for BW3-1, position 1

No image available

Figure D.77: Post Test Part 01 (WC_LOW_WL_SE) stability photograph for BW3-1, position 1

Figure D.78: Post Test Part 02 (WC_HIGH_WL_SE) stability photograph for BW3-1, position 1

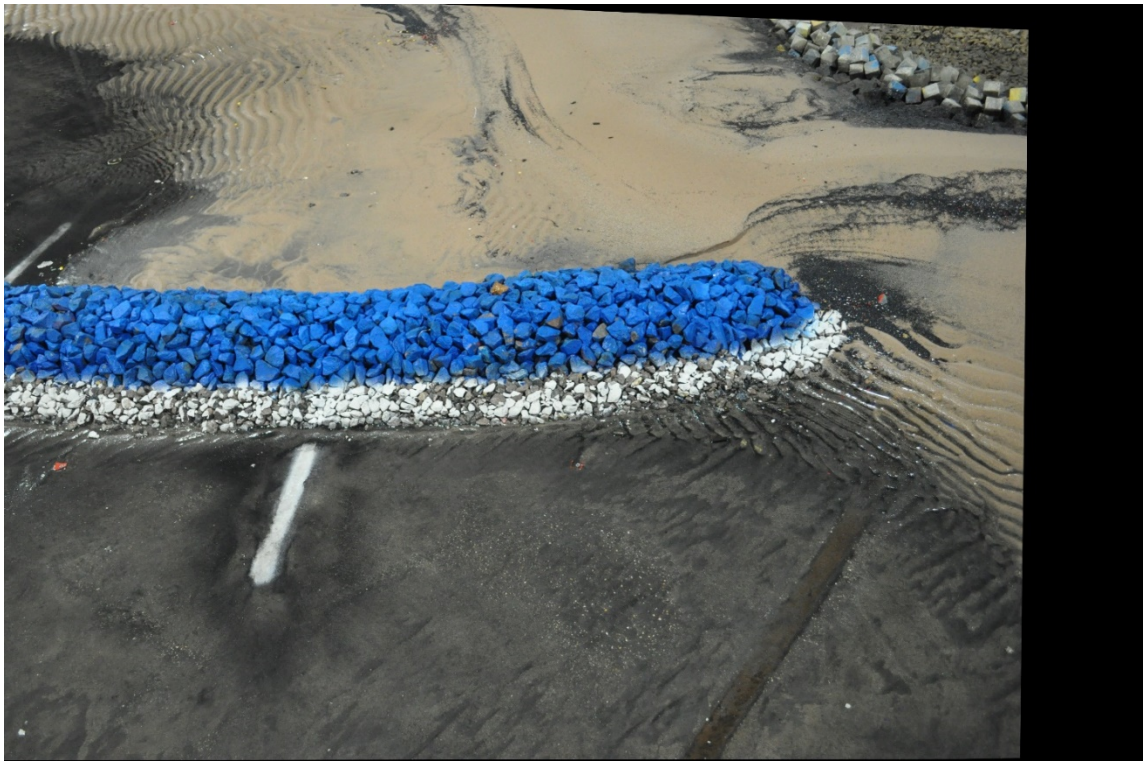

Figure D.79: Post Test Part 03 (WC_LOW_WL) stability photograph for BW3-1, position 1

Figure D.80: Post Test Part 04 (WC_HIGH_WL) stability photograph for BW3-1, position 1

Figure D.81: Post Test Part 05 (WC_EXT_WL_01) stability photograph for BW3-1, position 1

Figure D.82: Post Test Part 06 (WC_EXT_WL_02) stability photograph for BW3-1, position 1

Figure D.83: Pre-test stability photograph for BW3-1, position 2

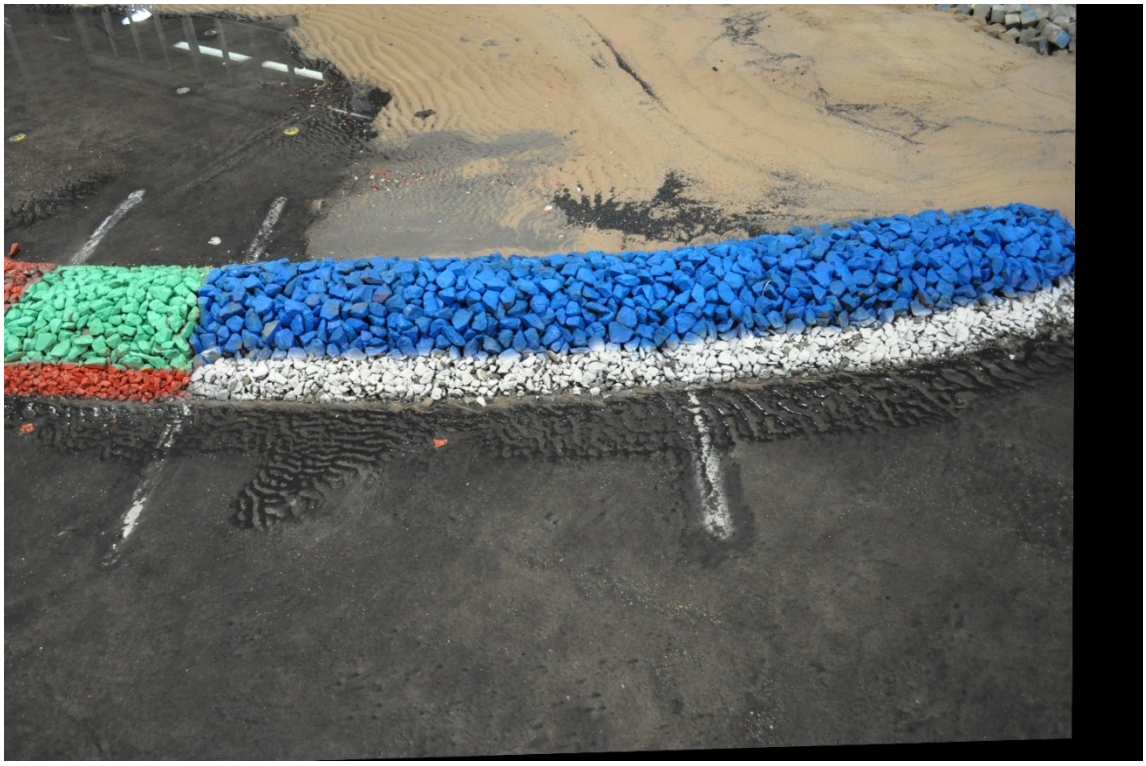

Figure D.84: Post Test Part 01 (WC_LOW_WL_SE) stability photograph for BW3-1, position 2

Figure D.85: Post Test Part 02 (WC_HIGH_WL_SE) stability photograph for BW3-1, position 2

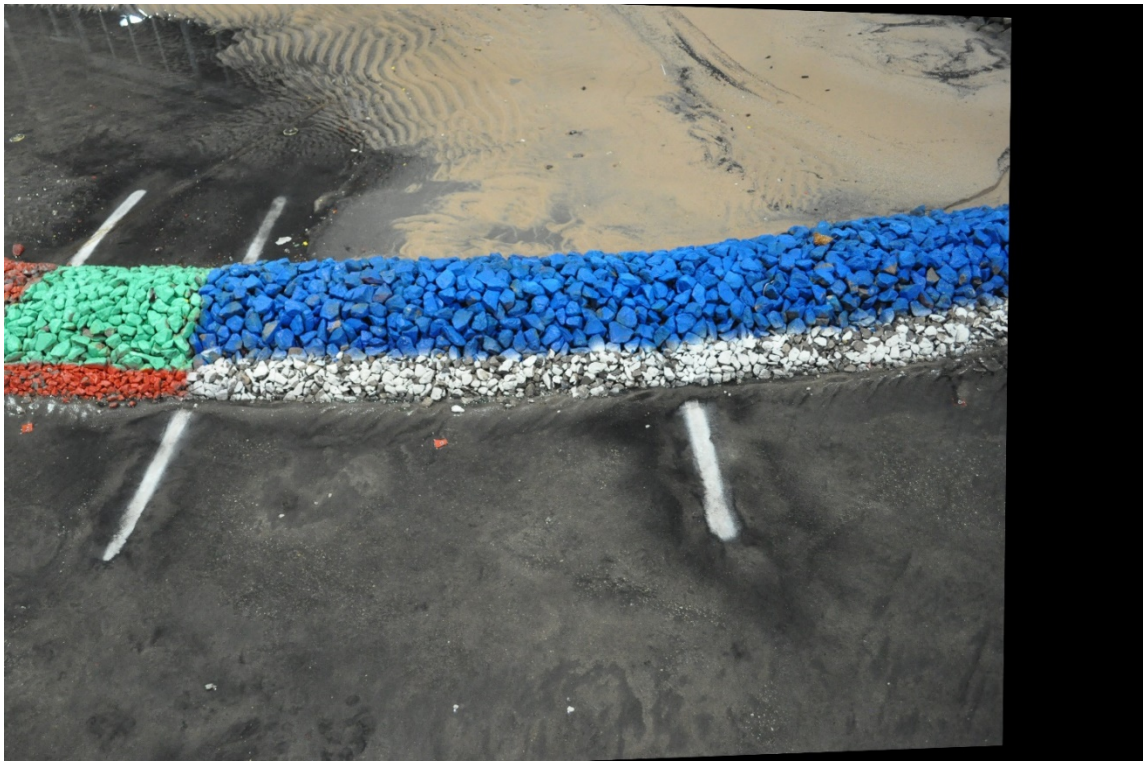

Figure D.86: Post Test Part 03 (WC_LOW_WL) stability photograph for BW3-1, position 2

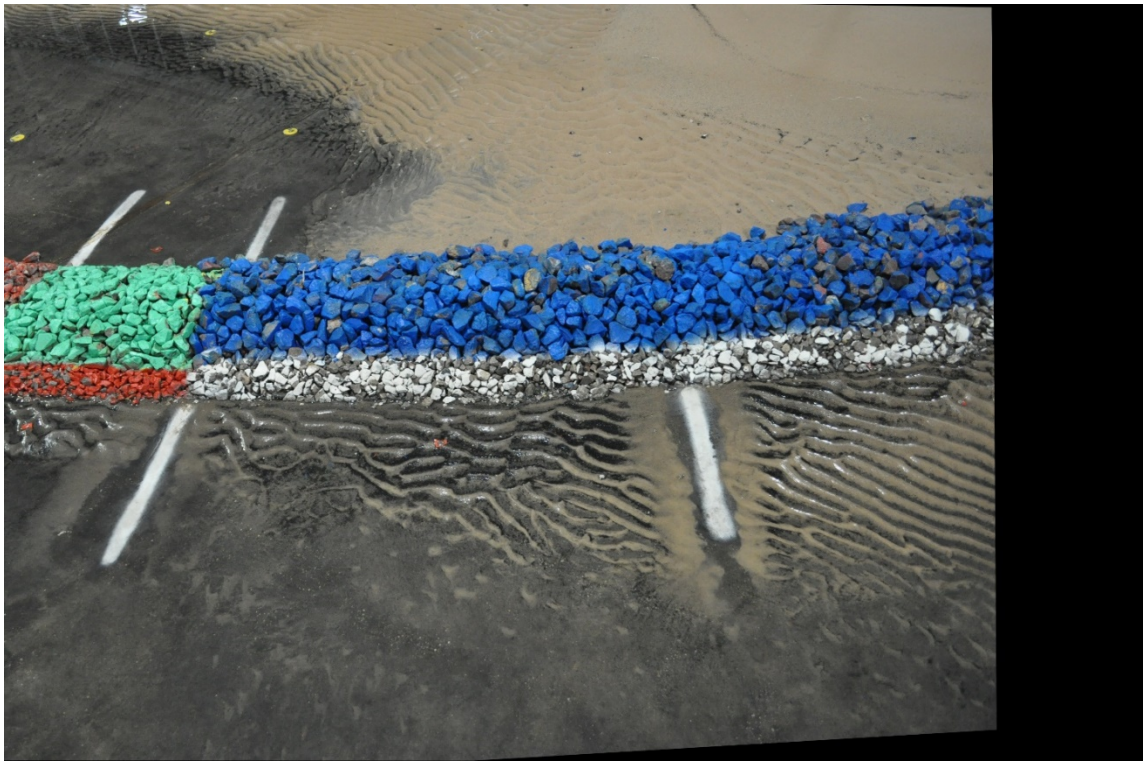

Figure D.87: Post Test Part 04 (WC_HIGH_WL) stability photograph for BW3-1, position 2

Figure D.88: Post Test Part 05 (WC_EXT_WL_01) stability photograph for BW3-1, position 2

Figure D.89: Post Test Part 06 (WC_EXT_WL_02) stability photograph for BW3-1, position 2

Figure D.90: Pre-test stability photograph for BW3-1, position 3

Figure D.91: Post Test Part 01 (WC_LOW_WL_SE) stability photograph for BW3-1, position 3

Figure D.92: Post Test Part 02 (WC_HIGH_WL_SE) stability photograph for BW3-1, position 3

Figure D.93: Post Test Part 03 (WC_LOW_WL) stability photograph for BW3-1, position 3

Figure D.94: Post Test Part 04 (WC_HIGH_WL) stability photograph for BW3-1, position 3

Figure D.95: Post Test Part 05 (WC_EXT_WL_01) stability photograph for BW3-1, position 3

Figure D.96: Post Test Part 06 (WC_EXT_WL_02) stability photograph for BW3-1, position 3

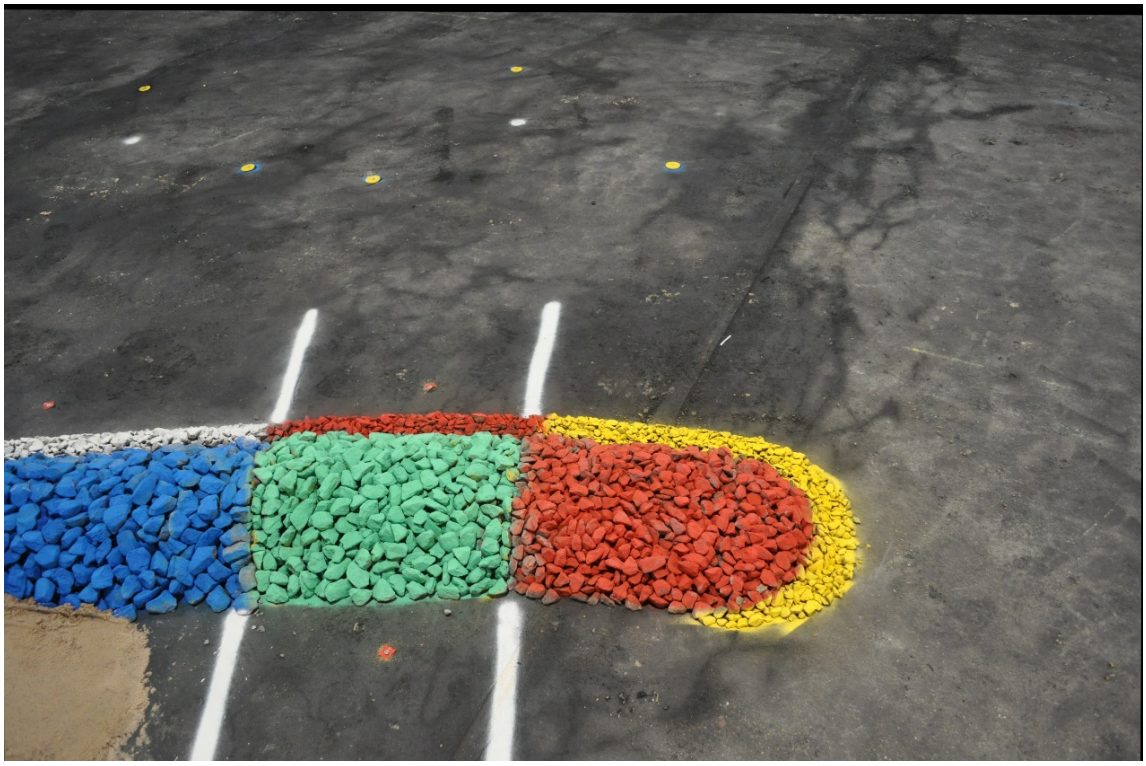

Figure D.97: Pre-test stability photograph for BW3-1, position 4

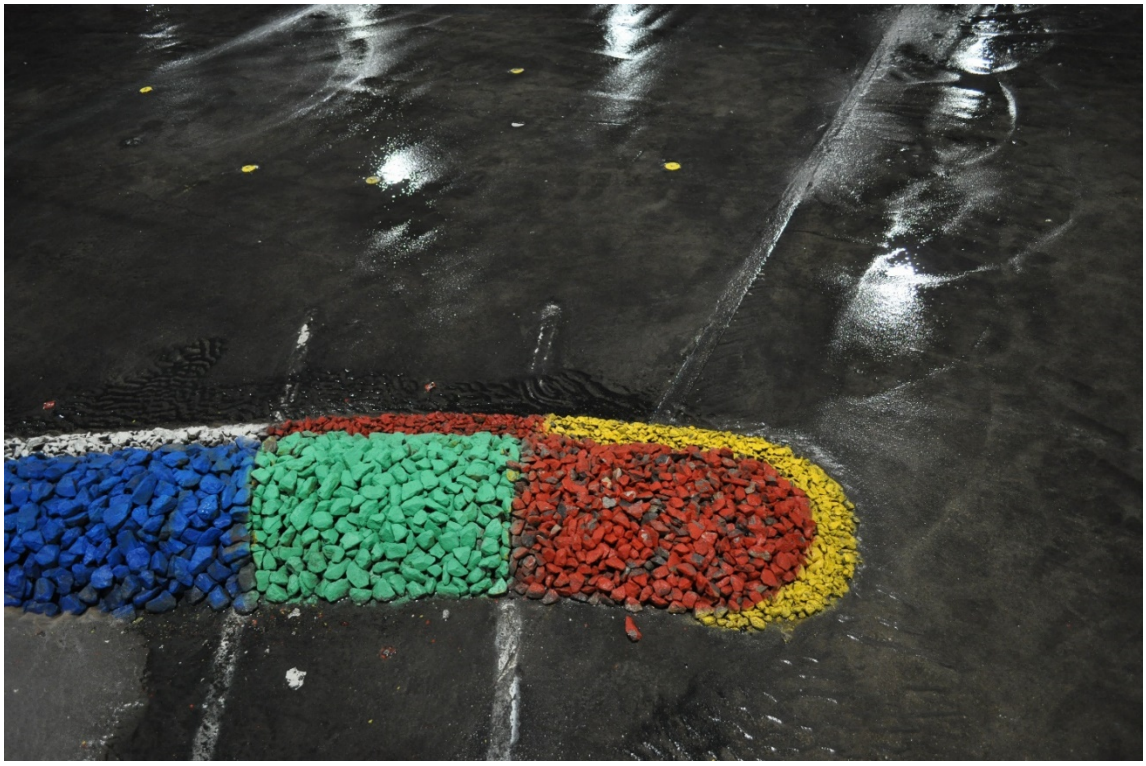

Figure D.98: Post Test Part 01 (WC_LOW_WL_SE) stability photograph for BW3-1, position 4

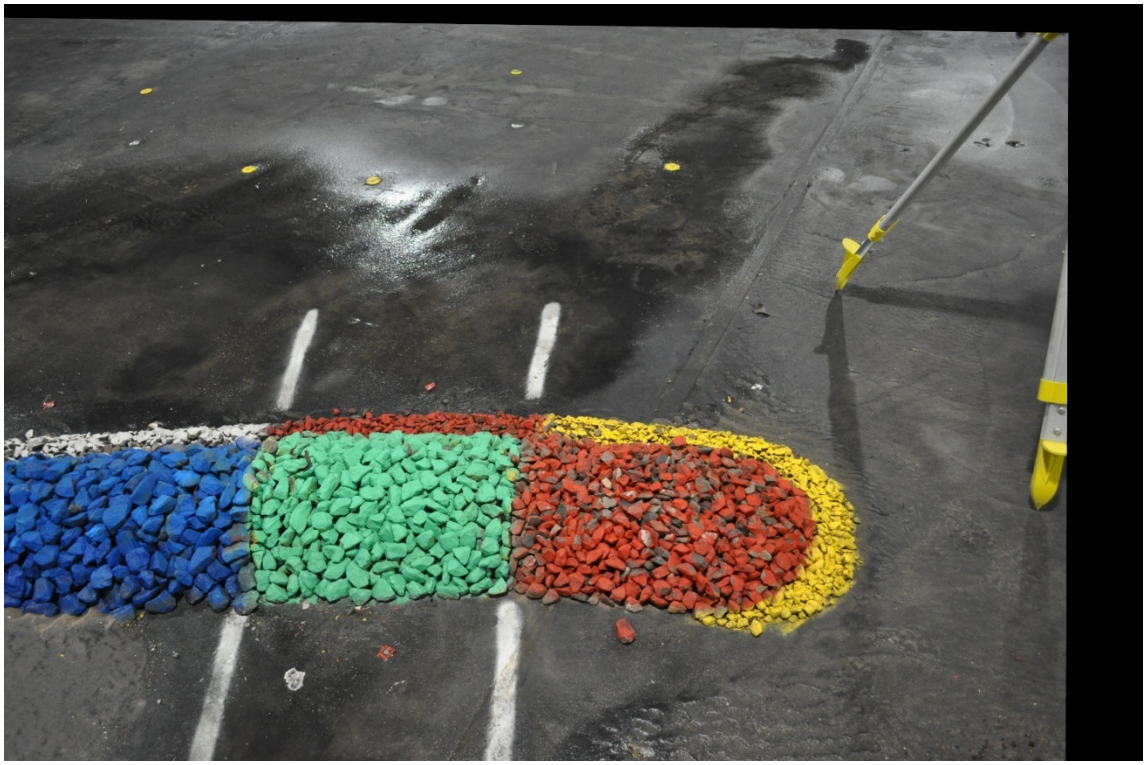

Figure D.99: Post Test Part 02 (WC_HIGH_WL_SE) stability photograph for BW3-1, position 4

Figure D.100: Post Test Part 03 (WC_LOW_WL) stability photograph for BW3-1, position 4

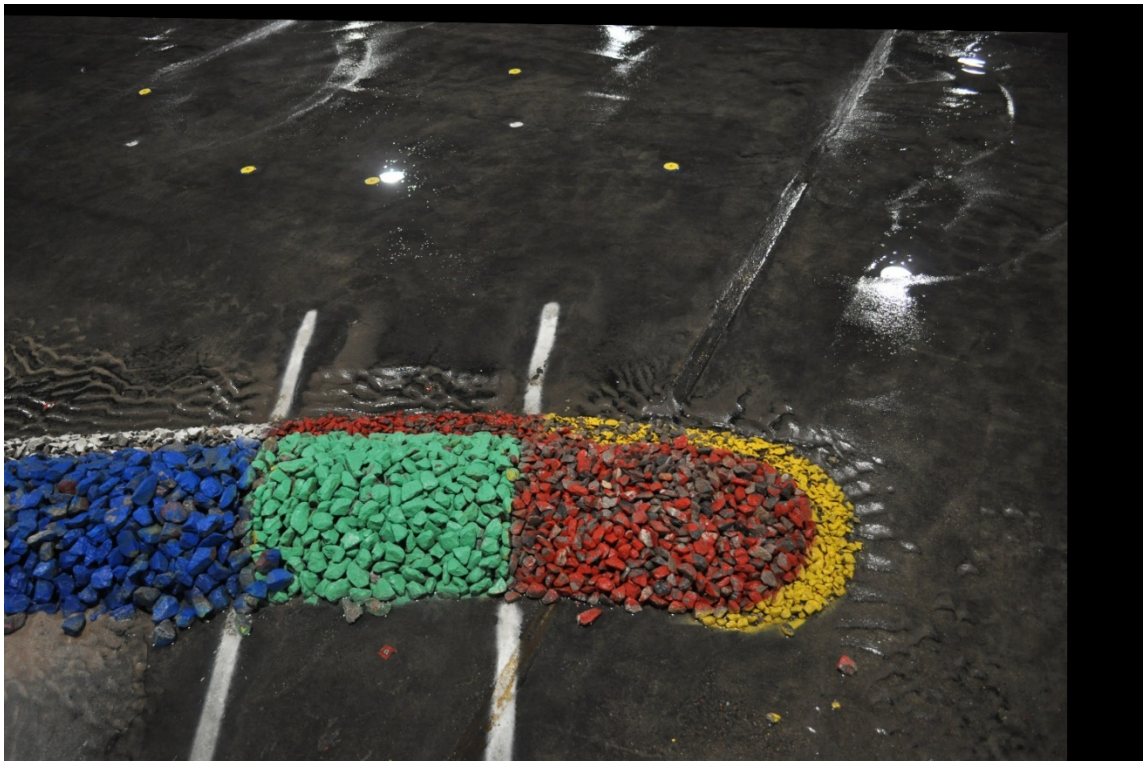

Figure D.101: Post Test Part 04 (WC_HIGH_WL) stability photograph for BW3-1, position 4

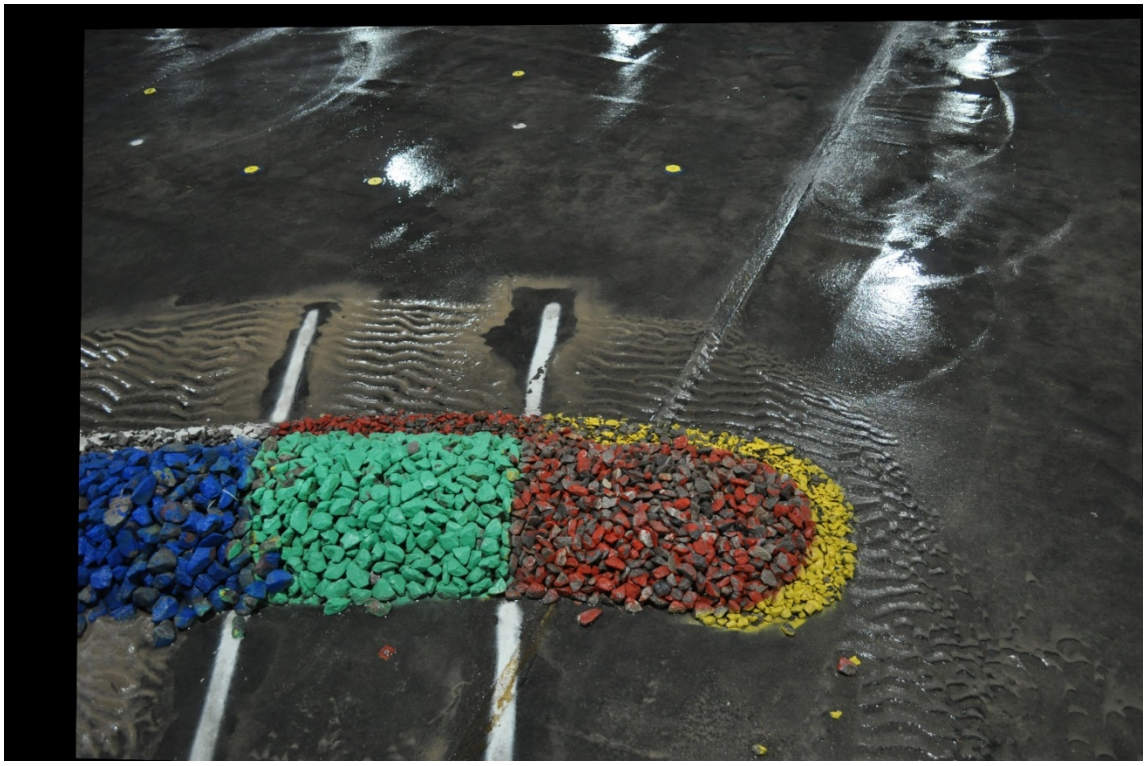

Figure D.102: Post Test Part 05 (WC_EXT_WL_01) stability photograph for BW3-1, position 4

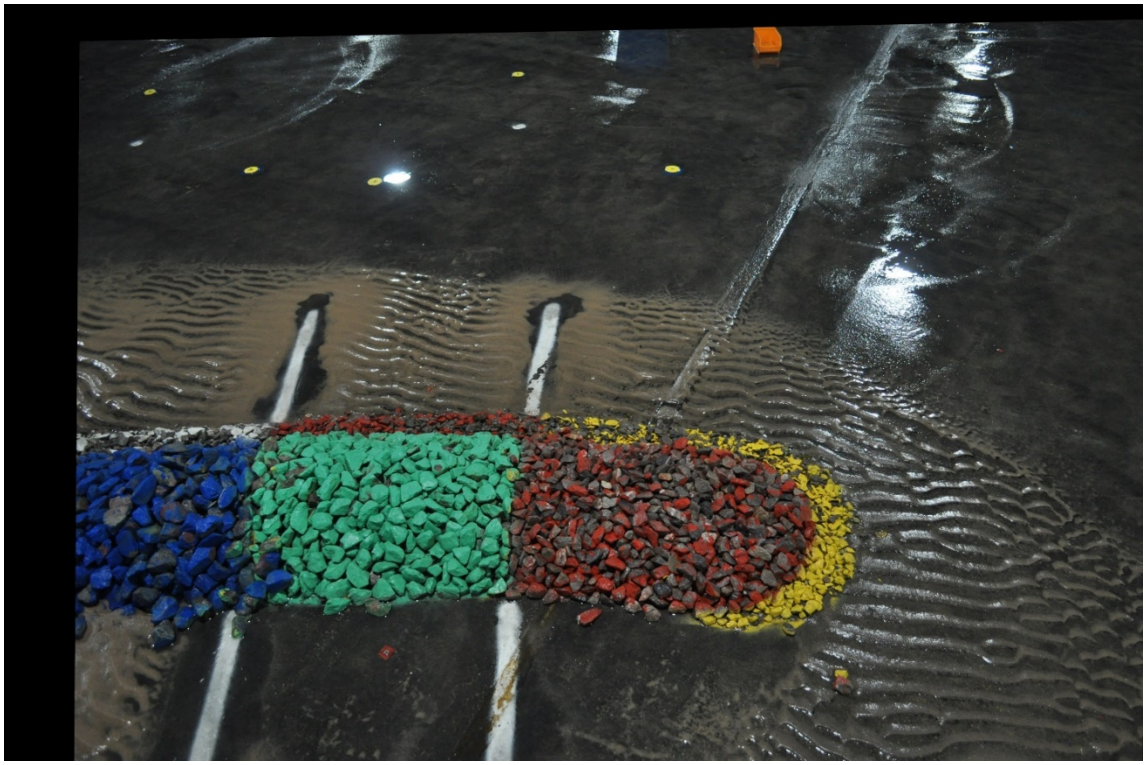

Figure D.103: Post Test Part 06 (WC_EXT_WL_02) stability photograph for BW3-1, position 4

## D.2.2. BW3-2

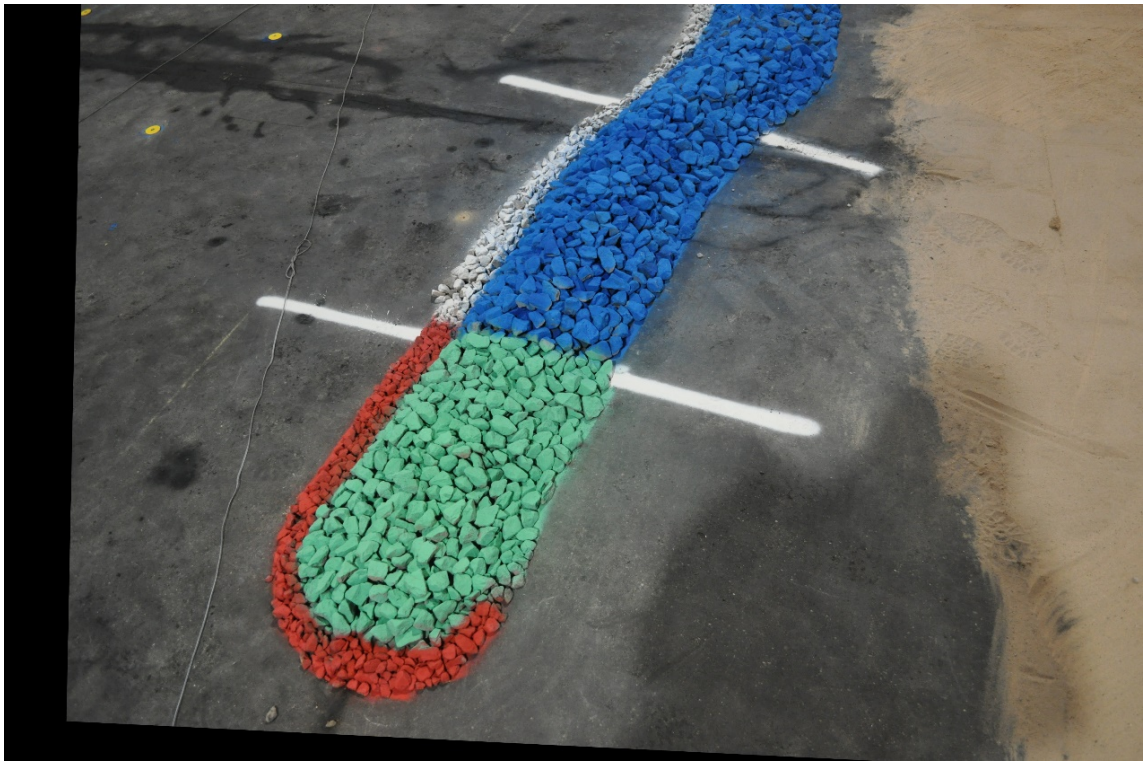

Figure D.104: Pre-test stability photograph for BW3-2, position 5

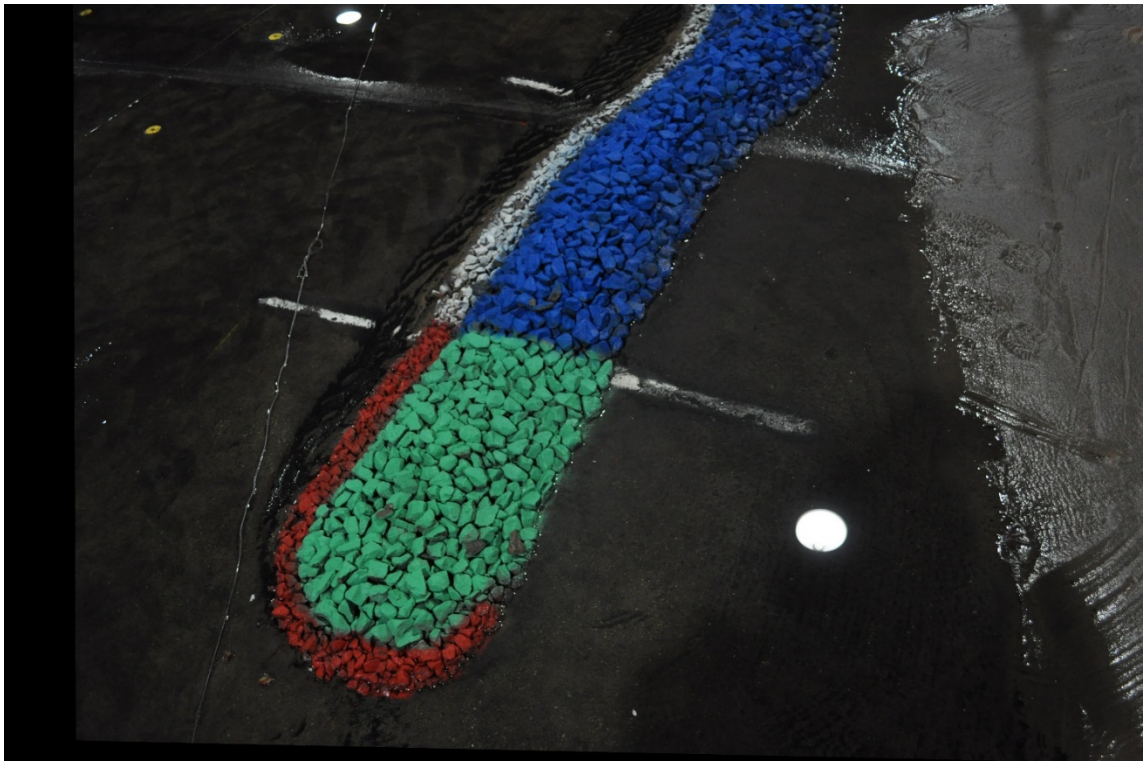

Figure D.105: Post Test Part 01 (WC_LOW_WL_SE) stability photograph for BW3-2, position 5

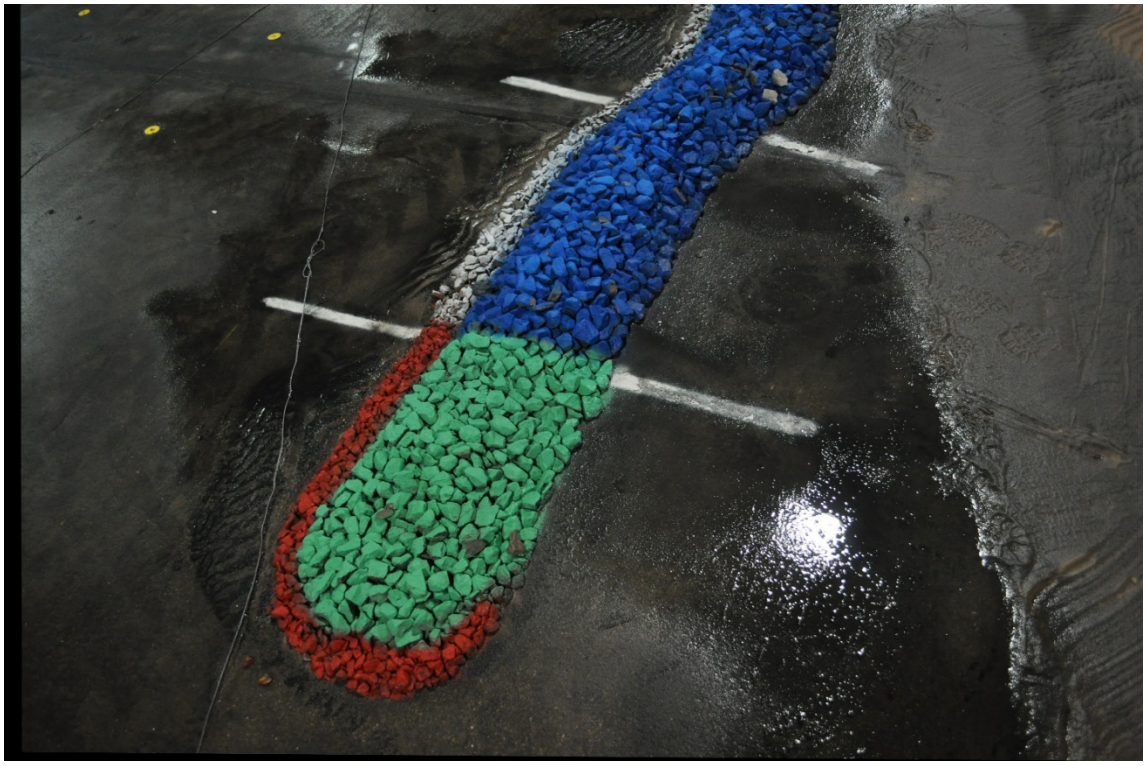

Figure D.106: Post Test Part 02 (WC_HIGH_WL_SE) stability photograph for BW3-2, position 5

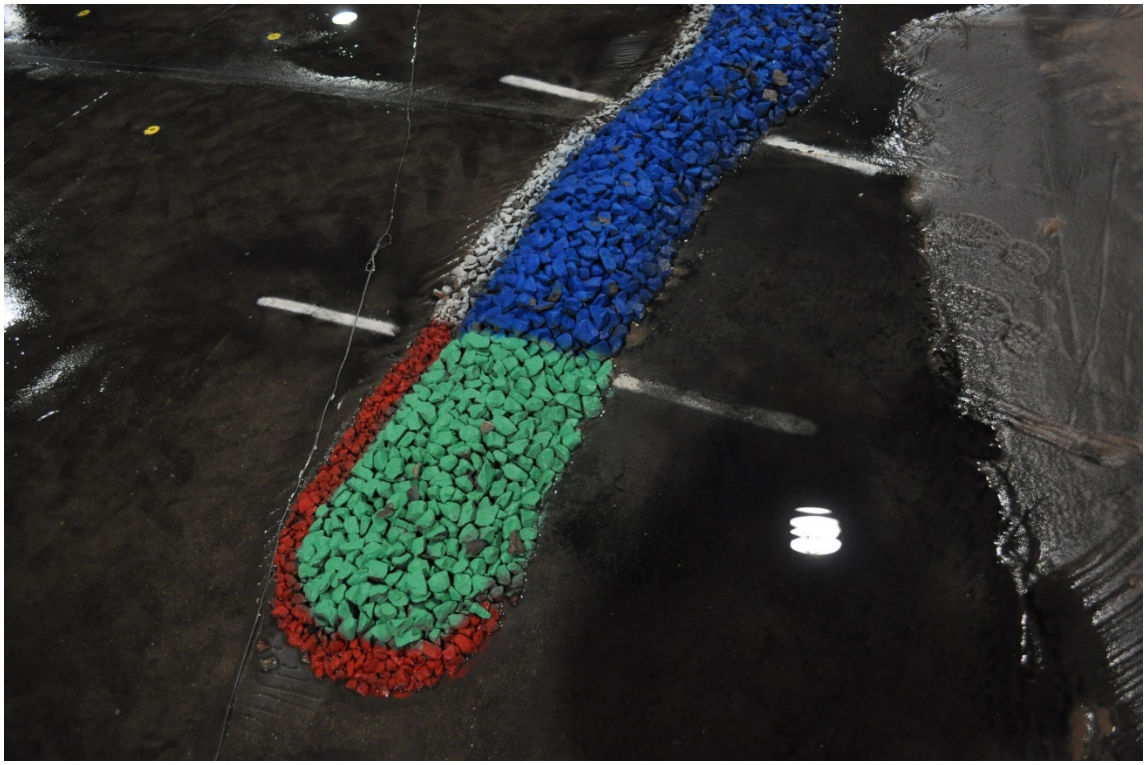

Figure D.107: Post Test Part 03 (WC_LOW_WL) stability photograph for BW3-2, position 5

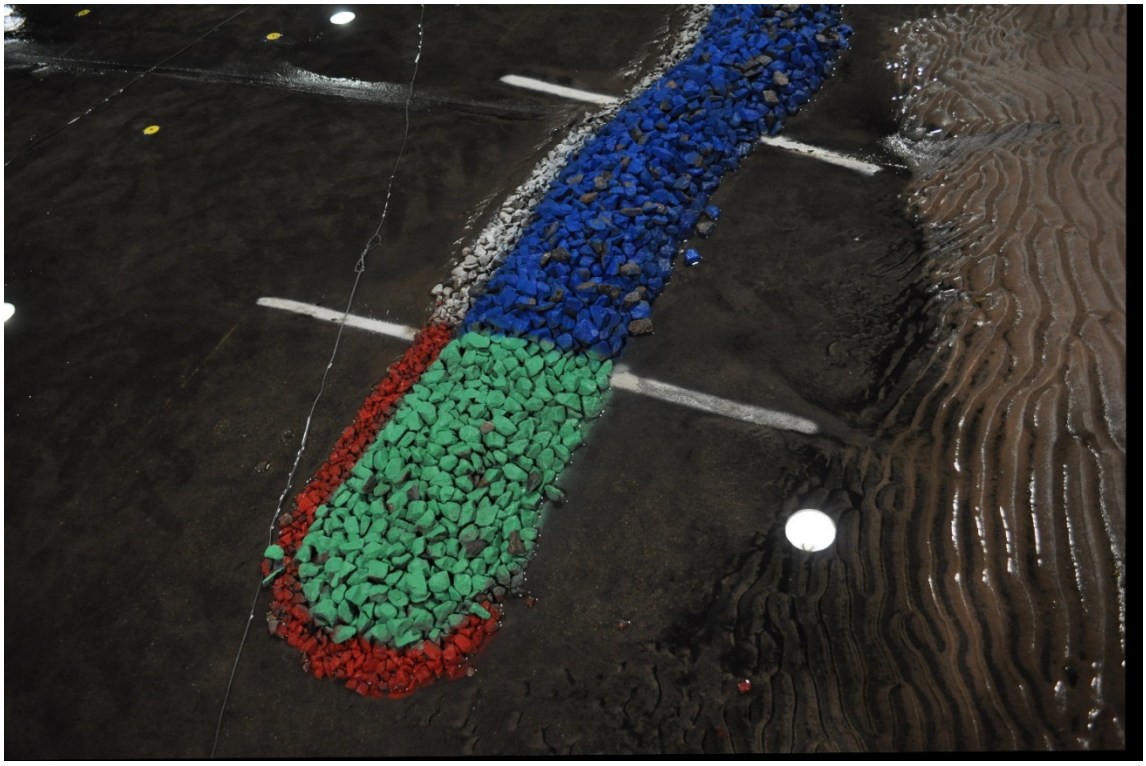

Figure D.108: Post Test Part 04 (WC_HIGH_WL) stability photograph for BW3-2, position 5

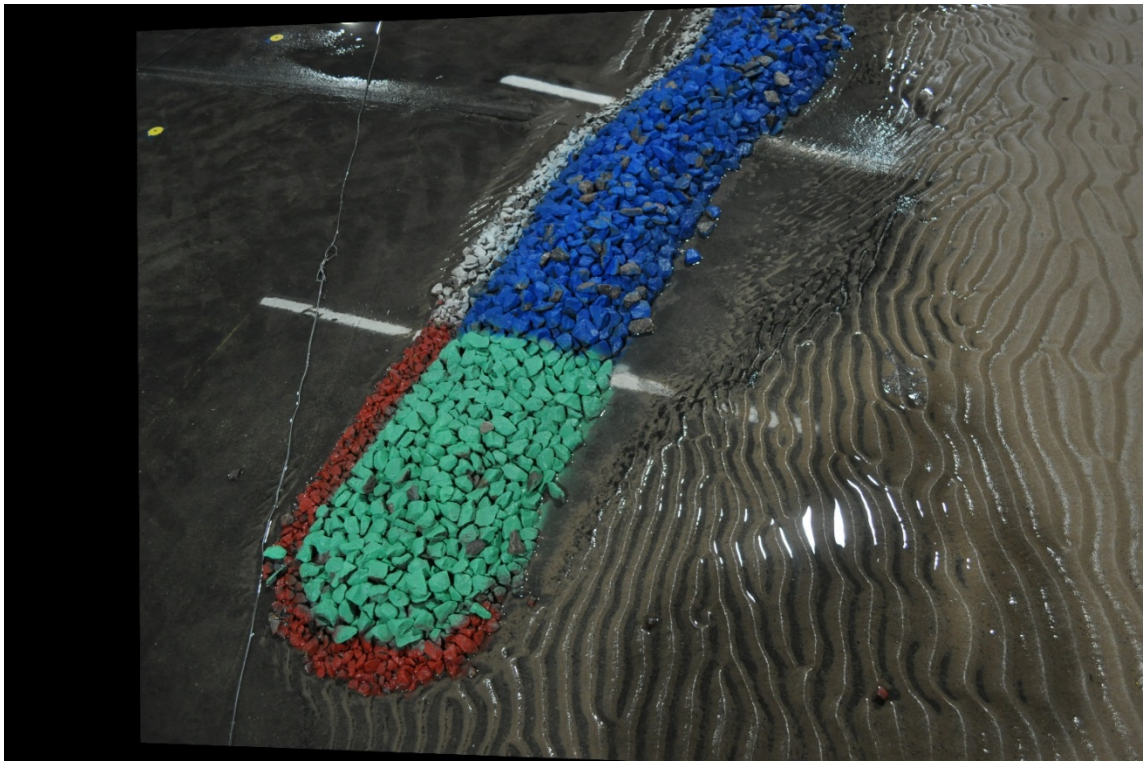

Figure D.109: Post Test Part 05 (WC_EXT_WL_01) stability photograph for BW3-2, position 5

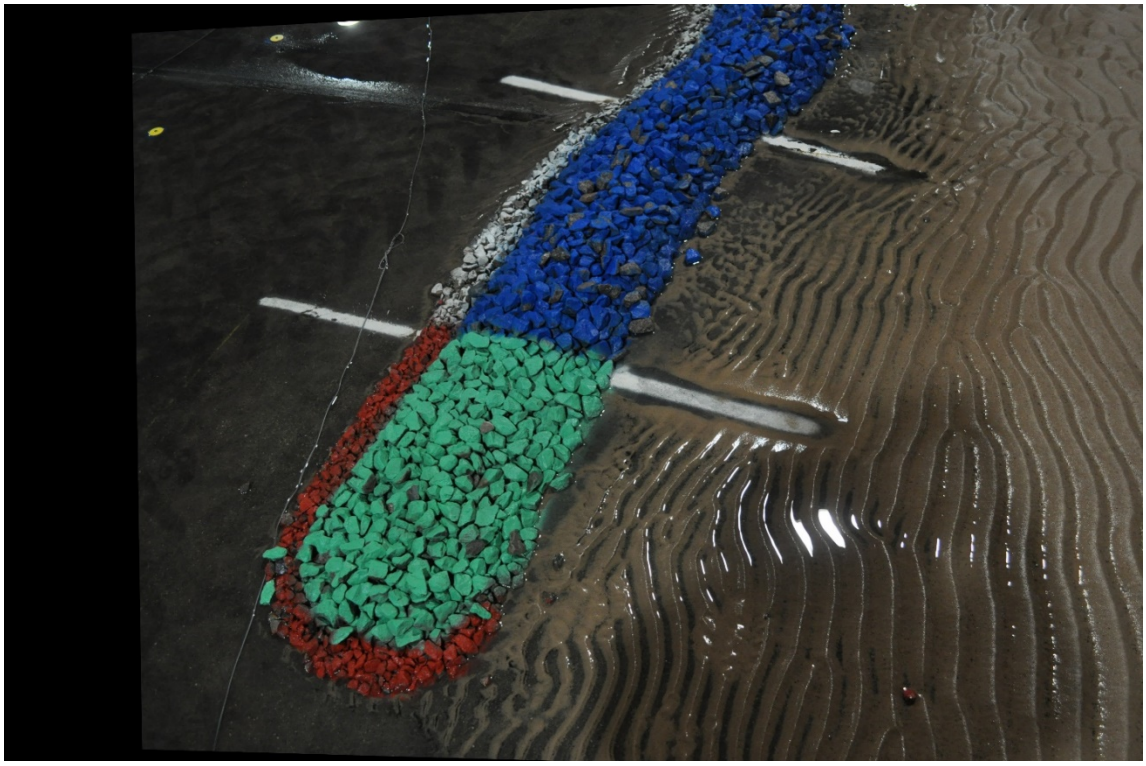

Figure D.110: Post Test Part 06 (WC_EXT_WL_02) stability photograph for BW3-2, position 5

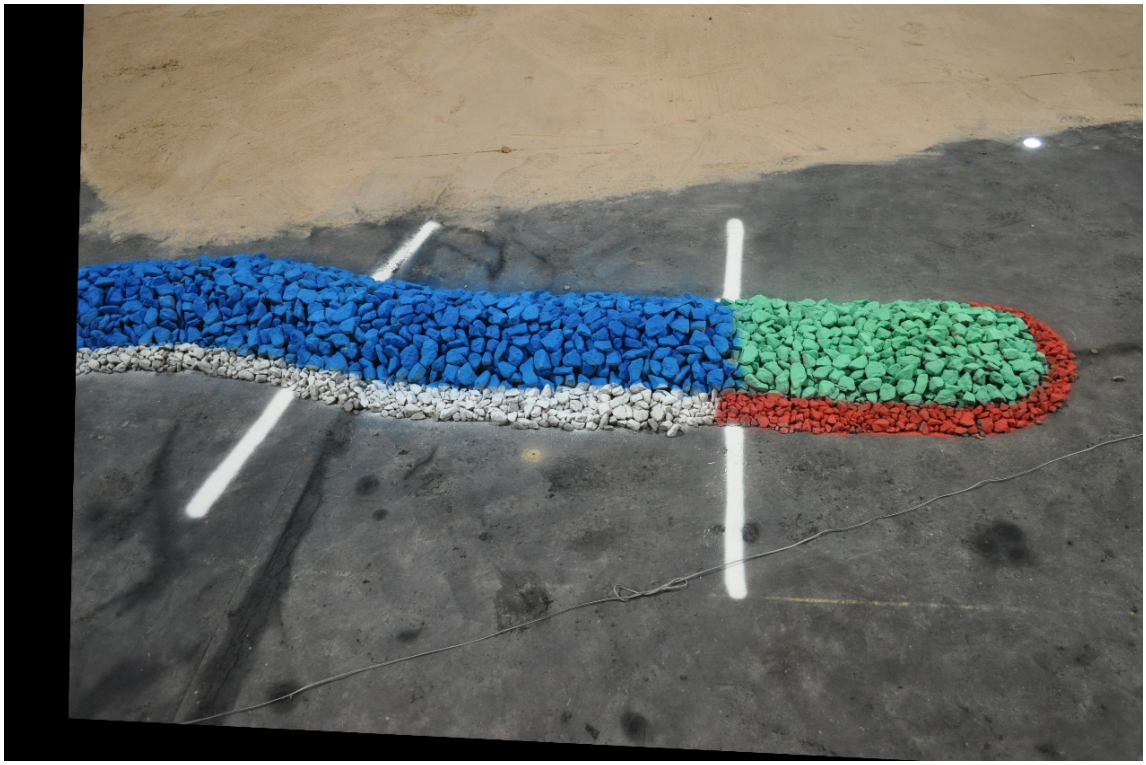

Figure D.111: Pre-test stability photograph for BW3-2, position 6

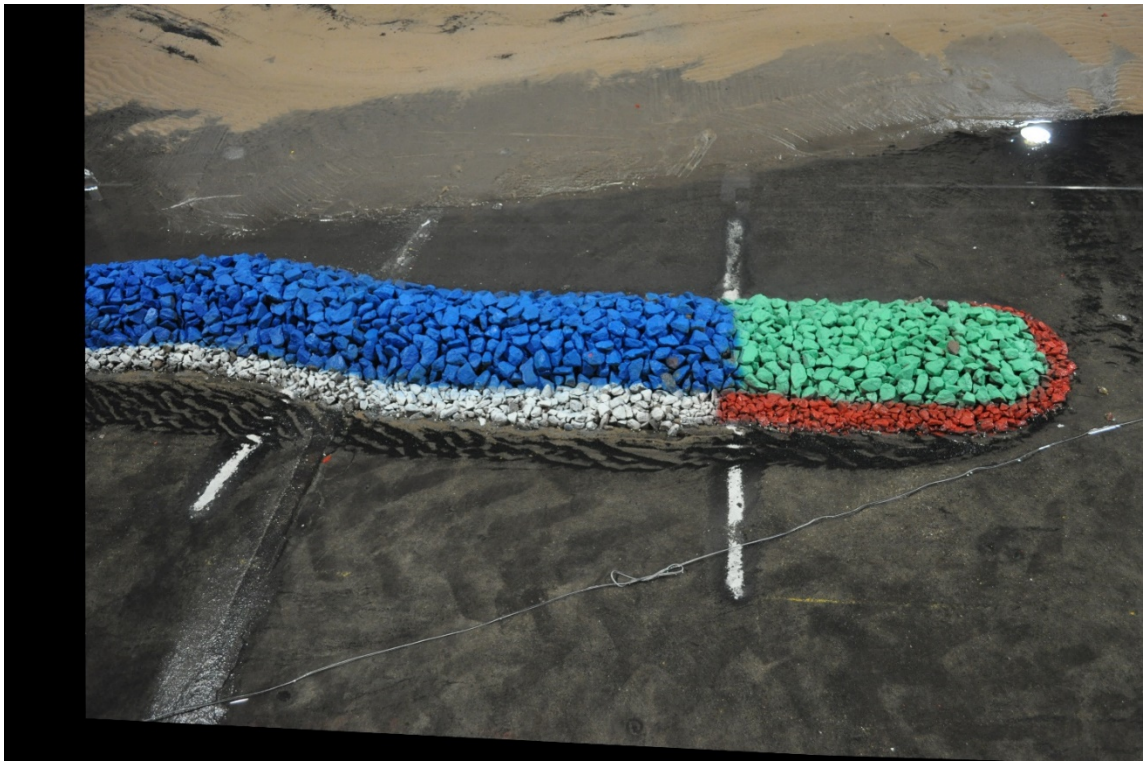

Figure D.112: Post Test Part 01 (WC_LOW_WL_SE) stability photograph for BW3-2, position 6

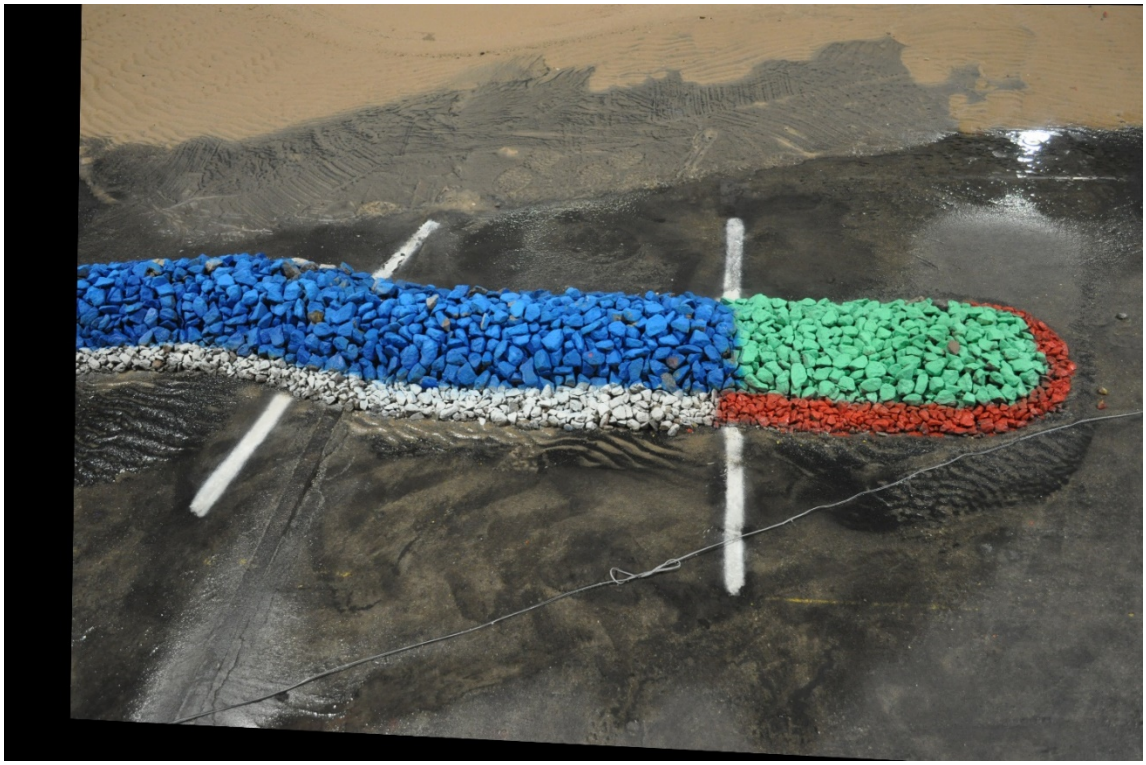

Figure D.113: Post Test Part 02 (WC_HIGH_WL_SE) stability photograph for BW3-2, position 6

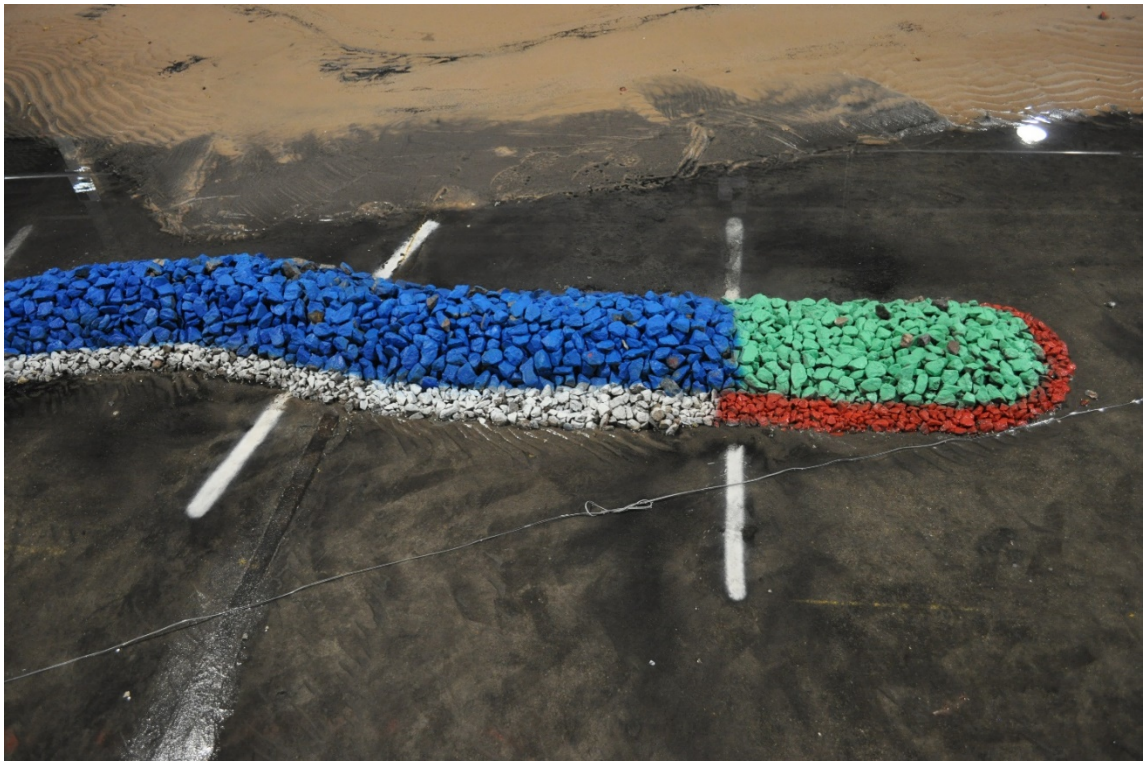

Figure D.114: Post Test Part 03 (WC_LOW_WL) stability photograph for BW3-2, position 6

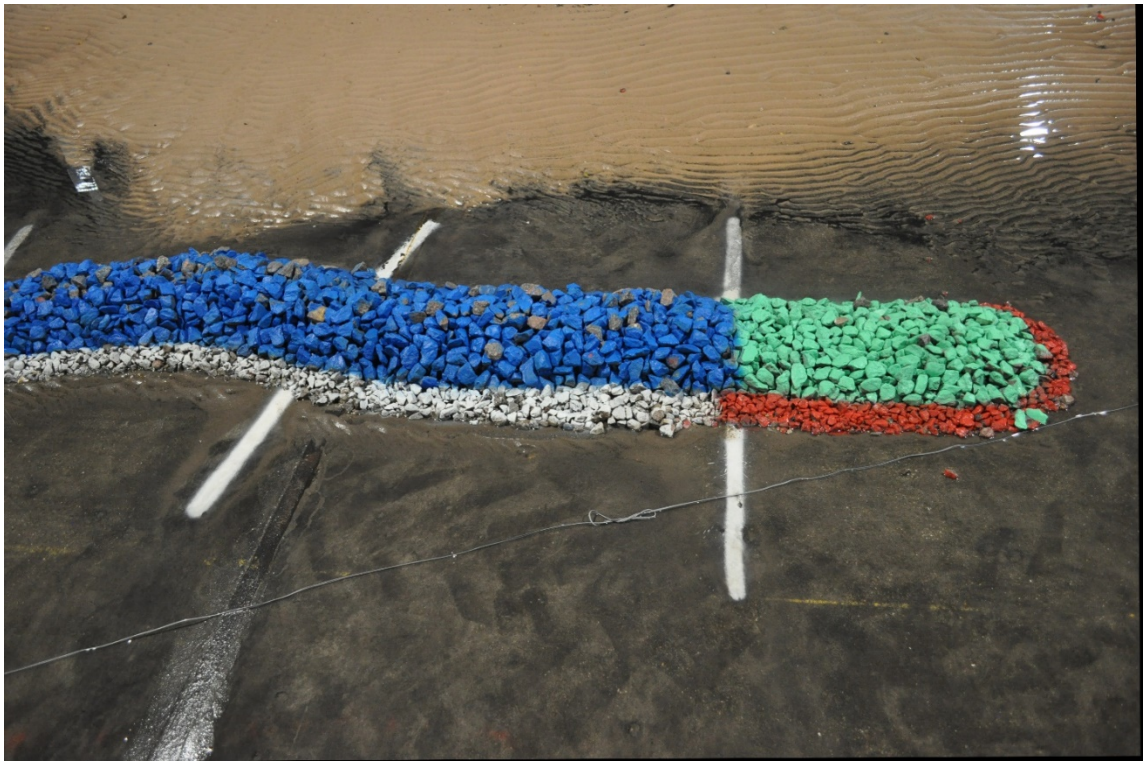

Figure D.115: Post Test Part 04 (WC_HIGH_WL) stability photograph for BW3-2, position 6

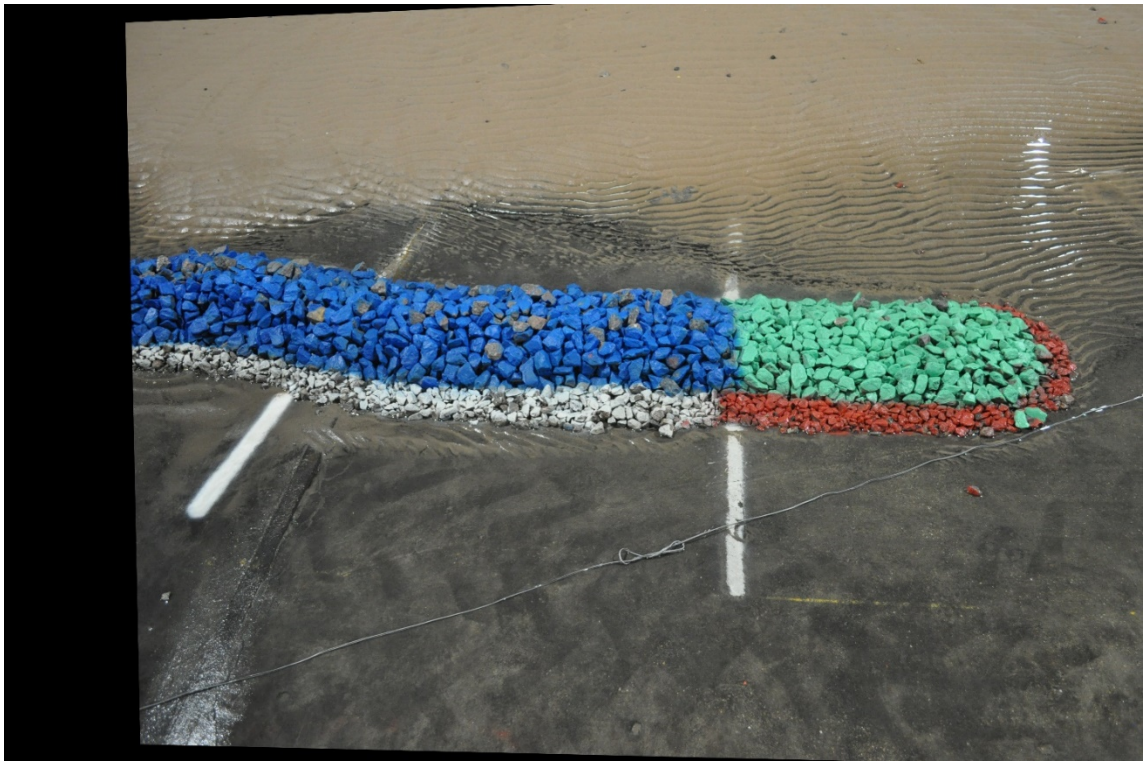

Figure D.116: Post Test Part 05 (WC_EXT_WL_01) stability photograph for BW3-2, position 6

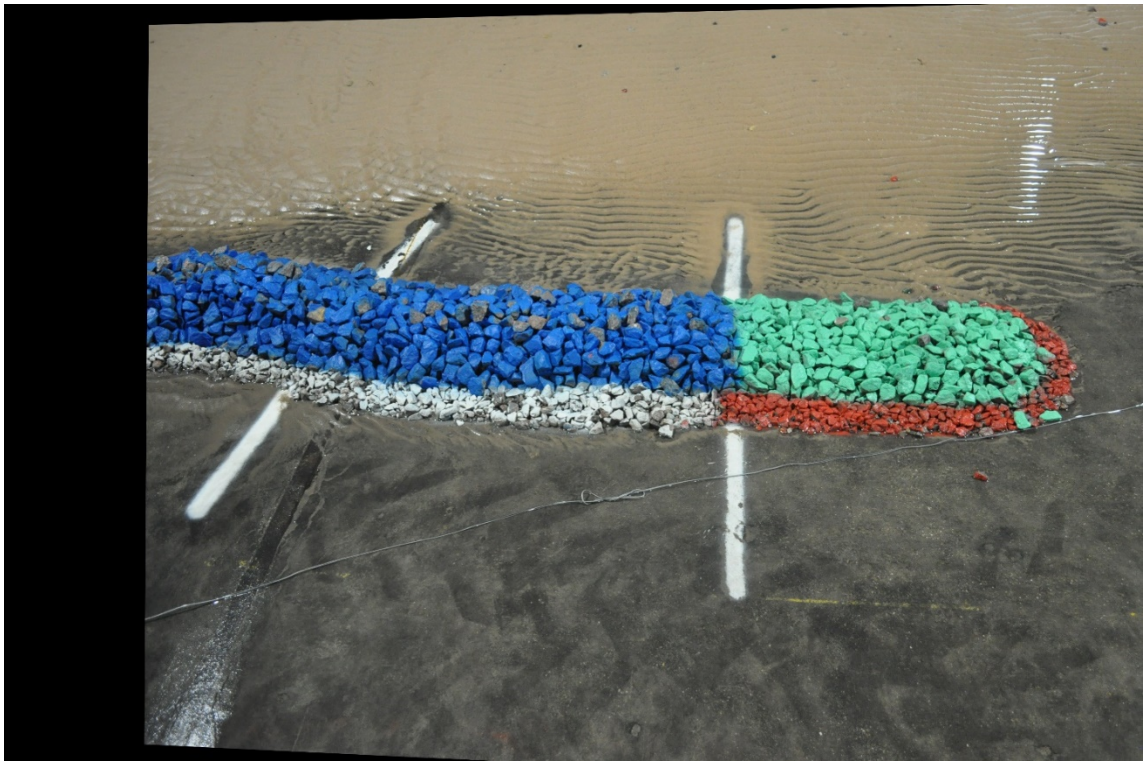

Figure D.117: Post Test Part 06 (WC_EXT_WL_02) stability photograph for BW3-2, position 6

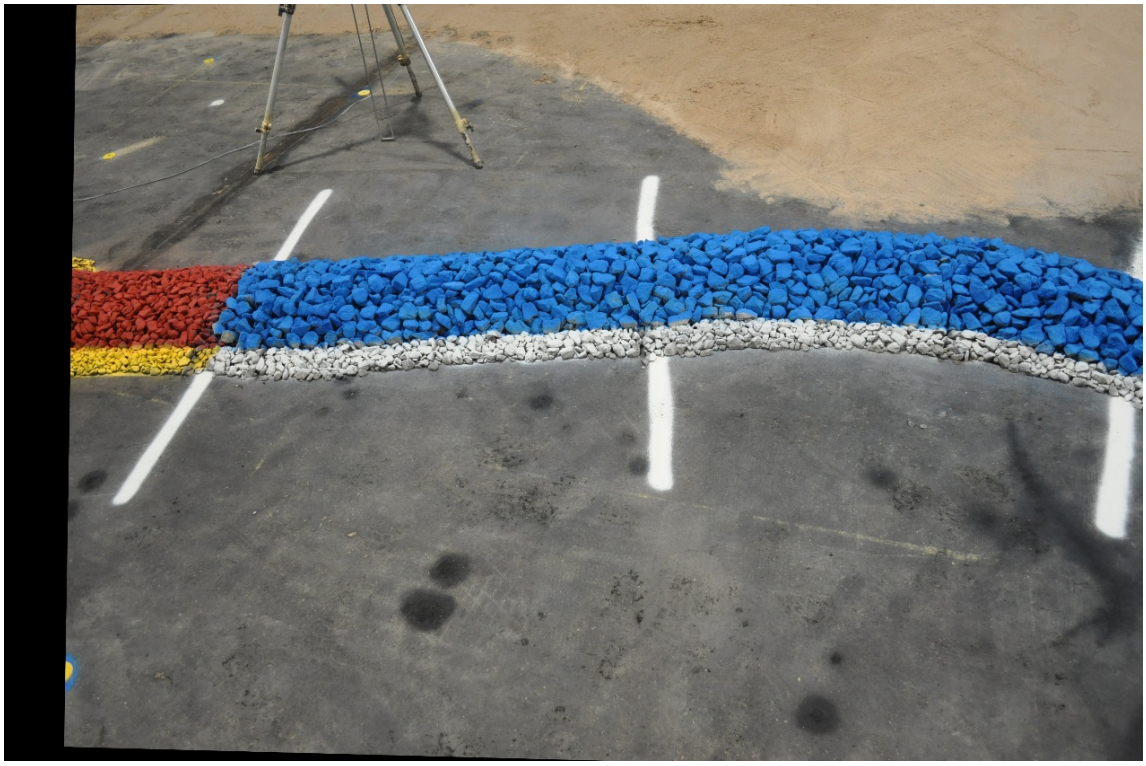

Figure D.118: Pre-test stability photograph for BW3-2, position 7

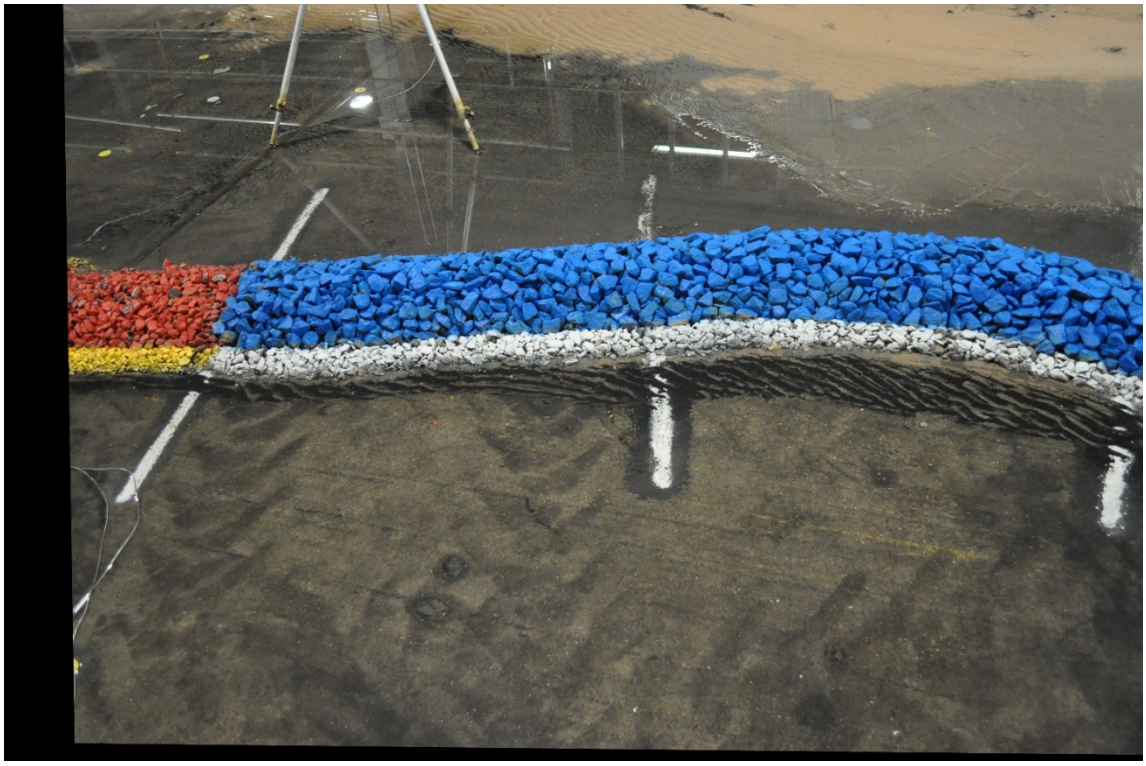

Figure D.119: Post Test Part 01 (WC_LOW_WL_SE) stability photograph for BW3-2, position 7

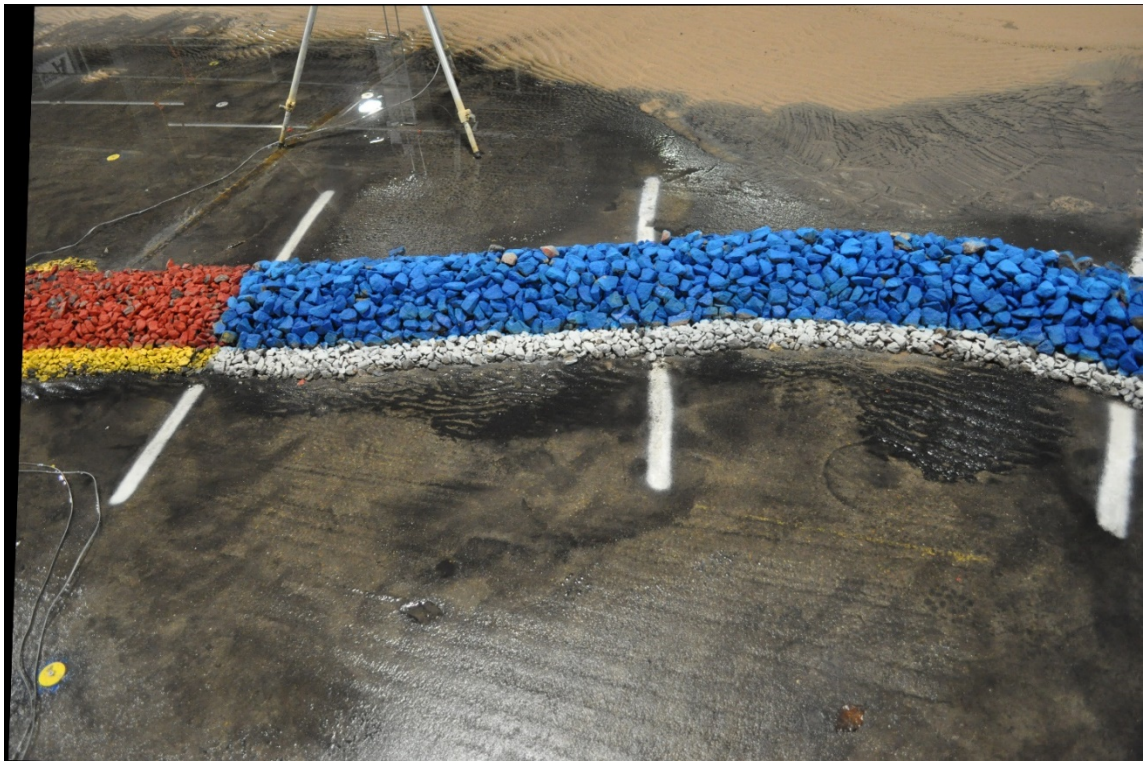

Figure D.120: Post Test Part 02 (WC_HIGH_WL_SE) stability photograph for BW3-2, position 7

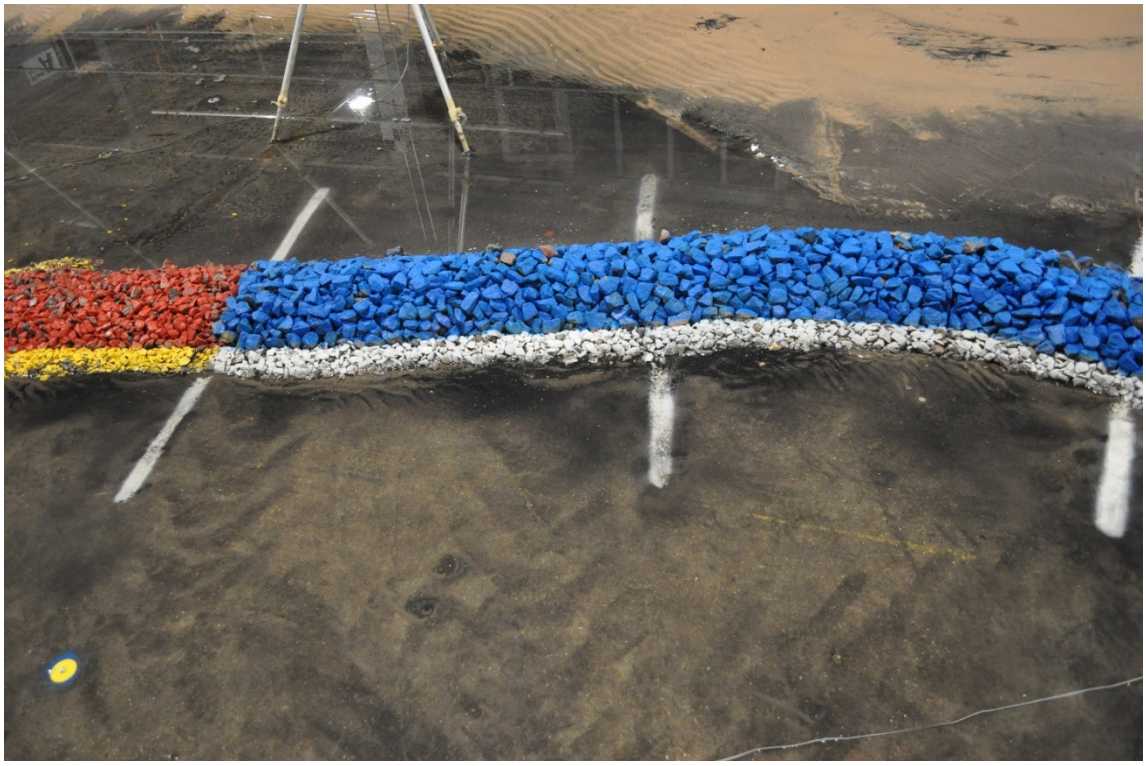

Figure D.121: Post Test Part 03 (WC_LOW_WL) stability photograph for BW3-2, position 7

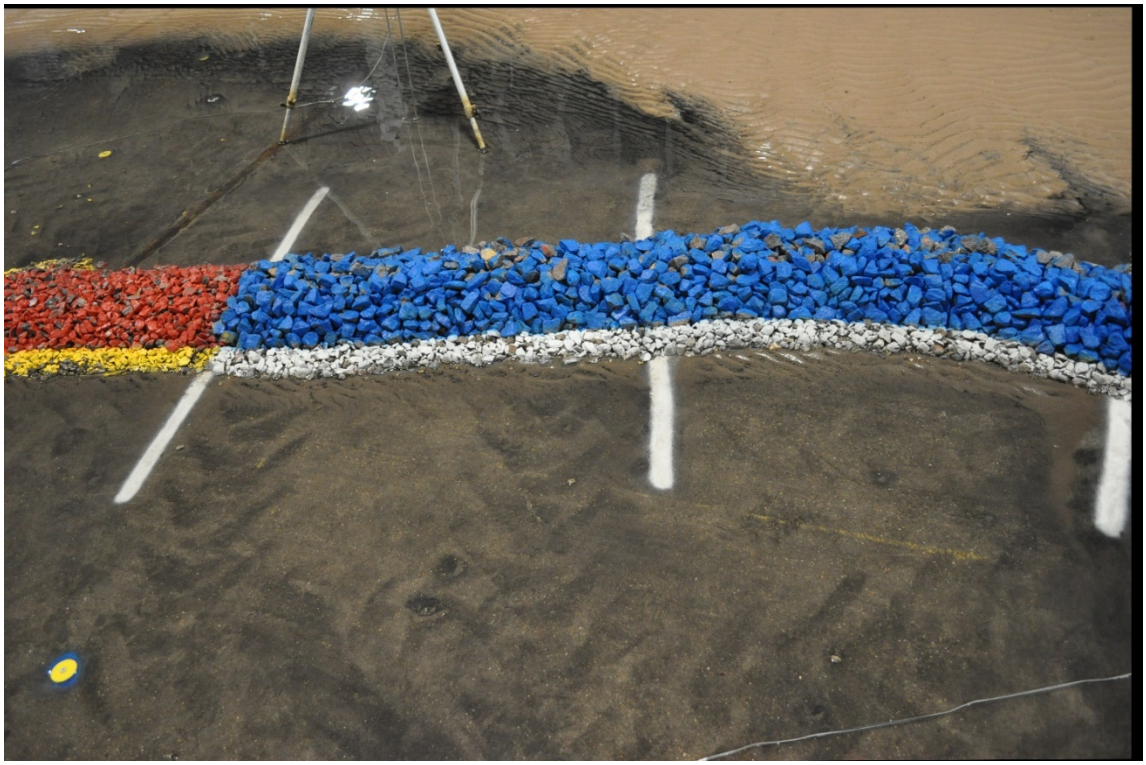

Figure D.122: Post Test Part 04 (WC_HIGH_WL) stability photograph for BW3-2, position 7

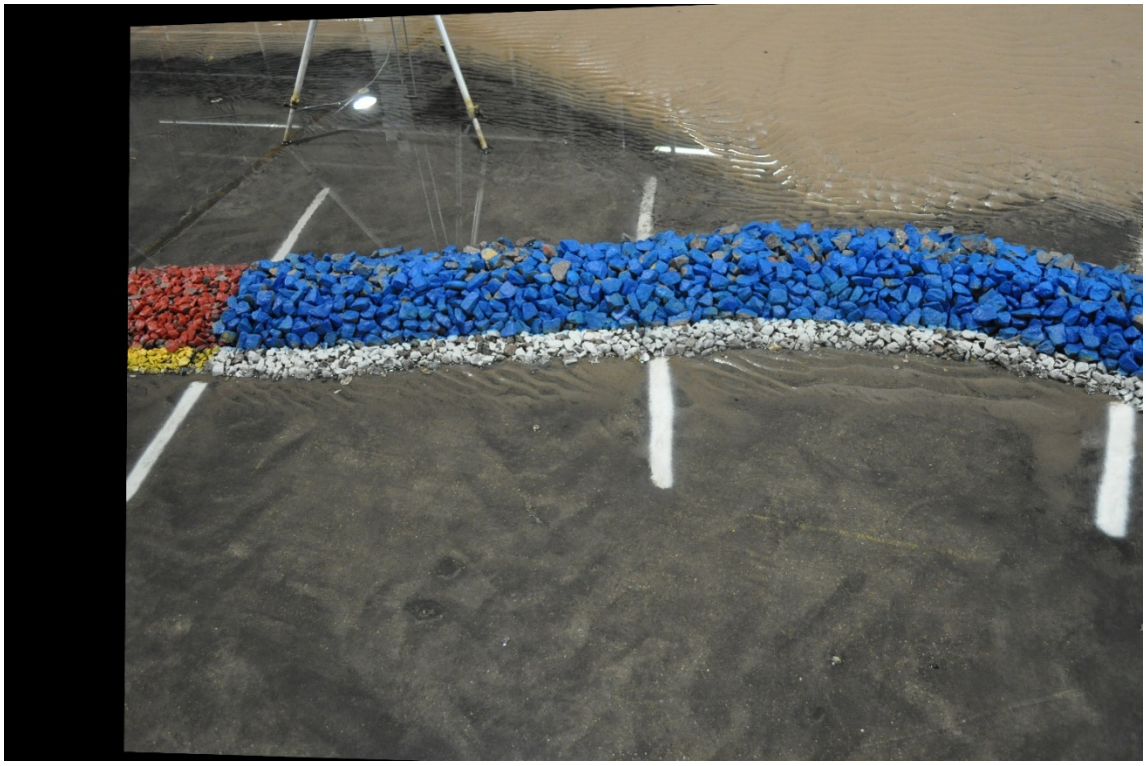

Figure D.123: Post Test Part 05 (WC_EXT_WL_01) stability photograph for BW3-2, position 7

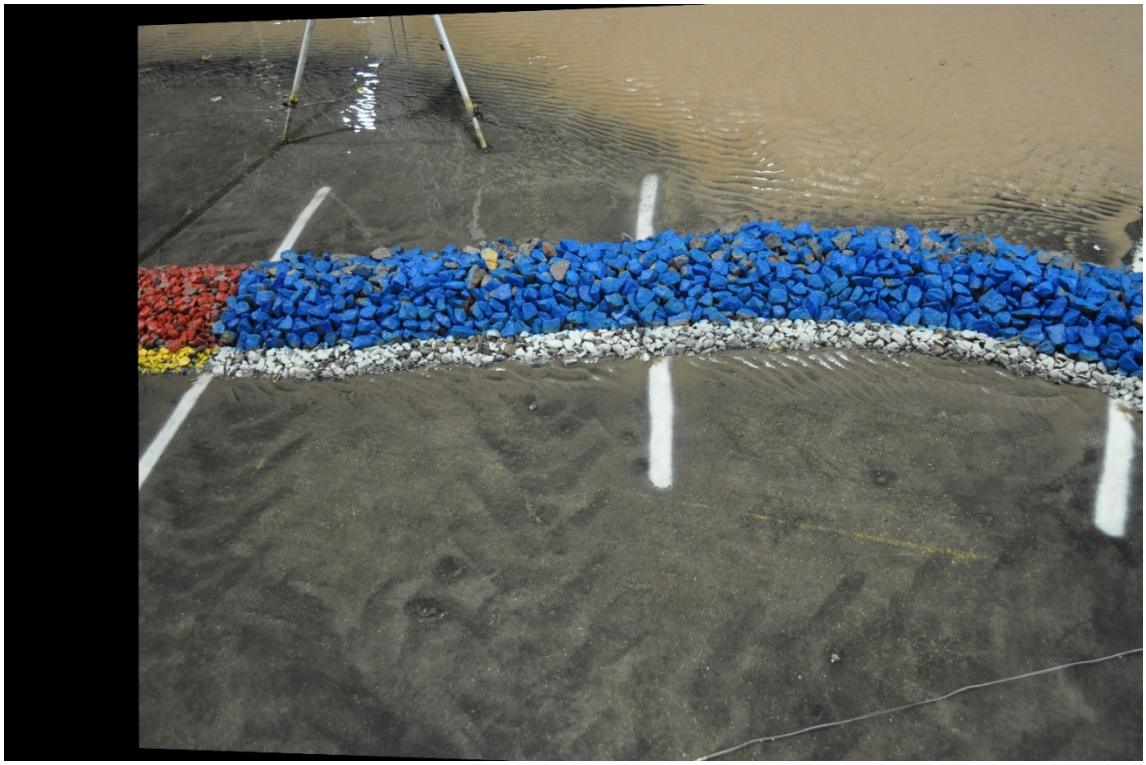

Figure D.124: Post Test Part 06 (WC_EXT_WL_02) stability photograph for BW3-2, position 7

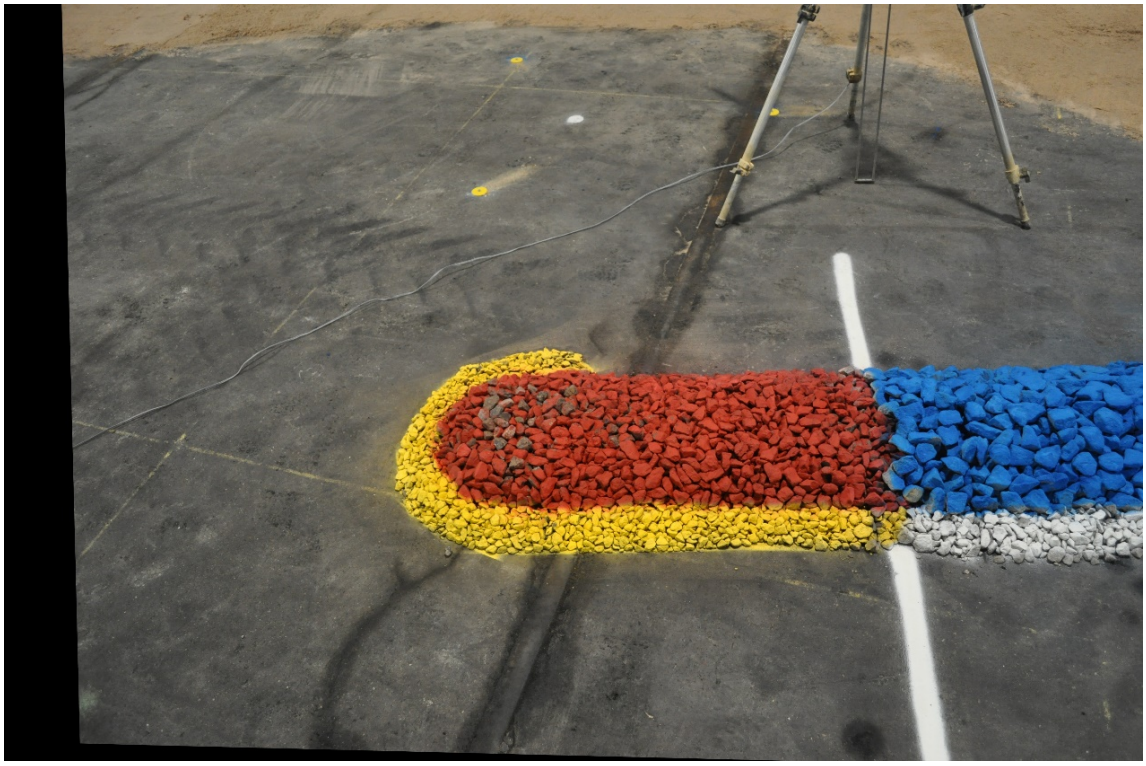

Figure D.125: Pre-test stability photograph for BW3-2, position 8

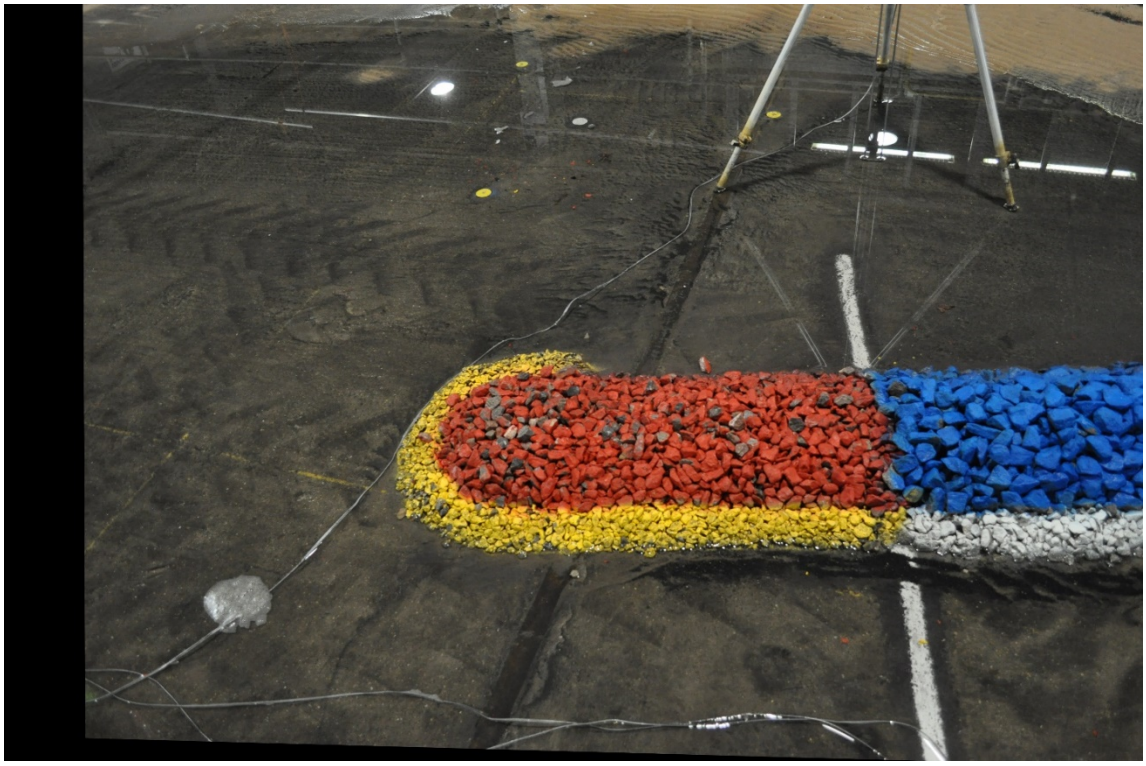

Figure D.126: Post Test Part 01 (WC_LOW_WL_SE) stability photograph for BW3-2, position 8

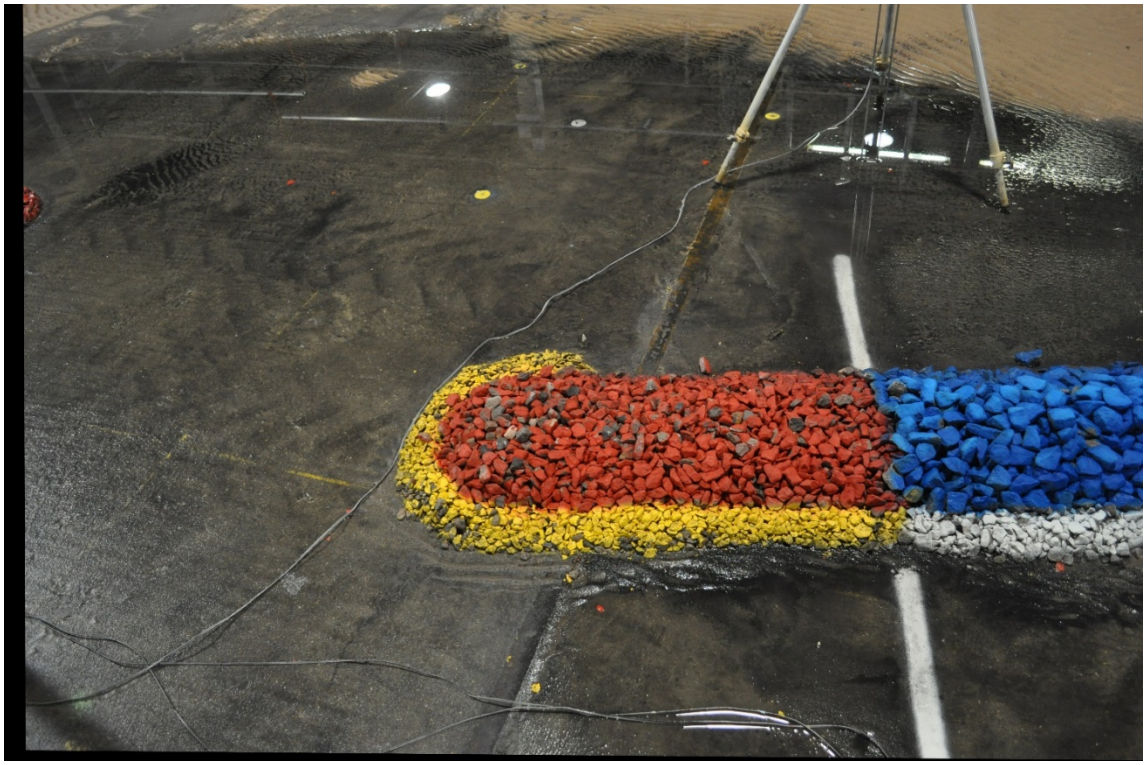

Figure D.127: Post Test Part 02 (WC_HIGH_WL_SE) stability photograph for BW3-2, position 8

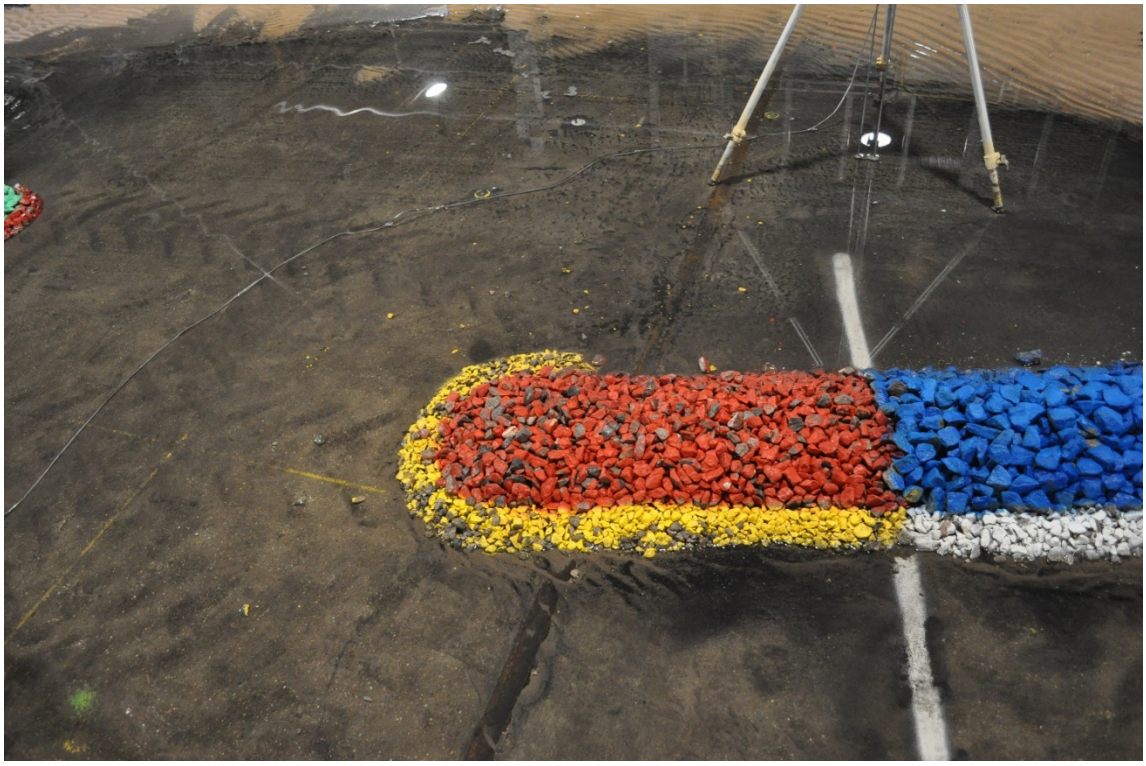

Figure D.128: Post Test Part 03 (WC_LOW_WL) stability photograph for BW3-2, position 8

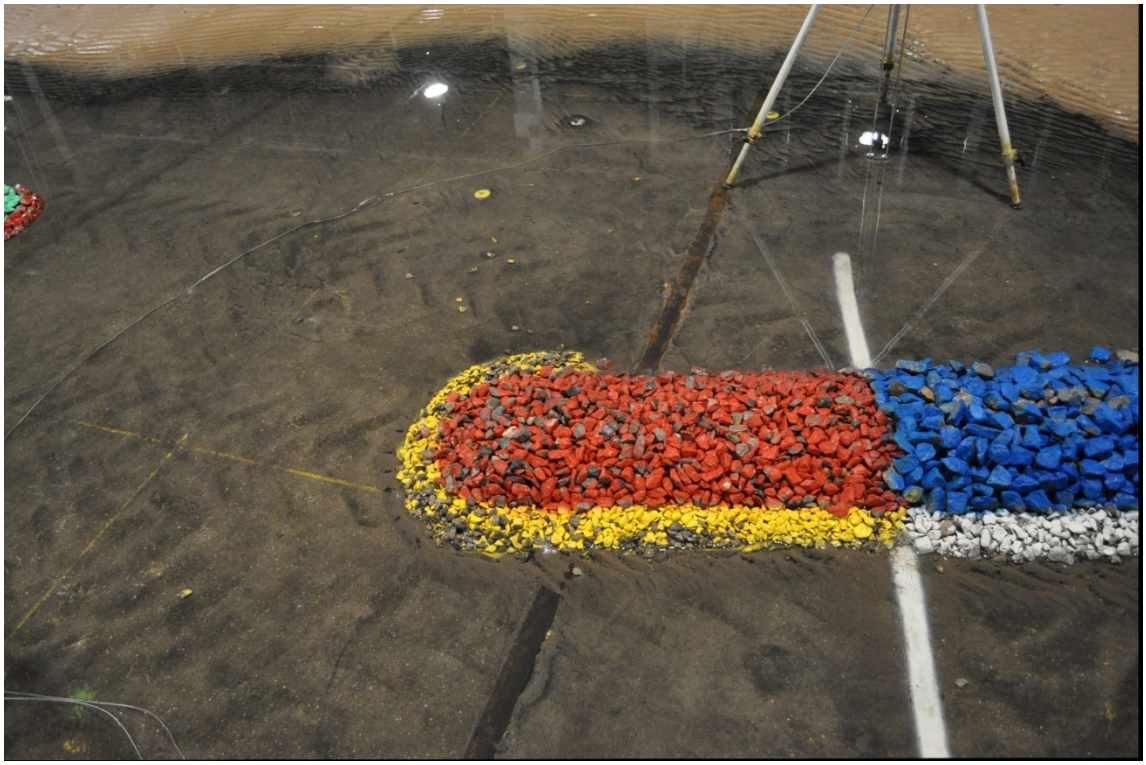

Figure D.129: Post Test Part 04 (WC_HIGH_WL) stability photograph for BW3-2, position 8

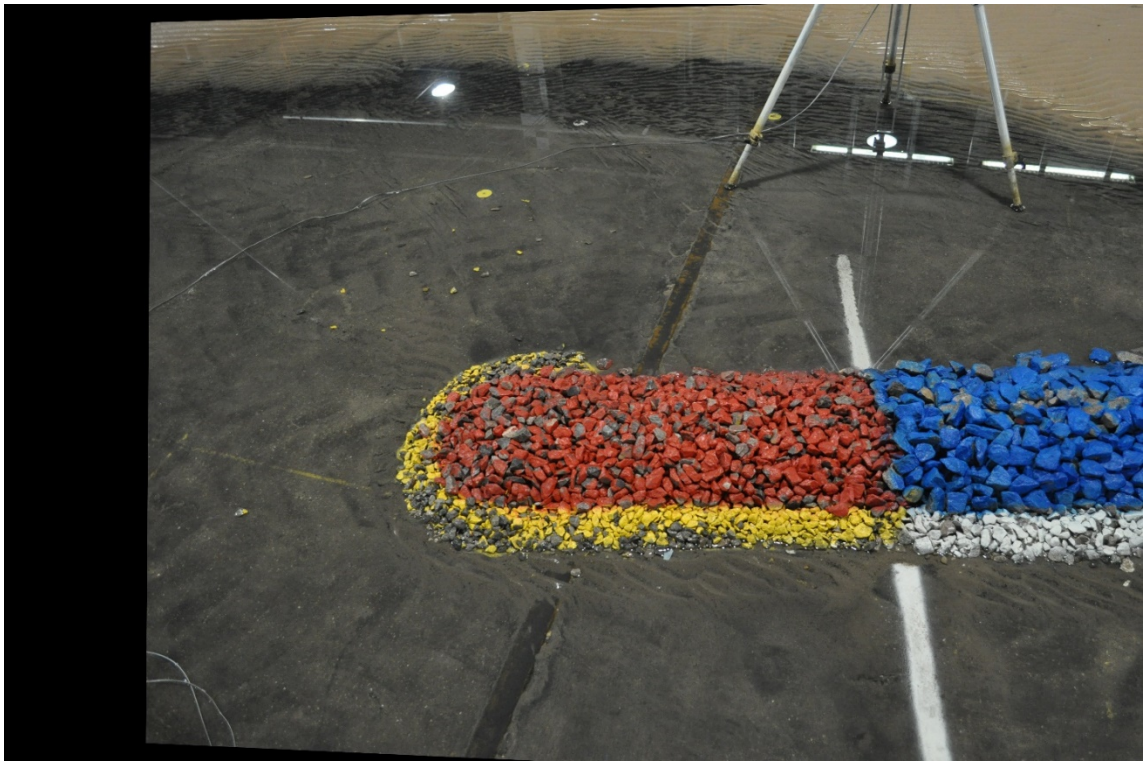

Figure D.130: Post Test Part 05 (WC_EXT_WL_01) stability photograph for BW3-2, position 8

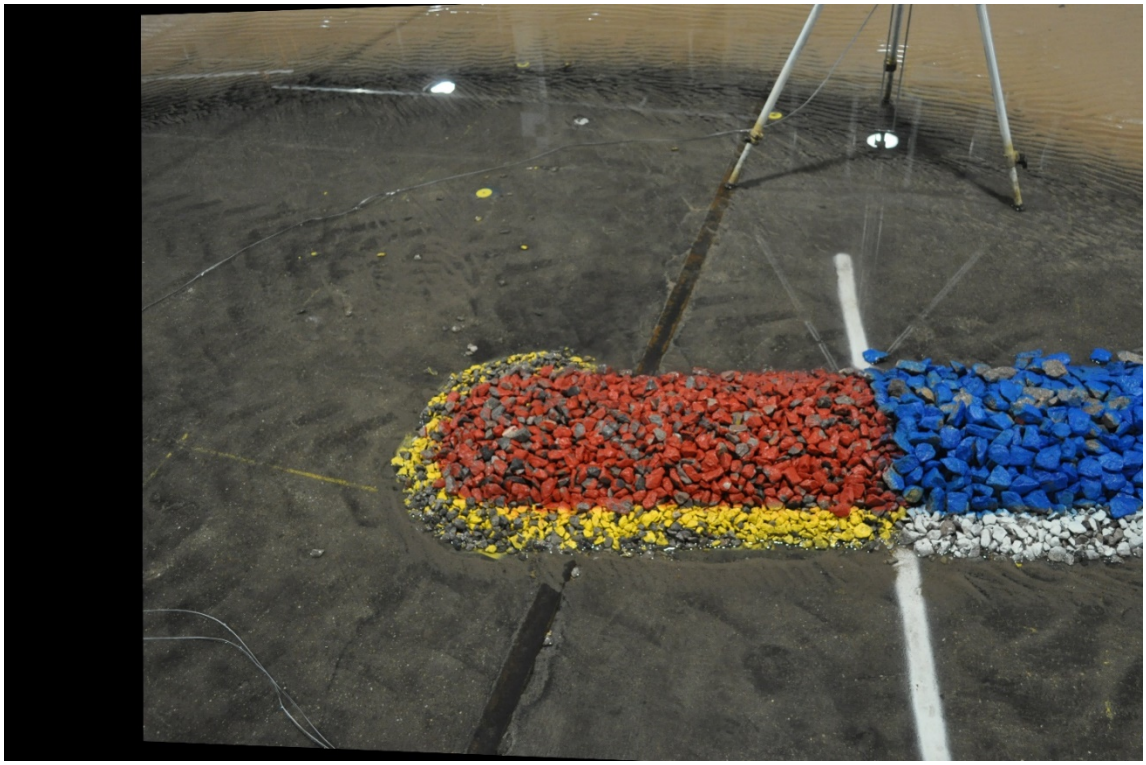

Figure D.131: Post Test Part 06 (WC_EXT_WL_02) stability photograph for BW3-2, position 8

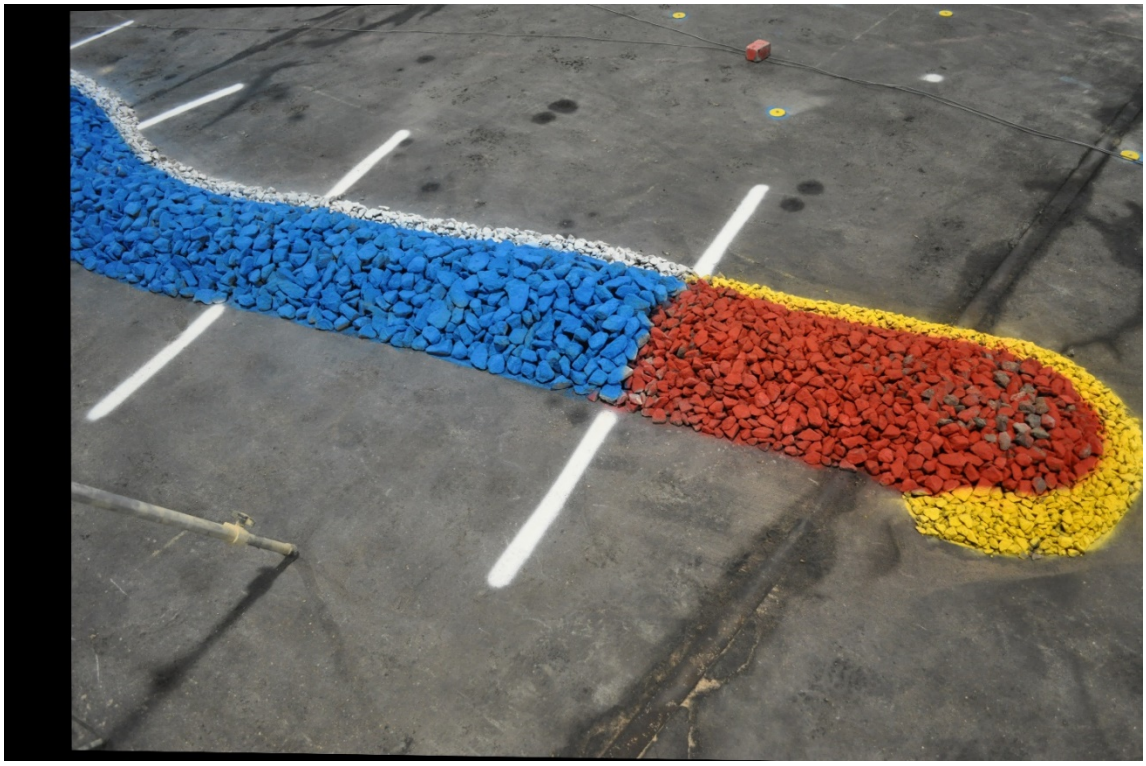

Figure D.132: Pre-test stability photograph for BW3-2, position 9

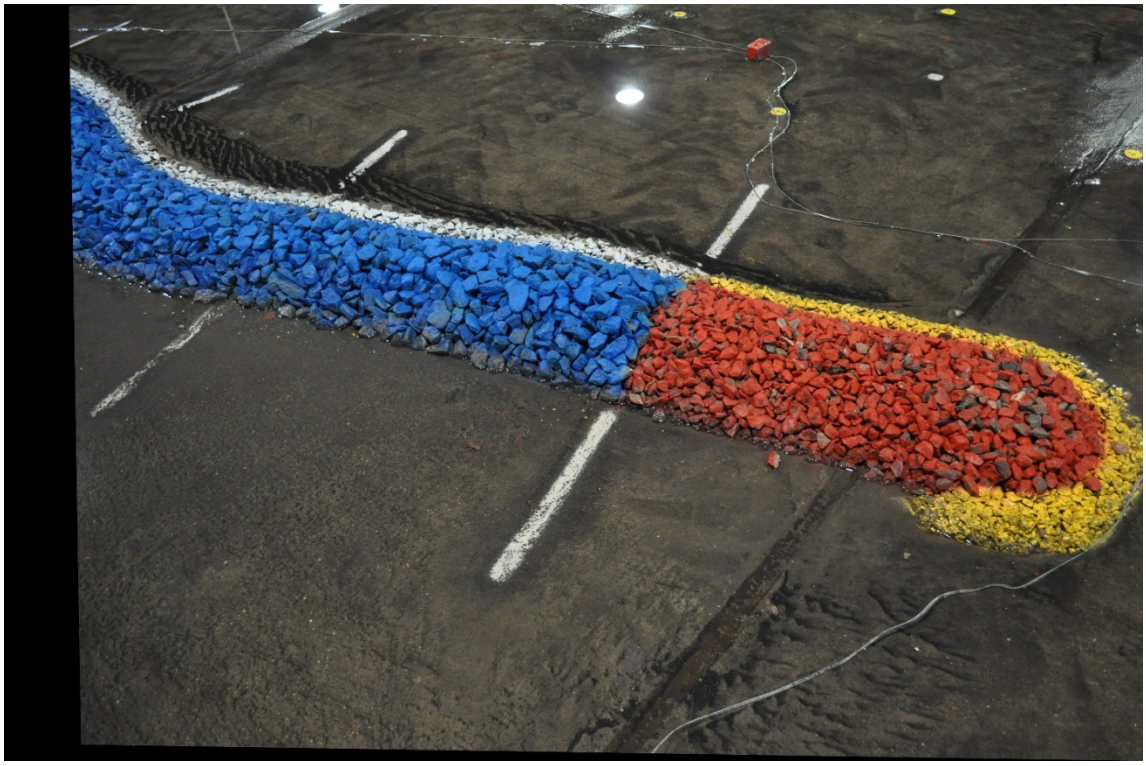

Figure D.133: Post Test Part 01 (WC_LOW_WL_SE) stability photograph for BW3-2, position 9

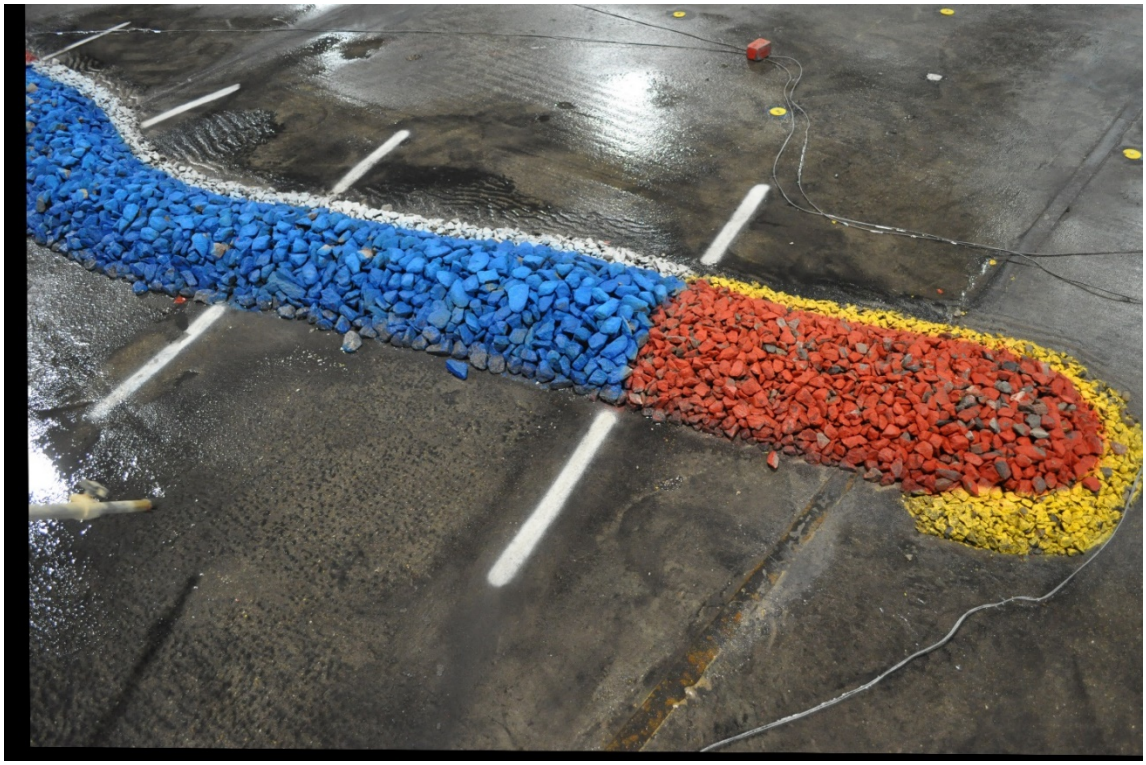

Figure D.134: Post Test Part 02 (WC_HIGH_WL_SE) stability photograph for BW3-2, position 9

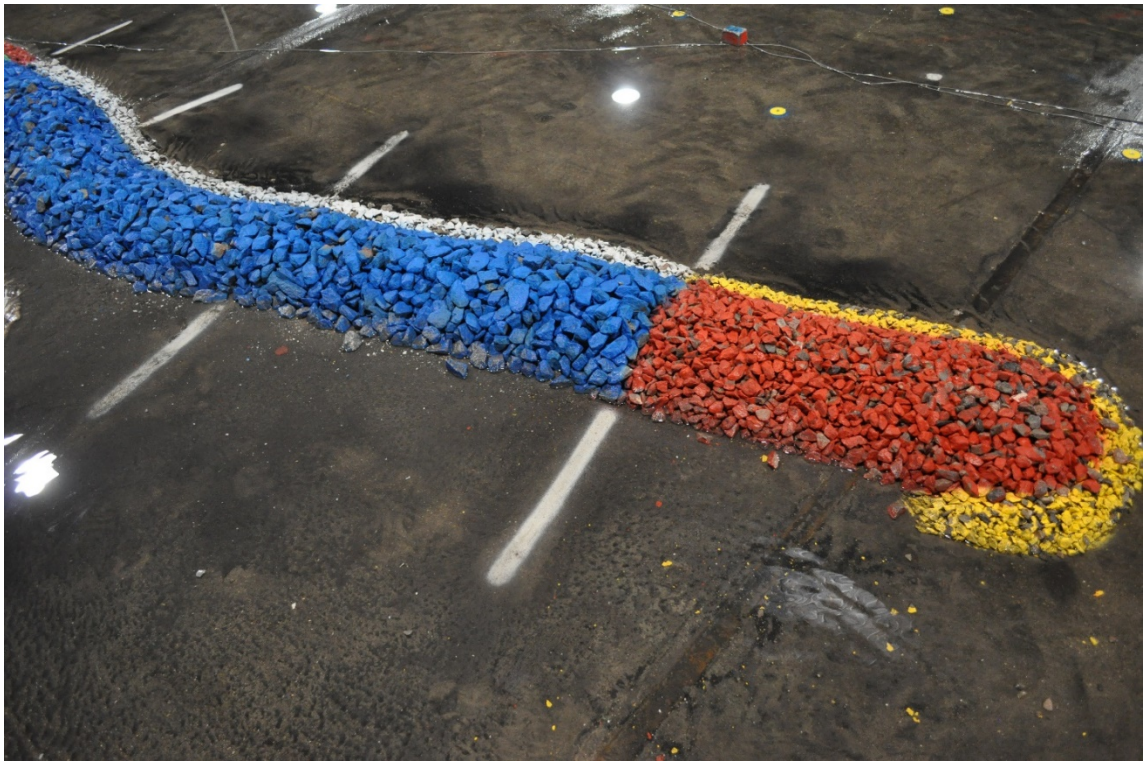

Figure D.135: Post Test Part 03 (WC_LOW_WL) stability photograph for BW3-2, position 9

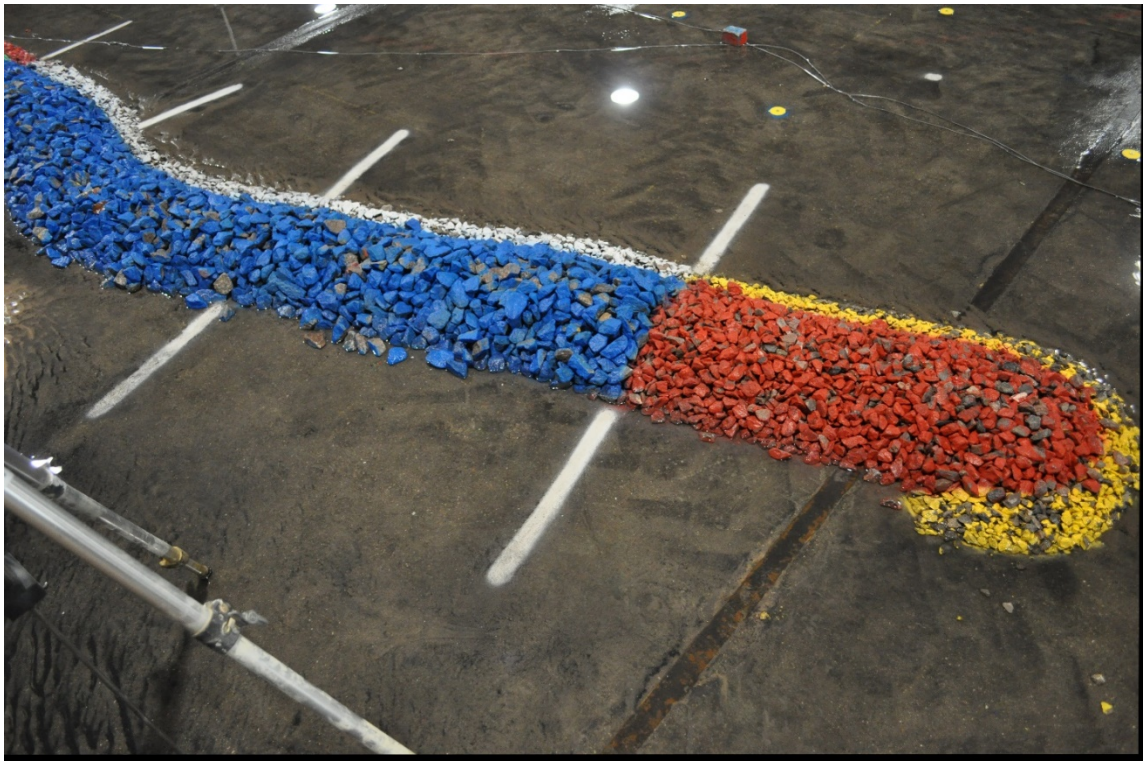

Figure D.136: Post Test Part 04 (WC_HIGH_WL) stability photograph for BW3-2, position 9

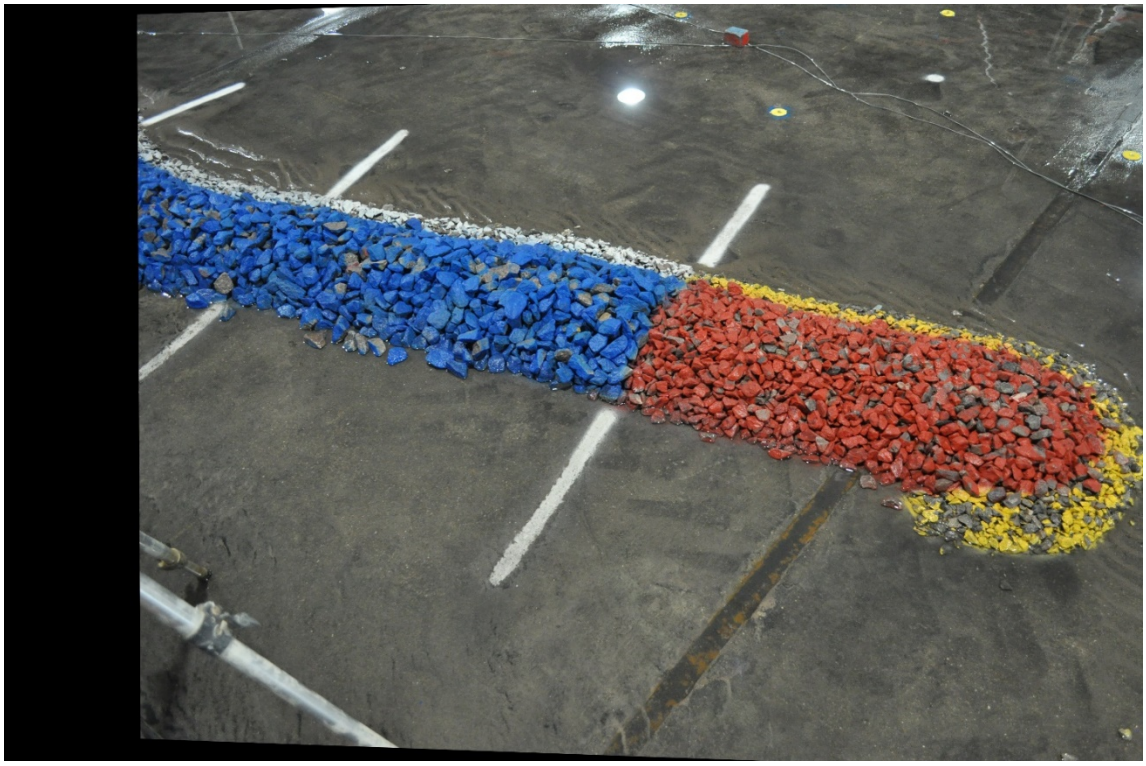

Figure D.137: Post Test Part 05 (WC_EXT_WL_01) stability photograph for BW3-2, position 9

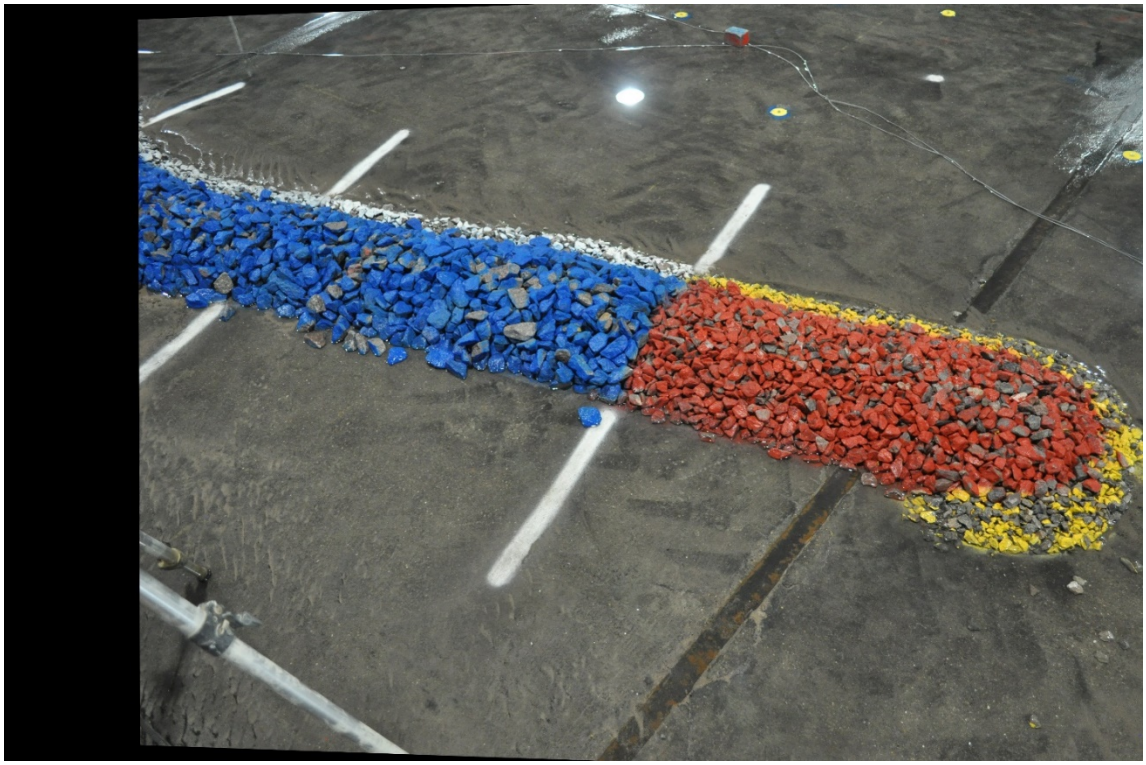

Figure D.138: Post Test Part 06 (WC_EXT_WL_02) stability photograph for BW3-2, position 9

## D.2.3. BW3-3

Figure D.139: Pre-test stability photograph for BW3-3, position 10

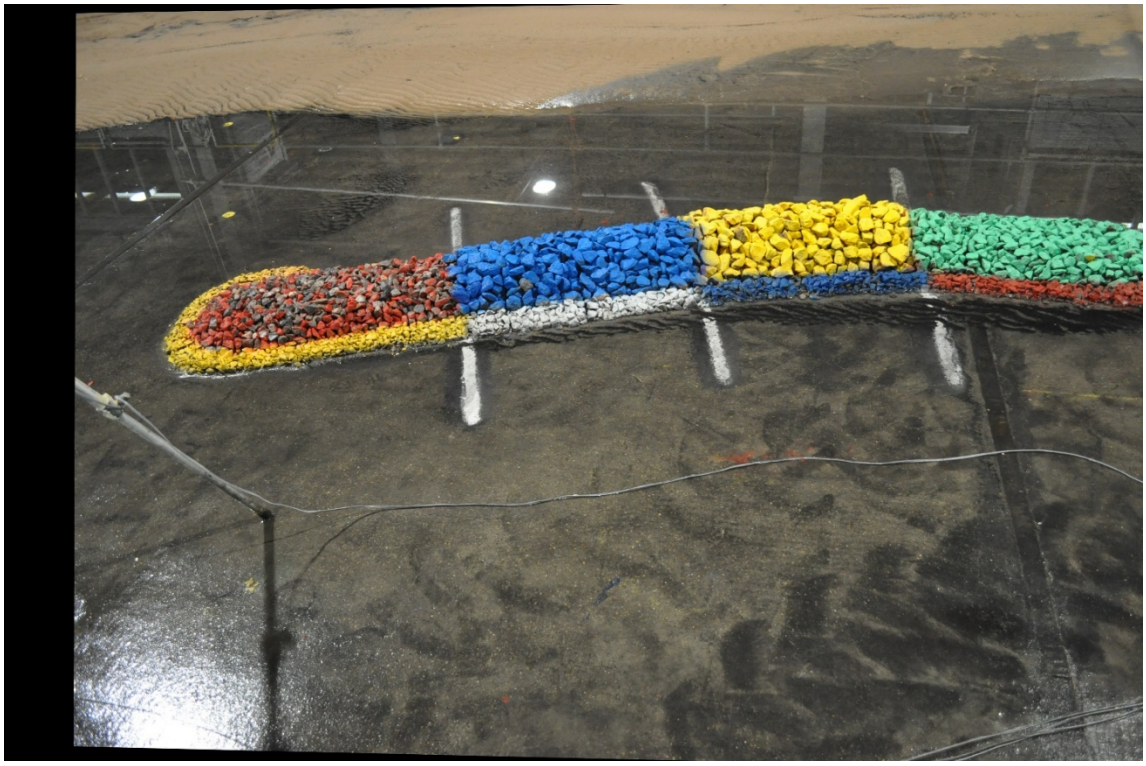

Figure D.140: Post Test Part 01 (WC_LOW_WL_SE) stability photograph for BW3-3, position 10

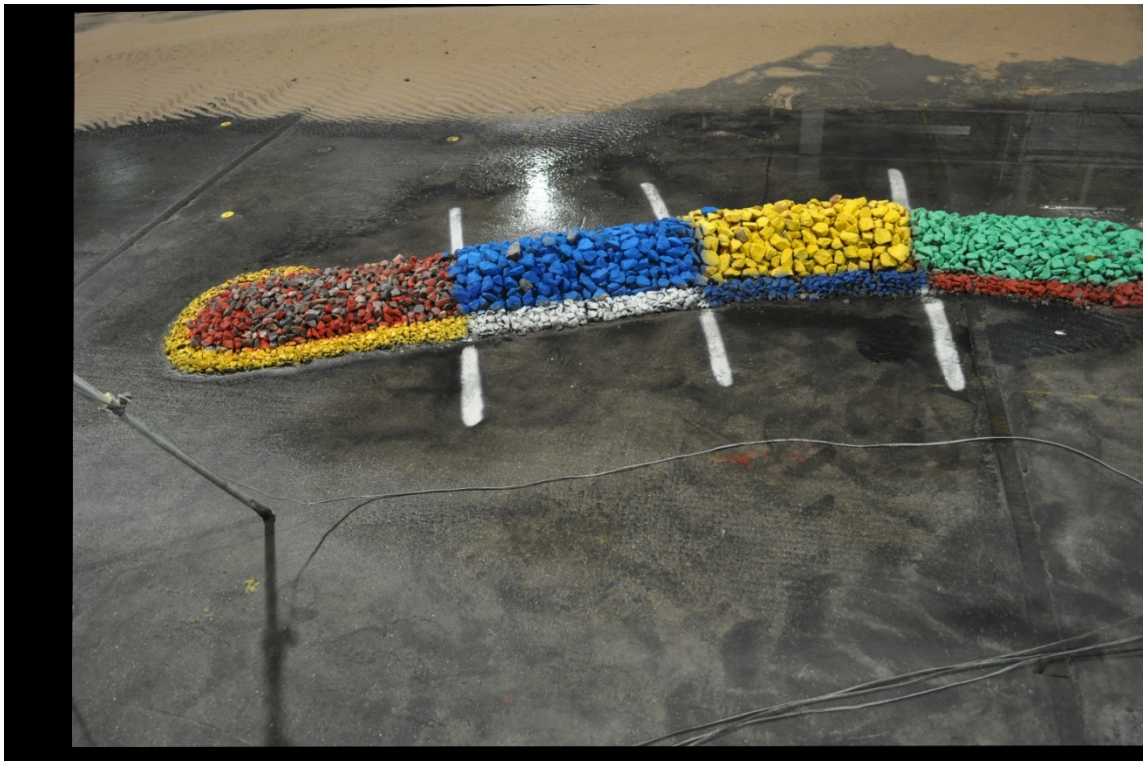

Figure D.141: Post Test Part 02 (WC_HIGH_WL_SE) stability photograph for BW3-3, position 10

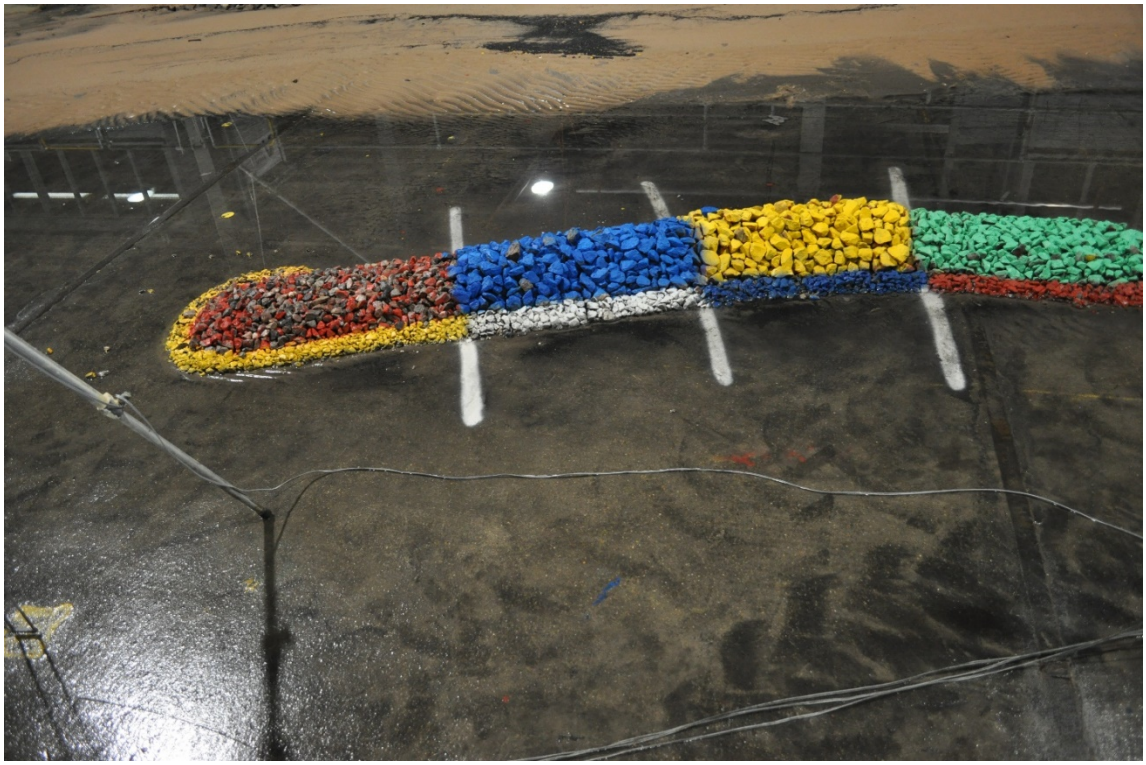

Figure D.142: Post Test Part 03 (WC_LOW_WL) stability photograph for BW3-3, position 10

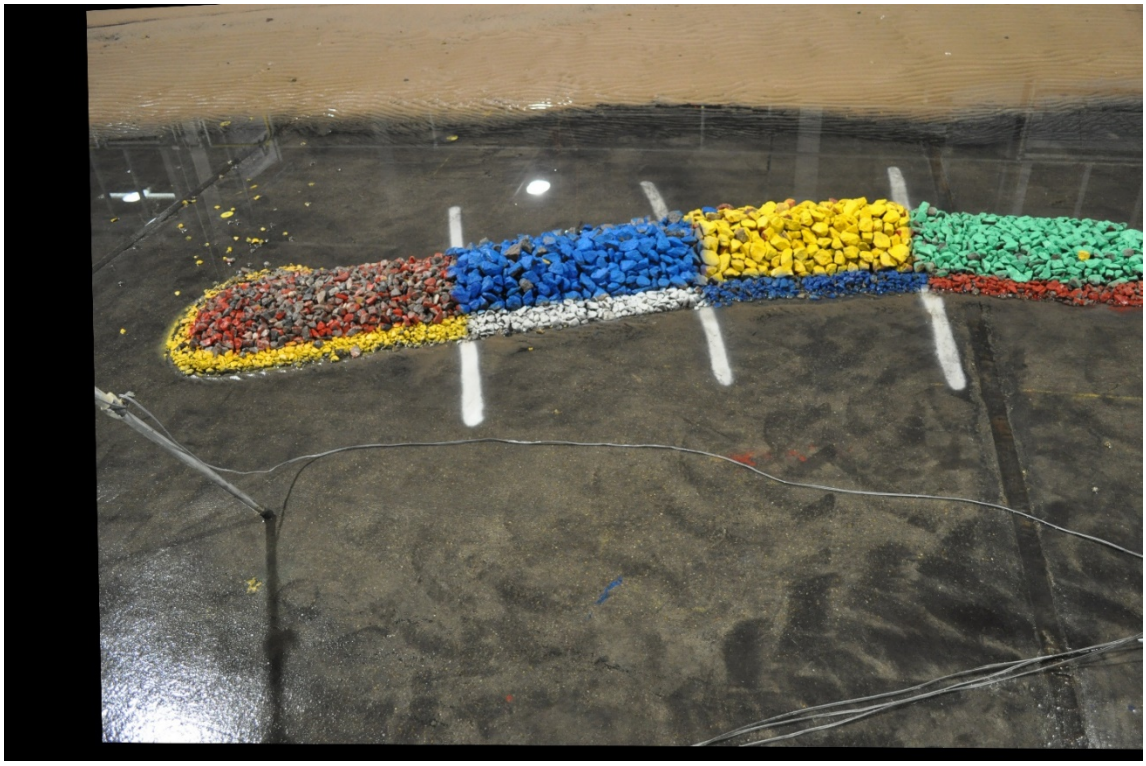

Figure D.143: Post Test Part 04 (WC_HIGH_WL) stability photograph for BW3-3, position 10

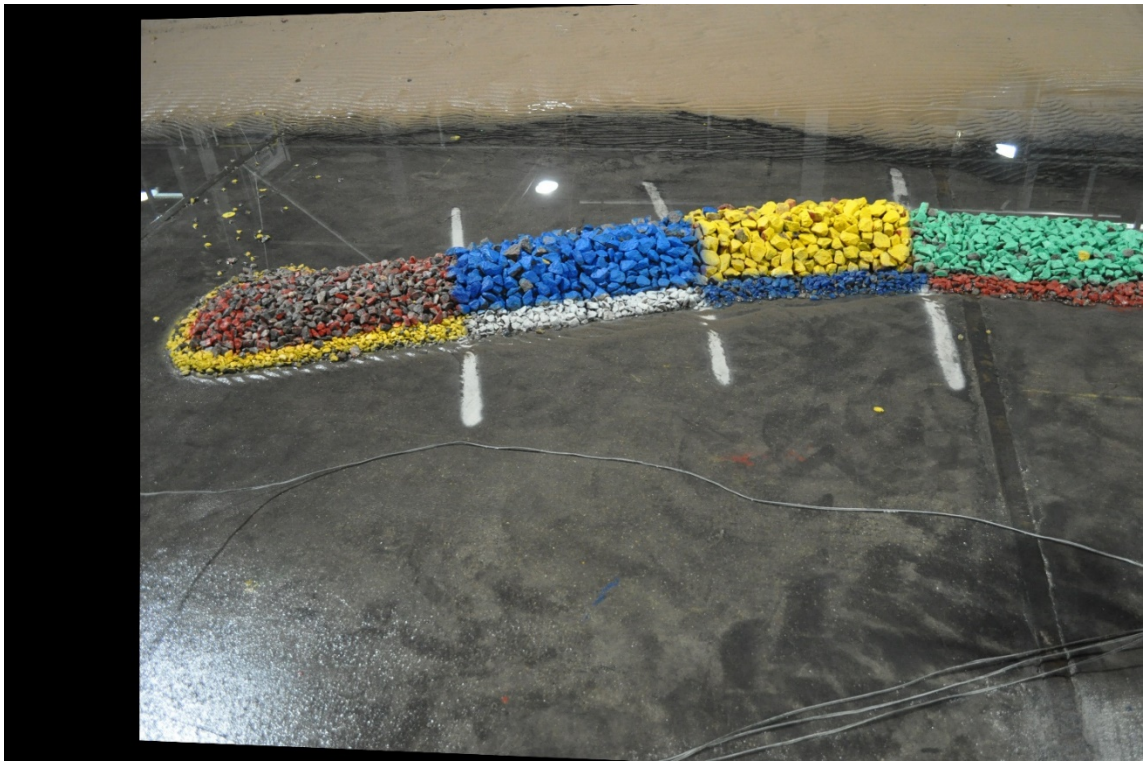

Figure D.144: Post Test Part 05 (WC_EXT_WL_01) stability photograph for BW3-3, position 10

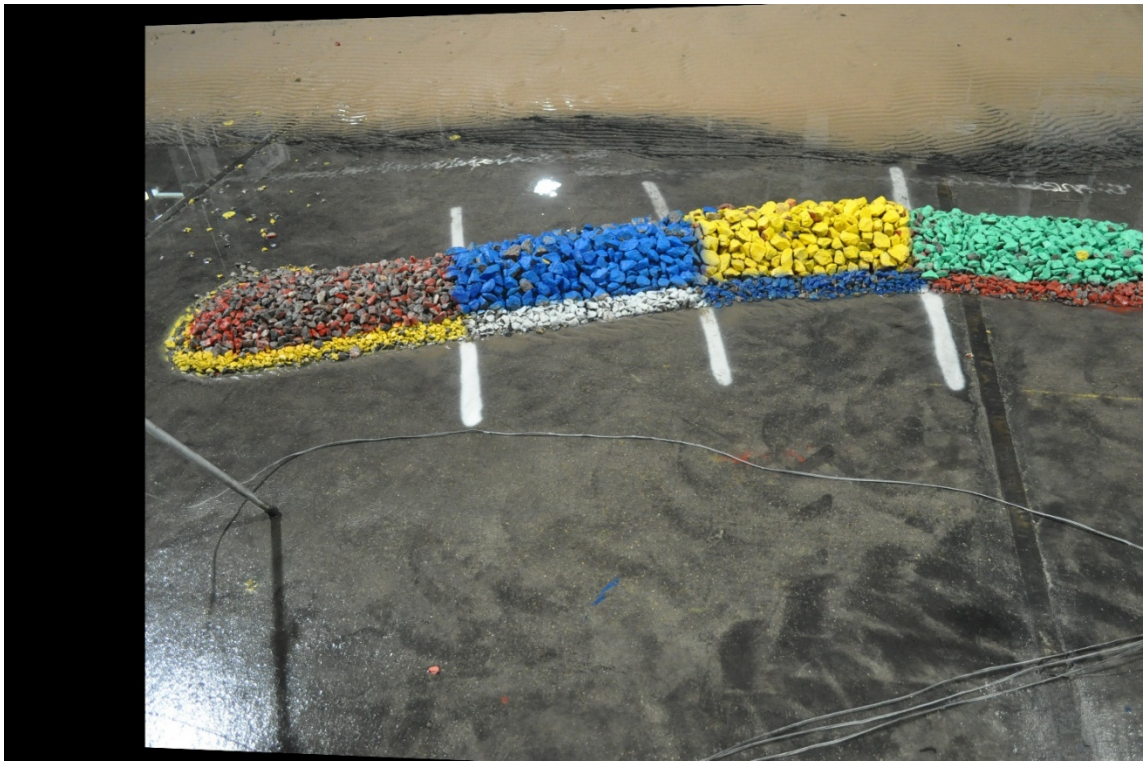

Figure D.145: Post Test Part 06 (WC_EXT_WL_02) stability photograph for BW3-3, position 10

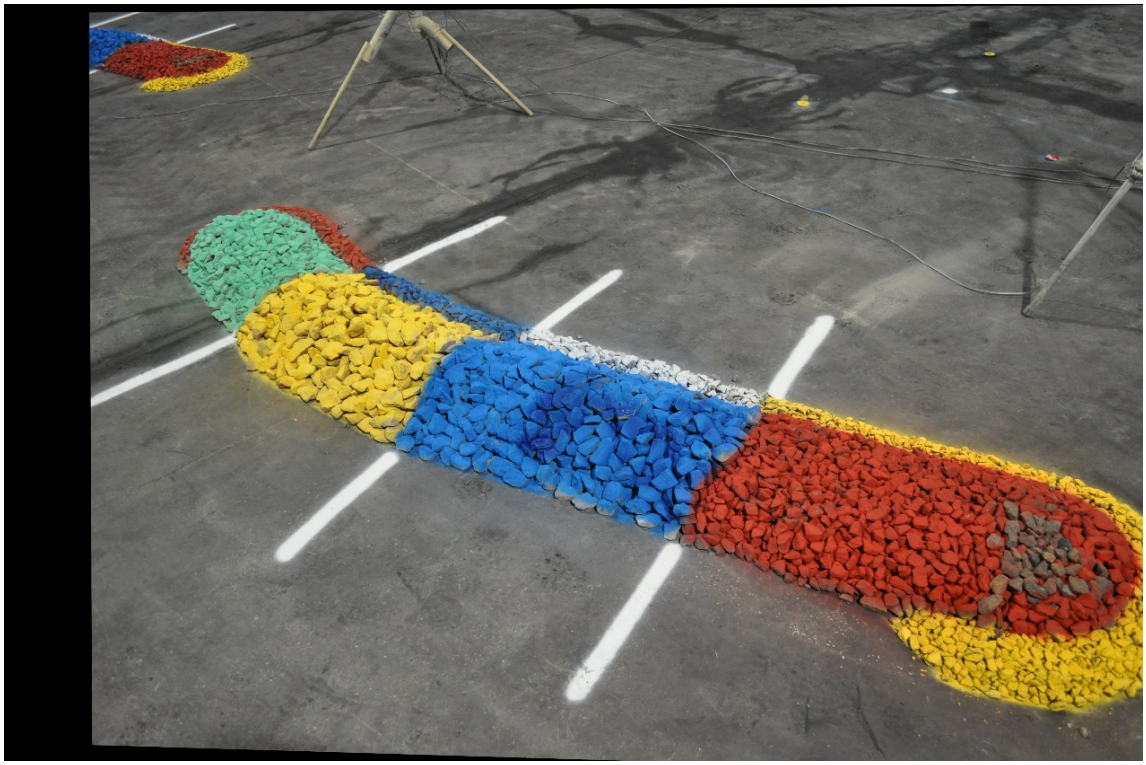

Figure D.146: Pre-test stability photograph for BW3-3, position 11

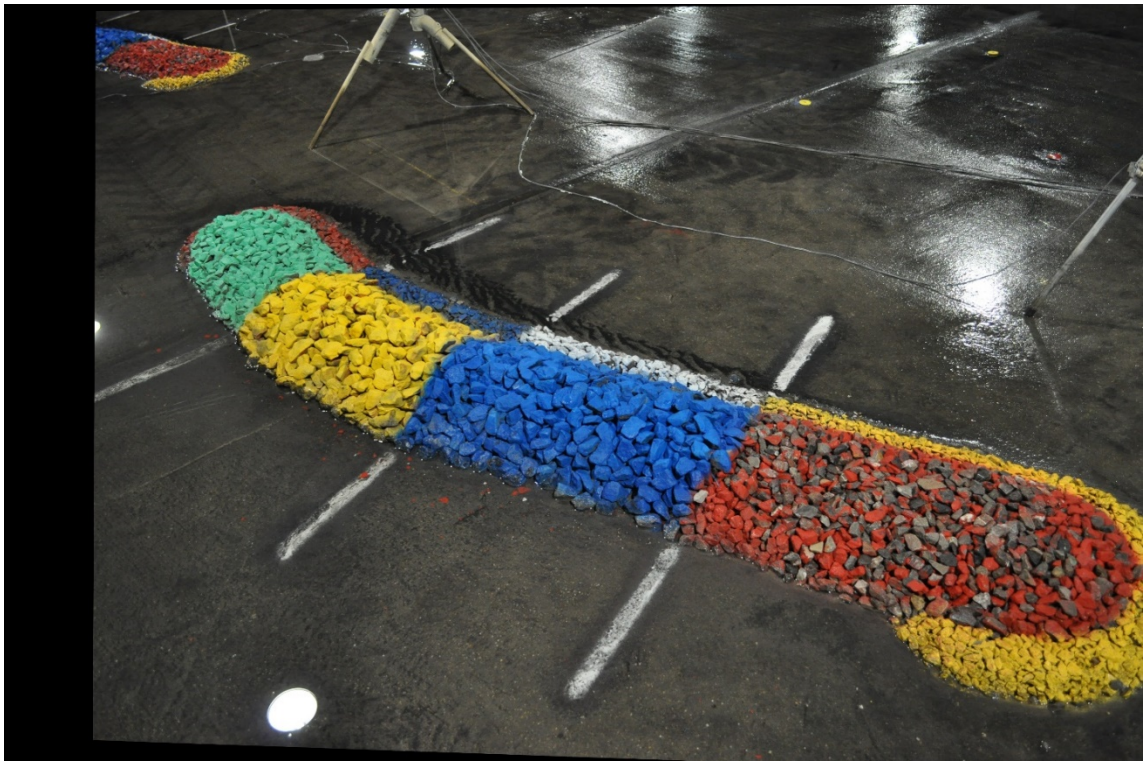

Figure D.147: Post Test Part 01 (WC_LOW_WL_SE) stability photograph for BW3-3, position 11

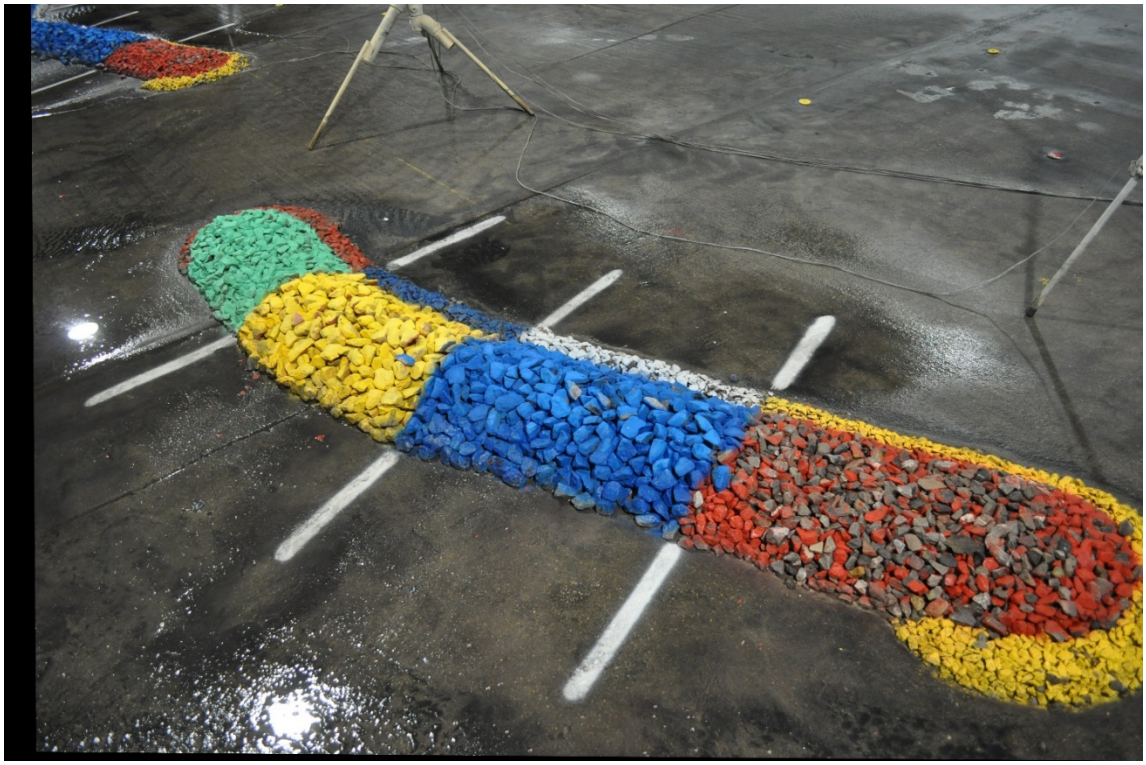

Figure D.148: Post Test Part 02 (WC_HIGH_WL_SE) stability photograph for BW3-3, position 11

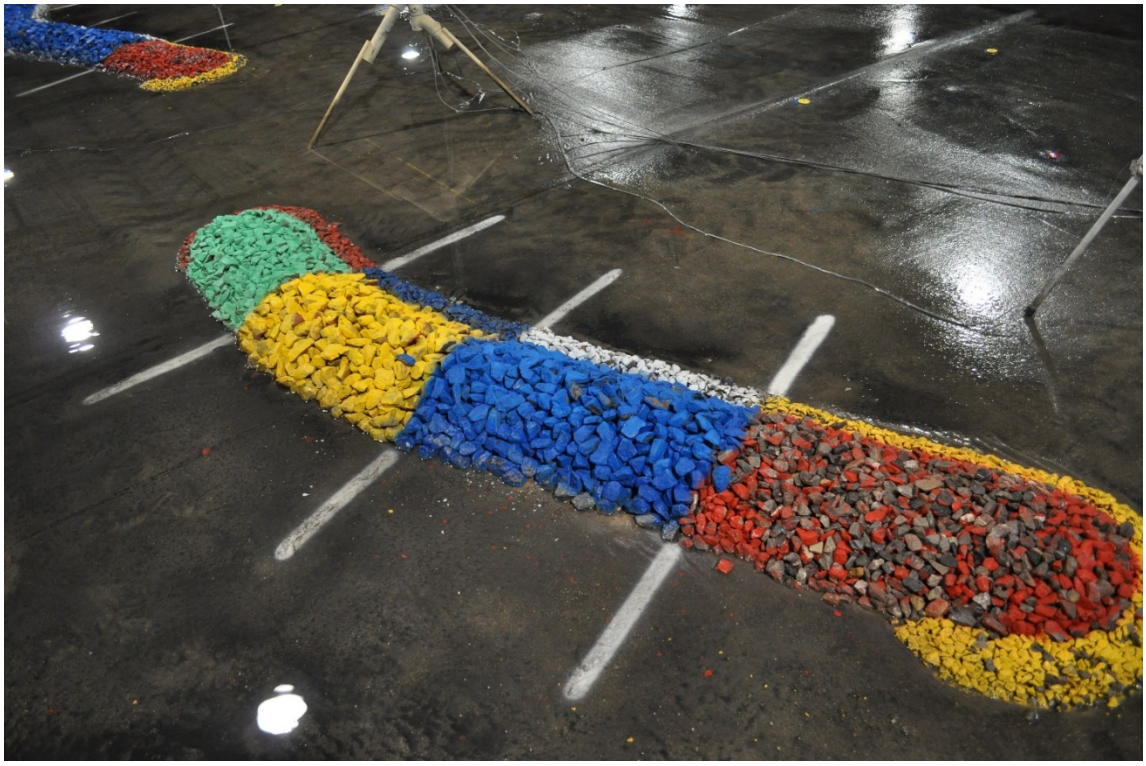

Figure D.149: Post Test Part 03 (WC_LOW_WL) stability photograph for BW3-3, position 11

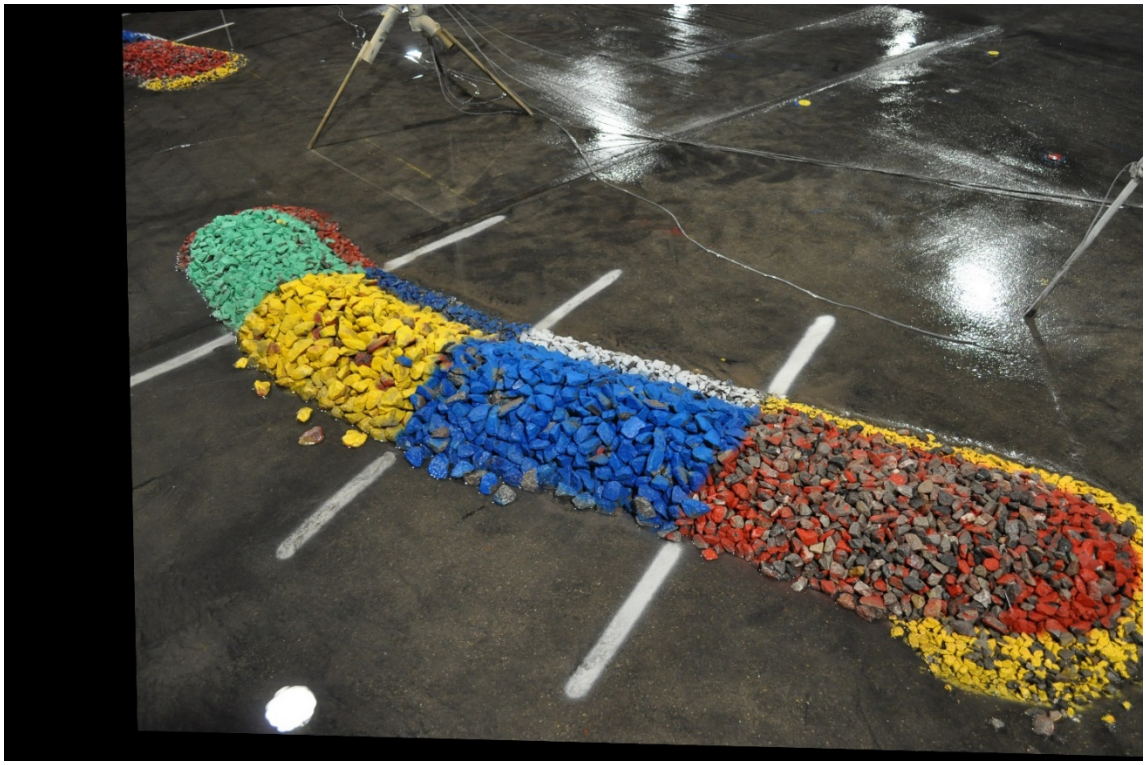

Figure D.150: Post Test Part 04 (WC_HIGH_WL) stability photograph for BW3-3, position 11

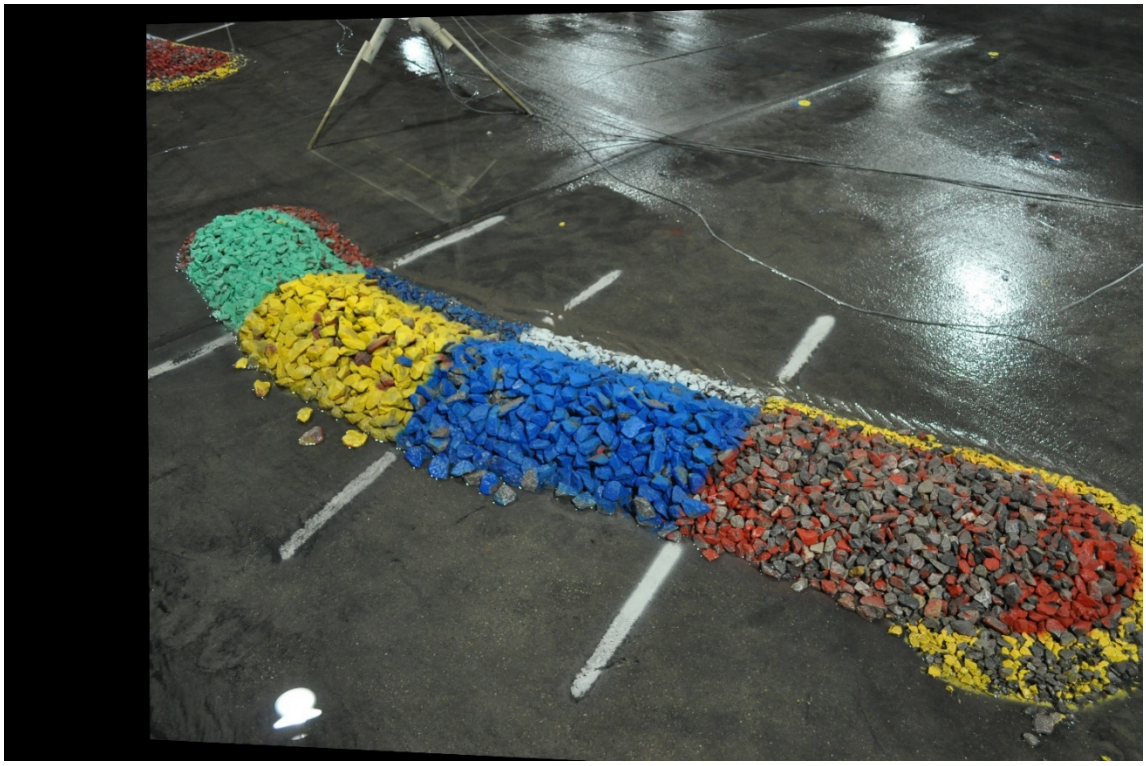

Figure D.151: Post Test Part 05 (WC_EXT_WL_01) stability photograph for BW3-3, position 11

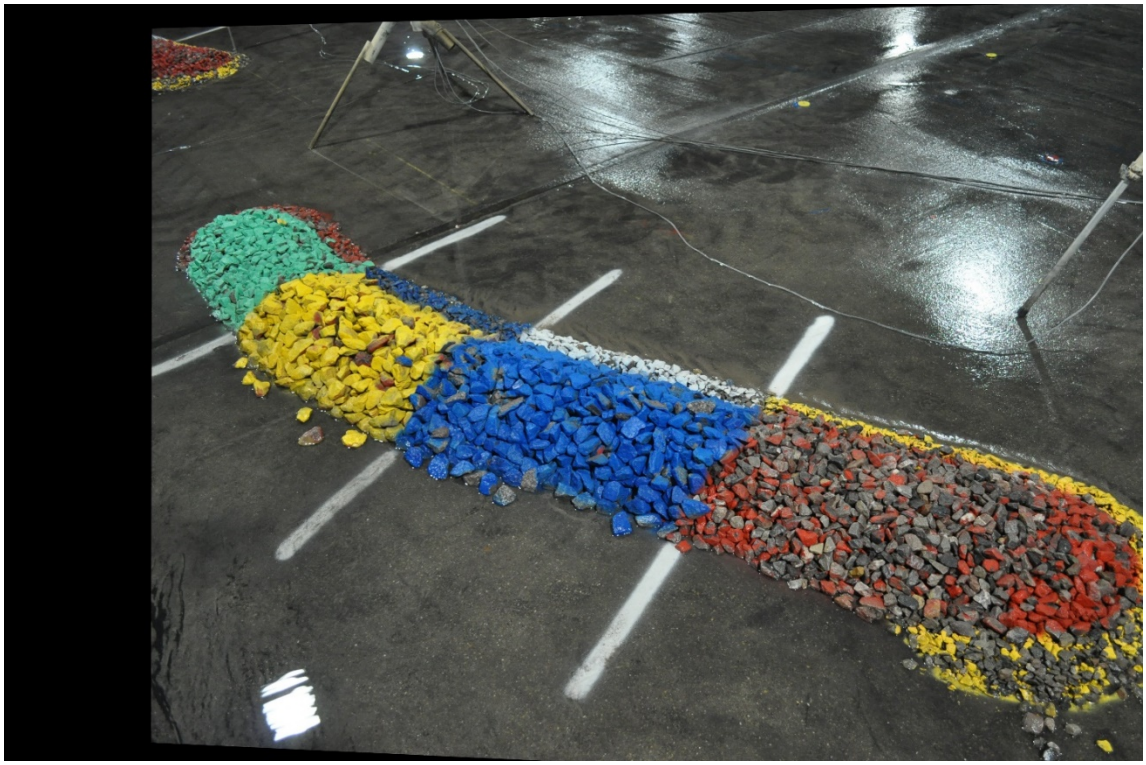

Figure D.152: Post Test Part 06 (WC_EXT_WL_02) stability photograph for BW3-3, position 11

## D.2.4. BW3-4

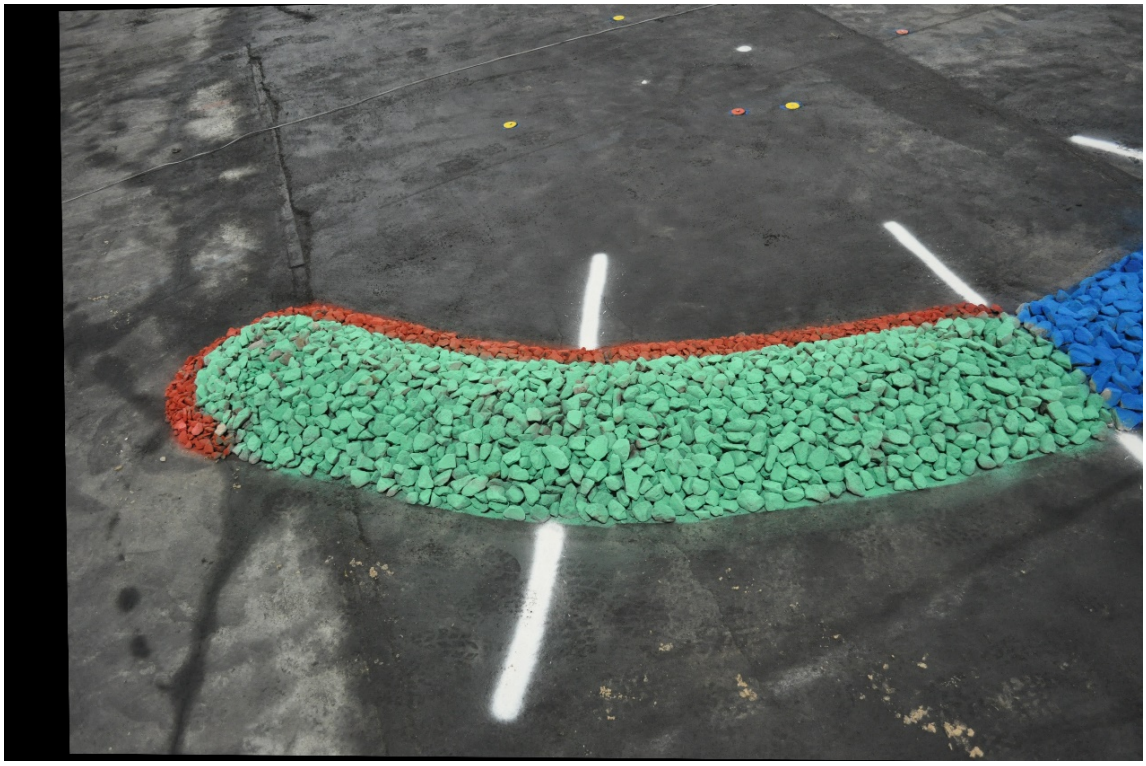

Figure D.153: Pre-test stability photograph for BW3-4, position 12

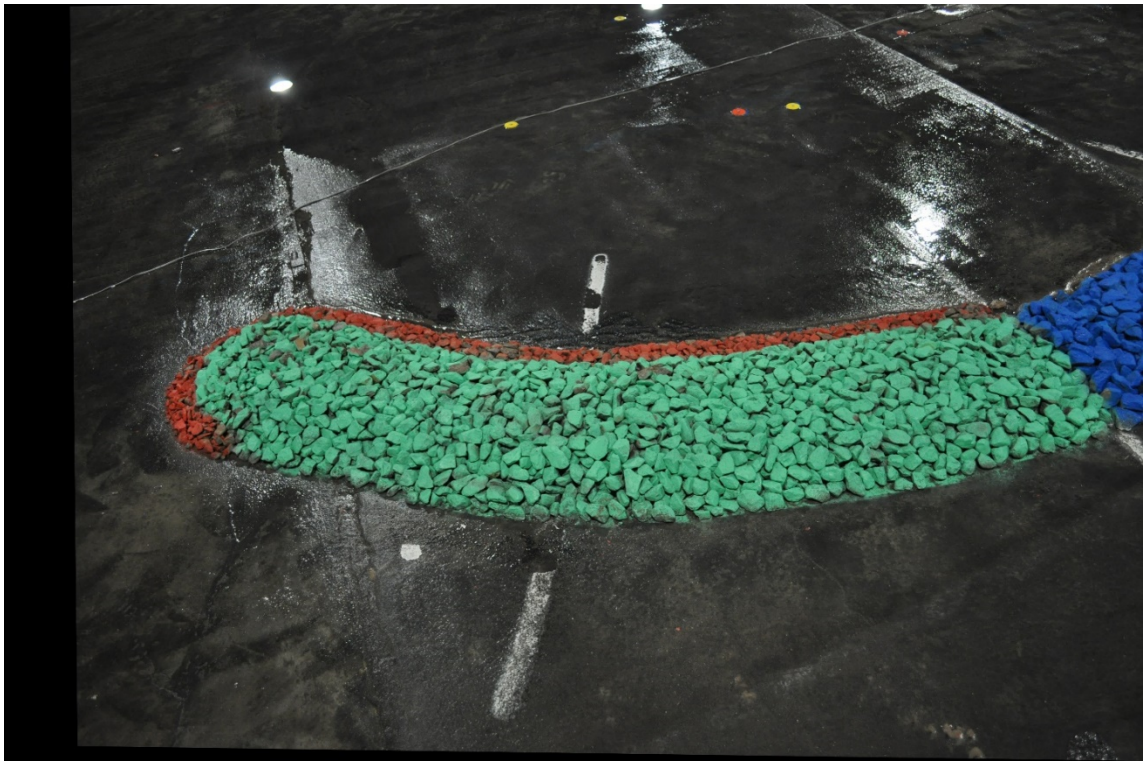

Figure D.154: Post Test Part 01 (WC_LOW_WL_SE) stability photograph for BW3-4, position 12

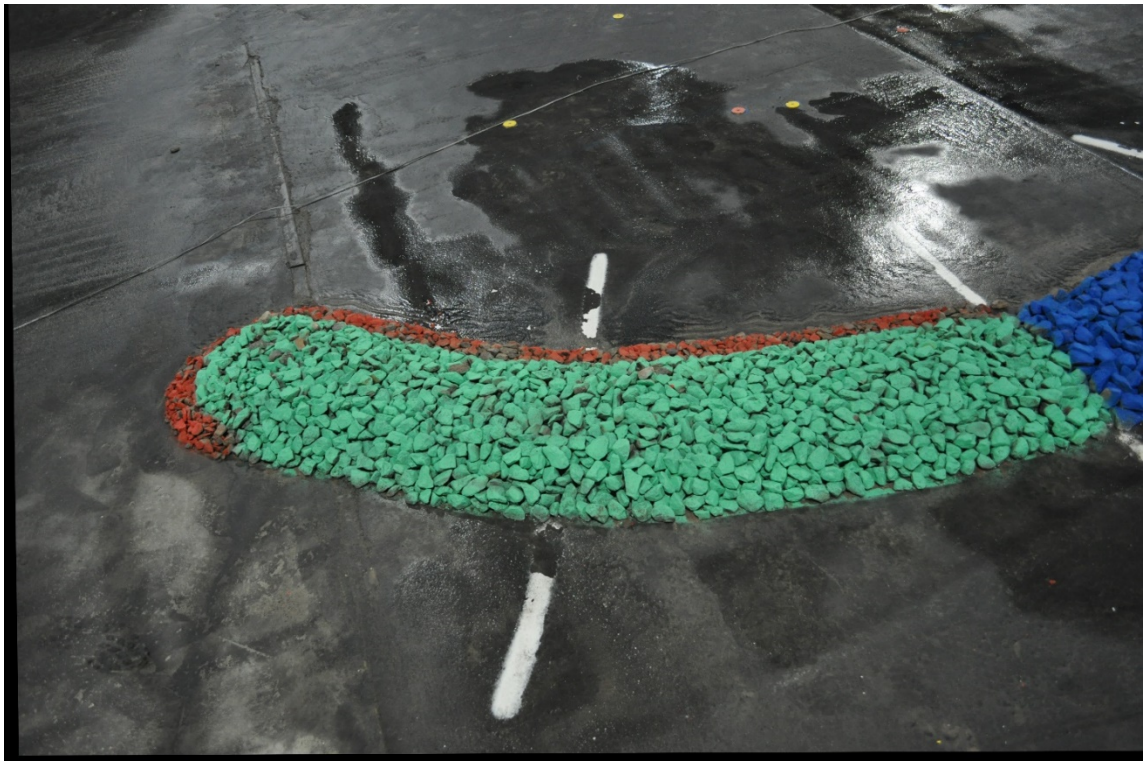

Figure D.155: Post Test Part 02 (WC_HIGH_WL_SE) stability photograph for BW3-4, position 12

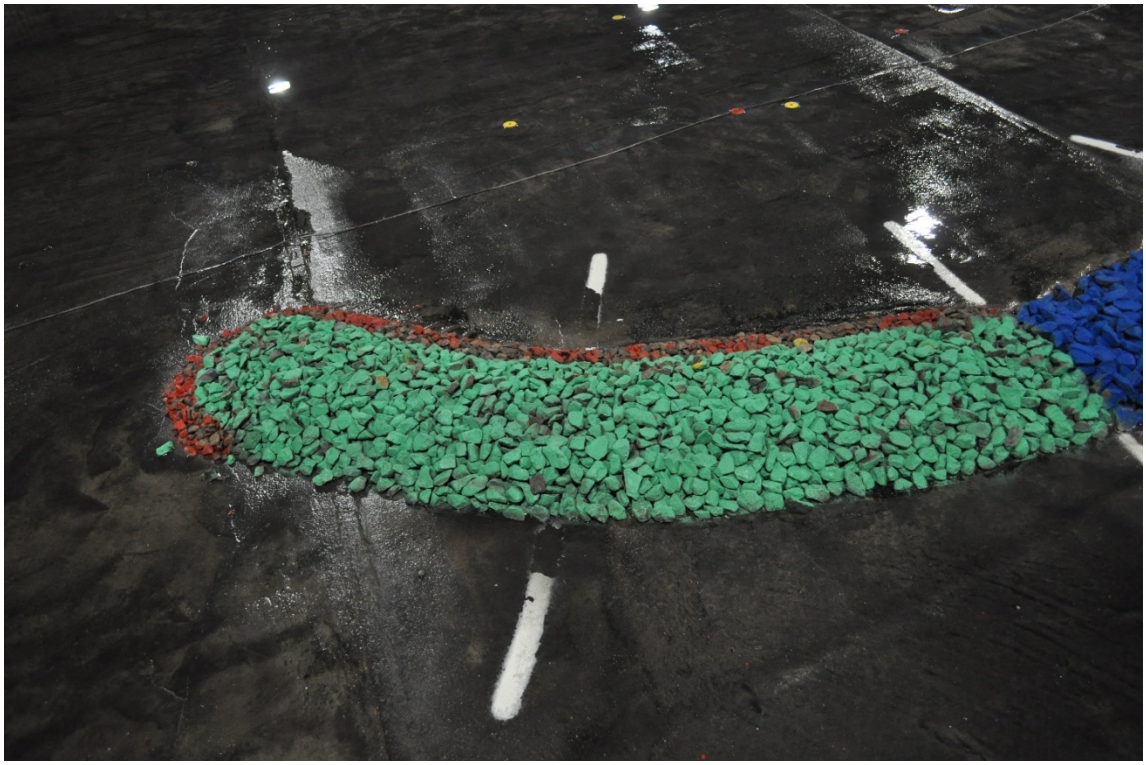

Figure D.156: Post Test Part 03 (WC_LOW_WL) stability photograph for BW3-4, position 12

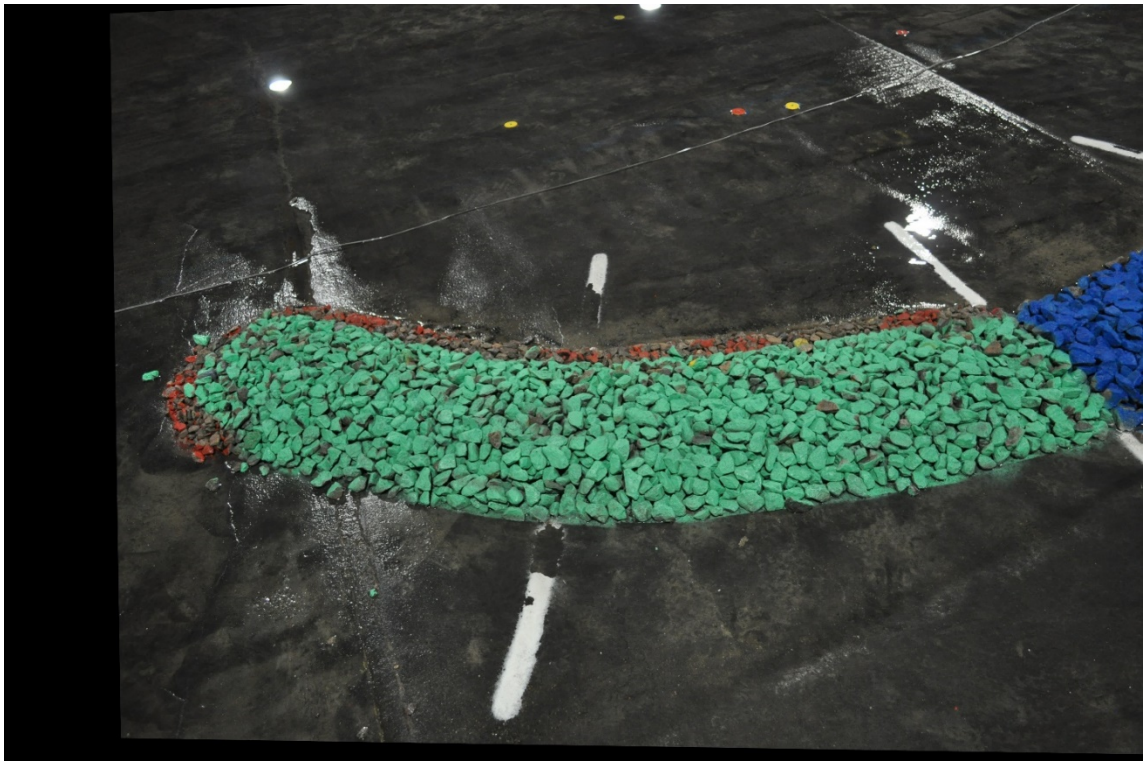

Figure D.157: Post Test Part 04 (WC_HIGH_WL) stability photograph for BW3-4, position 12

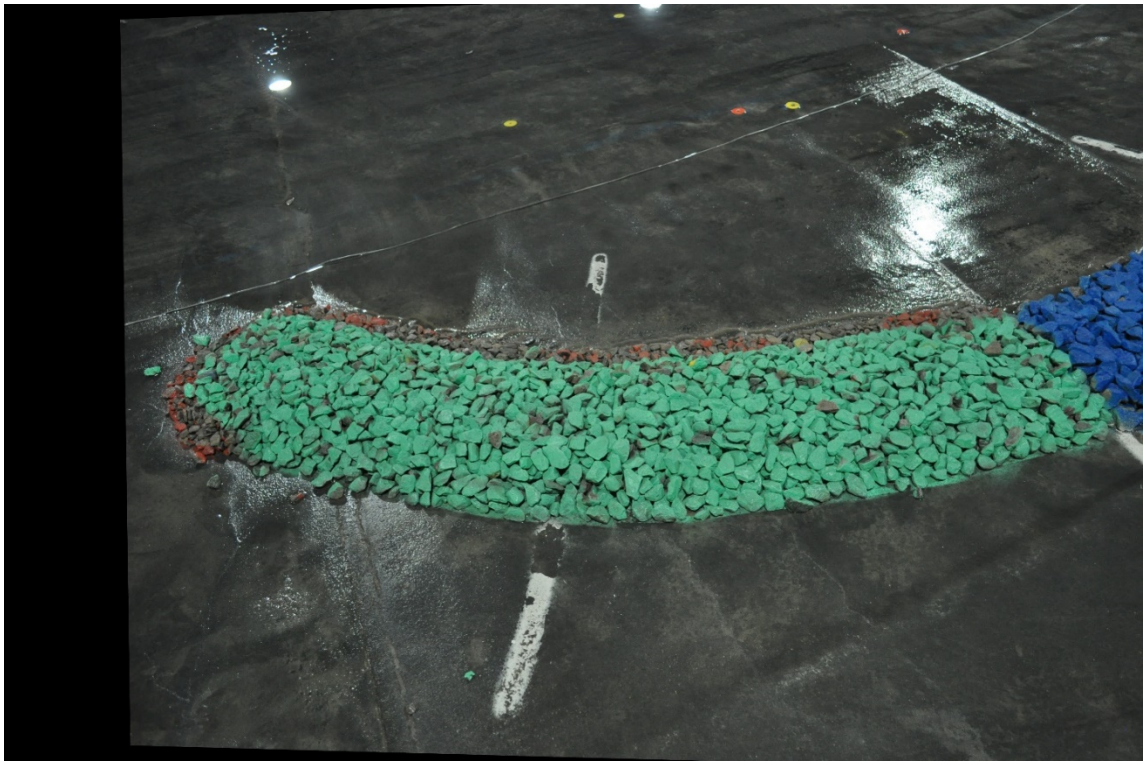

Figure D.158: Post Test Part 05 (WC_EXT_WL_01) stability photograph for BW3-4, position 12

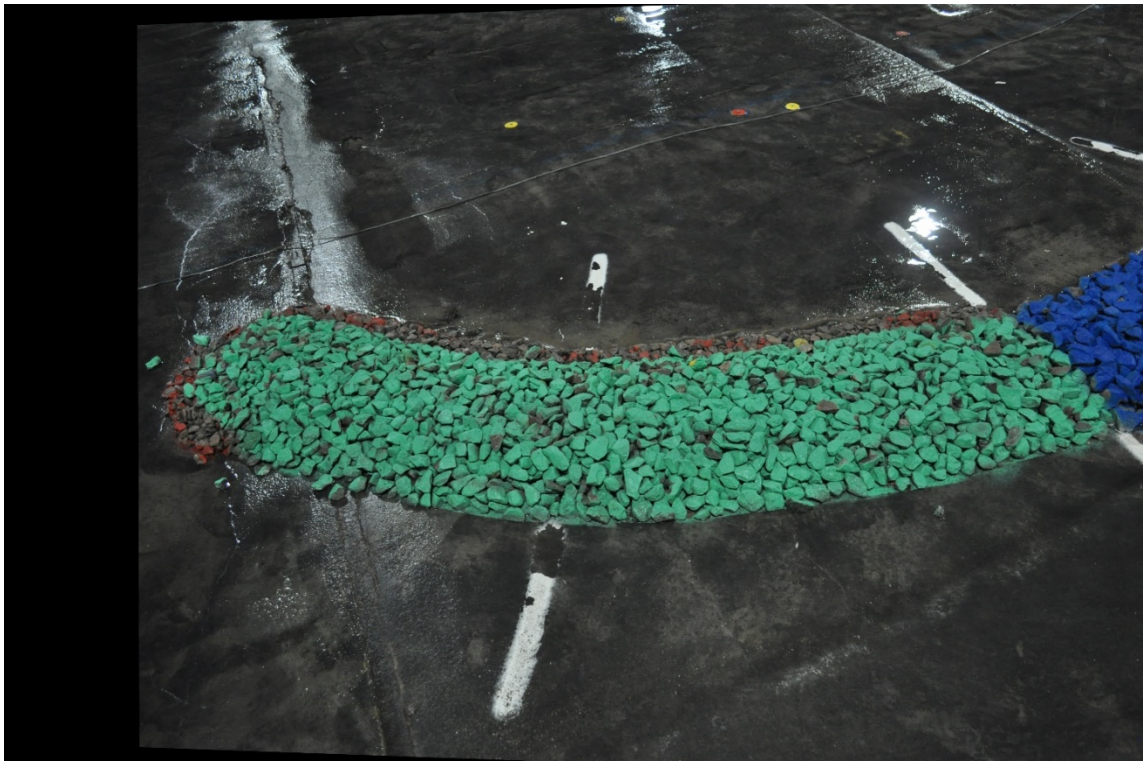

Figure D.159: Post Test Part 06 (WC_EXT_WL_02) stability photograph for BW3-4, position 12

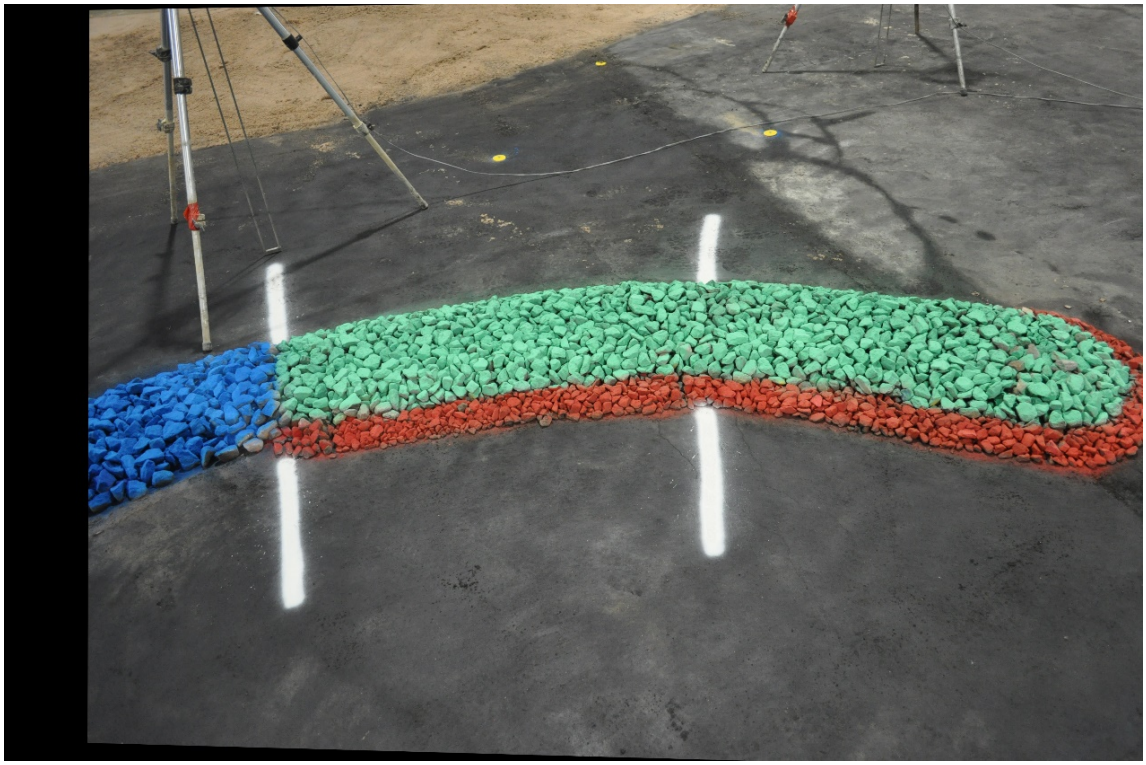

Figure D.160: Pre-test stability photograph for BW3-4, position 13

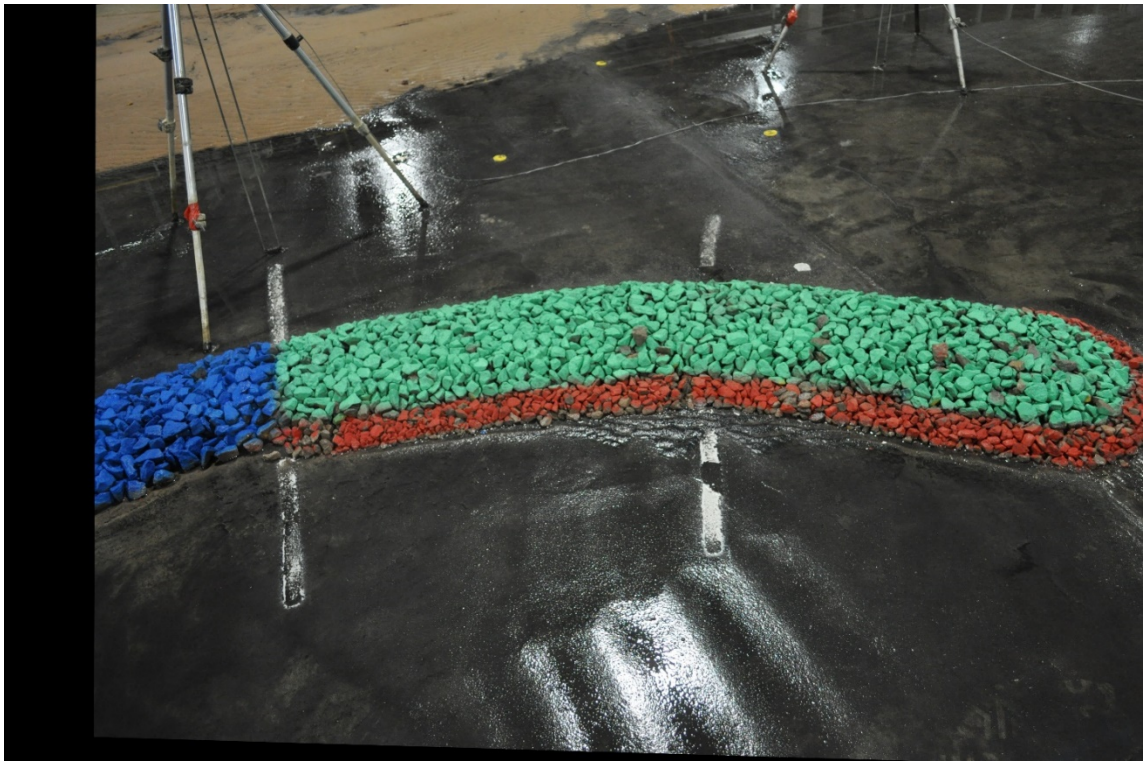

Figure D.161: Post Test Part 01 (WC_LOW_WL_SE) stability photograph for BW3-4, position 13

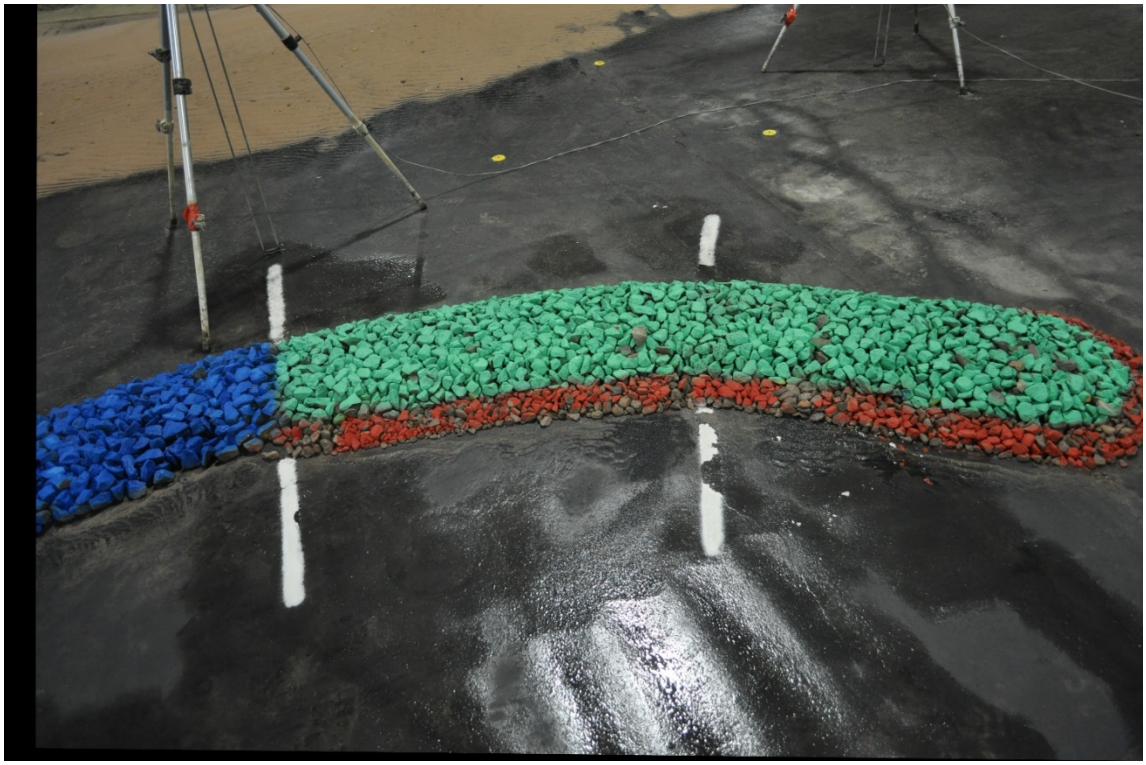

Figure D.162: Post Test Part 02 (WC_HIGH_WL_SE) stability photograph for BW3-4, position 13

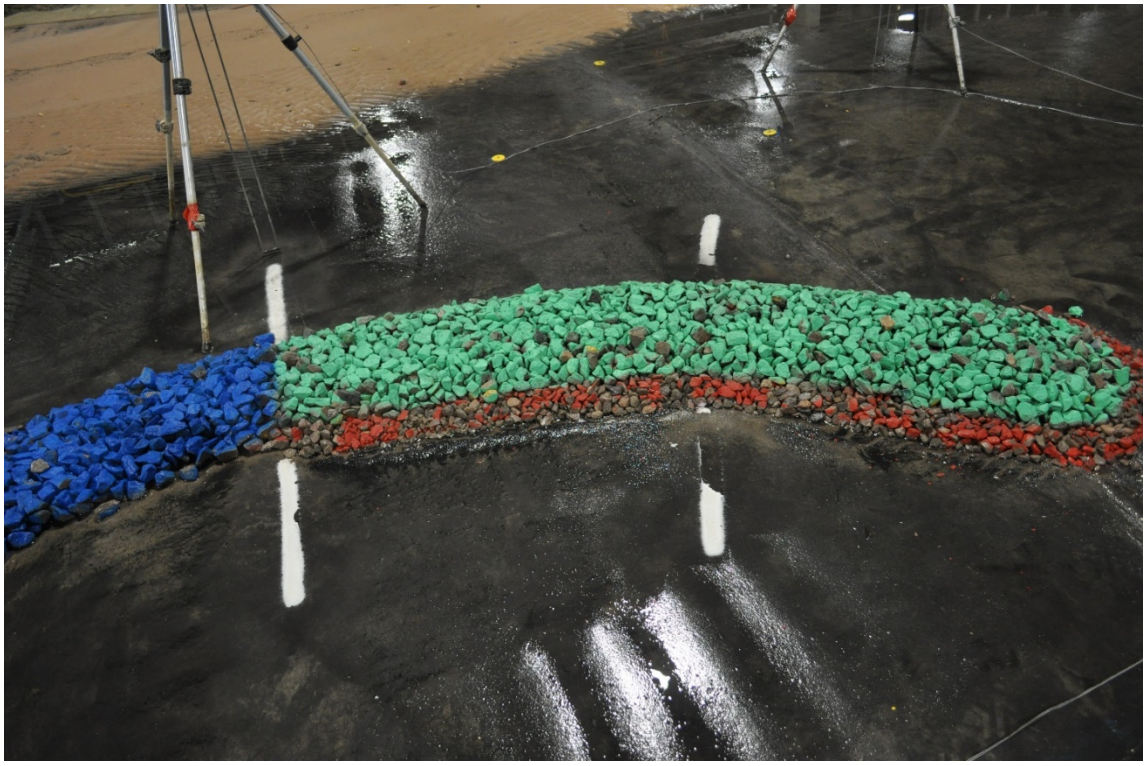

Figure D.163: Post Test Part 03 (WC_LOW_WL) stability photograph for BW3-4, position 13

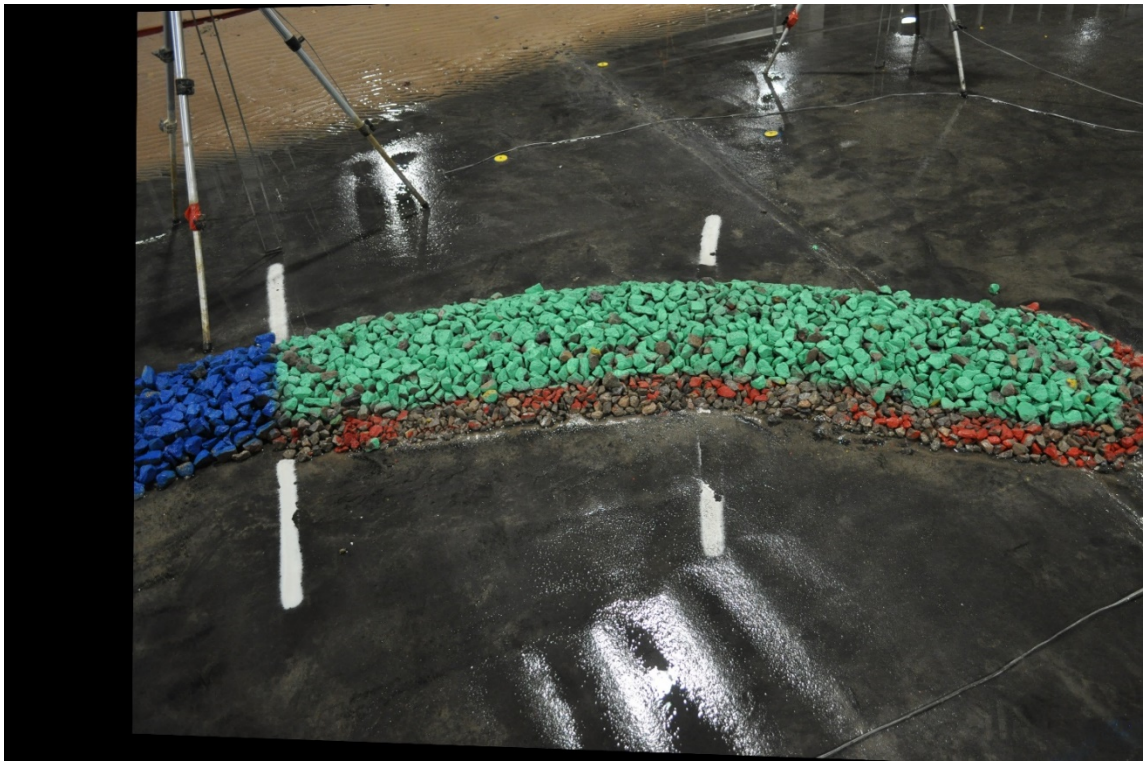

Figure D.164: Post Test Part 04 (WC_HIGH_WL) stability photograph for BW3-4, position 13

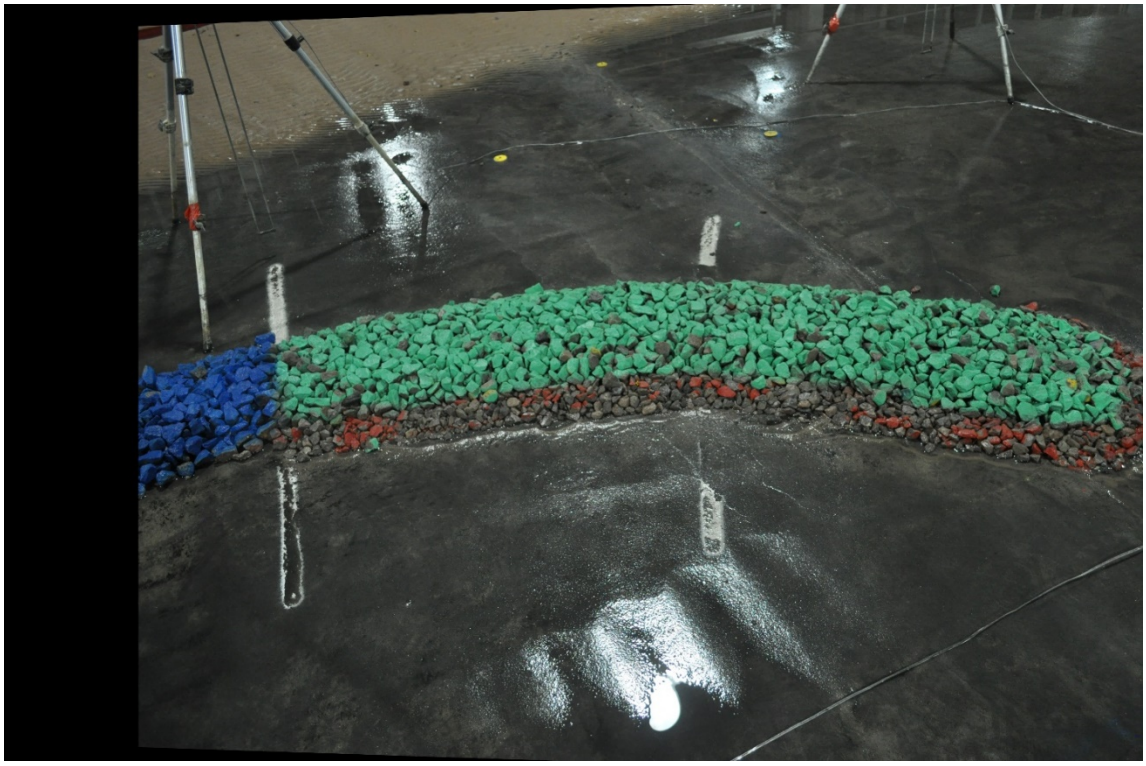

Figure D.165: Post Test Part 05 (WC_EXT_WL_01) stability photograph for BW3-4, position 13

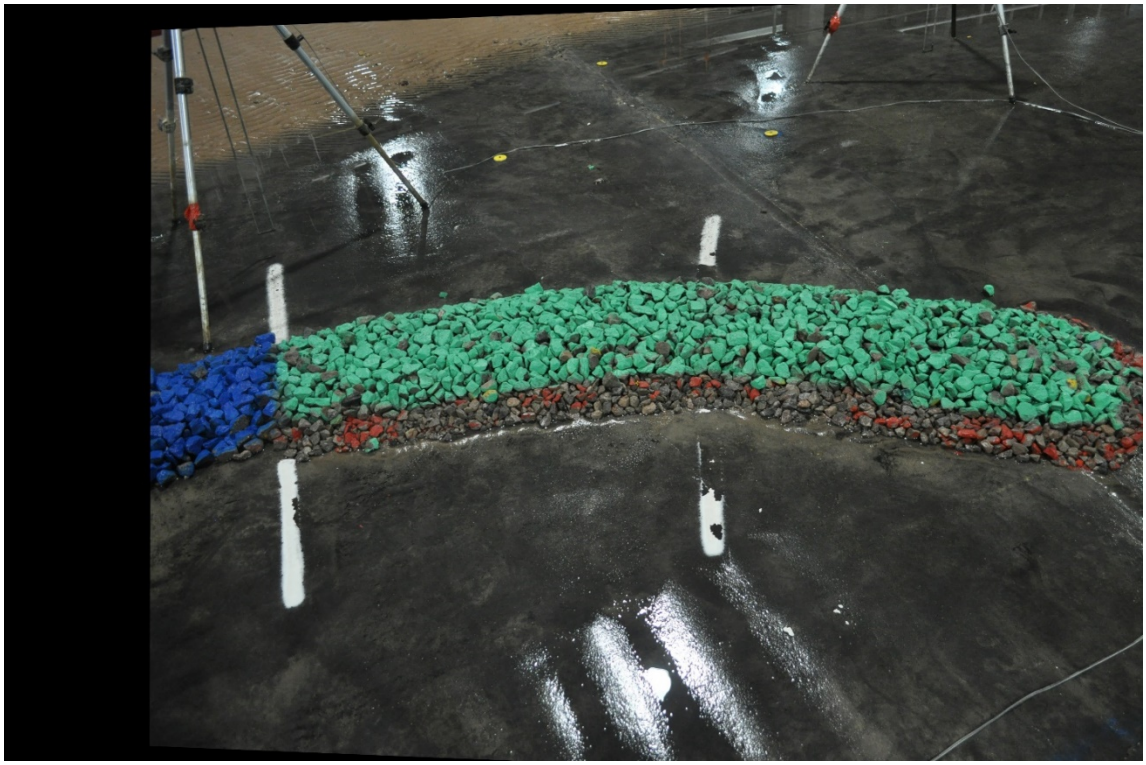

Figure D.166: Post Test Part 06 (WC_EXT_WL_02) stability photograph for BW3-4, position 13

Figure D.167: Pre-test stability photograph for BW3-4, position 14

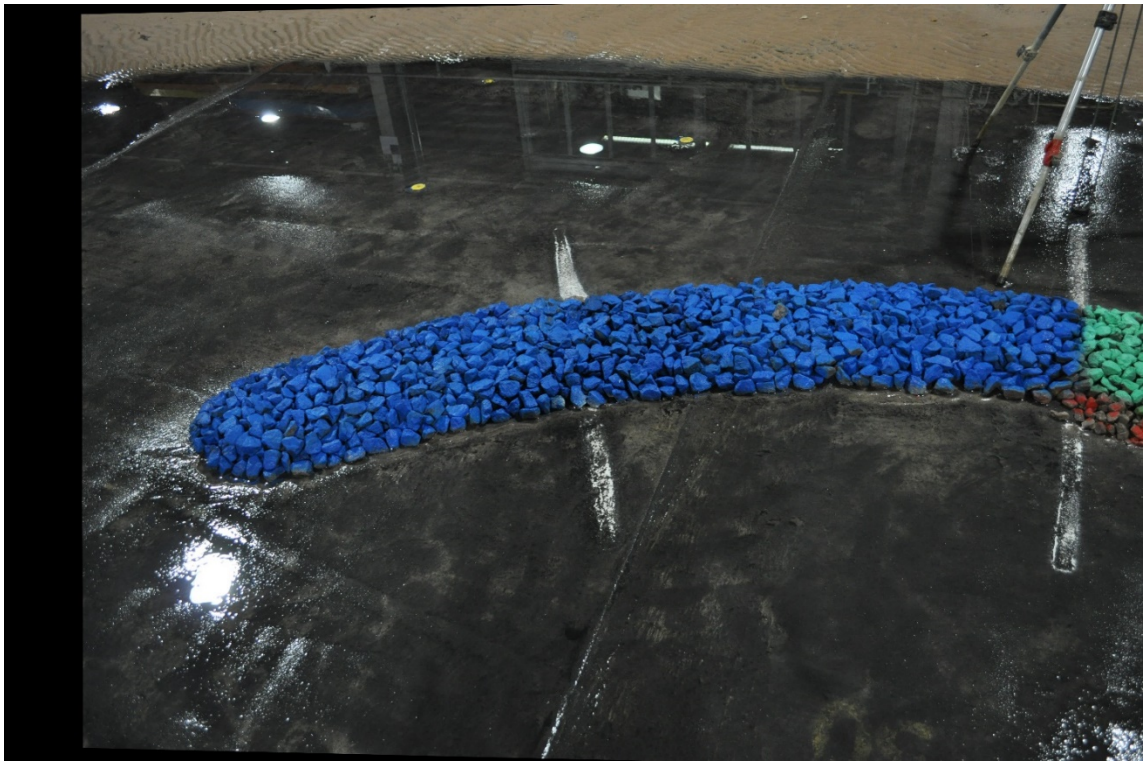

Figure D.168: Post Test Part 01 (WC_LOW_WL_SE) stability photograph for BW3-4, position 14

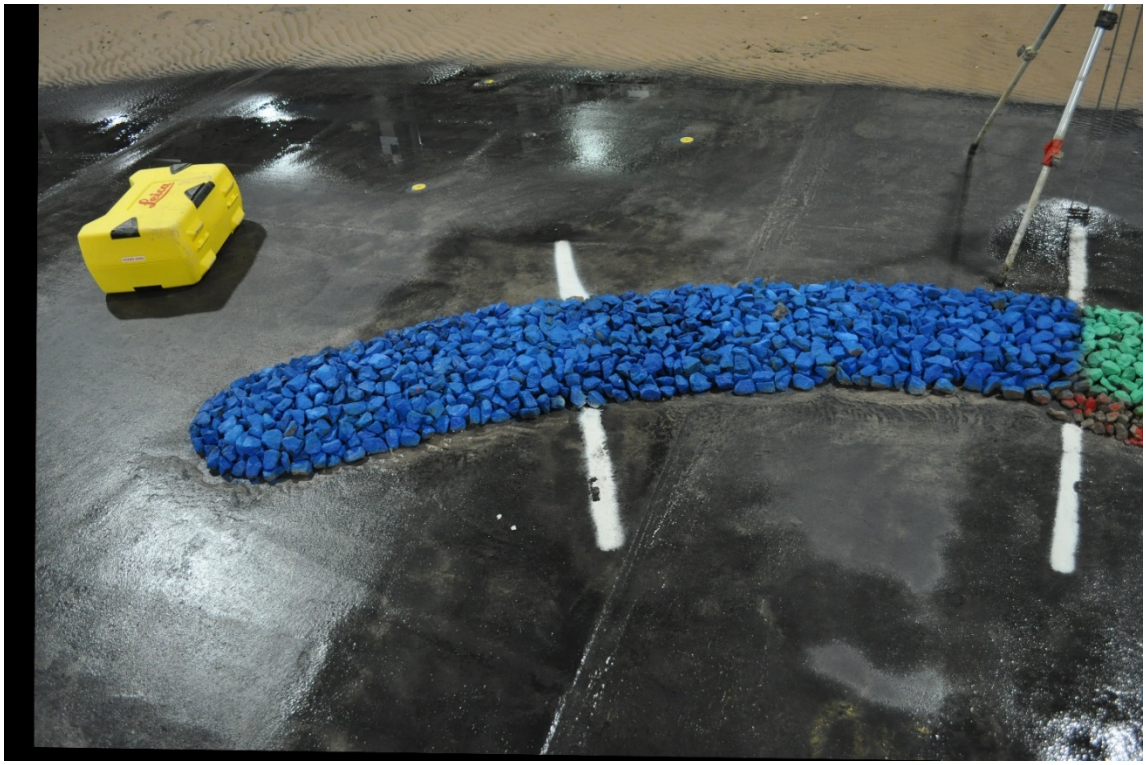

Figure D.169: Post Test Part 02 (WC_HIGH_WL_SE) stability photograph for BW3-4, position 14

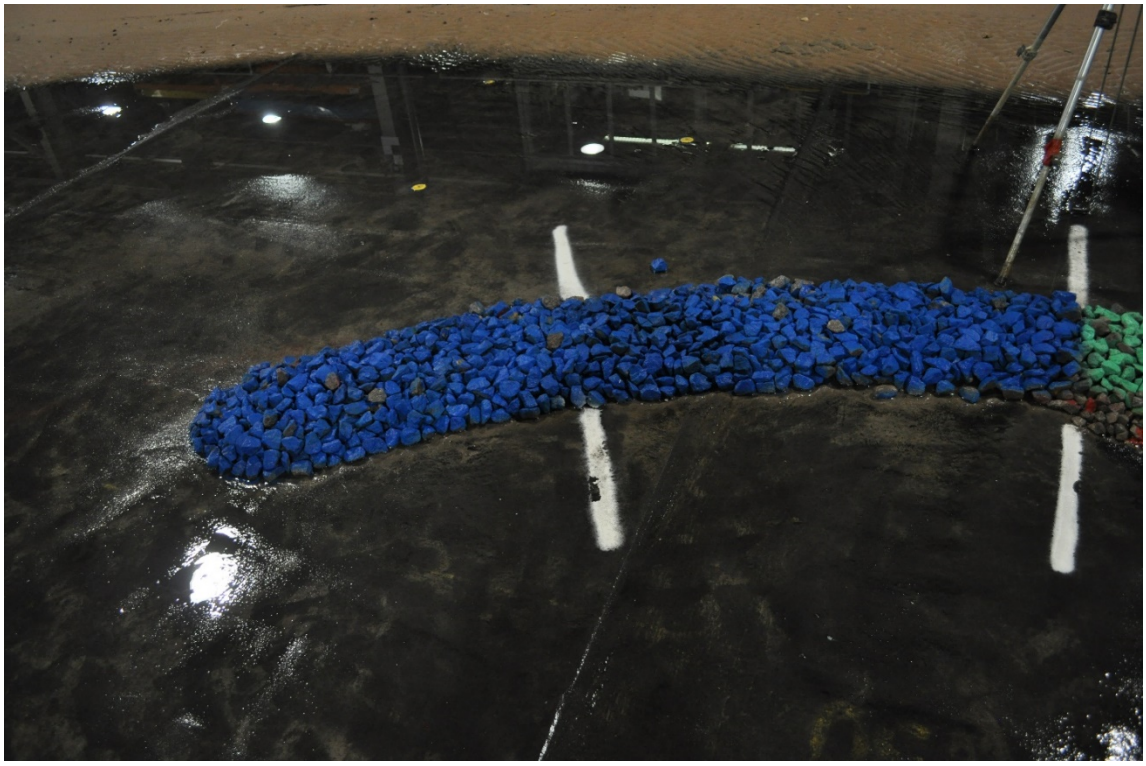

Figure D.170: Post Test Part 03 (WC_LOW_WL) stability photograph for BW3-4, position 14

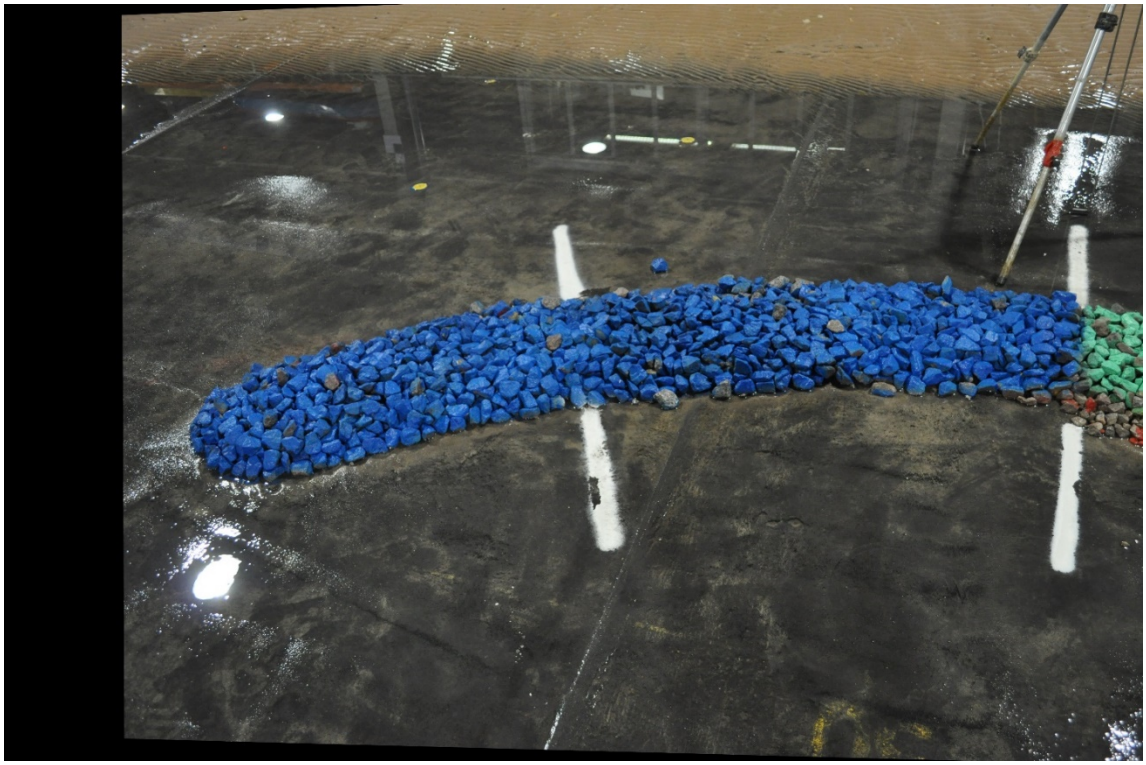

Figure D.171: Post Test Part 04 (WC_HIGH_WL) stability photograph for BW3-4, position 14

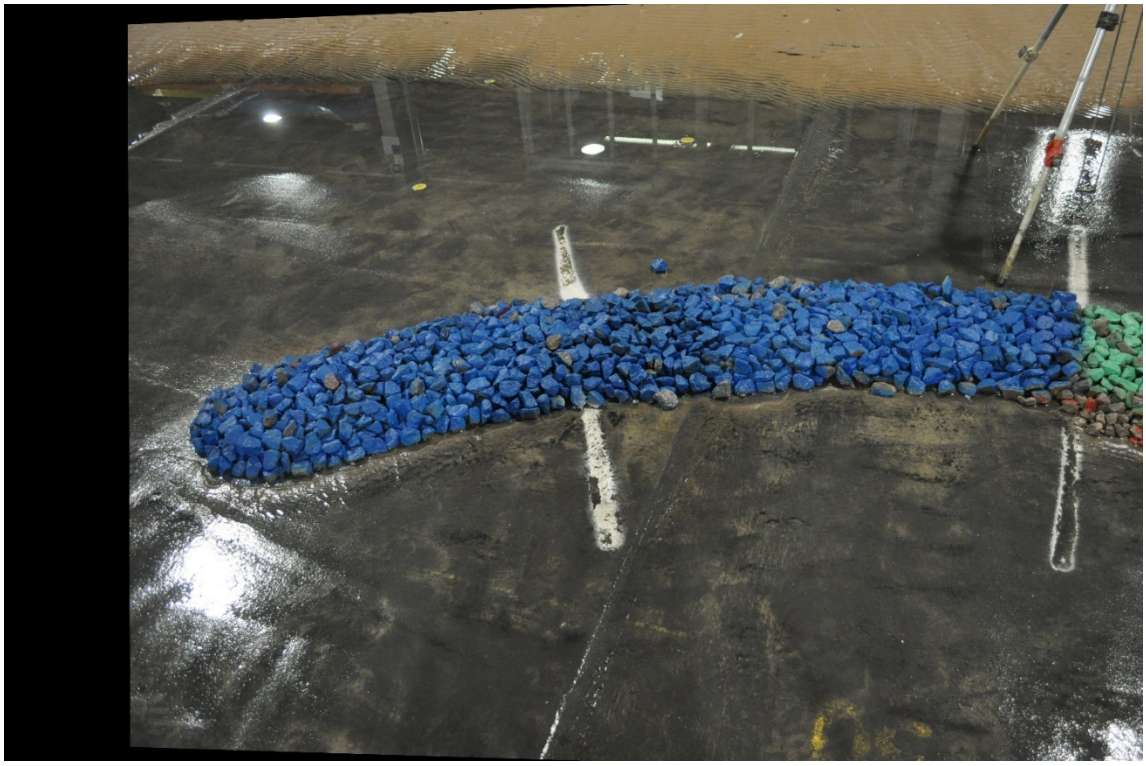

Figure D.172: Post Test Part 05 (WC_EXT_WL_01) stability photograph for BW3-4, position 14

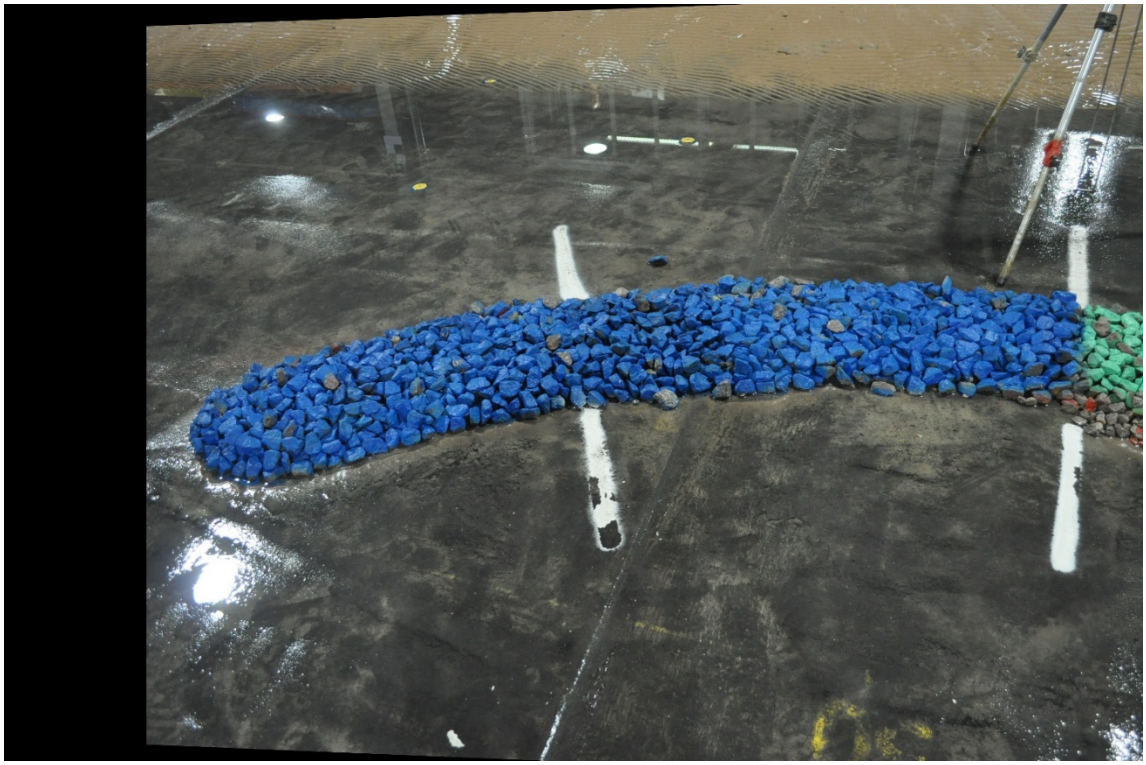

Figure D.173: Post Test Part 06 (WC_EXT_WL_02) stability photograph for BW3-4, position 14

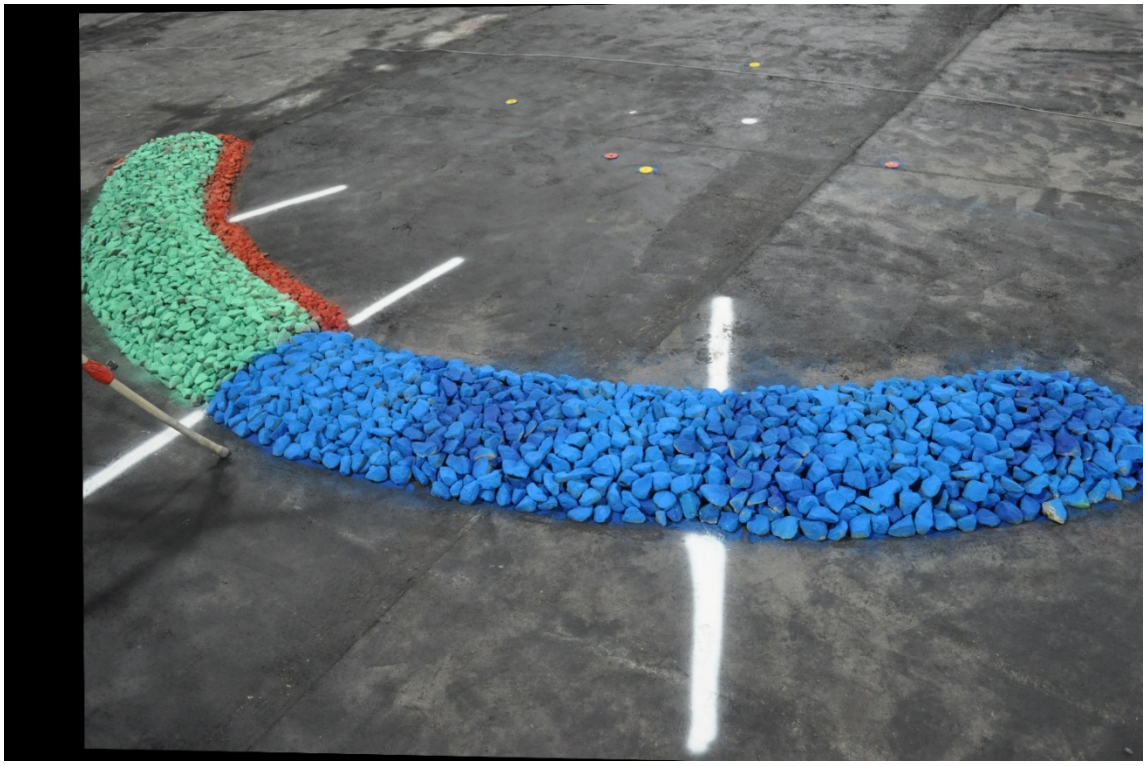

Figure D.174: Pre-test stability photograph for BW3-4, position 15

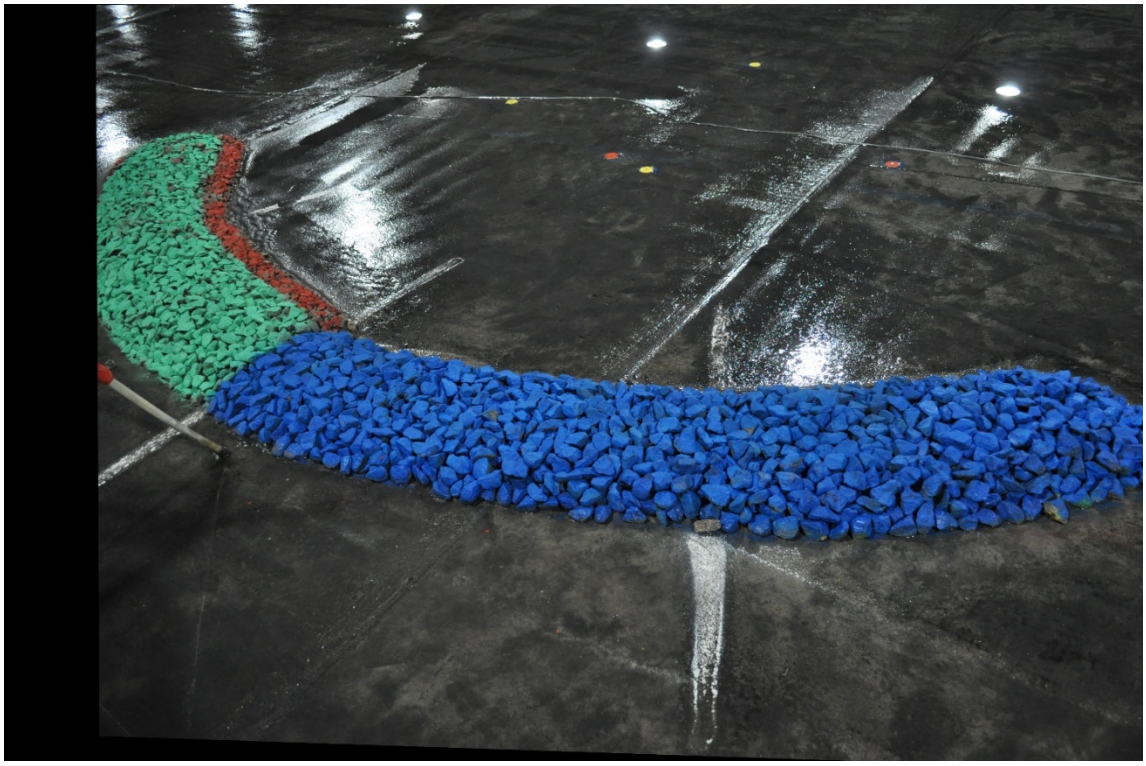

Figure D.175: Post Test Part 01 (WC_LOW_WL_SE) stability photograph for BW3-4, position 15

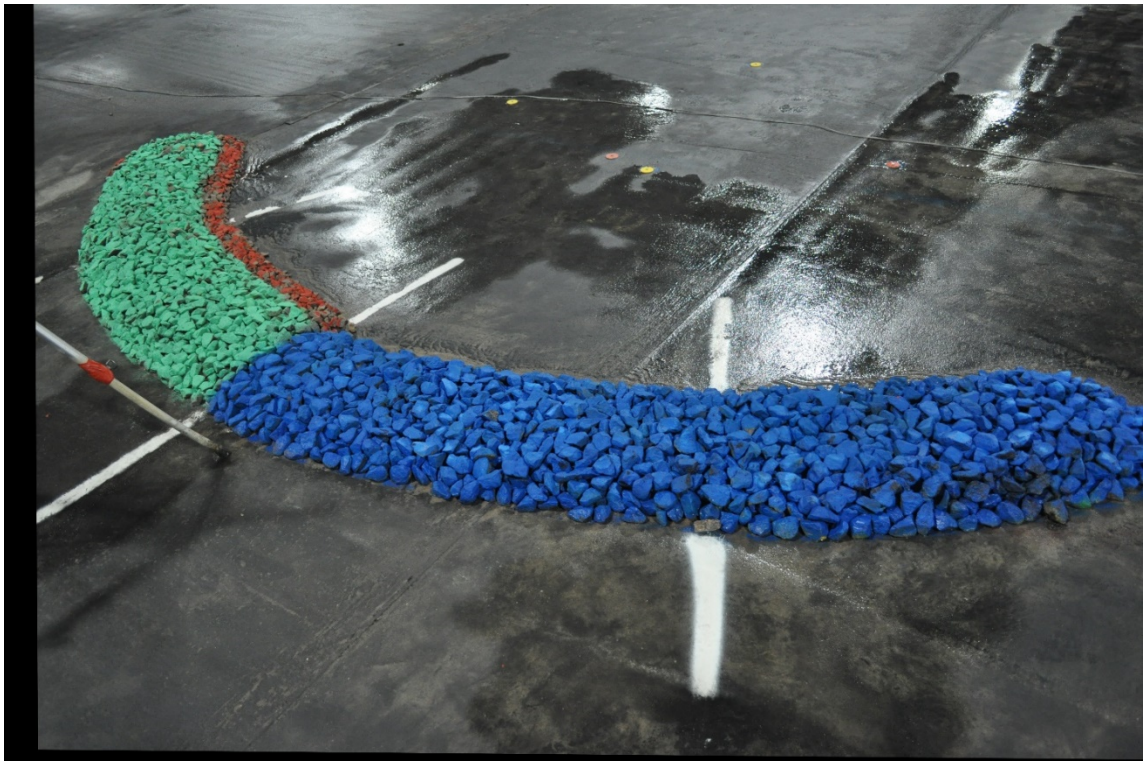

Figure D.176: Post Test Part 02 (WC_HIGH_WL_SE) stability photograph for BW3-4, position 15

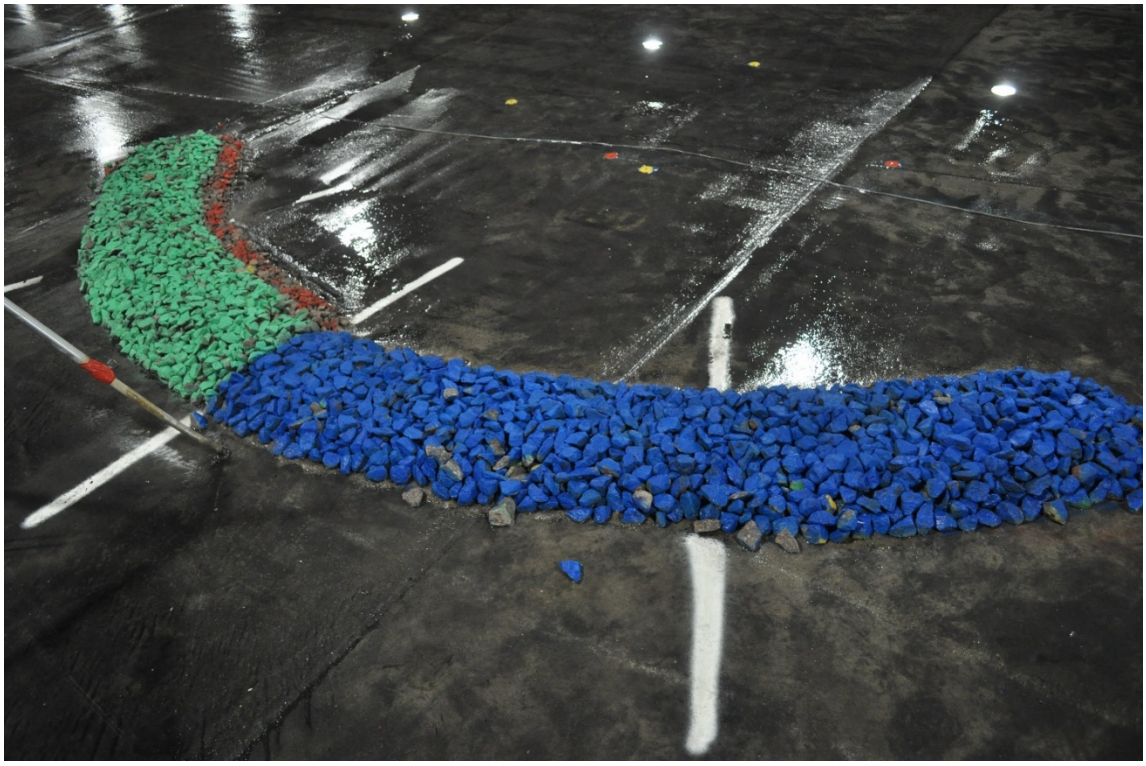

Figure D.177: Post Test Part 03 (WC_LOW_WL) stability photograph for BW3-4, position 15

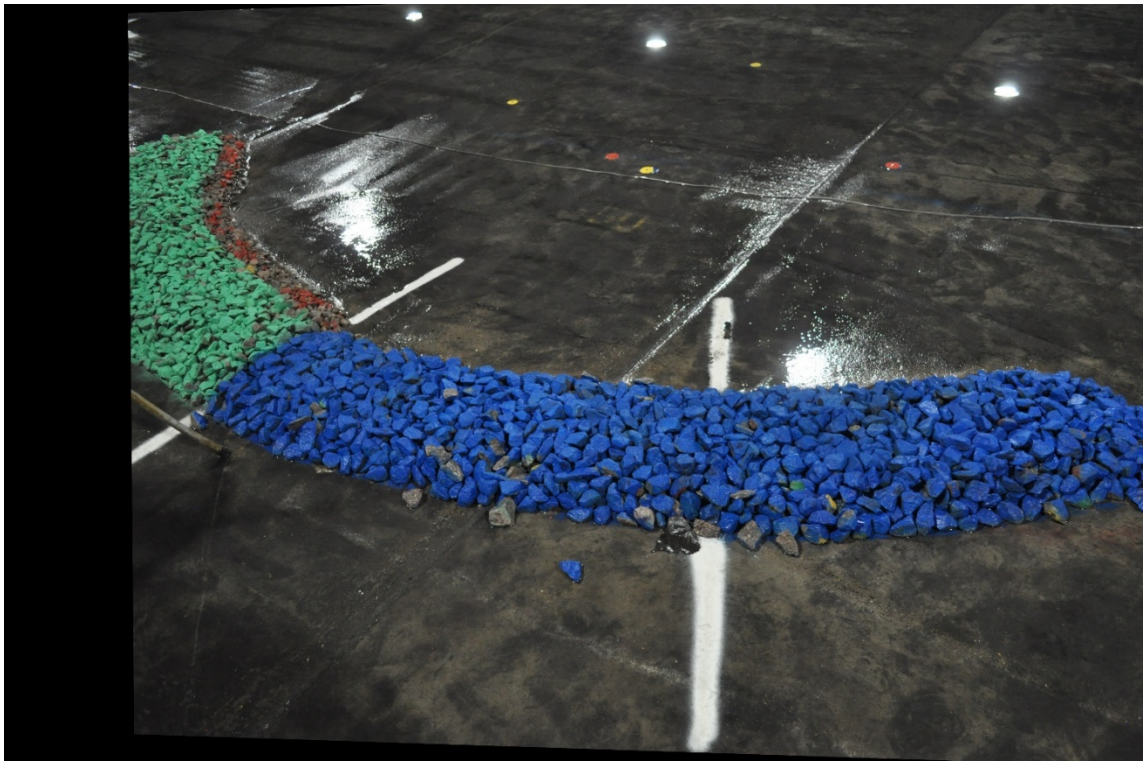

Figure D.178: Post Test Part 04 (WC_HIGH_WL) stability photograph for BW3-4, position 15

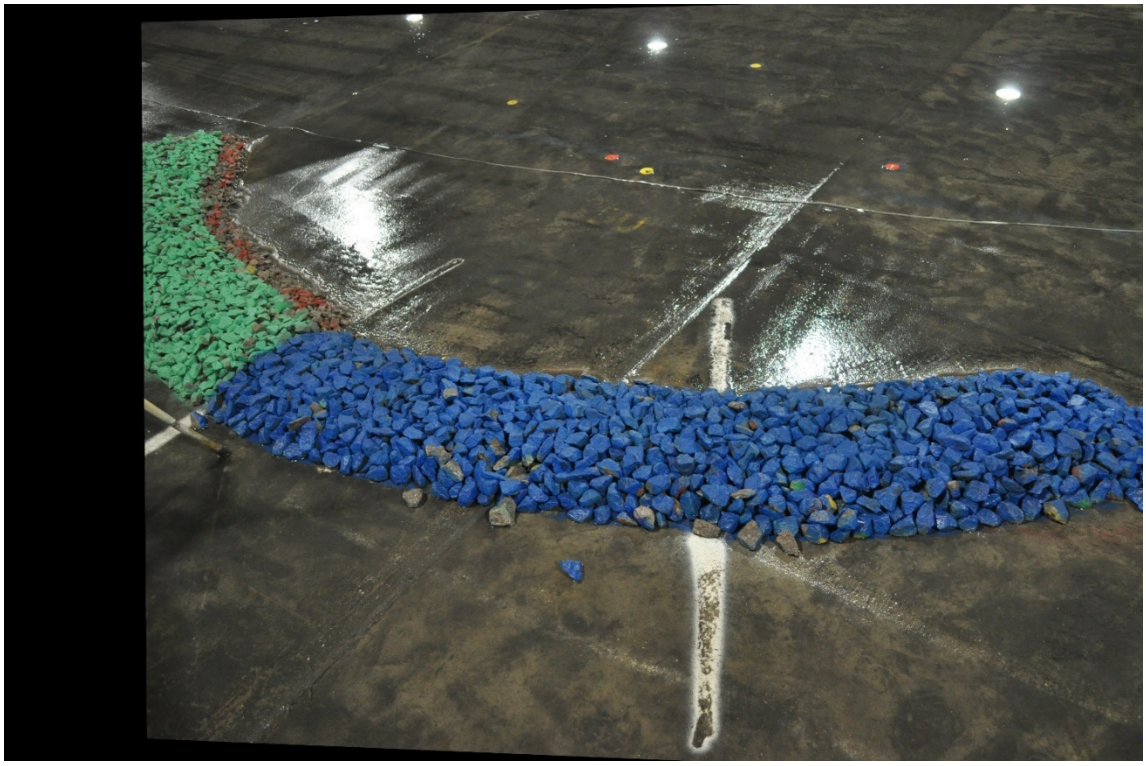

Figure D.179: Post Test Part 05 (WC_EXT_WL_01) stability photograph for BW3-4, position 15

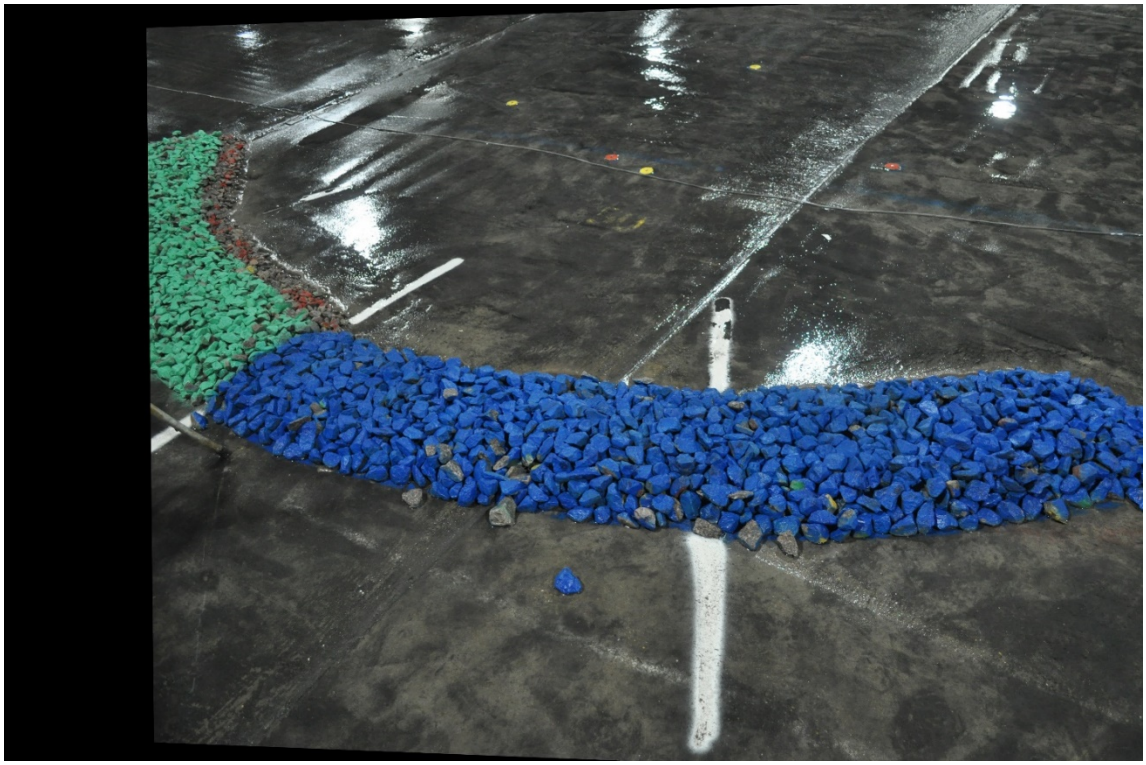

Figure D.180: Post Test Part 06 (WC_EXT_WL_02) stability photograph for BW3-4, position 15

## D.2.5. BW3-5

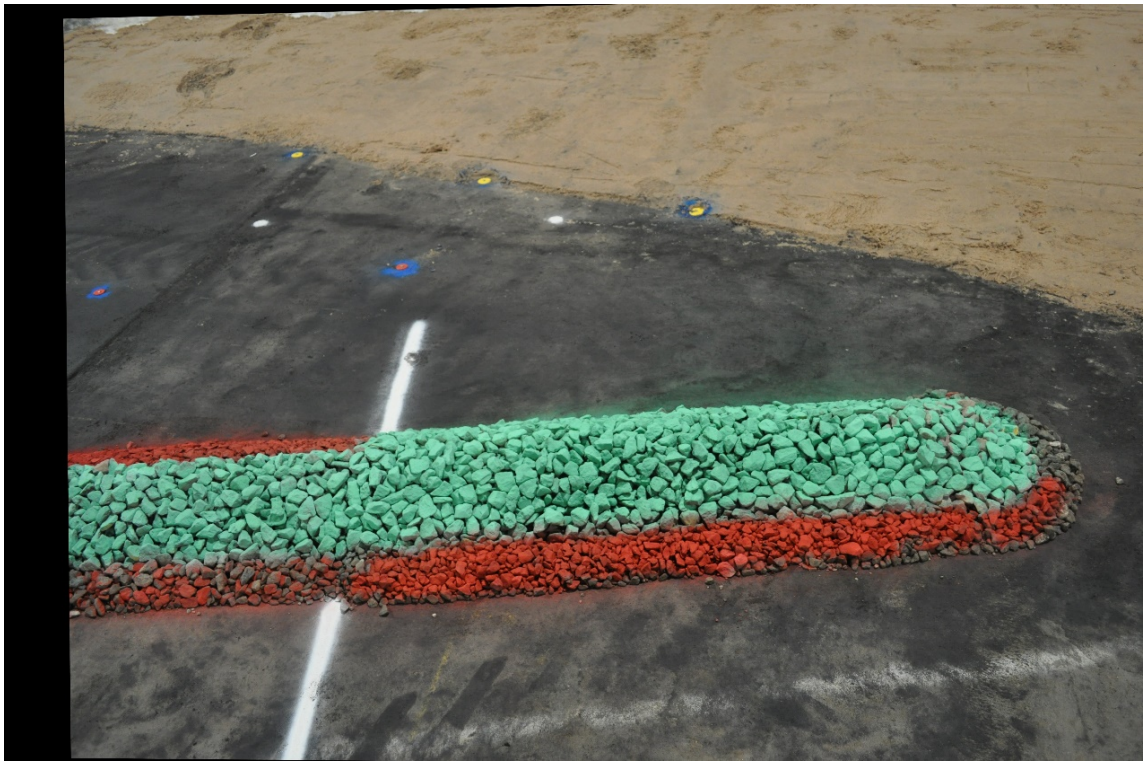

Figure D.181: Pre-test stability photograph for BW3-5, position 16

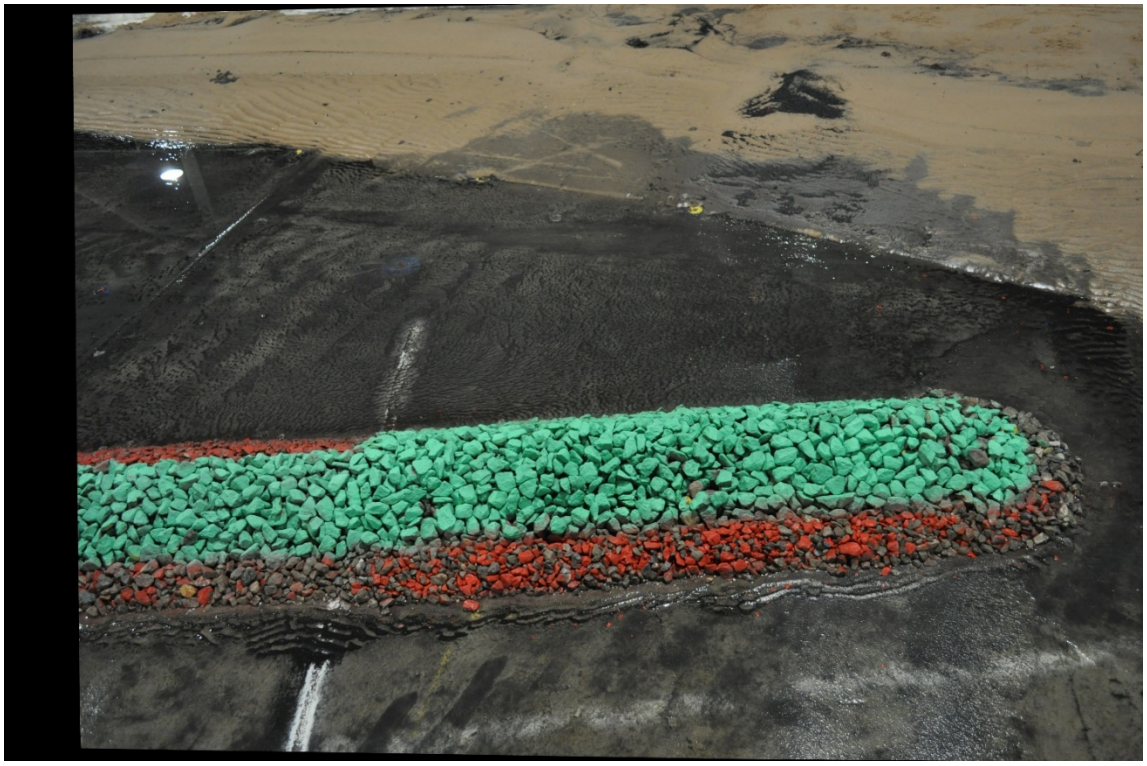

Figure D.182: Post Test Part 01 (WC_LOW_WL_SE) stability photograph for BW3-5, position 16

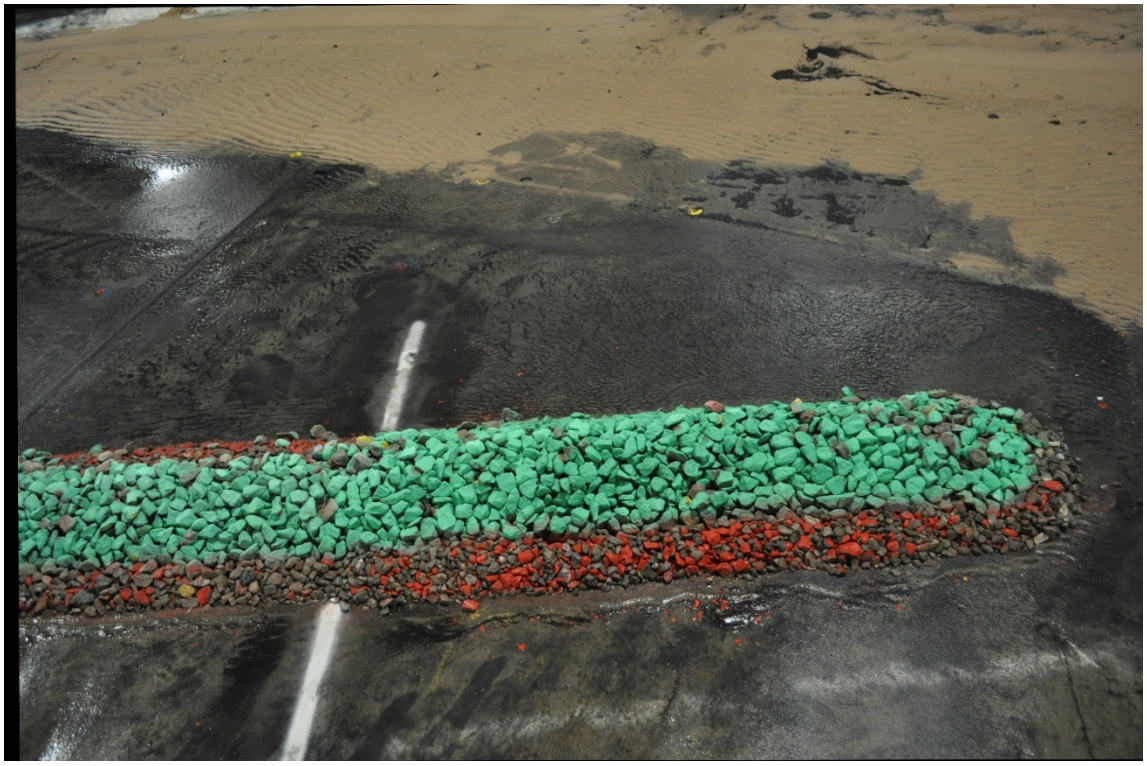

Figure D.183: Post Test Part 02 (WC_HIGH_WL_SE) stability photograph for BW3-5, position 16

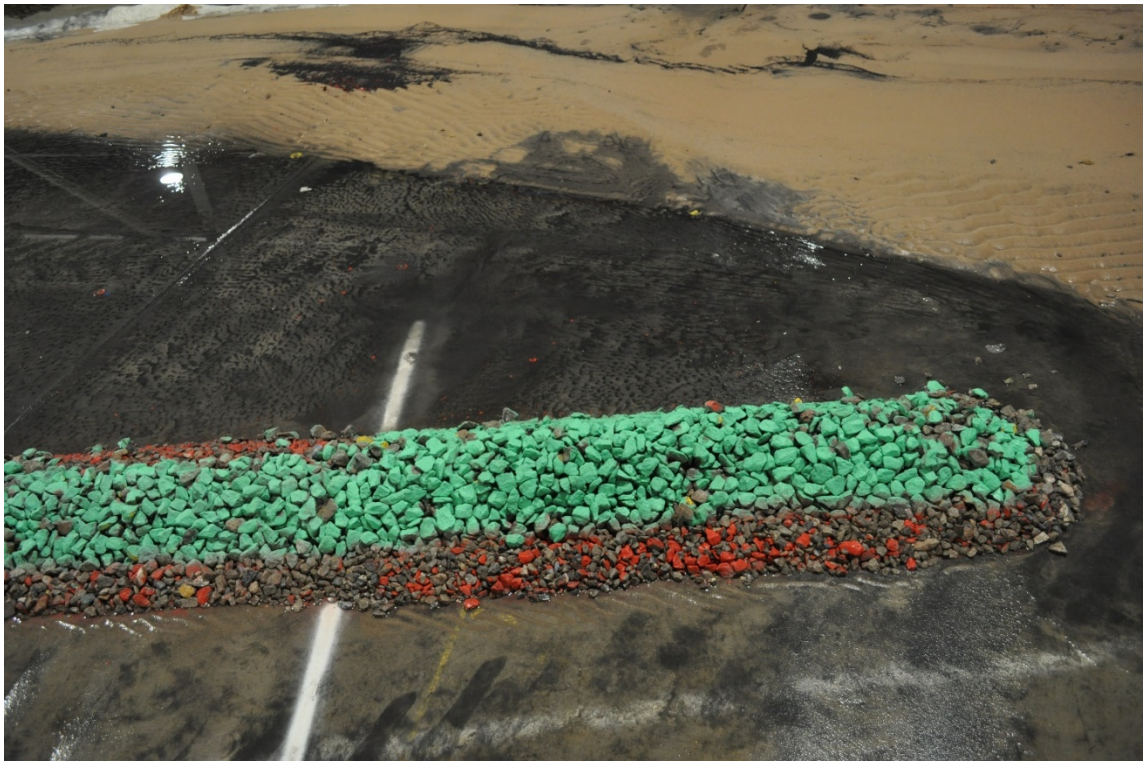

Figure D.184: Post Test Part 03 (WC_LOW_WL) stability photograph for BW3-5, position 16

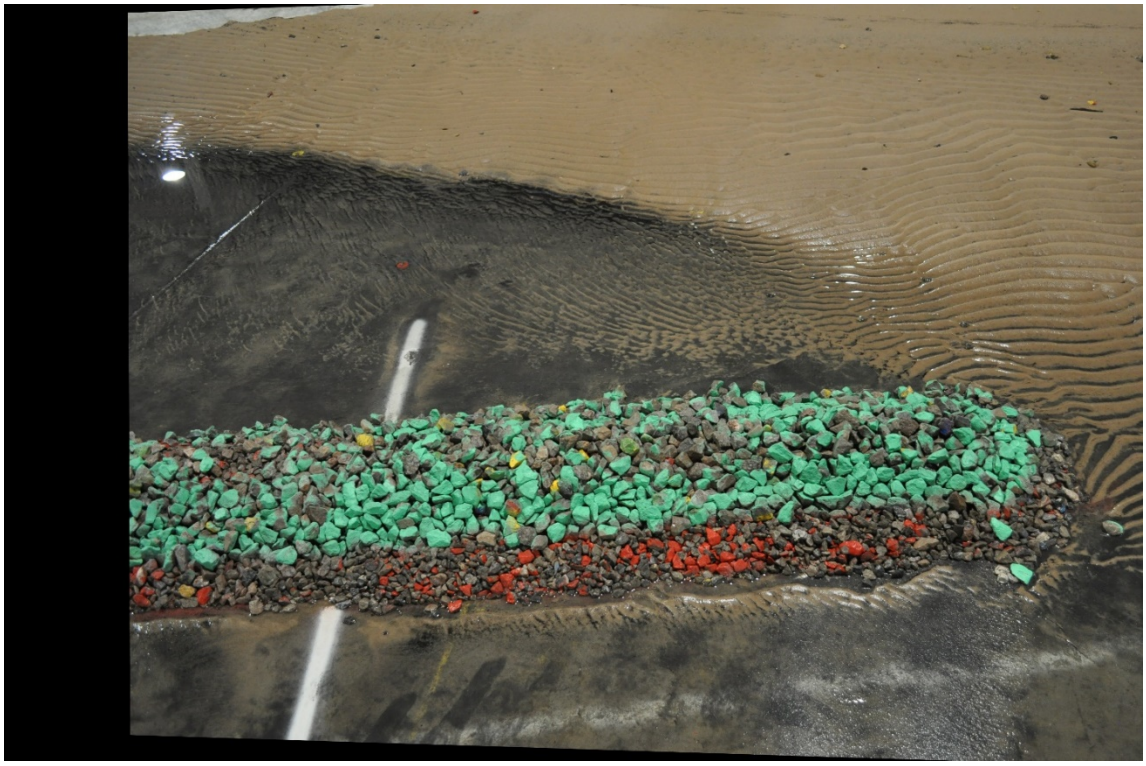

Figure D.185: Post Test Part 04 (WC_HIGH_WL) stability photograph for BW3-5, position 16

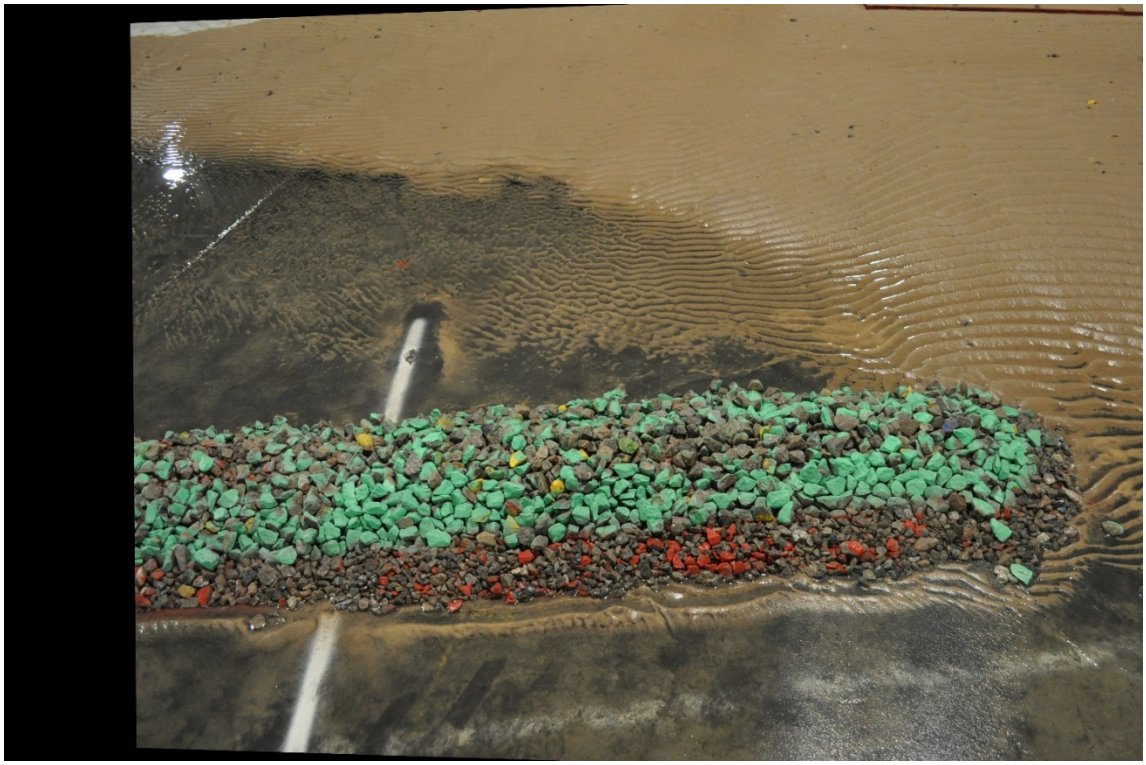

Figure D.186: Post Test Part 05 (WC_EXT_WL_01) stability photograph for BW3-5, position 16

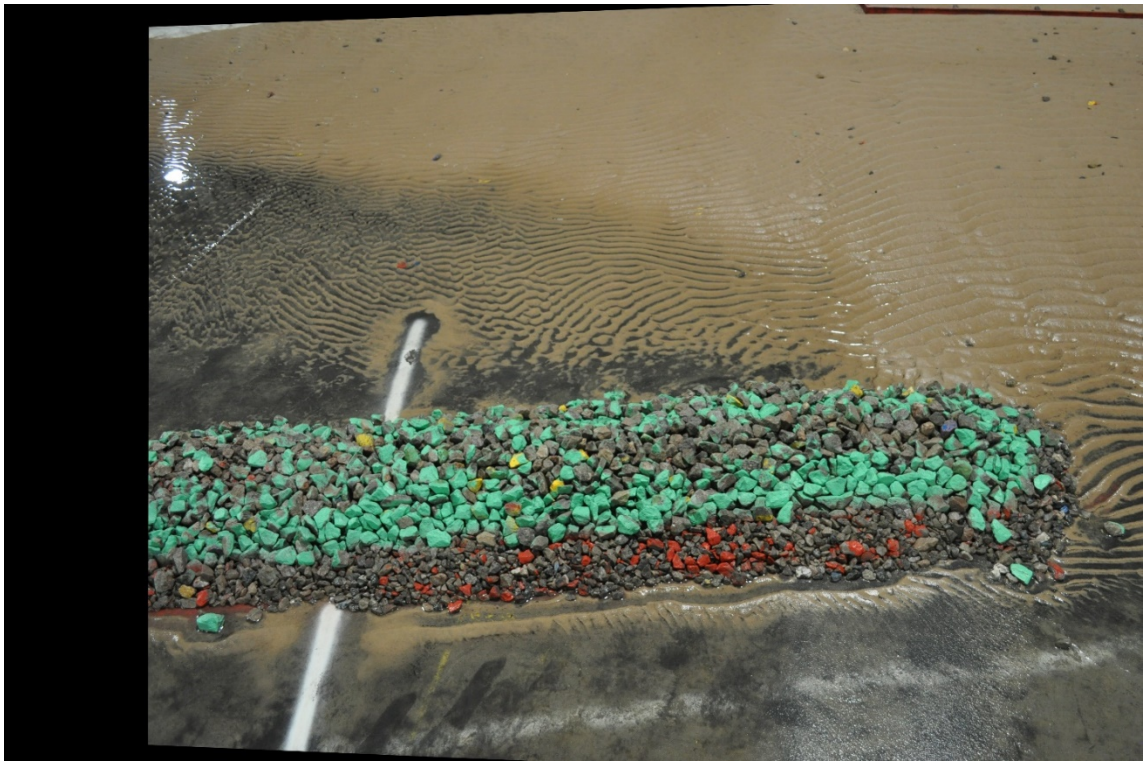

Figure D.187: Post Test Part 06 (WC_EXT_WL_02) stability photograph for BW3-5, position 16

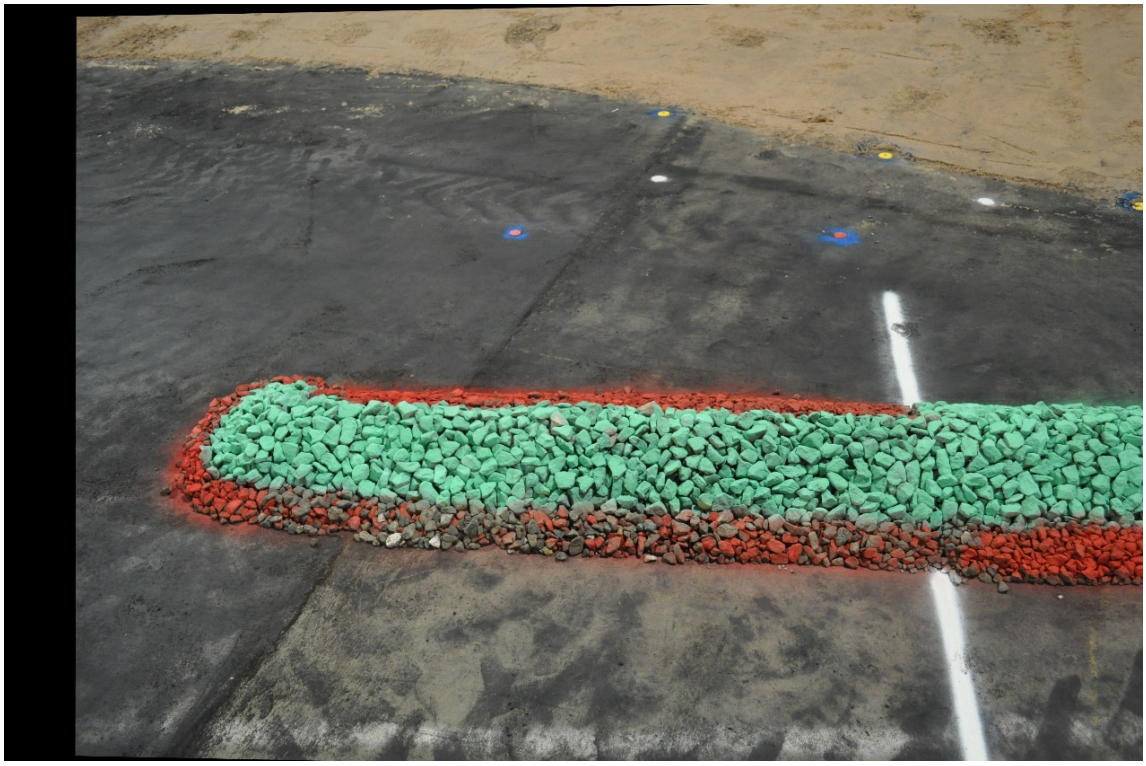

Figure D.188: Pre-test stability photograph for BW3-5, position 17

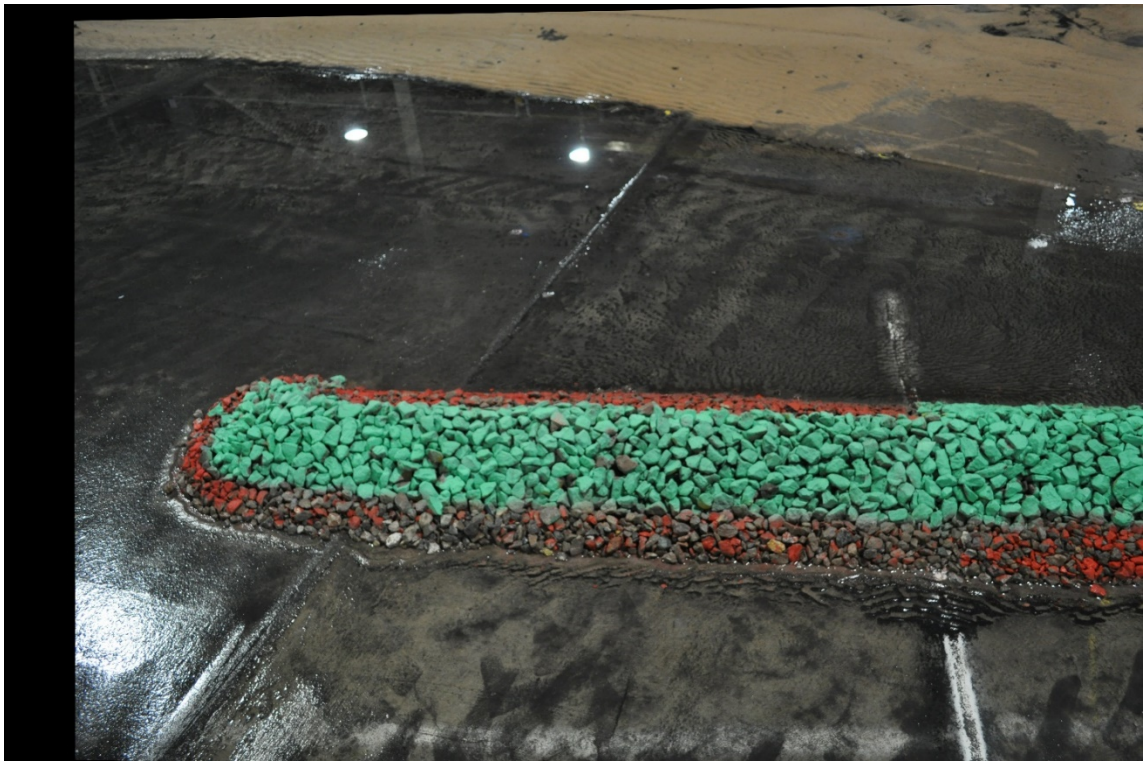

Figure D.189: Post Test Part 01 (WC_LOW_WL_SE) stability photograph for BW3-5, position 17

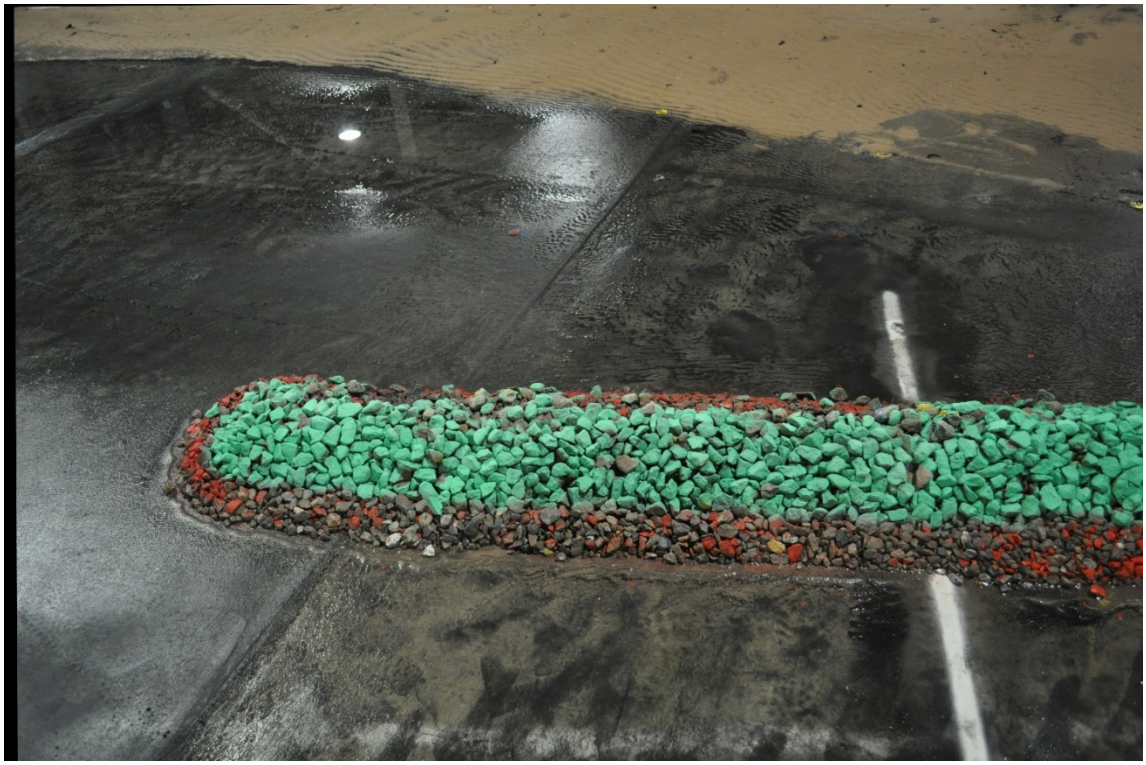

Figure D.190: Post Test Part 02 (WC_HIGH_WL_SE) stability photograph for BW3-5, position 17

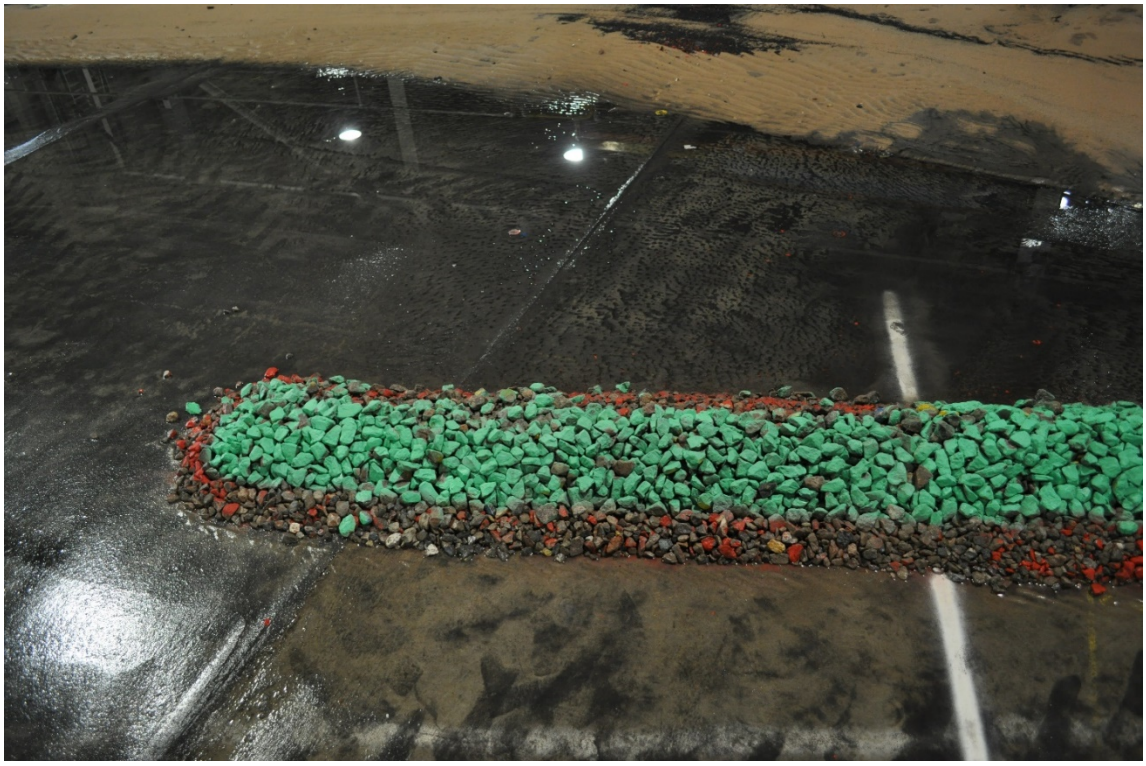

Figure D.191: Post Test Part 03 (WC_LOW_WL) stability photograph for BW3-5, position 17

Figure D.192: Post Test Part 04 (WC_HIGH_WL) stability photograph for BW3-5, position 17

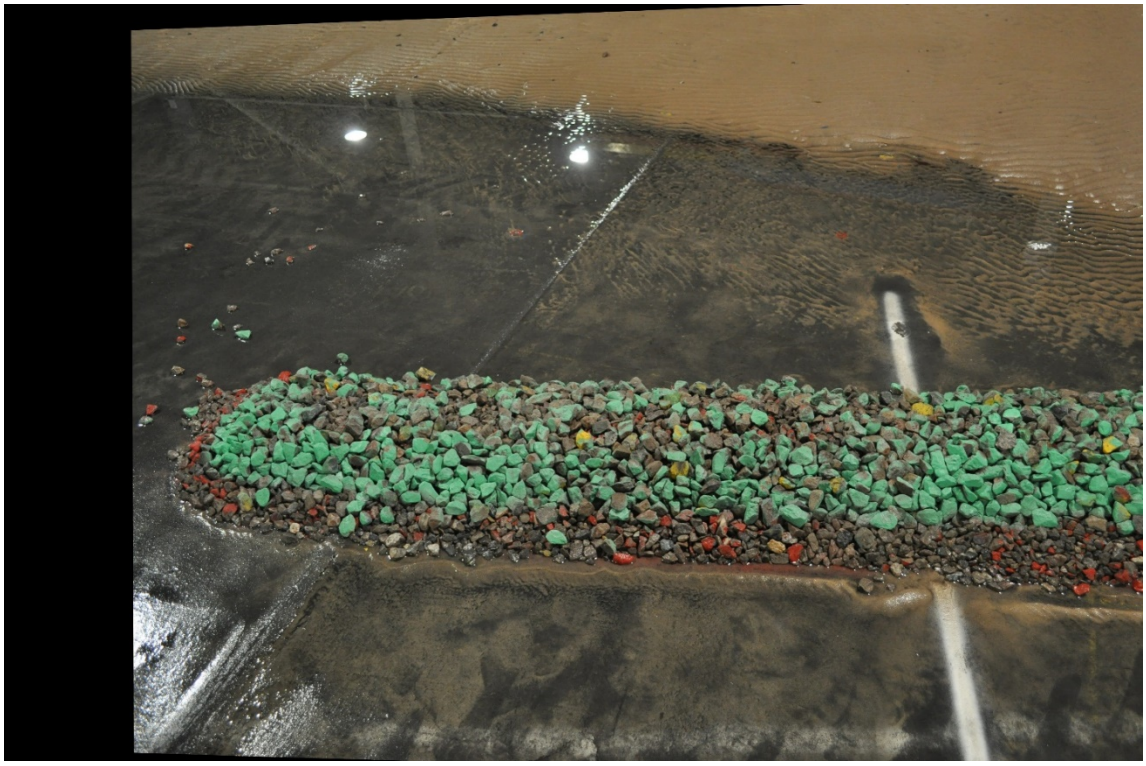

Figure D.193: Post Test Part 05 (WC_EXT_WL_01) stability photograph for BW3-5, position 17

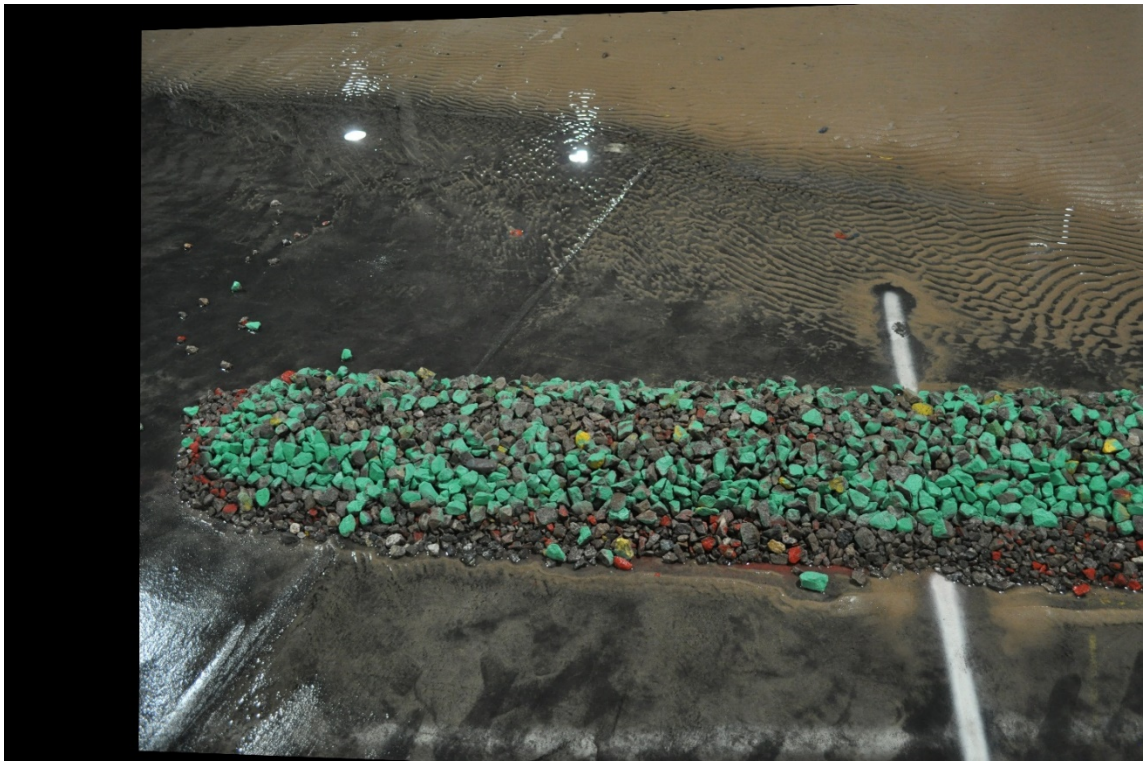

Figure D.194: Post Test Part 06 (WC_EXT_WL_02) stability photograph for BW3-5, position 17

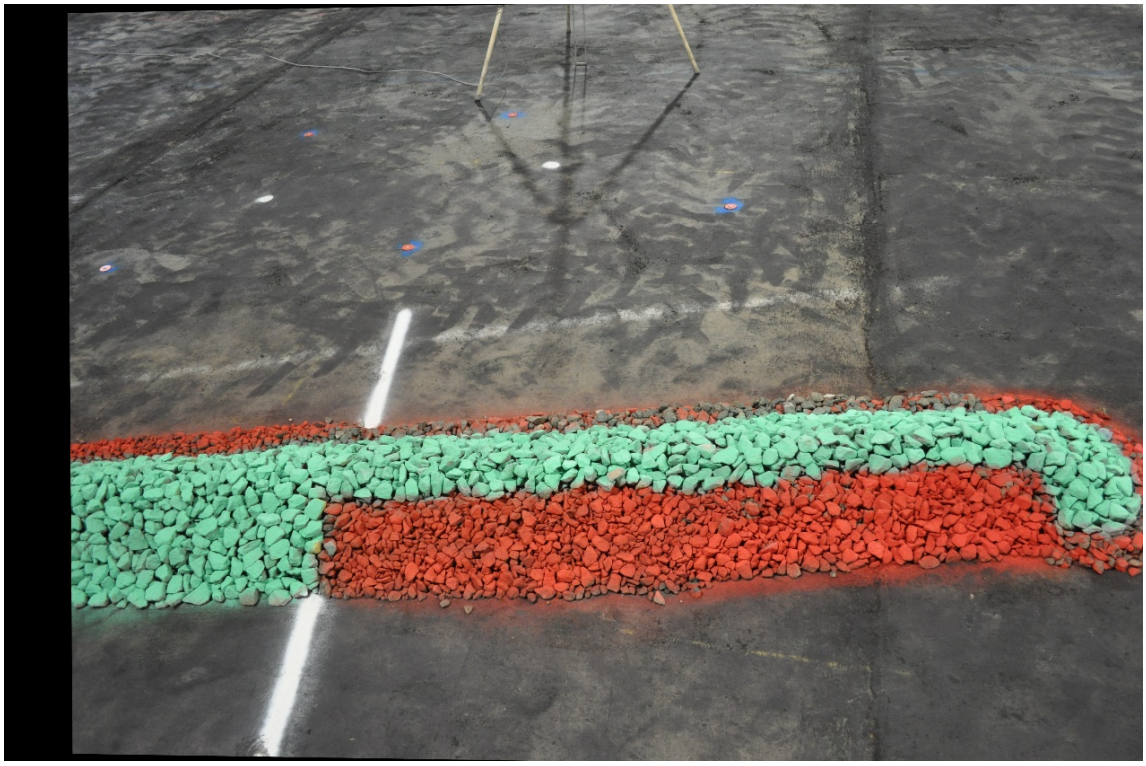

Figure D.195: Pre-test stability photograph for BW3-5, position 18

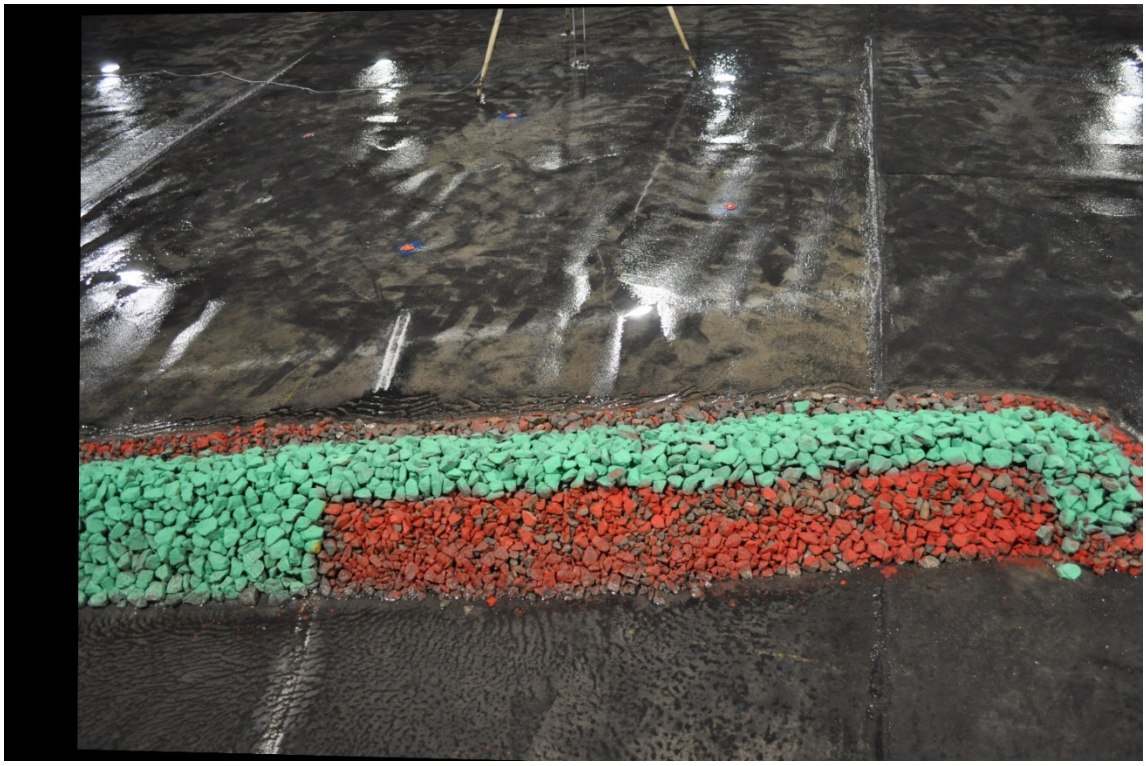

Figure D.196: Post Test Part 01 (WC_LOW_WL_SE) stability photograph for BW3-5, position 18

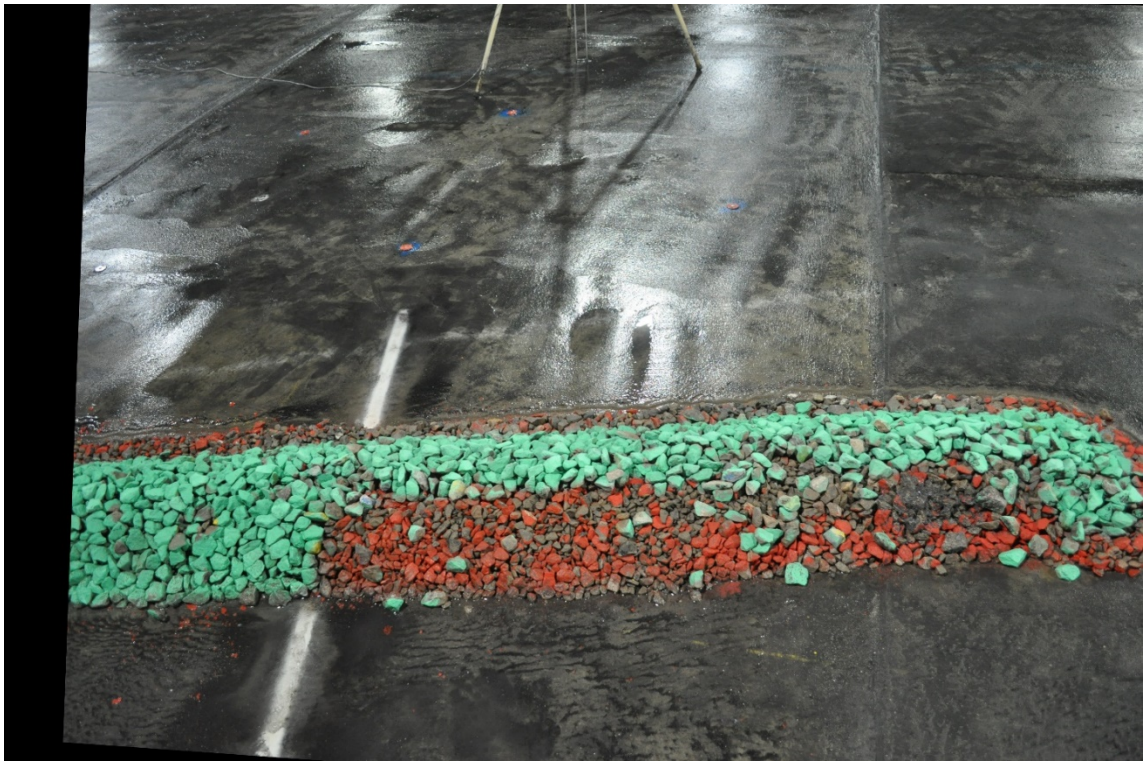

Figure D.197: Post Test Part 02 (WC_HIGH_WL_SE) stability photograph for BW3-5, position 18

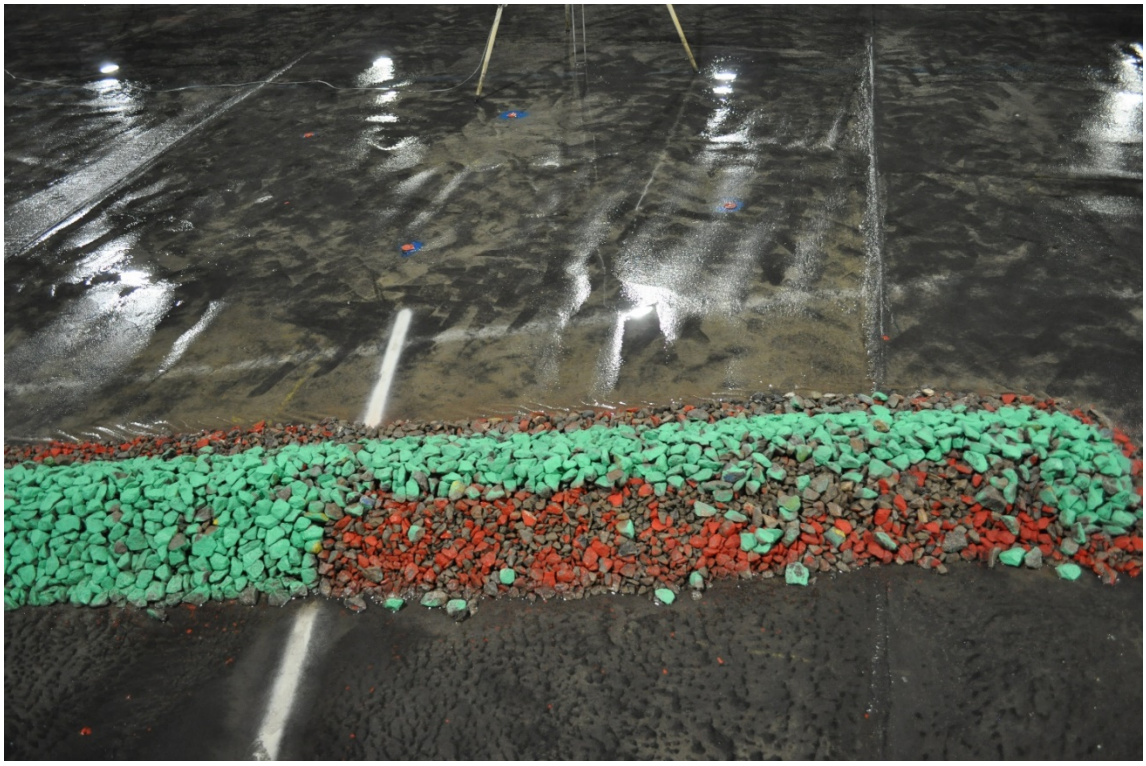

Figure D.198: Post Test Part 03 (WC_LOW_WL) stability photograph for BW3-5, position 18

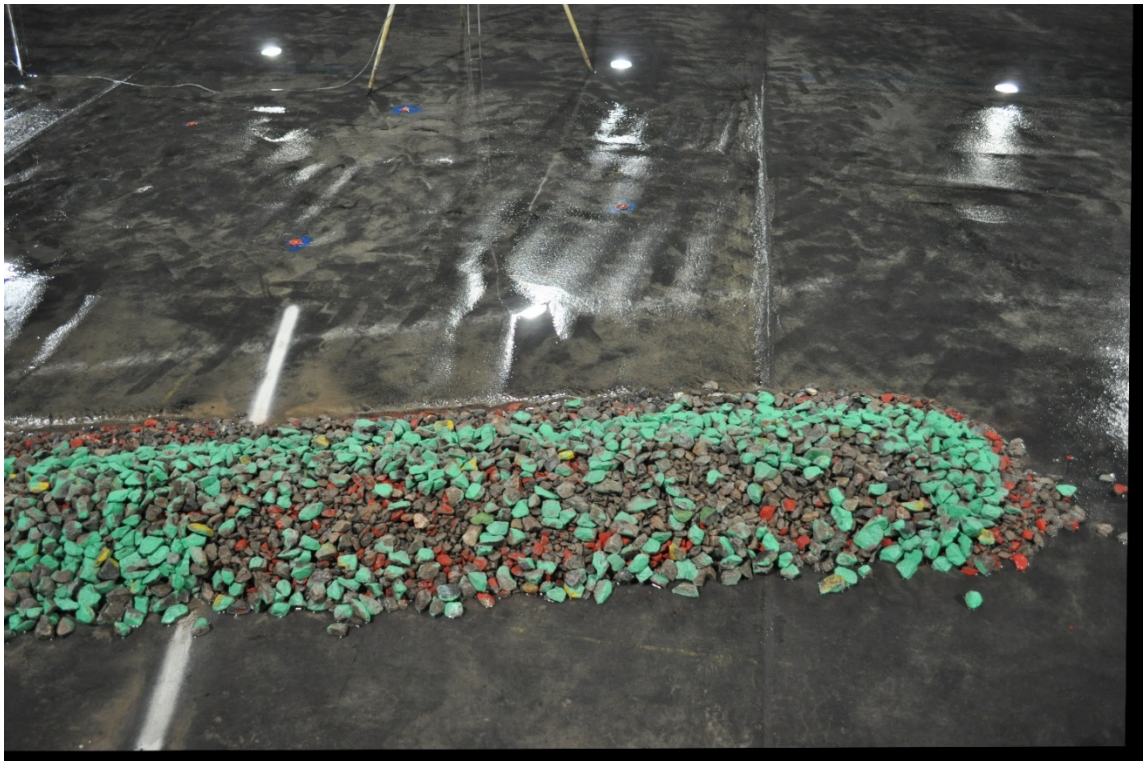

Figure D.199: Post Test Part 04 (WC_HIGH_WL) stability photograph for BW3-5, position 18

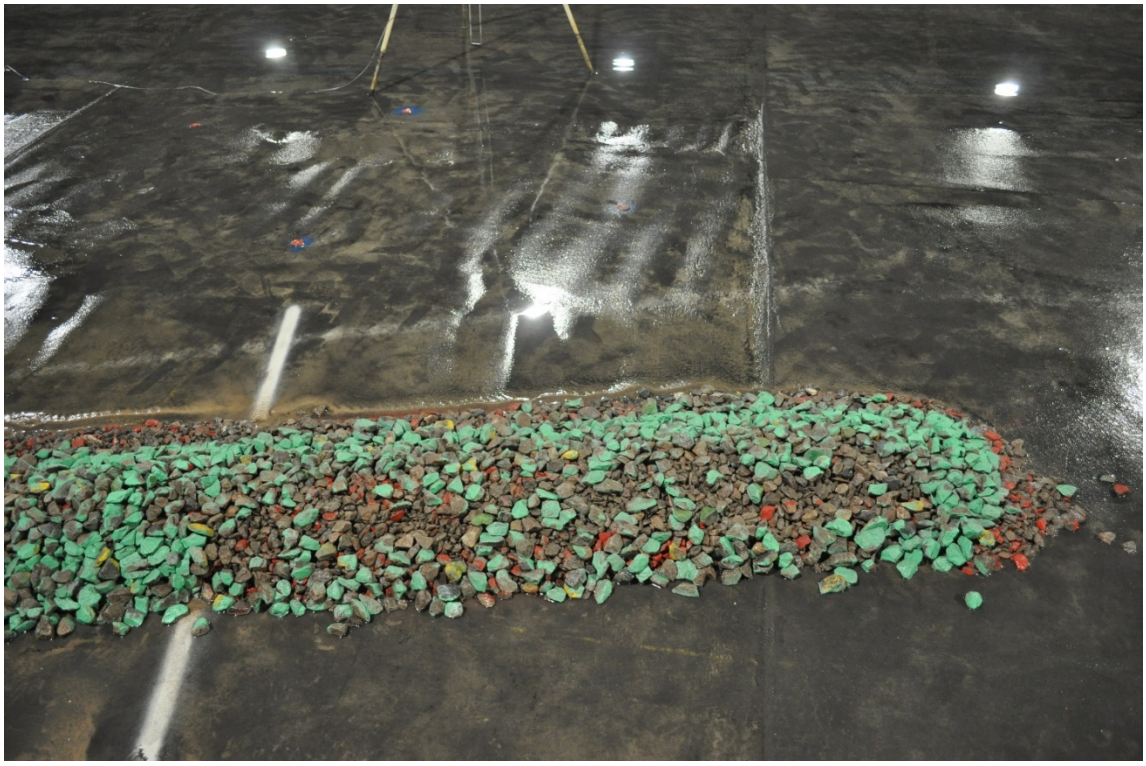

Figure D.200: Post Test Part 05 (WC_EXT_WL_01) stability photograph for BW3-5, position 18

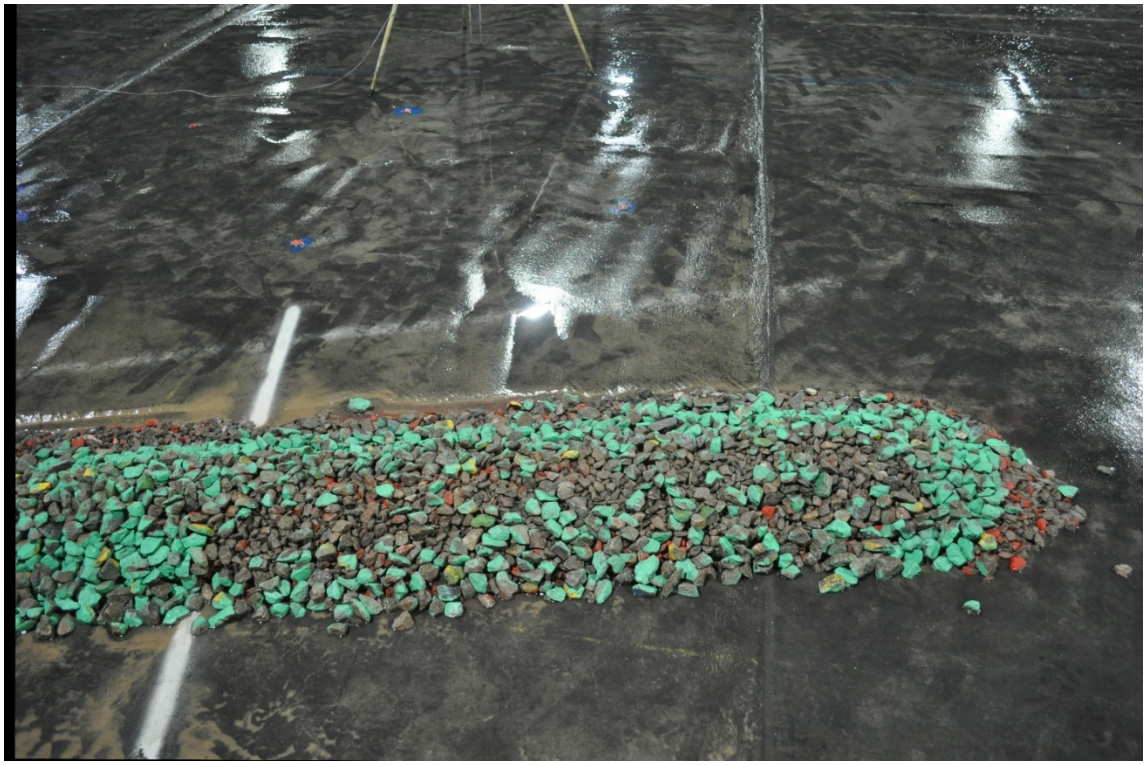

Figure D.201: Post Test Part 06 (WC_EXT_WL_02) stability photograph for BW3-5, position 18

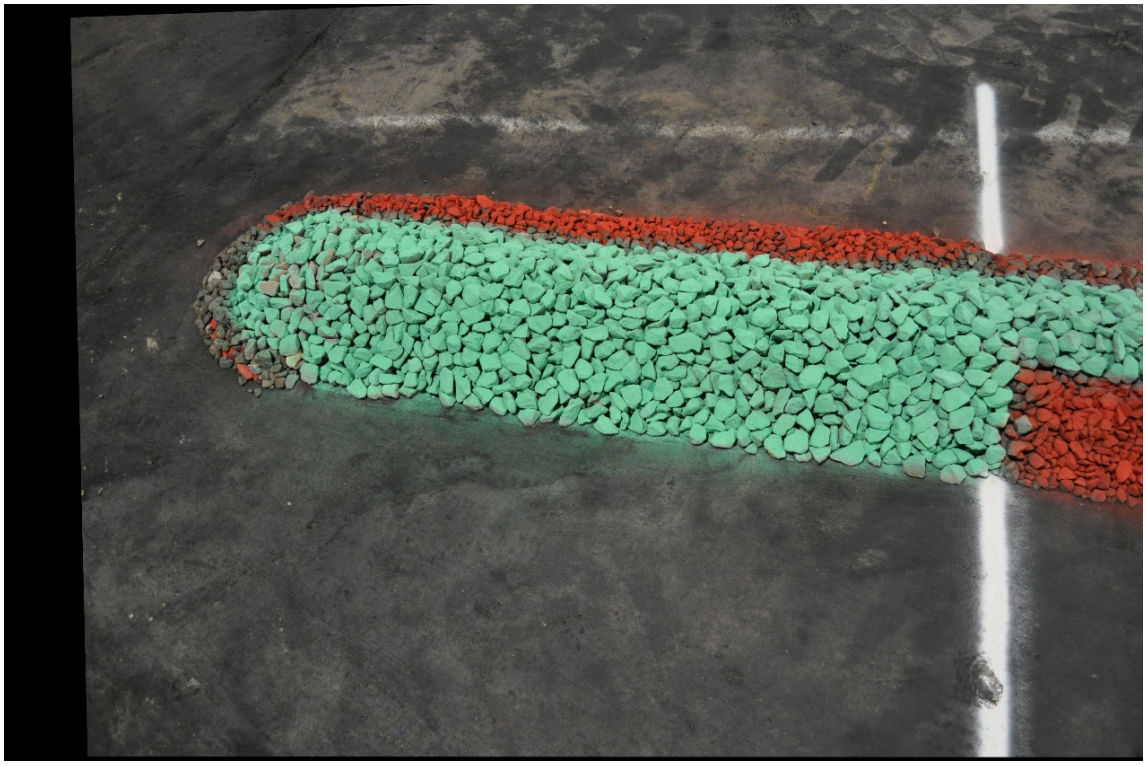

Figure D.202: Pre-test stability photograph for BW3-5, position 19

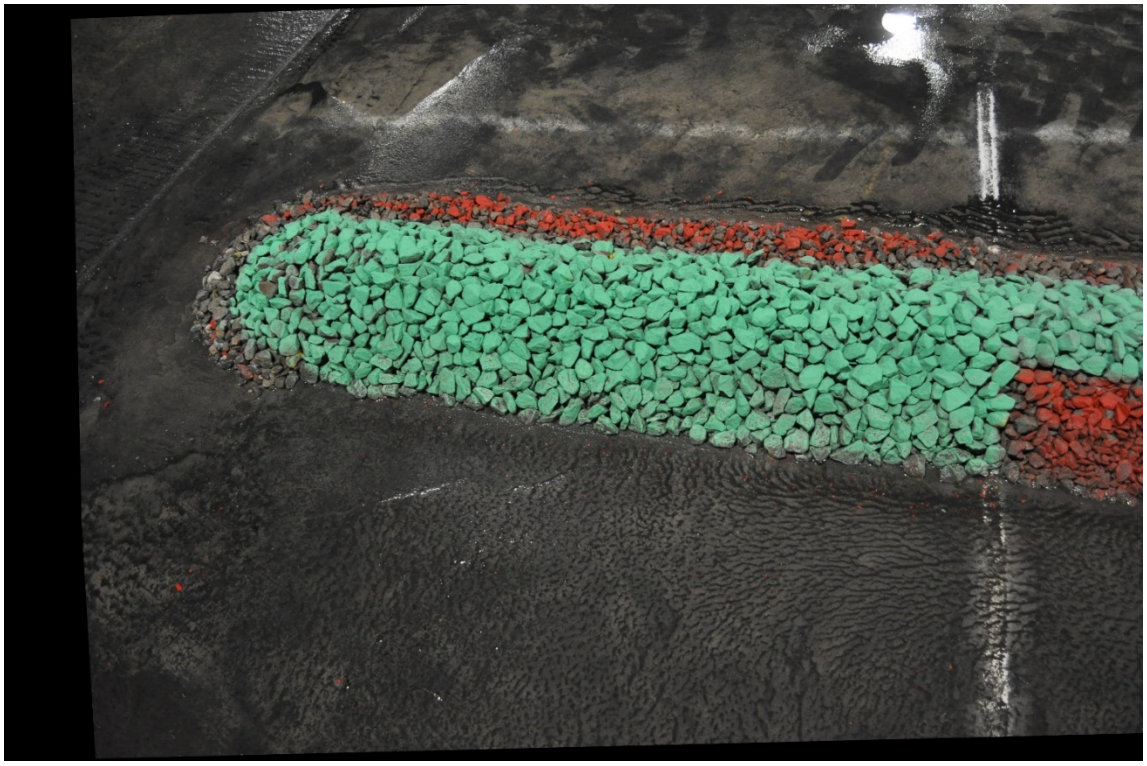

Figure D.203: Post Test Part 01 (WC_LOW_WL_SE) stability photograph for BW3-5, position 19

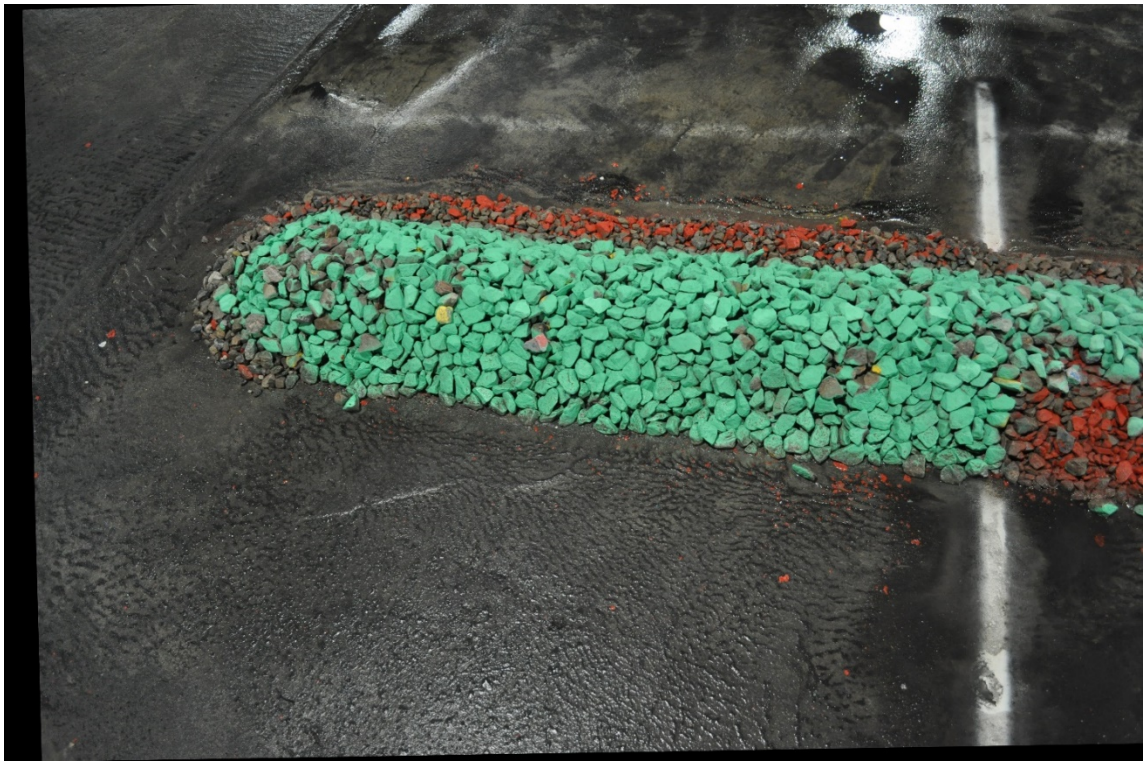

Figure D.204: Post Test Part 02 (WC_HIGH_WL_SE) stability photograph for BW3-5, position 19

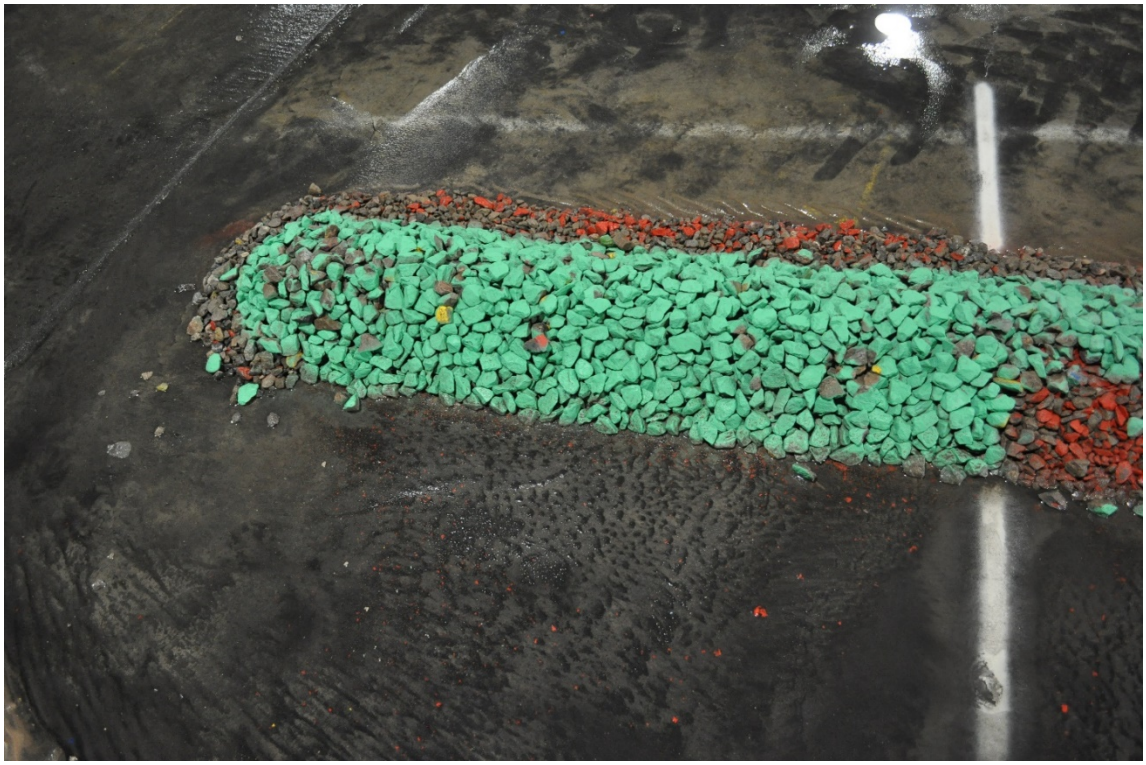

Figure D.205: Post Test Part 03 (WC_LOW_WL) stability photograph for BW3-5, position 19

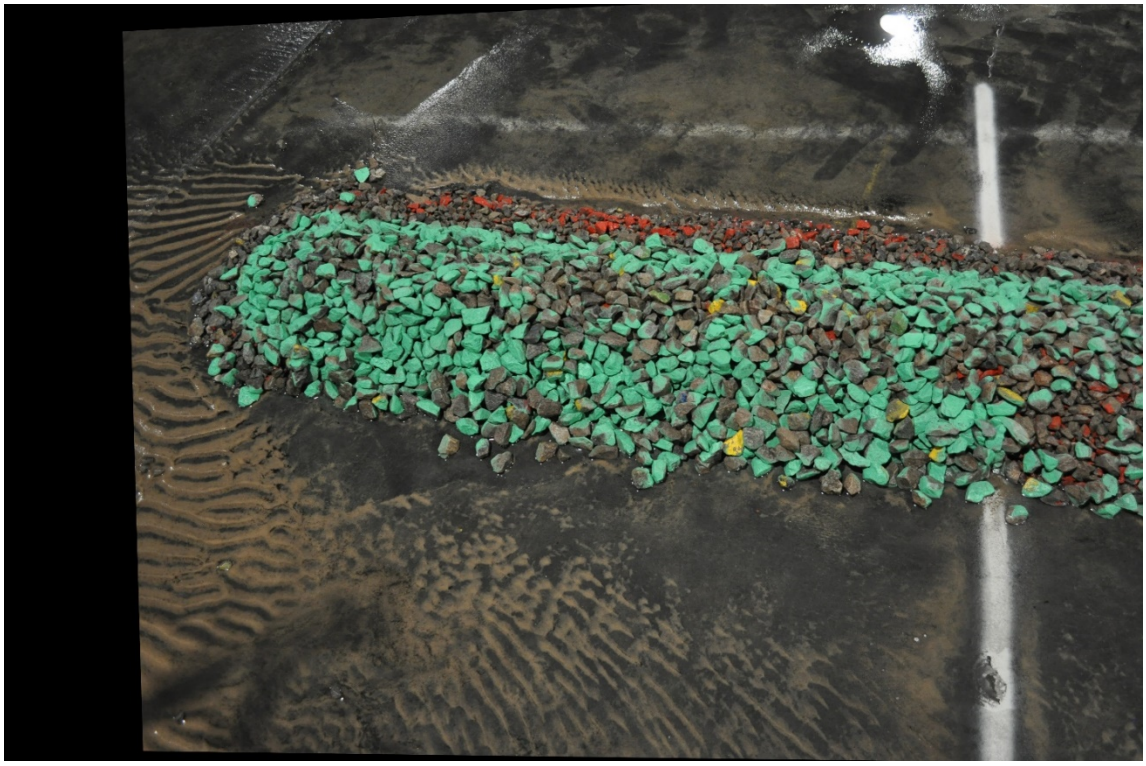

Figure D.206: Post Test Part 04 (WC_HIGH_WL) stability photograph for BW3-5, position 19

No image available

Figure D.207: Post Test Part 05 (WC_EXT_WL_01) stability photograph for BW3-5, position 19

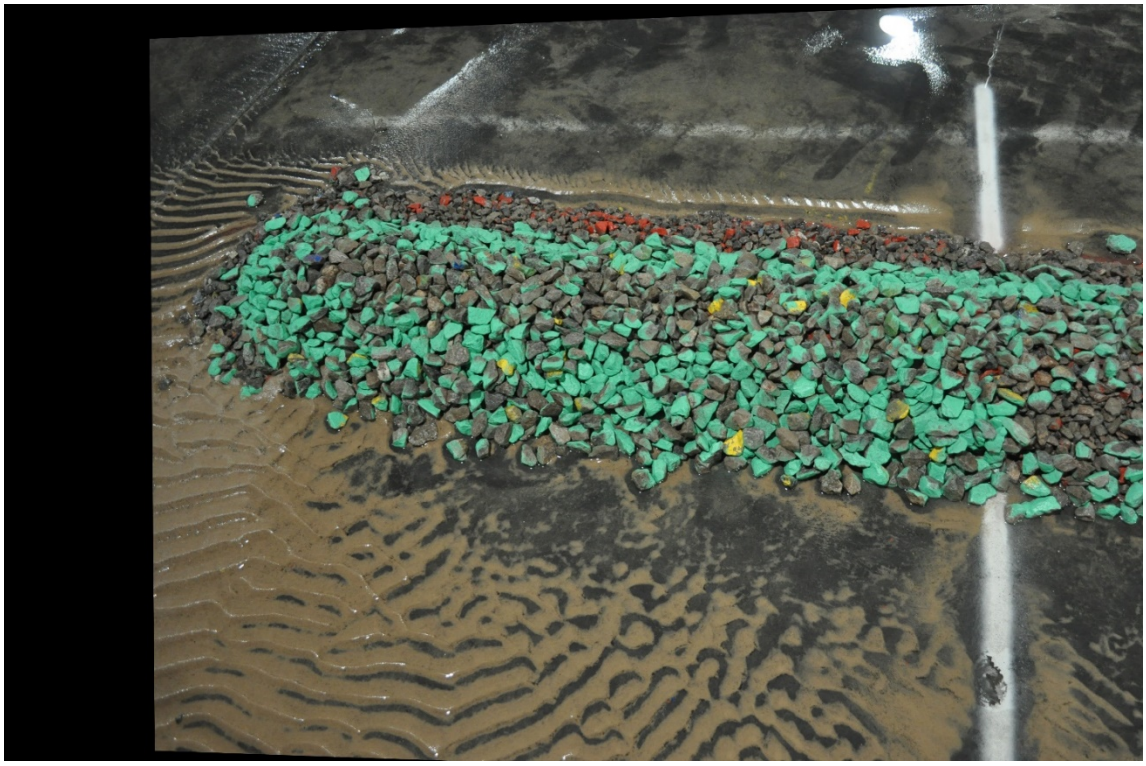

Figure D.208: Post Test Part 06 (WC_EXT_WL_02) stability photograph for BW3-5, position 19

HR Wallingford
*Working with water*

HR Wallingford is an independent engineering and environmental hydraulics organisation. We deliver practical solutions to the complex water-related challenges faced by our international clients. A dynamic research programme underpins all that we do and keeps us at the leading edge. Our unique mix of know-how, assets and facilities includes state of the art physical modelling laboratories, a full range of numerical modelling tools and, above all, enthusiastic people with world-renowned skills and expertise.

HR Wallingford, Howbery Park, Wallingford, Oxfordshire OX10 8BA, United Kingdom
tel +44 (0)1491 835381 fax +44 (0)1491 832233 email info@hrwallingford.com
www.hrwallingford.com

FS 516431
EMS 558310
OHS 595357

© HR Wallingford